

# **$C_{NHC}NC_{NHC}$ -Pincer Complexes of Group 9 and Their Catalytic Activities in Homogeneous Catalysis**

**Dissertation**

der Mathematisch-Naturwissenschaftlichen Fakultät  
der Eberhard Karls Universität Tübingen  
zur Erlangung des Grades eines  
Doktors der Naturwissenschaften  
(Dr. rer. nat.)

vorgelegt von  
M. Sc. Yingying Tian  
aus Bozhou, P. R. China

Tübingen  
2020



Gedruckt mit Genehmigung der Mathematisch-Naturwissenschaftlichen Fakultät der  
Eberhard Karls Universität Tübingen.

Tag der mündlichen Qualifikation: 25.05.2020

Dekan:

Prof. Dr. Wolfgang Rosenstiel

1. Berichterstatter:

Prof. Dr. Doris Kunz

2. Berichterstatter:

Prof. Dr. Reiner Anwander





The work presented currently was done from October 2016 to April 2020 in the Institute of Inorganic Chemistry under the supervision of Prof. Dr. Doris Kunz.

I am deeply grateful to Prof. Dr. Doris Kunz for providing such interesting research topics and a great working atmosphere in the whole group.



To spend life side by side, in the sway of our dreams: your patriotic dream, our humanitarian dream and our scientific dream.

Marie Curie



## Abstract (English)

With the interest in N-heterocyclic carbenes (NHCs), this thesis deals with the design and synthesis of  $C_{NHC}NC_{NHC}$ -pincer complexes with transition-metals of group 9 and their applications as catalysts in small molecule isomerization and semihydrogenation of alkynes. The details are as follows.

In the first chapter, the nucleophilic Meinwald rearrangement of functionalized terminal epoxides into methyl ketones under mild conditions was realized using  $[Rh(bimca^{Homo})]$ . An excellent regio- and chemoselectivity is obtained for the first time for aryl oxiranes.

In the second chapter, further development of the Meinwald rearrangement was made with the more reactive  $[Rh(bimca^{Me,Homo})]$  and the substrate scope was extended to internal epoxides. In addition, mechanistic investigations showed that the catalytic cycle follows a  $\beta$ -hydride elimination–reductive elimination pathway after the nucleophilic ring opening of the epoxide.

In the third chapter, two methods for the synthesis of the bis(imidazolin-2-ylidene)carbazolide cobalt(I) complex  $[Co(bimca^{Homo})]$  have been developed. The first route relies on the direct transmetalation of the *in situ* generated lithium complex  $[Li(bimca^{Homo})]$  with  $Co(PPh_3)_3Cl$ . The second one is a two-step synthesis that consists of the transmetalation of  $[Li(bimca^{Homo})]$  with  $CoCl_2$  followed by reduction of the Co(II) complex to yield the desired Co(I) complex. The analogous rhodium and iridium complexes were prepared by transmetalation of  $[Li(bimca^{Homo})]$  or  $[K(bimca^{Homo})]$  with  $[M(COD)(\mu-Cl)]_2$ . The catalytic activity of  $[Co(bimca^{Homo})]$  and  $[Ir(bimca^{Homo})]$  in the epoxide isomerization was tested with and without the presence of  $H_2$ . When  $[M(bimca^{Homo})]$  ( $M = Rh$  or  $Ir$ ) were exposed to 1 bar  $H_2$  at 80 °C single crystals formed whose X-ray structure analyses revealed the hydrogenation of the *N*-homoallyl moieties and formation the dimeric hydrido complexes  $[Ir(bimca^{n-Bu})(H)_2]_2$  and  $[Rh(bimca^{n-Bu})(H)_2]_2$ .

In the fourth chapter, the selective isomerization of various *N*-Boc protected terminal aziridines to enamides is presented using the highly reactive nucleophilic [Rh(bimca<sup>Me,Homo</sup>)] with the Lewis acid LiNTf<sub>2</sub> as co-catalyst under moderate conditions. The reaction proceeds smoothly with only 1 mol% catalyst loading and excellent yields were achieved. An intermediate containing an enamide with a non-conjugated terminal C=C double bond was detected during the course of the reaction, which isomerizes to form the thermodynamically favored 2-amido styrene. Mechanistic insight is gained based on these observations.

In the last chapter, the semihydrogenation of both terminal and internal alkynes was developed with [Co(bimca<sup>Homo</sup>)]. Catalytic reactions were performed under ambient conditions. Several terminal and internal alkynes were semihydrogenated to yield olefins without over-reduction. In the case of internal alkynes, *cis*-olefins were achieved exclusively after semihydrogenation. Full reduction of alkynes was realized by tuning the reaction conditions.

## Abstract (German)

Aufgrund des generellen Interesses an N-heterocyclischen Carbenen (NHCs) handelt diese Doktorarbeit vom Design und der Synthese von  $C_{NHC}NC_{NHC}$ -Pincer-Komplexen mit Übergangsmetallen der Gruppe 9. Zusätzlich wird ihre Anwendung in der Isomerisierung kleiner Moleküle und Teilhydrierung von Alkinen beschrieben. Die Details sind wie folgt:

Im ersten Kapitel wird die nucleophile Meinwald-Umlagerung von funktionalisierten terminalen Epoxiden zu Methylketone unter sehr milden Bedingungen mit der  $[Rh(bimca^{Homo})]$ -Katalysatorvorstufe dargestellt. Es liegt eine hervorragende, erstmalige Regio- und Chemoselektivität für Aryl-Oxirane vor.

Im zweiten Kapitel werden weitere Errungenschaften in der Meinwald-Umlagerung mittels des reaktiveren  $[Rh(bimca^{Me,Homo})]$ -Komplexes vorgestellt. Die Substratbandbreite konnte für interne Epoxide erweitert werden. Zusätzlich erfolgte der Nachweis, dass der Katalysezyklus nach einer nukleophilen Ringöffnung des Epoxids über einen  $\beta$ -Hydrideliminierung–reduktiven Eliminierungs-Mechanismus abläuft.

Im dritten Kapitel werden zwei Methoden zur Synthese des Bis(imidazolin-2-ylidene)carbazolid Cobalt(I)-Komplexes  $[Co(bimca^{Homo})]$  vorgestellt. Der erste Syntheseweg verläuft über die direkte Transmetallierung des *in situ* generierten Lithium-Komplexes  $[Li(bimca^{Homo})]$  mit  $Co(PPh_3)_3Cl$ . Die zweite Route geht über eine zweistufige Synthese mit einer Transmetallierung des Lithiumkomplexes  $[Li(bimca^{Homo})]$  mit  $CoCl_2$  und einer anschließenden Reduktion des Co(II) zu dem gewünschten Co(I)-Komplex. Die analogen Rhodium- und Iridiumkomplexe wurden über eine Transmetallierungsreaktion von  $[Li(bimca^{Homo})]$  oder  $[K(bimca^{Homo})]$  mittels  $[M(COD)(\mu-Cl)]_2$  dargestellt. Die katalytischen Aktivitäten von  $[Co(bimca^{Homo})]$  und  $[Ir(bimca^{Homo})]$  in der Epoxidisomerisierungs-Reaktion wurden sowohl in Anwesenheit von  $H_2$  als auch ohne durchgeführt. Durch das Vorhandensein von einem bar  $H_2$  bei  $80\text{ }^\circ\text{C}$  bei den Komplexen  $[M(bimca^{Homo})]$  ( $M = Rh$  or  $Ir$ ) konnten Einkristalle isoliert werden, welche Röntgenkristallographisch analysiert wurden. Die Molekülstrukturen

zeigten eine Hydrierung der *N*-Homoallyleinheiten und Bildung der dimerisierten Hydridokomplexe  $[\text{Ir}(\text{bimca}^{n\text{-Bu}})(\text{H})_2]_2$  und  $[\text{Rh}(\text{bimca}^{n\text{-Bu}})(\text{H})_2]_2$ .

Das vierte Kapitel dieser Arbeit behandelt die selektive Isomerisierung von verschiedenen *N*-Boc geschützten, endständigen Aziridinen zu Enaminen. Dies kann durch den hochreaktiven, nucleophilen  $[\text{Rh}(\text{bimca}^{\text{Me,Homo}})]$ -Komplex und der Lewis-Säure  $\text{LiNTf}_2$  als Cokatalysator unter moderaten Bedingungen erreicht werden. Die Reaktionen erfolgten mit einer Katalysatormenge von lediglich 1 mol% und exzellenten Ausbeuten. Eine Zwischenstufe, die ein Enamid mit einer nicht-konjugierten endständigen C=C-Doppelbindung enthält, konnte im Verlauf der Reaktion detektiert werden. Diese isomerisiert zu dem thermodynamisch stabileren 2-Amidostyrol. Anhand dieser Beobachtung können mechanistische Einblicke werden erhalten.

Im letzten Kapitel wird die Teilhydrierung sowohl von terminalen als auch von internen Alkinen behandelt, welche mit dem  $[\text{Co}(\text{bimca}^{\text{Homo}})]$ -Komplex entwickelt worden ist. Die katalytischen Reaktionen erfolgten unter Umgebungsbedingungen. Einige terminale und interne Alkine wurden teilhydriert um Olefine zu erhalten, ohne diese zu überreduzieren. Im Falle von internen Alkinen werden ausschließlich *cis*-Olefine erhalten. Die gesamte Reduktion von Alkinen zu Alkanen kann durch Anpassung der Reaktionsbedingungen erreicht werden.



# Contents

<b>Abstract</b> (English)	I
<b>Abstrakt</b> (German)	III
<b>Contents</b>	V
<b>Introduction</b>	1
<b>Research Purpose</b>	7
<b>Results and Discussion</b>	9
<b>Chapter 1</b> Regio- and Chemoselective Rearrangement of Terminal Epoxides into Methyl Alkyl and Aryl Ketones	33
<b>Chapter 2</b> Nucleophilic Isomerization of Epoxides by Pincer-Rhodium Catalysts: Activity Increase and Mechanistic Insights	45
<b>Chapter 3</b> Synthesis and Reactivity of Cobalt(I) and Iridium(I) Complexes Bearing a Pentadentate <i>N</i> -Homoallyl Substituted Bis(NHC) Pincer-Ligand	64
<b>Chapter 4</b> Nucleophilic Rh <sup>I</sup> Catalyzed Selective Isomerization of Terminal Aziridines to Enamides	85
<b>Chapter 5</b> Semihydrogenation of Alkynes	95
<b>Summary</b>	103
<b>Outlook</b>	106
<b>Publications</b>	107
<b>Abbreviations</b>	
<b>List of Publications</b>	
<b>Acknowledgement</b>	
<b>Personal Contribution</b>	
<b>Curriculum Vitae</b>	



## Introduction

### N-Heterocyclic Carbenes

A carbene is a molecule containing a neutral carbon atom with a valence of two and two unshared valence electrons. They are classified as either singlets or triplets, depending on their electronic structure. Singlet carbenes are spin-paired which means the molecule adopts an  $sp^2$  hybrid structure. Triplet carbenes have two unpaired electrons.<sup>[1]</sup> Most carbenes have a nonlinear triplet ground state, except for those with nitrogen, oxygen, or sulfur atoms, and halides directly bonded to the divalent carbon. In an N-heterocyclic carbene (NHC) generated from the imidazol-2-ylidene, the adjacent nitrogen atoms stabilize the singlet state of the NHC by  $\pi$ -electron donating and  $\sigma$ -electron withdrawing effects, which leads to a four electron 3-center  $\pi$ -system (Figure 1).<sup>[2]</sup>

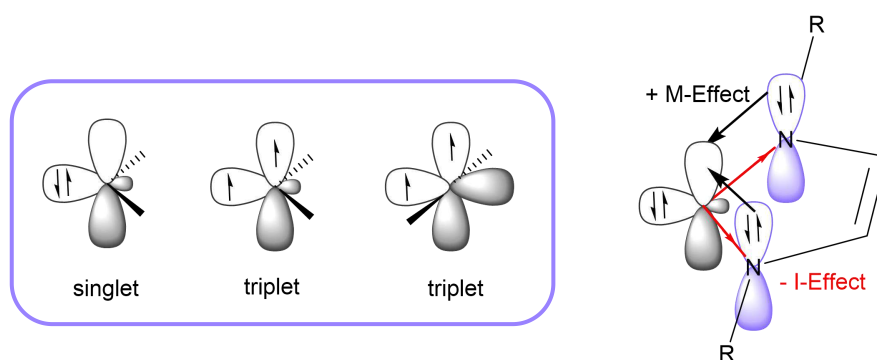
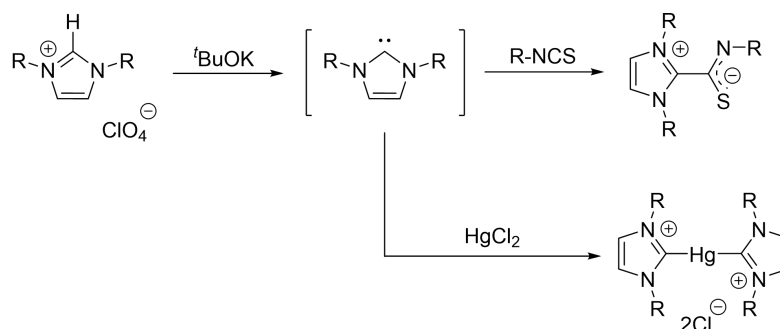


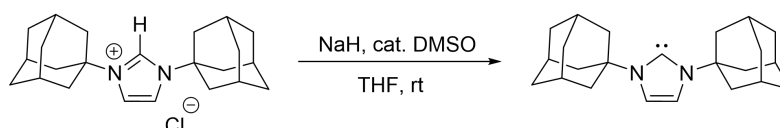
Figure 1. Carbenes of singlet and triplet types and an NHC (imidazol-2-ylidene).

NHCs, which mainly derived from imidazole, imidazoline, thiazole or triazole, are the best examples of stable carbenes, especially the ones derived from imidazole. In 1970, Wanzlick's group generated imidazol-2-ylidene carbenes by the deprotonation of an imidazolium salt.<sup>[3]</sup> However, they did not isolate imidazol-2-ylidenes, but instead the *in situ* generated carbenes were coordinated to mercury and isothiocyanate. Afterward, in 1991, a stable, isolated, and crystalline diaminocarbene was obtained by Arduengo and co-workers<sup>[4]</sup> through deprotonation of an imidazolium chloride with a strong base (Scheme 1). This work triggered the research interest of chemists to design versatile NHCs and to investigate the application of NHCs in various fields.

## Wanzlick's group



## Arduengo's group



Scheme 1. Pioneer work of generation of NHCs from Wanzlick and Arduengo.

## Bis(NHC)-Pincer Ligands

Due to the strong  $\sigma$ -donor and weak  $\pi$ -acceptor character, NHCs are extremely prevailing in the last decades as they are ideal ligands to coordinate to transition-metals, as they make a strong NHC-metal-bond. In addition, they increase the electron density of the metal center and thus lead to the generation of more nucleophilic metal centers.<sup>[5,6]</sup> There are three orbital contributions of the metal-(NHC) bond. The starting hypothesis that NHCs were simple  $\sigma$ -donors is abandoned, while it is clear that both  $d \rightarrow \pi^*$  ( $\pi^*$ -backdonation) as well as  $\pi \rightarrow d$  ( $\pi$ -donation) have to be considered to understand the details of the metal-(NHC) bond (Figure 2).<sup>[2]</sup>

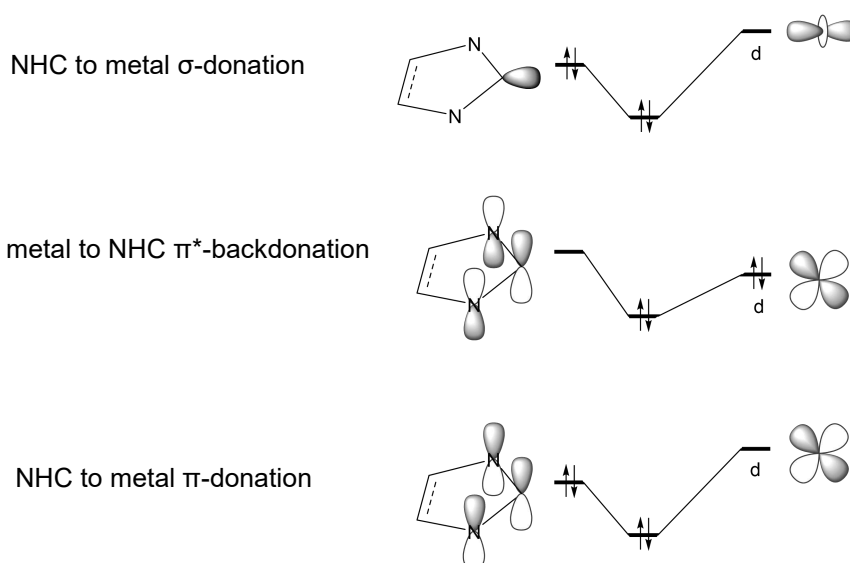


Figure 2. The three bonding contributions to the M-(NHC) bond.

The ease of modification of the imidazolium salt proligands leads to the incorporation of NHCs in polydentate ligand structures, usually in combination with other classical donors. The aim of this strategy is to develop stable transition-metal complexes and precisely tailor the metal coordination sphere, which are of importance for the generation of reactive species in homogeneous catalysis.<sup>[7]</sup>

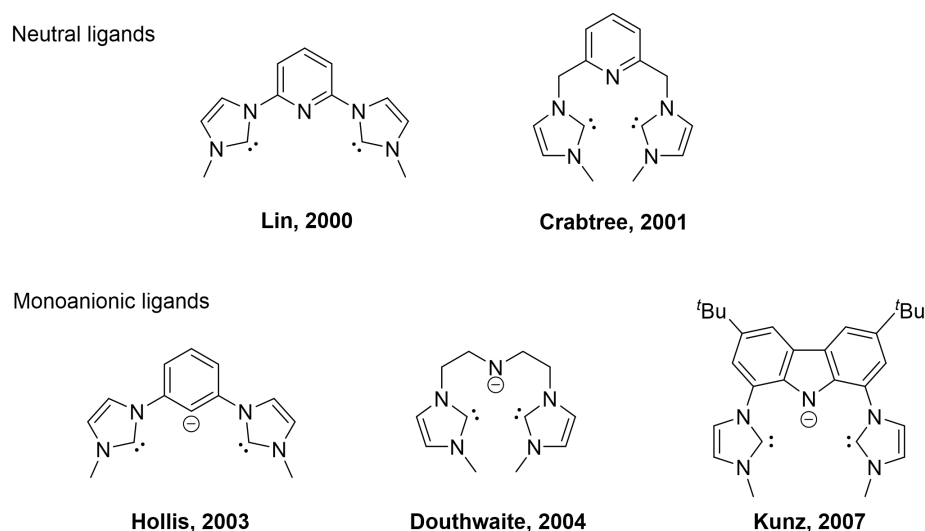
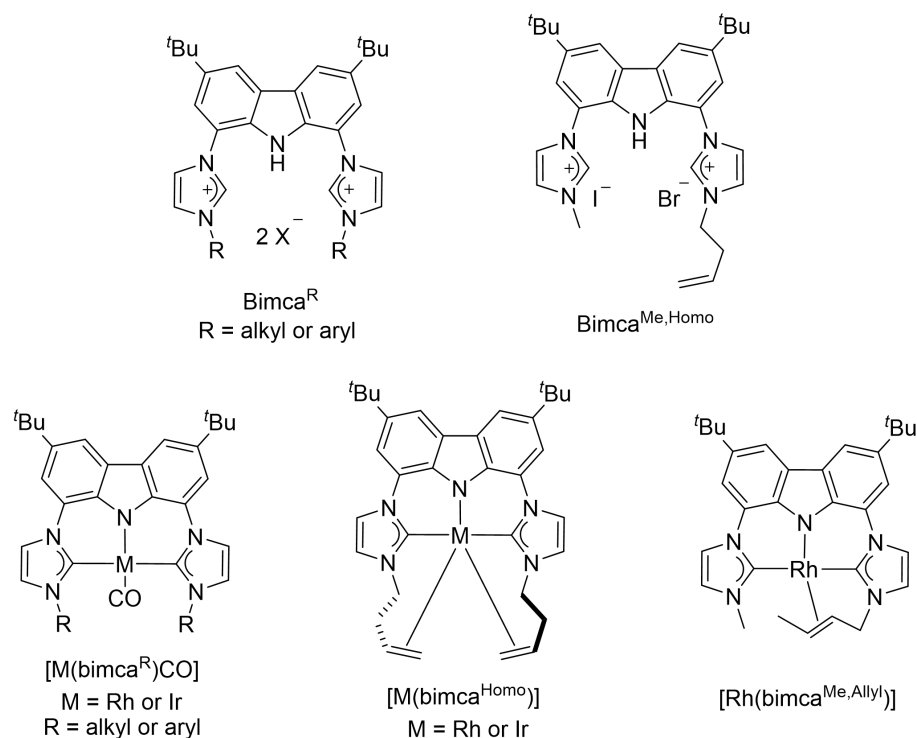


Figure 3. Diverse bis(NHC)-pincer ligands .

The pioneer work was initiated by the Lin group in 2000, of which the neutral  $C_{NHC}NC_{NHC}$ -pincer ligand was successfully generated and the corresponding helical dimercury compound was synthesized as well.<sup>[8]</sup> The year after, the Crabtree group reported the modified  $C_{NHC}NC_{NHC}$ -ligand with a  $CH_2$  moiety between the rings to enhance the solubility. Together with palladium, they behaved as an effective catalyst for the Heck cross-coupling reaction of activated aryl chlorides.<sup>[9]</sup> In addition to neutral bis(NHC) pincer ligands, monoanionic ones are also known. The Hollis group synthesized a monoanionic  $C_{NHC}CC_{NHC}$ -pincer ligand in 2003 and demonstrated its efficiency in Pd-catalyzed Suzuki–Miyaura cross-coupling reaction.<sup>[10]</sup> Afterward, the Douthwaite group succeeded in the generation of a  $C_{NHC}NC_{NHC}$ -pincer ligand in which the two NHC units are linked via an amido function and the corresponding palladium complexes were first generated as well.<sup>[11]</sup> In 2007, the Kunz group replaced the amido function with a carbazolidone backbone which makes the pincer ligand more rigid. The corresponding rhodium CO-containing complex was successfully applied in the Meinwald rearrangement (Figure 3).<sup>[12]</sup>

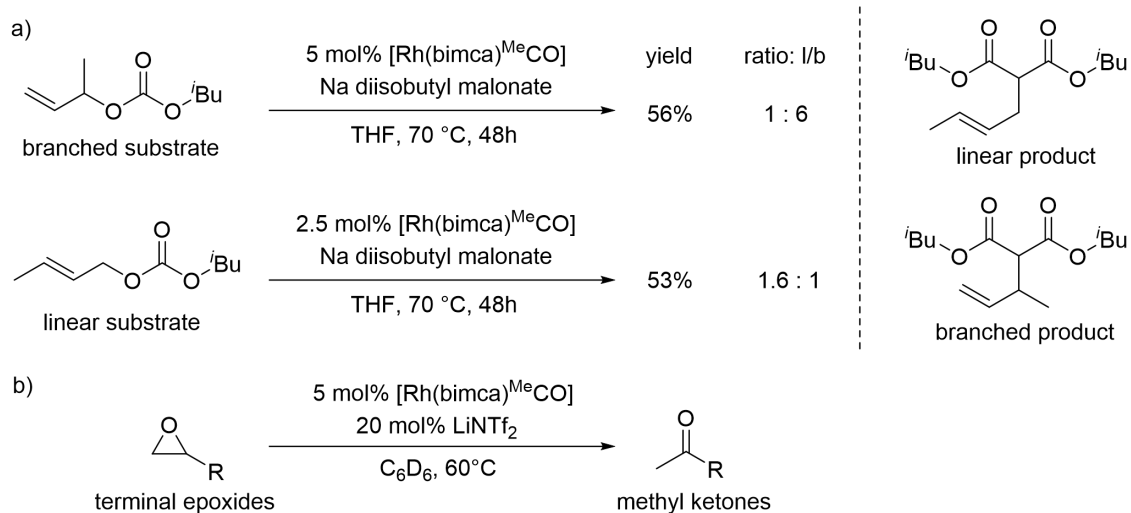
## Bimca Ligands



**Figure 4.** The disubstituted bimca salts and known group 9 transition-metal complexes.

The synthesis of 1,8-bis(imidazolin-2-ylidene)-3,6-di(*tert*-butyl)carbazolide (bimca) framework was initially developed by Michael Moser from the Kunz group in 2007.<sup>[12,13]</sup> Afterward, an optimized synthetic route to the structure was presented and this new route benefits from a streamlined workup and the elimination of air-sensitive techniques to afford the desired imidazolium salts in good yield over a short time frame. They have demonstrated that this framework provides a platform from which *N*-functionalized derivatives can be easily accessed by general protocols for the *N*-alkylation, *N*-arylation, and *N*-heteroarylation at both imidazole moieties. Thus, a small symmetric ligand library was constructed and fully characterized.<sup>[14]</sup> The synthesis of the unsymmetrically ligand bimca<sup>Me,Homo</sup> requires two separate monoalkylation steps which was tuned by different solvents.<sup>[13,15]</sup> Several new transition-metal complexes [M(bimca<sup>R</sup>)(CO)] and CO-free ones [M(bimca<sup>Homo</sup>)] and [Rh(bimca<sup>Me,Allyl</sup>)] based on the bimca ligands were obtained smoothly in our group.<sup>[15]</sup> The study of the [Rh(bimca<sup>Me</sup>)(CO)] complex showed a relatively small wavenumber in the IR spectrum for the  $\nu$  (CO) band, thus indicating strong  $\sigma$ -donor and weak  $\pi$ -acceptor properties of the bimca ligand. The highly nucleophilic character of the Rh(I)

center was proven by the formal oxidative addition of methyl iodide to  $[\text{Rh}(\text{bimca}^{\text{Me}})(\text{CO})]$ , a reaction that proceeded more quickly than with any other Rh(I) complex reported, indicating a strong nucleophilicity (Figure 4).<sup>[13]</sup>



**Scheme 2.** (a) Reaction of branched and linear allyl carbonates with sodium diisobutylmalonate using  $[\text{Rh}(\text{bimca}^{\text{Me}})\text{CO}]$  as a catalyst. (b) The isomerization of terminal epoxides into methyl ketones with  $[\text{Rh}(\text{bimca}^{\text{Me}})\text{CO}]$ .

The catalytic reactivity of  $[\text{Rh}(\text{bimca}^{\text{Me}})(\text{CO})]$  was first investigated with the allylic alkylation reaction. The results indicated that in the rhodium-catalyzed alkylation, mainly the *ipso* product is formed. However, quite a large amount of the isomeric branched product was also formed, which could result from the  $\text{S}_{\text{N}}2'$  metal-transfer isomerization.<sup>[16]</sup> Another homogeneous catalysis in which  $[\text{Rh}(\text{bimca}^{\text{Me}})(\text{CO})]$  was involved is the Meinwald rearrangement. Applying the rhodium catalyst together with a strong Lewis acid co-catalyst, the highly regioselective transformation of terminal epoxides into methyl ketones was realized under relatively mild conditions (Scheme 2).<sup>[17]</sup>

## References

- (1) Bourissou, D.; Guerret, O.; Gabbaï, F. P.; Bertrand, G. *Chem. Rev.* **2000**, *100*, 39–91.
- (2) Jacobsen, H.; Correa, A.; Poater, A.; Costabile, C.; Cavallo, L. *Coord. Chem. Rev.* **2009**, *253*, 687–703.
- (3) Wanzlick, H. W.; Schönherr, H. J. *Liebigs Ann. Chem.* **1970**, *731*, 176–179.
- (4) Arduengo, A. J.; Harlow, R. L.; Kline, M. *J. Am. Chem. Soc.* **1991**, *113*, 361–363.

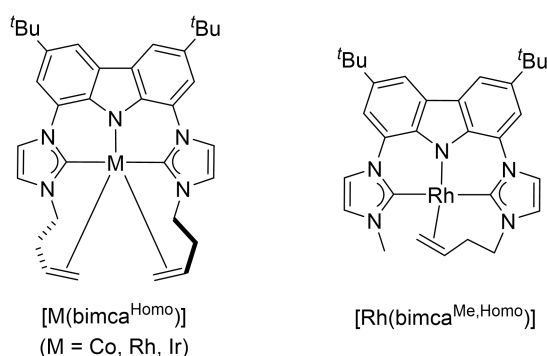
- (5) Herrmann, W. A. *Angew. Chem. Ed. Int.* **2002**, *41*, 1290–1309.
- (6) Díez-González, S.; Nolan, S. P. *Coord. Chem. Rev.* **2007**, *251*, 874–883.
- (7) Crabtree, R. H. *J. Organomet. Chem.* **2005**, *690*, 5451–5457.
- (8) Chen, J. C. C.; Lin, I. J. B. *J. Chem. Soc., Dalton Trans.* **2000**, 839–840.
- (9) Gründemann, S.; Albrecht, M.; Loch, J. A.; Faller, J. W.; Crabtree, R. H. *Organometallics* **2001**, *20*, 5485–5488.
- (10) Vargas, V. C.; Rubio, R. J.; Hollis, T. K.; Salcido, M. E. *Org. Lett.* **2003**, *5*, 4847–4849.
- (11) Douthwaite, R. E.; Houghton, J.; Kariuki, B. M. *Chem. Commun.* **2004**, 698–699.
- (12) Moser, M.; Wucher, B.; Kunz, D.; Rominger, F. *Organometallics* **2007**, *26*, 1024–1030.
- (13) Moser, M. *PhD Thesis*, University of Tübingen, **2007**.
- (14) Jürgens, E.; Buys, K. N.; Schmidt, A.-T.; Furfari, S. K.; Cole, M. L.; Moser, M.; Rominger, F.; Kunz, D. *New J. Chem.* **2016**, *40*, 9160–9169.
- (15) Jürgens, E. *PhD Thesis*, University of Tübingen, **2017**.
- (16) Wucher, B.; Moser, M.; Schumacher, S. A.; Rominger, F.; Kunz, D. *Angew. Chem. Int. Ed.* **2009**, *48*, 4417–4421.
- (17) Jürgens, E.; Wucher, B.; Rominger, F.; Törnroos, K. W.; Kunz, D. *Chem. Commun.* **2015**, *51*, 1897–1900.



## Research Purpose

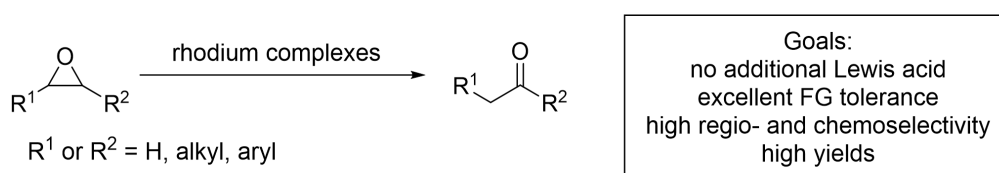
Based on the successful application of  $[\text{Rh}(\text{bimca}^{\text{Me}})\text{CO}]$  in the selective isomerization of terminal epoxides into methyl ketones,<sup>[1]</sup> the design and generation of more reactive and nucleophilic transition-metal catalysts and their utilities in homogeneous catalysis are of great interest. Therefore, my research purposes are as follows.

- Synthesis of the challenging group 9 complexes  $[\text{M}(\text{bimca}^{\text{Homo}})]$  ( $\text{M} = \text{Co}, \text{Rh}, \text{Ir}$ ), which are extremely air and moisture sensitive, and the more nucleophilic unsymmetric rhodium complex  $[\text{Rh}(\text{bimca}^{\text{Me,Homo}})]$ , which is supposed to be more reactive in the Meinwald rearrangement (Figure 1).



**Figure 1.** The synthesis of challenging  $[\text{M}(\text{bimca}^{\text{Homo}})]$  and unsymmetric rhodium(I) complexes.

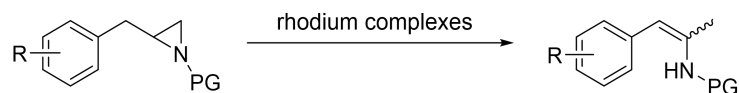
- Improving the catalytic reactivity and regio- and chemoselectivity of  $\text{C}_{\text{NHC}}\text{NC}_{\text{NHC}}$ -transition-metal complexes in the epoxide isomerization, enlarging the substrate scope and investigating the mechanism of this reaction with rhodium catalysts.



**Scheme 1.** Catalytic isomerization of epoxides with Rh-complexes.

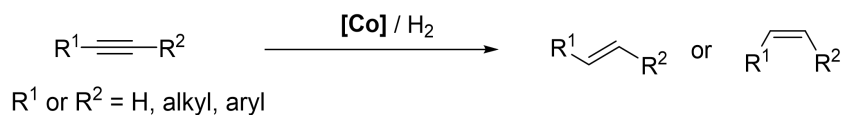
(1) Jürgens, E.; Wucher, B.; Rominger, F.; Törnroos, K. W.; Kunz, D. *Chem. Commun.* **2015**, 51,1897–1900.

- The isomerization of terminal aziridines, which is analogous to epoxides, will be studied with the highly nucleophilic rhodium catalysts in the transformation of terminal aziridines into enamides (Scheme 2).



**Scheme 2.** Catalytic isomerisation of terminal aziridines into enamides with Rh-complexes.

- The semihydrogenation of both terminal and internal alkynes to obtain (*E*)- or (*Z*)-olefins will be investigated with the novel C<sub>NHC</sub>NC<sub>NHC</sub>-pincer Co(I)-complex (Scheme 3).



**Scheme 3.** Selective semihydrogenation of both terminal and internal alkynes into olefins.

## Results and Discussion

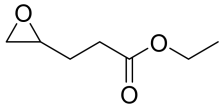
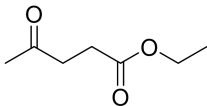
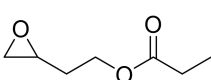
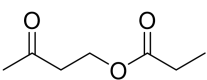
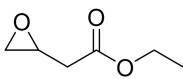
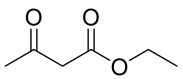
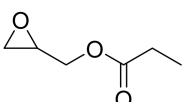
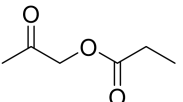
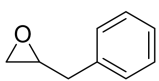
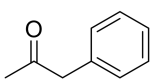
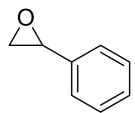
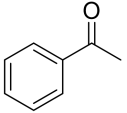
### Epoxide Isomerization with [Rh(bimca<sup>Hom</sup>)<sub>2</sub>CO]

The research started from [Rh(bimca<sup>Me</sup>)CO], which was confirmed to be an active catalyst for the Meinwald reaction. However, the drawbacks of this system are obvious as it requires elevated temperature and a relatively strong Lewis acid co-catalyst (LiNTf<sub>2</sub>) to achieve full conversion in the case of terminal alkyl oxiranes to methyl ketones. However, terminal epoxides bearing functional substituents were not tested in this publication, except phenyl oxirane.<sup>[1]</sup>

To continue the research, a substrate scope study was carried out first and it revealed a high functional group tolerance for some substrates (**1e–k**), such as hydroxyl, sulfonamide, ester and phenyl functionalized epoxides, but a substantial drop in conversion and/or yield and selectivity was recognized (Table 1). Notably, styrene oxides can not be rearranged regioselectively because of the Lewis acid catalyzed side reaction. The isomerization of phenyl oxirane (**3a**) with [Rh(bimca<sup>Me</sup>)CO] led only to a mixture of phenyl methyl ketone (**4a**) and phenyl ethanal (**5a**) (2 : 3), which indicates a competition between the Lewis acidic and the nucleophilic pathway. Therefore, enhancing the selectivity for phenyl oxiranes as well as increasing the activity of the catalyst was the primary goal.

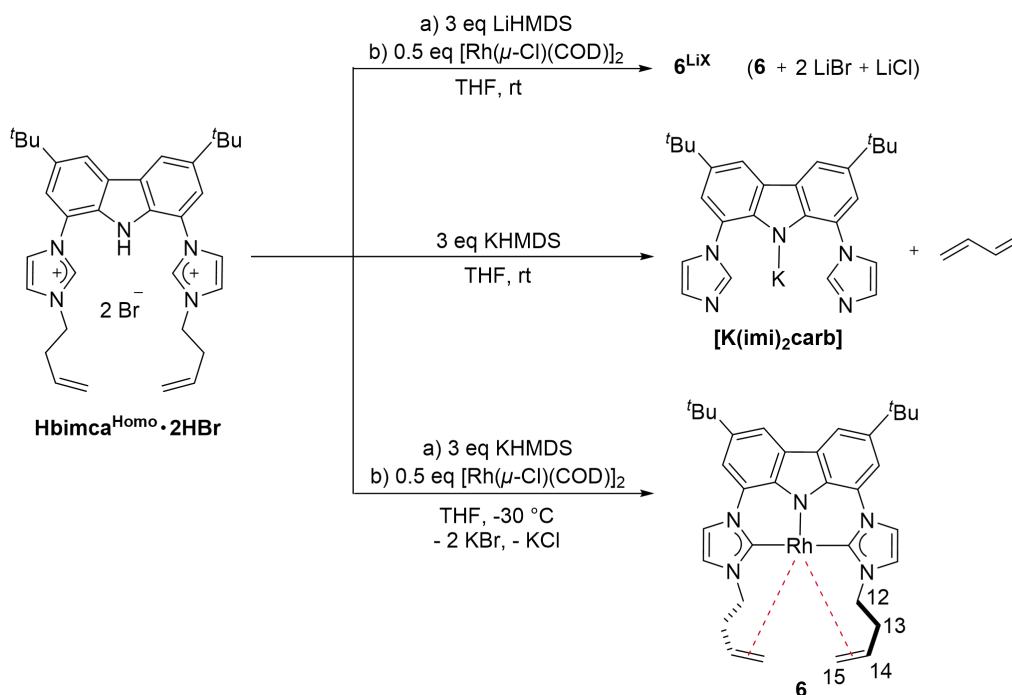
**Table 1.** Additional substrate scope of [Rh(bimca<sup>Me</sup>)CO] in the Meinwald reaction.

Epoxide	Methyl ketone	Time	Yield [%] <sup>[a,b]</sup>
<b>1c</b> 	<b>2c</b> 	9.7 d	50
<b>1e</b> 	<b>2e</b> 	3 h	98
<b>1f</b> 	<b>2f</b> 	2 h	50
<b>1g</b> 	<b>2g</b> 	24 h	20

<b>1h</b>		<b>2h</b>		24 h	67
<b>1i</b>		<b>2i</b>		24 h	37
<b>1j</b>		<b>2j</b>		24 h	33 <sup>[c]</sup>
<b>1k</b>		<b>2k</b>		24 h	17 <sup>[c]</sup>
<b>1l</b>		<b>2l</b>		24 h	99
<b>3a</b>		<b>4a</b>		24 h	26 (Ketone, <b>4a</b> ) 44 (Aldehyde, <b>5a</b> )

[a] Standard reaction conditions: Substrates (40  $\mu\text{mol}$ ),  $[\text{Rh}(\text{bimca}^{\text{Me}})\text{CO}]$  (2.0  $\mu\text{mol}$ ),  $\text{C}_6\text{D}_6$  (0.4 mL), 60  $^\circ\text{C}$ . All reactions were carried out using *J. Young* NMR tubes. [b] Yield of methyl ketones was determined by  $^1\text{H}$  NMR using 1,3,5-trimethoxybenzene as the internal standard. [c] at 80  $^\circ\text{C}$ .

To deal with these problems, a more reactive and nucleophilic catalyst was required. It was supposed that a CO-free Rh-catalyst would further increase the nucleophilicity of the metal centre and reduce the need for a Lewis acid co-catalyst.<sup>[2]</sup> The earlier reported *N*-homoallyl substituted ligand  $\text{Hbimca}^{\text{Homo}} \cdot 2\text{HBr}$ <sup>[3]</sup> would fulfil these criteria if the intramolecular olefin moieties would reversibly coordinate to the metal centre, which could also stabilize the complex during catalysis and increase its lifetime. Preparation of *in situ*  $[\text{Rh}(\text{bimca}^{\text{Homo}})]$  (**6<sup>LiX</sup>**) was achieved by deprotonation of  $\text{Hbimca}^{\text{Homo}} \cdot 2\text{HBr}$  with LiHMDS and subsequent addition of  $[\text{Rh}(\mu\text{-Cl})(\text{COD})]_2$ . To obtain the isolated complex, the deprotonation of  $\text{Hbimca}^{\text{Homo}} \cdot 2\text{HBr}$  was conducted initially with KHMDS at room temperature in order to generate  $[\text{K}(\text{bimca}^{\text{Homo}})]$ , however it would decompose at room temperature into butadiene and the bisimidazole carbazolidone  $[\text{K}(\text{imi})_2\text{carb}]$ . Isolation of complex **6** was achieved successfully *via* transmetalation from the potassium complex  $[\text{K}(\text{bimca}^{\text{Homo}})]$  generated *in situ* by deprotonation of  $\text{Hbimca}^{\text{Homo}} \cdot 2\text{HBr}$  with KHMDS at -30  $^\circ\text{C}$ . After filtering off potassium halides and removing volatile species, complex **6** was obtained in 63% yield (Scheme 1).



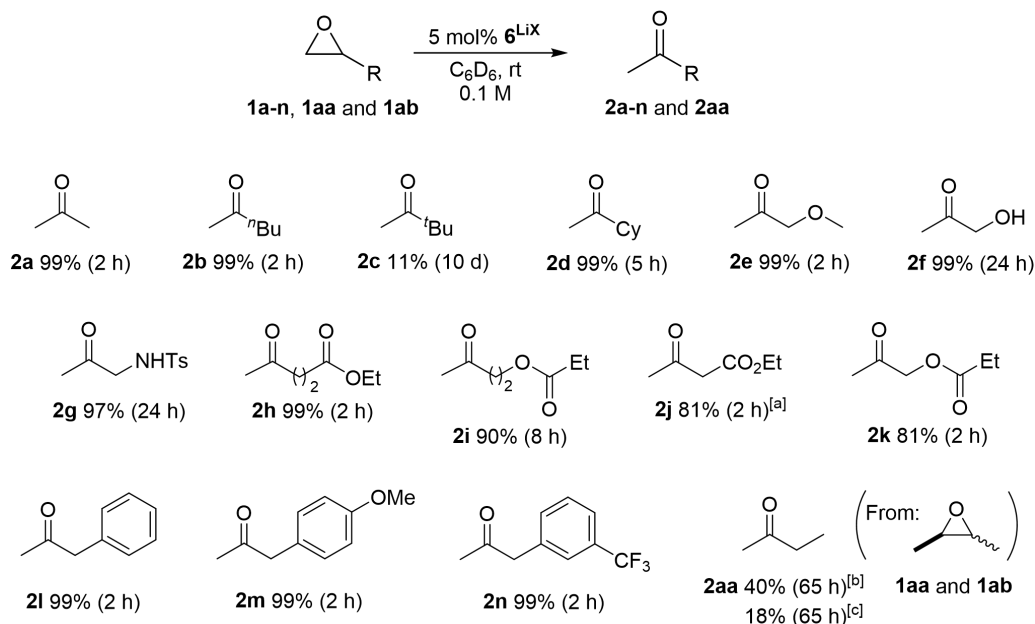
Scheme 1. Synthesis of both *in situ* and isolated  $[\text{Rh}(\text{bimca}^{\text{Homo}})]$  (**6**).

The molecular structure of **6** was characterized by NMR spectroscopic analysis and DFT calculations. The single signal set confirms a symmetric coordination mode of the ligand and the coordination of both double bonds and both carbene moieties to the Rh-centre is confirmed not only by the up-field shift of the respective signals in the  $^{13}\text{C}$  NMR spectrum to 185.5 ppm (carbene), 55.9 (C15) and 51.1 ppm (C14), but also by the  $^1J_{\text{RhC}}$  coupling of 33.9 (carbene), 6.7 (C15) and 11.3 Hz (C14). The four  $^1\text{H}$  NMR signals for the methylene protons (H-12, H-13) of the homoallyl moiety were assigned according to their coupling constants and an NOE experiment. The signals of the olefinic protons are strongly shielded (4.18–4.10 (H-14), 2.41 (H-15<sub>cis</sub>), 1.67 ppm (H-15<sub>trans</sub>)) and the reduced coupling constants of only 8.0 (*cis*) and 9.9 Hz (*trans*) can be explained by the reduced s-character due to the coordination with the Rh-centre. DFT calculations also confirmed the structure as described.

With the rhodium complex **6** and **6**<sup>LiX</sup>, the isomerization of 1,2-epoxyhexane (**1b**) as the model substrate was tested. No catalytic activity was found when the isolated complex **6** was applied without a Lewis acid co-catalyst and addition of 10 mol% of LiBr achieved no improvement as well. Nevertheless, small amounts of THF (20  $\mu\text{L}$ ) restored the catalytic activity fully as it enhanced the solubility of LiBr. After screening different solvents, Lewis acids, catalyst loadings, reaction temperatures and substrate concentrations, the optimized reaction conditions (5 mol% **6**<sup>LiX</sup>, 0.1 M

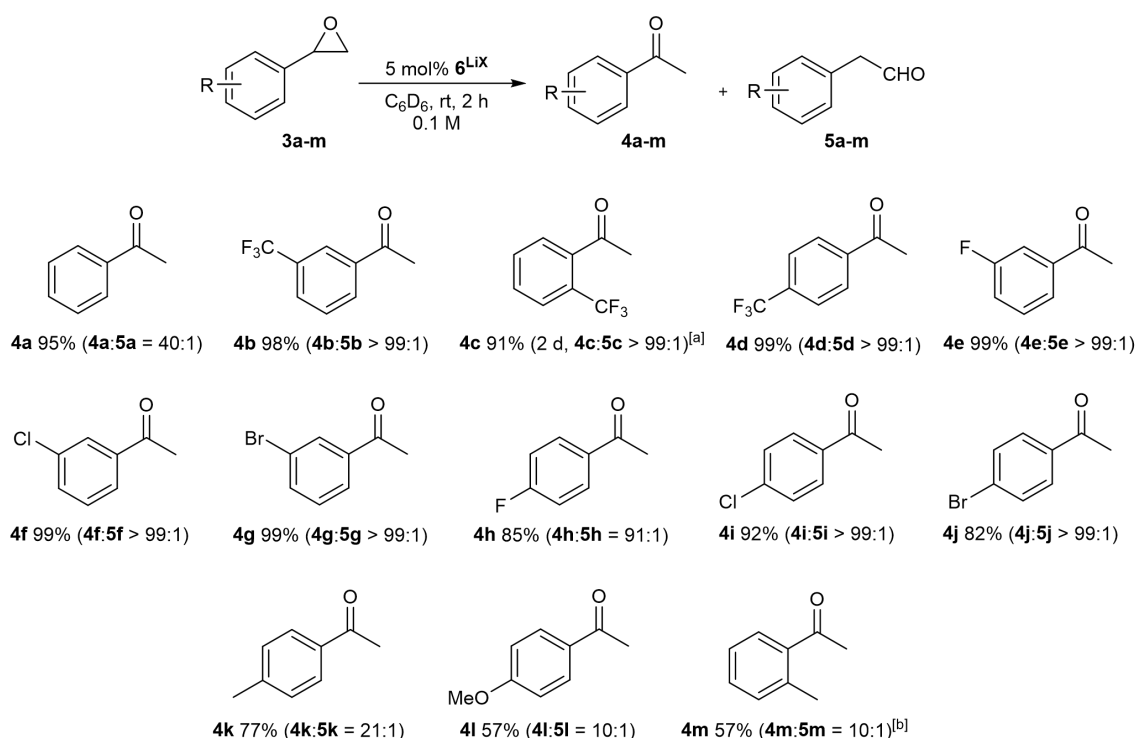
epoxide, C<sub>6</sub>D<sub>6</sub>, room temperature) were determined and applied to explore the generality of this protocol.

Diversely functionalized alkyl oxiranes were converted successfully into the desired methyl ketones using complex **6**<sup>LiX</sup> as the catalyst (Scheme 2). The alkyl substituted epoxides **1a–d** and the methoxy epoxide **1e** were transformed into the desired products **2a–e** almost quantitatively with full regioselectivity. The only exception was *tert*-butyloxirane (**1c**), which reacted extremely slow and only 11% yield was obtained after 10 days, possibly due to steric effects. In the case of hydroxyl (**1f**) and sulfonamide groups (**1g**), the isomerization progressed slowly, which revealed a competing influence of the acidic protons, nonetheless **2f** and **2g** were formed in 99% and 97% yields. Notably, ester groups are compatible with the system as well and the isomerization of epoxides **1h–k** afforded **2h–k** with high regio- and chemoselectivity. **1j** reacts a bit slower than **1h**, which might be due to its  $\alpha$ -acidity. Furthermore, 2-benzyloxirane (**1l**) and its congeners (**1m–n**) were isomerized to the methyl ketones **2l–n** almost quantitatively. Internal epoxides (**1aa** and **1ab**) react considerably slower in this case.



**Scheme 2.** The isomerization of alkyl oxiranes with catalyst **6**. Standard reaction conditions: Substrate (50.0  $\mu\text{mol}$ ), **6**<sup>LiX</sup> (5 mol%), C<sub>6</sub>D<sub>6</sub> (0.5 mL), r.t. at the given time. Carried out in *J. Young* NMR tubes. Yield (<sup>1</sup>H NMR) calibrated to 1,3,5-trimethoxybenzene (internal standard). <sup>[a]</sup> 14 % of epoxide **1j** left. <sup>[b]</sup> *cis*-2,3-epoxybutane (**1aa**), 80 °C. <sup>[c]</sup> *trans*-2,3-epoxybutane (**1ab**), 80 °C.

The selective rearrangement of aryl oxiranes to methyl ketones is extremely challenging and has not been achieved so far due to the Lewis acid catalyzed side reaction.<sup>[1,4]</sup> Therefore, the new catalyst **6<sup>LiX</sup>** was also applied in the isomerization of aryl oxiranes (Scheme 3). With styrene oxide (**3a**) an unprecedented good ratio was observed between acetophenone (**4a**) and 2-phenylacetaldehyde (**5a**) of 40 : 1. Furthermore, acetophenones **4b–j** bearing the electron-withdrawing substituents were obtained regioselectively (>99 : 1) in excellent yield. Aryl oxiranes containing electron-donating groups (methyl or methoxy) were converted into **4k** and **4l** with still very good regioselectivities of 21 : 1 and 10 : 1 favoring the methyl ketones over the aldehydes in good to moderate yields. Notably, epoxide **3l** is extremely sensitive towards Lewis acids in C<sub>6</sub>D<sub>6</sub> at room temperature and the Lewis acid itself would lead to the formation of the aldehyde **5l** and others, possibly polymerization products. The oxirane **3m** having a methyl group at the *ortho* position can be transformed into **4m** with still good regioselectivity and in good yield.

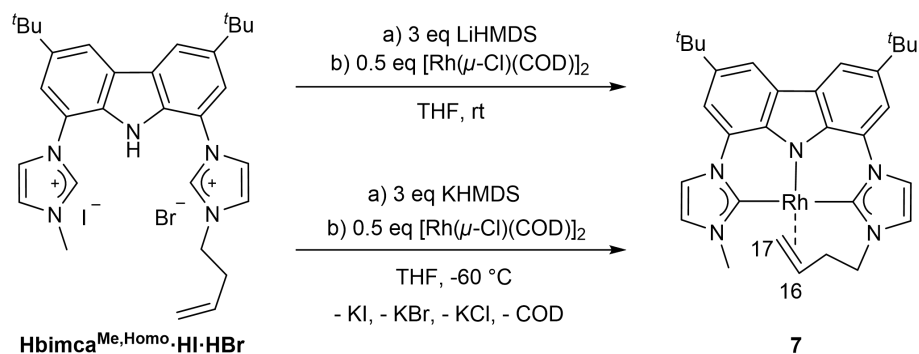


**Scheme 3.** The isomerization of terminal aryl oxiranes with catalyst **6**. Standard reaction conditions: epoxide (50.0  $\mu$ mol), **6<sup>LiX</sup>** (5 mol%), C<sub>6</sub>D<sub>6</sub> (0.5 mL), rt. Carried out in *J. Young* NMR tubes. Yields (<sup>1</sup>H NMR) calibrated to 1,3,5-trimethoxybenzene (internal standard). <sup>[a]</sup> At 80 °C for 2 days. <sup>[b]</sup> 22 h.

### Epoxide Isomerization with $[\text{Rh}(\text{bimca}^{\text{Me,Homo}})]$

Even though catalyst **6** is highly reactive in the Meinwald rearrangement and has a very good functional group tolerance, sterically demanding substrates such as *tert*-butyloxirane and *ortho*-substituted aryl oxiranes,  $-\text{NH}_2$ , or  $-\text{OH}$  containing substrates, or internal epoxides required quite long reaction times and/or elevated temperatures which in some cases still led to low yields. In addition, the regioselectivity for aryl oxiranes bearing electron-donating groups is not quite satisfying (the ratio of the methyl ketone and the aldehyde from 21:1 to 10:1 for **3k–m**). Therefore, more efforts needed to be taken to develop a more nucleophilic catalyst system and to gain more insight into the reaction mechanism.

During catalysis, the  $18\text{ e}^-$  rhodium(I) complex **6** requires the dissociation of one olefin moiety to react as a nucleophile, thus a new complex, such as a  $16\text{ e}^-$  Rh(I) complex, would be an interesting target to fulfill the purpose: The complex would be stabilized intramolecularly by one olefin moiety during catalysis but in addition exhibit a higher nucleophilicity and thus catalytic activity. Therefore, the synthesis of the unsymmetric Rh complex **7** as well as the catalytic activity of **7** toward the chemo- and regioselective epoxide isomerization are of great interest. In addition, the reaction mechanism should be investigated further.



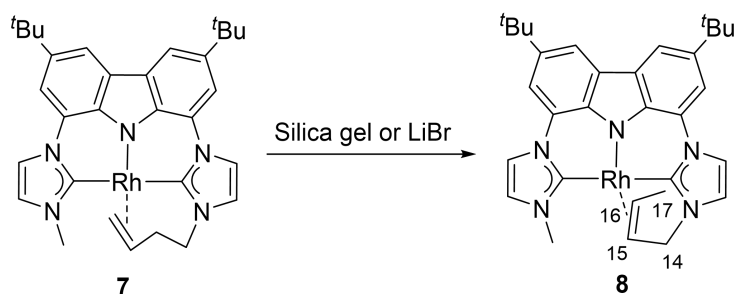
**Scheme 4.** Synthesis of both *in situ* and isolated  $[\text{Rh}(\text{bimca}^{\text{Me,Homo}})]$  (**7**).

The unsymmetrically substituted bimca ligand was generated according to the method discovered by E. Jürgens.<sup>[2]</sup> The preparation of  $\mathbf{7}^{\text{LiX}}$  was achieved by deprotonation of  $\text{Hbimca}^{\text{Me,Homo}} \cdot \text{HI} \cdot \text{HBr}$  with LiHMDS and subsequent addition of  $[\text{Rh}(\mu\text{-Cl})(\text{COD})]_2$  (Scheme 4). To obtain the isolated complex, the generated COD and HMDS during the reaction were removed *in vacuo* but decomposition of the



complex occurred, possibly due to the presence of the lithium salts. The isolation of complex **7** was achieved successfully *via* transmetalation from the potassium complex  $[K(\text{bimca}^{\text{Homo}})]$  generated *in situ* by deprotonation of  $\text{Hbimca}^{\text{Me,Homo}} \cdot \text{HI} \cdot \text{HBr}$  with KHMDS at  $-60\text{ }^\circ\text{C}$ . The potassium halides formed could be readily removed by filtration and complex **7** was isolated in 52% yield after removal of all volatiles *in vacuo*.

The molecular structure of complex **7** was identified by NMR experiments. Bonding of the terminal double bond to the rhodium center is proven by the  $^1J_{\text{RhC}}$  coupling constants of 13.2 Hz (C16) and 13.7 Hz (C17) in the  $^{13}\text{C}$  NMR spectrum and the 4 signals for the diastereotopic hydrogen atoms at the two methylene groups of the homoallyl substituent. The *cis/trans* assignment of the olefinic signals at 3.50 ppm ( $^3J = 7.7\text{ Hz}$ , H-17<sub>*cis*</sub>) and 2.94 ppm ( $^3J = 11.5\text{ Hz}$ , H-17<sub>*trans*</sub>) is based on the vicinal coupling constants, which are smaller than those typically observed in non-coordinated olefins, and can be explained with the lower s-character due to a rehybridization upon coordination of the metal ion. Furthermore, informations on the relative conformation of the metallacycle were obtained with an NOE experiment. DFT calculations also confirmed the structure as described.



**Scheme 5.** Isomerization of the terminal double bond of complex **7** to complex **8** with an internal double bond *cis*-configuration.

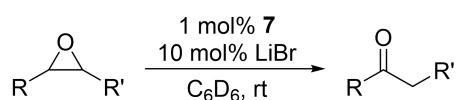
In addition, the isomerized complex **8** was isolated when catalyst **7** was purified by chromatography with silica gel under argon. The isomerization also takes place within 1 h at room temperature when 2 eq LiBr are added to a solution of the isolated complex **7** in  $\text{C}_6\text{D}_6$  (Scheme 5). Obviously, the Lewis acidity of the lithium cation in benzene is enhanced so that the isomerization of the double bond occurs. The molecular structure was characterized by NMR spectroscopy. The typical signal at 1.17 ppm with an integral of 3H shows a  $^3J$  (6.3 Hz) and a  $^4J$  coupling to the olefinic signals at 4.56 (H-15) and 4.09 ppm (H-16). The *cis*-conformation of the double bond

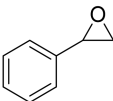
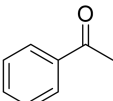
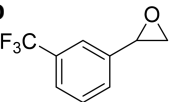
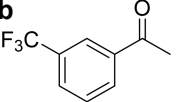
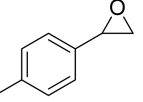
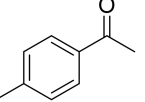
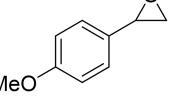
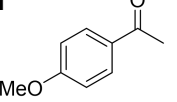
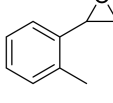
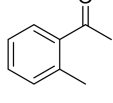
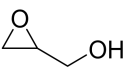
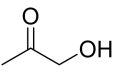
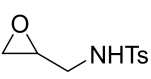
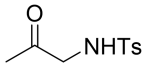
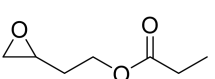
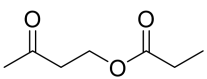
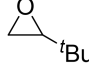
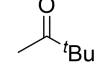

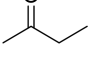

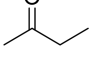
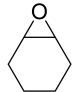
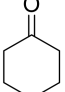
is not only confirmed by the  $^3J$  coupling constant of 6.3 Hz, but also by the NOE between methyl signal H-17 and one signal of the methylene group (H-14). Besides, an NOE cross-peak is observed between the signals of both olefinic protons and the *N*-methyl signal. The assignment of the peaks of the imidazole moieties and carbazole backbone are based on the observed NOE crosspeaks (Scheme 5).

With the novel rhodium complex **7**, the epoxide isomerization was studied using phenyl oxirane (**3a**) as the model substrate. After testing different catalyst loadings, Lewis acids, solvents, and substrate concentrations, the optimized reaction conditions (1 mol% catalyst **7**, 0.2 M epoxide,  $C_6D_6$ , room temperature) were determined and applied to study the generality of this system.

Using complex **7** as the catalyst, various functionalized epoxides were converted successfully into the desired methyl ketones (Table 2). Phenyl oxirane (**3a**) and its derivative **3b** bearing the strong electron-withdrawing trifluoromethyl substituent were transformed regioselectively in excellent yield. Surprisingly, epoxides **3k** and **3l** possessing electron-donating groups (methyl or methoxy) were converted with excellent regioselectivities of 50:1 and 22:1 favoring the methyl ketones over the aldehydes in good to moderate yields. Even the *ortho*-substituted methyl ketone **4m** was obtained from **3m** with excellent regioselectivity and high yield. According to the above results for aryl oxiranes, it is confirmed that catalyst **7** is much more reactive and regioselective for aryl oxiranes than the previously studied catalyst **6** with even a lower catalyst loading (1 mol%). Notably, complex **7** is the best catalyst reported for the regioselective isomerization of terminal aryl oxiranes until now.

Besides aryl ketones, epoxides bearing OH or NH groups like hydroxyl groups (**1f**) and sulfonamide (**1g**) were rearranged to the desired methyl ketones with 1 mol% catalyst loading in 90% (**2f**) and 83% (**2g**) yield, albeit with longer reaction time (24 h). The isomerization of epoxide **1i** possessing an ester group afforded **2i** in moderate yield with 5 mol% catalyst loading after 24 h. As the extended reaction times may derive from competing coordination of LiBr at the Lewis basic centers of functional groups, the amount of LiBr was increased to 50 mol% and full conversions were achieved already after 1 h at moderate to excellent yields (entries 6-8). Furthermore, the sterically demanding 2-(*tert*-butyl)oxirane (**1c**) can be also converted to the desired product **2c** in almost quantitative yield, albeit with higher catalyst loading (5 mol%) and reaction temperature.

**Table 2.** Substrate scope in the isomerization of epoxide catalyzed by rhodium complex **7**<sup>[a]</sup>.

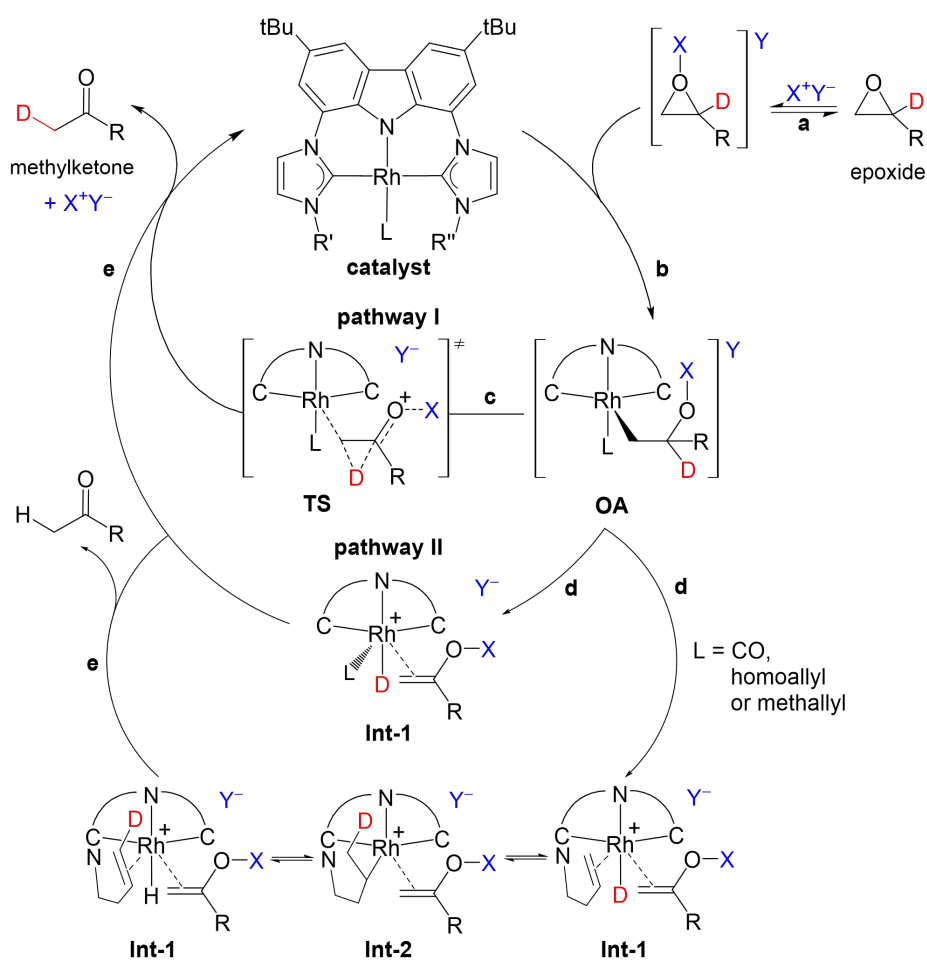
Entry	substrate	product	time	Yield [%] <sup>[b]</sup>	Ratio (4:5)
1	<b>3a</b> 	<b>4a</b> 	1 h	99	>99:1
2	<b>3b</b> 	<b>4b</b> 	1 h	98	>99:1
3	<b>3k</b> 	<b>4k</b> 	1 h	77	50:1
4	<b>3l</b> 	<b>4l</b> 	1 h	42	22:1
5	<b>3m</b> 	<b>4m</b> 	24 h	92	33:1
6	<b>1f</b> 	<b>2f</b> 	24 h 1 h	90 42 <sup>[e,g]</sup>	-
7	<b>1g</b> 	<b>2g</b> 	24 h 1 h	83 94 <sup>[e,g]</sup>	-
8	<b>1i</b> 	<b>2i</b> 	24 h 1 h	67 <sup>[c,e]</sup> 80 <sup>[e,g]</sup>	-
9 <sup>[d-f]</sup>	<b>1c</b> 	<b>2c</b> 	24 h	99	-
10 <sup>[d-f]</sup>	<b>1aa</b> 	<b>2aa</b> 	24 h	99	-
11 <sup>[d-f]</sup>	<b>1ab</b> 	<b>2aa</b> 	24 h	7	-
12 <sup>[d-f]</sup>	<b>1ac</b> 	<b>2ac</b> 	24 h	99	-

[a] Carried out in *J. Young* NMR tubes and with 10 mol% LiBr and 5  $\mu\text{L}$  THF- $d_8$ , 0.2 M concentration of epoxides. [b] Yield of ketones ( $^1\text{H}$  NMR) calibrated to 1,3,5-trimethoxybenzene (internal standard). [c] At 60  $^\circ\text{C}$ . [d] 20 mol% LiNTf<sub>2</sub> instead of LiBr. [e] 5 mol% catalyst **7**. [f] At 80  $^\circ\text{C}$ . [g] 50 mol% LiBr.

The internal epoxides were tested with catalyst **7** as well. Compared with rhodium catalyst **6**, *cis*-2,3-epoxybutane (**1aa**) was compatible with the catalytic system and

yielded 99% of butan-2-one (**2aa**) in 24 h. In contrast, the conversion of *trans*-2,3-epoxybutane (**1ab**) under otherwise identical conditions yielded only 7% of **2aa**. This outcome is of considerable interest as it is contrary to the results from Coates and coworkers, who obtained less than 40% conversion with *cis*-2-hexene oxide but 98% yield with *trans*-2-hexene oxide applying  $[(\text{salcy})\text{Al}(\text{THF})_2]^+[\text{Co}(\text{CO})_4]^-$  as the catalyst.<sup>[5]</sup> In addition, 7-oxabicyclo[4.1.0]heptane (**1ac**) was isomerized into cyclohexanone in almost quantitative yield at 80 °C.

To check whether complex **8** is an active catalyst as well, the Meinwald reaction of phenyl oxirane (**3a**) was carried out with the isolated complex **8** under the general conditions. The reaction rate is comparable to that when using complex **7**. It is assumed that the isomerization of complex **7** to **8** occurs under the catalytic conditions of the Meinwald reaction.

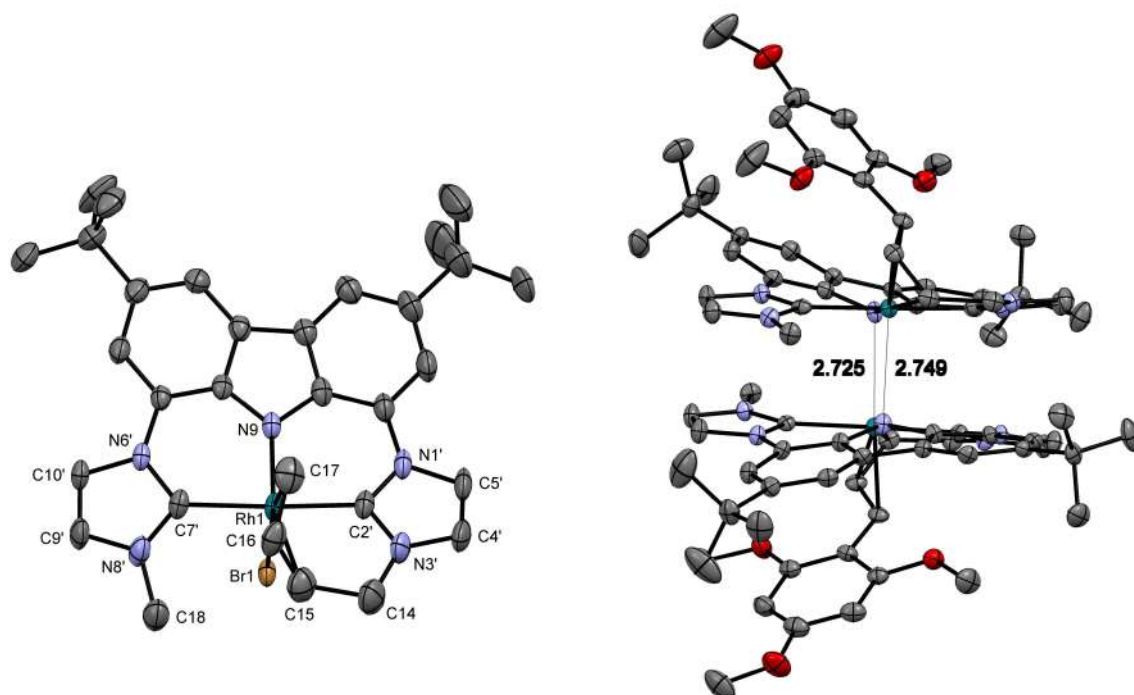


**Scheme 6.** The initially proposed catalytic cycle (pathway I and pathway II) for  $[\text{Rh}(\text{bimca}^{\text{Me}})\text{CO}]$  ( $\text{L} = \text{CO}$ ) and the evidence for pathway II due to the observed H/D exchange in case of the homoallyl complexes **6** and **7** (vide infra).

Apart from the investigation of rhodium catalysts in the epoxide isomerization, the mechanism of this reaction was studied further. A plausible mechanism was already proposed with  $[\text{Rh}(\text{bimca}^{\text{Me}})\text{CO}]$ , which starts with pre-activation of the epoxide by the Lewis acid additive followed by a nucleophilic attack of the  $\text{Rh}^{\text{I}}$  centre at the most electrophilic side of the epoxide (also the least hindered one) and the oxidative addition product was confirmed by NMR spectroscopy. From this intermediate two possible pathways can lead to the product: a concerted 1,2-H shift under reductive elimination of the catalyst (c) or  $\beta$ -hydride elimination (d) to form the Rh-hydride intermediate **Int-1**, which subsequently undergoes reductive elimination (e) to release the product and the catalyst (Scheme 6).<sup>[1]</sup>

As a hydride intermediate **Int-1** was not observed during the catalysis with  $[\text{Rh}(\text{bimca}^{\text{Me}})\text{CO}]$  ( $\text{L} = \text{CO}$ ), it was supposed that the *N*-homoallyl moiety of catalyst **1** or **7** could insert into the Rh-H intermediate **Int-1** to give the rhodium alkyl intermediate **Int-2**, which could undergo a D/H exchange in case deuterated phenyl oxirane was used. To prove this hypothesis, catalytic experiments using 1-D-phenyl oxirane as the substrate were performed with both catalysts **1** and **7** under catalytic as well as stoichiometric conditions. In all cases, an exchange of the deuterium by hydrogen in the methylphenyl ketone of **5** – **7** % was observed (deuteration degree of the phenyl oxirane: 98%). According to these observations, pathway II was favored for the catalytic cycle of the nucleophilic Meinwald reaction with the rhodium catalysts. During the mechanistic study of epoxide isomerization with catalyst **7**, two deactivation products of **7** were detected. One, as red crystals, was observed after finishing a VT NMR experiment of catalyst **7** with 1.0 eq phenyl oxirane at room temperature. The X-ray structure analysis reveals the formation of a bromido-Rh(III) complex **9** (Figure 1, left), in which the *N*-homoallyl substituent is coordinated in a  $\eta^3$ -allyl coordination mode to the oxidized metal center. As the isomerization of phenyl oxide **4a** is very fast, it is likely that the formation of this product occurs after the catalysis. C-H activation at the allylic position to form an allylhydrido complex and subsequent substitution of the hydrido by a bromido ligand can explain its formation. Another deactivation product was obtained from the testing of *cis*-1,2-diethoxycarboxyl)oxirane (5 mol% **7** (2.3 mg), 20 mol%  $\text{LiNTf}_2$  (4.6 mg), the epoxide (15.1 mg) and 1,3,5-trimethoxybenzene (4.3 mg), 24 h at 80 °C and 24 h at 100 °C). Red single crystals in the NMR tube were collected after several days at room temperature. The X-ray structure analysis reveals that under the elevated

temperature the internal standard 1,3,5-trimethoxybenzene has reacted with the *N*-homoallyl moiety of complex **7** in a formal dehydrogenation and C-C bond formation to the Rh(III)( $\eta^3$ -allyl) complex **10** (Figure 1, right). In the solid state the 16e<sup>-</sup> Rh-d<sup>6</sup> complex forms a Lewis-pair dimer between the rhodium and the carbazol nitrogen atoms with a mean distance of 2.74 Å. Thus, catalytic tests with substrates of low reactivity should be carried out either with an inert or without an internal standard to avoid erroneous catalytic results in the NMR experiments.



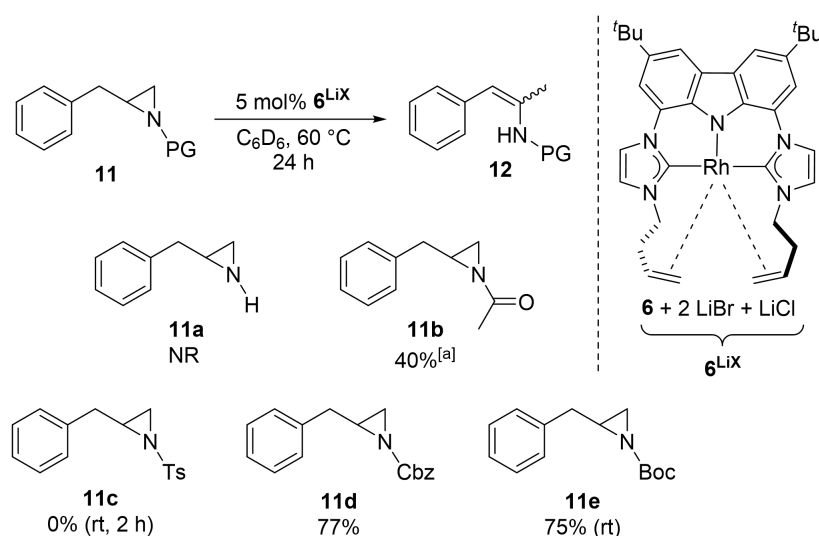
**Figure 1.** Molecular structure of the catalyst deactivation product **9** (left) and Molecular structure of the side product **10** (right). Atoms are shown with anisotropic atomic displacement parameters at the 50% probability level. Hydrogen atoms and co-crystallized molecules are omitted for clarity.

### Aziridine Isomerization with [Rh(bimca<sup>Me,Homo</sup>)]

With the successful application of the rhodium catalysts in the Meinwald rearrangement, the isomerization of other small molecules such as aziridines is of great interest. Moreover, the isomerization of aziridines has been rarely investigated and there are only two reports of transition-metal catalyzed reactions by the Wolfe group<sup>[6]</sup> and the groups of Lledós and Riera<sup>[7]</sup>. Therefore, the aziridine isomerization was studied as well with the bimca rhodium catalysts.

Different protecting groups on the nitrogen atom were tested at the beginning (Scheme 7). The general reaction conditions were 5 mol% *in situ* generated **6**<sup>LiX</sup> and aziridines in C<sub>6</sub>D<sub>6</sub> at 60 °C for 24 h. Non-protected aziridine **11a** did not react under

these conditions. *N*-Acetyl aziridine **11b** was isomerized to yield the desired product **12b** in only 40% yield along with 28% of dihydrooxazole, which was formed in a Lewis acid catalyzed side reaction with LiBr and confirmed in a blank reaction. Interestingly, with the *N*-tosyl protected substrate **11c**, the reaction went quite fast at room temperature and full conversion was achieved in 2 h. However, no desired enamides were obtained due to polymerization as a side reaction. Aziridines **11d** and **11e** were converted smoothly to obtain the corresponding enamides in comparable yields at 60 °C and room temperature, respectively. Finally, the *N*-Boc protecting group was chosen as aziridine **11e** can be isomerized already at room temperature.

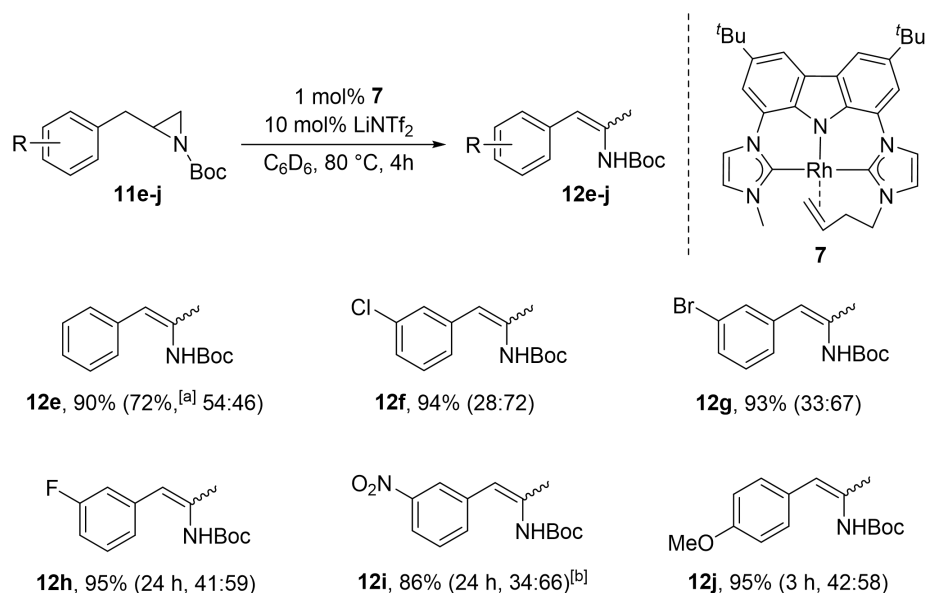


**Scheme 7.** Isomerization of terminal aziridines with different protecting groups (PG). <sup>[a]</sup> Along with 28% of dihydrooxazole.

The aziridine isomerization was investigated with *N*-Boc-2-benzylaziridine (**11e**) as the model substrate. Reaction parameters, such as rhodium catalysts, Lewis acids, solvents, catalyst loadings, Lewis acid loadings and aziridine concentrations, were tested in sequence. Besides, efforts were taken to control the *Z/E* ratio of the enamides as well, but failed because of the tendency of the isomerization of the kinetically favored *Z*-**12e** isomer into the thermodynamically favored *E*-**12e** isomer at the required temperature. The best catalytic result was obtained with 1 mol% **7** and 0.1 M aziridine in  $C_6D_6$  at 80 °C and the optimized reaction conditions were applied to probe the generality of this system.

Afterward, various *N*-Boc terminal aziridines were converted successfully into the desired enamides (Scheme 8). Terminal aziridines **11f** and **11g**, possessing weak electron-withdrawing chloro and bromo substituents on the phenyl ring, were

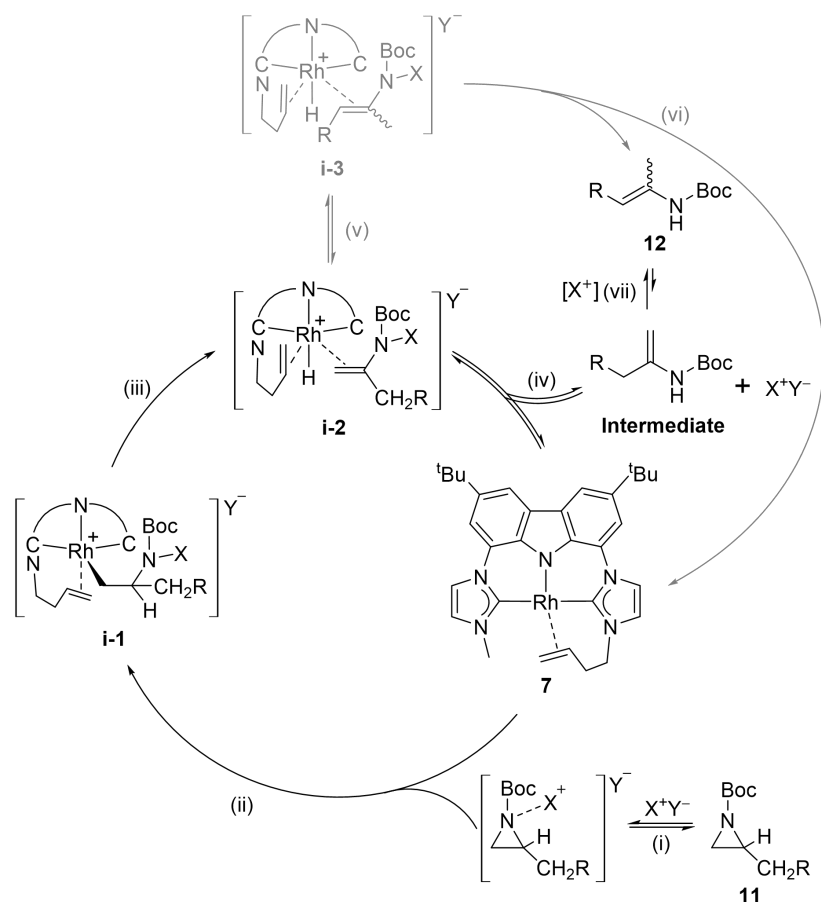
isomerized smoothly to yield the corresponding enamides in excellent yield (94% and 93%, respectively). Interestingly, aziridine **11h** bearing a moderate electron-withdrawing fluoro substituent was rearranged much slower and full conversion was obtained after 24 h in 95% yield. To confirm this tendency, substrate **11i** bearing a strong electron-withdrawing nitro group and **11j** with a strong electron-donating substituent (methoxy) were tested. Harsher reaction conditions were required with **11i** and the reaction can only be completed with 5 mol% catalyst **7** in 24 h with the yield of 86%. Notably, an intermediate bearing a terminal C=C double bond was observed, which would be fully rearranged to the desired product. In comparison, when aziridine **11j** was applied, the reaction proceeded much faster and was completed to obtain enamides **12j** in 95% yield after 3 h. A closer look at the  $^1\text{H}$  NMR spectra monitoring the reaction of substrates **11e** and **11h** revealed the formation of the respective intermediates as well. While the isomerization is fast for the substrate with an electron donating substituent (**11j**), it becomes even rate limiting in the case of **11h** and **11i** bearing electron-withdrawing substituents. The feasibility of this novel method was tested with a scaled-up reaction of **11e** and the desired enamide **12e** was isolated by column chromatography in 72% yield with the *Z/E* ratio of 54:46.



**Scheme 8.** Isomerization of diverse *N*-Boc terminal aziridines with rhodium catalyst **7**. The yield of **12** was determined by  $^1\text{H}$  NMR against the internal standard 1,3,5-trimethoxybenzene and *Z/E* ratios are given in brackets. <sup>[a]</sup> 0.3 g of **11e** (1.3 mmol) and 1 mol% catalyst **7** used; isolated yield of **12e** in brackets. <sup>[b]</sup> 5 mol% catalyst **7**.



According to the observations during the catalytic reactions, a plausible mechanism, similar to the rhodium catalyzed epoxide rearrangement, was proposed for the aziridine isomerization. The reaction starts with pre-activation of the terminal aziridines (Scheme 9, step (i)), and followed by a nucleophilic attack of the 16 e<sup>-</sup> Rh<sup>I</sup> catalyst **7** at the most electrophilic side of the aziridine (ii) and formation of intermediate **i-1** which is likely stabilized by the Lewis acid as well. Subsequent  $\beta$ -hydride elimination (iii) would lead to the Rh<sup>III</sup> hydrido complex **i-2** which can either release the **Intermediate** by reductive elimination (iv) under regeneration of complex **7** or isomerize directly to intermediate **i-3** (v) from which the thermodynamically favored product is released by reductive elimination (vi). The isomerization of the **Intermediate** to the product **12** can either occur by re-coordination to the catalyst **7** under formation of the Rh<sup>III</sup> hydrido complex **i-2**, or directly by a Lewis acid catalyzed isomerization (vii). As the isomerization rate of step vii is substrate depending and slows down in case of more electron-withdrawing substituents, this step is assumed to be Lewis-acid catalyzed.

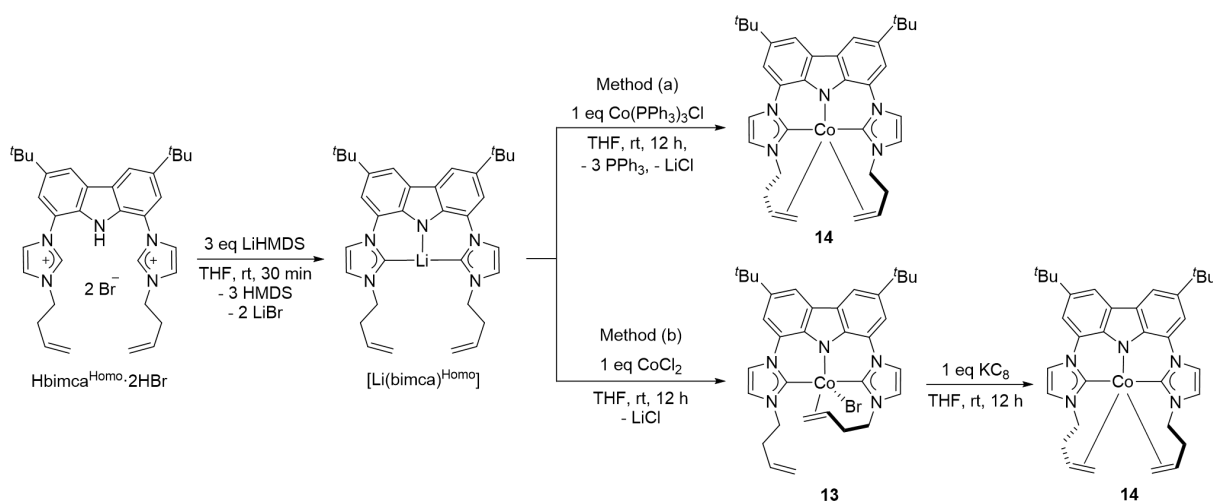


**Scheme 9.** Proposed mechanism for the isomerization of terminal aziridines with transition-metal complexes.

### Synthesis and Characterization of $[M(\text{bimca}^{\text{Homo}})]$ ( $M = \text{Co}$ and $\text{Ir}$ ) and Their Catalytic Reactivity toward the Meinwald Rearrangement

In comparison with rhodium complexes, the extreme air and moisture sensitive property of low-valent cobalt complexes inhibits its development. Thus well-defined cobalt complexes were less reported. With the reported  $\text{bimca}^{\text{Homo}}$  ligand, the synthesis and characterization of  $[\text{Co}(\text{bimca}^{\text{Homo}})]$  (**14**) was studied.

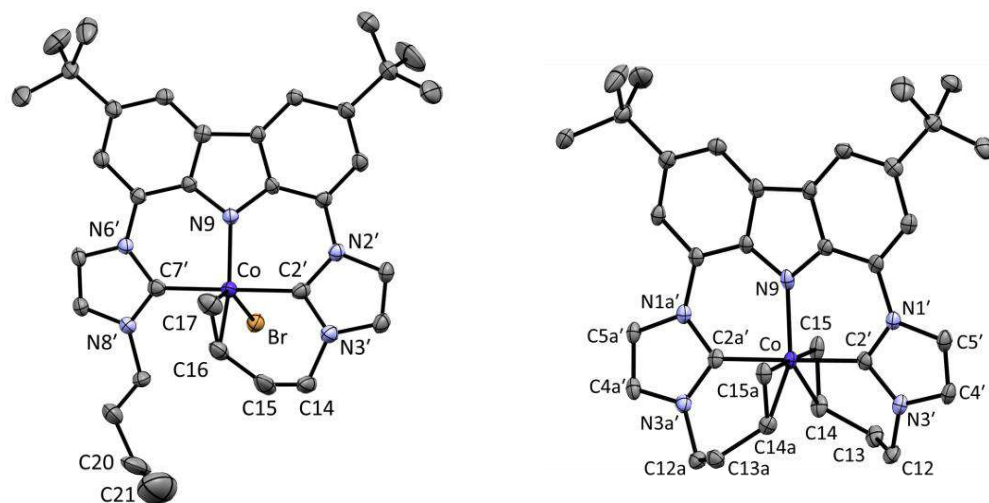
The preparation of complex **14** commenced with the generation of  $[\text{Li}(\text{bimca}^{\text{Homo}})]$  and followed by transmetalation with  $\text{CoCl}(\text{PPh}_3)_3$  in THF at room temperature (Scheme 10, method a). A color change from light yellow to red was observed immediately and the *in situ* generated compound **14** was confirmed by  $^1\text{H}$  NMR spectrum with a symmetric coordination mode of the ligand. However, the purpose to obtain pure complex failed as residual  $\text{PPh}_3$  could not be removed completely by chromatography at silica gel.



**Scheme 10.** Synthesis of  $[\text{Co}(\text{bimca}^{\text{Homo}})]$  (**14**) by two methods.

Triggered by the work of Braunstein<sup>[8]</sup> and Nishibayashi<sup>[9]</sup>, who obtained diamagnetic  $\text{Co}(\text{I})$  complexes *via* reduction of the corresponding  $\text{Co}(\text{II})$  complexes with  $\text{KC}_8$ , the paramagnetic  $[\text{Co}(\text{bimca}^{\text{Homo}})\text{Br}]$  (**13**) was prepared first by addition of solid  $\text{CoCl}_2$  into the freshly generated  $[\text{Li}(\text{bimca}^{\text{Homo}})]$  (Scheme 10, method b). Instant halogen exchange occurs to transform  $[\text{Co}(\text{bimca}^{\text{Homo}})\text{Cl}]$  into  $[\text{Co}(\text{bimca}^{\text{Homo}})\text{Br}]$  as bromide anions are still present in the solution. Brown single crystals of **13** suitable for X-ray diffraction were grown by slow evaporation from benzene at room temperature. Crystallographic characterization of the complex (Figure 2, left) reveals a distorted trigonal bipyramidal geometry at the cobalt center with one coordinated homoallyl

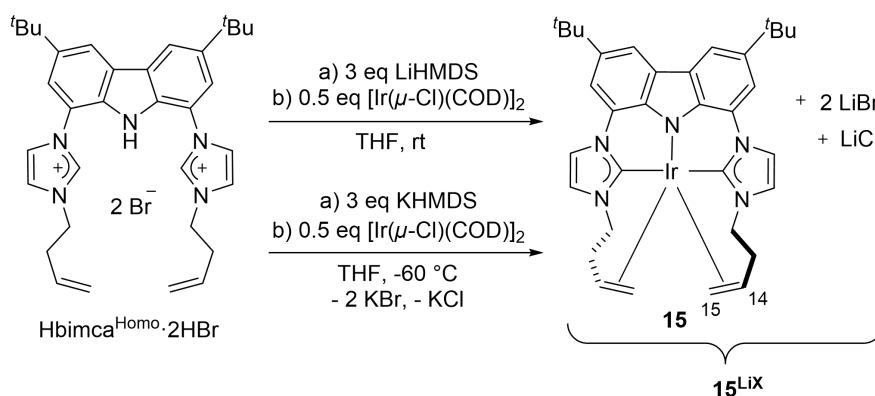
moiety. The NHC moieties take in the apical positions with a C2'-Co-C7' angle of 174.0(2)°. Both Co-C<sub>NHC</sub> bond lengths are within the range reported for Co(II)-C<sub>NHC</sub> bonds of 1.791-2.152 Å.<sup>[10]</sup> In the coordinated homoallyl moiety, the C=C bond is elongated (C16-C17 = 1.384(6) Å) due to a good  $\pi$ -backbonding ability of the cobalt center. This is the first structural report of a cobalt(II) NHC complex with a coordinated olefin. Besides, single crystals of the cobalt(III) complex [Co(bimca<sup>Homo</sup>)<sub>2</sub>]Br with two coordinated bimca<sup>Homo</sup> ligands in an octahedral fashion were generated as a side product, presumably resulting from traces of oxygen.



**Figure 2.** Solid-state molecular structure of **13** (left) and solid-state molecular structure of **14** (right). Atoms are shown with anisotropic atomic displacement parameters at the 50% probability level. Hydrogen atoms and co-crystallized solvent molecules are omitted for clarity.

Complex **14** was successfully obtained *via* reduction of **13** with KC<sub>8</sub>. After filtration and purification by chromatography, the desired complex **14** was isolated as a red solid. Complex **14** is extremely air sensitive and an obvious color change would be observed with traces of oxygen. The structure of **14** was initially confirmed by <sup>1</sup>H NMR spectrum which indicates a C<sub>2</sub>-symmetric ligand environment with both *N*-homoallyl substituents coordinated to the cobalt(I) center. The signals of the olefinic protons are strongly shifted up-field (4.09–4.02 (H-14), 3.21 (H-15<sub>cis</sub>), 2.54 ppm (H-15<sub>trans</sub>)). The <sup>13</sup>C NMR signal of the carbene carbon atoms at 191.1 ppm lie about 26 ppm at higher field than the signal of a comparable unsaturated free NHC (217.1 ppm<sup>[11]</sup>). Single crystals of **14** suitable for X-ray diffraction were grown from a concentrated solution of toluene and pentane at -30 °C and the solid state of the molecular structure is consistent with NMR spectroscopy (Figure 2, right). The

coordination geometry at the Co(I) center is trigonal bipyramidal with both olefin moieties and the carbazole nitrogen taking in the equatorial and both NHC moieties the axial positions ( $C2'-Co-C2a' = 179.0(3)^\circ$ ),  $c(C15,C14)-Co-c(C15',C14') = 139.2^\circ$ ; (c: mid-point of bond)). The Co-C<sub>NHC</sub> bond lengths (Co-C2' = 1.911(5) Å, Co-C2a' = 1.913(5) Å) are comparable to reported (C<sub>NHC</sub>NC<sub>NHC</sub>)-pincer cobalt(I) complexes,<sup>[9,12]</sup> while the Co-N bond (1.947(4) Å) in **2** is substantially longer than the pyridine Co-N bond (e.g. 1.839(4) Å<sup>[12]</sup>), possibly due to steric reasons. The bond lengths of C14-C15 (1.401(8) Å) and C14'-C15' (1.400(7) Å) are elongated compared to the non-coordinated olefinic bond in the Co(II) complex **13** (C20 - C21 = 1.274(10)Å), confirming a certain amount of metallacyclopropane character in **14**.



**Scheme 11.** Synthesis of both *in situ* generated **15**<sup>LiX</sup> and isolated [Ir(bimca<sup>Homo</sup>)] (**15**).

In addition, [Ir(bimca<sup>Homo</sup>)] (**15**) was generated as well to fulfill the generation of group 9 transition-metal complexes with the bimca<sup>Homo</sup> ligand. *In situ* generated iridium complex **15**<sup>LiX</sup> was achieved applying the same route as for [Rh(bimca<sup>Homo</sup>)] (**6**<sup>LiX</sup>), (Scheme 11). To obtain the pure complex **15**, the transmetalation was conducted with freshly generated [K(bimca<sup>Homo</sup>)] at -60 °C. The potassium halides formed could be readily removed by filtration and complex **15** was isolated by removal of all volatiles *in vacuo* in 55% yield.

According to NMR spectroscopy, the molecular structure of **15** shows the same symmetric coordination mode of the ligand as for **14** and **6**. All signals were assigned by means of 2D NMR and NOE experiments. Both double bonds and both carbene moieties are coordinated to the Ir-center, which is confirmed by the up-field shift of the respective signals in the <sup>1</sup>H NMR spectrum (3.77-3.69 (H-14), 1.63 (H-15<sub>cis</sub>), 0.78

ppm (H-15<sub>trans</sub>) as well as in the <sup>13</sup>C NMR spectrum, 39.7 (C15) and 27.7 ppm (C14). The carbene signal is found at typical 164.5 ppm. In comparison with the <sup>1</sup>H NMR spectra of the complexes **14** (Co) and **6** (Rh), the stronger metallacyclopropane character of complex **15** can be derived from the stronger high-field shift of the olefinic proton signals from **14**, **6** to **15** as well as the decreasing <sup>3</sup>J coupling constant of the olefinic protons from 8.0 (*cis*) and 11.3 Hz (*trans*) in **14** to only 7.6 (*cis*) and 8.0 Hz (*trans*) in **15** due to the reduced s-character of the olefinic carbon atoms. This reflects the tendency of 5d metals to form stronger metal-C bonds and the increased stability of the higher oxidation state. DFT calculations of the complexes (**6**, **14** and **15**) also confirmed the structure as described.

**Table 3.** Regioelective isomerization of terminal epoxides with [M(bimca<sup>Homo</sup>)]<sup>[a]</sup>

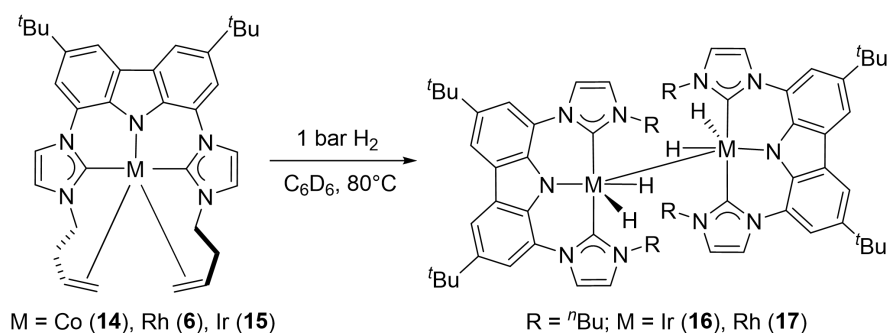
Entry	Epoxide	[Cat.]	H <sub>2</sub> (bar)	Time	Conversion (%)	Yield (%)
1		<b>14</b>	-	6 days	32	18
2	 <b>1b</b>	<b>6</b>	-	30 min	100	92
3		<b>15</b>	-	6 days	100	92
4		<b>14</b>	1	24 h	19	11
5		<b>15</b>	1	24 h	81	52
6		<b>14</b>	-	6 days	0	0
7	 <b>3a</b>	<b>6</b>	-	30 min	100	88
8		<b>15</b>	-	6 days	100	26
9		<b>14</b>	1	24 h	11	5
10		<b>15</b>	1	24 h	75	38

[a] Reactions were carried out in *J. Young* NMR tubes with 10  $\mu$ L THF-d<sub>8</sub> and yield of the products was calibrated to 1,3,5-trimethoxybenzene (internal standard).

In comparison with the highly reactive rhodium complex **6**, the catalytic reactivity of its analogs **14** and **15** were tested in the Meinwald reaction as well. The initial catalytic reactions with complexes **14** and **15** and 1,2-epoxyhexane (**1b**) were conducted at room temperature but no conversion was detected after 6 days.

Therefore, the reaction temperature was elevated to 80 °C and all the further catalytic reactions were performed with 5 mol% catalyst and 10 mol% LiBr in C<sub>6</sub>D<sub>6</sub> (Table 3). When **14** was applied using 1,2-epoxyhexane (**1b**) as the substrate, the isomerization was surprisingly slow and only 18% yield was obtained after 6 days (entry 1) and no conversion was obtained with styrene oxide **3a** (entry 6). Under identical conditions, the reactions with catalyst **6** were completed already within 30 min (entries 2 and 7) and high yields of 2-hexanone (**2b**) and acetophenone (**4a**) were obtained. Furthermore, complex **15** was used in the isomerization of **1b** to yield 2-hexanone in 92% yield (entry 3), but interestingly with a much slower rate compared with **6**. With substrate **3a**, only 26% yield was achieved despite full conversion (entry 8). It is supposed that the low reactivity of the Co(I) complex **14** results from a higher energy barrier of **14** in the nucleophilic ring opening to form the Co(III) intermediate and the higher stability of the coordinated *N*-homoallyl moieties (stronger metallacyclopropane character) in complex **15** leads as well to the low activity.

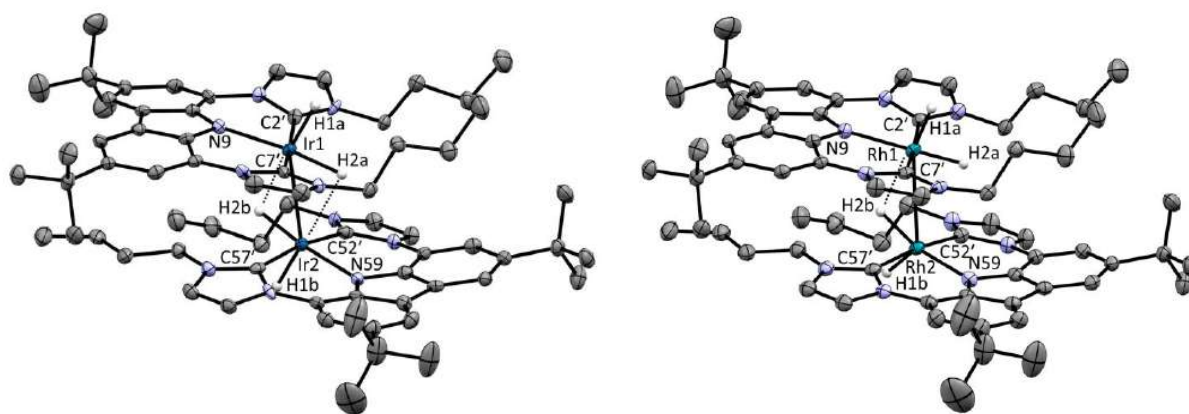
Therefore, the strategy of hydrogenation of the *N*-homoallyl moieties was utilized in order to form highly reactive nucleophilic metal complexes *in situ*. In contrast, the formation of hydrido complexes may reduce the activity or lead to side reactions as well. Indeed, an enhanced reactivity at the beginning with 11% and 52% yield for substrate **1b** (entries 4 and 5) and 5% and 38% yield for the less electrophilic substrate **3a** (entries 9 and 10) was observed after 24 h when the reactions were conducted with **14** or **15** in presence of 1 bar of hydrogen. However, the reaction stopped and could not be completed by extending the reaction time. The higher conversion with catalyst **15** was attributed to the formation of 2-phenylethanol, which was confirmed by <sup>1</sup>H NMR spectroscopy, as well as a polymerization side reaction. Therefore, neither complex **14** nor **15** were able to compete with rhodium catalyst **6**.



Scheme 12. Hydrogenation of [M(bimca<sup>Homo</sup>)].

To elucidate whether the *N*-homoallyl moieties of the complexes (**6**, **14** and **15**) can be hydrogenated in the presence of hydrogen under the catalytic conditions, they were exposed to 1 bar H<sub>2</sub> at 80 °C in C<sub>6</sub>D<sub>6</sub> (Scheme 12).

For iridium complex **15**, a color change from yellow to dark red was observed after 24 h and red crystals were formed after cooling the reaction to ambient temperature. The X-ray structure analysis reveals a dimeric structure in which the former *N*-homoallyl moieties are fully hydrogenated and residual electron density at the metal indicated the formation of the iridium(III) hydrido complex **16** (Figure 3, left). The Ir-H bond lengths were fixed at the value obtained from DFT calculations based on the X-ray structure as the hydrido ligands could not be identified with certainty from X-ray data. The Ir–Ir distance of 2.784 Å in **16** is comparable to those phosphine complexes containing the [Ir(H)(μ-H)]<sub>2</sub> motif (2.73 Å and 2.77 Å) [13], however, the hydride atoms in **16** are less symmetrically bridged, possibly due to steric reasons. The hydrogen bridges in **16** measure 2.50 Å (Ir1-H2b) and 2.53 Å (Ir2-H2a) and were also confirmed by DFT geometry optimizations. In addition, London dispersion<sup>[14]</sup> may play an important role for the dimer formation as the energy difference between the monomers and the dimer strongly favors the dimer. The metal carbene bond lengths Ir-C<sub>NHC</sub> (2.03 Å, mean) are comparable with those of a C<sub>NHC</sub>CC<sub>NHC</sub>-Ir complex from Braunstein.<sup>[15]</sup>



**Figure 3.** Solid-state molecular structure of **16** (left) and **17** (right). Atoms are shown with anisotropic atomic displacement parameters at the 50% probability level. The co-crystallized benzene molecule and the hydrogen atoms (except for the hydrido ligands) are omitted for clarity.

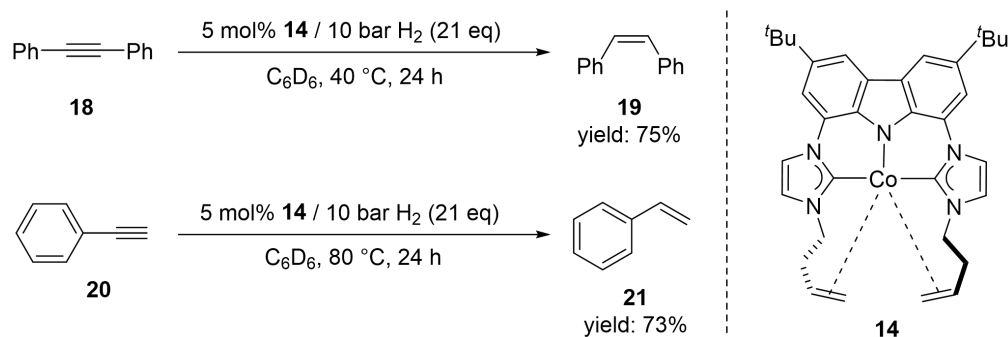
Under identical conditions, the reaction with rhodium complex **6** leads to the formation of red single crystals as well. The X-ray structure analysis shows the

generation of complex **17**, which possesses the same coordination mode as complex **16** (Figure 3, right). The only striking differences to complex **16** is the longer metal-metal distance of 2.934 Å. The Rh-H bond lengths and angles were determined by DFT calculations by fixing all bonds and angles based on the X-ray structure analysis except for the hydrido ligands. At Rh1, a square pyramidal arrangement and at Rh2 a Y-shaped distorted trigonal bipyramidal coordination geometry was found (the latter is also obtained by DFT calculations for a monomeric species). Thus only one intramolecular hydrogen bridge is found (Rh1-H2b = 2.54 Å; Rh2-H2a = 2.79 Å, which also explains the longer Rh1-Rh2 distance compared to complex **16**.

Unfortunately, for cobalt complex **14**, the reaction only led to formation of a dark green solution and no crystals were observed. The *in situ* generated solution shows broad peaks between 16 and -9 ppm in the  $^1\text{H}$  NMR spectrum, possibly due to a paramagnetic influence.

### Semihydrogenation of Alkynes with $[\text{Co}(\text{bimca}^{\text{Homo}})]$

With the successful synthesis of cobalt complex **14**, its application in homogeneous catalysis is extremely attractive and worthy to be investigated. Several cobalt complexes are known to be efficient catalysts for semihydrogenation of alkynes already,<sup>[16]</sup> but only one report from the Fout group studied the semihydrogenation of internal alkynes with a bis(NHC) cobalt catalyst (Figure 4).<sup>[16c]</sup> As complex **14** is structurally analogous to the reported bis(NHC) cobalt catalyst, it may present a similar catalytic reactivity toward this reaction. To confirm the hypothesis, complex **14** was applied in the semihydrogenation of both internal and terminal alkynes.



Scheme 13. Semihydrogenation with cobalt complex **14**.



As expected, complex **14** is highly active in the semihydrogenation reaction (Scheme 13). After screening the hydrogen pressure, reaction temperature, solvent and catalyst loading, the best result with internal alkyne 1,2-diphenylethyne (**18**) currently was 75% yield of (*Z*)-1,2-diphenylethene **19** exclusively. The molecular structure of **19** was determined by <sup>1</sup>H NMR spectroscopy and compared with the literature.<sup>[17]</sup> With the same strategy, the semihydrogenation of the terminal alkyne ethynylbenzene (**20**) was explored. The optimized conditions currently are 5 mol% **14**, 10 bar H<sub>2</sub> in C<sub>6</sub>D<sub>6</sub> at 80 °C. The desired styrene **21** was generated exclusively in 73% yield. Further investigations were not undertaken because of time reasons.

### References

- (1) Jürgens, E.; Wucher, B.; Rominger, F.; Törnroos, K. W.; Kunz, D. *Chem. Commun.* **2015**, *51*, 1897–1900.
- (2) Jürgens, E. *PhD Thesis*, Universität Tübingen, **2017**.
- (3) Jürgens, E.; Kunz, D. *Eur. J. Inorg. Chem.* **2017**, 233–236.
- (4) (a) Kulasegaram, S.; Kulawiec, R. J. *J. Org. Chem.* **1994**, *59*, 7195–7196. (b) Prandi, J.; Namy, J. L.; Menoret, G.; Kagan, H. B. *J. Organomet. Chem.* **1985**, *285*, 449–460.
- (5) Lamb, J. R.; Mulzer, M.; LaPointe, A. M.; Coates, G. W. *J. Am. Chem. Soc.* **2015**, *137*, 15049–15054.
- (6) Wolfe, J. P.; Ney, J. E. *Org. Lett.* **2003**, *5*, 4607–4610.
- (7) Cabré, A.; Sciortino, G.; Ujaque, G.; Verdaguer, X.; Lledós, A.; Riera, A. *Org. Lett.* **2018**, *20*, 5747–5751.
- (8) Simler, T.; Choua, S.; Danopoulos, A. A.; Braunstein, P. *Dalton Trans.* **2018**, *47*, 7888–7895.
- (9) Kuriyama, S.; Arashiba, K.; Tanaka, H.; Matsuo, Y.; Nakajima, K.; Yoshizawa, K.; Nishibayashi, Y. *Angew. Chem. Int. Ed.* **2016**, *55*, 14291–14295.
- (10) Allen, F. H. *Acta Cryst.* **2002**, *B58*, 380–388.
- (11) Fürstner, A.; Krause, H.; Ackermann, L.; Lehmann, C. W. *Chem. Commun.* **2001**, 2240–2241.
- (12) Yu, R. P.; Darmon, J. M.; Milsmann, C.; Margulieux, G. W.; Stieber, S. C. E.; DeBeer, S.; Chirik, P. J. *J. Am. Chem. Soc.* **2013**, *135*, 13168–13184.

(13) (a) Nakayama, S.; Morisako, S.; Yamashita, M. *Organometallics* **2018**, *37*, 1304–1313. (b) Choualeb, A.; Lough, A. J.; Gusev, D. G. *Organometallics* **2007**, *26*, 5224–5229. (c) Peloso, R.; Pattacini, R.; Cazin, C. S. J.; Braunstein P. *Inorg. Chem.* **2009**, *48*, 11415–11424. (d) Chadwick, F. M.; Olliff, N. Weller, A. S. *J. Organomet. Chem.* **2016**, *812*, 268–271. (e) Cano, I.; Martinez-Prieto, L. M.; Vendier, L.; van Leeuwen, P. W. N. M. *Cat. Sci. Tech.* **2018**, *8*, 221–228.

(14) (a) Grimme, S.; Huenerbein, R.; Ehrlich, S. *ChemPhysChem* **2011**, *12*, 1258–1261. (b) Wagner, J. P.; Schreiner, P. R. *J. Chem. Theory Comput.* **2016**, *12*, 231–237. (c) Liptrot, D. J.; Power, P. P. *Nat. Rev. Chem.* **2017**, *1*, 1–12.

(15) Raynal, M.; Pattacini, R.; Cazin, C. S. J.; Vallée, C.; Olivier-Bourbigou, H.; Braunstein, P. *Organometallics* **2009**, *28*, 4028–4047.

(16) (a) Zhang, G.; Yin, Z.; Tan, J. *RSC Adv.* **2016**, *6*, 22419–22423. (b) Fu, S.; Chen, N.; Liu, X.; Shao, Z.; Luo, S.; Liu, Q. *J. Am. Chem. Soc.* **2016**, *138*, 8588–8594. (c) Tokmic, K.; Fout, A. R. *J. Am. Chem. Soc.* **2016**, *138*, 13700–13705. (d) Landge, V.; Pitchaimani, J.; Midya, S.; Subaramanian, M.; Madhu, V.; Balaraman, E. *Catal. Sci. Technol.* **2018**, *8*, 428–433.

(17) Belger, C.; Neisius, N. M.; Plietker, B. *Chem. Eur. J.* **2010**, *16*, 12214–12220.

## Chapter 1

# Regio- and Chemoselective Rearrangement of Terminal Epoxides into Methyl Alkyl and Aryl Ketones

Yingying Tian, Eva Jürgens and Doris Kunz\*

Institut für Anorganische Chemie, Eberhard Karls Universität Tübingen, Auf der Morgenstelle 18, 72076 Tübingen, Germany

### Abstract

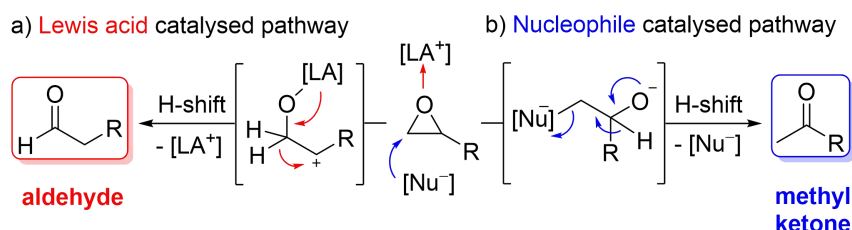
The development of the highly active pincer-type rhodium catalyst **2** for the nucleophilic Meinwald rearrangement of functionalized terminal epoxides into methyl ketones under mild conditions is presented. An excellent regio- and chemoselectivity is obtained for the first time for aryl oxiranes.

---

Tian, Y.; Jürgens, E.; Kunz, D. *Chem. Commun.* **2018**, 54, 11340–11343.

## Introduction

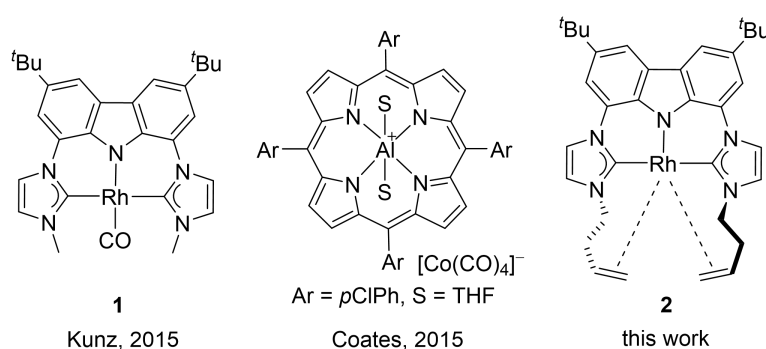
Epoxides are important intermediates in organic synthesis as they undergo various useful transformations.<sup>[1]</sup> Among those, the isomerization to carbonyl compounds (Meinwald reaction) has gained increased attention, and various kinds of catalysts have been reported so far.<sup>[2,3]</sup> Most abundant is the Lewis acid catalyzed isomerization in which the selectivity is determined by formation of the most stable carbenium intermediate followed by an H-shift that leads to aldehydes as the major product in the case of terminal epoxides (Scheme 1a).<sup>[4-6]</sup> The inverse selectivity is obtained with nucleophilic catalysts that attack the more electrophilic site (usually the less substituted one) of the epoxide. After rearrangement *via* a formal H-shift, methyl ketones are formed from terminal epoxides (Scheme 1b).<sup>[7]</sup> This selectivity is very attractive, as it could substitute the Wacker oxidation by a two-step epoxidation-isomerization sequence for temperature and/or Lewis acid-sensitive olefins.<sup>[7d]</sup> Moreover, combining the Johnson–Corey–Chaykovsky epoxidation with the isomerization would provide a very mild and oxidation-free transformation of aldehydes into methyl ketones, which is usually carried out by addition of a methyl-Grignard reagent to the aldehyde, followed by alcohol oxidation.



**Scheme 1.** Catalytic isomerisation pathways of terminal epoxides: formation of aldehydes versus methyl ketones.<sup>[10]</sup>

So far all nucleophilic Meinwald reactions require a pre-activation of the epoxide by Lewis acids. In the first report in 1962 by Eisenmann,<sup>[7a]</sup> the Co(II)–Lewis acid co-catalyst and the nucleophilic  $[\text{Co}(\text{CO})_4]$  catalyst are formed in situ by disproportionation of  $[\text{Co}_2(\text{CO})_8]$  in methanol. A similar principle is likely applicable to the case of Pd-catalysis, in which the Pd(0) catalyst is formed in situ from Pd(II).<sup>[7e]</sup> The presence of the latter can explain the Lewis acid catalyzed selectivity in favour of aldehydes in the case of aryl oxiranes. Nucleophiles like iodide and bromide can also serve as catalysts in combination with Lewis acids like  $\text{Li}^+$ <sup>[7b-d]</sup> or  $\text{Sm}^{2+}$ .<sup>[7f]</sup> Recently,

we have shown that the combination of the nucleophilic Rh-pincer complex **1**<sup>[8]</sup> (Figure 1) and LiNTf<sub>2</sub> is suitable for the regioselective isomerization of terminal alkyl epoxides to methyl ketones<sup>[9]</sup> and soon after Coates reported the highly active complex [Al(porphyrin)]<sup>+</sup> [Co(CO)<sub>4</sub>]<sup>-</sup>.<sup>[7g]</sup> In both cases, the isomerization of phenyl oxirane led only to mixtures of phenyl ethanal and phenyl methyl ketone (2 : 3 (Rh), 3 : 2 (Co)), which indicates a competition between the Lewis acidic and the nucleophilic pathway. Therefore, enhancing the selectivity for phenyl oxiranes as well as increasing the activity of the catalyst was the primary goal of our investigations, whose results are reported in the following.

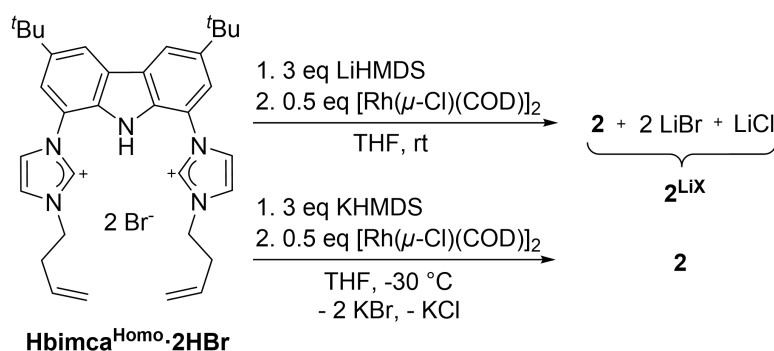


**Figure 1.** Examples of nucleophilic epoxide isomerisation catalysts.

Catalyst **1** requires elevated temperature (60 °C) and a co-catalyst (20 mol% LiNTf<sub>2</sub>) to achieve full conversion within 2 h in the case of terminal alkyl oxiranes.<sup>[9]</sup> An additional substrate scope revealed a high functional group tolerance for many substrates, but a substantial drop in conversion and/or yield was recognized. To overcome these drawbacks we supposed that a CO-free Rh-catalyst would further increase the nucleophilicity of the metal centre and thus reduce the need for a Lewis acid co-catalyst. However, all attempts to synthesize a CO-free version of **1** by using [Rh(μ-Cl)(COD)]<sub>2</sub> or [Rh(μ-Cl)(C<sub>2</sub>H<sub>4</sub>)<sub>2</sub>]<sub>2</sub> as starting material failed and revealed a complex product mixture in the NMR spectra. Increasing the steric bulk at the carbene by *N*-iPr groups lead only to a bridged dinuclear complex.<sup>[11]</sup> Therefore, we tried to reversibly coordinate olefin moieties intramolecularly, which could also stabilize the complex during catalysis and increase its lifetime.

## Results and Discussion

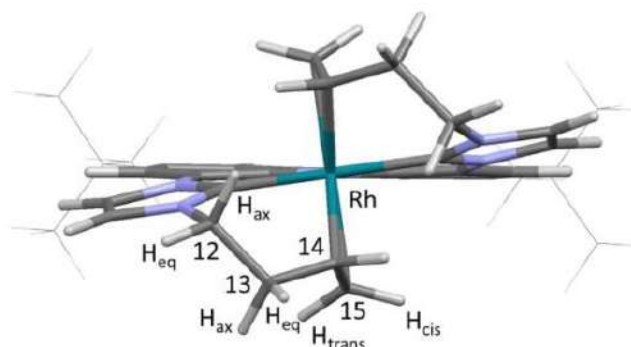
We found the earlier reported *N*-homoallyl substituted ligand  $\text{bimca}^{\text{Homo}}$ <sup>[12]</sup> to fulfil these criteria (Scheme 2). Preparation of **2** was achieved by deprotonation of  $\text{Hbimca}^{\text{Homo}} \cdot 2\text{HBr}$  with LiHMDS and subsequent addition of  $[\text{Rh}(\mu\text{-Cl})(\text{COD})]_2$ . Removal of COD in vacuo yielded **2** along with LiBr and LiCl quantitatively. As the lithium salts turned out to be necessary for the catalytic activity of **2** (vide infra), we did not remove them, but used this mixture  $\mathbf{2}^{\text{LiX}}$  for catalysis. To obtain the pure complex **2**, we transmetalated from the potassium complex  $[\text{K}(\text{bimca}^{\text{Homo}})]$  generated *in situ* by deprotonation of  $\text{Hbimca}^{\text{Homo}} \cdot 2\text{HBr}$  with KHMDS.<sup>[13]</sup> The potassium halides formed were readily removed by filtration.



**Scheme 2.** Synthesis of the rhodium pincer complex **2**.

The molecular structure of **2** (Figure 2) is revealed by NMR spectroscopic analysis and DFT calculations. The single signal set confirms a symmetric coordination mode of the ligand. Coordination of both double bonds and both carbene moieties to the Rh-centre is confirmed not only by the up-field shift of the respective signals in the <sup>13</sup>C NMR spectrum to 185.5 ppm (carbene), 55.9 (C15) and 51.1 ppm (C14), but also by the <sup>1</sup>J<sub>RhC</sub> coupling of 33.9 (carbene), 6.7 (C15) and 11.3 Hz (C14). DFT calculations also predict a pentacoordinating ligand with both olefin moieties contributing to the trigonal bipyramidal coordination mode at the Rh centre and an orientation in line with the trigonal base.<sup>[14]</sup> The four <sup>1</sup>H NMR signals for the methylene protons (H-12, H-13) of the homoallyl moiety were assigned according to their coupling constants and NOE to the axial and equatorial protons of the six membered metallacycles. The signals of the olefinic protons are strongly shielded (4.18–4.10 (H-14), 2.41 (H-15<sub>cis</sub>), 1.67 ppm (H-15<sub>trans</sub>)) and the reduced coupling

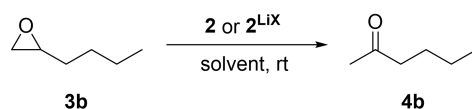
constants of only 8.0 (cis) and 9.9 Hz (trans) can be explained by the reduced s-character due to the coordination with the Rh-centre.



**Figure 2.** Calculated structure of **2** with *tert*-Bu groups depicted in wireframe for clarity.

With the rhodium complex **2** in hand, we tested the isomerization of 1,2-epoxyhexane (**3b**) as the model substrate. An initial test applying 5 mol% of complex **2**<sup>LiX</sup> in THF-*d*<sub>8</sub> revealed only low conversion at room temperature (Table 1, entry 1), which improved by raising the reaction temperature to 60 °C and adding LiNTf<sub>2</sub> as co-catalyst (Table 1, entry 2). Interestingly, full regioselectivity and quantitative yields were obtained in short reaction times at room temperature when toluene-*d*<sub>8</sub> (3 h) or C<sub>6</sub>D<sub>6</sub> (2 h) were used as solvent (Table 1, entries 3 and 4). We suppose that the poor conversion in THF-*d*<sub>8</sub> derives from competitive binding between THF and the substrate to the Lewis acid co-catalyst.<sup>[15]</sup> To test whether the residual lithium halides are still necessary as a Lewis acid co-catalyst we applied the isolated catalyst **2** in C<sub>6</sub>D<sub>6</sub>. No catalytic activity was found under these conditions (Table 1, entry 5). Surprisingly, addition of 10 mol% of LiBr achieved no improvement, but small amounts of THF (20 μL) restored the catalytic activity fully, which can be explained by the enhanced solubility of LiBr<sup>[16]</sup> (entries 6 and 7). As lithium halides are known catalysts for the Meinwald reaction, albeit at elevated temperature,<sup>[7b-d]</sup> we tested them under our conditions at room temperature. Neither lithium bromide nor solubilized lithium bromide (by 20 μL THF) were able to catalyse this reaction (entries 8 and 9). These results clearly show that catalyst **2** is much more active than catalyst **1** and that at least a weak Lewis acid co-catalyst is still necessary.

Lowering the catalyst loading from 5 mol% to 1 mol% at constant concentration of the substrate did not affect the regioselectivity but required a longer reaction time (Table

**Table 1.** Rh-catalyzed isomerization of 1,2-epoxyhexane (**3b**): Optimization of the reaction conditions.<sup>[a]</sup>

Entry	Catalyst [mol%] + additive [mol%]	Solvent	Conc. <b>3b</b> [mol/L]	Time	Yield [%] <sup>[b]</sup>
1	5 ( <b>2</b> <sup>LiX</sup> )	THF- <i>d</i> <sub>8</sub>	0.1	2 h	< 5
2 <sup>[c, f]</sup>	5 ( <b>2</b> <sup>LiX</sup> )	THF- <i>d</i> <sub>8</sub>	0.1	5.5 d	88
3	5 ( <b>2</b> <sup>LiX</sup> )	Toluene- <i>d</i> <sub>8</sub>	0.1	3 h	>99
4	5 ( <b>2</b> <sup>LiX</sup> )	C <sub>6</sub> D <sub>6</sub>	0.1	2 h	> 99
5	5 ( <b>2</b> )	C <sub>6</sub> D <sub>6</sub>	0.1	2 h	0
6	5 ( <b>2</b> ) + 10 (LiBr)	C <sub>6</sub> D <sub>6</sub>	0.1	1 h	0
7 <sup>[d]</sup>	5 ( <b>2</b> ) + 10 (LiBr)	C <sub>6</sub> D <sub>6</sub>	0.1	3 h	> 99
8	10 (LiBr)	C <sub>6</sub> D <sub>6</sub>	0.1	24 h	0
9 <sup>[d]</sup>	10 (LiBr)	C <sub>6</sub> D <sub>6</sub>	0.1	24 h	0
10	4 ( <b>2</b> <sup>LiX</sup> )	C <sub>6</sub> D <sub>6</sub>	0.1	3 h	> 99
11	3 ( <b>2</b> <sup>LiX</sup> )	C <sub>6</sub> D <sub>6</sub>	0.1	8 h	> 99
12	2 ( <b>2</b> <sup>LiX</sup> )	C <sub>6</sub> D <sub>6</sub>	0.1	9 h	> 99
13	1 ( <b>2</b> <sup>LiX</sup> )	C <sub>6</sub> D <sub>6</sub>	0.1	7 d	> 99
14 <sup>[e]</sup>	1 ( <b>2</b> <sup>LiX</sup> )	C <sub>6</sub> D <sub>6</sub>	0.1	4 d	87
15 <sup>[f]</sup>	1 ( <b>2</b> <sup>LiX</sup> )	C <sub>6</sub> D <sub>6</sub>	0.1	3 d	93
16	1 ( <b>2</b> <sup>LiX</sup> )	C <sub>6</sub> D <sub>6</sub>	0.2	24 h	> 99
17	1 ( <b>2</b> <sup>LiX</sup> )	C <sub>6</sub> D <sub>6</sub>	0.4	14 h	> 99
18	1 ( <b>2</b> <sup>LiX</sup> )	C <sub>6</sub> D <sub>6</sub>	1.0	3 h	98

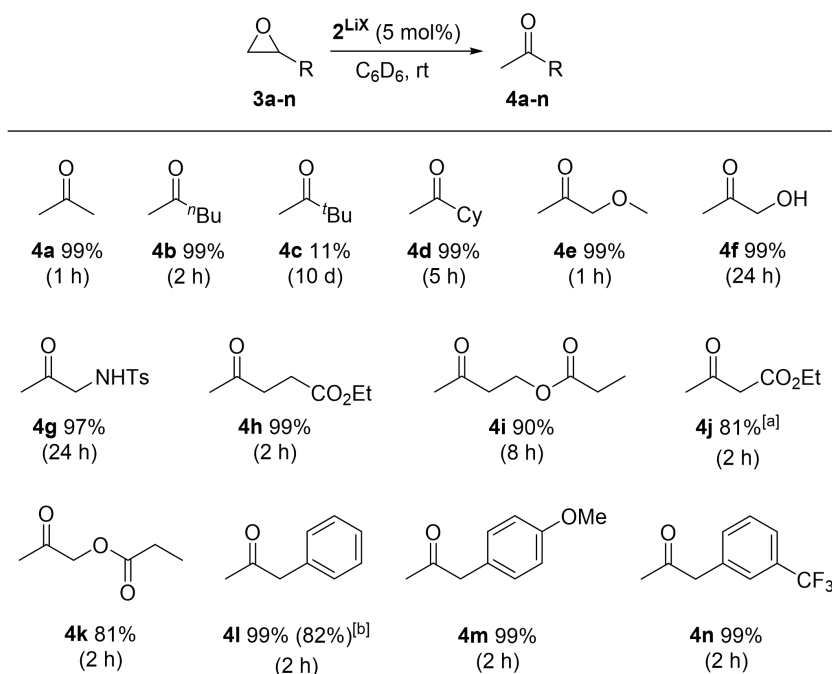
[a] Carried out in *J. Young* NMR tubes. [b] Yield (<sup>1</sup>H NMR) of **4b** calibrated to 1,3,5-trimethoxybenzene (internal standard); conversion = yield. [c] With 20 mol% LiTNf<sub>2</sub>. [d] With 20 μL THF. [e] At 40 °C. [f] At 60 °C.

1, entries 10–13). A higher temperature accelerated the reaction, but it still needed several days for completion using 1 mol% of catalyst (Table 1, entries 14 and 15). Epoxide concentrations of 0.4 mol/L and 1.0 mol/L (Table 1, entries 16–18) shortened the reaction time substantially and the reaction is about 10 times faster compared to literature.<sup>[7g]</sup> Even though 1 mol% of catalyst loading was sufficient for the model reaction at high concentrations, further experiments showed that it may lead to polymerization of functionalized epoxides (especially with ester groups). Thus,

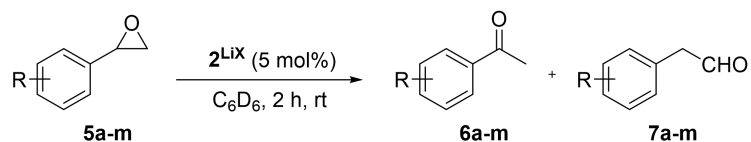


the optimized reaction conditions (5 mol% **2<sup>LiX</sup>**, 0.1 M epoxide, C<sub>6</sub>D<sub>6</sub>, room temperature) were applied to explore the generality of this protocol.

Using complex **2<sup>LiX</sup>** as the catalyst, 13 functionalized terminal epoxides were converted successfully into the desired methyl ketones (Scheme 3). The alkyl substituted epoxides **3a–d** and the methoxy epoxide **3e** were transformed into the desired products **4a–e** almost quantitatively with full regioselectivity. The only exception was *tert*-butyloxirane (**3c**), which could be obtained in only 11% yield after 10 days, possibly due to steric effects. In the case of hydroxyl (**3f**) and sulfonamide groups (**3g**) the isomerization progressed slowly, which might reveal a competing influence of the acidic protons, nonetheless **4f** and **4g** were formed in 99% and 97% yields. Notably, catalyst **2<sup>LiX</sup>** is well suited for the isomerization of terminal epoxides **3h–k** with ester groups and afforded **4h–k** with high regio- and chemoselectivity. **3j** reacts a bit slower than **3h**, which might be due to its  $\alpha$ -acidity. Furthermore, 2-benzyloxirane (**3l**) and its methoxy (**3m**) and trifluoromethyl (**3n**) congeners were isomerized to the methyl ketones **4l–n** quantitatively. Internal epoxides react considerably slower. §



**Scheme 3.** Rh-catalyzed regio- and chemoselective isomerisation of terminal epoxides. Standard reaction conditions: Substrate (50.0  $\mu$ mol), **2<sup>LiX</sup>** (5 mol%), C<sub>6</sub>D<sub>6</sub> (0.5 mL), r.t. at the given time. Carried out in *J. Young* NMR tubes. Yield (<sup>1</sup>H NMR) calibrated to 1,3,5-trimethoxybenzene (internal standard). [a] 14 % of unreacted epoxide left. [b] isolated yield after column chromatography of a 1 mmol scale experiment.

**Table 2.** Regio- and chemoselective isomerisation of aryl oxiranes **5a-m**.<sup>[a]</sup>

Entry	Epoxide <b>5</b>	<b>6</b> Yield [%] <sup>[b]</sup>	Ratio ( <b>6:7</b> )
1	<b>5a</b>	<b>6a</b> , 95	40:1
2	<b>5b</b>	<b>6b</b> , 98	> 99:1
3 <sup>[c]</sup>	<b>5c</b>	<b>6c</b> , 91	> 99:1
4	<b>5d</b>	<b>6d</b> , 99	> 99:1
5	<b>5e</b>	<b>6e</b> , 99	> 99:1
6	<b>5f</b>	<b>6f</b> , 99	> 99:1
7	<b>5g</b>	<b>6g</b> , 99	> 99:1
8	<b>5h</b>	<b>6h</b> , 85	91:1
9	<b>5i</b>	<b>6i</b> , 92	> 99:1
10	<b>5j</b>	<b>6j</b> , 82	> 99:1
11	<b>5k</b>	<b>6k</b> , 77	21:1
12	<b>5l</b>	<b>6l</b> , 57	10:1
13 <sup>[d]</sup>	<b>5m</b>	<b>6m</b> , 75	7:1

[a] Standard reaction conditions: epoxide (50.0  $\mu\text{mol}$ ),  $2\text{LiX}$  (5 mol%),  $\text{C}_6\text{D}_6$  (0.5 mL), rt. Carried out in *J. Young* NMR tubes. [b] Yields ( $^1\text{H}$  NMR) calibrated to 1,3,5-trimethoxybenzene (internal standard). [c] At 80  $^\circ\text{C}$  for 2 days. [d] 22 h.

The selective rearrangement of aryl oxiranes to methyl ketones has not been achieved so far due to the Lewis acid catalyzed side reaction.<sup>[7e, f, 9]</sup> Therefore, we applied our new catalyst **2**<sup>Li<sup>x</sup></sup> also in the isomerization of aryl oxiranes (Table 2). With styrene oxide (**5a**) we found an unprecedented good ratio between acetophenone (**6a**) and 2-phenylacetaldehyde (**7a**) of 40 : 1. To our delight, acetophenones **6b–d** bearing the strong electron-withdrawing trifluoromethyl substituent were obtained regioselectively in excellent yield. This counts also for the terminal epoxides **5e–j** possessing fluoro, chloro and bromo substituents (>99 : 1). Aryl oxiranes containing electron-donating groups (methyl or methoxy) were converted into **6k** and **6l** with still very good regioselectivities of 21 : 1 and 10 : 1 favoring the methyl ketones (**6k**, **6l**) over the aldehydes (**7k**, **7l**) in good to moderate yields. Notably, epoxide **5l** is extremely sensitive towards Lewis acids in C<sub>6</sub>D<sub>6</sub> at room temperature. In two control experiments without catalyst **2**, 10 mol% of LiBr and 5 mol% of LiCl as well as 10 mol% LiI were added to the aryl oxirane **5l** in C<sub>6</sub>D<sub>6</sub>. After few days (LiBr/Cl) or 23 h (LiI), only formation of the aldehyde **7l** and other, possibly polymerization products, was observed. The oxirane **5m** bearing a +I substituent in *ortho* position can be transformed into **6m** with still good regioselectivity and in good yield after 22 h.

### Conclusions

The new CO-free rhodium complex **2** led to significant improvement of the nucleophilic Meinwald reaction with respect to lower reaction temperature, catalyst loading and the absence of additional Lewis acids. It also shows a high functional group tolerance. The stronger nucleophilicity of complex **2** is crucial for the excellent regioselectivity achieved in the case of aryl oxiranes, which can get isomerized for the first time almost exclusively to the methyl ketones. Thus, we have broadened the scope of this reaction, which should be very valuable for organic synthesis, especially in combination with the Johnson–Corey–Chaykovsky reaction.

### Acknowledgement

Yingying Tian thanks the China Scholarship Council (CSC) for a predoctoral fellowship and Eva Jürgens the MWK-BW for funding (Landesgraduiertenförderung). We thank Alexander Klaiber, Nicolas Wiedmaier and Mario R. Rapp for help in synthesising some of the substrates and in the catalyst testing.

## Experimental procedure

*In situ* generation of catalyst  $2^{\text{LiX}}$ :  $\text{Li}(\text{N}(\text{SiMe}_3)_2)$  (7.4 mg, 44.0 mmol) was added to a suspension of  $\text{Hbimca}^{\text{Homo}}\cdot 2\text{HBr}$  (10.0 mg, 14.7 mmol) in 0.5 mL of  $\text{THF-d}_8$  at room temperature. After 10 min,  $[\text{Rh}(\mu\text{-Cl})(\text{COD})]_2$  (3.6 mg, 7.3 mmol) was added and the solution was stirred for another 10 min. After checking the successful formation of the catalyst by NMR, 85.0 mL (containing 2.5 mmol  $2^{\text{LiX}}$ ) of the freshly prepared catalyst solution were used for each NMR experiment and the THF was removed in oil-pump vacuum prior to the addition of the epoxide.

## Notes and References

§ At 80 °C, but under otherwise identical conditions, the conversion of 77 % *cis*-2,3-epoxybutane into methylethyl ketone was achieved after 10 days and only 34 % with *trans*-2,3-epoxybutane. No further optimization was attempted.

(1) Smith, J. G. *Synthesis*, **1984**, 1984, 629–656.

(2) (a) Hartman, B. C.; Rickborn, B. *J. Org. Chem.* **1972**, *37*, 943–946. (b) Rickborn, B. in *Compr. Org. Synth.*, Vol. 3, B. M. Trost (Ed.), Pergamon, Oxford, **1991**, pp. 733–775. (c) Kita, Y.; Kitagaki, S.; Yoshida, Y.; Mihara, S.; Fang, D.-F.; Kondo, M.; Okamoto, S.; Imai, R.; Akai, S.; Fujioka, H. *J. Org. Chem.* **1997**, *62*, 4991–4997. (d) Huang, C.-Y.; Doyle, A. G. *Chem. Rev.* **2014**, *114*, 8153–8198.

(3) Meinwald, J.; Labana, S. S.; Chadha, M. S. *J. Am. Chem. Soc.* **1963**, *85*, 582–585.

(4)  $\text{Ni}^{2+}$ : (a) Miyashita, A.; Shimada, T.; Sugawara, A.; Nohiya, H. *Chem. Lett.* **1986**, *15*, 1323–1326.  $\text{In}^{3+}$ : (b) Ranu, B. C.; Jana, U. *J. Org. Chem.* **1998**, *63*, 8212–8216.  $\text{Fe}^{3+}$ : (c) Suda, K.; Baba, K.; Nakajima, S.-i.; Takanami, T. *Tetrahedron Lett.* **1999**, *40*, 7243–7246.  $\text{Bi}^{3+}$ : (d) Anderson, A. M.; Blazek, J. M.; Garg, P.; Payne, B. J.; Mohan, R. S. *Tetrahedron Lett.* **2000**, *41*, 1527–1530.  $\text{Er}^{3+}$ : (e) Procopio, A.; Dalpozzo, R.; De Nino, A.; Nardi, M.; Sindona, G.; Tagarelli, A. *Synlett* **2004**, 2633–2635. Sn: (f) Banerjee, M.; Roy, U. K.; Sinha, P.; Roy, S. *J. Organomet. Chem.* **2005**, *690*, 1422–1428.  $\text{Cu}^{2+}$ : (g) Robinson, M. W. C.; Pillinger, K. S.; Mabbett, I.; Timms, D. A.; Graham, A. E. *Tetrahedron* **2010**, *66*, 8377–8382.  $[\text{ReBr}(\text{CO})_3]$ : (h) Umeda, R.; Muraki, M.; Nakamura, Y.; Tanaka, T.; Kamiguchi, K.; Nishiyama, Y. *Tetrahedron Lett.* **2017**, *58*, 2393–2395.

- (5) The chelation enhanced formation of methyl ketones from  $\alpha$ -keto oxiranes by a  $\text{Ru}^{2+}$  catalyst: Chang, C.-L.; Kumar, M. P.; Liu, R.-S. *J. Org. Chem.* **2004**, *69*, 2793–2796.
- (6)  $\text{Pd}^{2+}$ : (a) Vyas, D. J.; Larionov, E.; Besnard, C.; Guénée, L.; Mazet, C. *J. Am. Chem. Soc.* **2013**, *135*, 6177–6183. (b) Humbert, N., Vyas, D. J., Besnard, C., Mazet, C. *Chem. Commun.* **2014**, *50*, 10592–10595. (c) Kulasegaram, S.; Kulawiec, R. J. *J. Org. Chem.* **1997**, *62*, 6547–6561. (d) Kulasegaram, S.; Kulawiec, R. J. *Tetrahedron* **1998**, *54*, 1361–1374. Ni in a reaction sequence: (e) Desnoyer, A. N.; Geng, J. L.; Drover, M. W.; Patrick, B. O.; Love, J. A. *Chem. Eur. J.* **2017**, *23*, 11509–11512.
- (7) (a) Eisenmann, J. L. *J. Org. Chem.* **1962**, *27*, 2706–2706. (b) Rickborn, B.; Gerkin, R. M. *J. Am. Chem. Soc.* **1968**, *90*, 4193–4194. (c) Rickborn, B.; Gerkin, R. M. *J. Am. Chem. Soc.* **1971**, *93*, 1693–1700. (d) An, Z.-w. D'Aloisio, R.; Venturello, C. *Synthesis* **1992**, 1229–1231. (e) Kulasegaram, S.; Kulawiec, R. J. *J. Org. Chem.* **1994**, *59*, 7195–7196. (f) Prandi, J.; Namy, J. L.; Menoret, G.; Kagan, H. B. *J. Organomet. Chem.* **1985**, *285*, 449–460. (g) Lamb, J. R.; Jung, Y.; Coates, G. W. *Org. Chem. Front.* **2015**, *2*, 346–349.
- (8) Moser, M.; Wucher, B.; Kunz, D.; Rominger, F. *Organometallics* **2007**, *26*, 1024–1030.
- (9) Jürgens, E.; Wucher, B.; Rominger, F.; Törnroos, K. W.; Kunz, D. *Chem. Commun.* **2015**, *51*, 1897–1900.
- (10) The nucleophilic pathway (Scheme 1) follows an  $\text{S}_{\text{N}}2$  mechanism. Formation of metallaoxetanes by insertion into the  $\sigma$ -carbon oxygen bond: (a) Dauth, A.; Love, J. A. *Chem. Rev.* **2011**, *111*, 2010–2047. For  $\text{Ni}(0)$  see Lit. 4a and 6e as well as: (b) Desnoyer, A. N.; Bowes, E. G.; Patrick, B. O.; Love, J. A. *J. Am. Chem. Soc.* **2015**, *137*, 12748–12751. Rh: (c) Calhorda, M. J.; Galvao, A. M.; Unaleroglu, C.; Zlota, A. A.; Frolow, F.; Milstein, D. *Organometallics* **1993**, *12*, 3316–3325. and (d) de Bruin, B.; Boerakker, M. J.; Donners, J. J. J. M.; Christiaans, B. E. C.; Schlebos, P. P. J.; de Gelder, R.; Smits, J. M. M.; Spek, A. L.; Gal, A. W. *Angew. Chem. Int. Ed.* **1997**, *36*, 2063–2067. (e) de Bruin, B.; Boerakker, M. J.; Verhagen, J. A. W.; de Gelder, R.; Smits, J. M. M.; Gal, A. W. *Chem. Eur. J.* **2000**, *6*, 298–312. Without additional Lewis acid (2'-oxoalkyl)(hydrido)rhodium(III) intermediates were isolated reacting  $\text{RhCl}(\text{PMe}_3)_3$  in neat propylene or styrene oxide after 16 h: (f) Milstein, D. *J. Am. Chem. Soc.* **1982**, *104*, 5227–5228. Ir: (g) Milstein, D.; Calabrese, J. C. *J. Am. Chem. Soc.* **1982**, *104*, 3773–3774. We tested  $\text{RhCl}(\text{PMe}_3)_3$  under our conditions and found

it considerably slower than complex  $2^{LiX}$ : 5% yield for styrene oxide after 2 h (with or without addition of  $Br^-$ ); after 24 h still 5% yield without  $Br^-$  and 16% in presence of 10 mol% LiBr. For nucleophilic mechanisms *via* C-H bond activation: (h) Milstein, D.; Buchman, O.; Blum, J. *J. Org. Chem.* **1977**, 42, 2299–2308. (i) Wu, J.; Bergman, R. G. *J. Am. Chem. Soc.* **1989**, 111, 7628–7630.

(11) Jürgens, E. *PhD Thesis*, University of Tübingen, **2017**.

(12) Bicma ((3,6-di-*tert*-butyl-1,8-bis(imidazolin-2-ylidene)-9-carbazolide). E. Jürgens, D. Kunz, *Eur. J. Inorg. Chem.* **2017**, 233–236.

(13) In contrast to  $[Li(bimca^{Homo})]$ , complex  $[K(bimca^{Homo})]$  decomposes at room temperature into butadiene and the bisimidazole carbazolidine  $[K(imi)_2carb]$ .

(14) DCM and acetonitrile react already with **1**: M. Moser, *PhD Thesis*, Heidelberg University, **2007**.

(15)  $2^{LiX}$  is generated in THF, which is then removed (with COD) *in vacuo*. Some THF remains coordinated to  $Li^+$  so that the solubility of LiX is enhanced during catalysis in  $C_6D_6$  or toluene- $d_8$ .

## Chapter 2

### Nucleophilic Isomerization of Epoxides by Pincer-Rhodium

#### Catalysts: Activity Increase and Mechanistic Insights

Yingying Tian, Eva Jürgens, Katharina Mill, Ronja Jordan, Theo Maulbetsch, and  
Doris Kunz\*

Institut für Anorganische Chemie, Eberhard Karls Universität Tübingen, Auf der  
Morgenstelle 18, 72076 Tübingen, Germany

#### Abstract

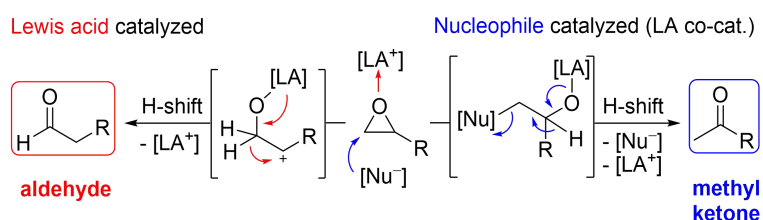
Herein, we present the efficient isomerization of epoxides into methyl ketones with a novel pincer-rhodium complex under very mild conditions. The catalyst system has an excellent functional group tolerance and a wide array of epoxides was tested. The corresponding methyl ketones were obtained in very high yields with excellent chemo- and regioselectivity. In addition, we investigated mechanistic details like the isomerization of the catalyst, and we obtained evidence that the catalytic cycle follows a  $\beta$ -hydride elimination-reductive elimination pathway after the nucleophilic ring opening of the epoxide.

---

Tian, Y.; Jürgens, E.; Mill, K.; Jordan, R.; Maulbetsch, T.; Kunz, D. *ChemCatChem* **2019**, *11*, 4028 – 4035.

## Introduction

In contrast to the common Lewis acid catalyzed isomerization of terminal epoxides (Meinwald reaction),<sup>[1]</sup> which leads to the formation of aldehydes via generation of the more stable carbenium intermediate,<sup>[2]</sup> the isomerization by nucleophilic catalysts is rare and results in the formation of methyl ketones (Scheme 1).<sup>[3]</sup> This pathway is very attractive because, in combination with the Corey-Chaykovsky reaction, it provides an oxidation-free route for the synthesis of methyl ketones from aldehydes or, together with the epoxidation of olefins, an alternative to the Wacker oxidation. Since the discovery of this opposite regioselectivity in 1962 by Eisenmann,<sup>[3a]</sup> it was evident that the catalysis is not only achieved by a nucleophilic catalyst on its own, but typically requires a Lewis acid co-catalyst [LA<sup>+</sup>] which pre-activates the epoxide by coordination, but does not lead to ring opening under carbocation formation.

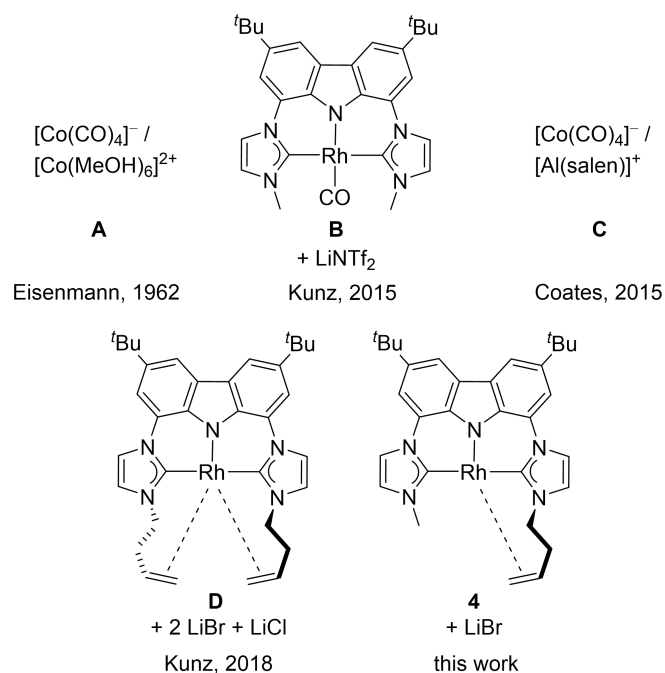


**Scheme 1.** Lewis acid (left) and nucleophile (right) catalyzed Meinwald reaction of terminal epoxides: formation of aldehydes versus methyl ketones.

In case of the results of Eisenmann, the catalytic system **A** (Figure 1) most likely consists of the  $[\text{Co}(\text{CO})_4]^-$  nucleophile and the Lewis acid  $[\text{Co}(\text{CH}_3\text{OH})_6]^{2+}$  formed *in situ* by disproportionation of  $[\text{Co}_2(\text{CO})_8]$  in methanol that is required as a solvent. In 2015 we have reported on a selective ring opening using the nucleophilic Rh-catalyst **B** (5 mol%) along with 20 mol% of the Lewis acid co-catalyst  $\text{LiNTf}_2$  at 60 °C.<sup>[3h]</sup> A more active system was reported by Coates using  $[\text{Al}(\text{salen})][\text{Co}(\text{CO})_4]$ .<sup>[3i]</sup> While both systems were highly selective with terminal alkyl epoxides, the isomerization of phenyl oxirane led to a mixture of the aldehyde and the ketone in almost equal amounts. This prompted us to develop the more nucleophilic CO-free rhodium catalyst **D**, in which the highly reactive metal center is intramolecularly stabilized by coordination of both *N*-homoallyl substituents of the so-called bimca<sup>Homo</sup> (1,8-bis(imidazolin-2-ylidene)-3,6-di(*tert*-butyl)carbazolide) carbene-pincer-ligand.<sup>[3j]</sup> Due to its higher nucleophilicity, a mixture of the weak Lewis acids LiBr and LiCl (2:1),



which are present from the synthesis of **D** in THF, is sufficient to act as a co-catalyst in benzene. With this system it was not only possible to achieve a selectivity of methylketone vs. aldehyde of 40:1 and 95% yield in the isomerization of phenyl oxirane after 2 h at room temperature (5 mol% **D**), but also to isomerize the highly sensitive *p*-methoxyphenyl oxirane to the corresponding ketone with a ratio of 10 :1 and in 57% yield.



**Figure 1.** Rhodium pincer complexes and suitable Lewis acid co-catalysts for the nucleophilic Meinwald rearrangement.

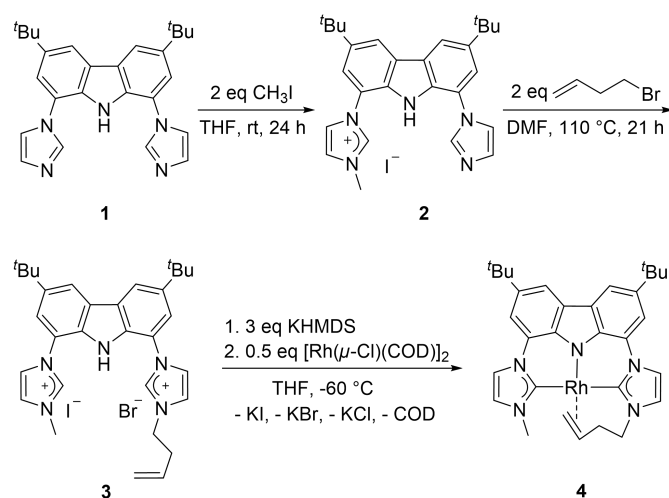
The functional group tolerance of catalyst **D** is very high, but sterically demanding substrates such as *tert*-butyloxirane, -NH<sub>2</sub>, or -OH containing substrates, some *ortho*-substituted aryl oxiranes or internal epoxides required very long reaction times and/or elevated temperatures, which in some cases still led to low yields. Therefore, we were interested in developing our catalyst system further along with gaining more insight into the reaction mechanism.

As the 18 e<sup>-</sup> rhodium complex **D** requires the dissociation of one olefin moiety to react as a nucleophile, we envisaged the 16 e<sup>-</sup> complex **4** being an interesting target to fulfill our purpose: The complex would still be stabilized intramolecularly by one olefin moiety during catalysis but in addition exhibit a higher nucleophilicity and thus catalytic activity. However, an unsymmetrically *N*-substituted bimca ligand or related systems have hitherto not yet been reported. In the following, we will report on the

synthesis of the unsymmetric bimca ligand **bimca**<sup>Me,Homo</sup> and its Rh complex **4** as well as the catalytic activity of **4** in the regioselective epoxide isomerization. In addition, more insight into the reaction mechanism and deactivation pathways will be provided.

## Results and Discussion

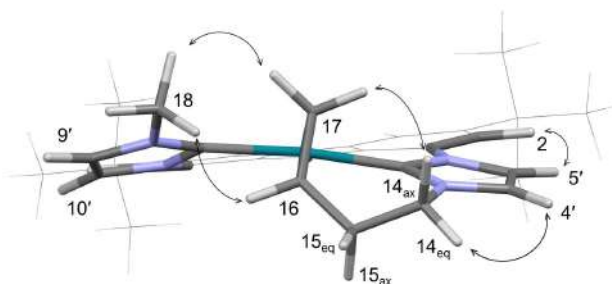
The synthesis of an unsymmetrically substituted bimca ligand requires the selective monoalkylation of bisimidazol **1**. Based on our observation that the monoalkylated product **2** was formed as a byproduct when reacting bisimidazol **1** with an excess methyl iodide in THF,<sup>[4]</sup> we investigated the monoalkylation further. In acetonitrile the reaction of equimolar amounts of bisimidazol **1** and methyl iodide or Meerwein's salt (Me<sub>3</sub>OBF<sub>4</sub>) leads to a 1:1 mixture of the dialkylated product and the starting material **1**. However, if the reaction is carried out with even a twofold excess of methyl iodide in THF at room temperature the desired product **2** is formed due to its precipitation under these conditions, which prevents further alkylation (Scheme 2). After workup by filtration, the imidazolium salt **2** was obtained in 90% yield as a yellow solid. The reduced symmetry leads to four signals for the carbazole moiety and six signals for the imidazolium moieties. The presence of only one NH signal with the same integral as the other aromatic peaks excludes a potential 1:1 mixture of **1** and the dimethylated product. The introduction of the *N*-homoallyl substituent was carried out with a twofold excess of 4-bromo-1-butene at 110 °C in dimethylformamide and the desired bisimidazolium salt **3** was isolated after workup in 95 % yield. The 10 signals



Scheme 2. Synthesis of unsymmetric rhodium catalyst **4**.

for the aromatic imidazolium and carbazole protons can be clearly assigned with the help of 2D NMR experiments including an NOE experiment to assign the peaks to the relative sides of the carbazole backbone.

The preparation of **4**<sup>LiX</sup> was achieved by deprotonation of **3** with LiHMDS and subsequent addition of  $[\text{Rh}(\mu\text{-Cl})(\text{COD})]_2$ . However, the generated COD and HMDS during the reaction cannot be removed *in vacuo* without decomposition of the complex, possibly due to the presence of the lithium salts. To obtain the pure complex **4**, we transmetalated the ligand from the potassium complex  $[\text{K}(\text{bimca}^{\text{Me,Homo}})]$  generated *in situ* by deprotonation of **3** with KHMDS. The potassium halides formed could be readily removed by filtration and complex **4** isolated by removal of all volatiles *in vacuo*.

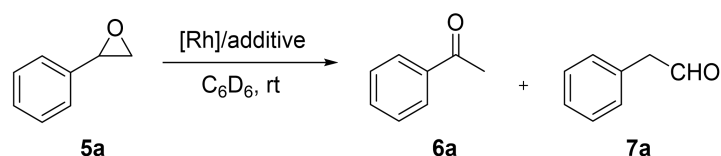


**Figure 2.** Minimum conformation of complex **4** based on DFT-D3 calculations (TurboMole: BP86/def2-TZVP) and observed NOE crosspeaks (indicated with arrows). For clarity reasons, part of the carbazole backbone is depicted in wireframe style.

The structure of complex **4** could be identified by NMR experiments. Bonding of the terminal double bond to the rhodium center is proven by the  $^1J_{\text{RhC}}$  coupling constants of 13.2 Hz (C16) and 13.7 Hz (C17) in the  $^{13}\text{C}$  NMR spectrum and the 4 signals for the diastereotopic hydrogen atoms at the two methylene groups of the homoallyl substituent. The *cis/trans* assignment of the olefinic signals at 3.50 ppm ( $^3J = 7.7$  Hz, H-17<sub>cis</sub>) and 2.94 ppm ( $^3J = 11.5$  Hz, H-17<sub>trans</sub>) is based on the vicinal coupling constants, which are smaller than those typically observed in non-coordinated olefins (e.g. in compound **3**:  $^3J_{\text{HH}} = 17.2$  Hz (*trans*) and 10.3 Hz (*cis*)), and can be explained with the lower s-character due to a rehybridization upon coordination of the metal ion. The relative assignment of axial and equatorial methylene signals is also based on the Karplus equation. Finally, informations on the relative conformation of the metallacycle were obtained with an NOE experiment, which confirmed the aforementioned assignments. Out of several minimum conformations of similar

energy obtained by DFT-calculations, the NOE data is in accordance with the structure that is second lowest in energy ( $\Delta = 1.5$  kJ/mol; Figure 2).

**Table 1.** Optimization of the reaction conditions for the isomerization of phenyl oxirane in presence of rhodium catalyst **4**.<sup>[a]</sup>



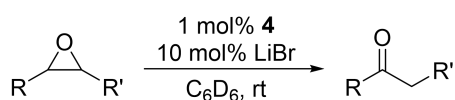
Entry	Catalyst [mol%]	Conc. <b>5a</b> [mol/L]	Time	Yield [%] <sup>[b]</sup>	Ratio ( <b>6a:7a</b> )
1	5	0.1	40 min	84	>99:1
2	3	0.1	70 min	89	>99:1
3	1	0.1	120 min	>99	>99:1
4 <sup>[c]</sup>	1	0.1	24 h	7	5:1
5 <sup>[d]</sup>	1	0.1	24 h	6	10:1
6	1	0.2	60 min	99	>99:1
7	1	0.4	50 min	95	>99:1
8	1	0.8	40 min	92	>99:1
9	-	0.8	60 min	<5	-

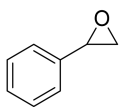
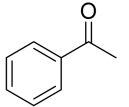
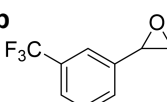
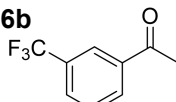
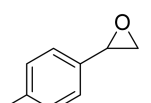
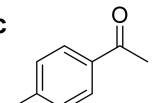
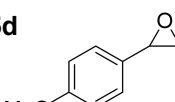
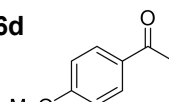
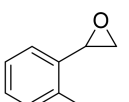
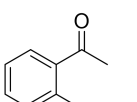
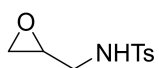
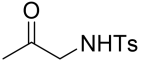
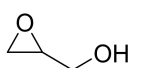
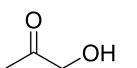
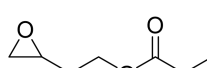
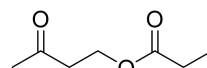
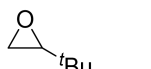
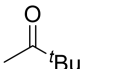
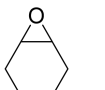
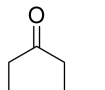

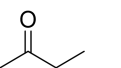

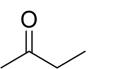
[a] Carried out in *J. Young* NMR tubes and with 10 mol% LiBr and 5  $\mu$ L THF- $d_8$ . [b] Yield ( $^1H$  NMR) of **6a** calibrated to 1,3,5-trimethoxybenzene (internal standard). [c] Without LiBr. [d] THF- $d_8$  as the solvent.

With the new rhodium complex **4** in hand, we were able to investigate the isomerization of phenyl oxirane (**5a**) as the model substrate. To our satisfaction, an initial test using 5 mol% of complex **4** together with 10 mol% LiBr (pre-activated with 5  $\mu$ L THF- $d_8$ ) in  $C_6D_6$  revealed full conversion at room temperature in a short time and demonstrated that the catalyst was more active than the previous catalyst **D** (Table 1, entry 1). Encouraged by this result, we tried to reduce the catalyst loading: 1 mol% of the catalyst was sufficient for a fast and quantitative rearrangement without influencing the excellent regioselectivity (Table 1, entries 2 and 3). To test whether lithium bromide was still necessary as a co-catalyst we applied the isolated

catalyst **4** without adding any Lewis acids. The catalytic activity was reduced dramatically under these conditions (Table 1, entry 4). This indicates that a Lewis acid is essential for the pre-activation of the substrates. Low conversion was also obtained using THF-d<sub>8</sub> as the solvent which most likely stems from competitive binding between THF and the substrate to the Lewis acid co-catalyst (Table 1, entry 5). Afterward, the concentration of phenyl oxirane was studied. Epoxide concentrations of 0.2 mol/L (Table 1, entry 6) shortened the reaction time substantially and the reaction was 10 times faster compared to catalyst **D**. Further increase of the concentration led to a reduced reaction time whereas the yields decreased slightly (Table 1, entries 7 and 8). In addition, the need for catalyst **4** was also tested. Without rhodium catalyst **4** the yield remained below 5% (Table 1, entry 9). Thus, the optimized reaction conditions (1 mol% catalyst **4**, 0.2 M epoxide, C<sub>6</sub>D<sub>6</sub>, room temperature) were applied to investigate the generality of this protocol.

Using complex **4** as the catalyst, various functionalized epoxides were converted successfully into the desired methyl ketones (Table 2). Phenyl oxirane (**5a**) and aryl oxirane **5b** bearing the strong electron-withdrawing trifluoromethyl substituent were transformed regioselectively in excellent yield. To our delight, epoxides **5c** and **5d** possessing electron-donating groups (methyl or methoxy) were converted into **6c** and **6d** with still very good regioselectivities of 50:1 and 22:1 favoring the methyl ketones (**6c**, **6d**) over the aldehydes (**7c**, **7d**) in good to moderate yields. Even the *ortho*-substituted methyl ketone **6e** was obtained from **5e** in high yield and with excellent regioselectivity. Besides aryl ketones, epoxides bearing NH or OH groups like sulfonamide (**5f**) and hydroxyl groups (**5g**) were rearranged to the desired methyl ketones with 1 mol% catalyst loading in 83% (**6f**) and 90% (**6g**) yield, albeit at longer reaction time (24 h). The high nucleophilicity of complex **4** is also compatible with an ester group. The isomerization of epoxide **5h** afforded **6h** albeit in moderate yield and after 24 h and 5 mol% catalyst loading. As the extended reaction times may derive from competing coordination of LiBr at the Lewis basic centers of functional groups, we have increased the amount of LiBr to 50 mol% and achieved full conversion already after 1 h reaction time at moderate to excellent yield (entries 6-8). In the case of **5g**, the moderate yield resulted from unknown side products which will be studied further. Furthermore, the sterically demanding 2-(*tert*-butyl)oxirane (**5i**) can be also

**Table 2.** Substrate scope in the isomerization of epoxide catalyzed by rhodium complex **4**<sup>[a]</sup>.

Entry	substrate	product	time	Yield [%] <sup>[b]</sup>	Ratio (6:7)
1	<b>5a</b> 	<b>6a</b> 	1 h	99	>99:1
2	<b>5b</b> 	<b>6b</b> 	1 h	98	>99:1
3	<b>5c</b> 	<b>6c</b> 	1 h	77	50:1
4	<b>5d</b> 	<b>6d</b> 	1 h	42	22:1
5	<b>5e</b> 	<b>6e</b> 	24 h	92	33:1
6	<b>5f</b> 	<b>6f</b> 	24 h 1 h	83 94 <sup>[e,g]</sup>	-
7	<b>5g</b> 	<b>6g</b> 	24 h 1 h	90 42 <sup>[e,g]</sup>	-
8	<b>5h</b> 	<b>6h</b> 	24 h 1 h	67 <sup>[c,e]</sup> 80 <sup>[e,g]</sup>	-
9 <sup>[d-f]</sup>	<b>5i</b> 	<b>6i</b> 	24 h	99	-
10 <sup>[d-f]</sup>	<b>5j</b> 	<b>6j</b> 	24 h	99	-
11 <sup>[d-f]</sup>	<b>5k</b> 	<b>6k</b> 	24 h	99	-
12 <sup>[d-f]</sup>	<b>5l</b> 	<b>6k</b> 	24 h	7	-

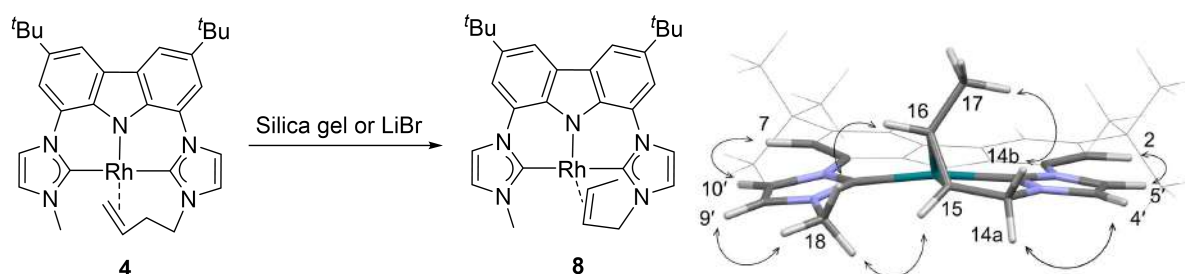
[a] Carried out in *J. Young* NMR tubes and with 10 mol% LiBr and 5  $\mu\text{L}$  THF- $d_6$ , 0.2 M concentration of epoxides. [b] Yield ( $^1\text{H}$  NMR) of ketones calibrated to 1,3,5-trimethoxybenzene (internal standard). [c] At 60  $^\circ\text{C}$ . [d] 20 mol% LiNTf<sub>2</sub> instead of LiBr. [e] 5 mol% catalyst **4**. [f] At 80  $^\circ\text{C}$ . [g] 50 mol% LiBr.

converted to the desired product **6i**, albeit with higher catalyst loading (5 mol%) and reaction temperature.

The internal epoxides **5j-l** react considerably faster compared with rhodium catalyst **D**. At 80 °C, 7-oxabicyclo[4.1.0]heptane (**5j**) was isomerized into cyclohexanone in almost quantitative yield. Furthermore, *cis*-2,3-epoxybutane (**5k**) was also compatible with the catalyst system and yielded 99% butan-2-one. In contrast, the conversion of *trans*-2,3-epoxybutane (**5l**) under otherwise identical conditions yielded only 7% of butan-2-one. This outcome is of considerable interest as it is contrary to the results from Coates and coworkers, who obtained less than 40% conversion with *cis*-2-hexene oxide but 98% yield with *trans*-2-hexene oxide applying  $[(\text{salcy})\text{Al}(\text{THF})_2]^+[\text{Co}(\text{CO})_4]^-$  as the catalyst.<sup>[5]</sup>

### Mechanistic investigation

When we tried to isolate catalyst **4** by chromatography at silica gel under argon, we isolated the isomerized complex **8** (Figure 3, left) as indicated by the characteristic substitution pattern in the NMR spectra. The signal at 1.17 ppm with an integral of 3H shows a  $^3J$  (6.3 Hz) and a  $^4J$  coupling to the olefinic signals at 4.56 (H-15) and 4.09 ppm (H-16). The *cis*-conformation of the double bond is not only confirmed by the  $^3J$  coupling constant of 6.3 Hz, but also by the NOE between methyl signal H-17 and the signal H-14b of the methylene group. In addition, an NOE cross-peak is observed between the signals of both olefinic protons and the *N*-methyl signal. The assignment of the peaks of the imidazole moieties and carbazole backbone are based on the observed NOE crosspeaks (Figure 3, right).



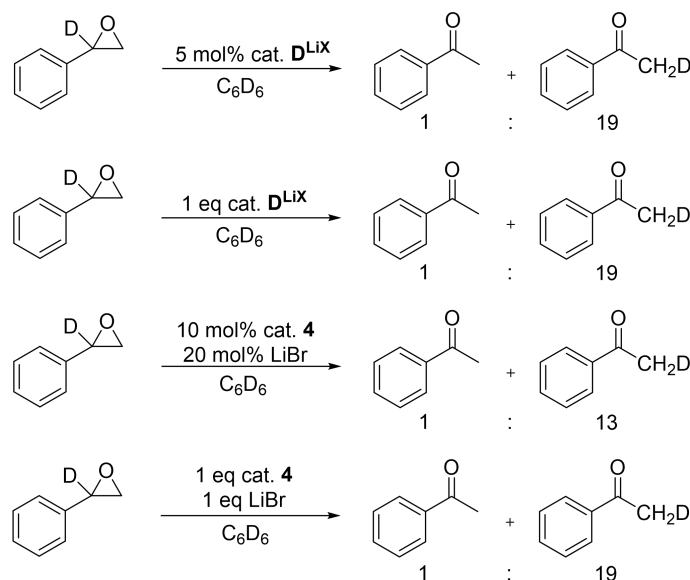
**Figure 3.** Left: Isomerization of the terminal double bond of complex **4** to an internal double bond *cis*-configuration in complex **8** by Lewis acids. Right: Minimum conformation of the isomerized complex **8** based on DFT calculations (TurboMole: BP86/def2-TZVP) and observed NOE crosspeaks (indicated with arrows). For clarity reasons, part of the carbazole moiety is depicted in wireframe style.





Earlier, we had proposed a catalytic cycle for catalyst **B**, in which the oxidative addition product **OA** was confirmed by NMR spectroscopy (Scheme 3).<sup>[3h]</sup> From this intermediate two possible pathways can lead to the product: a concerted 1,2-H shift under reductive elimination of the catalyst (c) or  $\beta$ -hydride elimination (d) to form the Rh-hydride intermediate (**Int-1**), which subsequently undergoes reductive elimination (e) to release the product and the catalyst.

As the hydride intermediate (**Int-1**) was not observed during the catalysis with complex **B** (L = CO), we envisaged that the *N*-homoallyl moiety of catalyst **D** or **4** could insert into the Rh-H intermediate **Int-1** to give the rhodium alkyl intermediate **Int-2**, which could undergo a D/H exchange in case deuterated phenyl oxirane was used. To prove this hypothesis we carried out catalytic experiments with 1-D-phenyl oxirane as substrate with both *N*-homoallyl-substituted catalysts **D** and **4** under catalytic as well as stoichiometric conditions (Scheme 4). In all cases, we found an exchange of the deuterium by hydrogen in the methylphenyl ketone of 5 – 7 %. (deuteration degree of the phenyl oxirane: 98%).



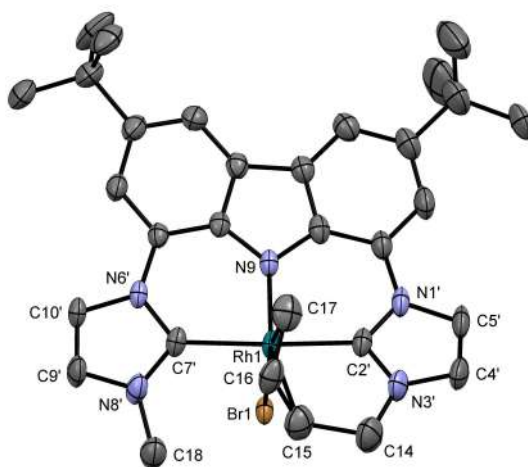
**Scheme 4.** D/H exchange during the isomerization of 1-D-phenyl oxirane with the *N*-homoallyl substituted catalysts **D** and **4** indicate a hydrido-Rh(III) intermediate **Int-1** in the catalytic cycle.

Based on these observations, we favor pathway II for the catalytic cycle of the nucleophilic Meinwald reaction with our rhodium catalysts. This pathway is also supported by the observations by Milstein, who isolated hydrido-2-oxoalkyl complexes when reacting  $\text{RhCl}(\text{PMe}_3)_3$  with neat methyl or phenyl oxirane.<sup>[3g]</sup> In this

case, the reductive elimination to the acetone or acetophenone is the rate limiting step.<sup>[6]</sup>

### Catalyst deactivation pathways

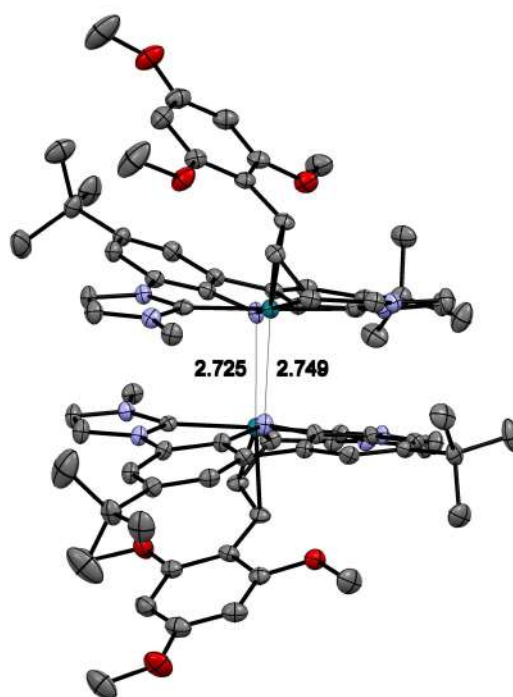
In addition, we observed two deactivation products of the catalyst. We recognized the formation of red crystals after finishing a VT NMR experiment of catalyst **4** with 1.0 equiv. of phenyl oxirane at room temperature. The X-ray structure analysis reveals the formation of a bromido-Rh(III) complex, in which the *N*-homoallyl substituent is coordinated in a  $\eta^3$ -allyl coordination mode to the oxidized metal center (Figure 4). The allyl-Rh bonds measure 2.137 (Rh-C17), 2.114 (Rh-C16) and 2.220 Å (Rh-C15). As the isomerization of phenyl oxide **5a** is very fast, it is likely that the formation of complex **9** occurs after the catalysis. C-H activation at the allylic position to form an allylhydrido complex and subsequent substitution of the hydrido by a bromido ligand can explain its formation.



**Figure 4.** Molecular structure of the catalyst deactivation product **9**. Atoms are shown with anisotropic atomic displacement parameters at the 50% probability level. Hydrogen atoms as well as 3.5 co-crystallized benzene molecules are omitted for clarity.

From the testing of *cis*-1,2-diethoxycarboxyl)oxirane (5 mol% **4** (2.3 mg), 20 mol% LiNTf<sub>2</sub> (4.6 mg), *cis*-1,2-(diethoxycarboxyl)oxirane (15.1 mg) and 1,3,5-trimethoxybenzene (4.3 mg), 24 h at 80 °C and 24 h at 100 °C) we obtained red single crystals in the NMR tube after several days at room temperature. The X-ray structure analysis reveals that under the elevated temperature the internal standard 1,3,5-trimethoxybenzene has reacted with the *N*-homoallyl moiety of complex **4** in a

formal dehydrogenation and C-C bond formation to the Rh(III)( $\eta^3$ -allyl) complex **10** (Figure 5). In the solid state the 16e<sup>-</sup> Rh-d<sup>6</sup> complex forms a Lewis-pair dimer between the rhodium and the carbazol nitrogen atoms with a mean distance of 2.74 Å. The allyl rhodium bonds measure 2.143 (Rh-C17), 2.124 (Rh-C16) and 2.243 Å (Rh-C15) (mean).



**Figure 5.** Molecular structure of the side product **10**. Atoms are shown with anisotropic atomic displacement parameters at the 50% probability level. Hydrogen atoms as well as the two NTf<sub>2</sub><sup>-</sup> counter ions and two co-crystallized benzene molecules are omitted for clarity.

To avoid erroneous catalytic results in the NMR experiments, catalytic tests with substrates of low reactivity should be carried out either with an inert or without an internal standard.

## Conclusions

Herein, we have presented the most active and selective catalyst system for the nucleophilic Meinwald reaction of terminal epoxides so far. The reactivity enhancement of catalyst **4** was achieved by providing only one coordinating *N*-homoallyl substituent at the ligand scaffold. The isolated complex **4** can undergo isomerization of the double bond in the presence of weak Lewis acids and benzene as solvent to yield the *N*-methallyl complex **8**, which is itself a comparably active

catalyst in the Meinwald reaction. D/H exchange experiments provide strong evidence for a  $\beta$ -hydride elimination/reductive elimination pathway via a hydrido-Rh intermediate for the Rh-catalyzed nucleophilic Meinwald reaction.

### Experimental procedure

**General information.** Unless otherwise noted, all reactions were carried out under an argon atmosphere in dried and degassed solvents using Schlenk technique. Toluene, pentane, dichloromethane and tetrahydrofuran were purchased from Sigma Aldrich and dried using an MBraun SPS-800 solvent purification system. All lithium salts used were obtained from commercial suppliers, dried in vacuum and used without further purification. Chemicals from commercial suppliers were degassed through freeze-pump-thaw cycles prior to use. Rhodium complex **D** was synthesized according to the literature procedure.<sup>[3j]</sup>  $^1\text{H}$  and  $^{13}\text{C}$  NMR spectra were recorded using a Bruker AVANCE II+ 400 spectrometer. Chemical shifts  $\delta$  (ppm) are given relative to the solvent's residual proton and carbon signal respectively: THF- $d_8$ : 3.58 ppm ( $^1\text{H}$  NMR) and 67.57 ppm ( $^{13}\text{C}\{\text{H}\}$  NMR);  $\text{C}_6\text{D}_6$ : 7.16 ppm ( $^1\text{H}$  NMR) and 128.39 ppm ( $^{13}\text{C}\{\text{H}\}$  NMR); DMSO- $d_6$ : 2.50 ppm ( $^1\text{H}$  NMR) and 39.51 ppm ( $^{13}\text{C}\{\text{H}\}$  NMR). Coupling constants ( $J$ ) are expressed in Hz. Signals were assigned as s (singlet), d (doublet), t (triplet), q (quartet), quint (quintet), m (multiplet) and variations thereof; (br) refers to a broad signal. The assignment of peaks is based on 2D NMR correlation and NOE spectra.

**Synthesis of Hbimca<sup>MeHomo</sup>-HI-HBr (3).** *a) Synthesis of 2:* To a suspension of **1** (0.74 g, 1.8 mmol) in 10 mL THF was added MeI (0.51 g, 3.6 mmol) dropwise. The reaction was stirred at room temperature for 24 h to form a pale precipitate. The mixture was filtered and dissolved in dichloromethane. After removal of solvent, product **2** was obtained as a light yellow solid (0.89 g, 1.6 mmol, yield: 90%).  $^1\text{H}$  NMR (250.13 MHz, DMSO- $d_6$ )  $\delta$  = 11.24 (s (br), 1H, NH), 9.69 (s (br), 1H, H-7'), 8.57 (d,  $^4J_{\text{HH}}$  = 1.7 Hz, 1H, H-5), 8.42 (d,  $^4J_{\text{HH}}$  = 1.7, 1H, H-4), 8.21 (s (br), 1H, H-2'), 8.19 (ps t,  $^3J_{\text{HH}}$  = 1.8 Hz, 1H, H-10'), 7.98 (ps t,  $^3J_{\text{HH}}$  = 1.7 Hz, 1H, H-9'), 7.73 (ps t,  $^3J_{\text{HH}}$  = 1.3 Hz, 1H, H-5'), 7.66 (d,  $^4J_{\text{HH}}$  = 1.7 Hz, 1H, H-7), 7.50 (d,  $^4J_{\text{HH}}$  = 1.7 Hz, 1H, H-2), 7.22 (ps t,  $^3J_{\text{HH}}$  = 1.0 Hz, 1H, H-4'), 3.99 (s, 3H, H-18), 1.45 (s, 18H, H-11 and H-13).  $^{13}\text{C}\{\text{H}\}$  NMR (62.90 MHz, DMSO- $d_6$ )  $\delta$  = 143.6 and 143.2 (C3 and C6), 138.0 (C7'), 137.2

(C2'), 132.7 (C8a), 132.1 (C1a), 129.1 (C4'), 125.7 (C4a), 125.0 (C5a), 123.7 (2x) (C10' and C9'), 121.7 (C1), 121.0 (C7), 120.2 (C5'), 120.0 (C2), 119.1 (C5), 118.9 (C8), 116.7 (C4), 36.0 (C18), 34.78 and 34.70 (C10 and C12), 31.65 and 31.62 (C11 and C13).  $C_{27}H_{32}N_5I$  (553.50): calcd C 58.59, H 5.83, N 12.65; found C 58.38, H 6.29, N 12.30. m.p.: 287 °C (dec.).

b) *Synthesis of 3*: To a solution of the monomethylated product **2** (0.89 g, 1.6 mmol) in 10 mL DMF was added 4-bromobutene (0.43 g, 3.2 mmol) in one portion. The reaction was stirred at 110 °C for 21 h. The solvent was removed via oil pump and a good precipitate was achieved after adding a bit of ethanol and diethyl ether. The mixture was filtered and the residue was resolved in dichloromethane. After removal of solvent, the product **3** was obtained as a light yellow solid (1.0 g, 1.5 mmol, yield: 95%).  $^1H$  NMR (250.13 MHz,  $DMSO-d_6$ )  $\delta$  = 11.63 (s (br), 1H, NH), 10.06 (s (br), 1H, H-2'), 10.01 (s (br), 1H, H-7'), 8.65 (s (br), 2H, H-4 and H-5), 8.32 (s (br), 1H, H-5'), 8.29 (s (br), 1H, H-10'), 8.17 (s (br), 1H, H-4'), 8.06 (s (br), 1H, H-9'), 7.76 (d,  $^4J_{HH}$  = 1.3 Hz) and 7.75 (d,  $^4J_{HH}$  = 1.4 Hz) (2H, H-2 and H-7), 5.92 (ddt,  $^3J_{HH}$  = 17.2 Hz,  $^3J_{HH}$  = 10.3 Hz,  $^3J_{HH}$  = 6.8 Hz, 1H, H-16), 5.23 (dd,  $^3J_{HH}$  = 17.2 Hz,  $^2J_{HH}$  = 1.0 Hz, 1H, H-17<sub>trans</sub>), 5.16 (d (br),  $^3J_{HH}$  = 10.3 Hz, 1H, H-17<sub>cis</sub>), 4.44 (t,  $^3J_{HH}$  = 7.2 Hz, 2H, H-14), 4.03 (s, 3H, H-18), 2.78 (dt,  $^3J_{HH}$  = 6.8 Hz,  $^3J_{HH}$  = 7.2 Hz, 2H, H-15), 1.47 (s, 18H, H-11 and H-13).  $^{13}C\{H\}$  NMR (62.90 MHz,  $DMSO-d_6$ )  $\delta$  = 143.7 (C3 and C6), 137.9 (C7'), 137.3 (C2'), 133.7 (C16), 132.3 and 132.2 (C1a and C8a), 125.5 and 125.4 (C4a and C5a), 123.9 (C9'), 123.3 (C5'), 123.2 (C10'), 122.9 (C4'), 120.92 and 120.89 (C2 and C7), 119.42 and 119.37 (C4 and C5), 119.0 (C1 and C8), 118.3 (C17), 48.4 (C14), 36.1 (C18), 34.9 (C10 and C12), 33.2 (C15), 31.6 (C11 and C13). m.p.: 263 °C.

**Preparation of catalysts 4<sup>LiX</sup>**. a) *In situ generation of [Li(bimca)<sup>Me,Homo</sup>]*: Lithium bis(trimethylsilyl)amide (7.3 mg, 44  $\mu$ mol) was added to the suspension of **3** (10.0 mg, 14.5  $\mu$ mol) in 0.5 mL of THF- $d_8$  at room temperature and a light yellow solution with blue fluorescence was formed. After 10 min, the quantitative formation of [Li(bimca)<sup>Me,Homo</sup>] was confirmed by  $^1H$  NMR spectroscopy.  $^1H$  NMR (400 MHz, THF- $d_8$ )  $\delta$  = 7.99 (s (br), 2H, H-4 and H-5), 7.73 (s (br), 2H, H-5' and H10'), 7.39 (s (br), 2H, H-2 and H-7), 7.21 and 7.15 (each s (br), each 1H, H-4' and H-9'), 5.80-6.05 (m, 1H, H-16), 5.15 (d,  $^3J_{HH}$  = 16.5 Hz, 1H, H-17<sub>trans</sub>), 5.04 (d,  $^3J_{HH}$  = 10.5 Hz, 1H, H-

17<sub>cis</sub>), 4.26-4.35 (m, 2H, H-14), 3.93 (s (br), 3H, H-18), 2.70-2.80 (m, 2H, H-15), 1.50 (s, 18H, H-11 and H-13).

*b) In situ generation of 4<sup>LiX</sup>*: [Rh( $\mu$ -Cl)(COD)]<sub>2</sub> (0.5 eq) was added to the previous prepared solution of [Li(bimca<sup>Me,Homo</sup>)] (1.0 eq) at room temperature. The solution was stirred for 10 min. Catalyst 4<sup>LiX</sup> was obtained as an orange solution in quantitative yield as determined by NMR spectroscopy. <sup>1</sup>H NMR (400 MHz, THF-*d*<sub>8</sub>)  $\delta$  = 8.17 (d, <sup>3</sup>J<sub>HH</sub> = 2.2 Hz, 1H, H-10'), 8.10 (d, <sup>3</sup>J<sub>HH</sub> = 2.3 Hz, 1H, H-5'), 8.08-8.09 (m, 2H, H-4 and H-5), 7.73 (d, <sup>4</sup>J<sub>HH</sub> = 1.5 Hz, 1H, H-2), 7.70 (d, <sup>4</sup>J<sub>HH</sub> = 1.5 Hz, 1H, H-7), 7.17 (d, <sup>3</sup>J<sub>HH</sub> = 2.3 Hz, 1H, H-4'), 7.16 (d, <sup>3</sup>J<sub>HH</sub> = 2.2 Hz, 1H, H-9'), 4.65-4.58 (m, 1H, H-16), 4.28 (ps td, <sup>2/3</sup>J<sub>HH</sub> = 12.4 Hz, <sup>3</sup>J<sub>HH</sub> = 2.2 Hz, 1H, H-14<sub>ax</sub>), 4.09 (d ps t, <sup>2</sup>J<sub>HH</sub> = 13.0 Hz, <sup>3</sup>J<sub>HH</sub> = 3.6 Hz, 1H, H-14<sub>eq</sub>), 3.92 (s, 3H, H-18), 3.50 (d, <sup>3</sup>J = 7.7 Hz, 1H, H-17<sub>cis</sub>), 2.94 (d, <sup>3</sup>J = 11.5 Hz, 1H, H-17<sub>trans</sub>), 2.67 (br dd, <sup>2</sup>J<sub>HH</sub> = 15.1 Hz, <sup>3</sup>J<sub>HH</sub> = 12.4 Hz, 1H, H-15<sub>ax</sub>), 2.33-2.25 (m, 1H, H-15<sub>eq</sub>) (overlap with COD signal), 1.53 and 1.52 (each s, 18H, H-11 and H-13). <sup>13</sup>C{H} NMR (101 MHz, THF-*d*<sub>8</sub>)  $\delta$  = 184.8 (d, <sup>1</sup>J<sub>RhC</sub> = 43.3 Hz, C7'), 179.0 (d, <sup>1</sup>J<sub>RhC</sub> = 45.7 Hz, C2'), 139.2 (C3), 139.1 (C6), 137.1 (C1a), 136.8 (C8a), 127.3 and 127.2 (C4a and C5a), 126.6 (C9'), 126.0 (C8), 125.7 (C1), 123.9 (C4'), 116.1 (C10'), 116.5 (C5'), 113.6 (C5), 113.4 (C4), 111.3 (C7), 110.2 (C2), 51.3 (d, <sup>1</sup>J<sub>RhC</sub> = 13.2 Hz, C16), 47.5 (C14), 38.9 (C18), 37.0 (d, <sup>1</sup>J<sub>RhC</sub> = 13.7 Hz, C17), 35.6 (C10 and C12), 32.8 (C11 and C13), 31.9 (C15).

**Preparation of catalyst 4.** Imidazolium salt **3** (100 mg, 145  $\mu$ mol), potassium bis(trimethylsilyl)amide (86.9 mg, 436  $\mu$ mol) and [Rh( $\mu$ -Cl)(COD)]<sub>2</sub> (35.8 mg, 72.6  $\mu$ mol) were added to a dry flask at room temperature. The flask was cooled down to -60 °C for 30 min. Cold THF was injected into the flask and the reaction was stirred for another 30 min at -60 °C. After completion, the reaction was filtered to remove potassium halides. Collected filtrate was dried under vacuum and the residue was washed with pentane (3  $\times$  5 mL). Pure catalyst **4** was obtained after removal of solvent as a yellow solid (43.6 mg, 75.0  $\mu$ mol, yield: 52%). The NMR data (THF-*d*<sub>8</sub>) correspond to the results obtained from using [Li(bimca<sup>Me,Homo</sup>)]. C<sub>31</sub>H<sub>36</sub>N<sub>5</sub>Rh (581.56): calcd C 64.02, H 6.24, N 12.04; found C 61.70, H 6.02, N 11.36. Possibly contains residual KBr: C<sub>31</sub>H<sub>36</sub>N<sub>5</sub>Rh $\cdot$ 0.2 KBr: calcd C 61.51, H 5.99, N 11.57.

**Synthesis of the isomerized rhodium complexes 8.** To a *J. Young* NMR tube containing LiBr (6.9 mg, 80  $\mu$ mol) and 20  $\mu$ L of THF-*d*<sub>8</sub>, was added catalyst **4** (23.2

mg, 40.0  $\mu\text{mol}$ ) with  $\text{C}_6\text{D}_6$  (0.8 mL). Catalyst **8** was generated at room temperature after 1 h in quantitative yield as determined by NMR spectroscopy. Another method for achieving complex **8** was to run a chromatography on silica gel with complex **4**.  $^1\text{H}$  NMR (400 MHz,  $\text{THF}-d_8$ )  $\delta$  = 8.19 (d,  $^3J_{\text{HH}}$  = 2.2 Hz, 1H, H-10'), 8.14 and 8.13 (each d, each  $^4J_{\text{HH}}$  = 1.6 Hz, each 1H, H-5 and H-4), 8.02 (d,  $^3J_{\text{HH}}$  = 2.2 Hz, 1H, H-5'), 7.81 (d,  $^4J_{\text{HH}}$  = 1.6 Hz, 1H, H-7), 7.73 (d,  $^4J_{\text{HH}}$  = 1.6 Hz, 1H, H-2), 7.27 (d,  $^3J_{\text{HH}}$  = 2.0 Hz, 1H, H-4'), 7.17 (d,  $^3J_{\text{HH}}$  = 2.0 Hz, 1H, H-9'), 4.56 (br ps t, 1H,  $^3J_{\text{HH}}$  = 7.2 Hz, H-15), 4.45 (dd,  $^2J_{\text{HH}}$  = 11.7 Hz,  $^3J_{\text{HH}}$  = 6.8 Hz, 1H, H-14<sub>a</sub>), 4.09 (d ps quint,  $^3J_{\text{HH}}$  = 6.2 Hz,  $^4J_{\text{HH}}$  = 2.3 Hz, 1H, H-16), 3.97 (br d,  $^2J$  = 11.7 Hz, 1H, H-14<sub>b</sub>), 3.71 (s, 3H, H-18), 1.55 and 1.54 (each s, 18H, H-11 and H-13), 1.17 (dd,  $^3J_{\text{HH}}$  = 6.3 Hz,  $^4J_{\text{HH}}$  = 0.6 Hz, 3H, H-17).  $^{13}\text{C}\{\text{H}\}$  NMR (101 MHz,  $\text{THF}-d_8$ )  $\delta$  = 187.9 (d,  $^1J_{\text{RhC}}$  = 42.4 Hz, C7'), 187.2 (d,  $^1J_{\text{RhC}}$  = 44.3 Hz, C2'), 139.5 and 139.2 (C3 and C6), 137.5 (C1a), 136.3 (C8a), 127.9 and 127.6 (C4a and C5a), 126.4 (C1), 126.2 (C8), 124.6 (C9'), 118.3 (C4'), 116.5 (C10'), 114.8 (C5'), 114.1 (C5), 113.8 (C4), 111.4 (C7), 109.7 (C2), 57.3 (d,  $^1J_{\text{RhC}}$  = 14.1 Hz, C16), 53.8 (d,  $^1J_{\text{RhC}}$  = 12.7 Hz, C15), 50.0 (C14), 37.6 (C18), 35.72 and 35.65 (C10 and C12), 32.93 and 32.90 (C11 and C13), 20.9 (C17).  $^1\text{H}$  NMR (400 MHz,  $\text{C}_6\text{D}_6$ )  $\delta$  = 8.46 (s, 2H), 7.67 (s, 1H), 7.59 (s, 1H), 7.49 (s, 1H), 7.23 (s, 1H), 6.36 (s, 1H), 6.14 (s, 1H), 4.48-4.40 (m, 1H, H-15), 4.31 (ps quint,  $^3J_{\text{HH}}$  = 6.0 Hz, 1H, H-16), 4.09 (dd,  $^2J_{\text{HH}}$  = 11.2 Hz,  $^3J_{\text{HH}}$  = 6.8 Hz, 1H, H-14<sub>a</sub>), 3.66 (br d,  $^2J_{\text{HH}}$  = 11.7 Hz, 1H, H-14<sub>b</sub>), 3.12 (s, 3H, H-18), 1.55 (br s, 18H, H-11 and H-13), 1.37 (br d,  $^3J_{\text{HH}}$  = 6.0 Hz, 3H, H-17).

**DFT calculations** Performed based on density functional theory at the BP86/def2-SVP and/or BP86/def2-TZVP<sup>[7]</sup> level implemented in Turbomole<sup>[8]</sup>. The RI-approximation<sup>[9]</sup> and the Grimme dispersion correction D3-BJ<sup>[10]</sup> were used all over. Several structures were optimized differing in the conformation of the rings formed by the coordination of the double bond. Minimum structures were verified at the BP86/def2-SVP level by calculating the Hessian matrix and ensuring that it has no imaginary frequency.

### Acknowledgement

Yingying Tian thanks the China Scholarship Council (CSC) for a predoctoral fellowship and Eva Jürgens the MWK-BW for funding (Landesgraduiertenförderung).

We are grateful to Prof. Karl W. Törnroos for assistance in the X-ray structure analyses and thank Mario R. Rapp for helpful discussions as well as Nina F. Liska for help with the substrate synthesis.

### References

- (1) Meinwald, J.; Labana, S. S.; Chadha, M. S. *J. Am. Chem. Soc.* **1963**, *85*, 582–585.
- (2) Ni<sup>2+</sup>: (a) Miyashita, A.; Shimada, T.; Sugawara, A.; Nohiya, H. *Chem. Lett.* **1986**, *15*, 1323–1326. In<sup>3+</sup>: (b) Ranu, B. C.; Jana, U. *J. Org. Chem.* **1998**, *63*, 8212–8216. Fe<sup>3+</sup>: (c) Suda, K.; Baba, K.; Nakajima, S.-i.; Takanami, T. *Tetrahedron Lett.* **1999**, *40*, 7243–7246. Bi<sup>3+</sup>: (d) Anderson, A. M.; Blazek, J. M.; Garg, P.; Payne, B. J.; Mohan, R. S. *Tetrahedron Lett.* **2000**, *41*, 1527–1530. Er<sup>3+</sup>: (e) Procopio, A.; Dalpozzo, R.; De Nino, A.; Nardi, M.; Sindona, G.; Tagarelli, A. *Synlett* **2004**, 2633–2635. Sn: (f) Banerjee, M.; Roy, U. K.; Sinha, P.; Roy, S. *J. Organomet. Chem.* **2005**, *690*, 1422–1428. Cu<sup>2+</sup>: (g) Robinson, M. W. C.; Pillinger, K. S.; Mabbett, I.; Timms, D. A.; Graham, A. E. *Tetrahedron* **2010**, *66*, 8377–8382. [ReBr(CO)<sub>3</sub>]: (h) Umeda, R.; Muraki, M.; Nakamura, Y.; Tanaka, T.; Kamiguchi, K.; Nishiyama, Y. *Tetrahedron Lett.* **2017**, *58*, 2393–2395. Ru<sup>2+</sup>: (i) Chang, C.-L.; Kumar, M. P., Liu, R.-S. *J. Org. Chem.* **2004**, *69*, 2793–2796 (although Lewis-acid catalyzed, methyl ketones from  $\alpha$ -keto oxiranes possibly due to chelation effects). Pd<sup>2+</sup>: (j) D. J. Vyas, E. Larionov, C. Besnard, L. Guénée, C. Mazet, *J. Am. Chem. Soc.* **2013**, *135*, 6177–6183; (k) N. Humbert, D. J. Vyas, C. Besnard, C. Mazet, *Chem. Commun.* **2014**, *50*, 10592–10595; (l) S. Kulasegaram, R. J. Kulawiec, *J. Org. Chem.* **1997**, *62*, 6547–6561; (m) S. Kulasegaram, R. J. Kulawiec, *Tetrahedron* **1998**, *54*, 1361–1374; Ni in a reaction sequence: (n) A. N. Desnoyer, J. L. Geng, M. W. Drover, B. O. Patrick, J. A. Love, *Chem. Eur. J.* **2017**, *23*, 11509–11512.
- (3) (a) Eisenmann, J. L. *J. Org. Chem.* **1962**, *27*, 2706–2706. (b) Rickborn, B.; Gerkin, R. M. *J. Am. Chem. Soc.* **1968**, *90*, 4193–4194. (c) Rickborn, B.; Gerkin, R. M. *J. Am. Chem. Soc.* **1971**, *93*, 1693–1700. (d) An, Z.-w. D'Aloisio, R.; Venturello, C. *Synthesis* **1992**, 1229–1231. (e) Kulasegaram, S.; Kulawiec, R. J. *J. Org. Chem.* **1994**, *59*, 7195–7196. (f) Prandi, J.; Namy, J. L.; Menoret, G.; Kagan, H. B. *J. Organomet. Chem.* **1985**, *285*, 449–460. (g) Milstein, D. *J. Am. Chem. Soc.* **1982**, *104*, 5227–5228; (h) Jürgens, E.; Wucher, B.; Rominger, F.; Törnroos, K. W.; Kunz, D. *Chem. Commun.* **2015**, *51*, 1897–1900; (i) Lamb, J. R.; Jung, Y.; Coates, G. W.



*Org. Chem. Front.* **2015**, *2*, 346–349. (j) Tian, Y.; Jürgens, E.; Kunz, D. *Chem. Commun.* **2018**, *54*, 11340–11343.

(4) Moser, M. *PhD Thesis*, Heidelberg University, **2007**.

(5) Lamb, J. R.; Mulzer, M.; LaPointe, A. M.; Coates, G. W. *J. Am. Chem. Soc.* **2015**, *137*, 15049–15054.

(6) Milstein, D. *Acc. Chem. Res.* **1984**, *17*, 221–226.

(7) (a) Becke, A. *Phys. Rev. A* **1988**, *38*, 3098–3100. (b) Perdew, J. P. *Phys. Rev. B* **1986**, *33*, 8822–8824. (c) Schäfer, A.; Horn, H.; Ahlrichs, R. *J. Chem. Phys.* **1992**, *97*, 2571–2577. (d) Schäfer, A.; Huber, C.; Ahlrichs, R. *J. Chem. Phys.* **1994**, *100*, 5829–5835. (e) Weigend, F.; Ahlrichs, R. *Phys. Chem. Chem. Phys.* **2005**, *7*, 3297–3305. (f) Weigend, F. *Phys. Chem. Chem. Phys.* **2006**, *8*, 1057–1065.

(8) (a) TURBOMOLE V6.3.1 2011, a development of University of Karlsruhe and Forschungszentrum Karlsruhe GmbH, 1989–2007, TURBOMOLE GmbH, since 2007; available from <http://www.turbomole.com>. (b) Treutler, O.; Ahlrichs, R. *J. Chem. Phys.* **1995**, *102*, 346–354. (c) Arnim, M. von; Ahlrichs, R. *J. Comp. Chem.* **1998**, *19*, 1746–1757. (d) Wüllen, C. van *J. Comp. Chem.* **2011**, *32*, 1195–1201. (e) Deglmann, P.; Furche, F.; Ahlrichs, R. *Chem. Phys. Lett.* **2002**, *362*, 511–518. (f) Deglmann, P.; Furche, F. *J. Chem. Phys.* **2002**, *117*, 9535–9538. (g) Ahlrichs, R.; Bär, M.; Häser, M.; Horn, H.; Kölmel, C. *Chem. Phys. Lett.* **1989**, *162*, 165–169. (h) Armbruster, M. K.; Weigend, F.; Wüllen, C. van; Klopper, W. *Phys. Chem. Chem. Phys.* **2008**, *10*, 1748–1756. (i) Peng, D.; Middendorf, N.; Weigend, F.; Reiher, M. *J. Chem. Phys.* **2013**, *138*, 184105.

(9) (a) Eichkorn, K.; Treutler, O.; Öhm, H.; Häser, M.; Ahlrichs, R. *Chem. Phys. Lett.* **1995**, *240*, 283–290. (b) Eichkorn, K.; Treutler, O.; Öhm, H.; Häser, M.; Ahlrichs, R. *Chem. Phys. Letters* **1995**, *242*, 652–660; (c) Eichkorn, K.; Weigend, F.; Treutler, O.; Ahlrichs, R. *Theor. Chem. Acc.* **1997**, *97*, 119–124. (d) Deglmann, P.; May, K.; Furche, F.; Ahlrichs, R. *Chem. Phys. Lett.* **2004**, *384*, 103–107. (e) Weigend, F. *Phys. Chem. Chem. Phys.* **2002**, *4*, 4285–4291. (f) Sierka, M.; Hogekamp, A.; Ahlrichs, R. *J. Chem. Phys.* **2003**, *118*, 9136–9148.

(10) (a) Grimme, S.; Antony, J.; Ehrlich, S.; Krieg, H. *J. Chem. Phys.* **2010**, *132*, 154104. (b) Grimme, S.; Ehrlich, S.; Goerigk, L. *J. Comput. Chem.* **2011**, *32*, 1456–1465.

## Chapter 3

### Synthesis and Reactivity of Cobalt(I) and Iridium(I)

#### Complexes Bearing a Pentadentate *N*-Homoallyl

#### Substituted Bis(NHC) Pincer-Ligand

Yingying Tian,<sup>†</sup> Theo Maulbetsch,<sup>†</sup> Ronja Jordan,<sup>†</sup> Karl W. Törnroos,<sup>‡</sup> and Doris Kunz\*

<sup>†</sup>Institut für Anorganische Chemie, Eberhard Karls Universität Tübingen, Auf der Morgenstelle 18, 72076 Tübingen, Germany

<sup>‡</sup> Department of Chemistry, University of Bergen, Allégaten 41, 5007 Bergen, Norway

#### Abstract

Two methods for the synthesis of the bis(imidazolin-2-ylidene)carbazolide cobalt(I) complex [Co(bimca<sup>Homo</sup>)] (**2**) have been developed. The first route relies on the direct transmetallation of the *in situ* generated lithium complex [Li(bimca<sup>Homo</sup>)] with CoCl(PPh<sub>3</sub>)<sub>3</sub>. The second one is a two-step synthesis that consists of the transmetallation of [Li(bimca<sup>Homo</sup>)] with CoCl<sub>2</sub> followed by reduction of the Co(II) complex to yield the desired Co(I) complex **2**. The analogous iridium complex [Ir(bimca<sup>Homo</sup>)] (**4**) was prepared by transmetallation of [Li(bimca<sup>Homo</sup>)] or [K(bimca<sup>Homo</sup>)] with [Ir(μ-Cl)(COD)]<sub>2</sub>. The catalytic activity of complexes **2** and **4** in the epoxide isomerization was tested in the absence and presence of H<sub>2</sub>. When [M(bimca<sup>Homo</sup>)] (M = Ir (**4**), Rh (**3**)) were exposed to 1 bar H<sub>2</sub> at 80 °C single crystals formed whose X-ray structure analyses revealed the hydrogenation of the *N*-homoallyl moieties and formation of the dimeric hydrido complexes [Ir(bimca<sup>*n*-Bu</sup>)(H)<sub>2</sub>]<sub>2</sub> (**7**) and [Rh(bimca<sup>*n*-Bu</sup>)(H)<sub>2</sub>]<sub>2</sub> (**8**).

---

Tian, Y.; Maulbetsch, T.; Jordan, R.; Törnroos, K. W.; Kunz, D. *Organometallics* **2020**, *39*, 1221-1229.

## Introduction

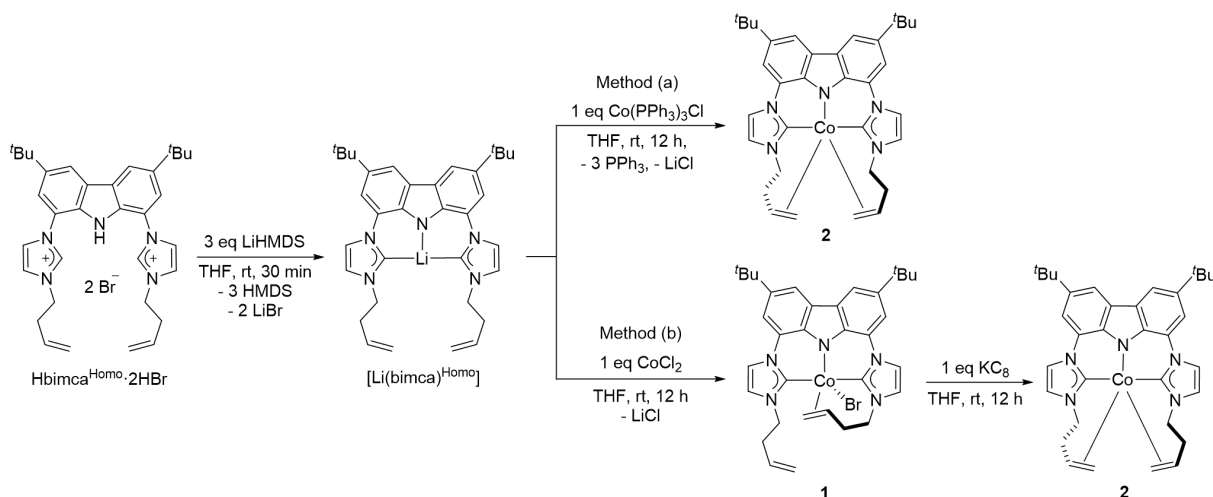
N-heterocyclic carbenes (NHCs) have experienced a huge success in the last decades due to their use as ligands for metal catalysts or as organocatalysts in various kinds of catalytic reactions.<sup>[1]</sup> Electronically, NHCs usually possess strong  $\sigma$ -donor and weak  $\pi$ -acceptor properties. This leads to strong metal-ligand bonds and electron-rich metal centers and imparts these complexes nucleophilic character.<sup>[2]</sup> Incorporation of more than one NHC unit in one ligand increases the stability of the complex due to the chelate effect. In addition, it stabilizes metal centers in high oxidation states and activates metal centers in low oxidation states.

Well-defined bis(NHC)-pincer transition-metal complexes have been widely applied as catalysts in versatile homogeneous catalytic reactions, for example, Chirik's cobalt catalyst with a (C<sub>NHC</sub>NC<sub>NHC</sub>)-pincer ligand represents one of the most active base metal catalysts for the hydrogenation of unactivated, sterically hindered olefins and (C<sub>NHC</sub>C<sub>aryl</sub>C<sub>NHC</sub>)-pincer cobalt complexes from the Fout group are used for the hydrogenation of unsaturated bonds.<sup>[3,4]</sup> We reported on several highly reactive nucleophilic Rh(I) complexes bearing the electron-rich bis(NHC)-pincer ligand called bimca, such as bimca<sup>Me</sup>, bimca<sup>Homo</sup> and bimca<sup>Me,Homo</sup> (bimca = 1,8-bis(imidazolin-2-ylidene)-3,6-di(*tert*-butyl)carbazolide; the superscript denotes the *N*-substituents methyl or homoallyl). They are e. g. efficient catalysts for the regio- and chemoselective isomerization of diversely functionalized epoxides to yield methyl ketones and are the only regioselective catalysts for the isomerization of aryl oxiranes to acetophenone derivatives to date. This selectivity is very attractive as it could substitute the Wacker oxidation by a two-step epoxidation-isomerization sequence for temperature and Lewis acid sensitive substrates.<sup>[5]</sup> Rh complexes with the neutral, macrocyclic C<sub>NHC</sub>N<sub>aryl</sub>C<sub>NHC</sub> ligands from the Chaplin group were found to be active in the selective en-yne dimerization.<sup>[6]</sup> (C<sub>NHC</sub>C<sub>aryl</sub>C<sub>NHC</sub>)-pincer complexes of iridium are well studied by Chianese and coworkers and are active in the acceptorless alkane dehydrogenation and in the alkene isomerization.<sup>[7]</sup>

To continue our interest in low-valent, nucleophilic transition-metal catalysts, we report herein the synthesis and characterization of both [Co(bimca<sup>Homo</sup>)] (**2**) and [Ir(bimca<sup>Homo</sup>)] (**4**), and their catalytic activity together with the earlier reported Rh-complex [Rh(bimca<sup>Homo</sup>)] (**3**)<sup>[5b]</sup> in the nucleophilic epoxide isomerization is discussed.

## Results and Discussion

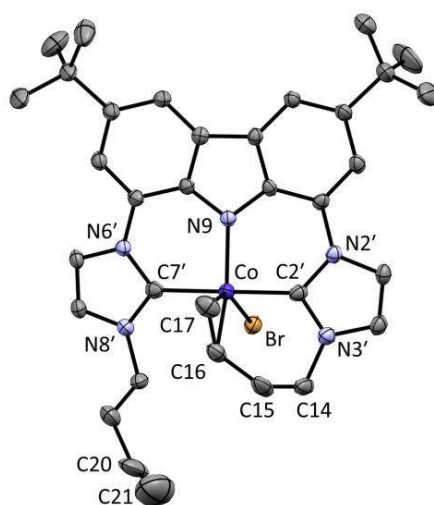
Our studies commenced with the preparation of complex **2** (Scheme 1). One challenge associated with the synthesis of cobalt(I) complexes is their extreme air and moisture sensitivity. The ligand precursor  $\text{Hbimca}^{\text{Homo}} \cdot 2\text{HBr}$  and its lithium complex were generated according to previously reported methods.<sup>[5b]</sup> The transmetalation of  $[\text{Li}(\text{bimca}^{\text{Homo}})]$  was initially explored with the addition of 1.0 equiv of  $\text{CoCl}(\text{PPh}_3)_3$  in THF at room temperature. A color change from light yellow to red was observed immediately and the single signal set in the  $^1\text{H}$  NMR spectrum of the *in situ* generated compound **2** confirmed a symmetric coordination mode of the ligand. However, the complex obtained by this method always contained residual  $\text{PPh}_3$ , even after chromatography on silica in the glovebox.



**Scheme 1.** Synthesis of  $[\text{Co}(\text{bimca}^{\text{Homo}})]$  by two methods.

An alternative route was inspired by the work of Braunstein<sup>[8]</sup> and Nishibayashi<sup>[9]</sup>, who demonstrated that addition of alkali-metal complexes to a solution of the  $\text{Co}(\text{II})$  precursor resulted in the formation of four-coordinate cobalt halogen complexes. Reduction with  $\text{KC}_8$  at room temperature afforded the corresponding diamagnetic  $\text{Co}(\text{I})$  complexes. To explore the analogous chemistry with our own ligand, paramagnetic  $[\text{Co}(\text{bimca}^{\text{Homo}})\text{Br}]$  (**1**) was prepared by treatment of freshly generated  $[\text{Li}(\text{bimca}^{\text{Homo}})]$  in THF with solid  $\text{CoCl}_2$ . We suppose that  $[\text{Co}(\text{bimca}^{\text{Homo}})\text{Cl}]$  is generated firstly, but instant halogen exchange occurs with the bromide anion still present in the solution from the ligand precursor  $\text{Hbimca}^{\text{Homo}} \cdot 2\text{HBr}$ . Brown single crystals of **1** suitable for X-ray diffraction were grown by slow evaporation from

benzene at room temperature. Crystallographic characterization of the complex (Fig. 1) reveals a distorted trigonal bipyramidal geometry at the cobalt center with one coordinated homoallyl moiety, the bromide ligand and the carbazole nitrogen atom in the equatorial positions ( $\text{Br1-Co-c(C16,C17)} = 129.0^\circ$ ; c: mid-point of bond). The NHC moieties take in the apical positions with a  $\text{C2'-Co-C7'}$  angle of  $174.0(2)^\circ$ . Both  $\text{Co-C}_{\text{NHC}}$  bond lengths are within the range reported for  $\text{Co(II)-C}_{\text{NHC}}$  bonds of 1.791-2.152 Å.<sup>[10]</sup>



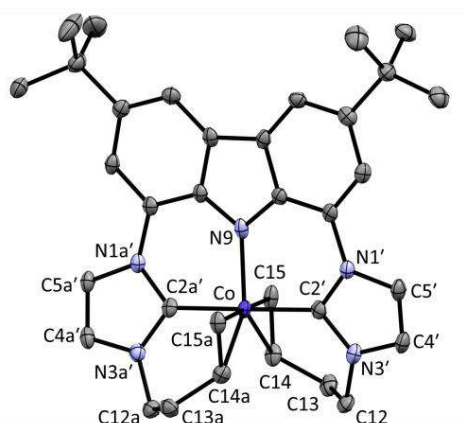
**Figure 1.** Solid-state molecular structure of **1**. Atoms are shown with anisotropic atomic displacement parameters at the 50% probability level. Hydrogen atoms are omitted for clarity. Selected bond lengths (Å) and angles (deg):  $\text{Co-N9} = 1.915(3)$ ,  $\text{Co-C2'} = 1.917(4)$ ,  $\text{Co-C7'} = 1.978(4)$ ,  $\text{Co-c(C16,C17)} = 1.950$ ,  $\text{Co-Br} = 2.515(1)$ ,  $\text{C16-C17} = 1.384(6)$ ,  $\text{C20-C21} = 1.274(10)$ ;  $\text{N9-Co-c(C16,C17)} = 119.3$ ,  $\text{N9-Co-Br} = 111.45(9)$ ;  $\text{C2'-Co1-C7'} = 173.95(15)$ ,  $\text{Br-Co-c(C16,C17)} = 129.0$  (c: mid-point of bond).

Due to the coordinating homoallyl substituent, one  $\text{Co-C}_{\text{NHC}}$  bond ( $\text{Co-C2'} = 1.917(4)$  Å) is shorter than the other ( $\text{Co-C7'} = 1.978(4)$  Å). Danopoulos<sup>[11]</sup> reported an intermediate bond length for the symmetric complex  $\text{Co(C}_{\text{NHC}}\text{NC}_{\text{NHC}}\text{)Br}_2$  ( $\text{CNC} = 2,6$ -bis(arylimidazolin-2-ylidene)pyridine) of 1.942(6) Å. In the coordinated homoallyl moiety, the  $\text{C=C}$  bond is elongated ( $\text{C16-C17} = 1.384(6)$  Å) due to a good  $\pi$ -backbonding ability of cobalt center. This is the first structural report of a cobalt(II) NHC complex with a coordinated olefin.

DFT optimized structures fit very well with a low-spin state ( $S = 1/2$ ) at the cobalt center, which is reasonable as the five donor atoms require at least one empty d-orbital for this  $d^7$  electron configuration. Attempts to calculate a high spin complex ( $S = 3/2$ ) resulted in dissociation of the olefin moiety and larger deviations from the

experimentally determined bond lengths of the obtained structure (see Supporting Information).

In addition, single crystals of the cobalt(III) complex **[Co(bimca<sup>Homo</sup>)<sub>2</sub>Br]** with two coordinated bimca<sup>Homo</sup> ligands in an octahedral fashion were generated as a side product in one of the experiments (see Supporting Information, p. S39 for further description). Only very few cobalt complexes bearing two bis(NHC)pincer ligands are known, all of them in the oxidation state +III.<sup>[12]</sup> Starting from Co(II) they are presumably formed with traces of oxygen.

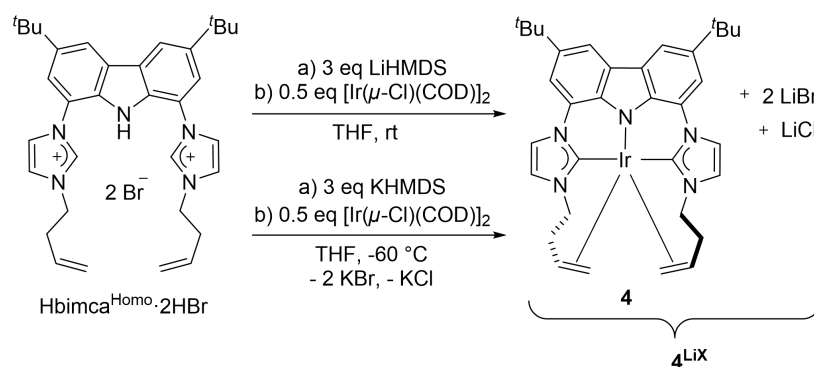


**Figure 2.** Solid-state molecular structure of **2**. Atoms are shown with anisotropic atomic displacement parameters at the 50% probability level. One co-crystallized toluene and the hydrogen atoms are omitted for clarity. Selected bond lengths (Å) and angles (deg) (mean of the two independent enantiomers in the unit cell): Co–N9 = 1.947(4), Co–C2' = 1.911(5), Co–C2a' = 1.913(5), Co–C15 = 2.043(5), Co–C14 = 2.092(5), Co–C15a = 2.037(5), Co–C14a = 2.084(5), C14–C15 = 1.401(8), C14a–C15a = 1.400(7); N9–Co–c(C15,C14) = 110.0, N9–Co–c(C15a,C14a) = 110.8(5), c(C15,C14)–Co–c(C15a,C14a) = 139.2, C2'–Co–C2a' = 179.0(3) (c: mid-point of bond).

Complex **1** was successfully reduced with  $\text{KC}_8$  in THF at room temperature and a red solution was obtained after completion. The raw product was purified by chromatography to yield the desired complex **2** as a red solid. Complex **2** is extremely air sensitive and an obvious color change would be observed with traces of oxygen. The  $^1\text{H}$  NMR spectrum of **2** in THF- $d_8$  is consistent with a  $C_2$ -symmetric ligand environment with both *N*-homoallyl substituents coordinated to the cobalt(I) center. The signals of the olefinic protons are strongly shifted up-field (4.09–4.02 (H-14), 3.21 (H-15<sub>cis</sub>), 2.54 ppm (H-15<sub>trans</sub>)). The  $^{13}\text{C}$  NMR signal of the carbene carbon atoms at 191.1 ppm lie about 26 ppm at higher field than the signal of a comparable unsaturated free NHC (217.1 ppm<sup>[13]</sup>). About the same difference ( $\Delta \sim 22$  ppm) is found when the reported  $\text{Co}(\text{C}_{\text{NHC}}\text{C}_{\text{aryl}}\text{C}_{\text{NHC}})\text{N}_2$  complex<sup>[14]</sup> is compared.

Single crystals of **2** suitable for X-ray diffraction were grown from a concentrated solution of toluene and pentane at  $-30\text{ }^{\circ}\text{C}$ . The molecular structure confirms the structure derived from the NMR spectra in solution (Figure 2). The coordination geometry at the Co(I) center is trigonal bipyramidal with both olefin moieties and the carbazole nitrogen taking in the equatorial and both NHC moieties the axial positions ( $\text{C}2'-\text{Co}-\text{C}2\text{a}' = 179.0(3)^{\circ}$ ),  $\text{c}(\text{C}15,\text{C}14)-\text{Co}-\text{c}(\text{C}15',\text{C}14') = 139.2^{\circ}$ ; (c: mid-point of bond)). The Co–C<sub>NHC</sub> bond lengths (Co–C2' = 1.911(5) Å, Co–C2a' = 1.913(5) Å) are comparable to reported (C<sub>NHC</sub>NC<sub>NHC</sub>)-pincer cobalt(I) complexes,<sup>[3,9]</sup> while the Co–N bond (1.947(4) Å) in **2** is substantially longer than the pyridine Co–N bond (e.g. 1.839(4) Å<sup>[9]</sup>), possibly due to steric reasons. The bond lengths of C14–C15 (1.401(8) Å) and C14'–C15' (1.400(7) Å) are pronouncedly elongated compared to the non-coordinated olefinic bond in the Co(II) complex **1** or in the respective imidazolium salt<sup>[15]</sup> (1.28 - 1.32 Å), which confirms a certain amount of metallacyclopropane character in **2**.

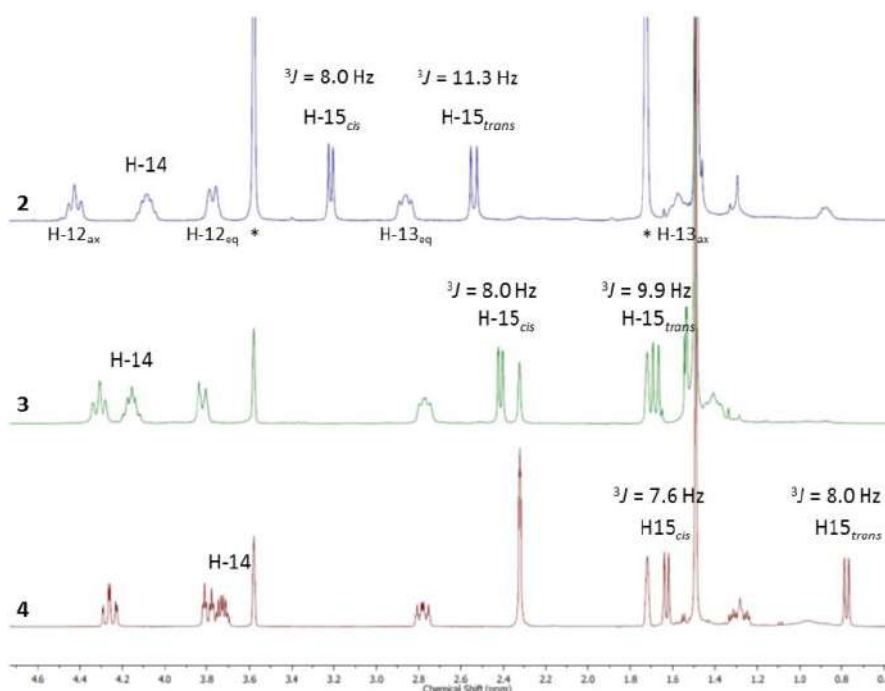
*In situ* generation of the iridium complex **4**<sup>LiX</sup> was achieved applying the same route as for [Rh(bimca<sup>Homo</sup>)] (**3**),<sup>[5b]</sup> which is deprotonation of Hbimca<sup>Homo</sup>·2HBr with LiHMDS and subsequent transmetalation with [Ir(μ-Cl)(COD)]<sub>2</sub> (Scheme 2). To obtain the pure complex **4**, the transmetalation step was conducted at low temperature using the potassium complex [K(bimca<sup>Homo</sup>)] generated *in situ* by deprotonation of Hbimca<sup>Homo</sup>·2HBr with KHMDS at  $-60\text{ }^{\circ}\text{C}$ . In contrast to lithium halides, the potassium halides formed could be readily removed by filtration.



**Scheme 2.** Synthesis of both *in situ* generated **4**<sup>LiX</sup> and Isolated [Ir(bimca<sup>Homo</sup>)] (**4**).

The molecular structure of **4** is isostructural to **2** as revealed by NMR spectroscopy showing a symmetric coordination mode of the ligand. All signals could be assigned by means of 2D and NOE experiments. The coordination of both double bonds and

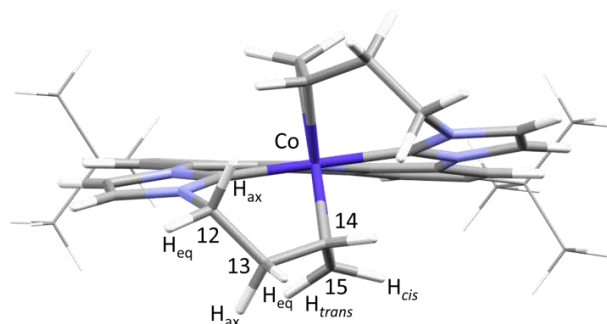
both carbene moieties to the Ir-center is confirmed by the up-field shift of the respective signals in the  $^1\text{H}$  NMR spectrum (3.77-3.69 (H-14), 1.63 (H-15<sub>cis</sub>), 0.78 ppm (H-15<sub>trans</sub>)) as well as in the  $^{13}\text{C}$  NMR spectrum, 39.7 (C15) and 27.7 ppm (C14). The carbene signal is found at typical 164.5 ppm. In comparison with the  $^1\text{H}$  NMR spectra of the complexes **2** (Co) and **3** (Rh) (Figure 3) the stronger metallacyclopropane character of complex **4** can be derived from the stronger high-field shift of the olefinic proton signals from **2** to **4** as well as the decreasing  $^3J$  coupling constant of the olefinic protons from 8.0 (*cis*) and 11.3 Hz (*trans*) in **2** to only 7.6 (*cis*) and 8.0 Hz (*trans*) in **4** due to the reduced s-character of the olefinic carbon atoms (from  $\text{sp}^2$  to partial  $\text{sp}^3$  hybridization). This reflects the tendency of 5d metals to form stronger metal-C bonds and the increased stability of the higher oxidation state.



**Figure 3.**  $^1\text{H}$  NMR spectra (section) of the *N*-homoallyl signals of **2** (Co), **3** (Rh) and **4** (Ir), and the  $^3J_{\text{HH}}$  coupling constants in comparison (\* THF- $\text{d}_7$ ).

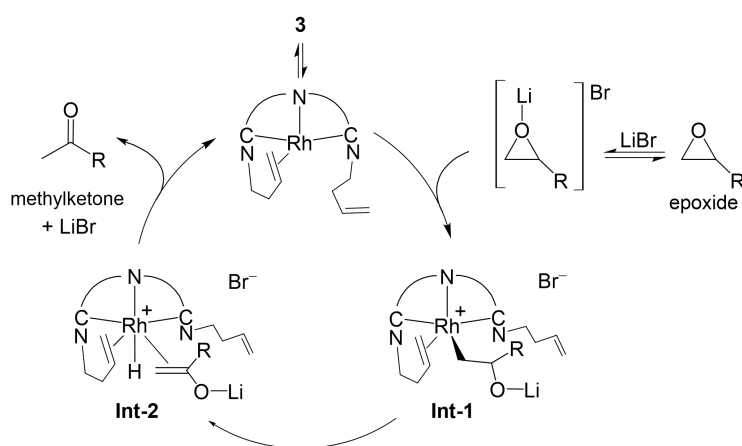
DFT calculations of the complexes **2** - **4** confirm the experimental results of the bond lengths and angles from the X-ray structure analysis of **2**. The increasing metallacyclopropane character from the cobalt to the iridium complex is also displayed in the increasing C=C bond lengths of the coordinated homoallyl moieties from 1.413 (**2**) to 1.446 Å (**4**) (Figure 4).





**Figure 4.** Calculated structure (DFT-D3) of **2** with *tert*-Bu groups depicted in wireframe for clarity. The geometry optimized structures of **3** and **4** are isostructural. The olefinic bond length C14-C15 (mean) is increasing from **2** (1.413 Å) over **3** (1.424 Å) to **4** (1.446 Å).

As the rhodium complex **3** was found to be a highly reactive nucleophilic catalyst for rearrangement of terminal epoxides into methyl ketones already at room temperature, we were eager to test the catalytic reactivity of its analogs **2** and **4** in the same reaction. The general mechanism for the nucleophilic isomerization of terminal epoxides catalyzed by **3** requires the dissociation of one homoallyl moiety from the rhodium center to generate the nucleophilic, catalytically active species (Scheme 3).<sup>[5b]</sup> This is followed by nucleophilic ring opening of the epoxide preactivated by the Lewis acid co-catalyst to generate the Rh(III) intermediate **Int-1**.<sup>[5c]</sup> After  $\beta$ -hydride elimination to **Int-2**,<sup>[5a]</sup> the desired methyl ketone is obtained by a formal reductive elimination and release of the catalytic active species, which can be stabilized by recoordination of the *N*-homoallyl moiety.

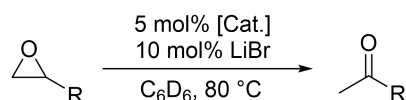


**Scheme 3.** Mechanism of the nucleophilic epoxide isomerization with catalyst [Rh(bimca<sup>Homo</sup>)] (**3**).

As initial catalytic attempts with complexes **2** and **4** and 1,2-epoxyhexane (**5a**) at room temperature did not lead to any conversion after 6 days, further catalytic experiments were conducted at 80 °C with 5 mol% catalyst and 10 mol% LiBr in C<sub>6</sub>D<sub>6</sub>. The results of the epoxide isomerizations with catalysts **2** and **4** are summarized in Table 1. When **2** was applied using 1,2-epoxyhexane (**5a**) as the substrate, the isomerization was surprisingly slow and only 18% yield was obtained after 6 days (entry 1). No conversion was obtained with the more challenging styrene oxide **5b**, which contains a less electrophilic  $\beta$ -C atom and can be easily isomerized by Lewis acids to the aldehyde (entry 6). Under identical conditions (80 °C), the reactions with catalyst **3** were completed already within 30 min (entries 2 and 7) and high yields of 2-hexanone (**6a**) and acetophenone (**6b**) were obtained.<sup>[16]</sup> We suppose that the low reactivity of the Co(I) complex **2** results from a higher energy barrier of **2** in the nucleophilic ring opening to form the Co(III) intermediate. In reports from Eisenman and Coates on the nucleophilic epoxide isomerization, the active species is [Co(CO)<sub>4</sub>]<sup>-</sup> (Co(-I)), which explains the higher reactivity apart from using a stronger Lewis acid.<sup>[17]</sup> Iridium(I) complexes, who have a considerable lower redox potential, should react much easier, as the oxidative addition of the epoxide (e.g. by a nucleophilic ring opening mechanism) is the rate limiting step in the Rh catalysis. Therefore, we tested **4** in the isomerization of **5a** to yield 2-hexanone in 92% yield (entry 3), but surprisingly, the reaction proceeded much slower (6 days) than with **3** ( $\leq$  30 min). With substrate **5b**, only 26 % yield was achieved despite full conversion (entry 8). This can be explained with a higher degree of side reactions: a polymerization might arise from more stable Ir(III) intermediates analogous to **Int-1** or **Int-2** (Scheme 3) that in addition slow down the  $\beta$ -hydride elimination step. The lower activity of complex **4** (6 d for full conversion) can be rationalized with the higher stability of the coordinated *N*-homoallyl moieties (stronger metallacyclopropane character), of which one has to dissociate to form the nucleophilic active species. Therefore, we tried to run the reactions in presence of 1 bar of hydrogen, so that the homoallyl moieties get hydrogenated *in situ* and a highly reactive nucleophilic metal complex could form. On the other hand, the formation of hydrido complexes could reduce the activity or lead to side reactions. Indeed, when the reactions with **2** or **4** were conducted in presence of 1 bar of hydrogen, we observed an enhanced reactivity at the beginning with 11% and 52% yield for substrate **5a** (entries 4 and 5) and 5% and 38% for the less electrophilic substrate **5b** (entries 9 and 10) after 24 h.

However, the reaction stops and cannot be completed by extending the reaction time. The higher conversion with catalyst **4** can be attributed to formation of 2-phenylethanol (confirmed by  $^1\text{H}$  NMR spectroscopy) as well as some degree of polymerization. Unfortunately, neither complex **2** nor **4** were able to compete with our previously reported rhodium catalyst **3**.<sup>[5b]</sup>

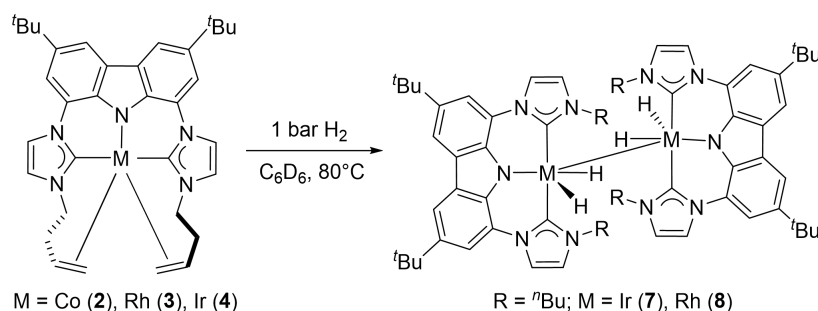
**Table 1.** Regioelective Isomerization of Terminal Epoxides with  $[\text{M}(\text{bimca}^{\text{Homo}})]^{\text{[a]}}$



Entry	Epoxide	[Cat.]	H <sub>2</sub> (bar)	Time	Conversion (%)	Yield (%)
1		<b>2</b>	-	6 days	32	18
2	 <b>5a</b>	<b>3</b>	-	30 min	100	92
3		<b>4</b>	-	6 days	100	92
4		<b>2</b>	1	24 h	19	11
5		<b>4</b>	1	24 h	81	52
6		<b>2</b>	-	6 days	0	0
7	 <b>5b</b>	<b>3</b>	-	30 min	100	88
8		<b>4</b>	-	6 days	100	26
9		<b>2</b>	1	24 h	11	5
10		<b>4</b>	1	24 h	75	38

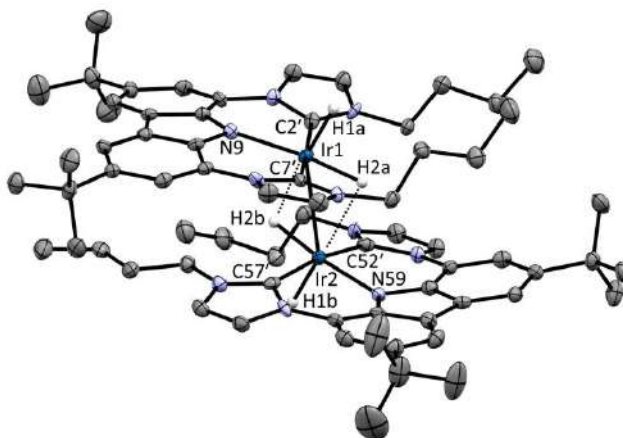
[a] Reactions were carried out in *J. Young* NMR tubes with 10  $\mu\text{L}$  THF- $d_8$  and yield of the products was calibrated to 1,3,5-trimethoxybenzene (internal standard).

To elucidate whether the *N*-homoallyl moieties of the complexes **2** – **4** can indeed be hydrogenated in the presence of hydrogen under the catalytic conditions, we exposed a solution of **4** in benzene- $d_6$  to 1 bar H<sub>2</sub> at 80 °C (Scheme 4), which resulted in a color change from yellow to dark red after 24 h and the formation of red crystals upon cooling to ambient temperature.



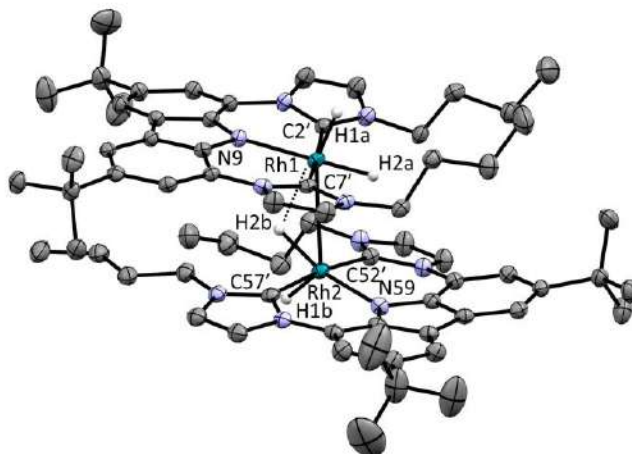
**Scheme 4.** Hydrogenation of [M(bimca<sup>Homo</sup>)].

The X-ray structure analysis reveals a dimeric structure in which the former *N*-homoallyl moieties are fully hydrogenated and residual electron density at the metal indicates the formation of the iridium(III) hydrido complex **7** (Figure 5). As it can be expected that the hydrido ligands cannot be identified with certainty from X-ray data, the Ir-H bond lengths were fixed at the value obtained from DFT calculations based on the X-ray structure (with all bonds and angles fixed, except of those of the hydrido ligands, see Supporting Information). The structural motif [Ir(H)( $\mu$ -H)]<sub>2</sub> has been found before e.g. in phosphine complexes<sup>[18,19]</sup> and the Ir-Ir distance of 2.784 Å in **7** is comparable to those complexes (2.73 Å and 2.77 Å), but in contrast, the hydride atoms in **7** are less symmetrically bridged, possibly for steric reasons. It is also noteworthy that the more flexible bis(phosphinomethyl)carbazolide ligand (PNP) in an analogous complex by Yamashita and coworkers lead to a bridging instead of a pincer-type ligand coordination.<sup>[18]</sup> The hydrogen bridges in **7** measure 2.50 Å (Ir1-H2b) and 2.53 (Ir2-H2a), which was also confirmed by DFT geometry optimizations without constraints. In addition, London dispersion<sup>[20]</sup> seems to play an important role for the dimer formation, as the energy difference between the monomers and the dimer strongly favors the dimer (see Supporting Information). The intramolecular distances of the carbazolidine planes at Ir1 and Ir2 are between 3.71 and 4.15 Å (measured from the respective pyrrolide centers). However, intermolecular London dispersion is pronounced in the crystal. The distance between the co-planar carbazolidine planes at Ir2 and Ir2# measures only 2.63 Å. The metal carbene bond lengths Ir-C<sub>NHC</sub> (2.03 Å, mean) are comparable with those of a C<sub>NHC</sub>CC<sub>NHC</sub>-Ir complex from Braunstein.<sup>[21]</sup>



**Figure 5.** Solid-state molecular structure of **7**. Atoms are shown with anisotropic atomic displacement parameters at the 50% probability level. The co-crystallized benzene molecule and the hydrogen atoms (except for the hydrido ligands) are omitted for clarity. Selected bond lengths (Å) and angles (deg): Ir1–N9 = 2.059(3), Ir1–C2' = 2.035(4), Ir1–C7' = 2.027(4), Ir2–N59 = 2.059(3), Ir2–C52' = 2.035(4), Ir2–C57' = 2.027(4), Ir1–Ir2 = 2.7836(2); N9–Ir1–Ir2 = 115.21(9), N59–Ir2–Ir1 = 114.10(9); the metal-hydrogen bond lengths and angles were fixed (Ir1–H1a = 1.58, Ir1–H2a = 1.63, Ir2–H1b = 1.58, Ir2–H2b = 1.63) based on DFT calculations; (hydrogen bridges) 2.50 Å (Ir1–H2b) and 2.53 (Ir2–H2a).

Also with bis(NHC)Rh(I) complexes, the formation of hydrido Rh(III) complexes is to be expected.<sup>[22]</sup> Under analogous conditions, the reaction with rhodium complex **3** leads to the formation of red single crystals as well. The X-ray structure analysis confirms the successful hydrogenation of the *N*-homoallyl moieties and formation of the dimer **8** that is isostructural with complex **7** (Figure 6). All intra- (3.64 and 4.10 Å) and intermolecular (2.63 Å) distances of the carbazolide planes are comparable with those of the iridium complex **7**. The only striking differences to complex **7** is the longer metal-metal distance of 2.934 Å that also comes with the 6° more acute N-Rh-Rh angles of 107.5° (N9-Rh1-Rh2) and 109.0° (N59-Rh2-Rh1). As already performed in X-ray data refinement of complex **7**, the Rh-H bond lengths and angles were calculated by DFT methods by fixing all bonds and angles based on the X-ray structure analysis except for the hydrido ligands. At Rh1, a square pyramidal arrangement and at Rh2 a Y-shaped distorted trigonal bipyramidal coordination geometry was found (the latter is also obtained by DFT calculations for a monomeric species). Thus only one intramolecular hydrogen bridge is found (Rh1–H2b = 2.54 Å; Rh2–H2a = 2.79 Å, which explains the longer Rh1–Rh2 distance compared to complex **7**.



**Figure 6.** Solid-state molecular structure of **8**. Atoms are shown with anisotropic atomic displacement parameters at the 50% probability level. The co-crystallized benzene molecule and the hydrogen atoms (except for the hydrido ligands) are omitted for clarity. The crystal structures of **7** and **8** are isomorphous. Selected bond lengths (Å) and angles (deg): Rh1–N9 = 2.062(2), Rh1–C2' = 2.037(2), Rh1–C7' = 2.029(2), Rh2–N59 = 2.035(2), Rh2–C52' = 2.036(2), Rh2–C57' = 2.029(2), Rh1–Rh2 = 2.9335(3); N9–Rh1–Rh2 = 107.53(5), N59–Rh2–Rh1 = 108.97(5); The metal-hydrogen bond lengths and angles were fixed at Rh1–H1a = 1.54, Rh1–H2a = 1.58, Rh2–H1b = 1.54, Rh2–H2b = 1.58 based on DFT calculations; (hydrogen bridges) 2.54 Å (Rh1–H2b) and 2.79 (Rh2–H2a).

Hydrogenation of the cobalt complex **2** under identical conditions led to formation of a dark green solution whose  $^1\text{H}$  NMR spectrum shows broad peaks between 16 and  $-9$  ppm possibly due to a paramagnetic influence. More detailed analyses would lead beyond the scope of this investigation.

## Conclusions

Based on the pentadentate pincer bis-NHC ligand  $\text{bimca}^{\text{Homo}}$ , the corresponding cobalt complex **2** was successfully synthesized by a deprotonation-transmetallation-reduction sequence starting from  $\text{CoCl}_2$  which involves  $[\text{Co}(\text{bimca}^{\text{Homo}})\text{Br}]$  (**1**) in which the  $\text{bimca}^{\text{Homo}}$  ligand shows a tetradentate coordination mode. The iridium catalyst **4** was synthesized straightforwardly by transmetallation of  $[\text{Li}(\text{bimca}^{\text{Homo}})]$  with  $[\text{Ir}(\mu\text{-Cl})(\text{COD})_2]$ . In contrast to the highly reactive rhodium analogue **3**, complexes **2** and **4** were much less active in the nucleophilic epoxide isomerization. This can be ascribed to the lower oxidation potential of **2** compared to **3** and in the case of **4** to the higher oxidation potential, which is also displayed in the increasing metallacyclopropane character of the coordinated *N*-homoallyl moieties. When the reaction was carried out in presence of 1 bar  $\text{H}_2$  an increased activity was observed, however, on the cost of side reactions. The successful hydrogenation of the *N*-

homoallyl to *N-n*-butyl substituents and the formation of hydrido pincer complexes under these conditions was confirmed with the X-ray structure analyses of **7** (Ir) and **8** (Rh). Further investigations of these interesting complexes will be the subject of future work in our group.

### Experimental procedure

**General Information.** Unless otherwise noted, all reactions were carried out under an argon atmosphere in dried and degassed solvents using Schlenk technique. All glassware was stored in a preheated oven prior to use. Toluene, pentane, benzene and tetrahydrofuran were purchased from Sigma Aldrich and dried using an MBraun SPS-800 solvent purification system. The lithium and potassium bases used were obtained from commercial suppliers, dried in vacuum and used without further purification.  $\text{KC}_8$ <sup>[23]</sup> and  $\text{Rh}(\text{bimca}^{\text{Homo}})$ <sup>[5b]</sup> were synthesized, and  $[\text{Li}(\text{bimca}^{\text{Homo}})]$ <sup>[5b]</sup> and  $[\text{K}(\text{bimca}^{\text{Homo}})]$ <sup>[5b]</sup> were generated *in situ* according to the literature. Liquid Chemicals from commercial suppliers were degassed through freeze-pump-thaw cycles prior to use. <sup>1</sup>H and <sup>13</sup>C NMR spectra were recorded using a Bruker AVANCE II+ 400 spectrometer. Chemical shifts  $\delta$  (ppm) are given relative to the solvent's residual proton and carbon signal respectively: THF-*d*<sub>8</sub>: 3.58 ppm (<sup>1</sup>H NMR) and 67.57 ppm (<sup>13</sup>C NMR); C<sub>6</sub>D<sub>6</sub>: 7.16 ppm (<sup>1</sup>H NMR) and 128.39 ppm (<sup>13</sup>C NMR). <sup>1</sup>H NMR data for diamagnetic compounds are reported as follows: chemical shift, multiplicity (s = singlet, d = doublet, t = triplet, q = quartet, br = broad, m = multiplet), coupling constants (Hz), integration, assignment. The assignment of peaks is based on 2D NMR correlation and NOE spectra.

**X-ray Data Collection and Structure Analysis.** Suitable crystals for the X-ray analysis were obtained as described below. Data collection (except for  $[\text{Co}(\text{bimca}^{\text{Homo}})_2]\text{Br}$ ) was carried out on a Bruker APEX Duo CCD with an Incoatec  $\mu\text{S}$  Microsource with a Quazar MX mirror using Mo  $K_\alpha$  radiation ( $\lambda = 0.71073 \text{ \AA}$ ) and a graphite monochromator. Corrections for absorption effects were applied using SADABS.<sup>[24a]</sup> All structures were solved by direct methods using SHELXS and refined using SHELXL.<sup>[24]</sup> In the case of structure **1** and  $[\text{Co}(\text{bimca}^{\text{Homo}})_2]\text{Br}$  the SQUEEZE routine<sup>[25]</sup> was applied for disordered solvent.

**Synthesis of [Co(bimca<sup>Homo</sup>)Br] (1).** CoCl<sub>2</sub> (9.5 mg, 73 μmol, 1 eq) was added to the previous prepared solution of [Li(bimca<sup>Homo</sup>)] (73.4 μmol) at room temperature. The solution was shaken for 2 min. After 12 h, brown crystals appeared and were filtered, washed with THF (0.5 mL × 3) and dried *in vacuo*. Single crystals suitable for X-ray diffraction were obtained (39.1 mg). Although C,H,N analysis reveals residual impurity, most probably LiBr and THF, the material can be used directly in the next step. Anal. Calcd for C<sub>34</sub>H<sub>40</sub>BrCoN<sub>5</sub>·0.25 LiBr·1.25 C<sub>4</sub>H<sub>8</sub>O: C: 60.88, H:6.55, N: 9.10; found: C: 61.02, H: 6.30, N: 8.95.

**Synthesis of [Co(bimca<sup>Homo</sup>)] (2) from [Co(bimca<sup>Homo</sup>)Br] (1).** To a suspension of [Co(bimca<sup>Homo</sup>)Br] (1) (39.1 mg from the material obtained above) in THF (2.0 mL) was added KC<sub>8</sub> (8.0 mg, 59 μmol). The suspension was stirred at room temperature for 12 h in an argon-filled glovebox. After completion, the mixture was filtered with a syringe filter and purified by column chromatography using THF as eluent in the glovebox. [Co(bimca<sup>Homo</sup>)] (2) containing 0.75 mol THF (13.0 mg, 21 μmol, 28% yield over two steps) was obtained as a red solid after removal of the solvent. Single crystals suitable for X-ray diffraction were grown from a concentrated solution of **2** in toluene and pentane at -30 °C. <sup>1</sup>H NMR (400 MHz, THF-d<sub>8</sub>) δ 8.00 (d, <sup>4</sup>J<sub>HH</sub> = 1.3 Hz, 2H, H-4/5), 7.79 (d, <sup>3</sup>J<sub>HH</sub> = 1.0 Hz, 2H, H-5'), 7.37 (d, <sup>4</sup>J<sub>HH</sub> = 1.3 Hz, 2H, H-2/7), 6.91 (d, <sup>3</sup>J<sub>HH</sub> = 1.0 Hz, 2H, H-4'), 4.38 (br ps t, <sup>2/3</sup>J<sub>HH</sub> = 12.6 Hz, 2H, H-12<sub>ax</sub>), 4.11–4.02 (m, 2H, H-14), 3.72 (br d, <sup>2</sup>J<sub>HH</sub> = 12.3 Hz, 2H, H-12<sub>eq</sub>), 3.21 (d, <sup>3</sup>J<sub>HH</sub> = 8.0 Hz, 2H, H-15<sub>cis</sub>), 2.86–2.80 (m, 2H, H-13<sub>eq</sub>), 2.54 (br d, <sup>3</sup>J<sub>HH</sub> = 11.3 Hz, 2H, H-15<sub>trans</sub>), 1.59–1.50 (m, 2H, H-13<sub>ax</sub>), 1.50 (s, 18H, H-11). <sup>13</sup>C NMR (101 MHz, THF-d<sub>8</sub>) δ 191.1 (C2'), 138.6 (C3/6), 136.5 (C1a/8a), 128.5 (C4a/5a), 125.4 (C1/8), 122.4 (C4'), 115.9 (C5'), 115.0 (C4/5), 107.6 (C2/7), 66.1 (C15), 57.5 (C14), 50.8 (C12), 35.6 (C13 and C10), 33.0 (C11). Anal. Calcd for C<sub>34</sub>H<sub>40</sub>N<sub>5</sub>Co·0.75 C<sub>4</sub>H<sub>8</sub>O: C:70.35, H: 7.34, N: 11.09; found: C: 70.49, H: 7.47, N: 11.08.

**Synthesis of [Co(bimca<sup>Homo</sup>)] (2) from [Co(PPh<sub>3</sub>)<sub>3</sub>Cl].** To a freshly generated solution of [Li(bimca<sup>Homo</sup>)] (29.3 μmol) in THF (0.6 mL) was added [Co(PPh<sub>3</sub>)<sub>3</sub>Cl] (25.6 mg, 29.3 μmol). The mixture was shaken until the cobalt precursor was fully dissolved. After completion, the mixture was purified by column chromatography using THF as eluent in an argon-filled glovebox. [Co(bimca<sup>Homo</sup>)] (2) was obtained as red solid after removal of the solvent, however, containing residual PPh<sub>3</sub>. The NMR data correspond to the results obtained from starting with **1**.



**In situ generation of LiX containing [Ir(bimca<sup>Homo</sup>)] (4<sup>LiX</sup>).** [Ir( $\mu$ -Cl)(COD)]<sub>2</sub> (9.7 mg, 15  $\mu$ mol) was added to the previous prepared solution of [Li(bimca<sup>Homo</sup>)] (29  $\mu$ mol) in THF (0.6 mL) at room temperature. The solution was stirred for 30 min. *In situ* generated [Ir(bimca<sup>Homo</sup>)] (4<sup>LiX</sup>) was obtained as an orange solution in quantitative yield as determined by NMR spectroscopy. <sup>1</sup>H NMR (400 MHz, THF-d<sub>8</sub>)  $\delta$  8.02 (d, <sup>4</sup>J<sub>HH</sub> = 1.5 Hz, 2H, H-4/5), 7.94 (d, <sup>3</sup>J<sub>HH</sub> = 2.3 Hz, 2H, H-5'), 7.53 (d, <sup>4</sup>J<sub>HH</sub> = 1.5 Hz, 2H, H-2/7), 7.11 (d, <sup>3</sup>J<sub>HH</sub> = 2.3 Hz, 2H, H-4'), 4.26 (dt, <sup>2</sup>J<sub>HH</sub> = 12.6 Hz, <sup>3</sup>J<sub>HH</sub> = 2.7 Hz, 2H, H-12<sub>ax</sub>), 3.80 (dt, <sup>2</sup>J<sub>HH</sub> = 12.6 Hz, <sup>3</sup>J<sub>HH</sub> = 3.2 Hz, 2H, H-12<sub>eq</sub>), 3.77–3.69 (m, 2H, H-14), 2.82–2.75 (m, 2H, H-13<sub>eq</sub>), 1.63 (d, <sup>3</sup>J<sub>HH</sub> = 7.6 Hz, 2H, H-15<sub>cis</sub>), 1.49 (s, 18H, H-11), 1.33–1.24 (m, 2H, H-13<sub>ax</sub>), 0.78 (br d, <sup>3</sup>J<sub>HH</sub> = 8.0 Hz, 2H, H-15<sub>trans</sub>). <sup>13</sup>C NMR (101 MHz, THF-d<sub>8</sub>)  $\delta$  164.5 (C2'), 137.3 (C1a/8a), 136.1 (C3/6), 128.1 (C4a/5a), 126.4 (C1/8), 121.1 (C4'), 115.7 (C5'), 115.2 (C4/5), 109.6 (C2/7), 53.8 (C12), 39.7 (C15), 35.6 (C10), 35.3 (C13), 32.9 (C11), 27.7 (C14).

**Synthesis of salt-free [Ir(bimca<sup>Homo</sup>)] (4).** [Ir( $\mu$ -Cl)(COD)]<sub>2</sub> (9.8 mg, 15  $\mu$ mol) was added to an *in situ* generated solution of [K(bimca<sup>Homo</sup>)] (29.3  $\mu$ mol) at -60 °C. The solution was stirred for 30 min. The potassium salts formed were filtered off and the filtrate was dried *in vacuo*. The residue was washed with pentane (2 mL  $\times$  3) and dried again *in vacuo* to yield complex **4** as a yellow solid (5.7 mg, 8.1  $\mu$ mol, 55% yield). The NMR data correspond to the results obtained from using [Li(bimca<sup>Homo</sup>)]. Anal. Calcd for C<sub>34</sub>H<sub>40</sub>IrN<sub>5</sub>·0.85 C<sub>4</sub>H<sub>8</sub>O: C: 58.17, H: 6.11, N: 9.07; found: C: 58.04, H: 6.75, N: 9.24.

**General procedure for epoxide isomerization with [M(bimca<sup>Homo</sup>)].** In a argon-filled glovebox a *J. Young* NMR tube was charged with a solution of the epoxide (40  $\mu$ mol), LiBr (4.0  $\mu$ mol with 10  $\mu$ L THF-d<sub>8</sub>), [M(bimca<sup>Homo</sup>)] (2.0  $\mu$ mol) and a certain amount of 1,3,5 trimethoxybenzene as internal standard in C<sub>6</sub>D<sub>6</sub> (0.4 mL). The reaction was heated at 80 °C for the given reaction time and analyzed by <sup>1</sup>H NMR spectroscopy.

**General procedure for epoxide isomerization with [M(bimca<sup>Homo</sup>)] in presence of 1 bar H<sub>2</sub>.** In an argon-filled glovebox a *J. Young* NMR tube was charged with a solution of the epoxide (40  $\mu$ mol), LiBr (4.0  $\mu$ mol with 10  $\mu$ L THF-d<sub>8</sub>), [M(bimca<sup>Homo</sup>)] (2.0  $\mu$ mol) and a certain amount of the internal standard (1,3,5 trimethoxybenzene) in C<sub>6</sub>D<sub>6</sub> (0.4 mL). The tube was sealed, brought outside of the glovebox, and attached

to a Schlenk line. After a freeze-pump-thaw cycle with liquid nitrogen, the tube was charged with 1 bar of H<sub>2</sub> at room temperature. The reaction mixture was heated at 80 °C for 24 h and analyzed by <sup>1</sup>H NMR spectroscopy.

**Formation of [Ir(bimca<sup>n-Bu</sup>)(H)<sub>2</sub>]<sub>2</sub> (7).** In a argon-filled glovebox a *J. Young* NMR tube was charged with a solution of [Ir(bimca<sup>Homo</sup>)] (5.7 mg, 8.0 μmol) in C<sub>6</sub>D<sub>6</sub> (0.5 mL). The tube was sealed, brought outside of the glovebox, and attached to a Schlenk line. After a freeze-pump-thaw cycle with liquid nitrogen, the tube was charged with 1 bar of H<sub>2</sub> at room temperature and heated at 80 °C for 24 h. Red single crystals suitable for X-ray diffraction were obtained upon cooling to room temperature that confirm full hydrogenation of the homoallyl chain under the reaction conditions of the epoxide isomerization as a preliminary result. Further characterization was hampered by their slow solubility.

**Formation of [Rh(bimca<sup>n-Bu</sup>)(H)<sub>2</sub>]<sub>2</sub> (8).** In an argon-filled glovebox a *J. Young* NMR tube was charged with a solution of [Rh(bimca<sup>Homo</sup>)] (5.0 mg, 8.0 μmol) in C<sub>6</sub>D<sub>6</sub> (0.5 mL). The tube was sealed, brought outside of the glovebox, and attached to a Schlenk line. After a freeze-pump-thaw cycle with liquid nitrogen, the tube was charged with 1 bar of H<sub>2</sub> at room temperature and heated at 80 °C for 24 h. Red single crystals suitable for X-ray diffraction were obtained upon cooling to room temperature that confirm full hydrogenation of the homoallyl chain under the reaction conditions of the epoxide isomerization as a preliminary result. Further characterization was hampered by their slow solubility.

The identical procedure using the cobalt complex (2) resulted in a green solution, whose <sup>1</sup>H NMR spectrum showed broad peaks between 16 and -9 ppm indicating paramagnetic character.

**DFT calculations** Performed based on density functional theory at the BP86/def2-SVP and/or BP86/def2-TZVP<sup>[26]</sup> level implemented in Turbomole<sup>[27]</sup>. The RI-approximation<sup>[28]</sup> was used all over and the Grimme dispersion correction D3-BJ<sup>[29]</sup> where indicated. Minimum structures (except for the dimeric structures) were verified at the BP86/def2-SVP level by calculating the Hessian matrix and ensuring that it has no imaginary frequency.

### Acknowledgement

Yingying Tian thanks the China Scholarship Council (CSC) for a predoctoral fellowship. T.M. thanks the MWK-BW for a fellowship (Landesgraduiertenförderung). We are grateful to the Swiss-Norwegian beamlines at the ESRF, Grenoble, France and to Dr. D. Chernyshov for assistance on beamline BM01A and thank Prof. Kazushi Mashima for a helpful discussion.

### References

- (1) (a) Arduengo, A. J., III; Harlow, R. L.; Kline, M. *J. Am. Chem. Soc.* **1991**, *113*, 361–363. (b) Díez-González, S.; Marion, N.; Nolan, S. P. *Chem. Rev.* **2009**, *109*, 3612–3676. (c) Bourissou, D.; Guerret, O.; Gabbaï, F. P.; Bertrand, G. *Chem. Rev.* **2000**, *100*, 39–91. (d) Herrmann, W. A. *Angew. Chem. Int. Ed.* **2002**, *41*, 1290–1309. (e) Hahn, F. E.; Jahnke, M. C. *Angew. Chem. Int. Ed.* **2008**, *47*, 3122–3172. (f) Enders, D.; Niemeier, O.; Henseler, A. *Chem. Rev.* **2007**, *107*, 5606–5655. (g) Hopkinson, M. N.; Richter, C.; Schedler, M.; Glorius, F. *Nature* **2014**, *510*, 485–496.
- (2) (a) Danopoulos, A. A.; Simler, T.; Braunstein, P. *Chem. Rev.* **2019**, *119*, 3730–3961. (b) Iglesias, M.; Oro, L. A. *Chem. Soc. Rev.* **2018**, *47*, 2772–2808.
- (3) Yu, R. P.; Darmon, J. M.; Milsman, C.; Margulieux, G. W.; Stieber, S. C. E.; DeBeer, S.; Chirik, P. J. *J. Am. Chem. Soc.* **2013**, *135*, 13168–13184.
- (4) (a) Ibrahim, A. D.; Entsminger, S. W.; Zhu, L.; Fout, A. R. *ACS Catal.* **2016**, *6*, 3589–3593. (b) Tokmic, K.; Markus, C. R.; Zhu, L.; Fout, A. R. *J. Am. Chem. Soc.* **2016**, *138*, 11907–11913. (c) Ibrahim, A. D.; Entsminger, S. W.; Fout, A. R. *ACS Catal.* **2017**, *7*, 3730–3734. (d) Tokmic, K.; Jackson, B. J.; Salazar, A.; Woods, T. J.; Fout, A. R. *J. Am. Chem. Soc.* **2017**, *139*, 13554–13561.
- (5) (a) Tian, Y.; Jürgens, E.; Mill, K.; Jordan, R.; Maulbetsch, T.; Kunz, D. *ChemCatChem* **2019**, *11*, 4028–4035. (b) Tian, Y.; Jürgens, E.; Kunz, D. *Chem. Commun.* **2018**, *54*, 11340–11343. (c) Jürgens, E.; Wucher, B.; Rominger, F.; Törnroos, K. W.; Kunz, D. *Chem. Commun.* **2015**, *51*, 1897–1900.
- (6) Storey, C. M.; Gyton, M. R.; Andrew, R. E.; Chaplin, A. B. *Angew. Chem. Int. Ed.* **2018**, *57*, 12003–12006.
- (7) (a) Chianese, A. R.; Mo, A.; Lampland, N. L.; Swartz, R. L.; Bremer, P. T. *Organometallics* **2010**, *29*, 3019–3026. (b) Chianese, A. R.; Shaner, S. E.; Tendler, J. A.; Pudalov, D. M.; Shopov, D. Y.; Kim, D.; Rogers, S. L.; Mo, A. *Organometallics*

- 2012**, 31, 7359–7367. (c) Chianese, A. R.; Drance, M. J.; Jensen, K. H.; McCollom, S. P.; Yusufova, N.; Shaner, S. E.; Shopov, D. Y.; Tendler, J. A. *Organometallics* **2014**, 33, 457–464. (d) Knapp, S. M. M.; Shaner, S. E.; Kim, D.; Shopov, D. Y.; Tendler, J. A.; Pudalov, D. M.; Chianese, A. R. *Organometallics* **2014**, 33, 473–484.
- (8) Simler, T.; Choua, S.; Danopoulos, A. A.; Braunstein, P. *Dalton Trans.* **2018**, 47, 7888–7895.
- (9) Kuriyama, S.; Arashiba, K.; Tanaka, H.; Matsuo, Y.; Nakajima, K.; Yoshizawa, K.; Nishibayashi, Y. *Angew. Chem. Int. Ed.* **2016**, 55, 14291–14295.
- (10) Allen, F. H. *Acta Cryst.* **2002**, B58, 380–388.
- (11) Danopoulos, A. A.; Wright, J. A.; Motherwell, W. B.; Ellwood, S. *Organometallics* **2004**, 23, 4807–4810.
- (12) (a) Reilly, S. W.; Webster, C. E.; Hollis, T. K.; Valle, H. U. *Dalton Trans.* **2016**, 45, 2823–2828. (b) Denny, J. A.; Lamb, R. W.; Reilly, S. W.; Donnadieu, B.; Webster, C. E.; Hollis, T. K. *Polyhedron* **2018**, 151, 568–574. (c) Xi, Z.; Liu, B.; Lu, C.; Chen, W. *Dalton Trans.* **2009**, 7008–7014.
- (13) Fürstner, A.; Krause, H.; Ackermann, L.; Lehmann, C. W. *Chem. Commun.* **2001**, 2240–2241.
- (14) Ibrahim, A. D.; Tokmic, K.; Brennan, M. R.; Kim, D.; Matson, E. M.; Nilges, M. J.; Bertke, J. A.; Fout, A. R. *Dalton Trans.* **2016**, 45, 9805–9811.
- (15) Jürgens, E.; Kunz, D. *Eur. J. Inorg. Chem.* **2017**, 233–236.
- (16) In earlier results we showed that catalyst **3** is already very active at room temperature and full conversion is achieved within 2 h with substrate **5a** (99% yield) and substrate **5b** (95% yield) (under comparable conditions). Because of this high activity at room temperature catalytic reactions with **3** under H<sub>2</sub> have not been carried out as the reaction would already proceed before H<sub>2</sub> can be added in our setup.
- (17) (a) Eisenmann, J. L. *J. Org. Chem.* **1962**, 27, 2706; (b) Lamb, J. R.; Jung, Y.; Coates, G. W. *Org. Chem. Front.* **2015**, 2, 346–349.
- (18) Nakayama, S.; Morisako, S.; Yamashita, M. *Organometallics* **2018**, 37, 1304–1313.
- (19) (a) Choualeb, A.; Lough, A. J.; Gusev, D. G. *Organometallics* **2007**, 26, 5224–5229. (b) Peloso, R.; Pattacini, R.; Cazin, C. S. J.; Braunstein P. *Inorg. Chem.* **2009**, 48, 11415–11424. (c) Chadwick, F. M.; Olliff, N. Weller, A. S. *J. Organomet. Chem.* **2016**, 812, 268–271. (d) Cano, I.; Martinez-Prieto, L. M.; Vendier, L.; van Leeuwen, P. W. N. M. *Cat. Sci. Tech.* **2018**, 8, 221–228.

- (20) (a) Grimme, S.; Huenerbein, R.; Ehrlich, S. *ChemPhysChem* **2011**, *12*, 1258–1261. (b) Wagner, J. P.; Schreiner, P. R. *J. Chem. Theory Comput.* **2016**, *12*, 231–237. (c) Liptrot, D. J.; Power, P. P. *Nat. Rev. Chem.* **2017**, *1*, 1–12.
- (21) Raynal, M.; Pattacini, R.; Cazin, C. S. J.; Vallée, C.; Olivier-Bourbigou, H.; Braunstein, P. *Organometallics* **2009**, *28*, 4028–4047.
- (22) (a) Huang, J.; Stevens, E. D.; Nolan, S. P. *Organometallics* **2000**, *19*, 1194–1197. (b) Praetorius, J. M.; Wang, R.; Crudden, C. M. *Eur. J. Inorg. Chem.* **2009**, *2009*, 1746–1751.
- (23) Chakraborty, S.; Chattopadhyay, J.; Guo, W.; Billups, W. E. *Angew. Chem. Int. Ed.* **2007**, *46*, 4486–4488.
- (24) (a) Sheldrick, G. M. SADABS 2012/1; University of Göttingen, Göttingen, Germany, **2012**. (b) Sheldrick, G. M. *Acta Cryst.* **2008**, *A64*, 112–122. (c) Sheldrick, G. M. *Acta Cryst.* **2015**, *C71*, 3–8. (d) Hübschle, C. B.; Sheldrick, G. M.; Dittrich, B. *J. Appl. Cryst.* **2011**, *44*, 1281–1284. (e) Sheldrick, G. M. *Acta Cryst.* **2015**, *A71*, 3–8.
- (25) Spek, A. L. *Acta Cryst.* **2015**, *C71*, 9–18.
- (26) (a) Becke, A. *Phys. Rev. A* **1988**, *38*, 3098–3100. (b) Perdew, J. P. *Phys Rev. B* **1986**, *33*, 8822–8824. (c) Schäfer, A.; Horn, H.; Ahlrichs, R. *J. Chem. Phys.* **1992**, *97*, 2571–2577. (d) Weigend, F.; Ahlrichs, R. *Phys. Chem. Chem. Phys.* **2005**, *7*, 3297–3305. (e) Weigend, F. *Phys. Chem. Chem. Phys.* **2006**, *8*, 1057–1065.
- (27) (a) TURBOMOLE V6.3.1 2011, a development of University of Karlsruhe and Forschungszentrum Karlsruhe GmbH, 1989–2007, TURBOMOLE GmbH, since 2007; available from <http://www.turbomole.com>. (b) Treutler, O.; Ahlrichs, R. *J. Chem. Phys.* **1995**, *102*, 346–354. (c) von Arnim, M.; Ahlrichs, R. *J. Comp. Chem.* **1998**, *19*, 1746–1757. (d) van Wüllen, C. *J. Comp. Chem.* **2011**, *32*, 1195–1201. (e) Deglmann, P.; Furche, F.; Ahlrichs, R. *Chem. Phys. Lett.* **2002**, *362*, 511–518. (f) Deglmann, P.; Furche, F. *J. Chem. Phys.* **2002**, *117*, 9535–9538. (g) Ahlrichs, R.; Bär, M.; Häser, M.; Horn, H.; Kölmel, C. *Chem. Phys. Lett.* **1989**, *162*, 165–169. (h) Armbruster, M. K.; Weigend, F.; van Wüllen, C.; Klopper, W. *Phys. Chem. Chem. Phys.* **2008**, *10*, 1748–1756. (i) Peng, D.; Middendorf, N.; Weigend, F.; Reiher, M. *J. Chem. Phys.* **2013**, *138*, 184105–184114.
- (28) (a) Eichkorn, K.; Treutler, O.; Öhm, H.; Häser, M.; Ahlrichs, R. *Chem. Phys. Lett.* **1995**, *240*, 283–290. (b) Eichkorn, K.; Weigend, F.; Treutler, O.; Ahlrichs, R. *Theor. Chem. Acc.* **1997**, *97*, 119–124. (c) Deglmann, P.; May, K.; Furche, F.; Ahlrichs, R. *Chem. Phys. Lett.* **2004**, *384*, 103–107. (d) Weigend, F. *Phys. Chem. Chem. Phys.*

**2002**, 4, 4285–4291. (e) Sierka, M.; Hogekamp, A.; Ahlrichs, R. *J. Chem. Phys.* **2003**, 118, 9136–9148.

(29) (a) Grimme, S.; Antony, J.; Ehrlich S.; Krieg, H. *J. Chem. Phys.* **2010**, 132, 154104. (b) Grimme, S.; Ehrlich, S.; Goerigk, L. *J. Comput. Chem.* **2011**, 32, 1456-1465.

## Chapter 4

# Nucleophilic Rh<sup>I</sup> Catalyzed Selective Isomerization of Terminal Aziridines to Enamides

Yingying Tian, and Doris Kunz\*

Institut für Anorganische Chemie, Eberhard Karls Universität Tübingen, Auf der  
Morgenstelle 18, 72076 Tübingen, Germany

### Abstract

The selective isomerization of various terminal *N*-Boc protected aziridines to enamides was realized using the highly reactive nucleophilic rhodium catalyst **C** with the Lewis acid LiNTf<sub>2</sub> as co-catalyst under moderate conditions. The reaction proceeds smoothly with only 1 mol% catalyst loading and excellent yields were achieved. An intermediate containing an enamide with a non-conjugated terminal C=C double bond was detected during the course of the reaction, which isomerizes to form the thermodynamically favored 2-amido styrene. Mechanistic insight is gained based on these observations.

---

Tian, Y.; Kunz, D. *ChemCatChem* **2020**, DOI: 10.1002/cctc.202000597.

## Introduction

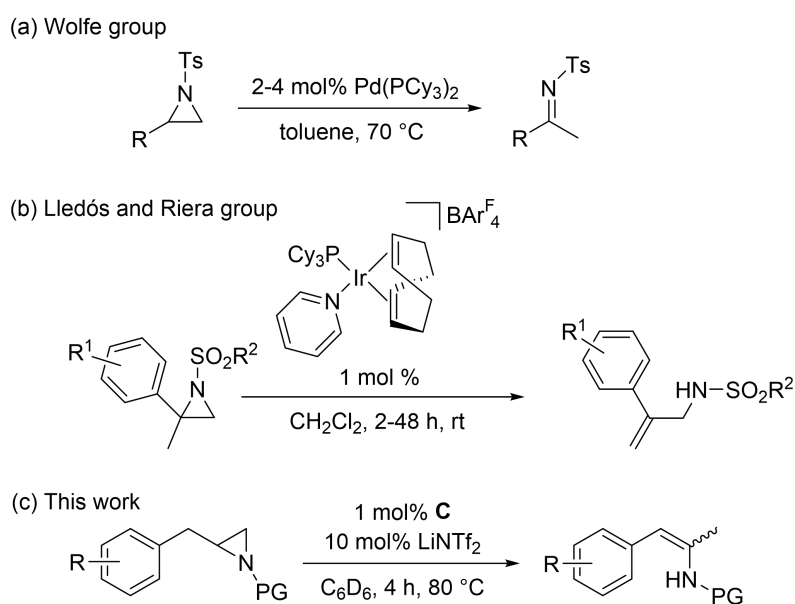
Catalytic isomerizations of small molecules are of great importance for synthetic chemistry due to the ready availability of the substrates and the ideal atom economy of the transformation. The isomerization of epoxides, known as the Meinwald rearrangement, is an efficient method for the conversion of epoxides to carbonyl compounds, such as aldehydes and methyl ketones, which is catalyzed by Lewis acids to obtain aldehydes<sup>[1]</sup> and promoted by Lewis acids with nucleophilic catalysts to yield methyl ketones.<sup>[2]</sup> Recently, our group has realized the chemo- and regioselective isomerization of a diverse range of epoxides including the challenging  $\alpha$ -aryl oxiranes, with the highly nucleophilic rhodium bis(NHC) pincer catalysts **A-C** to obtain almost exclusively methyl ketones in excellent yields under very mild conditions.<sup>[2b,d-e]</sup> Aziridines, the analogue of epoxides, are quite useful building blocks in both organic and pharmaceutical chemistry.<sup>[3]</sup> The most popular reaction for an aziridine transformation is the generation of  $\beta$ -lactams catalyzed by transition-metal complexes under the exposure of carbon monoxide.<sup>[4]</sup> Most recently, the ring opening of aziridines was well-studied and it behaves as an effective pathway to gain  $\beta$ -functionalized amines which can easily be transformed further.<sup>[5]</sup>

However, the isomerization of aziridines has been rarely investigated. In 2002, the Nakayama group reported a Lewis acid catalyzed aza-pinacol rearrangement of various *N*-tosyl aziridines to *N*-tosyl imines with  $\text{BF}_3$ .<sup>[6]</sup> One year later, the Wolfe group introduced the palladium-catalyzed isomerization of terminal *N*-tosyl aziridines to sulfonyl ketimines (Scheme 1, (a)).<sup>[7]</sup> Recently, Lledós, Riera and coworkers described an iridium-catalyzed isomerization of geminal disubstituted *N*-sulfonyl aziridines to allyl amines (Scheme 1, (b)).<sup>[8]</sup>

The potential products of the aziridine isomerization are manifold, such as the mentioned *N*-tosyl imines and allyl amines. Another kind of products expected are enamides which are valuable substrates for the asymmetric hydrogenation to gain access to optically pure amides.<sup>[9]</sup> Common methods to generate enamides usually include reacting ketones with amides<sup>[10]</sup> or applying its derivatives such as vinyl halides, triflates and tosylates with amides through transition-metal catalyzed cross-coupling reactions.<sup>[11]</sup> Recently, the Beller group described the Pd-catalyzed carbonylation reaction of imines to enamides.<sup>[12]</sup> Herein, we provide an alternative synthetic strategy for the preparation of various enamides via the selective



isomerization of terminal aziridines catalyzed by highly nucleophilic rhodium catalysts (Scheme 1, (c)).



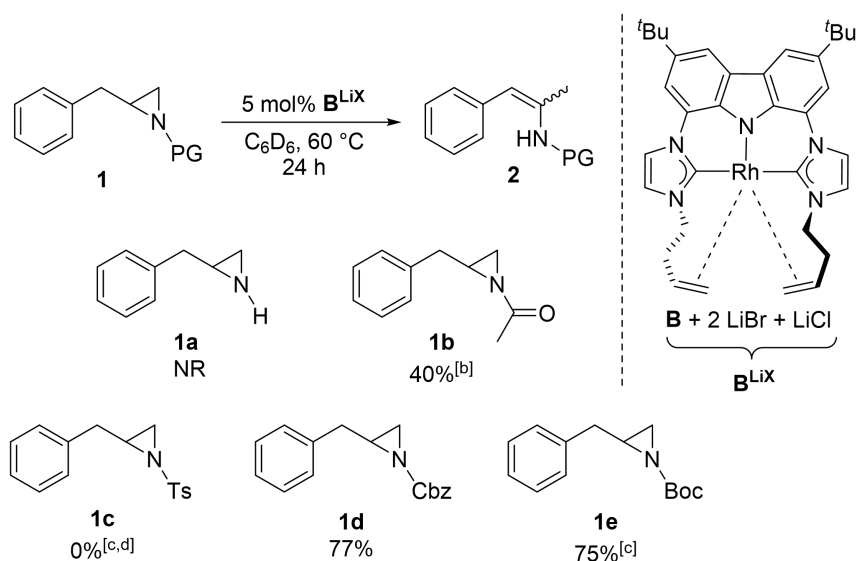
**Scheme 1.** Isomerization of terminal aziridines with transition-metal complexes.

## Results and Discussion

The synthesis of the aziridine candidates usually started from commercially available phenylalanine derivatives. They were reduced firstly with  $\text{NaBH}_4$  as the reducing agent and  $\text{I}_2$  as the catalyst to obtain the corresponding amino alcohols in almost quantitative yields.<sup>[13]</sup> Afterward, the amino substituent of the amino alcohols was protected with the respective protecting group.<sup>[14]</sup> The last step was a one pot reaction that consisted of converting the hydroxyl group into a better leaving group by tosylation and the ring closure with the strong base  $\text{KOH}$  in refluxing  $\text{THF}$ .<sup>[15]</sup> All desired terminal aziridines were generated in moderate to good yields.

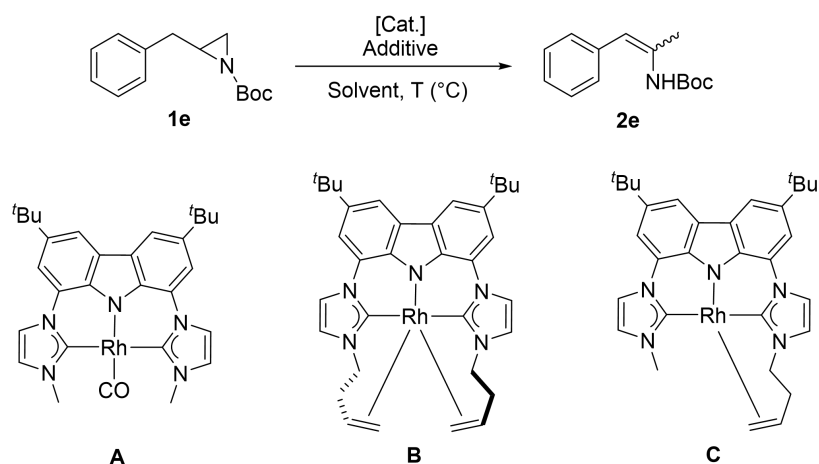
With the successfully prepared terminal aziridines, different protecting groups on the nitrogen atom were tested at the beginning (Scheme 2). The initial reaction conditions were 5 mol% *in situ* generated  $\mathbf{B}^{\text{LiX}}$  [2d] and aziridines in  $\text{C}_6\text{D}_6$  at 60 °C for 24 h. Non-protected aziridine **1a** was not reactive under these conditions. *N*-Acetyl aziridine **1b** was isomerized, but the desired product **2b** was only formed in 40% yield along with 28% of dihydrooxazole. The latter is formed in a Lewis acid catalyzed side reaction with  $\text{LiBr}$ , as confirmed in a blank reaction. When the *N*-tosyl protected substrate **1c** was applied, the reaction went quite fast even at room temperature and

full conversion was achieved after 2 h. However, the desired enamides were not obtained due to polymerization as a side reaction. At 60 °C, **1d** possessing the *N*-Cbz group was converted smoothly to obtain the desired **2d** in 77% yield. To our delight, the *N*-Boc aziridine **1e** can be rearranged at room temperature to yield the corresponding enamides in 75% yield. Therefore, the *N*-Boc protecting group was chosen for all further aziridines.



**Scheme 2.** Isomerization of terminal aziridines with different protecting groups (PG).<sup>[a]</sup> <sup>[a]</sup> The yield of **2** was determined by <sup>1</sup>H NMR calibrated to 1,3,5-trimethoxybenzene (internal standard). <sup>[b]</sup> Along with 28% of dihydrooxazole. <sup>[c]</sup> rt. <sup>[d]</sup> 2 h.

We tested the isomerization of *N*-Boc-2-benzylaziridine (**1e**) as the model substrate. A series of isolated rhodium catalysts efficient for epoxide rearrangement was applied. With the CO-containing catalyst **A**, only traces of the desired enamide were detected after 24 h (Table 1, entry 1). Under the identical conditions, a better yield (28%) was obtained with the more nucleophilic CO-free catalyst **B** and the best result was achieved using catalyst **C** to yield enamide **2e** in 57% yield (Table 1, entries 2 and 3). This can be rationalized with the enhanced nucleophilicity of the 16 e<sup>-</sup> complex **C** with a high-lying HOMO, while the 18 e<sup>-</sup> catalyst **B** requires the dissociation of one olefin moiety to react as a nucleophile. A stronger Lewis acid, necessary for the pre-activation of the aziridine was beneficial for the catalytic reaction and the yield was increased to 66% when LiNTf<sub>2</sub> was used as the co-catalyst (Table 1, entry 4). Furthermore, the reaction proceeds considerably fast when it is carried out at elevated temperatures and the desired product **2e** is

**Table 1.** Rh-catalyzed isomerization of **1e**: Optimization of the reaction conditions.<sup>[a]</sup>

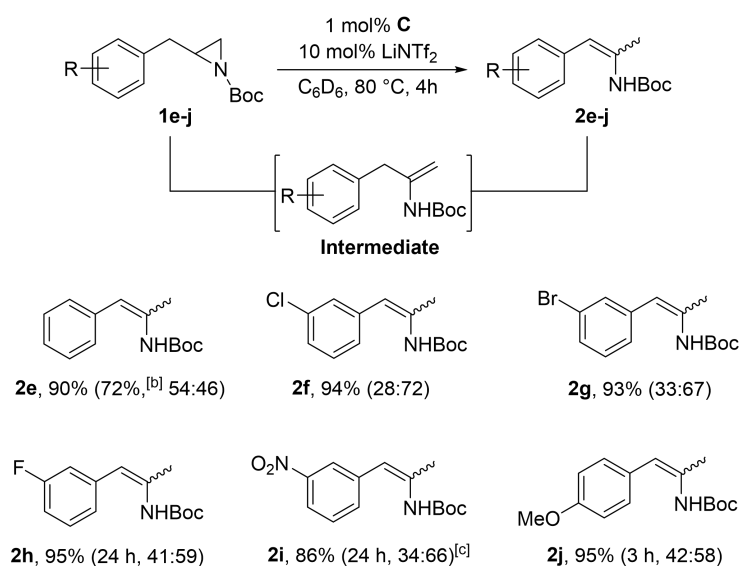
Entry	Catalyst [mol%]	Additive [mol%]	T (°C)	Time	Yield	
					[%] <sup>[b]</sup>	(Z:E)
1	5 ( <b>A</b> )	10 (LiBr)	rt	24 h	< 5	-
2	5 ( <b>B</b> )	10 (LiBr)	rt	24 h	28	50:50
3	5 ( <b>C</b> )	10 (LiBr)	rt	24 h	57	50:50
4	5 ( <b>C</b> )	10 (LiINTf <sub>2</sub> )	rt	24 h	66	47:53
5	5 ( <b>C</b> )	10 (LiINTf <sub>2</sub> )	40	4 h	87	47:53
6	5 ( <b>C</b> )	10 (LiINTf <sub>2</sub> )	60	4 h	87	45:55
7	5 ( <b>C</b> )	10 (LiINTf <sub>2</sub> )	80	4 h	96	41:59
8	5 ( <b>C</b> )	-	80	4 h	0	-
9 <sup>[c]</sup>	5 ( <b>C</b> )	10 (LiINTf <sub>2</sub> )	rt	24 h	<5	-
10 <sup>[d]</sup>	5 ( <b>C</b> )	10 (LiINTf <sub>2</sub> )	rt	24 h	<5	-
11	3 ( <b>C</b> )	10 (LiINTf <sub>2</sub> )	80	4 h	91	40:60
<b>12</b>	<b>1 (C)</b>	<b>10 (LiINTf<sub>2</sub>)</b>	<b>80</b>	<b>4 h</b>	<b>90</b>	<b>54:46</b>
				24 h	90	33:67
13	1 ( <b>C</b> )	20 (LiINTf <sub>2</sub> )	80	4 h	93	45:55
14	1 ( <b>C</b> )	5 (LiINTf <sub>2</sub> )	80	7 h	86	28:72
15	1 ( <b>C</b> )	70 (B(C <sub>6</sub> F <sub>5</sub> ) <sub>3</sub> )	rt	2 h	23 <sup>[e]</sup>	57:43
16 <sup>[f]</sup>	1 ( <b>C</b> )	10 (LiINTf <sub>2</sub> )	80	4 h	88	35:65
17 <sup>[g]</sup>	1 ( <b>C</b> )	10 (LiINTf <sub>2</sub> )	80	4 h	88	36:64
18	-	10 (LiINTf <sub>2</sub> )	80	4 h	0	-

[a] All the reactions were carried out in *J. Young* NMR tubes and the additive was pre-activated with 10  $\mu$ L THF-*d*<sub>8</sub>. [b] The yield (<sup>1</sup>H NMR) of **2e** was determined using 1,3,5-trimethoxybenzene as internal standard. [c] THF-*d*<sub>8</sub> as the solvent. [d] CD<sub>3</sub>CN as the solvent. [e] along with 40 % *N*-Boc deprotected product; full conversion of **1e**. [f] 0.2 M of **1e**. [g] 0.4 M of **1e**.

obtained in 96% after 4 h at 80 °C (Table 1, entries 5, 6 and 7). To check the role of the additive, LiNTf<sub>2</sub> was omitted and no reaction was observed after 4 h at 80 °C, which shows that the Lewis acid is essential for the catalytic reaction (Table 1, entry 8). This also explains why the reaction almost stands still when the solvent C<sub>6</sub>D<sub>6</sub> is replaced by THF-d<sub>8</sub> or CD<sub>3</sub>CN, which indicates competitive binding between THF-d<sub>8</sub> or CD<sub>3</sub>CN and the substrate to the Lewis acid co-catalyst (Table 1, entries 9 and 10). Surprisingly, full conversions were also obtained with lower catalyst loadings and 1 mol% catalyst **C** proved sufficient for a fast and selective isomerization (Table 1, entries 11 and 12). Interestingly, the *Z/E* ratio was reversed when extending the reaction time from 4 h to 24 h (with the *Z/E* ratio 54:46 and 33:67, respectively) without influencing the reaction yield, which indicates the transformation of the dynamically favored *Z*-(**2e**) isomer into the thermodynamically favored *E*-(**2e**) isomer. The loadings of the Lewis acid co-catalyst were examined as well. The yield of enamide **2e** improved slightly with 20 mol% LiNTf<sub>2</sub> and a longer reaction time was needed when only 5 mol% Lewis acid were used (Table 1, entries 13 and 14). Usually strong Lewis acids are not compatible with carbamate protecting groups. Nevertheless, we used 70 mol% of B(C<sub>6</sub>F<sub>5</sub>)<sub>3</sub> and found full conversion after 2 h room temperature, but besides 23 % of the product, also 40 % of the deprotected product was obtained (entry 15). Higher aziridine concentrations (0.2 mol/L and 0.4 mol/L, respectively) rarely influence the reaction rate and the desired enamide was obtained in comparable yields (Table 1, entries 16 and 17). Finally, a blank test without rhodium catalyst **C** showed no conversion (Table 1, entry 18). The geometrical selectivity was not so high (*Z/E*), which varied between 54:46 and 28:72. Thus, the optimized reaction conditions (1 mol% **C**, 0.1 M aziridine, C<sub>6</sub>D<sub>6</sub>, 80 °C) were applied to explore the generality of this protocol.

With the optimized conditions in hand, various *N*-Boc terminal aziridines were converted successfully into the desired enamides (Scheme 3). The terminal aziridines **1f** and **1g**, possessing weak electron-withdrawing chloro and bromo substituents on the phenyl ring, were isomerized smoothly to yield the corresponding enamides in excellent yield (94% and 93%, respectively). Interestingly, aziridine **1h** bearing a moderate electron-withdrawing fluoro group was rearranged much slower and full conversion was obtained after 24 h in 95% yield. To confirm this tendency, substrate **1i** bearing a strong electron-withdrawing nitro group was tested. Harsher reaction conditions were required and the reaction can only be completed with 5

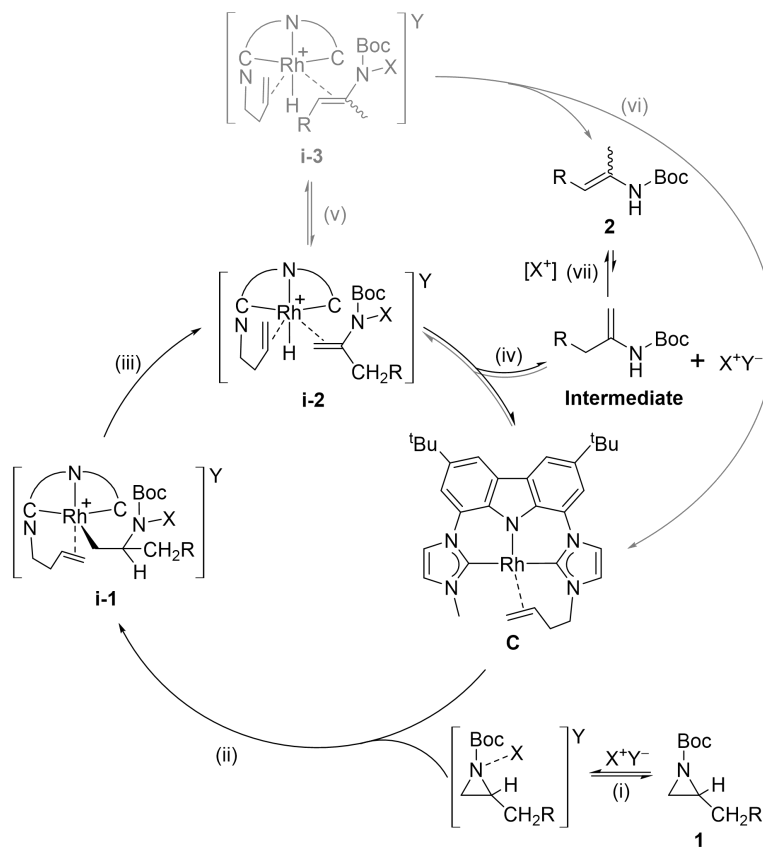
mol% catalyst **C** in 24 h (86% yield for **1i**). Notably, an intermediate bearing a terminal C=C double bond was observed, which is fully rearranged to the desired product. In comparison, aziridine **1j** with a strong electron-donating substituent (methoxy) was converted considerably fast and the reaction was finished in 3 h. The corresponding enamides **2j** were obtained in 95% yield. A closer look at the <sup>1</sup>H NMR spectra monitoring the reaction of the other substrates **1e** and **1h** revealed the formation of the respective intermediates as well. While the isomerization is fast for the substrate with an electron donating substituent (**1j**), it becomes even rate limiting in the case of **1h** (14% left after 18 h) and **1i** bearing electron-withdrawing substituents. To check the feasibility of this novel method for synthetic chemistry, a scaled-up reaction using **1e** (1.3 mmol) and 1 mol% catalyst **C** was prepared and the desired enamide **2e** was isolated by column chromatography in 72% yield with the *Z/E* ratio of 54:46.



**Scheme 3.** Substrate scope of the rhodium-catalyzed isomerization of *N*-Boc terminal aziridines.<sup>[a]</sup> <sup>[a]</sup> The yield of **2** was determined by <sup>1</sup>H NMR against the internal standard 1,3,5-trimethoxybenzene and *Z:E* ratios are given in brackets. <sup>[b]</sup> 0.3 g of **1e** (1.3 mmol) and 1 mol% catalyst **C** used; isolated yield of **2e** in brackets. <sup>[c]</sup> 5 mol% catalyst **C**.

A nucleophilic mechanism for the aziridine isomerization by a palladium(0) catalyst was suggested by the Wolfe group.<sup>[7]</sup> Together with the nucleophilic dual-activation mechanism (substrate pre-activation by a Lewis acid) we have reported for the epoxide isomerization, an analogous mechanism for the aziridines was proposed.<sup>[2b,e]</sup> The fact that the Lewis acid additive and non-coordinating solvents are required indicates a pre-activation of the terminal aziridines (Scheme 4, step (i)). This is

followed by a nucleophilic attack of the 16 e<sup>-</sup> Rh<sup>I</sup> catalyst **C** at the most electrophilic side of the aziridine, which is also the least hindered position in this case (ii) and formation of intermediate **i-1** which is likely stabilized by the Lewis acid as well. Subsequent  $\beta$ -hydride elimination (iii) could lead to the Rh<sup>III</sup> hydrido complex **i-2** which can either release the **Intermediate** by reductive elimination (iv) under regeneration of complex **C** as observed for substrates containing electron withdrawing groups, or isomerize directly to intermediate **i-3** (v) from which the thermodynamically favored product is released by reductive elimination under recovery of catalyst **C** (vi). The isomerization of the **Intermediate** to the product **2** can either occur by re-coordination to the catalyst **C** under formation of the Rh<sup>III</sup> hydrido complex **i-2**, or directly by, e.g. a Lewis acid catalyzed isomerization (vii). As the isomerization rate of step vii is substrate depending and slows down in case of more electron-withdrawing substituents, we assume that this step is Lewis-acid catalyzed. [1,3]-H shifts are thermally forbidden and a resting state that requires the oxidative addition of the **Intermediate** to the nucleophilic catalyst **C** under reformation of the Rh<sup>III</sup> hydrido complex **i-2** would require the breaking of a strong NH bond and thus seems less likely.



**Scheme 4.** Proposed mechanism for the isomerization of terminal aziridines with transition-metal complexes.

## Conclusions

We have presented the selective isomerization of a series of terminal aziridines to yield the desired enamides using the highly reactive nucleophilic rhodium catalyst **C** under moderate conditions. Most of the tested aziridines were converted smoothly with only 1 mol% catalyst loading and excellent yields were obtained. Intermediates containing the terminal C=C double bond were detected during the course of the reaction with substrates containing an electron poor group. The double bond migrates to the internal C=C double bond to complete the reaction. Based on these observations, a dual-activation mechanism including the activation of the substrate by the Lewis acid and the nucleophilic opening by Rh catalyst is proposed. This novel transformation provides an alternative strategy for the synthesis of enamides.

## References

- (1) (a) Meinwald, J.; Labana, S. S.; Chadha, M. S. *J. Am. Chem. Soc.* **1963**, *85*, 582–585. (b) Miyashita, A.; Shimada, T.; Sugawara, A.; Nohira, H. *Chem. Lett.* **1986**, 1323–1326. (c) Kulasegaram, S.; Kulawiec, R. J. *J. Org. Chem.* **1997**, *62*, 6547–6561. (d) Chang, C.-L.; Kumar, M. P.; Liu, R.-S. *J. Org. Chem.* **2004**, *69*, 2793–2796. (e) Robinson, M. W. C.; Pillinger, K. S.; Mabbett, I.; Timms, D. A.; Graham, A. E. *Tetrahedron* **2010**, *66*, 8377–8382. (f) Vyas, D. J.; Larionov, E.; Besnard, C.; Guénée, L.; Mazet, C. *J. Am. Chem. Soc.* **2013**, *135*, 6177–6183. (g) Humbert, N.; Vyas, D. J.; Besnard, C.; Mazet, C. *Chem. Commun.* **2014**, *50*, 10592–10595.
- (2) (a) Eisenmann, J. L. *J. Org. Chem.* **1962**, *27*, 2704–2710. (b) Jürgens, E.; Wucher, B.; Rominger, F.; Törnroos, K. W.; Kunz, D. *Chem. Commun.* **2015**, *51*, 1897–1900. (c) Lamb, J. R.; Jung, Y.; Coates, G. W. *Org. Chem. Front.* **2015**, *2*, 346–349. (d) Tian, Y.; Jürgens, E.; Kunz, D. *Chem. Commun.* **2018**, *54*, 11340–11343. (e) Tian, Y.; Jürgens, E.; Mill, K.; Jordan, R.; Maulbetsch, T.; Kunz, D. *ChemCatChem* **2019**, *11*, 4028–4035.
- (3) (a) Sweeney, J. B. *Chem. Soc. Rev.* **2002**, *31*, 247–258. (b) Huang, C.-Y.; Doyle, A. G. *Chem. Rev.* **2014**, *114*, 8153–8198.
- (4) (a) Alper, H.; Urso, F.; Smith, D. J. H. *J. Am. Chem. Soc.* **1983**, *105*, 6737–6738. (b) Chamchaang, W.; Pinhas, A. R. *J. Org. Chem.* **1990**, *55*, 2943–2950. (c) Piotti, M. E.; Alper, H. *J. Am. Chem. Soc.* **1996**, *118*, 111–116. (d) Ardura, D.; López, R.;

- Sordo, T. L. *J. Org. Chem.* **2006**, *71*, 7315–7321. (e) Pitts, C. R.; Lectka, T. *Chem. Rev.* **2014**, *114*, 7930–7953.
- (5) (a) Lin, B. L.; Clough, C. R.; Hillhouse, G. L. *J. Am. Chem. Soc.* **2002**, *124*, 2890–2891. (b) Lu, P. *Tetrahedron* **2010**, *66*, 2549–2560. (c) Huang, C.-Y.; Doyle, A. G. *J. Am. Chem. Soc.* **2012**, *134*, 9541–9544. (d) Takeda, Y.; Kuroda, A.; Sameera, W. M. C.; Morokuma, K.; Minakata, S. *Chem. Sci.* **2016**, *7*, 6141–6152. (e) Yi, H.; Oestreich, M. *Chem. Eur. J.* **2019**, *25*, 6505–6507.
- (6) Sugihara, Y.; Imura, S.; Nakayama, J. *Chem. Commun.* **2002**, 134–135.
- (7) Wolfe, J. P.; Ney, J. E. *Org. Lett.* **2003**, *5*, 4607–4610.
- (8) Cabré, A.; Sciortino, G.; Ujaque, G.; Verdaguer, X.; Lledós, A.; Riera, A. *Org. Lett.* **2018**, *20*, 5747–5751.
- (9) (a) Burk, M. J.; Casy, G.; Johnson, N. B. *J. Org. Chem.* **1998**, *63*, 6084–6085. (b) Zhang, Z.; Zhu, G.; Jiang, Q.; Xiao, D.; Zhang, X. *J. Org. Chem.* **1999**, *64*, 1774–1775. (c) Chen, J.; Zhang, W.; Geng, H.; Li, W.; Hou, G.; Lei, A.; Zhang, X. *Angew. Chem. Int. Ed.* **2009**, *48*, 800–802. (d) Nugent, T. C.; El-Shazly, M. *Adv. Synth. Catal.* **2010**, *352*, 753–819. (e) Zhu, S.-F.; Liu, T.; Yang, S.; Song, S.; Zhou, Q.-L. *Tetrahedron* **2012**, *68*, 7685–7690. (f) Liu, G.; Liu, X.; Cai, Z.; Jiao, G.; Xu, G.; Tang, W. *Angew. Chem. Int. Ed.* **2013**, *52*, 4235–4238.
- (10) (a) Tschaen, D. M.; Abramson, L.; Cai, D.; Desmond, R.; Dolling, U.-H.; Frey, L.; Karady, S.; Shi, Y.-J.; Verhoeven, T. R. *J. Org. Chem.* **1995**, *60*, 4324–4330. (b) Dupau, P.; Le Gendre, P.; Bruneau, C.; Dixneuf, P. H. *Synlett* **1999**, 1832–1834.
- (11) (a) Takuji, O.; Toshiyuki, K.; Kazuo, H.; Hitomi, S. *Chem. Lett.* **1991**, *20*, 1443–1446. (b) Shen, R.; Porco, J. A. *Org. Lett.* **2000**, *2*, 1333–1336. (c) Jiang, L.; Job, G. E.; Klapars, A.; Buchwald, S. L. *Org. Lett.* **2003**, *5*, 3667–3669. (d) Coleman, R. S.; Liu, P.-H. *Org. Lett.* **2004**, *6*, 577–580. (e) Wallace, D. J.; Klauber, D. J.; Chen, C.-y.; Volante, R. P. *Org. Lett.* **2003**, *5*, 4749–4752. (f) Klapars, A.; Campos, K. R.; Chen, C.-y.; Volante, R. P. *Org. Lett.* **2005**, *7*, 1185–1188.
- (12) Wang, L.; Neumann, H.; Spannenberg, A.; Beller, M. *Chem. Eur. J.* **2018**, *24*, 2164–2172.
- (13) Villa, R.; Mandel, A. L.; Jones, B. D.; La Clair, J. J.; Burkart, M. D. *Org. Lett.* **2012**, *14*, 5396–5399.
- (14) Chong, H.-S.; Song, H. A.; Dadwal, M.; Sun, X.; Sin, I.; Chen, Y. *J. Org. Chem.* **2010**, *75*, 219–221.
- (15) Wessig, P.; Schwarz, J. *Synlett* **1997**, 893–894.



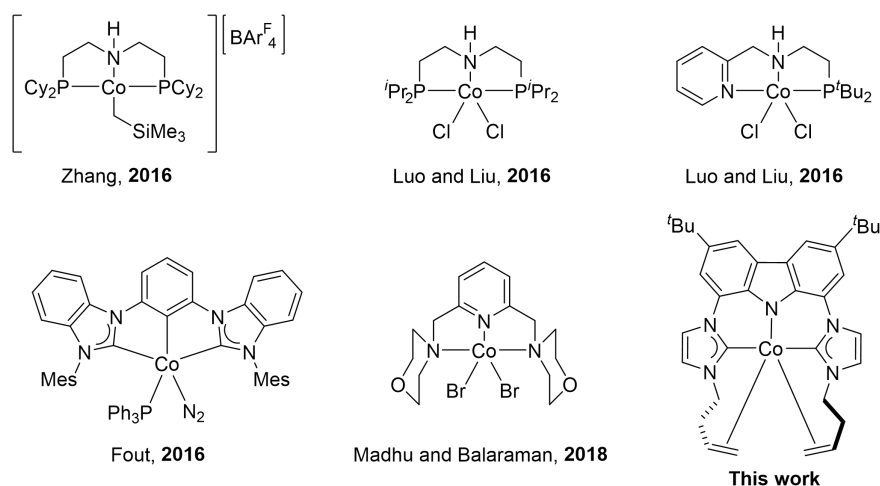
## Chapter 5

## Semihydrogenation of Alkynes

(Unpublished results)

## Introduction

C=C double bonds are among the most valuable functional groups in organic chemistry and the semihydrogenation of alkynes represents the most straightforward strategy to form alkenes.<sup>[1]</sup> Since the reduction of C≡C triple bonds to alkenes may potentially lead to the formation of (*E*)- or (*Z*)-alkenes as well as saturated hydrocarbons *via* over-reduction, it remains a great challenge to control the chemo- and stereoselectivity of this reaction.<sup>[2]</sup> Concerning the stereoselectivity of the reaction, recent examples showed that (*E*)-alkenes were mainly delivered due to secondary isomerization processes<sup>[3]</sup>, except in some cases.<sup>[4]</sup> Therefore, the development of new and selective homogeneous semihydrogenation catalysts that are able to produce (*Z*)-alkenes exclusively would still be of great advantages.



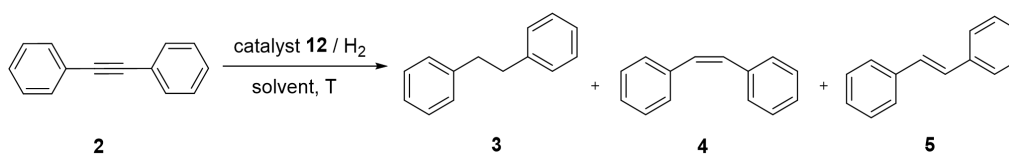
**Figure 1.** The semihydrogenation of alkynes with well-defined cobalt complexes.

The semihydrogenation of alkynes based on transition-metals has experienced a great development in the last decade. The major investigations have focused on noble metals such as Pd,<sup>[5]</sup> Ru,<sup>[6]</sup> Rh,<sup>[7]</sup> Au,<sup>[8]</sup> and Ir<sup>[9]</sup>, however, the number of well-defined catalysts that apply H<sub>2</sub> as the hydrogen source directly is surprisingly low.<sup>[10]</sup>

Although several cobalt complexes have been confirmed to be efficient catalysts for this reaction, only one report from the Fout group studied the semihydrogenation of internal alkynes using bis(NHC) cobalt catalyst (Figure 1).<sup>[10]</sup> To continue our interest in homogeneous catalysis with an array of the successfully generated  $[M(\text{bimca})^{\text{Homo}}]$  complexes,<sup>[11]</sup> we decided to investigate the semihydrogenation of alkynes with the novel  $\text{C}_{\text{NHC}}\text{NC}_{\text{NHC}}$ -pincer Co(I)-complex (**1**).

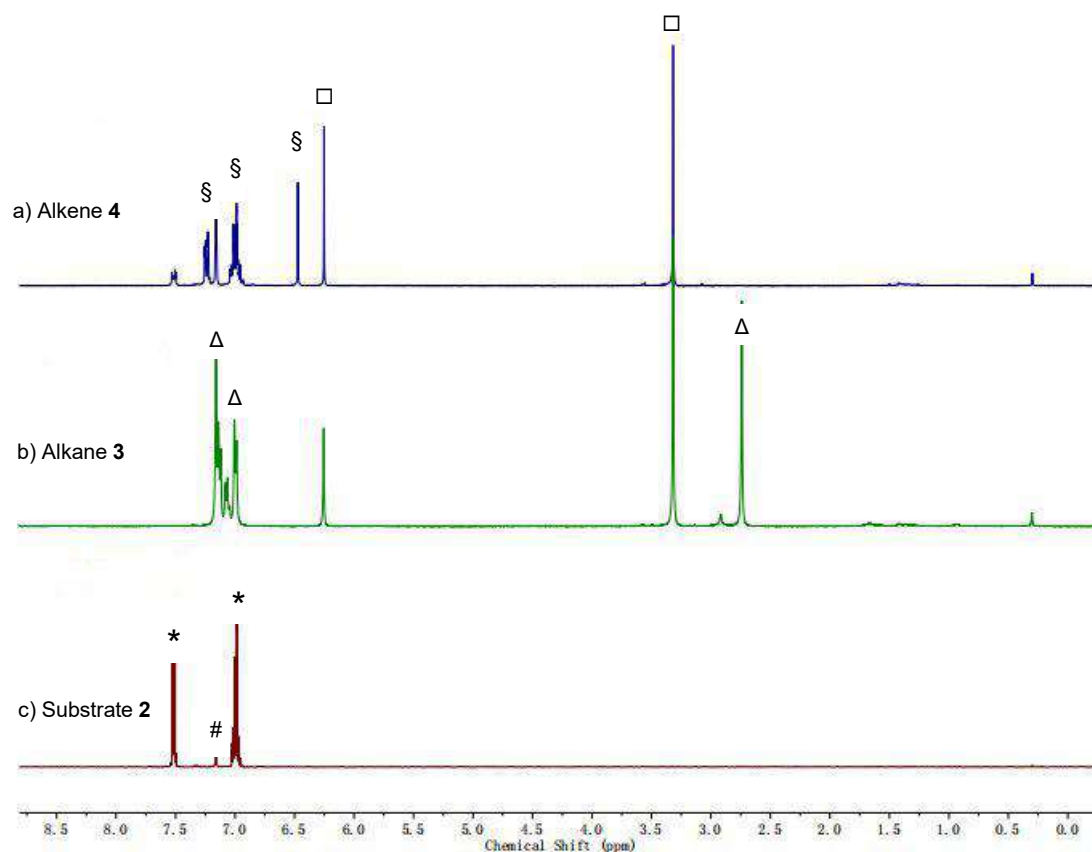
### Semihydrogenation of Internal Alkynes

We tested the semihydrogenation of internal alkynes with 1,2-diphenylethyne (**2**) as the model substrate. An initial test applying 10 mol% of **1** with 4 bar  $\text{H}_2$  in  $\text{C}_6\text{D}_6$  only yielded over-reduced product **3** at 80 °C (Table 1, entry 1). The reaction was improved with lower hydrogen pressures and the desired product **4** was obtained exclusively with 1 bar  $\text{H}_2$  (Table 1, entries 2 and 3). Extending the reaction time to 72 h increased the conversion slightly (Table 1, entry 4). A lower temperature would lead to the generation of **4** and a better result was obtained at 50 °C with a ratio of 26 : 74 (**3** : **4**) (Table 1, entries 5 and 6). Afterward, different solvents were tested. Interestingly, almost the reverse ratio of **3** : **4** was gained when the coordinated solvent THF- $d_8$  was used instead of  $\text{C}_6\text{D}_6$ , and no reactions were observed with  $\text{CD}_3\text{OD}$  or  $\text{CD}_3\text{CN}$  as the solvent (Table 1, entries 7-9). Reasonably, lower conversion was obtained when the reaction took place at 40 °C (Table 1, entry 10). Increasing the hydrogen pressure from 4 bar to 8 bar at 40 °C resulted in the formation of the (*Z*)-alkene (**4**), however over-reduced product was mainly formed with 10 bar  $\text{H}_2$  (Table 1, entries 11-13). The over-reduction may result from the transformation of the desired product **4** to the alkane **3**, thus the reaction mixture was analyzed after 16 h at 10 bar  $\text{H}_2$ . To our delight, the ratio of **3** and **4** was reversed and **4** was obtained as the main product (Table 1, entry 14). To prohibit over-reduction, a lower catalyst loading was applied. Surprisingly, the desired (*Z*)-1,2-diphenylethene (**4**) was obtained exclusively in 75% yield (Table 1, entry 15). For comparison, the  $^1\text{H}$  NMR spectra of substrate **2**, the generated alkane **3** and the (*Z*)-alkene **4** are presented in Figure 2. Further modification of the reaction conditions was not undertaken because of time reasons.

**Table 1.** The semihydrogenation of 1,2-diphenylethyne (**2**): Optimization of the reaction conditions.<sup>[a]</sup>

Entry	[Co]	H <sub>2</sub>	Solvent	T (°C)	Time	<b>3</b> : <b>4</b> : <b>5</b>	Conv.
1	10 mol%	4 bar	C <sub>6</sub> D <sub>6</sub>	80 °C	24 h	100 : - : -	100%
2	10 mol%	2 bar	C <sub>6</sub> D <sub>6</sub>	80 °C	24 h	91 : 9 : -	94%
3	10 mol%	1 bar	C <sub>6</sub> D <sub>6</sub>	80 °C	24 h	- : 100 : -	40%
4	10 mol%	1 bar	C <sub>6</sub> D <sub>6</sub>	80 °C	72 h	- : 100 : -	45%
5	10 mol%	4 bar	C <sub>6</sub> D <sub>6</sub>	60 °C	24 h	100 : - : -	93%
6	10 mol%	4 bar	C <sub>6</sub> D <sub>6</sub>	50 °C	24 h	26 : 74 : -	67%
7	10 mol%	4 bar	THF-d <sub>8</sub>	50 °C	24 h	72 : 28 : -	73%
8	10 mol%	4 bar	CD <sub>3</sub> OD	50 °C	24 h	-	NR
9	10 mol%	4 bar	CD <sub>3</sub> CN	50 °C	24 h	-	NR
10	10 mol%	4 bar	C <sub>6</sub> D <sub>6</sub>	40 °C	24 h	- : 100 : -	25%
11	10 mol%	6 bar	C <sub>6</sub> D <sub>6</sub>	40 °C	24 h	- : 100 : -	54%
12	10 mol%	8 bar	C <sub>6</sub> D <sub>6</sub>	40 °C	24 h	- : 100 : -	58%
13	10 mol%	10 bar	C <sub>6</sub> D <sub>6</sub>	40 °C	24 h	87 : 13 : -	100%
14	10 mol%	10 bar	C <sub>6</sub> D <sub>6</sub>	40 °C	16 h	29 : 71 : -	67%
15	5 mol%	10 bar	C <sub>6</sub> D <sub>6</sub>	40 °C	24 h	- : 100 : -	76% (75%) <sup>[b]</sup>

[a] All the reactions were carried out in high pressure *J. Young* NMR tubes. [b] In the brackets was the yield of **4** calibrated to 1,3,5-trimethoxybenzene (internal standard) with <sup>1</sup>H NMR.



**Figure 2.** a) Substrate **2** (\*) in C<sub>6</sub>D<sub>6</sub> (C<sub>6</sub>HD<sub>5</sub>: #). b) The generated alkane **3** (Δ) with the reaction conditions of entry 1 in table 1. c) The generated (Z)-alkane **4** (§) with the reaction conditions of entry 15 in table 1 with 1,3,5-trimethoxybenzene (□) as the internal standard.

### Semihydrogenation of Terminal Alkynes

Similarly, the semihydrogenation of terminal alkynes with ethynylbenzene (**6**) as the model substrate was explored. An initial test applying 10 mol% of cobalt catalyst **1** with 4 bar H<sub>2</sub> in C<sub>6</sub>D<sub>6</sub> was tested and the desired product styrene **8** was obtained without over-reduction with the conversion of 32% (Table 2, entry 1). To increase the conversion, the reaction time was extended to 7 days. To our delight, the reaction was completed with a ratio of 1 to 99 (**7** and **8**) (Table 2, entry 2). We supposed that the reaction rate would be even faster if it was rotated. Thus the NMR tube was rotated with an evaporator rotary. Unfortunately, no improvement was made (Table 2, entry 3). Increasing the hydrogen pressure from 4 bar to 10 bar resulted in the formation of more over-reduced alkane product. (Table 2, entries 4-6). Surprisingly, a much better result was obtained with 5 mol% catalyst loading and the desired styrene **8** was generated in 73% yield (Table 2, entry 7). For comparison, the <sup>1</sup>H NMR spectra of substrate **6** and the generated styrene **8** are presented in Figure 3. Further modification of the reaction conditions was not undertaken because of time reasons.

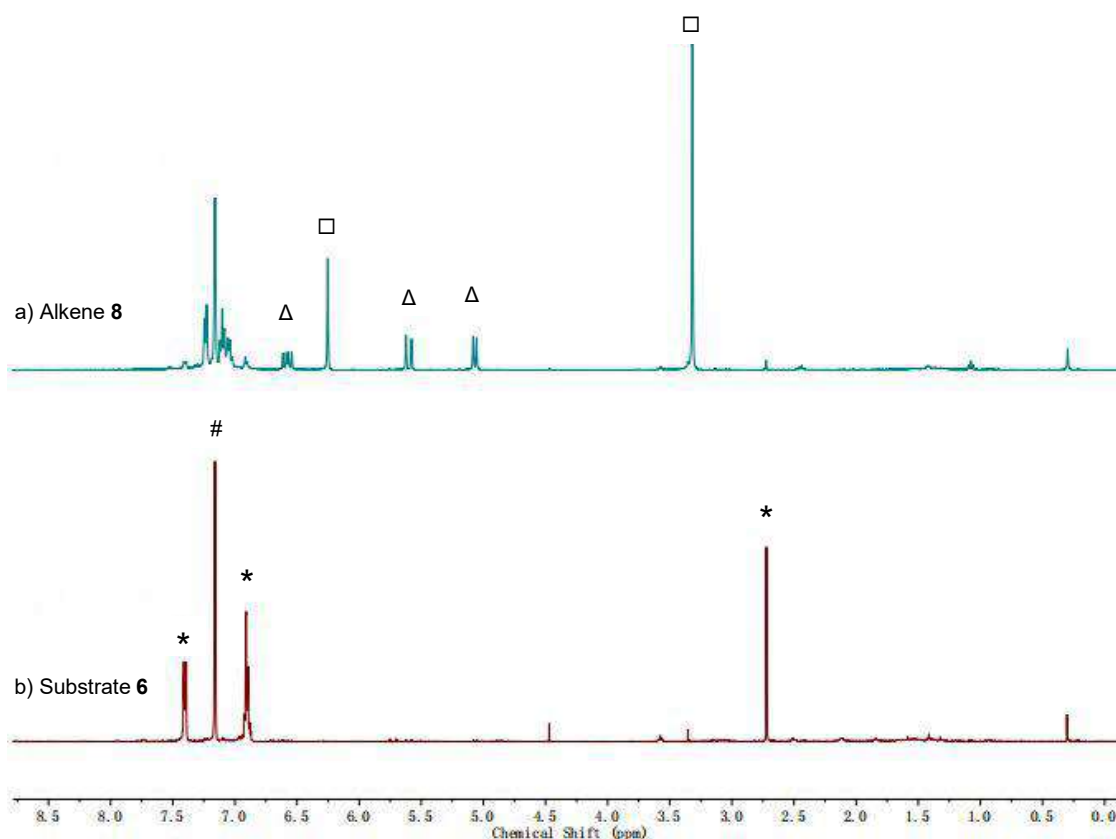
**Table 2.** The semihydrogenation of ethynylbenzene (**6**): Optimization of the reaction conditions.<sup>[a]</sup>

c1ccc(cc1)C#C  $\xrightarrow[\text{solvent, 80 } ^\circ\text{C}]{\text{catalyst 1 / H}_2}$  c1ccc(cc1)CC + c1ccc(cc1)C=C

**6** **7** **8**

Entry	[Co]	H <sub>2</sub>	Time	<b>38 : 39</b>	Conv.
1	10 mol%	4 bar	24 h	- : 100	32%
2	10 mol%	4 bar	7 d	1 : 99	100%
3 <sup>[b]</sup>	10 mol%	4 bar	7 d	1 : 99	100%
4	10 mol%	6 bar	24 h	13 : 87	69%
5	10 mol%	8 bar	24 h	13 : 87	62%
6	10 mol%	10 bar	24 h	35 : 65	100%
7	5 mol%	10 bar	24 h	7 : 93	89% (73%) <sup>[c]</sup>

[a] All the reactions were carried out in high pressure *J. Young* NMR tubes. [b] The reaction was rotated with an evaporator rotary. [c] In the brackets was the yield of **8** calibrated to 1,3,5-trimethoxybenzene (internal standard) with <sup>1</sup>H NMR.



**Figure 3.** a) Substrate **6** (\*) in C<sub>6</sub>D<sub>6</sub> (C<sub>6</sub>HD<sub>5</sub>: #). b) The generation of styrene **8** (Δ) with the reaction conditions of entry 7 in table 2 with 1,3,5-trimethoxybenzene (□) as the internal standard.

## Conclusions

With the novel cobalt complex **1**, the semihydrogenation of both internal and terminal alkynes using **2** and **6** as the model substrates was studied. Excellent selectivity was achieved from **2** to generate exclusively (*Z*)-alkene **4** under very mild conditions in 75% yield. In the case of terminal alkyne **6**, elevated temperature was needed and the desired product **8** was obtained in 73% yield with very good selectivity as well. The results are extremely promising.

## Experimental procedure

In an argon-filled glovebox a *J. Young* NMR tube was charged with a solution of the alkyne (40  $\mu\text{mol}$ ), catalyst **1** (*x* mol%) and a certain amount of the internal standard (1,3,5-trimethoxybenzene) in  $\text{C}_6\text{D}_6$  (0.4 mL). The tube was sealed, brought outside of the glovebox, and attached to a Schlenk line. After a freeze-pump-thaw cycle with liquid nitrogen, the tube was charged with  $\text{H}_2$  (*x* bar) at room temperature. The reaction mixture was heated at the given temperature and analyzed by  $^1\text{H}$  NMR spectroscopy.

## References

- (1) Oger, C.; Balas, L.; Durand, T.; Galano, J. M. *Chem. Rev.* **2013**, *113*, 1313–1350.
- (2) Swamy, K. C. K.; Reddy, A. S.; Sandeep, K.; Kalyani, A. *Tetrahedron Lett.* **2018**, *59*, 419–429.
- (3) (a) Srimani, D.; Diskin-Posner, Y.; Ben-David, Y.; Milstein, D. *Angew. Chem. Int. Ed.* **2013**, *52*, 14131–14134. (b) Karunananda, M. K.; Mankad, N. P. *J. Am. Chem. Soc.* **2015**, *137*, 14598–14601. (c) Tokmic, K.; Fout, A. R. *J. Am. Chem. Soc.* **2016**, *138*, 13700–13705. (d) Higashida, K.; Mashima, K. *Chem. Lett.* **2016**, *45*, 866–868.
- (4) (a) Fürstner, A. *J. Am. Chem. Soc.* **2019**, *141*, 11–24. (b) Radkowski, K.; Sundararaju, B.; Fürstner, A. *Angew. Chem. Int. Ed.* **2013**, *52*, 355–360. (c) Leutzsch, M.; Wolf, L. M.; Gupta, P.; Fuchs, M.; Thiel, W.; Farès, C.; Fürstner, A. *Angew. Chem. Int. Ed.* **2015**, *54*, 12431–12436. (d) Schleyer, D.; Niessen, H. G.; Bargon, J. *New J. Chem.* **2001**, *25*, 423–426.
- (5) (a) Shirakawa, E.; Otsuka, H.; Hayashi, T. *Chem. Commun.* **2005**, 5885–5886. (b) Hauwert, P.; Maestri, G.; Sprengers, J. W.; Catellani, M.; Elsevier, C. J. *Angew. Chem. Int. Ed.* **2008**, *47*, 3223–3226. (c) Shen, R.; Chen, T.; Zhao, Y.; Qiu, R.; Zhou,

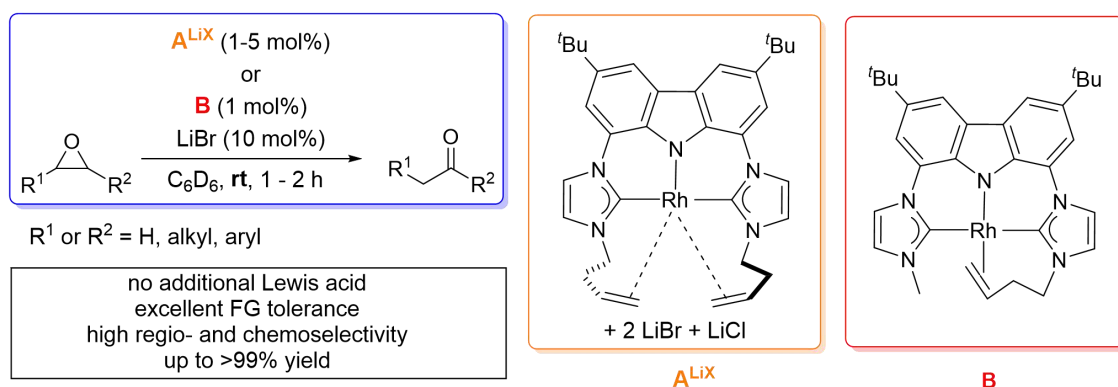
- Y.; Yin, S.; Wang, X.; Goto, M.; Han, L. *J. Am. Chem. Soc.* **2011**, *133*, 17037–17044.
- (d) Li, J.; Hua, R.; Liu, T. *J. Org. Chem.* **2010**, *75*, 2966–2970. (e) Verho, O.; Zheng, H.; Gustafson, K. P. J.; Nagendiran, A.; Zou, X.; Bäckvall, J.-E. *ChemCatChem* **2016**, *8*, 773–778. (f) Lu, Y.; Feng, X.; Takale, B. S.; Yamamoto, Y.; Zhang, W.; Bao, M. *ACS Catal.* **2017**, *7*, 8296–8303. (g) Furukawa, S.; Komatsu, T. *ACS Catal.* **2016**, *6*, 2121–2125. (h) Maazaoui, R.; Abderrahim, R.; Chemla, F.; Ferreira, F.; Perez-Luna, A.; Jackowski, O. *Org. Lett.* **2018**, *20*, 7544–7549.
- (6) (a) Guthertz, A.; Leutzsch, M.; Wolf, L. M.; Gupta, P.; Rummelt, S. M.; Goddard, R.; Fares, C.; Thiel, W.; Fürstner, A. *J. Am. Chem. Soc.* **2018**, *140*, 3156–3169. (b) Kusy, R.; Grela, K. *Org. Lett.* **2016**, *18*, 6196–6199. (c) Neumann, K. T.; Klimczyk, S.; Burhardt, M. N.; Bang-Andersen, B.; Skrydstrup, T.; Lindhardt, A. T. *ACS Catal.* **2016**, *6*, 4710–4714. (d) Radkowski, K.; Sundararaju, B.; Fürstner, A. *Angew. Chem. Int. Ed.* **2013**, *52*, 355–360. (e) Michaelides, I. N.; Dixon, D. J. *Angew. Chem. Int. Ed.* **2013**, *52*, 806–808. (f) Li, J.; Hua, R. *Chem. Eur. J.* **2011**, *17*, 8462–8465. (g) Musa, S.; Ghosh, A.; Vaccaro, L.; Ackermann, L.; Gelman, D. *Adv. Synth. Catal.* **2015**, *357*, 2351–2357. (h) Karunananda, M. K.; Mankad, N. P. *J. Am. Chem. Soc.* **2015**, *137*, 14598–14601.
- (7) (a) Jagtap, S. A.; Bhanage, B. M. *ChemistrySelect* **2018**, *3*, 713–718. (b) Furukawa, S.; Yokoyama, A.; Komatsu, T. *ACS Catal.* **2014**, *4*, 3581–3585.
- (8) (a) Fiorio, J. L.; Gonçalves, R. V.; Teixeira-Neto, E.; Ortuño, M. A.; López, N.; Rossi, L. M. *ACS Catal.* **2018**, *8*, 3516–3524. (b) Wagh, Y. S.; Asao, N. *J. Org. Chem.* **2015**, *80*, 847–851.
- (9) (a) Tani, K.; Iseki, A.; Yamagata, T. *Chem. Commun.* **1999**, 1821–1822. (b) Yang, J.; Wang, C.; Sun, Y.; Man, X.; Li, J.; Sun, F. *Chem. Commun.* **2019**, *55*, 1903–1906.
- (10) (a) Konnerth, H.; Prechtel, M. H. G. *Chem. Commun.* **2016**, *52*, 9129–9132. (b) Richmond, E.; Moran, J. *J. Org. Chem.* **2015**, *80*, 6922–6929. (c) Wen, X.; Shi, X.; Qiao, X.; Wu, Z.; Bai, G. *Chem. Commun.* **2017**, *53*, 5372–5375. (d) Barrios-Francisco, R.; Garcia, J. *J. Inorg. Chem.* **2009**, *48*, 386–393. (e) Chen, C.; Huang, Y.; Zhang, Z.; Dong, X.; Zhang, X. *Chem. Commun.* **2017**, *53*, 4612–4615. (f) Chen, F.; Kreyenschulte, C.; Radnik, J.; Lund, H.; Surkus, A. -E.; Junge, K.; Beller, M. *ACS Catal.* **2017**, *7*, 1526–1532. (g) Zhang, G.; Yin, Z.; Tan, J. *RSC Adv.* **2016**, *6*, 22419–22423. (h) Landge, V.; Pitchaimani, J.; Midya, S.; Subaramanian, M.; Madhu, V.; Balaraman, E. *Catal. Sci. Technol.* **2018**, *8*, 428–433. (i) Tokmic, K.; Fout, A. R. *J. Am. Chem. Soc.* **2016**, *138*, 13700–13705. (j) Fu, S.; Chen, N.; Liu, X.; Shao, Z.; Luo,

S.; Liu, Q. *J. Am. Chem. Soc.* **2016**, *138*, 8588–8594. (k) Srimani, D.; Diskin-Posner, Y.; Ben-David, Y.; Milstein, D. *Angew. Chem. Int. Ed.* **2013**, *52*, 14131–14134. (l) Bart, S. C.; Lobkovsky, E.; Chirik, P. J. *J. Am. Chem. Soc.* **2004**, *126*, 13794–13807. (m) Wienhçfer, G.; Westerhaus, F. A.; Jagadeesh, R. V.; Junge, K.; Junge, H.; Beller, M.; *Chem. Commun.* **2012**, *48*, 4827–4829. (n) Wei, D.; Darcel, C. *Chem. Rev.* **2019**, *119*, 2550–2610. (o) Gorgas, N.; Brünig, J.; Stöger, B.; Vanicek, S.; Tilset, M.; Veiros, L. F.; Kirchner, K. *J. Am. Chem. Soc.* **2019**, *141*, 17452–17458. (p) Kaeffer, N.; Liu, H.; Lo, H.-K.; Fedorov, A.; Copéret, C. *Chem. Sci.* **2018**, *9*, 5366–5371. (q) Wakamatsu, T.; Nagao, K.; Ohmiya, H.; Sawamura, M. *Organometallics* **2016**, *35*, 1354–1357. (r) Fedorov, A.; Liu, H.; Lo, H. -K.; Copéret, C. *J. Am. Chem. Soc.* **2016**, *138*, 16502–16507. (s) Brzozowska, A.; Azofra, L. M.; Zubar, V.; Atodiresei, I.; Cavallo, L.; Rueping, M.; El-Sepelgy, O. *ACS Catal.* **2018**, *8*, 4103–4109. (t) Zhou, Y.; Mo, Z.; Luecke, M. P.; Driess, M. *Chem. Eur. J.* **2018**, *24*, 4780–4784. (11) Tian, Y.; Maulbetsch, T.; Jordan, R.; Törnroos, K. W.; Kunz, D. *Organometallics*, **2020**, *39*, 1221-1229.



## Summary

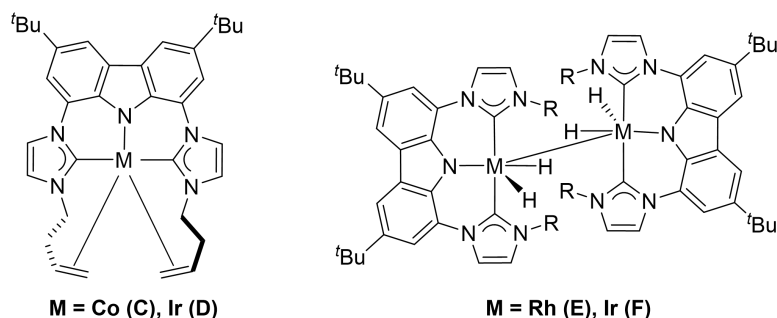
The novel  $C_{NHC}NC_{NHC}$ -pincer rhodium complexes (**A** and **B**), bearing two homoallyl moieties and one homoallyl moiety, were generated successfully. Afterward, the regio- and chemoselective isomerization of various epoxides was tested. A wide array of functionalized epoxides was tolerant with the Rh-catalyst systems and the desired methyl ketones were generated almost exclusively from terminal epoxides with excellent yields under very mild conditions, especially for  $\alpha$ -aryl oxiranes. D/H exchange experiments provide strong evidence for a  $\beta$ -hydride elimination/reductive elimination pathway via a hydrido-Rh intermediate for the Rh-catalyzed nucleophilic Meinwald reaction. Moreover, combining the Johnson-Corey-Chaykovsky epoxidation with the isomerization would provide a very mild and oxidation-free transformation of aldehydes into methyl ketones (Scheme 1).



**Scheme 1.** Catalytic isomerization of epoxides with Rh-catalysts.

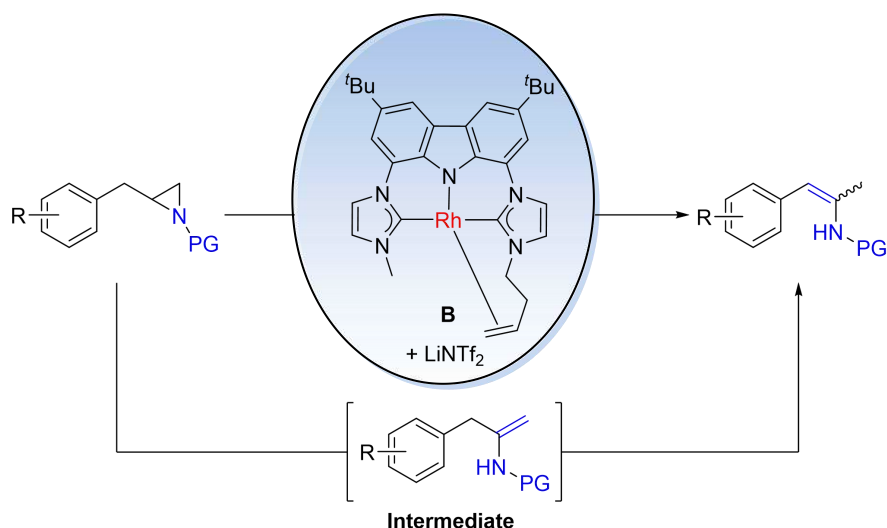
The air and moisture sensitive cobalt(I) complex (**C**), based on the pentadentate pincer bis-NHC ligand  $bimca^{Homo}$ , was successfully synthesized by two different pathways and characterized with X-ray analysis and NMR spectroscopy. In addition, the corresponding iridium complex (**D**) was generated as well. In contrast to the highly reactive rhodium analogue (**A**), complexes **C** and **D** were much less active in the nucleophilic epoxide isomerization. When the reaction was carried out in presence of 1 bar  $H_2$  an increased activity was observed, however, on the cost of side reactions. Furthermore, the hydrogenation of the *N*-homoallyl to *N*-*n*-butyl substituents in complexes **A** and **D**, and the formation of hydrido pincer complexes (**E**

and **F**) under these conditions were confirmed with X-ray structure analyses (Figure 1).



**Figure 1.** Left: Cobalt and iridium complexes (**C** and **D**) with the bimca<sup>Homo</sup> ligand. Right: The products (**E** and **F**) from the hydrogenation of complexes (**A** and **D**).

The selective isomerization of aziridines, which is analogous to epoxides, was studied with the highly active Rh-catalyst **B**. The reaction proceeds smoothly with only 1 mol% catalyst loading and excellent yields of enamides were achieved. An intermediate containing an enamide with a non-conjugated terminal C=C double bond was detected during the course of the reaction, which isomerizes to form the thermodynamically favored 2-amido styrene. A plausible mechanism was proposed based on these observations (Scheme 2).



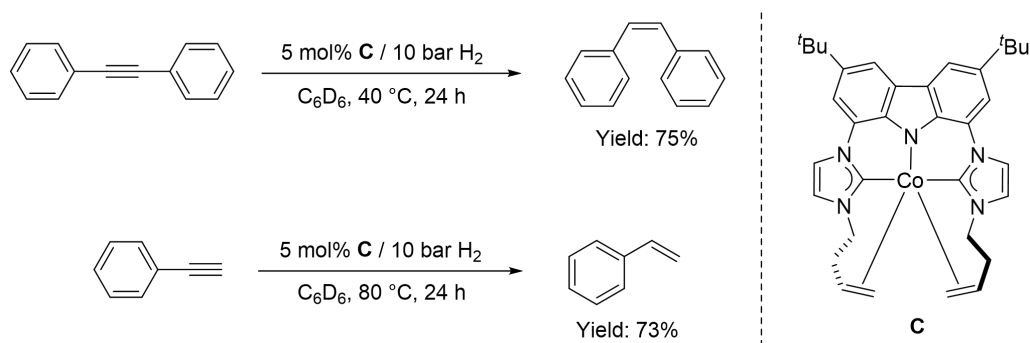
**Scheme 2.** Catalytic isomerization of various terminal aziridines into enamides.

With the novel cobalt(I) complex **C**, the semihydrogenation of both internal and terminal alkynes using 1,2-diphenylethyne and ethynylbenzene as the model

## Summary

---

substrates was studied. Excellent selectivity was achieved with 1,2-diphenylethyne to generate exclusively (*Z*)-1,2-diphenylethene under very mild conditions in 75% yield. In the case of ethynylbenzene, elevated temperature was needed and the desired styrene was obtained in 73% yield with excellent selectivity as well. The results are extremely promising (Scheme 3).



**Scheme 3.** Selective semihydrogenation of both terminal and internal alkynes into olefins.

## Outlook

Considering the successful utilities of group 9 transition-metal complexes based on the substituted bimca ligand in homogeneous catalysis, there is still a great potential for further studies.

First of all, the results for the semihydrogenation of alkynes with the novel  $[\text{Co}(\text{bimca}^{\text{Homo}})]$  complex are extremely promising, thus more efforts should be taken to screen the reaction conditions, broaden the substrate scope and study the mechanism of the reaction.

Next, the hydrogenated complexes  $[\text{Rh}(\text{bimca}^{n\text{-Bu}})(\text{H})_2]_2$  and  $[\text{Ir}(\text{bimca}^{n\text{-Bu}})(\text{H})_2]_2$  should be isolated. As the generation of alcohols was observed in the Meinwald rearrangement when 1 bar  $\text{H}_2$  was present, the hydrogenated complexes should be tested on the hydrogenation of ketones, aldehydes and other compounds containing unsaturated bonds.

Moreover, the reported  $[\text{Rh}(\text{bimca}^{\text{Homo}})]$  and  $[\text{Rh}(\text{bimca}^{\text{Me,Homo}})]$  complexes are very nucleophilic and they should be tested in other catalytic reactions as well that need a nucleophile to initiate the reaction such as ring opening and ring expansion reactions.

Furthermore, well-defined chiral transition metal complexes are quite rare and attractive. The modification of the bimca ligand should be studied with some chiral substituents to obtain chiral ligands. They can coordinate with transition metals and may be able to catalyze reactions in an asymmetric manner.

## **Publications**

### **Part 1**

Regio- and Chemoselective Rearrangement of Terminal Epoxides into Methyl Alkyl and Aryl Ketones

### **Part 2**

Nucleophilic Isomerization of Epoxides by Pincer-Rhodium Catalysts: Activity Increase and Mechanistic Insights

### **Part 3**

Synthesis and Reactivity of Cobalt(I) and Iridium(I) Complexes Bearing a Pentadentate *N*-Homoallyl Substituted Bis(NHC) Pincer-Ligand

### **Part 4**

Nucleophilic Rh<sup>I</sup> Catalyzed Selective Isomerization of Terminal Aziridines to Enamides



Cite this: *Chem. Commun.*, 2018, 54, 11340

Received 9th August 2018,  
Accepted 18th September 2018

DOI: 10.1039/c8cc06503a

rsc.li/chemcomm

## Regio- and chemoselective rearrangement of terminal epoxides into methyl alkyl and aryl ketones†

Yingying Tian,<sup>1</sup> Eva Jürgens and Doris Kunz<sup>1\*</sup>

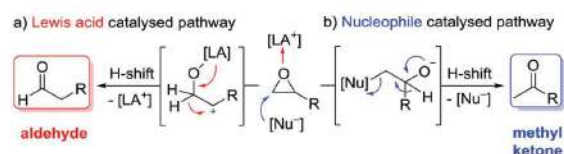
**The development of the highly active pincer-type rhodium catalyst **2** for the nucleophilic Meinwald rearrangement of functionalised terminal epoxides into methyl ketones under mild conditions is presented. An excellent regio- and chemoselectivity is obtained for the first time for aryl oxiranes.**

Epoxides are important intermediates in organic synthesis as they undergo various useful transformations.<sup>1</sup> Among those, the isomerisation to carbonyl compounds (Meinwald reaction) has gained increased attention, and various kinds of catalysts have been reported so far.<sup>2,3</sup> Most abundant is the Lewis acid catalysed isomerisation in which the selectivity is determined by formation of the most stable carbenium intermediate followed by an H-shift that leads to aldehydes as the major product in the case of terminal epoxides (Scheme 1a).<sup>4–6</sup> The inverse selectivity is obtained with nucleophilic catalysts that attack the more electrophilic site (usually the less substituted one) of the epoxide. After rearrangement *via* a formal H-shift, methyl ketones are formed from terminal epoxides (Scheme 1b).<sup>7</sup> This selectivity is very attractive, as it could substitute the Wacker oxidation by a two-step epoxidation-isomerisation sequence for temperature and/or Lewis acid-sensitive olefins.<sup>7d</sup> Moreover, combining the Johnson–Corey–Chaykovsky epoxidation with the isomerisation would provide a very mild and oxidation-free transformation of aldehydes into methyl ketones, which is usually carried out by

addition of a methyl-Grignard reagent to the aldehyde, followed by alcohol oxidation.

So far all nucleophilic Meinwald reactions require a pre-activation of the epoxide by Lewis acids. In the first report in 1962 by Eisenmann,<sup>7a</sup> the Co(II)–Lewis acid co-catalyst and the nucleophilic  $[\text{Co}(\text{CO})_4]^-$  catalyst are formed *in situ* by disproportionation of  $[\text{Co}_2(\text{CO})_8]$  in methanol. A similar principle is likely applicable to the case of Pd-catalysis, in which the Pd(0) catalyst is formed *in situ* from Pd(II).<sup>7e</sup> The presence of the latter can explain the Lewis acid catalysed selectivity in favour of aldehydes in the case of aryl oxiranes. Nucleophiles like iodide and bromide can also serve as catalysts in combination with Lewis acids like  $\text{Li}^+$ <sup>7b–d</sup> or  $\text{Sm}^{2+}$ .<sup>7f</sup> Recently, we have shown that the combination of the nucleophilic Rh-pincer complex **1**<sup>8</sup> (Fig. 1) and  $\text{LiNTf}_2$  is suitable for the regioselective isomerisation of terminal alkyl epoxides to methyl ketones<sup>9</sup> and soon after Coates reported the highly active complex  $[\text{Al}(\text{porphyrin})]^+ [\text{Co}(\text{CO})_4]^-$ .<sup>7g</sup> In both cases, the isomerisation of phenyl oxirane led only to mixtures of phenyl ethanal and phenyl methyl ketone (2 : 3 (Rh), 3 : 2 (Co)), which indicates a competition between the Lewis acidic and the nucleophilic pathway. Therefore, enhancing the selectivity for phenyl oxiranes as well as increasing the activity of the catalyst was the primary goal of our investigations, whose results are reported in the following.

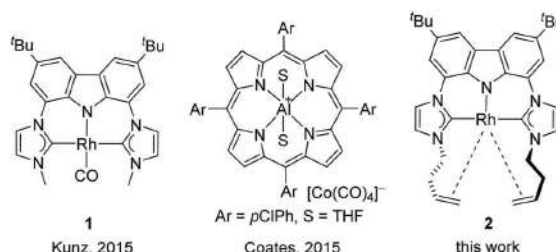
Catalyst **1** requires elevated temperature (60 °C) and a co-catalyst (20 mol%  $\text{LiNTf}_2$ ) to achieve full conversion within 2 h in the



**Scheme 1** Catalytic isomerisation pathways of terminal epoxides: formation of aldehydes versus methyl ketones.<sup>10</sup>

Institut für Anorganische Chemie, Eberhard Karls Universität Tübingen, Auf der Morgenstelle 18, 72076 Tübingen, Germany. E-mail: Doris.Kunz@uni-tuebingen.de

† Electronic supplementary information (ESI) available. See DOI: 10.1039/c8cc06503a



**Fig. 1** Examples of nucleophilic epoxide isomerisation catalysts.



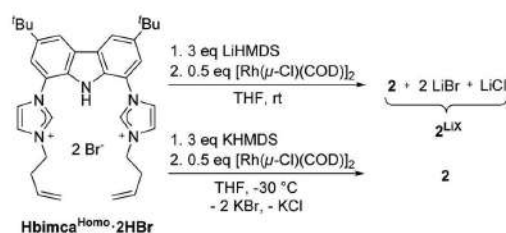
case of terminal alkyl oxiranes.<sup>9</sup> An additional substrate scope (see ESI†) revealed a high functional group tolerance for many substrates, but a substantial drop in conversion and/or yield was recognised. To overcome these drawbacks we supposed that a CO-free Rh-catalyst would further increase the nucleophilicity of the metal centre and thus reduce the need for a Lewis acid co-catalyst. However, all attempts to synthesise a CO-free version of **1** by using  $[\text{Rh}(\mu\text{-Cl})(\text{COD})_2]$  or  $[\text{Rh}(\mu\text{-Cl})(\text{C}_2\text{H}_4)_2]_2$  as starting material failed and revealed a complex product mixture in the NMR spectra. Increasing the steric bulk at the carbene by *N*-iPr groups lead only to a bridged dinuclear complex.<sup>11</sup> Therefore, we tried to reversibly coordinate olefin moieties intramolecularly, which could also stabilise the complex during catalysis and increase its lifetime.

We found the earlier reported *N*-homoallyl substituted ligand **bimca**<sup>Homo</sup><sup>12</sup> to fulfil these criteria (Scheme 2). Preparation of **2** was achieved by deprotonation of **Hbimca**<sup>Homo</sup>-2HBr with LiHMDS and subsequent addition of  $[\text{Rh}(\mu\text{-Cl})(\text{COD})_2]$ . Removal of COD *in vacuo* yielded **2** along with LiBr and LiCl quantitatively. As the lithium salts turned out to be necessary for the catalytic activity of **2** (*vide infra*), we did not remove them, but used this mixture **2**<sup>Lix</sup> for catalysis. To obtain the pure complex **2**, we transmetalated from the potassium complex  $[\text{K}(\text{bimca}^{\text{Homo}})]$  generated *in situ* by deprotonation of **Hbimca**<sup>Homo</sup>-2HBr with KHMDS.<sup>13</sup> The potassium halides formed were readily removed by filtration.

The molecular structure of **2** (Fig. 2) is revealed by NMR spectroscopic analysis and DFT calculations. The single signal set confirms a symmetric coordination mode of the ligand. Coordination of both double bonds and both carbene moieties to the Rh-centre is confirmed not only by the up-field shift of the respective signals in the <sup>13</sup>C NMR spectrum to 185.5 ppm (carbene), 55.9 (C15) and 51.1 ppm (C14), but also by the <sup>1</sup>J<sub>RhC</sub>

coupling of 33.9 (carbene), 6.7 (C15) and 11.3 Hz (C14). DFT calculations also predict a pentacoordinating ligand with both olefin moieties contributing to the trigonal bipyramidal coordination mode at the Rh centre and an orientation in line with the trigonal base.<sup>14</sup> The four <sup>1</sup>H NMR signals for the methylene protons (H-12, H-13) of the homoallyl moiety were assigned according to their coupling constants and NOE to the axial and equatorial protons of the six membered metallacycles. The signals of the olefinic protons are strongly shielded (4.18–4.10 (H-14), 2.41 (H-15<sub>cis</sub>), 1.67 ppm (H-15<sub>trans</sub>)) and the reduced coupling constants of only 8.0 (*cis*) and 9.9 Hz (*trans*) can be explained by the reduced *s*-character due to the coordination with the Rh-centre.

With the rhodium complex **2** in hand, we tested the isomerisation of 1,2-epoxyhexane (**3b**) as the model substrate. An initial test applying 5 mol% of complex **2**<sup>Lix</sup> in THF-*d*<sub>8</sub> revealed only low conversion at room temperature (Table 1, entry 1), which improved by raising the reaction temperature to 60 °C and adding LiNTf<sub>2</sub> as co-catalyst (Table 1, entry 2). Interestingly, full regioselectivity and quantitative yields were obtained in short reaction times at room temperature when toluene-*d*<sub>8</sub> (3 h) or C<sub>6</sub>D<sub>6</sub> (2 h) were used as solvent (Table 1, entries 3 and 4). We suppose that the poor conversion in THF-*d*<sub>8</sub> derives from competitive binding between THF and the substrate to the Lewis acid co-catalyst.<sup>15</sup> To test whether the residual lithium halides are still necessary as a Lewis acid co-catalyst we applied the isolated catalyst **2** in C<sub>6</sub>D<sub>6</sub>. No catalytic activity was found under these conditions (Table 1, entry 5). Surprisingly, addition of 10 mol% of LiBr achieved no improvement, but small amounts of THF (20 μL) restored the catalytic activity fully,



Scheme 2 Synthesis of the rhodium pincer complex **2**.

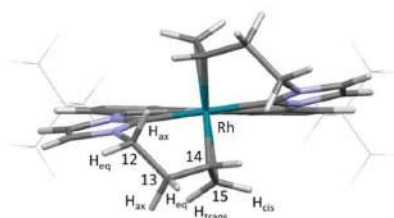


Fig. 2 Calculated structure of **2** with *tert*-Bu groups depicted in wire-frame for clarity.

Table 1 Rh-Catalyzed isomerisation of 1,2-epoxyhexane (**3b**): optimisation of the reaction conditions<sup>a</sup>

Entry	Catalyst [mol%] + additive [mol%]	Solvent	Conc. <b>3b</b> [mol L <sup>-1</sup> ]	Time	Yield <sup>b</sup> [%]
1	5 ( <b>2</b> <sup>Lix</sup> )	THF- <i>d</i> <sub>8</sub>	0.1	2 h	<5
2 <sup>c,f</sup>	5 ( <b>2</b> <sup>Lix</sup> )	THF- <i>d</i> <sub>8</sub>	0.1	5.5 d	88
3	5 ( <b>2</b> <sup>Lix</sup> )	Toluene- <i>d</i> <sub>8</sub>	0.1	3 h	>99
4	5 ( <b>2</b> <sup>Lix</sup> )	C <sub>6</sub> D <sub>6</sub>	0.1	2 h	>99
5	5 ( <b>2</b> )	C <sub>6</sub> D <sub>6</sub>	0.1	2 h	0
6	5 ( <b>2</b> ) + 10 (LiBr)	C <sub>6</sub> D <sub>6</sub>	0.1	1 h	0
7 <sup>d</sup>	5 ( <b>2</b> ) + 10 (LiBr)	C <sub>6</sub> D <sub>6</sub>	0.1	3 h	>99
8	10 (LiBr)	C <sub>6</sub> D <sub>6</sub>	0.1	24 h	0
9 <sup>d</sup>	10 (LiBr)	C <sub>6</sub> D <sub>6</sub>	0.1	24 h	0
10	4 ( <b>2</b> <sup>Lix</sup> )	C <sub>6</sub> D <sub>6</sub>	0.1	3 h	>99
11	3 ( <b>2</b> <sup>Lix</sup> )	C <sub>6</sub> D <sub>6</sub>	0.1	8 h	>99
12	2 ( <b>2</b> <sup>Lix</sup> )	C <sub>6</sub> D <sub>6</sub>	0.1	9 h	>99
13	1 ( <b>2</b> <sup>Lix</sup> )	C <sub>6</sub> D <sub>6</sub>	0.1	7 d	>99
14 <sup>e</sup>	1 ( <b>2</b> <sup>Lix</sup> )	C <sub>6</sub> D <sub>6</sub>	0.1	4 d	87
15 <sup>f</sup>	1 ( <b>2</b> <sup>Lix</sup> )	C <sub>6</sub> D <sub>6</sub>	0.1	3 d	93
16	1 ( <b>2</b> <sup>Lix</sup> )	C <sub>6</sub> D <sub>6</sub>	0.2	24 h	>99
17	1 ( <b>2</b> <sup>Lix</sup> )	C <sub>6</sub> D <sub>6</sub>	0.4	14 h	>99
18	1 ( <b>2</b> <sup>Lix</sup> )	C <sub>6</sub> D <sub>6</sub>	1.0	3 h	98

<sup>a</sup> Carried out in *J. Young* NMR tubes. <sup>b</sup> Yield (<sup>1</sup>H NMR) of **4b** calibrated to 1,3,5-trimethoxybenzene (internal standard); conversion = yield. <sup>c</sup> With 20 mol% LiNTf<sub>2</sub>. <sup>d</sup> With 20 μL THF. <sup>e</sup> At 40 °C. <sup>f</sup> At 60 °C.

which can be explained by the enhanced solubility of LiBr<sup>16</sup> (entries 6 and 7). As lithium halides are known catalysts for the Meinwald reaction, albeit at elevated temperature,<sup>7b-d</sup> we tested them under our conditions at room temperature. Neither lithium bromide nor solubilised lithium bromide (by 20  $\mu\text{L}$  THF) were able to catalyse this reaction (entries 8 and 9). These results clearly show that catalyst 2 is much more active than catalyst 1 and that at least a weak Lewis acid co-catalyst is still necessary.

Lowering the catalyst loading from 5 mol% to 1 mol% at constant concentration of the substrate did not affect the regioselectivity but required a longer reaction time (Table 1, entries 10–13). A higher temperature accelerated the reaction, but it still needed several days for completion using 1 mol% of catalyst (Table 1, entries 14 and 15). Epoxide concentrations of 0.4 mol L<sup>-1</sup> and 1.0 mol L<sup>-1</sup> (Table 1, entries 16–18) shortened the reaction time substantially and the reaction is about 10 times faster compared to literature.<sup>7g</sup> Even though 1 mol% of catalyst loading was sufficient for the model reaction at high concentrations, further experiments showed that it may lead to polymerisation of functionalised epoxides (especially with ester groups). Thus, the optimised reaction conditions (5 mol% 2<sup>LIX</sup>, 0.1 M epoxide, C<sub>6</sub>D<sub>6</sub>, room temperature) were applied to explore the generality of this protocol.‡

Using complex 2<sup>LIX</sup> as the catalyst, 13 functionalised terminal epoxides were converted successfully into the desired methyl ketones (Scheme 3). The alkyl substituted epoxides 3a–d and the methoxy epoxide 3e were transformed into the desired products 4a–e almost quantitatively with full regioselectivity. The only exception was *tert*-butyloxirane (3c), which could be obtained in only 11% yield after 10 days, possibly due to steric effects. In the case of hydroxyl (3f) and sulfonamide groups (3g) the isomerisation progressed slowly, which might reveal a competing influence of the

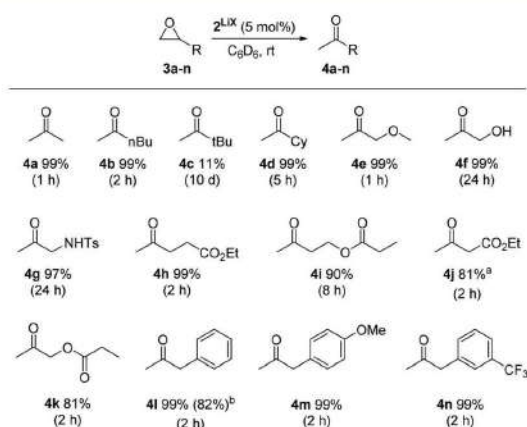
acidic protons, nonetheless 4f and 4g were formed in 99% and 97% yields. Notably, catalyst 2<sup>LIX</sup> is well suited for the isomerisation of terminal epoxides 3h–k with ester groups and afforded 4h–k with high regio- and chemoselectivity. 3j reacts a bit slower than 3h, which might be due to its  $\alpha$ -acidity. Furthermore, 2-benzyloxirane (3l) and its methoxy (3m) and trifluoromethyl (3n) congeners were isomerised to the methyl ketones 4l–n quantitatively. Internal epoxides react considerably slower.§

The selective rearrangement of aryl oxiranes to methyl ketones has not been achieved so far due to the Lewis acid catalysed side reaction.<sup>7e,f,g</sup> Therefore, we applied our new catalyst 2<sup>LIX</sup> also in the isomerisation of aryl oxiranes (Table 2). With styrene oxide (5a) we found an unprecedented good ratio between acetophenone (6a) and 2-phenylacetaldehyde (7a) of 40:1. To our delight, acetophenones 6b–d bearing the strong electron-withdrawing trifluoromethyl substituent were obtained regioselectively in excellent yield. This counts also for the terminal epoxides 5e–j possessing fluoro, chloro and bromo substituents (>99:1). Aryl oxiranes containing electron-donating groups (methyl or methoxy) were converted into 6k and 6l with still very good regioselectivities of 21:1 and 10:1 favouring the methyl ketones (6k, 6l) over the aldehydes (7k, 7l) in good to moderate yields. Notably, epoxide 5l is extremely sensitive towards Lewis acids in C<sub>6</sub>D<sub>6</sub> at room temperature. In two control experiments without catalyst 2, 10 mol% of LiBr and 5 mol% of LiCl as well as 10 mol% LiI were added to the aryl oxirane 5l in C<sub>6</sub>D<sub>6</sub>. After few days (LiBr/Cl) or

Table 2 Regio- and chemoselective isomerisation of aryl oxiranes 5a–m<sup>a</sup>

Entry	Epoxide 5	6 yield <sup>b</sup> [%]	Ratio (6:7)
1	5a	6a, 95	40:1
2	5b	<i>m</i> -6b, 98	>99:1
3 <sup>c</sup>	5c	<i>o</i> -6c, 91	>99:1
4	5d	<i>p</i> -6d, 99	>99:1
5	5e	F-6e, 99	>99:1
6	5f	Cl-6f, 99	>99:1
7	5g	Br-6g, 99	>99:1
8	5h	F-6h, 85	91:1
9	5i	Cl-6i, 92	>99:1
10	5j	Br-6j, 82	>99:1
11	5k	6k, 77	21:1
12	5l	6l, 57	10:1
13 <sup>d</sup>	5m	6m, 75	7:1

<sup>a</sup> Standard reaction conditions: epoxide (50.0  $\mu\text{mol}$ ), 2<sup>LIX</sup> (5 mol%), C<sub>6</sub>D<sub>6</sub> (0.5 mL), r.t. Carried out in *J. Young* NMR tubes. <sup>b</sup> Yields (<sup>1</sup>H NMR) calibrated to 1,3,5-trimethoxybenzene (internal standard). <sup>c</sup> At 80 °C for 2 days. <sup>d</sup> 22 h.



Scheme 3 Rh-Catalyzed regio- and chemoselective isomerisation of terminal epoxides. Standard reaction conditions: substrate (50.0  $\mu\text{mol}$ ), 2<sup>LIX</sup> (5 mol%), C<sub>6</sub>D<sub>6</sub> (0.5 mL), r.t. at the given time. Carried out in *J. Young* NMR tubes. Yield (<sup>1</sup>H NMR) calibrated to 1,3,5-trimethoxybenzene (internal standard). <sup>a</sup> 14% of unreacted epoxide left. <sup>b</sup> Isolated yield after column chromatography of a 1 mmol scale experiment.



23 h (LiI), only formation of the aldehyde **7l** and other, possibly polymerisation products (Fig. S5, ESI<sup>†</sup>), was observed. The oxirane **5m** bearing a +I substituent in *ortho* position can be transformed into **6m** with still good regioselectivity and in good yield after 22 h.

In conclusion, the new CO-free rhodium complex **2** led to significant improvement of the nucleophilic Meinwald reaction with respect to lower reaction temperature, catalyst loading and the absence of additional Lewis acids. It also shows a high functional group tolerance. The stronger nucleophilicity of complex **2** is crucial for the excellent regioselectivity achieved in the case of aryl oxiranes, which can get isomerised for the first time almost exclusively to the methyl ketones. Thus, we have broadened the scope of this reaction, which should be very valuable for organic synthesis, especially in combination with the Johnson–Corey–Chaykovsky reaction.

Yingying Tian thanks the China Scholarship Council (CSC) for a predoctoral fellowship and Eva Jürgens the MWK-BW for funding (Landesgraduiertenförderung). We thank Alexander Klaiber, Nicolas Wiedmaier and Mario R. Rapp for help in synthesising some of the substrates and in the catalyst testing.

## Conflicts of interest

The authors declare no conflict of interest.

## Notes and references

‡ Experimental procedure for *in situ* generation of catalyst **2**<sup>LiX</sup>: Li[N(SiMe<sub>3</sub>)<sub>2</sub>] (7.4 mg, 44.0 μmol) was added to a suspension of **Hbimca**<sup>Homo</sup>-**2HBr** (10.0 mg, 14.7 μmol) in 0.5 mL of THF-*d*<sub>8</sub> at room temperature. After 10 min, [Rh(μ-Cl)(COD)]<sub>2</sub> (3.6 mg, 7.3 μmol) was added and the solution was stirred for another 10 min. After checking the successful formation of the catalyst by NMR, 85.0 μL (containing 2.5 μmol **2**<sup>LiX</sup>) of the freshly prepared catalyst solution were used for each NMR experiment and the THF was removed in oil-pump vacuum prior to the addition of the epoxide (see ESI<sup>†</sup> for details).

§ At 80 °C, but otherwise identical conditions, 77% *cis*-2,3-epoxybutane and 34% *trans*-2,3-epoxybutane were converted into the ketone after 10 d. No further optimisation was attempted.

- J. G. Smith, *Synthesis*, 1984, 629.
- (a) B. C. Hartman and B. Rickborn, *J. Org. Chem.*, 1972, 37, 943; (b) B. Rickborn, in *Compr. Org. Synth.*, ed. B. M. Trost, Pergamon, Oxford, 1991, vol. 3, pp. 733–775; (c) Y. Kita, S. Kitagaki, Y. Yoshida, S. Mihara, D.-F. Fang, M. Kondo, S. Okamoto, R. Imai, S. Akai and H. Fujioka, *J. Org. Chem.*, 1997, 62, 4991; (d) C.-Y. Huang and A. G. Doyle, *Chem. Rev.*, 2014, 114, 8153.
- J. Meinwald, S. S. Labana and M. S. Chadha, *J. Am. Chem. Soc.*, 1963, 85, 582.
- Ni<sup>2+</sup>: (a) A. Miyashita, T. Shimada, A. Sugawara and H. Nohiya, *Chem. Lett.*, 1986, 1323; In<sup>3+</sup>: (b) B. C. Ranu and U. Jana, *J. Org. Chem.*, 1998, 63, 8212; Fe<sup>3+</sup>: (c) K. Suda, K. Baba, S.-I. Nakajima and T. Takanami, *Tetrahedron Lett.*, 1999, 40, 7243; Bi<sup>3+</sup>: (d) A. M. Anderson, J. M. Blazek, P. Garg, B. J. Payne and R. S. Mohan, *Tetrahedron Lett.*, 2000, 41, 1527; Er<sup>3+</sup>: (e) A. Procopio, R. Dalpozzo, A. De Nino, M. Nardi, G. Sindona and A. Tagarelli, *Synlett*, 2004, 2633; Sn: (f) M. Banerjee, U. K. Roy, P. Sinha and S. Roy, *J. Organomet. Chem.*, 2005, 690, 1422; Cu<sup>2+</sup>: (g) M. W. C. Robinson, K. S. Pillinger, I. Mabbett, D. A. Timms and A. E. Graham, *Tetrahedron*, 2010, 66, 8377; [ReBr(CO)<sub>3</sub>]: (h) R. Umeda, M. Muraki, Y. Nakamura, T. Tanaka, K. Kamiguchi and Y. Nishiyama, *Tetrahedron Lett.*, 2017, 58, 2393.
- The chelation enhanced formation of methyl ketones from α-keto oxiranes by a Ru<sup>2+</sup> catalyst: C.-L. Chang, M. P. Kumar and R.-S. Liu, *J. Org. Chem.*, 2004, 69, 2793.
- Pd<sup>2+</sup>: (a) D. J. Vyas, E. Larionov, C. Besnard, L. Guénee and C. Mazet, *J. Am. Chem. Soc.*, 2013, 135, 6177; (b) N. Humbert, D. J. Vyas, C. Besnard and C. Mazet, *Chem. Commun.*, 2014, 50, 10592; (c) S. Kulasegaram and R. J. Kulawiec, *J. Org. Chem.*, 1997, 62, 6547; (d) S. Kulasegaram and R. J. Kulawiec, *Tetrahedron*, 1998, 54, 1361; Ni in a reaction sequence: (e) A. N. Desnoyer, J. L. Geng, M. W. Drover, B. O. Patrick and J. A. Love, *Chem. – Eur. J.*, 2017, 23, 11509.
- (a) J. L. Eisenmann, *J. Org. Chem.*, 1962, 27, 2706; (b) B. Rickborn and R. M. Gerkin, *J. Am. Chem. Soc.*, 1968, 90, 4193; (c) B. Rickborn and R. M. Gerkin, *J. Am. Chem. Soc.*, 1971, 93, 1693; (d) Z.-w. An, R. D'Alaisio and C. Venturello, *Synthesis*, 1992, 1229; (e) S. Kulasegaram and R. J. Kulawiec, *J. Org. Chem.*, 1994, 59, 7195; (f) J. Prandi, J. L. Namy, G. Menoret and H. B. Kagan, *J. Organomet. Chem.*, 1985, 285, 449; (g) J. R. Lamb, Y. Jung and G. W. Coates, *Org. Chem. Front.*, 2015, 2, 346.
- M. Moser, B. Wucher, D. Kunz and F. Rominger, *Organometallics*, 2007, 26, 1024.
- E. Jürgens, B. Wucher, F. Rominger, K. W. Törnroos and D. Kunz, *Chem. Commun.*, 2015, 51, 1897.
- The nucleophilic pathway (Scheme 1) follows an S<sub>N</sub>2 mechanism. Formation of metallaoxetanes by insertion into the σ-carbon oxygen bond: (a) A. Dauth and J. A. Love, *Chem. Rev.*, 2011, 111, 2010. For Ni(0) see Lit. 4a and 6e as well as: (b) A. N. Desnoyer, E. G. Bowes, B. O. Patrick and J. A. Love, *J. Am. Chem. Soc.*, 2015, 137, 12748; Rh: (c) M. J. Calhorda, A. M. Galvao, C. Unaleroğlu, A. A. Zlota, F. Frolow and D. Milstein, *Organometallics*, 1993, 12, 3316; and; (d) B. de Bruin, M. J. Boerakker, J. J. J. M. Donners, B. E. C. Christiaans, P. P. J. Schlebos, R. de Gelder, J. M. M. Smits, A. L. Spek and A. W. Gal, *Angew. Chem., Int. Ed.*, 1997, 36, 2063; (e) B. de Bruin, M. J. Boerakker, J. A. W. Verhagen, R. de Gelder, J. M. M. Smits and A. W. Gal, *Chem. – Eur. J.*, 2000, 6, 298. Without additional Lewis acid (2'-oxoalkyl)(hydrido)rhodium(III) intermediates were isolated reacting RhCl(PMe<sub>3</sub>)<sub>3</sub> in neat propylene or styrene oxide after 16 h: (f) D. Milstein, *J. Am. Chem. Soc.*, 1982, 104, 5227; Ir: (g) D. Milstein and J. C. Calabrese, *J. Am. Chem. Soc.*, 1982, 104, 3773. We tested RhCl(PMe<sub>3</sub>)<sub>3</sub> under our conditions and found it considerably slower than complex **2**<sup>LiX</sup>: 5% yield for styrene oxide after 2 h (with or without addition of Br<sup>-</sup>); after 24 h still 5% yield without Br<sup>-</sup> and 16% in presence of 10 mol% LiBr. For nucleophilic mechanisms *via* C–H bond activation: (h) D. Milstein, O. Buchman and J. Blum, *J. Org. Chem.*, 1977, 42, 2299; (i) J. Wu and R. G. Bergman, *J. Am. Chem. Soc.*, 1989, 111, 7628.
- E. Jürgens, PhD thesis, University of Tübingen, Tübingen, 2017.
- Bimca (3,6-di-*tert*-butyl-1,8-bis(imidazolin-2-ylidene)-9-carbazolidine). E. Jürgens and D. Kunz, *Eur. J. Inorg. Chem.*, 2017, 2333.
- In contrast to [Li(bimca<sup>Homo</sup>)], complex [K(bimca<sup>Homo</sup>)] decomposes at room temperature into butadiene and the bisimidazole carbazolidine [K(imid)<sub>2</sub>carb] (see ESI<sup>†</sup>).
- See ESI<sup>†</sup> for another, but energetically disfavoured minimum.
- DCM and acetonitrile react already with **1**: M. Moser, PhD thesis, Heidelberg University, Heidelberg, 2007.
- 2**<sup>LiX</sup> is generated in THF, which is then removed (with COD) *in vacuo*. Some THF remains coordinated to Li<sup>+</sup> so that the solubility of LiX is enhanced during catalysis in C<sub>6</sub>D<sub>6</sub> or toluene-*d*<sub>8</sub>.

## Supporting Information

# Regio- and Chemoselective Rearrangement of Terminal Epoxides into Methyl Alkyl and Aryl Ketones

Yingying Tian, Eva Jürgens, and Doris Kunz\*

*Institut für Anorganische Chemie, Auf der Morgenstelle 18, 72076 Tübingen, Germany*

### Table of Contents

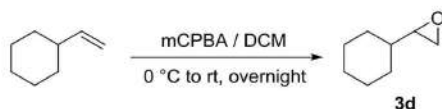
1. General information .....	2
2. Synthesis of terminal epoxides .....	3
3. Preparation of the rhodium complexes <b>2</b> and <b>2<sup>LiX</sup></b> .....	11
4. Reactivity comparison between catalyst <b>1</b> and catalyst <b>2</b> .....	14
5. Additional substrate scope for catalyst <b>1</b> in the Meinwald reaction .....	16
6. Stability of 2-(4-methoxyphenyl)oxirane ( <b>5l</b> ) against lithium halides and catalyst <b>2</b> .....	17
7. Experimental procedures for the Meinwald reaction of terminal epoxides with catalyst <b>2<sup>LiX</sup></b> .....	18
8. NMR spectra .....	24
9. DFT calculations .....	74
10. References .....	75

## 1. General information

Unless otherwise noted, all reactions were carried out under an argon atmosphere in dried and degassed solvents using Schlenk technique. Toluene, Pentane, dichloromethane and tetrahydrofuran were purchased from Sigma Aldrich and dried using an MBraun SPS-800 solvent purification system. All lithium salts used were obtained from commercial suppliers, dried in vacuum and used without further purification. Epoxides obtained from commercial suppliers and synthesised epoxides were degassed through freeze-pump-thaw cycles prior to use. **Hbimca<sup>Homo</sup>-2HBr**<sup>[1,2]</sup> and rhodium complex **1**<sup>[3]</sup> were synthesised according to the literature procedures. <sup>1</sup>H and <sup>13</sup>C NMR spectra were recorded using a Bruker ARX 250 and AVANCE II+ 400 spectrometer. Chemical shifts  $\delta$  (ppm) are given relative to the solvent's residual proton and carbon signal respectively: THF-*d*<sub>6</sub>: 3.58 ppm (<sup>1</sup>H NMR) and 67.57 ppm (<sup>13</sup>C NMR); C<sub>6</sub>D<sub>6</sub>: 7.16 ppm (<sup>1</sup>H NMR) and 128.39 ppm (<sup>13</sup>C NMR); CDCl<sub>3</sub>: 7.27 ppm (<sup>1</sup>H NMR) and 77.00 ppm (<sup>13</sup>C NMR); DMSO-*d*<sub>6</sub>: 2.50 ppm (<sup>1</sup>H NMR) and 39.51 ppm (<sup>13</sup>C NMR). Coupling constants (*J*) are expressed in Hz. Multiplets were assigned as br s (broad singlet), d (doublet), dd (doublet of doublets), ddd (doublet of doublet of doublets), dt (doublet of triplets), m (multiplet), q (quartet), qd (quartet of doublets) s (singlet), t (triplet) and tt (triplet of triplets). Assignment of peaks was made using 2D NMR correlation and NOE spectra.

## 2. Synthesis of terminal epoxides

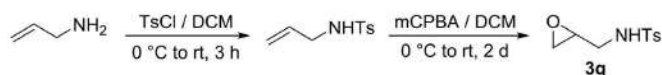
### 2-Cyclohexyloxirane (**3d**)<sup>[4]</sup>



To a solution of vinylcyclohexane (1.10 g, 10.0 mmol) in DCM (30 mL), *meta*-chloroperoxybenzoic acid (2.72 g, <77 % purity, 11.0 mmol) was added at 0 °C and the resulting mixture was stirred overnight at room temperature. The reaction mixture was filtered and the solvent was removed under reduced pressure. The residue was dissolved in ethyl acetate (50 mL) and washed with 10% Na<sub>2</sub>SO<sub>3</sub> (3 × 25 mL), 10% NaHCO<sub>3</sub> (4 × 25 mL), water (25 mL) and brine (25 mL). The organic phase was dried over Na<sub>2</sub>SO<sub>4</sub>, filtered and evaporated *in vacuo* to obtain **3d** (59%) as a colorless liquid.

<sup>1</sup>H NMR (400 MHz, CDCl<sub>3</sub>) δ = 2.72–2.70 (m, 2H), 2.53–2.51 (m, 1H), 1.89–1.86 (m, 1H), 1.76–1.63 (m, 4H), 1.30–1.05 (m, 6H). <sup>13</sup>C NMR (101 MHz, CDCl<sub>3</sub>) δ = 56.6, 46.0, 40.4, 29.7, 28.8, 26.3, 25.7, 25.5.

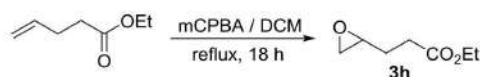
### 4-Methyl-*N*-(oxiran-2-ylmethyl)benzenesulfonamide (**3g**)<sup>[5]</sup>



To a solution of 4-toluenesulfonyl chloride (1.90 g, 10.0 mmol) in anhydrous dichloromethane (50 mL), allylamine (1.20 g, 21.0 mmol) was added dropwise at 0 °C and the resulting mixture was stirred for 3 h at room temperature. The reaction mixture was washed with 10% citric acid (2 × 25 mL), water (25 mL) and brine (25 mL). The organic phase was dried over Na<sub>2</sub>SO<sub>4</sub>, filtered and evaporated *in vacuo* to obtain *N*-allyl-4-methylbenzenesulfonamide. The compound obtained was used directly without purification. To a solution of *N*-allyl-4-methylbenzenesulfonamide in DCM (30 mL), *meta*-chloroperoxybenzoic acid (2.72 g, <77% purity, 11.0 mmol) was added at 0 °C and the resulting mixture was stirred for 48 h at room temperature. The reaction mixture was filtered and the solvent was removed under reduced pressure. The residue was dissolved in ethyl acetate (50 mL) and washed with 10% Na<sub>2</sub>SO<sub>3</sub> (3 × 25 mL), 10% NaHCO<sub>3</sub> (4 × 25 mL), water (25 mL) and brine (25 mL). The organic phase was dried over Na<sub>2</sub>SO<sub>4</sub>, filtered and evaporated *in vacuo* to obtain **3g** (87%) as a white solid.

$^1\text{H}$  NMR (400 MHz,  $\text{CDCl}_3$ )  $\delta$  = 7.77–7.74 (m, 2H), 7.33–7.31 (m, 2H), 4.76–4.74 (m, 1H), 3.38–3.32 (m, 1H), 3.09–3.01 (m, 2H), 2.77–2.75 (m, 1H), 2.64 (dd,  $J$  = 4.7, 2.3 Hz, 1H), 2.44 (s, 3H).  $^{13}\text{C}$  NMR (101 MHz,  $\text{CDCl}_3$ )  $\delta$  = 143.7, 136.8, 129.8, 127.0, 50.2, 45.1, 44.3, 21.5.

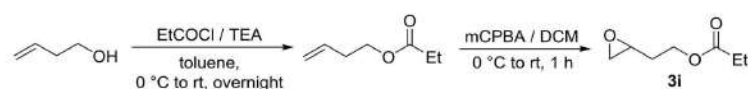
### Ethyl 3-(oxiran-2-yl)propanoate (**3h**)<sup>[4]</sup>



Ethyl pent-4-enoate (3.00 g, 23.4 mmol) and *meta*-chloroperoxybenzoic acid (5.77 g, <77% purity, 23.4 mmol) were dissolved in  $\text{CH}_2\text{Cl}_2$  (90 mL) and stirred for 18 h in an oil bath at 50 °C. The white solid was filtered off and the filtrate was washed with 10%  $\text{NaHSO}_3$  (100 mL), 10%  $\text{NaHCO}_3$  (3  $\times$  50 mL) and  $\text{H}_2\text{O}$  (2  $\times$  50 mL). The crude product was dried over  $\text{Na}_2\text{SO}_4$  then carefully concentrated without external heating. The desired product **3h** (59%) was obtained as a colorless liquid by distillation, b.p. 30–33 °C ( $9.0 \times 10^{-2}$  mbar).

$^1\text{H}$  NMR (400 MHz,  $\text{DMSO}-d_6$ )  $\delta$  = 4.06 (q,  $J$  = 7.1 Hz, 2H), 2.93–2.90 (m, 1H), 2.68–2.66 (m, 1H), 2.46 (dd,  $J$  = 5.1, 2.7 Hz, 1H), 2.39 (t,  $J$  = 7.4 Hz, 2H), 1.82–1.64 (m, 2H), 1.18 (t,  $J$  = 7.1 Hz, 3H).  $^{13}\text{C}$  NMR (101 MHz,  $\text{CDCl}_3$ )  $\delta$  = 172.8, 60.5, 51.2, 47.1, 30.4, 27.6, 14.2.

### 2-(Oxiran-2-yl)ethyl propionate (**3i**)<sup>[6]</sup>



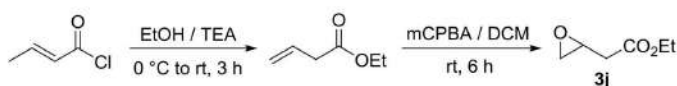
To a mixture of 3-buten-1-ol (3.00 g, 41.6 mmol) and triethylamine (5.06 g, 50.0 mmol) in toluene (30 mL), propionyl chloride (4.04 g, 43.7 mmol) was added dropwise with vigorous stirring at 0 °C. The reaction was allowed to warm to room temperature and stirred overnight. The solution was washed with cold water (3  $\times$  20 mL) and brine (100 mL). After drying over  $\text{Na}_2\text{SO}_4$ , the solvent was removed under reduced pressure to yield but-3-en-1-yl propionate as a crude oil. To a stirred solution of crude but-3-en-1-yl propionate (2.75 g, 21.5 mmol) in  $\text{CH}_2\text{Cl}_2$  (20 mL) at 0 °C, *meta*-chloroperoxybenzoic acid (5.55 g, <77% purity, 23.2 mmol) was added and the reaction was allowed to warm to room temperature. After stirred for 1 h, excess peroxide was quenched by the slow addition of 10%  $\text{NaHSO}_3$



(50 mL) at 0 °C, followed by slow addition of NaHCO<sub>3</sub> until bubbling ceased. The product was extracted with CH<sub>2</sub>Cl<sub>2</sub> (3 × 30 mL) and washed with brine (50 mL). The organic phase was dried over Na<sub>2</sub>SO<sub>4</sub> and the solvent was removed under reduced pressure. The crude product was purified by distillation and the desired product **3i** (26%) was obtained as a colorless liquid, b.p. 27-33 °C (9.0 × 10<sup>-2</sup> mbar).

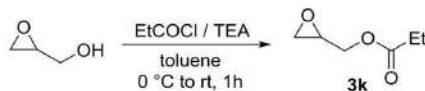
<sup>1</sup>H NMR (400 MHz, CDCl<sub>3</sub>) δ = 4.24 (t, *J* = 6.2, 2H), 3.04–2.99 (m, 1H), 2.80–2.78 (m, 1H), 2.51 (dd, *J* = 5.0, 2.7 Hz, 1H), 2.35 (q, *J* = 7.6 Hz, 2H), 1.97–1.78 (m, 2H), 1.15 (t, *J* = 7.6 Hz, 3H). <sup>13</sup>C NMR (101 MHz, CDCl<sub>3</sub>) δ = 174.3, 61.2, 49.5, 46.8, 31.9, 27.5, 9.1.

### Ethyl 2-(oxiran-2-yl)acetate (**3j**)<sup>[7]</sup>



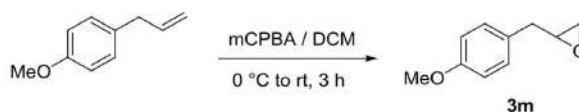
To the cooled mixture of triethylamine (4.84 g, 47.8 mmol) and ethanol (3.31 g, 71.7 mmol), crotonoyl chloride (4.50 g, 47.8 mmol) was added dropwise at 0 °C and the reaction was allowed to warm to room temperature. After stirring for 3 h, 10% NaHCO<sub>3</sub> (10 mL) was added to the reaction mixture, followed by water (20 mL). The reaction mixture was extracted with diethyl ether and pentane (70 mL). The organic layers were combined and washed with brine. The crude product was dried over Na<sub>2</sub>SO<sub>4</sub> then carefully concentrated without external heating. The compound obtained was used directly without further purification. To a stirred solution of crude ethyl but-3-enoate (3.54 g, 31.0 mmol) in CH<sub>2</sub>Cl<sub>2</sub> (20 mL), *meta*-chloroperoxybenzoic acid (7.64 g, <77% purity, 31.0 mmol) was added and the solution was stirred for 6 h. The reaction mixture was washed with 10% NaHSO<sub>3</sub> (30 mL), NaHCO<sub>3</sub> (sat., 30 mL) and brine (3 × 30 mL). The organic phase was dried over Na<sub>2</sub>SO<sub>4</sub> and the solvent was removed under reduced pressure. The crude product was purified by distillation and the desired product **3j** (32%) was obtained as a colorless liquid, b.p. 25-27 °C (3.1 × 10<sup>-2</sup> mbar).

<sup>1</sup>H NMR (400 MHz, C<sub>6</sub>D<sub>6</sub>) δ = 3.89 (q, *J* = 7.1 Hz, 2H), 3.03–2.99 (m, 1H), 2.30–2.26 (m, 1H), 2.09–2.21 (m, 2H), 2.00 (dd, *J* = 5.1, 2.5 Hz, 1H), 0.90 (t, *J* = 7.1 Hz, 3H). <sup>13</sup>C NMR (101 MHz, CDCl<sub>3</sub>) δ = 170.4, 60.9, 48.0, 46.7, 38.1, 14.2.

**Oxiran-2-ylmethyl propionate (3k)**<sup>[6]</sup>

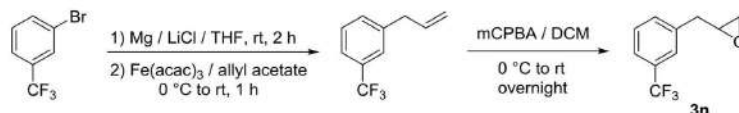
Propionyl chloride (6.24 g, 67.5 mmol) was added dropwise with vigorous stirring to a mixture of glycidol (5.00 g, 67.5 mmol) and triethylamine (8.26 g, 81.0 mmol) in toluene (30 mL) at 0 °C. After 1 h, the mixture was allowed to warm to room temperature. The solution was rapidly washed with cold water (3 × 20 mL) and brine (20 mL). The organic phase was collected, dried over Na<sub>2</sub>SO<sub>4</sub> and distilled twice to obtain the desired product **3k** (53%) as a colorless liquid, b.p. 82-85 °C (12.0 mbar).

<sup>1</sup>H NMR (400 MHz, CDCl<sub>3</sub>) δ = 4.42 (dd, *J* = 12.3, 3.1 Hz, 1H), 3.93 (dd, *J* = 12.3, 6.3 Hz, 1H), 3.23–3.19 (m, 1H), 2.85 (t, *J* = 4.5 Hz, 1H), 2.65 (dd, *J* = 4.9, 2.6 Hz, 1H), 2.39 (q, *J* = 7.6 Hz, 2H), 1.18–1.14 (t, *J* = 7.6 Hz, 3H). <sup>13</sup>C NMR (101 MHz, CDCl<sub>3</sub>) δ = 174.2, 64.8, 49.4, 44.6, 27.3, 9.0.

**2-(4-Methoxybenzyl)oxirane (3m)**<sup>[8]</sup>

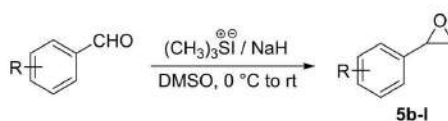
A solution of 1-allyl-4-methoxybenzene (3.00 g, 20.3 mmol) in CH<sub>2</sub>Cl<sub>2</sub> (75 mL) was cooled to 0 °C with an ice bath and *meta*-chloroperoxybenzoic acid (3.50 g, <77% purity; 20.3 mmol) was added portion wise. The mixture was allowed to warm to room temperature and then stirred until TLC indicated complete consumption of the starting material. After completion, NaHCO<sub>3</sub> (sat., 75 mL) was slowly added and the mixture was stirred vigorously until bubbling ceased. The organic layer was separated and washed with 10% NaHSO<sub>3</sub> (100 mL) and brine (70 mL), and then dried over Na<sub>2</sub>SO<sub>4</sub>. After removal of the solvent by rotary evaporation, the crude product was purified by chromatography on silica gel (EtOAc/hexane, gradient 5:95 to 20:80) to afford the desired product **3m** (87%) as a colorless liquid.

<sup>1</sup>H NMR (400 MHz, CDCl<sub>3</sub>) δ = 7.20–7.16 (m, 2H), 6.89–6.85 (m, 2H), 3.81 (s, 3H), 3.16–3.13 (m, 1H), 2.91–2.75 (m, 3H), 2.55–2.53 (m, 1H). <sup>13</sup>C NMR (101 MHz, CDCl<sub>3</sub>) δ = 158.4, 130.0, 129.1, 113.9, 55.2, 52.6, 46.8, 37.8.

**2-(3-(Trifluoromethyl)benzyl)oxirane (3n)**<sup>[8,9]</sup>

Freshly distilled THF (40 mL) and 1-bromo-3-(trifluoromethyl)benzene (6.14 g, 27.3 mmol) were added dropwise to a mixture of magnesium ribbons (822 mg, 33.8 mmol), dry LiCl (1.45 g, 33.8 mmol) and THF under argon protection. The mixture was stirred at room temperature for 2 h and then cooled to 0 °C in an ice bath. A solution of Fe(acac)<sub>3</sub> (473 mg, 1.30 mmol, 5 mol %) in dry THF (20 mL) was added, the solution stirred for 5 min, and allyl acetate (2.63 g, 26.0 mmol) was added. After stirring for 45 min at 0 °C, the reaction was quenched with saturated aqueous NaHCO<sub>3</sub> (5 mL) and extracted with ethyl acetate (3 × 10 mL). The combined organic phases were dried over Na<sub>2</sub>SO<sub>4</sub>, concentrated in vacuo and the crude product was purified by vacuum distillation. A solution of 1-allyl-3-(trifluoromethyl)benzene (7.41 g, 50.0 mmol) in CH<sub>2</sub>Cl<sub>2</sub> (75 mL) was cooled to 0 °C with an ice bath. *Meta*-chloroperoxybenzoic acid (12.1 g, <77% purity, 50.0 mmol) was added portion wise. The mixture was allowed to warm to room temperature and then stirred until TLC indicated complete consumption of the starting material. After completion, NaHCO<sub>3</sub> (sat., 75 mL) was slowly added and the mixture was stirred vigorously until bubbling ceased. The organic layer was separated and washed with 10% NaHSO<sub>3</sub> (100 mL), brine (70 mL), and then dried over Na<sub>2</sub>SO<sub>4</sub>. After removal of the solvent by rotary evaporation, the crude product was purified by chromatography on silica gel (EtOAc/hexane, gradient 5:95 to 20:80) to afford the desired product **3n** (36%) as a colorless liquid.

<sup>1</sup>H NMR (400 MHz, CDCl<sub>3</sub>) δ = 7.53–7.51 (m, 2H), 7.48–7.44 (m, 2H), 3.21–3.16 (m, 1H), 3.00–2.89 (m, 2H), 2.85–2.82 (m, 1H), 2.56 (dd, *J* = 4.9, 2.6 Hz, 1H). <sup>13</sup>C NMR (101 MHz, CDCl<sub>3</sub>) δ = 138.1, 132.4, 130.9 (q, <sup>2</sup>*J*<sub>CF</sub> = 32.0 Hz), 128.9, 125.7 (q, <sup>3</sup>*J*<sub>CF</sub> = 3.8 Hz), 124.1 (q, <sup>1</sup>*J*<sub>CF</sub> = 272.3 Hz), 123.6 (q, <sup>3</sup>*J*<sub>CF</sub> = 3.8 Hz), 51.9, 46.7, 38.4. <sup>19</sup>F NMR (376 MHz, CDCl<sub>3</sub>) δ = -62.62.

**α-Aryl oxiranes (5b-I)**<sup>[10]</sup>



Trimethylsulfonium iodide (20.0 mmol) and sodium hydride (60% in oil, 20.0 mmol) were dissolved in DMSO (15 mL) at 0 °C under an argon atmosphere. After stirring for 20 minutes, the corresponding aldehyde (12.0 mmol) dissolved in DMSO (20 mL) was added dropwise. The reaction was then stirred at room temperature overnight. The mixture was poured into cold water (60 mL), and extracted with ethyl acetate (3 × 30 mL). The combined organic layers were washed with water (30 mL) and brine (30 mL × 2), and dried over Na<sub>2</sub>SO<sub>4</sub>. The crude epoxide was purified using flash chromatography.

The desired product 2-(3-(trifluoromethyl)phenyl)oxirane (**5b**) was obtained as a colorless liquid (73%). <sup>1</sup>H NMR (400 MHz, CDCl<sub>3</sub>) δ = 7.59–7.55 (m, 2H), 7.49–7.48 (m, 2H), 3.94–3.93 (m, 1H), 3.21–3.18 (m, 1H), 2.81–2.79 (m, 1H). <sup>13</sup>C NMR (101 MHz, CDCl<sub>3</sub>) δ = 138.8, 131.1 (q, <sup>2</sup>J<sub>CF</sub> = 32.5 Hz), 129.0, 128.8, 125.0 (q, <sup>3</sup>J<sub>CF</sub> = 3.8 Hz), 124.0 (q, <sup>1</sup>J<sub>CF</sub> = 270.0 Hz), 122.3 (q, <sup>2</sup>J<sub>CF</sub> = 3.8 Hz), 51.8, 51.3. <sup>19</sup>F NMR (376 MHz, CDCl<sub>3</sub>) δ = -62.79.

The desired product 2-(2-(trifluoromethyl)phenyl)oxirane (**5c**) was obtained as a colorless liquid (58%). <sup>1</sup>H NMR (400 MHz, CDCl<sub>3</sub>) δ = 7.66 (dd, *J* = 7.8, 0.6 Hz, 1H), 7.57–7.53 (m, 1H), 7.49–7.46 (m, 1H), 7.43–7.39 (m, 1H), 4.24–4.22 (m, 1H), 3.21–3.18 (m, 1H), 2.67–2.65 (m, 1H). <sup>13</sup>C NMR (101 MHz, CDCl<sub>3</sub>) δ = 136.6, 132.3, 128.3 (q, <sup>2</sup>J<sub>CF</sub> = 31.1 Hz), 127.7, 125.5 (q, <sup>3</sup>J<sub>CF</sub> = 5.7 Hz), 125.3, 124.3 (q, <sup>1</sup>J<sub>CF</sub> = 273.6 Hz), 51.1, 49.2 (q, <sup>4</sup>J<sub>CF</sub> = 3.1 Hz). <sup>19</sup>F NMR (376 MHz, CDCl<sub>3</sub>) δ = -59.92.

The desired product 2-(4-(trifluoromethyl)phenyl)oxirane (**5d**) was obtained as a colorless liquid (80%). <sup>1</sup>H NMR (400 MHz, CDCl<sub>3</sub>) δ = 7.62 (d, *J* = 8.0 Hz, 2H), 7.41 (d, *J* = 8.0 Hz, 2H), 3.93 (dd, *J* = 4.1, 2.5 Hz, 1H), 3.20 (dd, *J* = 5.5, 4.1 Hz, 1H), 2.78 (dd, *J* = 5.5, 2.5 Hz, 1H). <sup>13</sup>C NMR (101 MHz, CDCl<sub>3</sub>) δ = 141.8, 130.4 (q, <sup>2</sup>J<sub>CF</sub> = 32.5 Hz), 125.7, 125.4 (q, <sup>3</sup>J<sub>CF</sub> = 3.8 Hz), 124.0 (q, <sup>1</sup>J<sub>CF</sub> = 272.2 Hz), 51.7, 51.4. <sup>19</sup>F NMR (376 MHz, CDCl<sub>3</sub>) δ = -62.62.

The desired product 2-(3-fluorophenyl)oxirane (**5e**) was obtained as a colorless liquid (80%). <sup>1</sup>H NMR (400 MHz, CDCl<sub>3</sub>) δ = 7.35–7.29 (m, 1H), 7.10 (dt, *J* = 7.7, 1.0 Hz, 1H), 7.03–6.96 (m, 2H), 3.87 (dd, *J* = 4.0, 2.8 Hz, 1H), 3.16 (dd, *J* = 5.6, 4.0 Hz, 1H), 2.77 (dd, *J* = 5.6, 2.8 Hz, 1H). <sup>13</sup>C NMR (101 MHz, CDCl<sub>3</sub>) δ = 163.1 (d, <sup>1</sup>J<sub>CF</sub> = 246.3 Hz), 140.4 (d, <sup>3</sup>J<sub>CF</sub> = 7.5 Hz), 130.1 (d, <sup>3</sup>J<sub>CF</sub> = 8.0 Hz), 121.3 (d,

$^4J_{CF} = 2.8$  Hz), 115.2 (d,  $^2J_{CF} = 21.2$  Hz), 112.2 (d,  $^2J_{CF} = 22.6$  Hz), 51.8 (d,  $^4J_{CF} = 2.4$  Hz), 51.2.  $^{19}F$  NMR (376 MHz,  $CDCl_3$ )  $\delta = -112.93$ .

The desired product 2-(3-chlorophenyl)oxirane (**5f**) was obtained as a colorless liquid (76%).

$^1H$  NMR (400 MHz,  $CDCl_3$ )  $\delta = 7.30-7.27$  (m, 3H), 7.21-7.16 (m, 1H), 3.85 (dd,  $J = 4.0, 2.5$  Hz, 1H), 3.16 (dd,  $J = 5.5, 4.0$  Hz, 1H), 2.77 (dd,  $J = 5.5, 2.5$  Hz, 1H).  $^{13}C$  NMR (101 MHz,  $CDCl_3$ )  $\delta = 139.8, 134.6, 129.8, 128.3, 125.5, 123.7, 51.7, 51.2$ .

The desired product 2-(3-bromophenyl)oxirane (**5g**) was obtained as a colorless liquid (82%).

$^1H$  NMR (400 MHz,  $CDCl_3$ )  $\delta = 7.46-7.42$  (m, 2H), 7.24-7.21 (m, 2H), 3.83 (dd,  $J = 4.0, 2.5$  Hz, 1H), 3.15 (dd,  $J = 5.5, 4.0$  Hz, 1H), 2.76 (dd,  $J = 5.5, 2.5$  Hz, 1H).  $^{13}C$  NMR (101 MHz,  $CDCl_3$ )  $\delta = 140.1, 131.2, 130.0, 128.4, 124.2, 122.7, 51.6, 51.2$ .

The desired product 2-(4-fluorophenyl)oxirane (**5h**) was obtained as a colorless liquid (71%).

$^1H$  NMR (400 MHz,  $CDCl_3$ )  $\delta = 7.28-7.23$  (m, 2H), 7.07-7.02 (m, 2H), 3.86 (dd,  $J = 4.0, 2.6$  Hz, 1H), 3.15 (dd,  $J = 5.4, 4.0$ , 1H), 2.78 (dd,  $J = 5.4, 2.6$  Hz, 1H).  $^{13}C$  NMR (101 MHz,  $CDCl_3$ )  $\delta = 162.7$  (d,  $^1J_{CF} = 246.3$  Hz), 133.3 (d,  $^4J_{CF} = 2.8$  Hz), 127.2 (d,  $^3J_{CF} = 8.5$  Hz), 115.5 (d,  $^2J_{CF} = 21.7$  Hz), 51.8, 51.2.  $^{19}F$  NMR (376 MHz,  $CDCl_3$ )  $\delta = -113.94$ .

The desired product 2-(4-chlorophenyl)oxirane (**5i**) was obtained as a colorless liquid (48%).

$^1H$  NMR (400 MHz,  $CDCl_3$ )  $\delta = 7.36-7.30$  (m, 2H), 7.26-7.20 (m, 2H), 3.90-3.82 (m, 1H), 3.19-3.13 (m, 1H), 2.76 (dd,  $J = 5.5, 2.5$  Hz, 1H).  $^{13}C$  NMR (101 MHz,  $CDCl_3$ )  $\delta = 136.2, 133.9, 128.7, 126.8, 51.8, 51.2$ .

The desired product 2-(4-bromophenyl)oxirane (**5j**) was obtained as a colorless liquid (71%).

$^1H$  NMR (400 MHz,  $CDCl_3$ )  $\delta = 7.51-7.46$  (m, 2H), 7.18-7.15 (m, 2H), 3.84 (dd,  $J = 4.0, 2.5$  Hz, 1H), 3.16 (dd,  $J = 5.5, 4.0$  Hz, 1H), 2.76 (dd,  $J = 5.5, 2.5$  Hz, 1H).  $^{13}C$  NMR (101 MHz,  $CDCl_3$ )  $\delta = 136.7, 131.6, 127.1, 122.0, 51.8, 51.2$ .

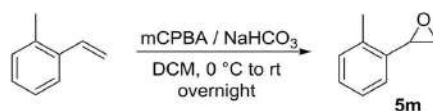
The desired product 2-(*p*-tolyl)oxirane (**5k**) was obtained as a colorless liquid (39%) and stored in fridge.

$^1\text{H}$  NMR (400 MHz,  $\text{CDCl}_3$ )  $\delta$  = 7.21–7.15 (m, 4H), 3.84 (dd,  $J$  = 4.1, 2.6 Hz, 1H), 3.14 (dd,  $J$  = 5.4, 4.1, 1H), 2.81 (dd,  $J$  = 5.4, 2.6 Hz, 1H), 2.36 (s, 3H).  $^{13}\text{C}$  NMR (101 MHz,  $\text{CDCl}_3$ )  $\delta$  = 138.0, 134.5, 129.2, 125.5, 52.3, 51.1, 21.2.

The desired product 2-(4-methoxyphenyl)oxirane (**5l**) was obtained as a colorless liquid (78%) and stored in fridge.

$^1\text{H}$  NMR (400 MHz,  $\text{DMSO}-d_6$ )  $\delta$  = 7.23–7.20 (m, 2H), 6.93–6.90 (m, 2H), 3.86 (dd,  $J$  = 4.1, 2.6 Hz, 1H), 3.74 (s, 3H), 3.07 (dd,  $J$  = 5.3, 4.1 Hz, 1H), 2.84 (dd,  $J$  = 5.3, 2.6 Hz, 1H).  $^{13}\text{C}$  NMR (101 MHz,  $\text{CDCl}_3$ )  $\delta$  = 159.7, 129.4, 126.8, 114.0, 55.3, 52.2, 51.0.

#### 2-(*o*-Tolyl)oxirane (**5m**)<sup>[11]</sup>

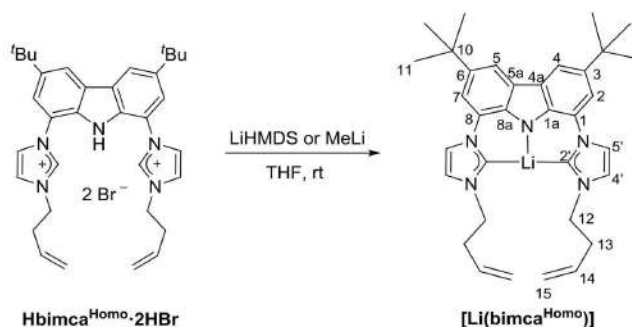


To a solution of 1-methyl-2-vinylbenzene (2.00 g, 16.9 mmol) in  $\text{CH}_2\text{Cl}_2$  (75 mL) was added solid  $\text{NaHCO}_3$  (2.80 g, 33.8 mmol). The reaction was cooled to 0 °C with an ice bath and *meta*-chloroperoxybenzoic acid (4.60 g, <77% purity; 18.6 mmol) dissolved in  $\text{CH}_2\text{Cl}_2$  (70 mL) was added dropwise. The mixture was allowed to warm to room temperature and then stirred until TLC indicated complete consumption of the starting material. After completion, the mixture was washed with aqueous  $\text{NaHCO}_3$  solution (sat., 75 mL), aqueous  $\text{Na}_2\text{S}_2\text{O}_3$  solution (sat., 100 mL) and then dried over  $\text{Na}_2\text{SO}_4$ . After removal of the solvent by rotary evaporation, the crude product was purified by distillation to afford the desired product **5m** (82%) as a light yellow liquid.

$^1\text{H}$  NMR (400 MHz,  $\text{CDCl}_3$ )  $\delta$  = 7.25–7.16 (m, 4H), 4.02 (dd,  $J$  = 4.1, 2.7 Hz, 1H), 3.18 (dd,  $J$  = 5.7, 4.1, 1H), 2.71 (dd,  $J$  = 5.7, 2.7 Hz, 1H), 2.44 (s, 3H).  $^{13}\text{C}$  NMR (101 MHz,  $\text{CDCl}_3$ )  $\delta$  = 136.1, 135.8, 129.8, 127.6, 126.1, 124.1, 50.4, 50.1, 18.7.

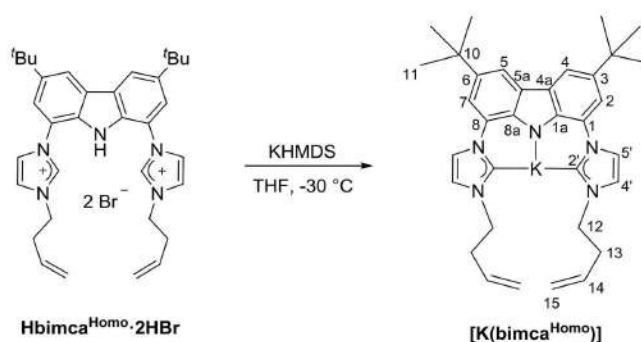
### 3. Preparation of the rhodium complexes **2** and **2<sup>LiX</sup>**

#### 3.1. Deprotonation of **Hbimca<sup>Homo</sup>·2HBr** with different bases



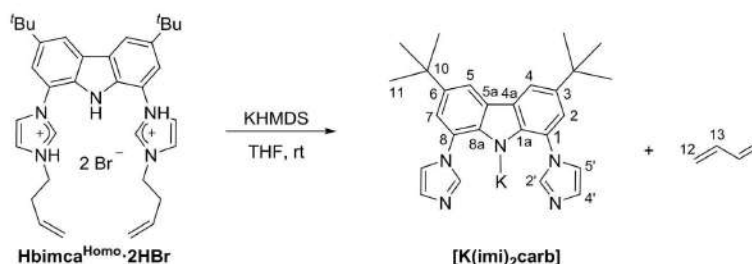
Lithium bis(trimethylsilyl)amide (7.4 mg, 44  $\mu\text{mol}$ ) or methyl lithium (1.0 mg, 44  $\mu\text{mol}$ ) was added to the suspension of **Hbimca<sup>Homo</sup>·2HBr** (10.0 mg, 14.7  $\mu\text{mol}$ ) in 0.5 mL of THF-*d*<sub>8</sub> at room temperature and a light yellow solution with blue fluorescence was formed. After 30 min, the quantitative formation of **[Li(bimca<sup>Homo</sup>)]** was confirmed by <sup>1</sup>H NMR spectroscopy.<sup>[1]</sup>

<sup>1</sup>H NMR (400 MHz, THF-*d*<sub>8</sub>)  $\delta$  = 8.00 (s, 2H, H-4/5), 7.73 (s, 2H, H-5'), 7.40 (s, 2H, H-2/7), 7.21 (s, 2H, H-4'), 5.98-5.88 (m, 2H, H-14), 5.15 (d, <sup>3</sup>*J*<sub>HH</sub> = 17.1 Hz, 2H, H-15<sub>trans</sub>), 5.04 (d, <sup>3</sup>*J*<sub>HH</sub> = 10.1 Hz, 2H, H-15<sub>cis</sub>), 4.29 (t, <sup>3</sup>*J*<sub>HH</sub> = 7.2 Hz, 4H, H-12), 2.72 (q, <sup>3</sup>*J*<sub>HH</sub> = 6.3 Hz, 4H, H-13), 1.50 (s, 18H, H-11). <sup>13</sup>C NMR (101 MHz, THF-*d*<sub>8</sub>)  $\delta$  = 205.3 (C2'), 143.8 (C1a/8a), 136.4 (C14), 135.8 (C3/6), 128.6 (C4a/5a), 128.4 (C1/8), 119.6 (C5'), 119.4 (C15), 117.3 (C4'), 114.3 (C4/5), 111.8 (C2/7), 51.9 (C12), 37.0 (C13), 35.4 (C10), 33.1 (C11).



Potassium bis(trimethylsilyl)amide (10.4 mg, 52.0  $\mu\text{mol}$ ) was added to the suspension of **Hbimca<sup>Homo</sup>·2HBr** (10.0 mg, 14.7  $\mu\text{mol}$ ) in 0.5 mL of THF-*d*<sub>8</sub> at  $-30$  °C and a yellow solution formed. After 10 min, the formation of **[K(bimca<sup>Homo</sup>)]** was checked by low temperature <sup>1</sup>H NMR spectroscopy at  $-30$  °C.

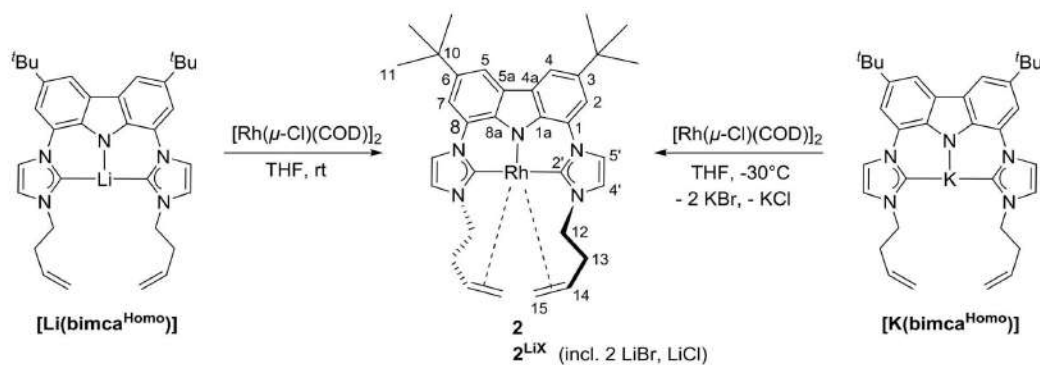
$^1\text{H}$  NMR (400 MHz,  $\text{THF-}d_8$ )  $\delta$  = 8.02 (s, 2H, H-4/5), 7.50 (br s, 2H, H-5'), 7.24 (s, 2H, H-2/7), 7.12 (s, 2H, H-4'), 5.91-5.83 (m, 2H, H-14), 5.12 (d,  $^3J_{\text{HH}}$  = 17.2 Hz, 2H, H-15<sub>trans</sub>), 5.03 (d,  $^3J_{\text{HH}}$  = 10.3 Hz, 2H, H-15<sub>cis</sub>), 4.13 (t,  $^3J_{\text{HH}}$  = 7.6 Hz, 4H, H-12), 2.57 (ps q,  $^3J_{\text{HH}}$  = 7.0 Hz, 4H, H-13), 1.46 (s, 18H, H-11).  $^{13}\text{C}$  NMR (101 MHz,  $\text{THF-}d_8$ )  $\delta$  = 146.5 (C1a/8a), 136.7 (C14), 134.3 (C3/6), 130.0 (C4a/5a), 128.5 (C1/8), 122.6 (C5'), 118.5 (C15), 117.0 (C4'), 116.3 (C4/5), 114.6 (C2/7), 51.2 (C12), 37.6 (C13), 35.3 (C10), 33.1 (C11). The signal of C2' is not observed.



Potassium bis(trimethylsilyl)amide (8.8 mg, 44  $\mu\text{mol}$ ) was added to the suspension of **Hbimca**<sup>Homo</sup>-2HBr (10.0 mg, 14.7  $\mu\text{mol}$ ) in 0.5 mL of  $\text{THF-}d_8$  at room temperature and a yellow solution was formed. After 10 min, the formation of **[K(imi)<sub>2</sub>carb]** and 1,3-butadiene was confirmed by  $^1\text{H}$  NMR spectroscopy.

$^1\text{H}$  NMR (400 MHz,  $\text{THF-}d_8$ )  $\delta$  = 8.93 (s, 2H, H-2'), 8.03 (d,  $^3J_{\text{HH}}$  = 1.9 Hz, 2H, H-4/5), 7.72 (t,  $^3J_{\text{HH}}$  = 1.2 Hz, 2H, H-5'), 7.28 (d,  $^3J_{\text{HH}}$  = 1.9 Hz, 2H, H-2/7), 7.04 (d,  $^3J_{\text{HH}}$  = 1.2 Hz, 2H, H-4'), 6.42-6.25 (m, 2H, H-13), 5.21-5.14 (m, 2H, H-12<sub>trans</sub>), 5.10-5.02 (m, 2H, H-12<sub>cis</sub>), 1.47 (s, 18H, H-11).  $^{13}\text{C}$  NMR (101 MHz,  $\text{THF-}d_8$ )  $\delta$  = 145.9 (C1a/8a), 139.9 (C2'), 138.9 (C13), 135.4 (C3/6), 128.7 (C4'), 128.6 and 124.9, (C1/8 and C4a/5a), 119.9 (C5'), 117.9 (C12), 115.2 (C4/5), 113.5 (2/7), 35.3 (C10), 33.1 (C11).

### 3.2. Preparation of catalysts **2** and **2**<sup>LiX</sup>



From **[Li(bimca<sup>Homo</sup>)]**:

[Rh( $\mu$ -Cl)(COD)]<sub>2</sub> (0.5 eq) was added to the previous prepared solution of **[Li(bimca<sup>Homo</sup>)]** (1.0 eq) at the given temperature. The solution was stirred for 1 h. Catalyst **2** was obtained as an orange solution in quantitative yield as determined by NMR spectroscopy.

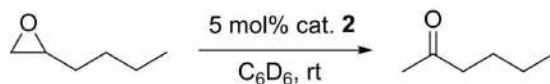
<sup>1</sup>H NMR (400 MHz, THF-*d*<sub>8</sub>)  $\delta$  = 8.02 (d, <sup>4</sup>J<sub>HH</sub> = 1.5 Hz, 2H, H-4/5), 7.92 (d, <sup>3</sup>J<sub>HH</sub> = 2.2 Hz, 2H, H-5'), 7.52 (d, <sup>4</sup>J<sub>HH</sub> = 1.5 Hz, 2H, H-2/7), 7.11 (d, <sup>3</sup>J<sub>HH</sub> = 2.2 Hz, 2H, H-4'), 4.21 (br ps t, <sup>2/3</sup>J = 12.0 Hz, 2H, H-12<sub>ax</sub>), 4.14–4.06 (m, 2H, H-14), 3.77 (br d, <sup>2</sup>J = 12.7 Hz, 2H, H-12<sub>eq</sub>), 2.74–2.65 (m, 2H, H-13<sub>eq</sub>), 2.38 (dd, <sup>3</sup>J<sub>HH</sub> = 8.0, <sup>2</sup>J<sub>HH</sub> = 1.3 Hz, 2H, H-15<sub>cis</sub>), 1.64 (br d, <sup>3</sup>J<sub>HH</sub> = 9.9 Hz, 2H, H-15<sub>trans</sub>), 1.48 (s, 18H, H-11), 1.41–1.32 (m, 2H, H-13<sub>ax</sub>). <sup>13</sup>C NMR (101 MHz, THF-*d*<sub>8</sub>)  $\delta$  = 185.5 (d, <sup>1</sup>J<sub>RhC</sub> = 33.9 Hz, C2'), 137.8 (C3/6), 136.6 (C1a/8a), 128.4 (C4a/5a), 126.2 (C1/8), 121.7 (C4'), 116.3 (C5'), 115.0 (C4/5), 109.1 (C2/7), 55.9 (d, <sup>1</sup>J<sub>RhC</sub> = 6.7 Hz, C15), 52.6 (C12), 51.1 (d, <sup>1</sup>J<sub>RhC</sub> = 11.3 Hz, C14), 36.0 (C13), 35.5 (C10), 33.0 (C11).

From **[K(bimca<sup>Homo</sup>)]**:

[Rh( $\mu$ -Cl)(COD)]<sub>2</sub> (0.5 eq) was added to the previous prepared solution of **[K(bimca<sup>Homo</sup>)]** (1.0 eq) at –30 °C. The solution was stirred for 1 h. After completion, the solvent was removed in vacuo. The residue was washed with pentane (3 × 1 mL) and redissolved in THF (1 mL). The solution was dried in vacuo to obtain catalyst **2** as a yellow solid. The NMR data correspond to the results obtained from using **[Li(bimca<sup>Homo</sup>)]**.

C<sub>34</sub>H<sub>40</sub>N<sub>5</sub>Rh (621.62): calcd C 65.69, H 6.49, N 11.27; found C 65.19, H 6.36, N 11.03. m.p.: 183–187 °C (dec). (From **[K(bimca<sup>Homo</sup>)]**)

#### 4. Reactivity comparison between catalyst 1 and catalyst 2



To a solution of catalyst 2 (2.0  $\mu\text{mol}$ ) and 1,3,5-trimethoxybenzene (certain amount) as the internal standard in  $\text{C}_6\text{D}_6$  (0.4 mL), 1,2-epoxyhexane (4.1 mg, 40  $\mu\text{mol}$ ) was added. The reaction at room temperature was followed by  $^1\text{H}$  NMR spectroscopy every 30 min.

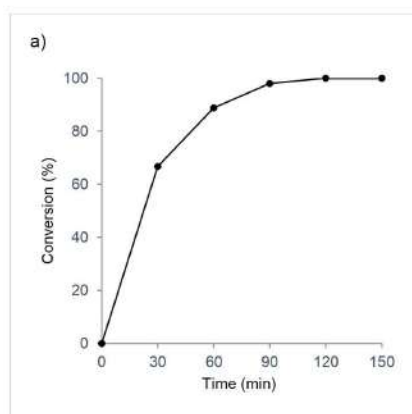


Figure S1. Monitoring the conversion of 1,2-epoxyhexane with catalyst 2.

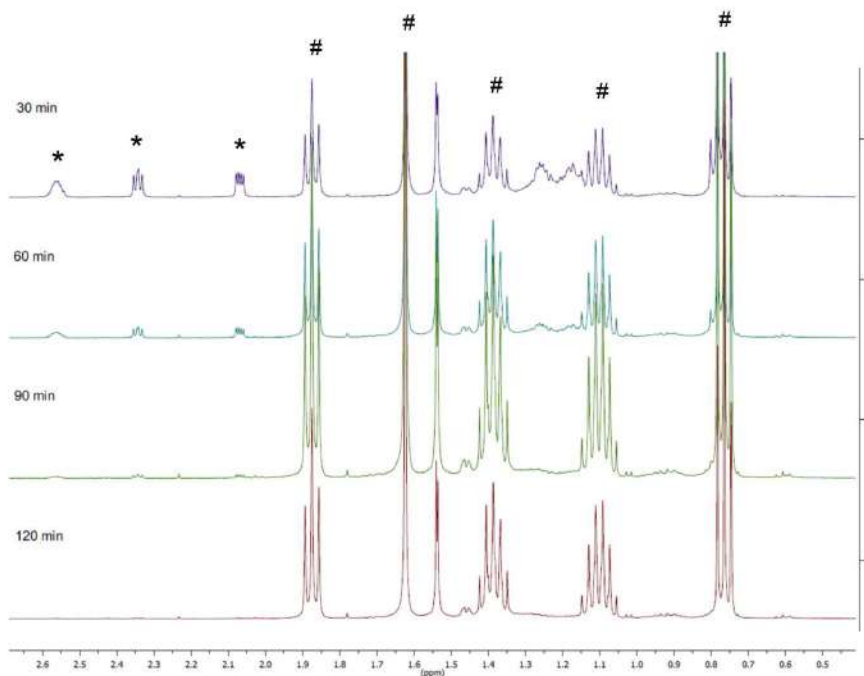
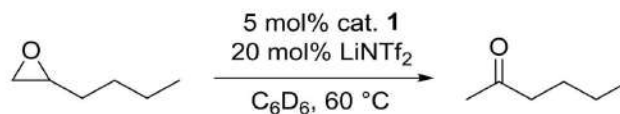


Figure S2. Monitoring the rearrangement of 1,2-epoxyhexane (\*) into hexan-2-one (#) with catalyst 2 by  $^1\text{H}$  NMR spectroscopy.



1,2-Epoxyhexane (4.1 mg, 40  $\mu\text{mol}$ ), catalyst **1** (1.1 mg, 2.0  $\mu\text{mol}$ ) and LiNTf<sub>2</sub> (2.3 mg, 8.0  $\mu\text{mol}$ ) were added into a *J. Young* NMR tube. 1,3,5-trimethoxybenzene (certain amount) was added as the internal standard and C<sub>6</sub>D<sub>6</sub> was used as the solvent. The reaction was carried out at 60 °C and monitored by <sup>1</sup>H NMR spectroscopy every 30 min.

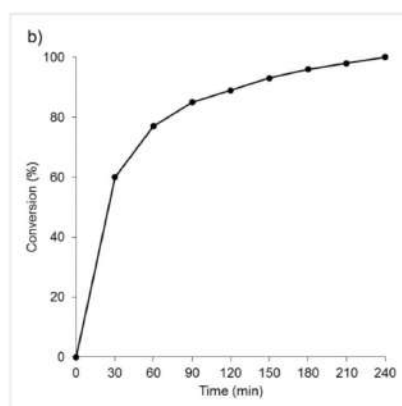


Figure S3. Monitoring the conversion of 1,2-epoxyhexane with catalyst **1**.

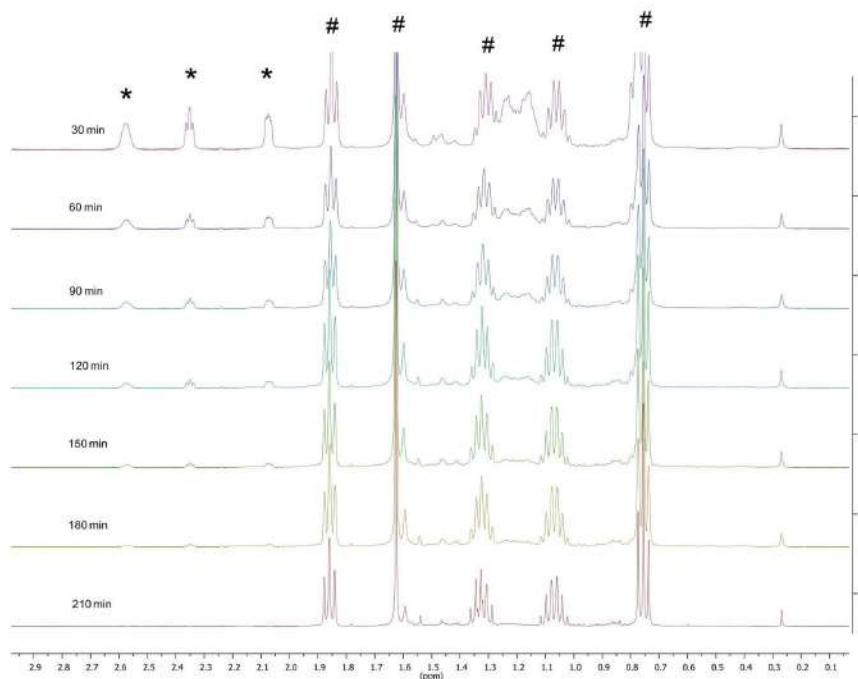


Figure S4. Monitoring the rearrangement of 1,2-epoxyhexane (\*) into hexan-2-one (#) with catalyst **1** by <sup>1</sup>H NMR spectroscopy.



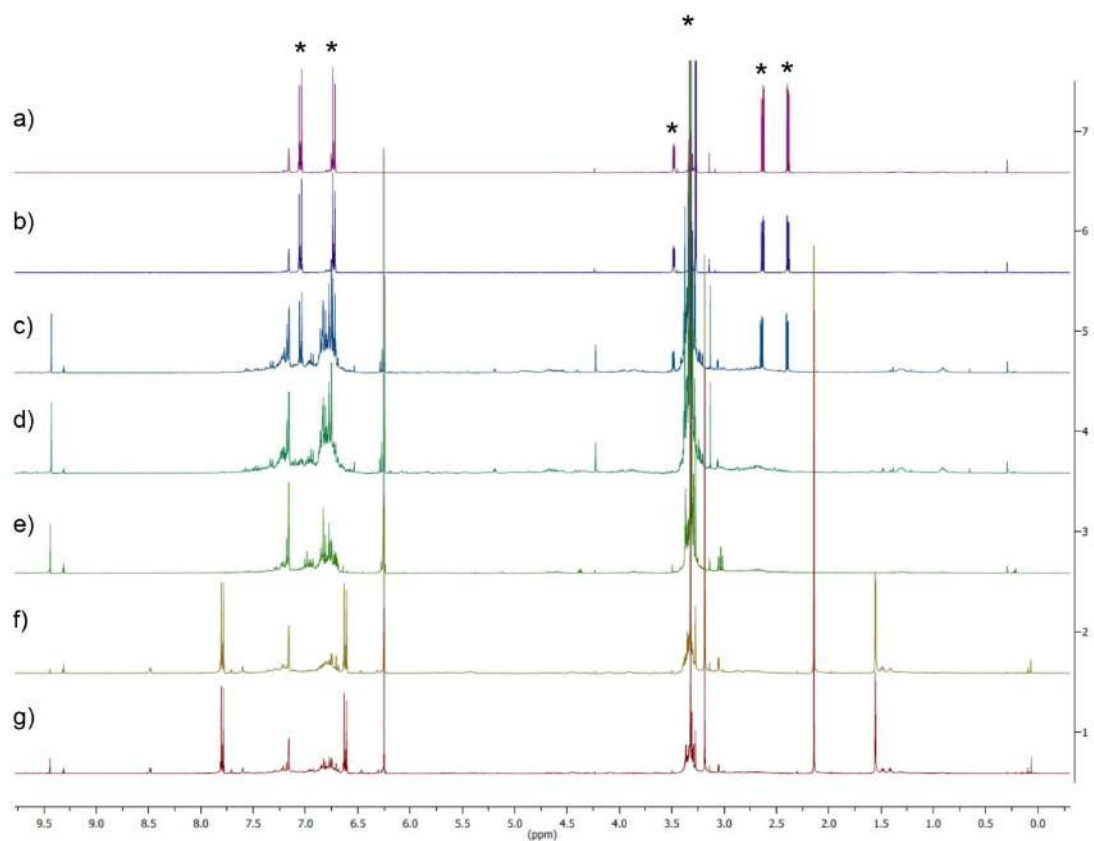
## 5. Additional substrate scope for catalyst 1 in the Meinwald reaction

5 mol% cat. 1  
20 mol% LiNTf<sub>2</sub>  
C<sub>6</sub>D<sub>6</sub>, 60 °C

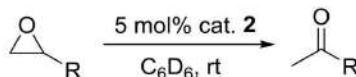
	Epoxide	Methyl ketone	Time	Yield [%] <sup>[a,b]</sup>
<b>3a</b>		<b>4a</b>	3 h	95
<b>3b</b>		<b>4b</b>	3 h	95
<b>3c</b>		<b>4c</b>	9.7 d	50
<b>3d</b>		<b>4d</b>	24 h	92
<b>3e</b>		<b>4e</b>	3 h	98
<b>3f</b>		<b>4f</b>	2 h	50
<b>3g</b>		<b>4g</b>	24 h	20
<b>3h</b>		<b>4h</b>	24 h	67
<b>3i</b>		<b>4i</b>	24 h	37
<b>3j</b>		<b>4j</b>	24 h	33 <sup>[c]</sup>
<b>3k</b>		<b>4k</b>	24 h	17 <sup>[c]</sup>
<b>3l</b>		<b>4l</b>	24 h	99
<b>5a</b>		<b>6a</b>	24 h	26 (Ketone) 44 (Aldehyde)

[a] Standard reaction conditions: Substrates (40  $\mu$ mol), Cat. 1 (2.0  $\mu$ mol), C<sub>6</sub>D<sub>6</sub> (0.4 mL), 60 °C. All reactions were carried out using a *J. Young* NMR tube. [b] Yield of methyl ketones was determined by <sup>1</sup>H NMR using 1,3,5-trimethoxybenzene as the internal standard. [c] at 80 °C.

6. Stability of 2-(4-methoxyphenyl)oxirane (**5I**) against lithium halides and catalyst **2**

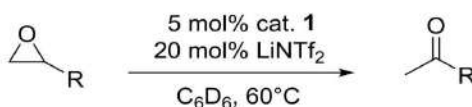


**Figure S5.** a) **5I** (\*) in C<sub>6</sub>D<sub>6</sub>; b) **5I** in C<sub>6</sub>D<sub>6</sub> after 8 days; c) **5I** in C<sub>6</sub>D<sub>6</sub> with 10 mol% LiBr and 5 mol% LiCl after 4 days; d) **5I** in C<sub>6</sub>D<sub>6</sub> with 10 mol% LiBr and 5 mol% LiCl after 18 days; e) **5I** in C<sub>6</sub>D<sub>6</sub> with 10 mol% LiI after 23 h; f) **5I** in C<sub>6</sub>D<sub>6</sub> with 5 mol% catalyst **2** after 2 h; g) **5I** in C<sub>6</sub>D<sub>6</sub> with 5 mol% catalyst **2** after 48 h.

7. Experimental procedures for the Meinwald reaction of terminal epoxides with catalyst **2**<sup>Lix</sup>**Method 1**

A defined amount of an in situ prepared solution containing catalyst **2**<sup>Lix</sup> (2.5  $\mu\text{mol}$ ) was injected into a *J. Young* NMR tube containing a defined amount of the internal standard 1,3,5-trimethoxybenzene and THF was removed under vacuum.  $\text{C}_6\text{D}_6$  (0.5 mL) and the respective epoxide (50  $\mu\text{mol}$ ) were added successively. The reaction at room temperature was monitored by  $^1\text{H}$  NMR spectroscopy. All yields were determined by 1,3,5-trimethoxybenzene (certain amount) as the internal standard. The NMR signals of the obtained ketones were confirmed with literature data.

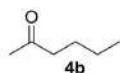
The up-scaling of this method was tested with **3I** (1.0 mmol). Lithium bis(trimethylsilyl)amide (25.1 mg, 150.0  $\mu\text{mol}$ ) was added to a suspension of **Hbimca**<sup>Hom</sup>**·2HBr** (34.1 mg, 50.0  $\mu\text{mol}$ ) in 0.7 mL of THF-*d*8 at room temperature. After 10 min,  $[\text{Rh}(\mu\text{-Cl})(\text{COD})]_2$  (12.3 mg, 25.0  $\mu\text{mol}$ ) was added and the solution was stirred for another 10 min. The successful formation of the catalyst was checked by  $^1\text{H}$  NMR. After the THF-*d*8 was removed in the oil-pump vacuum, the catalyst was transferred to a dry round flask with toluene (10 mL) and the epoxide **3I** (134.2 mg, 1.0 mmol) was added. The reaction was stirred for 2 h. After removal of the solvent by rotary evaporation, the crude product was purified by column chromatography on silica gel (EtOAc/hexane, 1:8) to afford the desired product **4I** (82%) as a colourless liquid.

**Method 2**

Catalyst **1** (1.1 mg, 2.0  $\mu\text{mol}$ ), lithium bis(trifluoromethanesulfonimide) (2.3 mg, 8.0  $\mu\text{mol}$ ) and 1,3,5-trimethoxybenzene (certain amount) were added into a *J. Young* NMR tube.  $\text{C}_6\text{D}_6$  (0.4 mL) was added as the solvent. The solution was then mixed with the respective epoxide (40  $\mu\text{mol}$ ) and heated at 60  $^\circ\text{C}$  for a defined period of time. The reaction was monitored by  $^1\text{H}$  NMR spectroscopy and the yields were determined by 1,3,5-trimethoxybenzene as the internal standard. The NMR signals of the obtained ketones were compared with literature values.



Propan-2-one (**4a**).  $^1\text{H}$  NMR (400 MHz,  $\text{C}_6\text{D}_6$ )  $\delta$  = 1.57 (s, 3H).



Hexan-2-one (**4b**).  $^1\text{H}$  NMR (400 MHz,  $\text{C}_6\text{D}_6$ )  $\delta$  = 1.89 (t,  $J$  = 7.4 Hz, 2H), 1.64 (s, 3H), 1.44–1.37 (m, 2H), 1.17–1.07 (m, 2H), 0.78 (t,  $J$  = 7.4 Hz, 3H).



3,3-Dimethylbutan-2-one (**4c**).  $^1\text{H}$  NMR (400 MHz,  $\text{C}_6\text{D}_6$ )  $\delta$  = 1.73 (s, 3H), 0.89 (s, 9H).



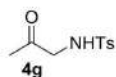
1-Cyclohexylethan-1-one (**4d**).  $^1\text{H}$  NMR (400 MHz,  $\text{C}_6\text{D}_6$ )  $\delta$  = 1.88 (tt,  $J$  = 11.4, 3.5 Hz, 1H), 1.71 (s, 3H), 1.64–1.42 (m, 5H), 1.26–1.16 (m, 2H), 1.07–0.96 (m, 3H).



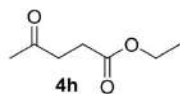
1-Methoxypropan-2-one (**4e**).  $^1\text{H}$  NMR (400 MHz,  $\text{C}_6\text{D}_6$ )  $\delta$  = 3.43 (s, 2H), 2.96 (s, 3H), 1.71 (s, 3H).



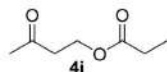
1-Hydroxypropan-2-one (**4f**).  $^1\text{H}$  NMR (400 MHz,  $\text{C}_6\text{D}_6$ )  $\delta$  = 3.57 (s, 2H), 2.97 (br s, 1H), 1.27 (s, 3H).



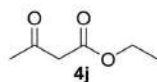
4-Methyl-*N*-(2-oxopropyl)benzenesulfonamide (**4g**).  $^1\text{H}$  NMR (400 MHz,  $\text{C}_6\text{D}_6$ )  $\delta$  = 7.79 (d,  $J$  = 8.1 Hz, 2H), 6.81 (d,  $J$  = 8.1 Hz, 2H), 5.71 (s, 1H), 3.38 (s, 2H), 1.87 (s, 3H), 1.32 (s, 3H).



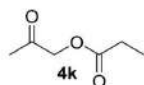
Ethyl-4-oxopentanoate (**4h**).  $^1\text{H NMR}$  (400 MHz,  $\text{C}_6\text{D}_6$ )  $\delta$  = 3.93 (q,  $J$  = 7.1 Hz, 2H), 2.34 (t,  $J$  = 6.4 Hz, 2H), 2.16 (t,  $J$  = 6.4 Hz, 2H), 1.62 (s, 3H), 0.94 (t,  $J$  = 7.1 Hz, 3H).



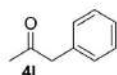
3-Oxobutyl-propionate (**4i**).  $^1\text{H NMR}$  (400 MHz,  $\text{C}_6\text{D}_6$ )  $\delta$  = 4.18 (t,  $J$  = 6.3 Hz, 2H), 2.07 (t,  $J$  = 6.3 Hz, 2H), 1.98 (q,  $J$  = 7.6 Hz, 2H), 1.55 (s, 3H), 0.93 (t,  $J$  = 7.6 Hz, 3H).



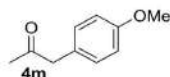
Ethyl-3-oxobutanoate (**4j**).  $^1\text{H NMR}$  (400 MHz,  $\text{C}_6\text{D}_6$ )  $\delta$  = 3.88 (q,  $J$  = 7.1 Hz, 2H), 2.90 (s, 2H), 1.66 (s, 3H), 0.89 (t,  $J$  = 7.1 Hz, 3H).



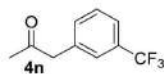
2-Oxopropylpropionate (**4k**).  $^1\text{H NMR}$  (400 MHz,  $\text{C}_6\text{D}_6$ )  $\delta$  = 4.11 (s, 2H), 2.12 (q,  $J$  = 7.6 Hz, 2H), 1.42 (s, 3H), 0.96 (t,  $J$  = 7.6 Hz, 3H).



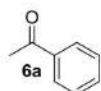
1-Phenylpropan-2-one (**4l**).  $^1\text{H NMR}$  (400 MHz,  $\text{C}_6\text{D}_6$ )  $\delta$  = 7.11–7.01 (m, 3H), 6.98–6.96 (m, 2H), 3.20 (s, 2H), 1.63 (s, 3H). Up-scaling result: 82% isolated yield.  $^1\text{H NMR}$  (400 MHz,  $\text{CDCl}_3$ )  $\delta$  = 7.37–7.33 (m, 2H), 7.30–7.26 (m, 1H), 7.23–7.21 (m, 2H), 3.71 (s, 2H), 2.16 (s, 3H).  $^{13}\text{C NMR}$  (101 MHz,  $\text{CDCl}_3$ )  $\delta$  = 206.4, 134.2, 129.4, 128.7, 127.0, 51.0, 29.2.



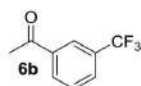
1-(4-Methoxyphenyl)propan-2-one (**4m**).  $^1\text{H NMR}$  (400 MHz,  $\text{C}_6\text{D}_6$ )  $\delta$  = 6.91 (dt,  $J$  = 8.0, 4.0 Hz, 2H), 6.73 (dt,  $J$  = 8.0, 4.0 Hz, 2H), 3.29 (s, 3H), 3.21 (s, 2H), 1.68 (s, 3H).



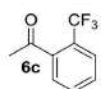
1-(3-(Trifluoromethyl)phenyl)propan-2-one (**4n**).  $^1\text{H}$  NMR (400 MHz,  $\text{C}_6\text{D}_6$ )  $\delta$  = 7.23–7.23 (m, 2H), 6.92–6.85 (m, 2H), 2.97 (s, 2H), 1.54 (s, 3H).



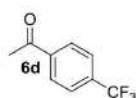
Acetophenone (**6a**).  $^1\text{H}$  NMR (400 MHz,  $\text{C}_6\text{D}_6$ )  $\delta$  = 7.77–7.74 (m, 2H), 7.13–7.09 (m, 1H), 7.06–7.00 (m, 2H), 2.09 (s, 3H).



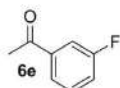
1-(3-(Trifluoromethyl)phenyl)ethan-1-one (**6b**).  $^1\text{H}$  NMR (400 MHz,  $\text{C}_6\text{D}_6$ )  $\delta$  = 8.00 (s, 1H), 7.64 (d,  $J$  = 7.8 Hz, 1H), 7.29 (d,  $J$  = 7.8 Hz, 1H), 6.80 (t,  $J$  = 7.8 Hz, 1H), 1.90 (s, 3H).



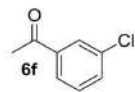
1-(2-(Trifluoromethyl)phenyl)ethan-1-one (**6c**).  $^1\text{H}$  NMR (400 MHz,  $\text{C}_6\text{D}_6$ )  $\delta$  = 7.26 (d,  $J$  = 7.7 Hz, 1H), 6.85–6.76 (m, 3H), 2.06 (s, 3H).



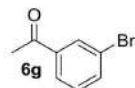
1-(4-(Trifluoromethyl)phenyl)ethan-1-one (**6d**).  $^1\text{H}$  NMR (400 MHz,  $\text{C}_6\text{D}_6$ )  $\delta$  = 7.48 (d,  $J$  = 8.0 Hz, 2H), 7.22 (d,  $J$  = 8.0 Hz, 2H), 1.95 (s, 3H).



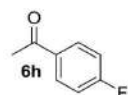
1-(3-Fluorophenyl)ethan-1-one (**6e**).  $^1\text{H}$  NMR (400 MHz,  $\text{C}_6\text{D}_6$ )  $\delta$  = 7.47–7.44 (m, 1H), 7.38–7.34 (m, 1H), 6.79–6.76 (m, 2H), 1.94 (s, 3H).



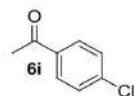
1-(3-Chlorophenyl)ethan-1-one (**6f**).  $^1\text{H}$  NMR (400 MHz,  $\text{C}_6\text{D}_6$ )  $\delta$  = 7.75 (t,  $J$  = 1.7 Hz, 1H), 7.45-7.43 (m, 1H), 7.08-7.06 (m, 1H), 6.71 (t,  $J$  = 7.9, 1H), 1.91 (s, 3H).



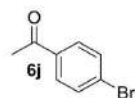
1-(3-Bromophenyl)ethan-1-one (**6g**).  $^1\text{H}$  NMR (400 MHz,  $\text{C}_6\text{D}_6$ )  $\delta$  = 7.92-7.91 (m, 1H), 7.49-7.46 (dt,  $J$  = 7.6, 1.0 Hz, 1H), 7.24-7.21 (m, 1H), 6.64 (t,  $J$  = 7.9, 1H), 1.89 (s, 3H).



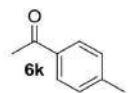
1-(4-Fluorophenyl)ethan-1-one (**6h**).  $^1\text{H}$  NMR (400 MHz,  $\text{C}_6\text{D}_6$ )  $\delta$  = 7.56-7.51 (m, 2H), 6.66-6.60 (m, 2H), 1.99 (s, 3H).



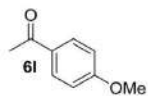
1-(4-Chlorophenyl)ethan-1-one (**6i**).  $^1\text{H}$  NMR (400 MHz,  $\text{C}_6\text{D}_6$ )  $\delta$  = 7.43 (dt,  $J$  = 8.7, 2.3 Hz, 2H), 6.98 (dt,  $J$  = 8.7, 2.3 Hz, 2H), 1.95 (s, 3H).



1-(4-Bromophenyl)ethan-1-one (**6j**).  $^1\text{H}$  NMR (400 MHz,  $\text{C}_6\text{D}_6$ )  $\delta$  = 7.34 (dt,  $J$  = 8.8, 2.3 Hz, 2H), 7.15 (dt,  $J$  = 8.8, 2.3 Hz, 2H), 1.94 (s, 3H).



1-(p-Tolyl)ethan-1-one (**6k**).  $^1\text{H}$  NMR (400 MHz,  $\text{C}_6\text{D}_6$ )  $\delta$  = 7.76-7.73 (m, 2H), 6.89-6.86 (m, 2H), 2.13 (s, 3H), 1.99 (s, 3H).



1-(4-Methoxyphenyl)ethan-1-one (**6l**).  $^1\text{H}$  NMR (400 MHz,  $\text{C}_6\text{D}_6$ )  $\delta$  = 7.80 (dt,  $J$  = 8.9, 2.9 Hz, 2H), 6.62 (dt,  $J$  = 8.9, 2.9 Hz, 2H), 3.18 (s, 3H), 2.14 (s, 3H).



1-(*o*-Tolyl)ethan-1-one (**6m**).  $^1\text{H}$  NMR (400 MHz,  $\text{C}_6\text{D}_6$ )  $\delta$  = 7.26 (d,  $J$  = 7.5 Hz, 1H), 7.05-7.01 (m, 1H), 6.93-6.91 (m, 2H), 2.53 (s, 3H), 2.11 (s, 3H).





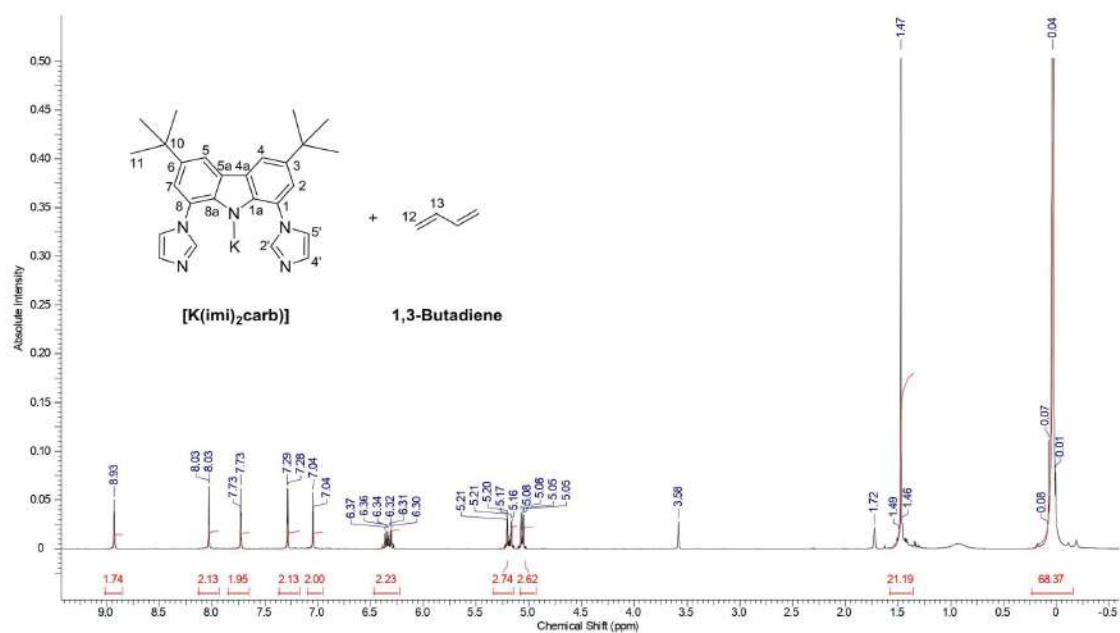


Figure S8. <sup>1</sup>H NMR (THF-*d*<sub>8</sub>, 400 MHz) spectrum: deprotonation of Hbimca<sup>Homo</sup>-2HBr with KHMDS at room temperature.

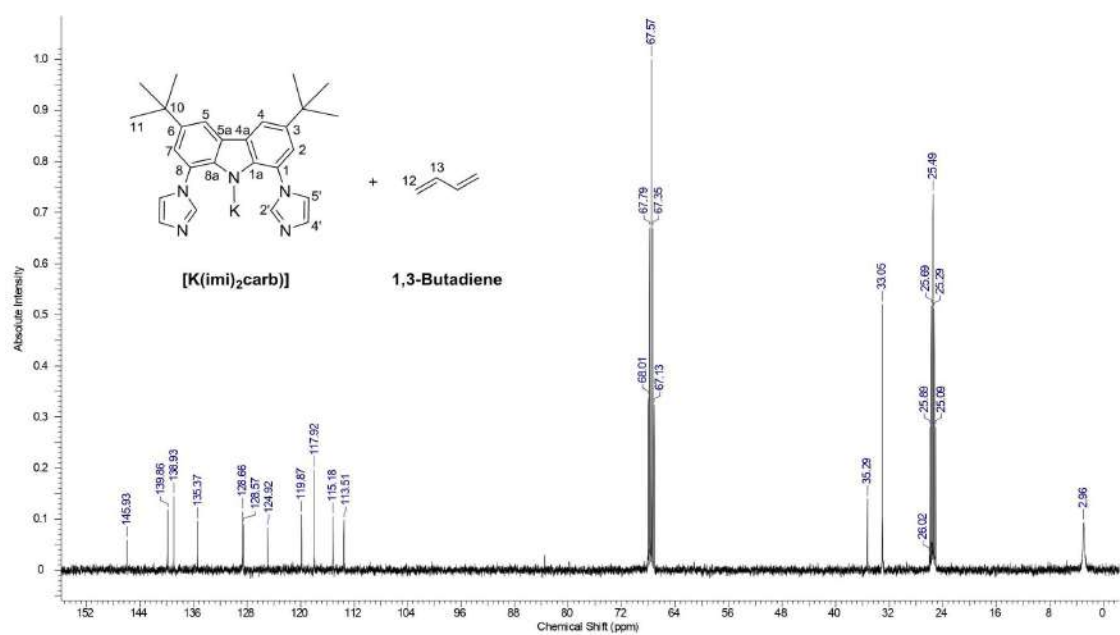


Figure S9. <sup>13</sup>C NMR (THF-*d*<sub>8</sub>, 101 MHz) spectrum: deprotonation of Hbimca<sup>Homo</sup>-2HBr with KHMDS at room temperature.

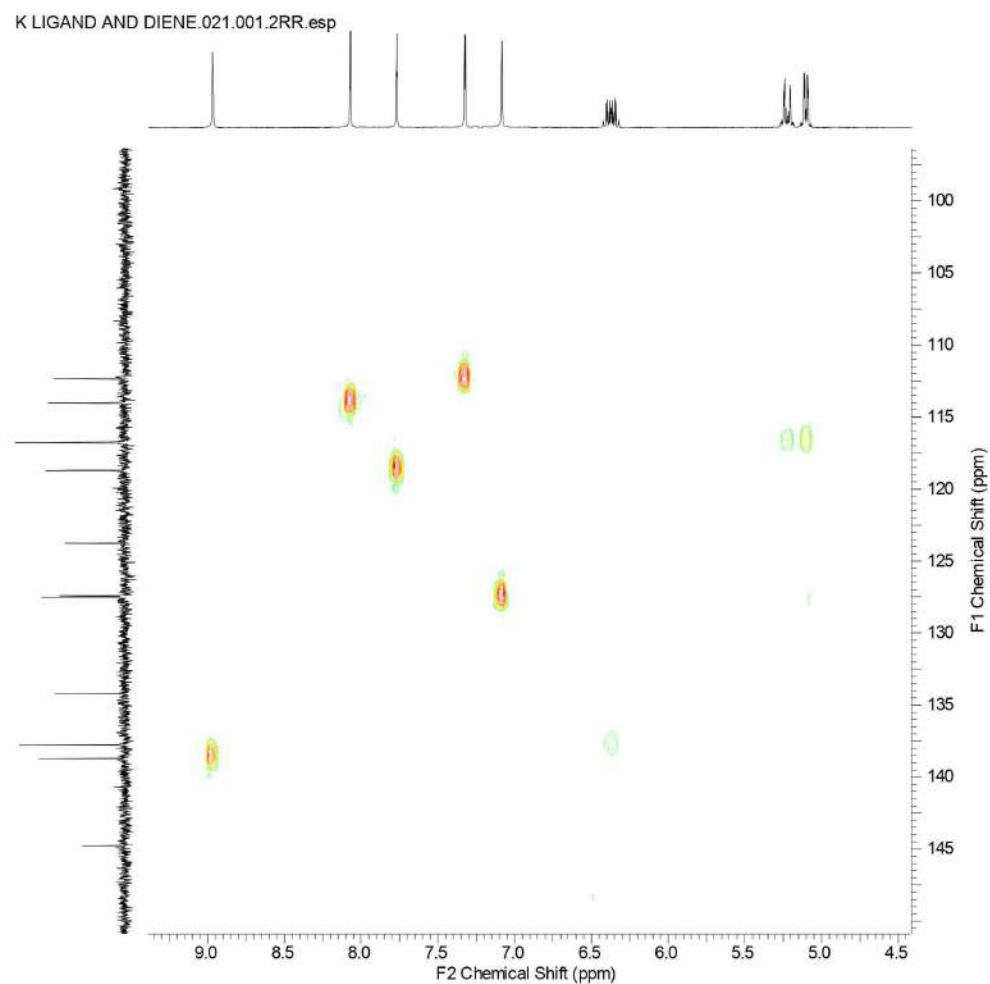


Figure S10. <sup>1</sup>H-<sup>13</sup>C HSQC (THF-*d*<sub>6</sub>, 400 MHz) spectrum: deprotonation of **Hbimca**<sup>Homo</sup>-**2HBr** with KHMDS at room temperature.

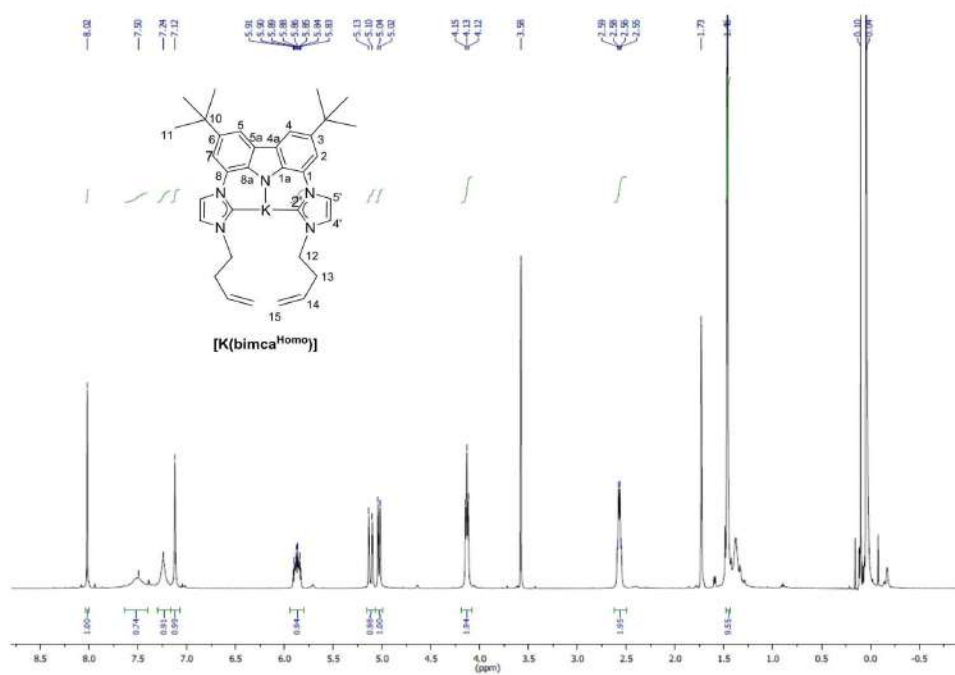


Figure S11.  $^1H$  NMR (THF- $d_8$ , 400 MHz) spectrum: deprotonation of  $Hbimca^{Homo}\cdot 2HBr$  with KHMDS at  $-30$   $^{\circ}C$ .

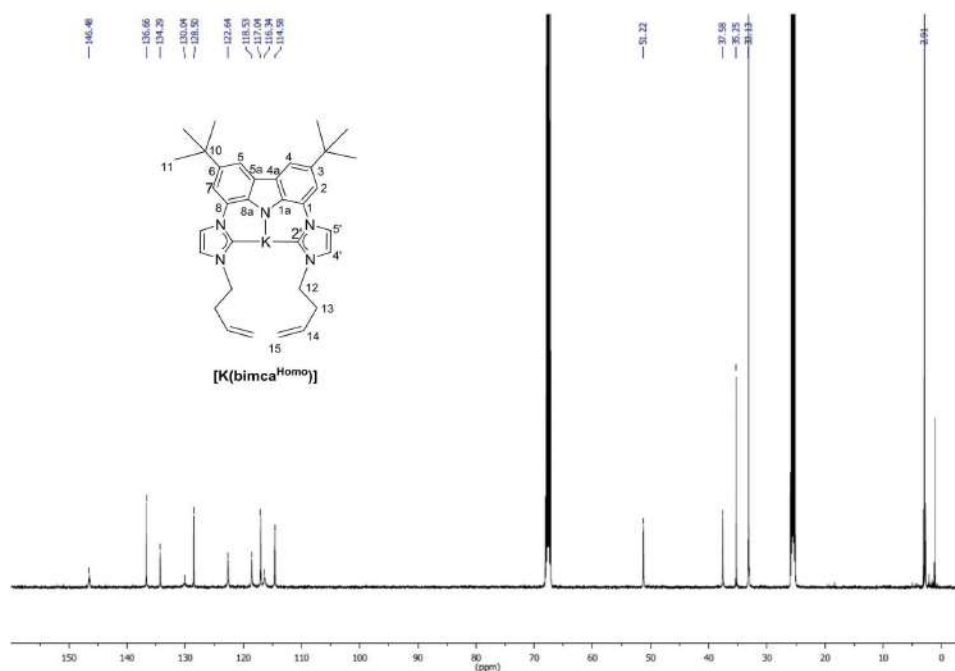


Figure S12.  $^{13}C$  NMR (THF- $d_8$ , 101 MHz) spectrum: deprotonation of  $Hbimca^{Homo}\cdot 2HBr$  with KHMDS at  $-30$   $^{\circ}C$ .



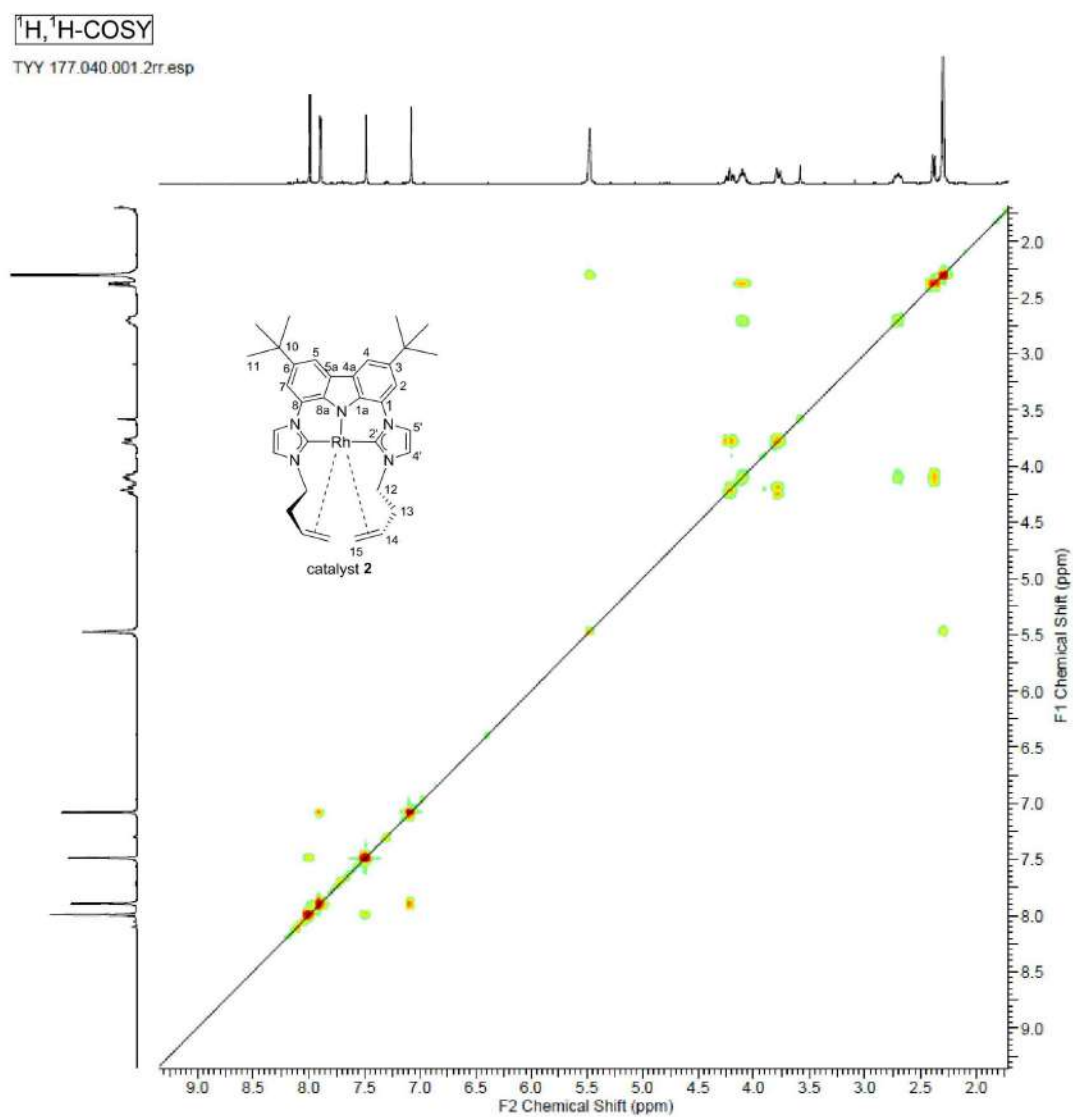
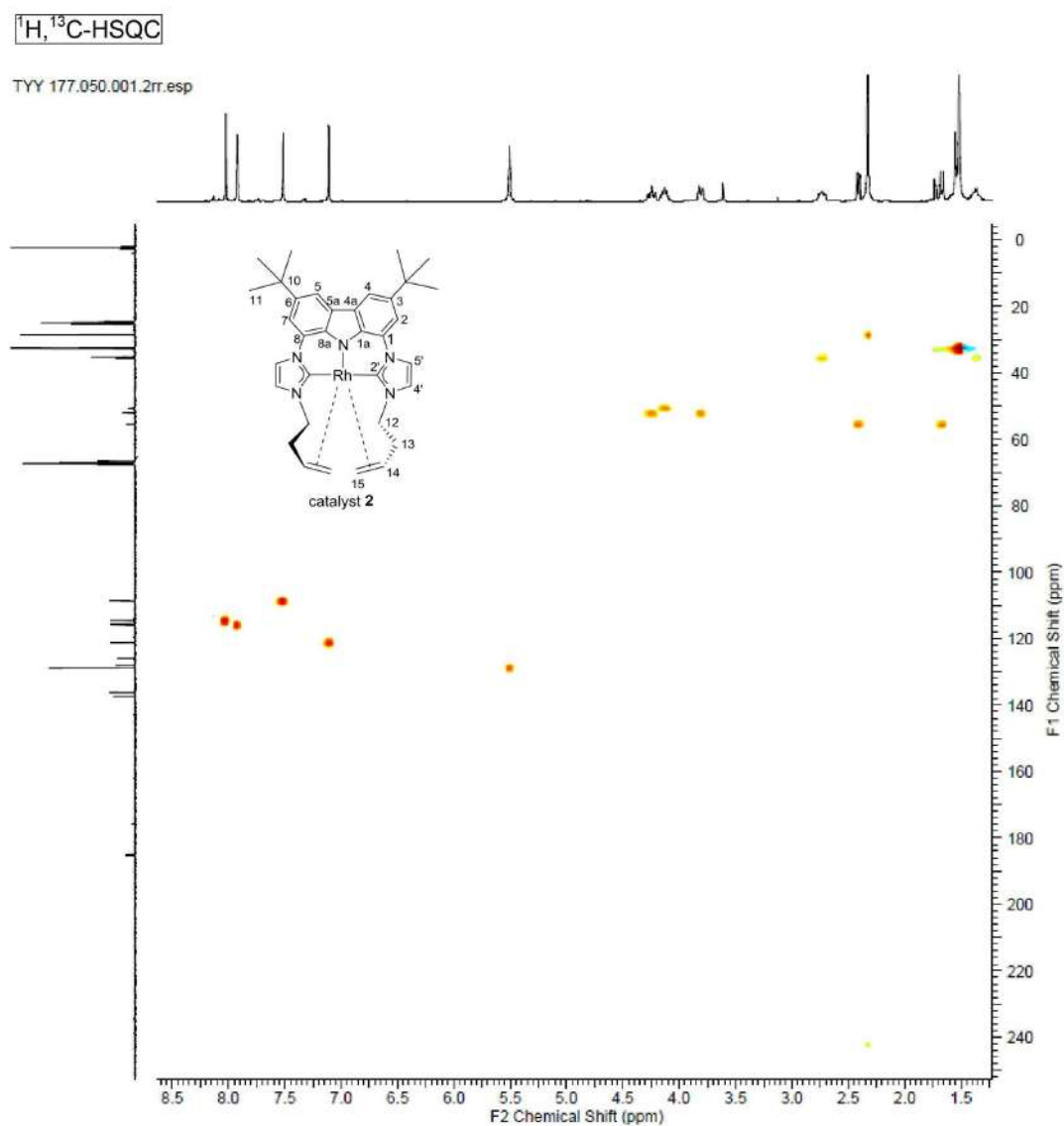


Figure S15.  $^1\text{H}, ^{13}\text{C}$ -COSY NMR ( $\text{THF}-d_6$ , 400 MHz) spectrum: transmetalation of  $[\text{Li}(\text{bimca}^{\text{Homo}})]$  with  $[\text{Rh}(\mu\text{-Cl})(\text{COD})]_2$ .



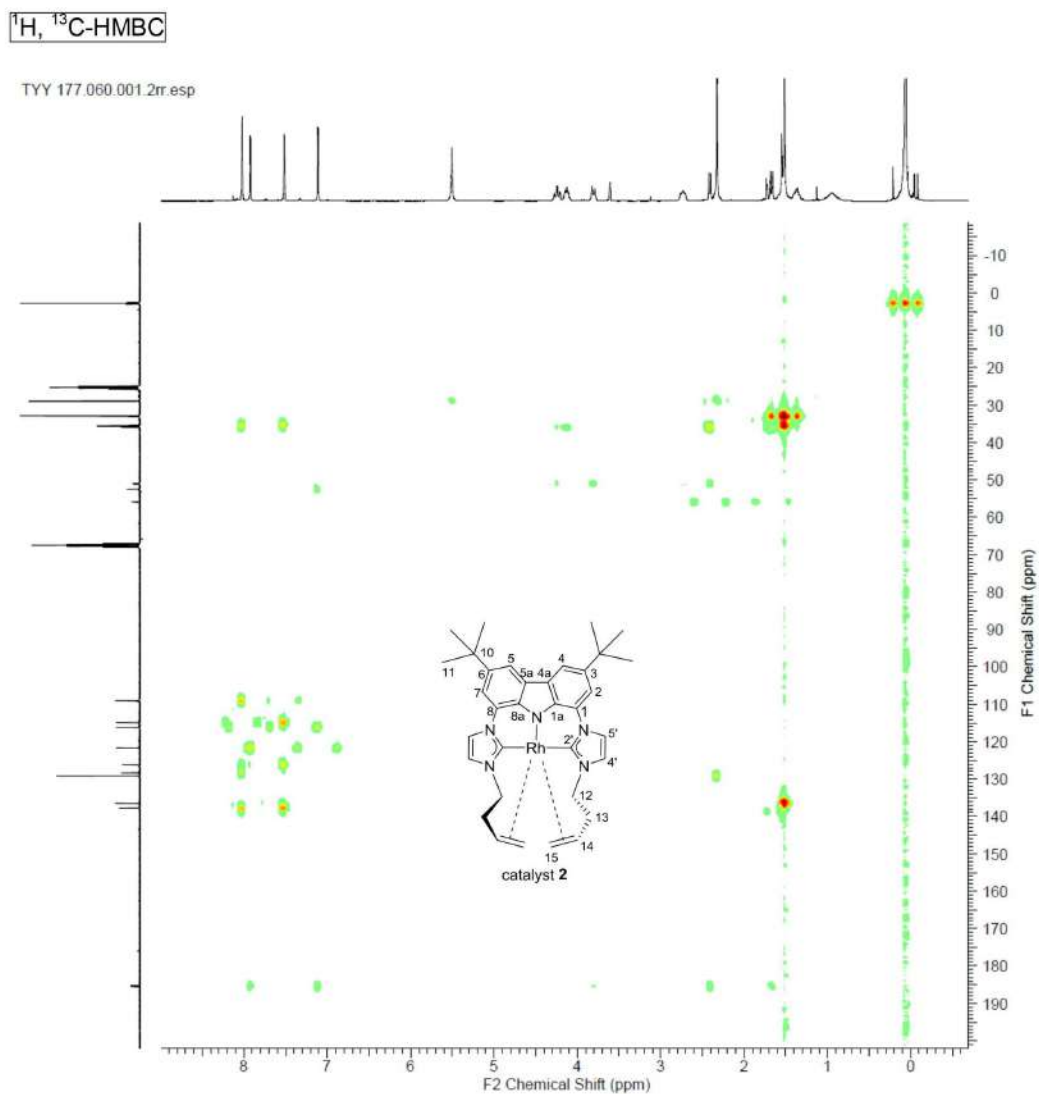


Figure S17.  $^1\text{H}, ^{13}\text{C}$ -HMBC NMR ( $\text{THF}-d_8$ , 400 MHz) spectrum: transmetalation of  $[\text{Li}(\text{bimca}^{\text{Homo}})]$  with  $[\text{Rh}(\mu\text{-Cl})(\text{COD})]_2$ .



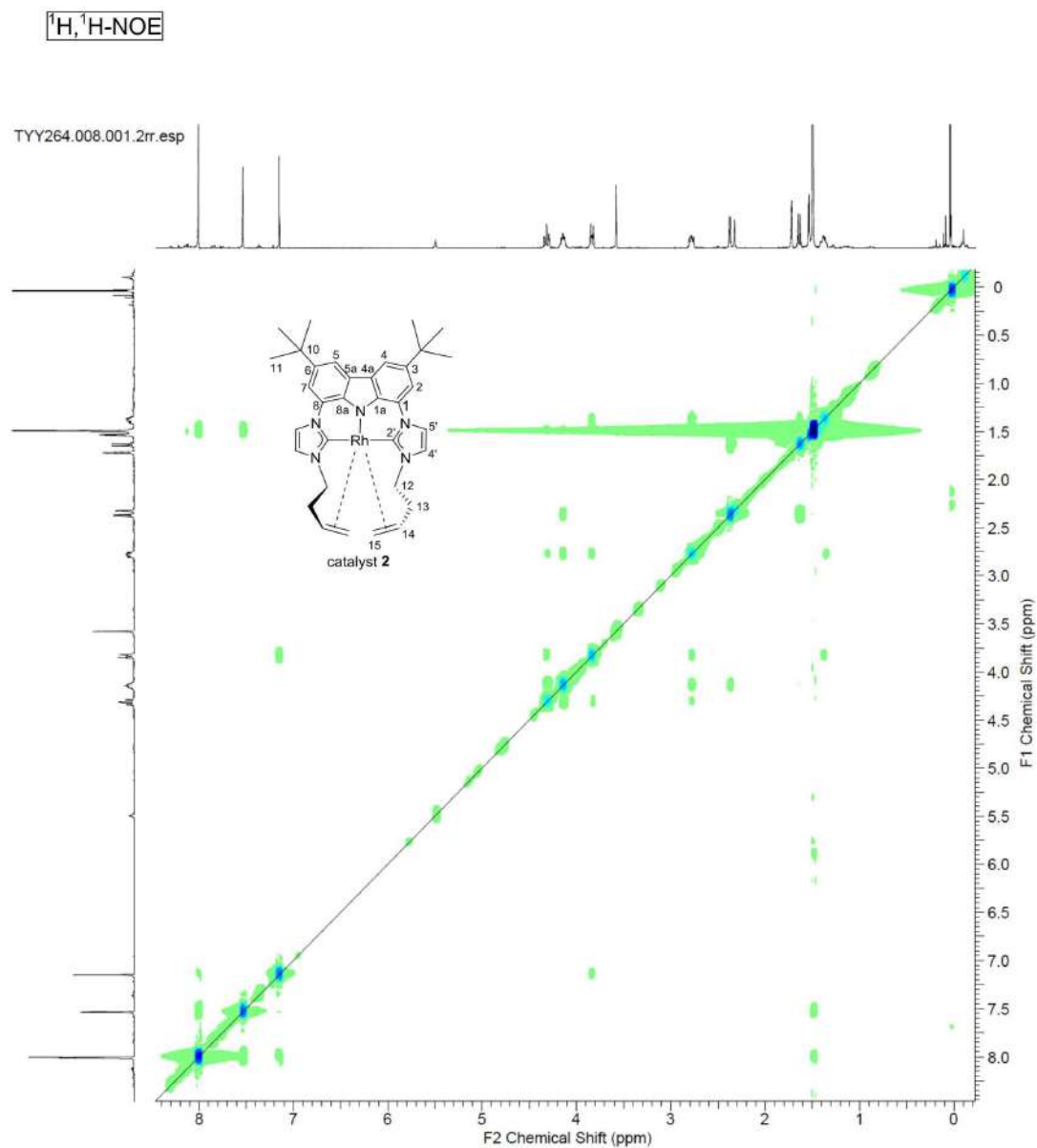


Figure S18.  $^1\text{H}, ^1\text{H}\text{-NOE}$  NMR ( $\text{THF-}d_6$ , 400 MHz) spectrum at 0 °C: transmetalation of  $[\text{Li}(\text{bimca}^{\text{Hom}o})]$  with  $[\text{Rh}(\mu\text{-Cl})(\text{COD})_2]$ .

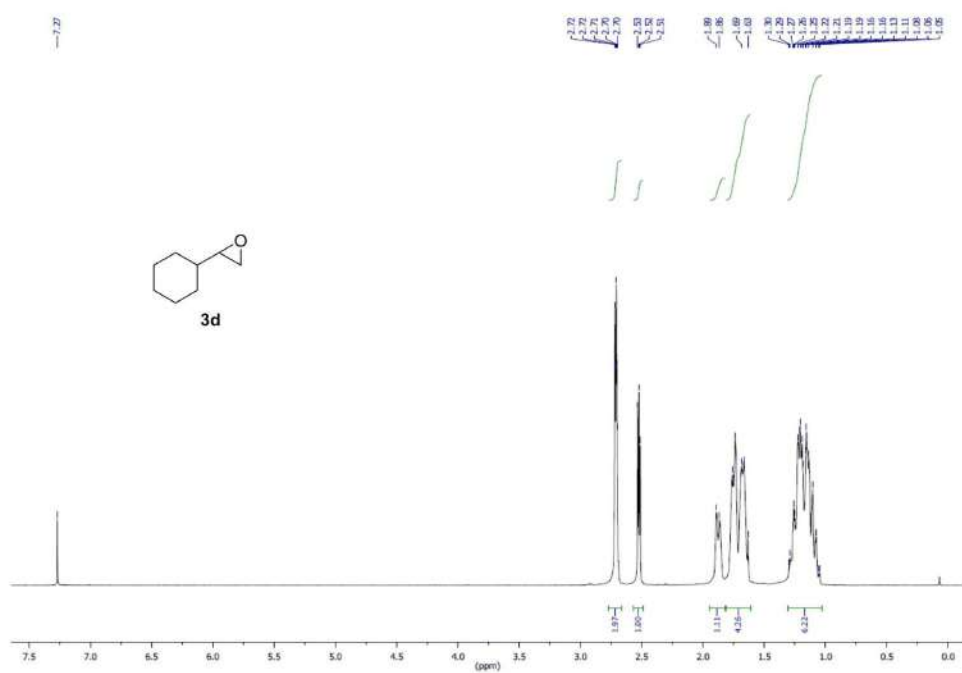


Figure S19. <sup>1</sup>H NMR (CDCl<sub>3</sub>, 400 MHz) spectrum: compound 3d.

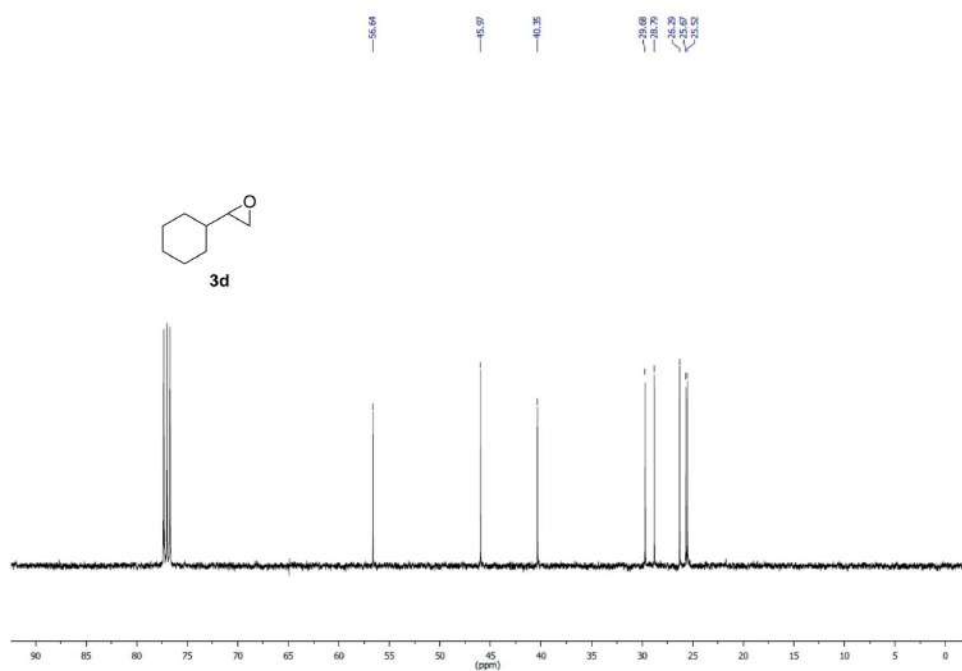


Figure S20. <sup>13</sup>C NMR (CDCl<sub>3</sub>, 101 MHz) spectrum: compound 3d.

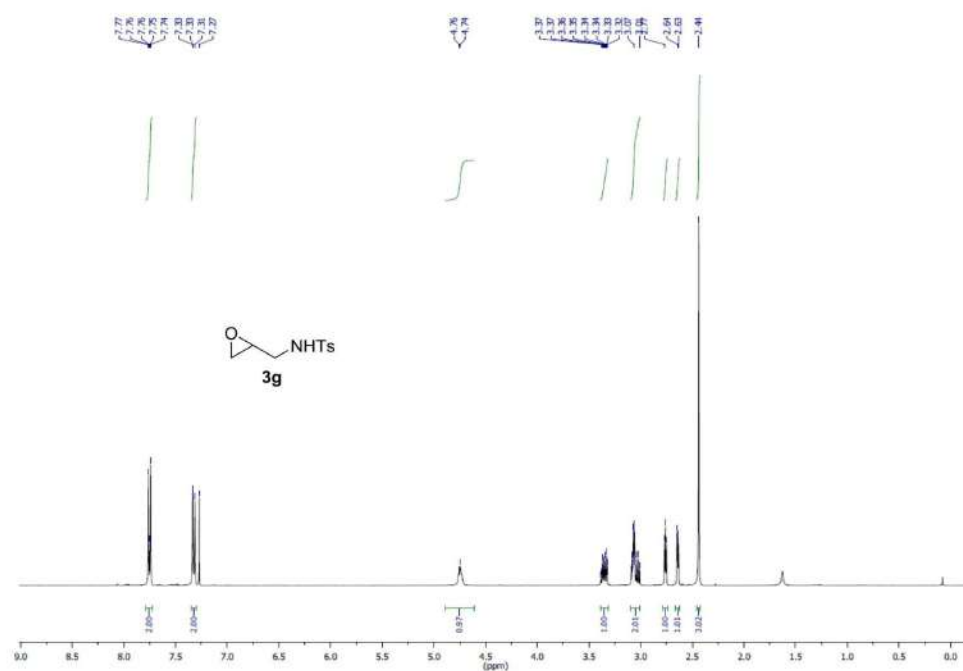


Figure S21. <sup>1</sup>H NMR (CDCl<sub>3</sub>, 400 MHz) spectrum: compound 3g.

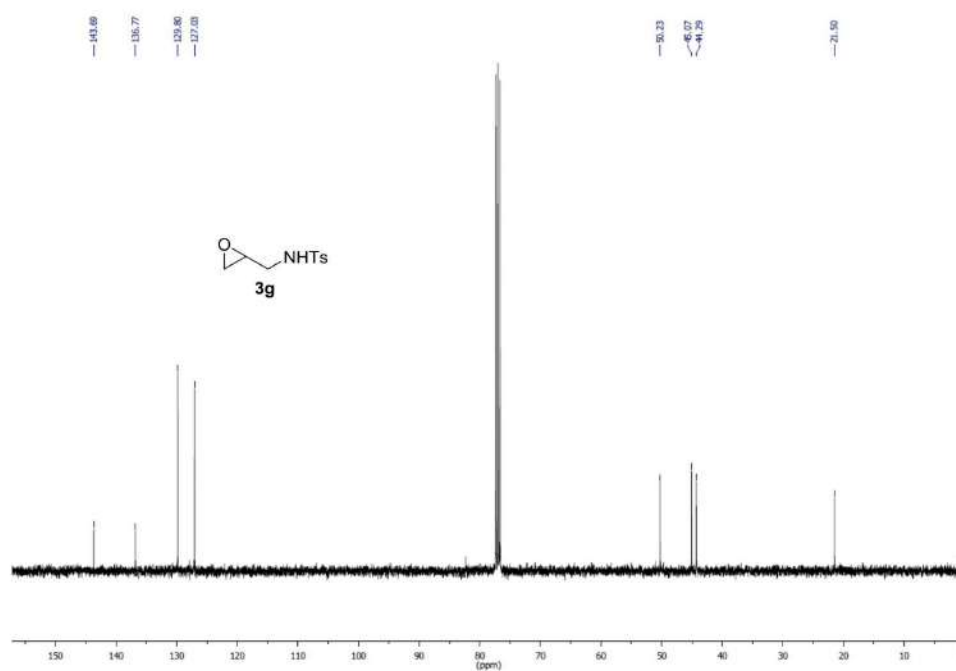


Figure S22. <sup>13</sup>C NMR (CDCl<sub>3</sub>, 101 MHz) spectrum: compound 3g.

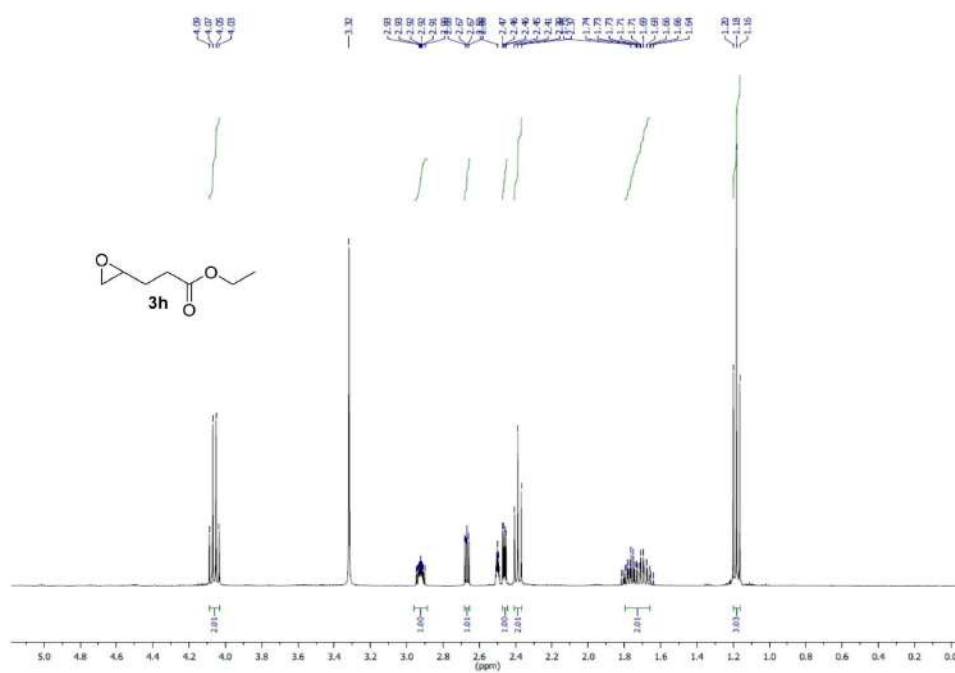


Figure S23. <sup>1</sup>H NMR (d<sub>6</sub>-DMSO, 400 MHz) spectrum: compound 3h.

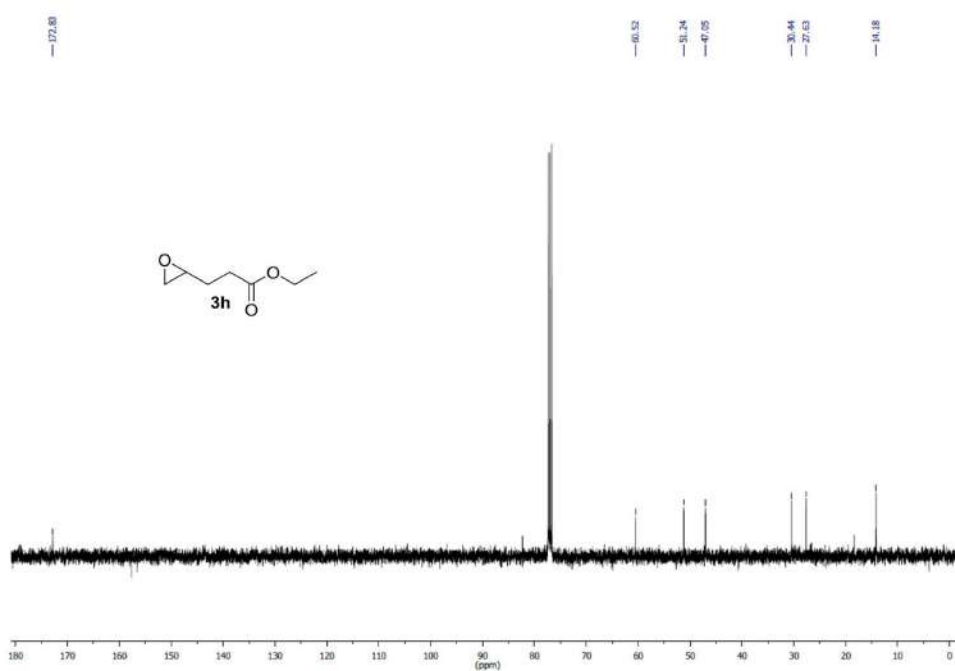


Figure S24. <sup>13</sup>C NMR (CDCl<sub>3</sub>, 101 MHz) spectrum: compound 3h.

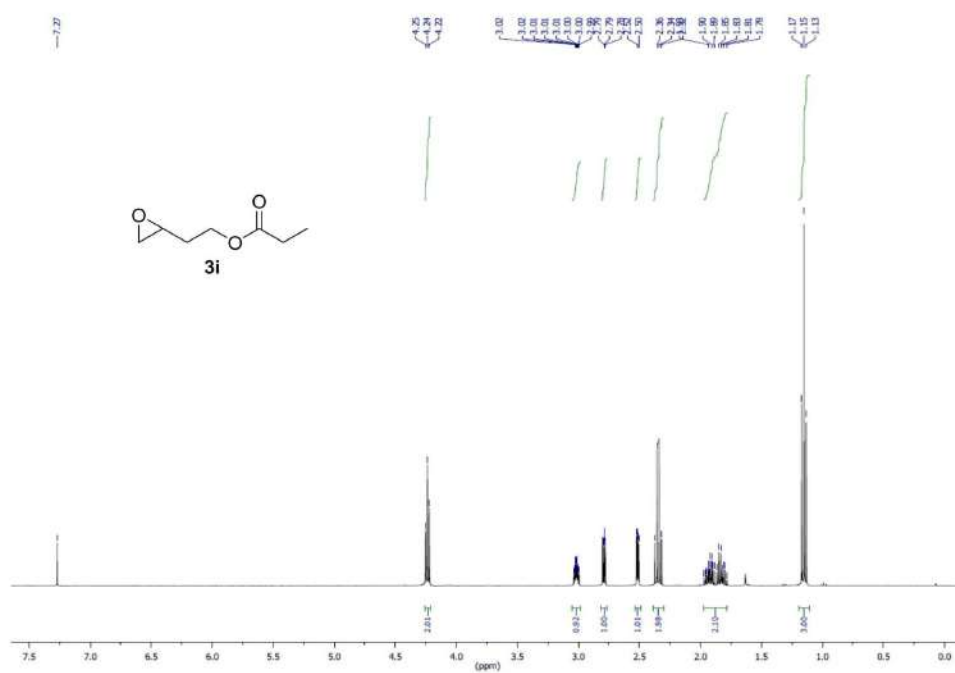


Figure S25. <sup>1</sup>H NMR (CDCl<sub>3</sub>, 400 MHz) spectrum: compound 3i.

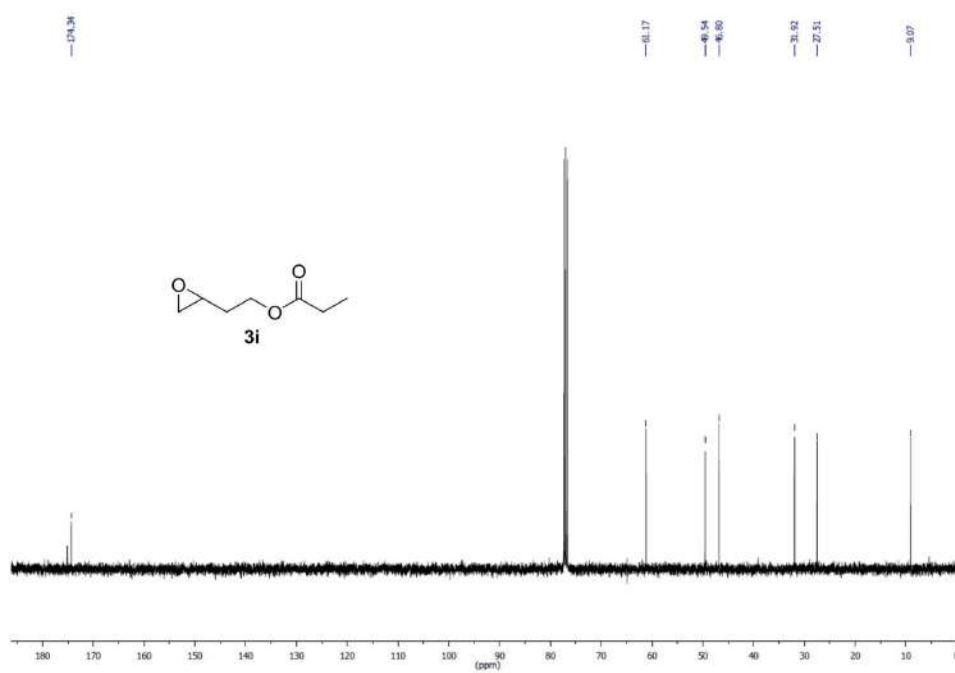
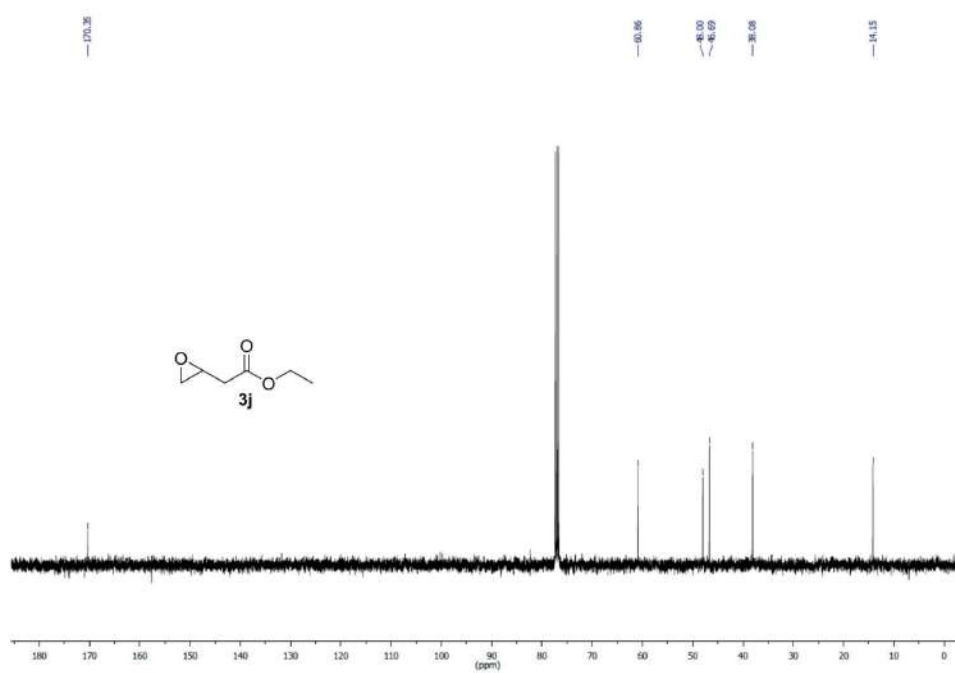
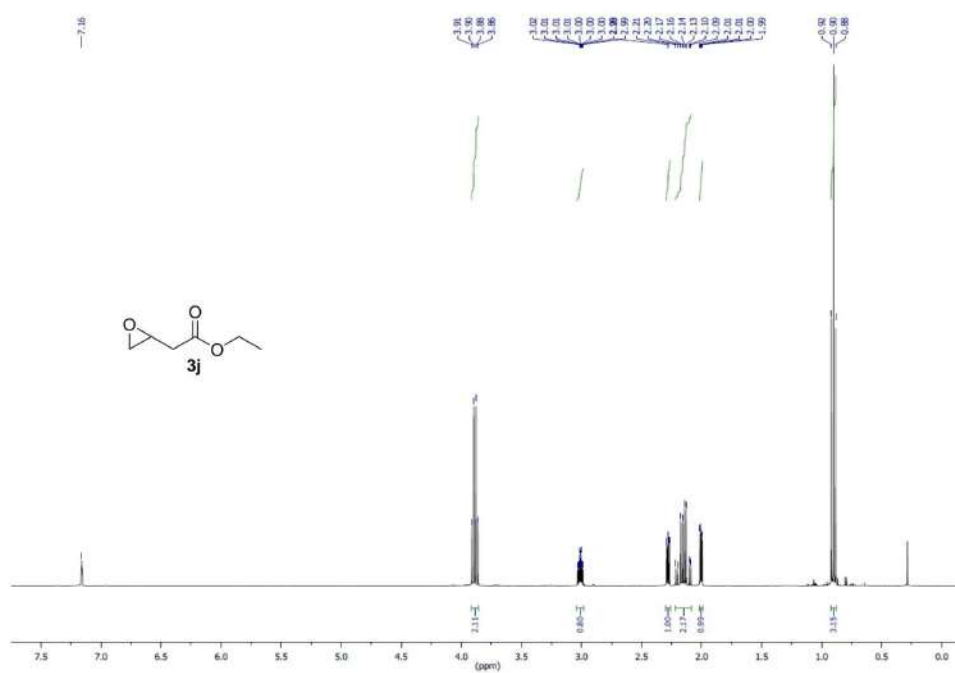


Figure S26. <sup>13</sup>C NMR (CDCl<sub>3</sub>, 101 MHz) spectrum: compound 3i.



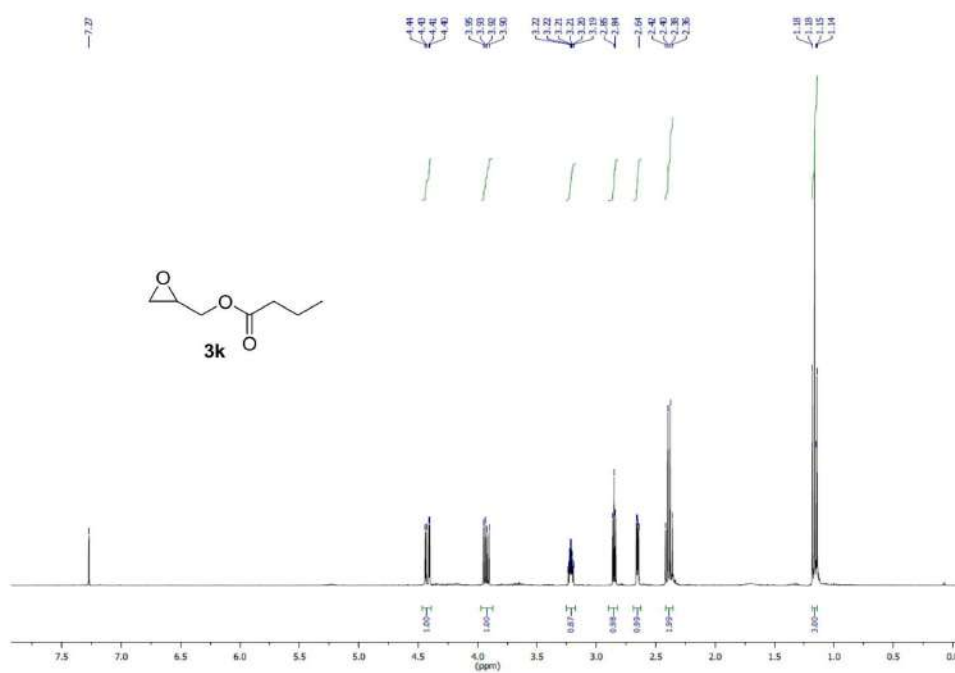


Figure S29. <sup>1</sup>H NMR (CDCl<sub>3</sub>, 400 MHz) spectrum: compound 3k.

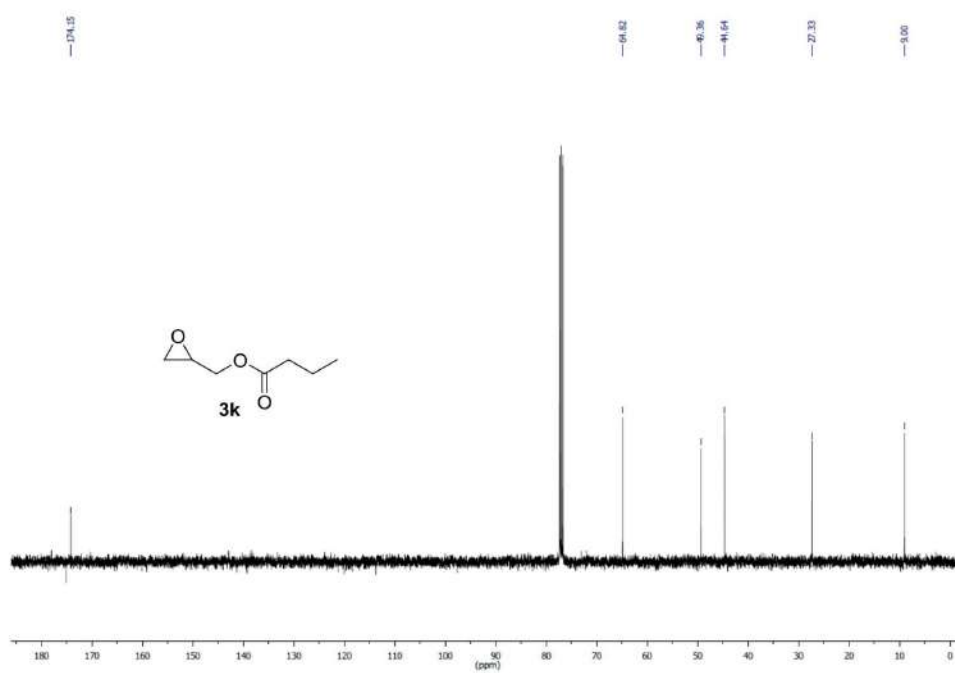


Figure S30. <sup>13</sup>C NMR (CDCl<sub>3</sub>, 101 MHz) spectrum: compound 3k.

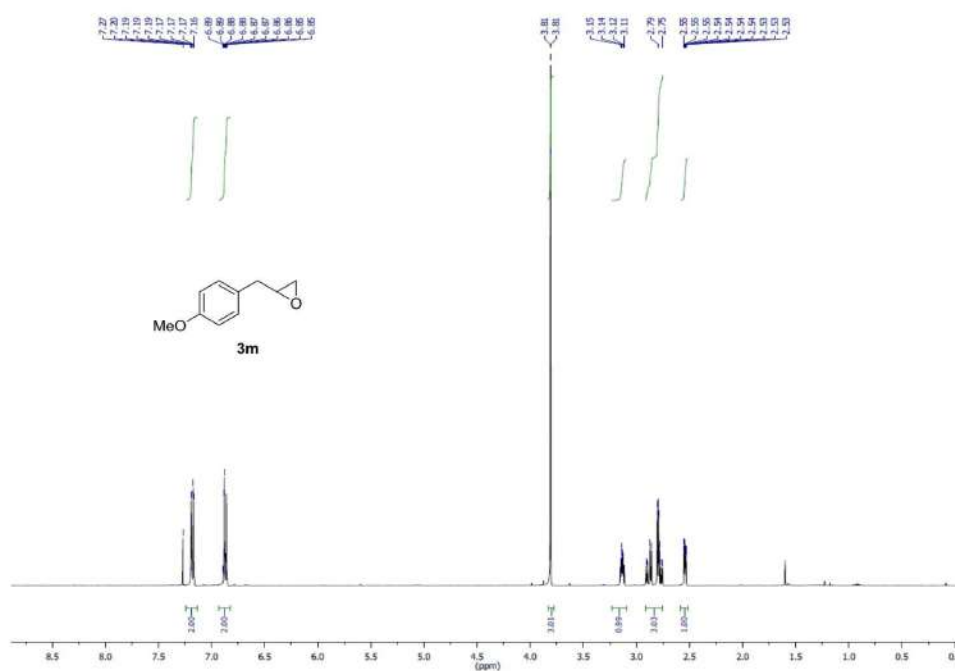


Figure S31. <sup>1</sup>H NMR (CDCl<sub>3</sub>, 400 MHz) spectrum: compound **3m**.

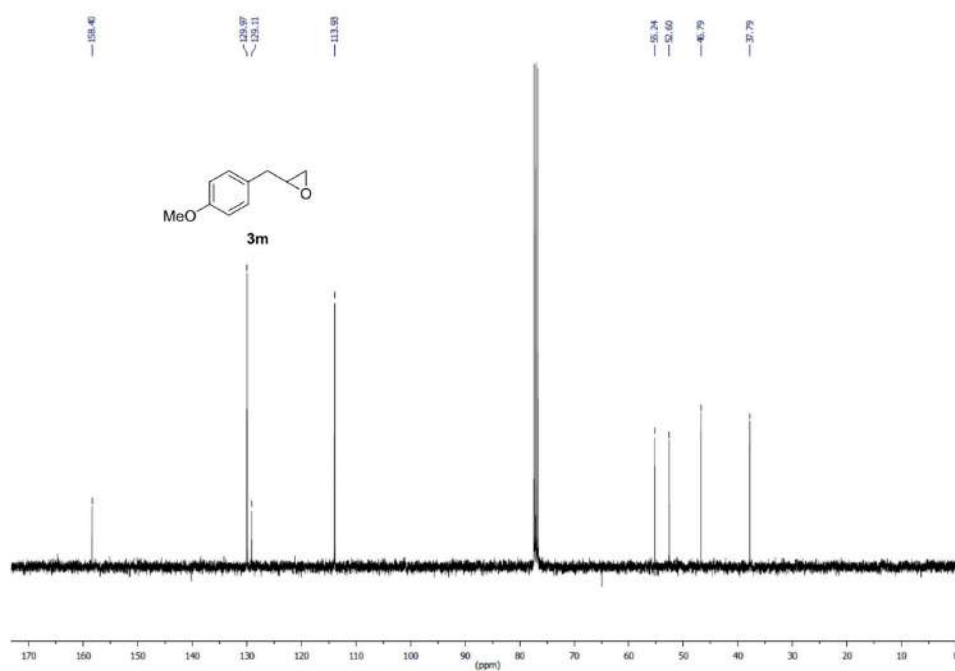


Figure S32. <sup>13</sup>C NMR (CDCl<sub>3</sub>, 101 MHz) spectrum: compound **3m**.



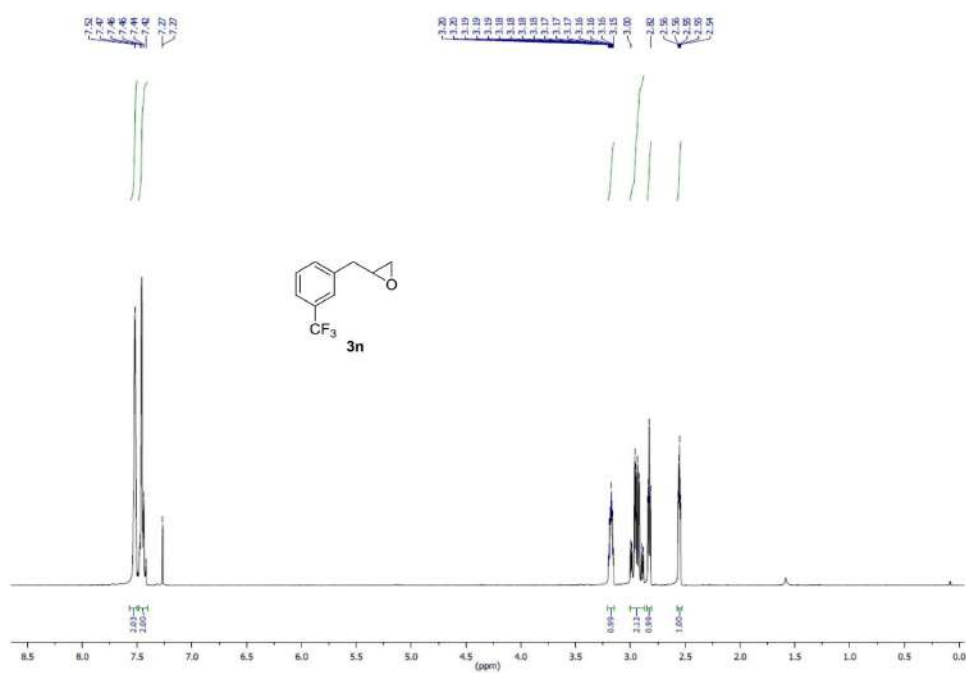


Figure S33. <sup>1</sup>H NMR (CDCl<sub>3</sub>, 400 MHz) spectrum: compound **3n**.

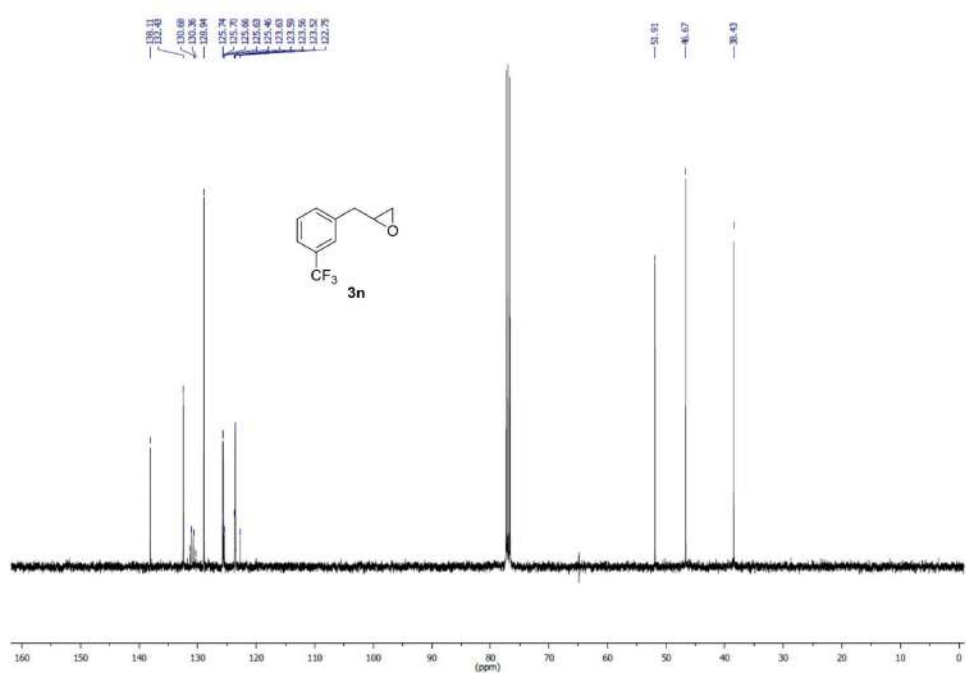


Figure S34. <sup>13</sup>C NMR (CDCl<sub>3</sub>, 101 MHz) spectrum: compound **3n**.

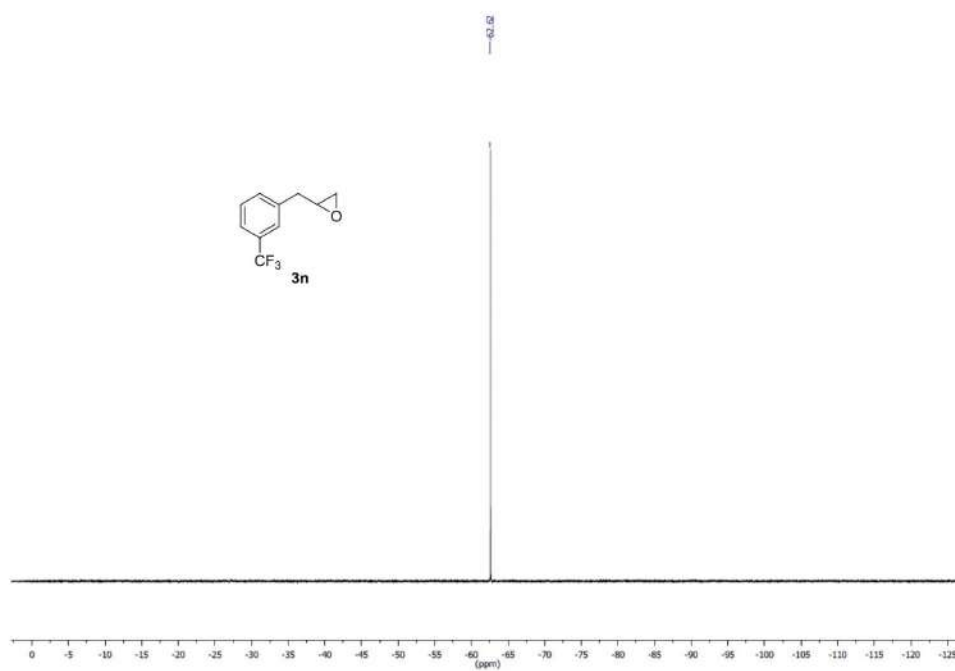


Figure S35.  $^{19}\text{F}$  NMR ( $\text{CDCl}_3$ , 376 MHz) spectrum: compound **3n**.

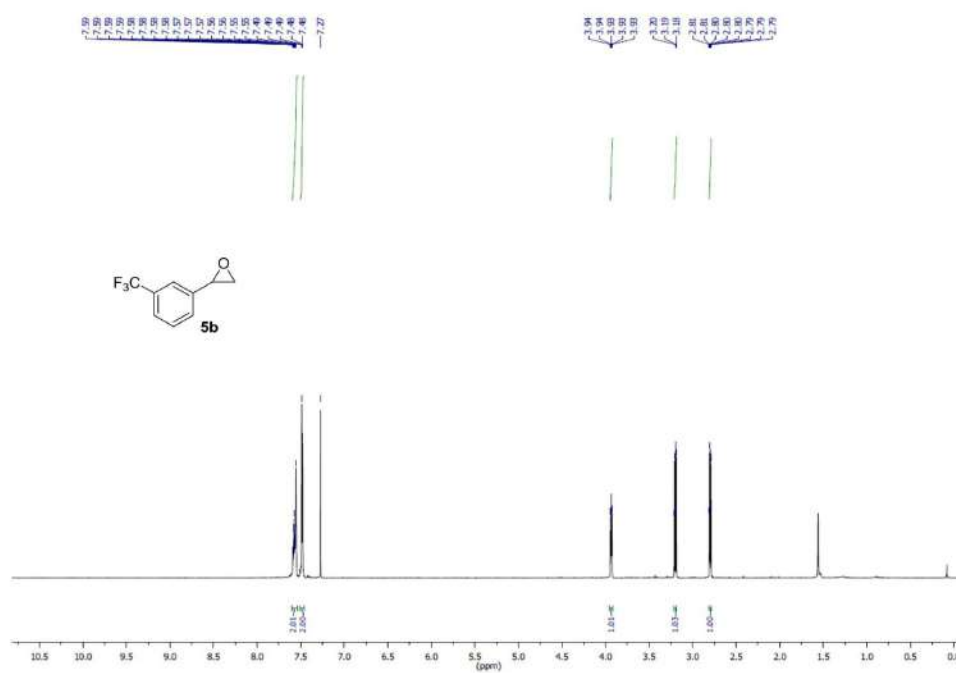


Figure S36. <sup>1</sup>H NMR (CDCl<sub>3</sub>, 400 MHz) spectrum: compound **5b**.

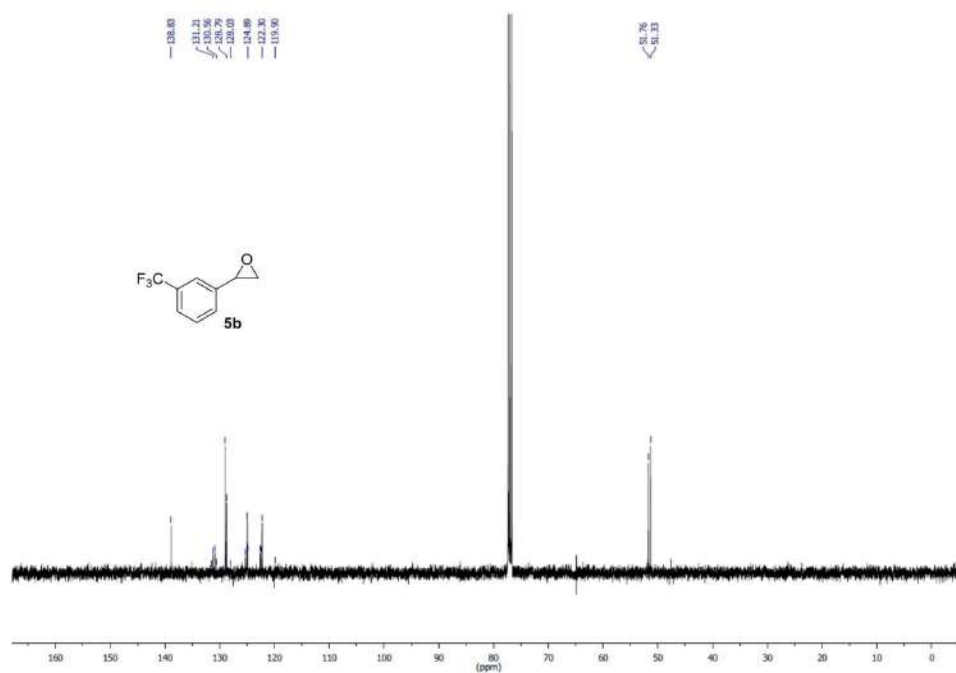


Figure S37. <sup>13</sup>C NMR (CDCl<sub>3</sub>, 101 MHz) spectrum: compound **5b**.

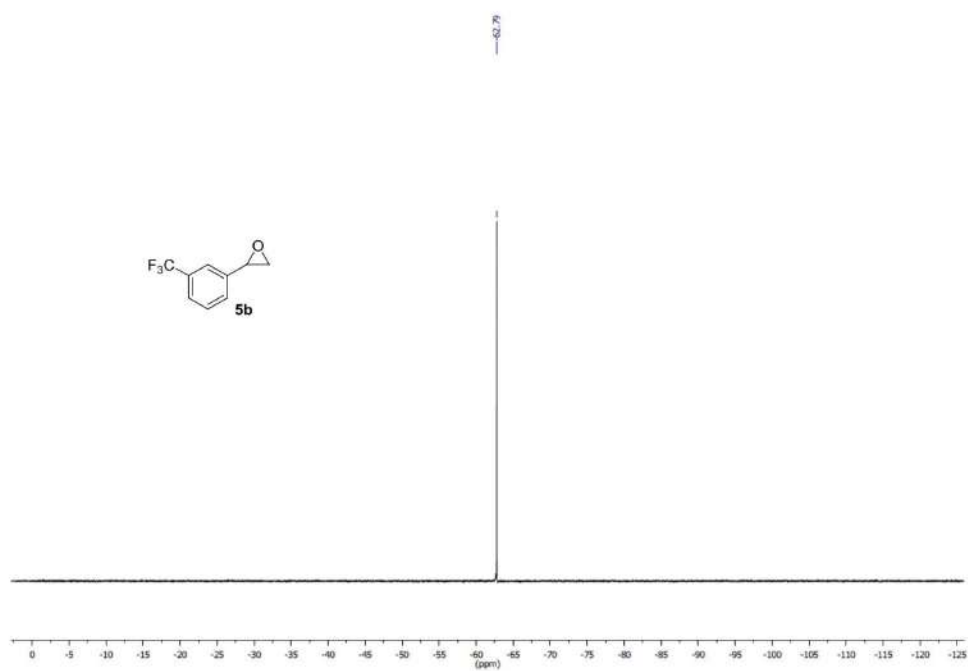


Figure S38.  $^{19}\text{F}$  NMR ( $\text{CDCl}_3$ , 376 MHz) spectrum: compound **5b**.

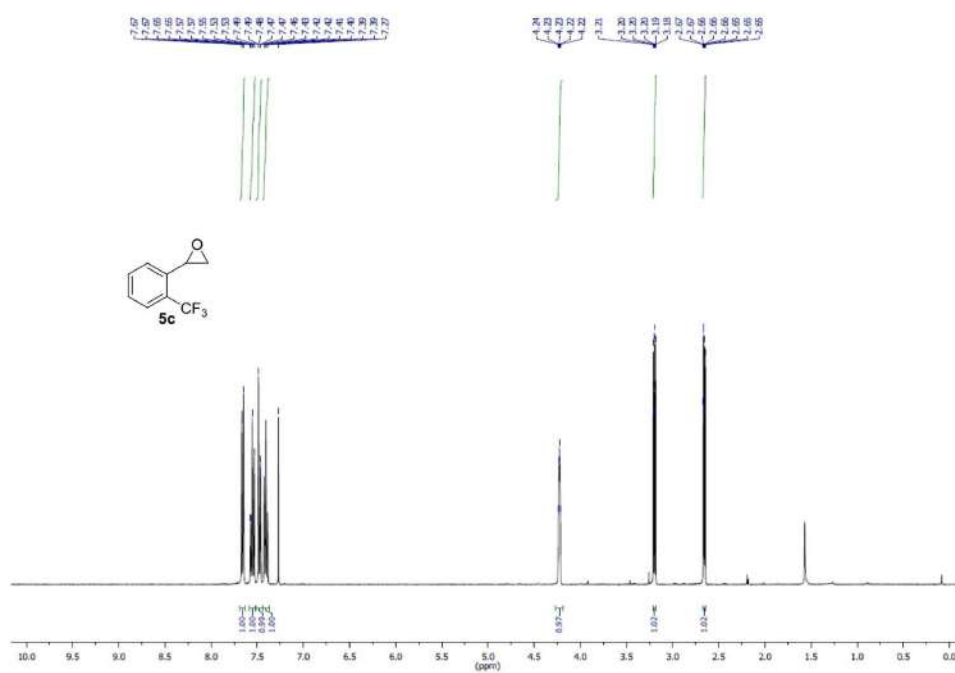


Figure S39.  $^1\text{H}$  NMR ( $\text{CDCl}_3$ , 400 MHz) spectrum: compound **5c**.

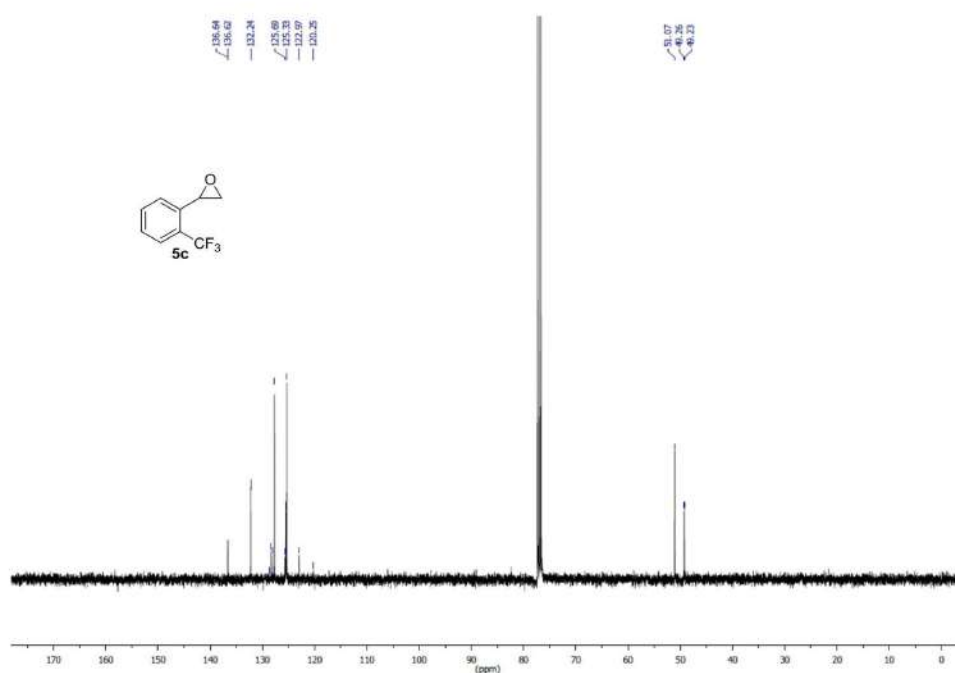


Figure S40.  $^{13}\text{C}$  NMR ( $\text{CDCl}_3$ , 101 MHz) spectrum: compound **5c**.

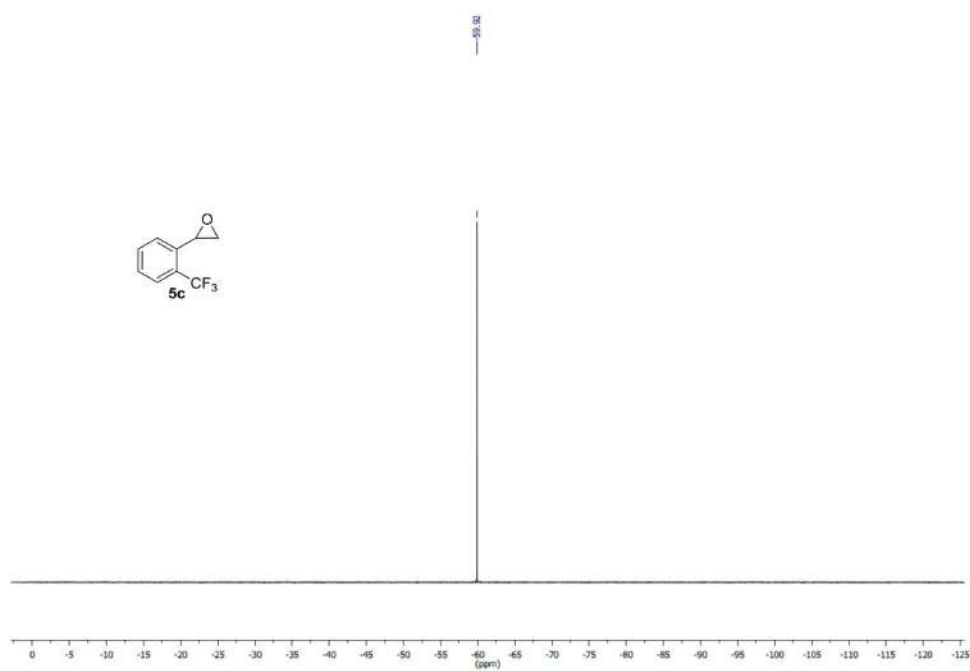


Figure S41.  $^{19}\text{F}$  NMR ( $\text{CDCl}_3$ , 376 MHz) spectrum: compound **5c**.

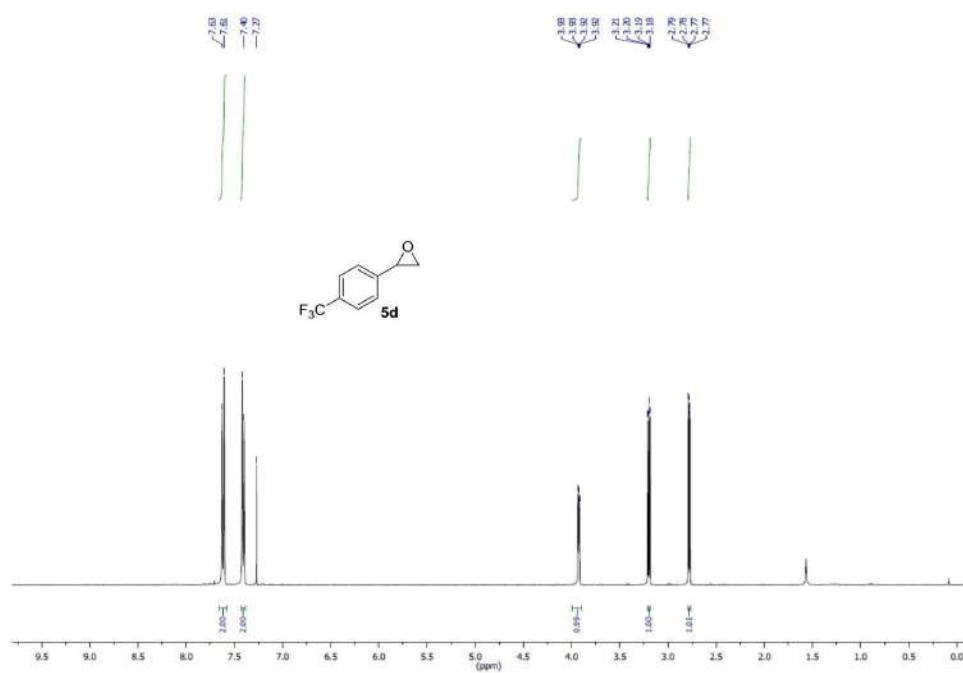


Figure S42. <sup>1</sup>H NMR (CDCl<sub>3</sub>, 400 MHz) spectrum: compound **5d**.

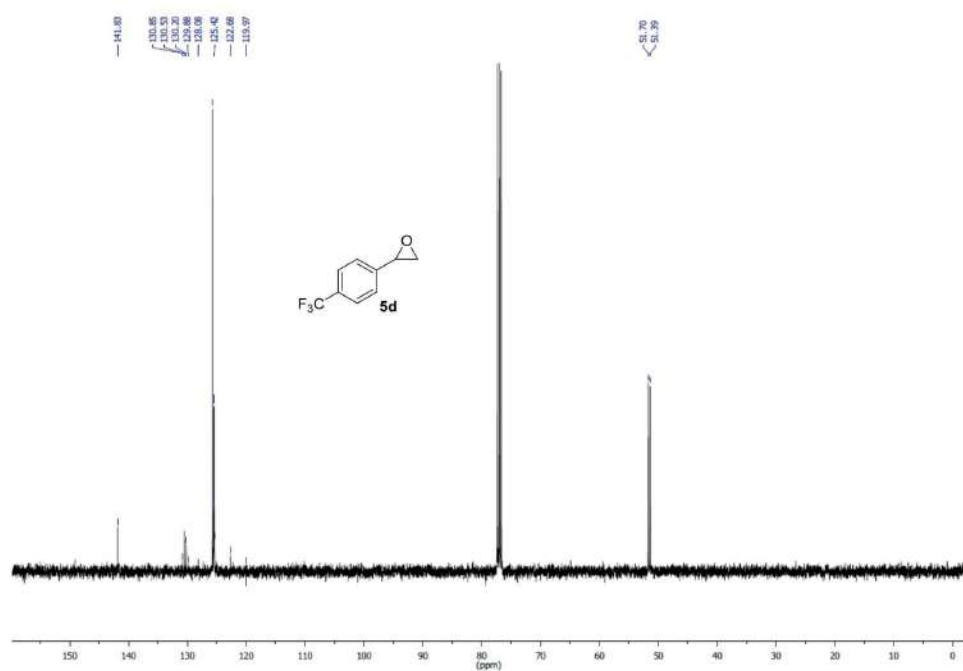


Figure S43. <sup>13</sup>C NMR (CDCl<sub>3</sub>, 101 MHz) spectrum: compound **5d**.

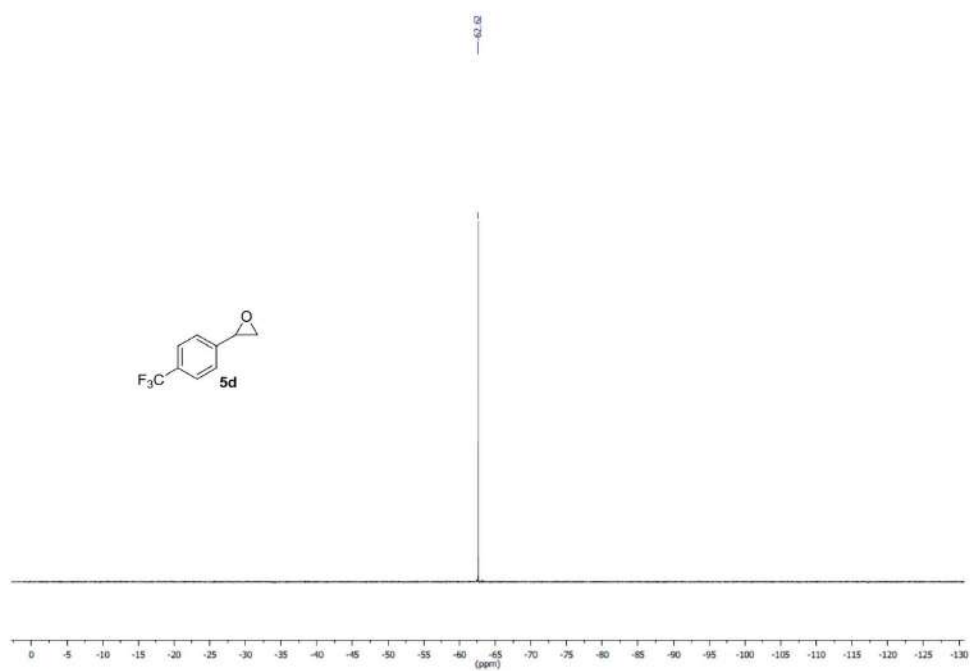


Figure S44.  $^{19}\text{F}$  NMR ( $\text{CDCl}_3$ , 376 MHz) spectrum: compound **5d**.





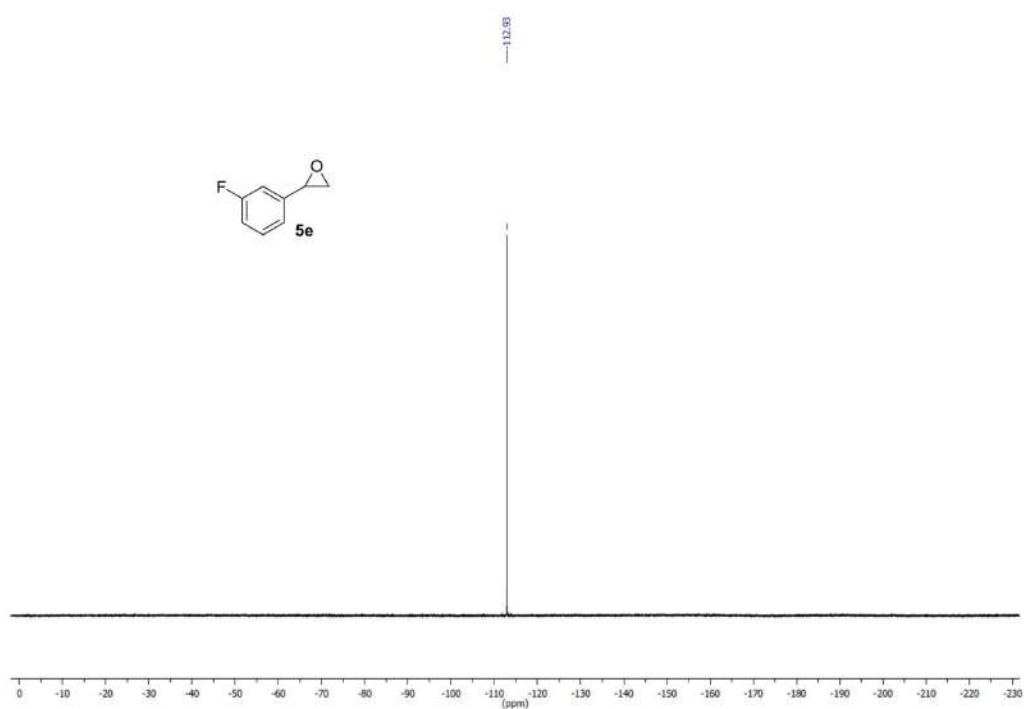


Figure S47.  $^{19}\text{F}$  NMR ( $\text{CDCl}_3$ , 376 MHz) spectrum: compound **5e**.

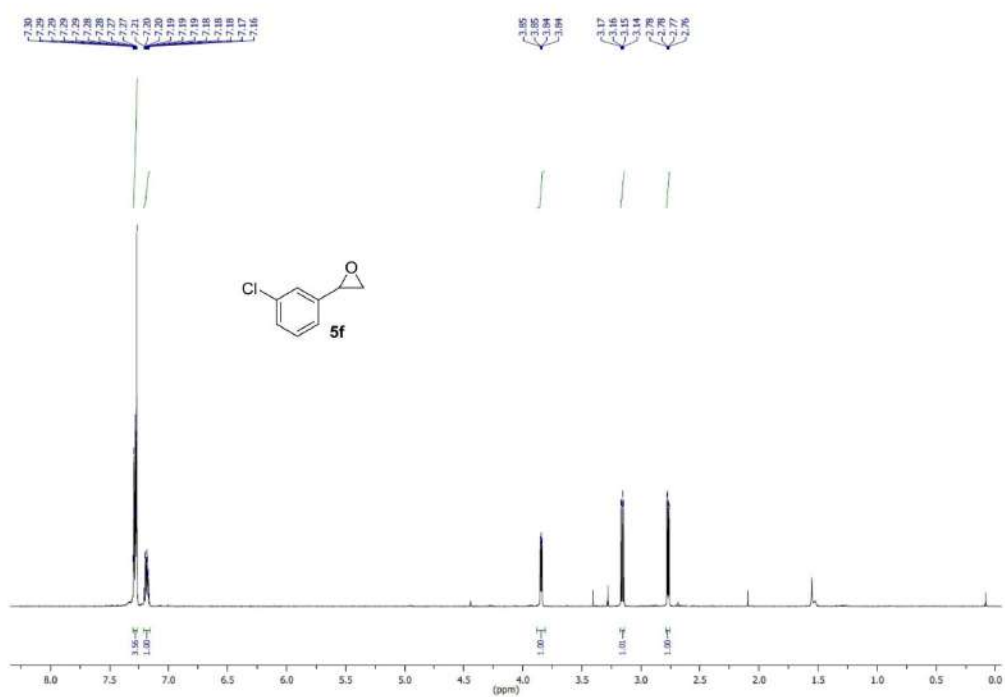


Figure S48. <sup>1</sup>H NMR (CDCl<sub>3</sub>, 400 MHz) spectrum: compound **5f**.

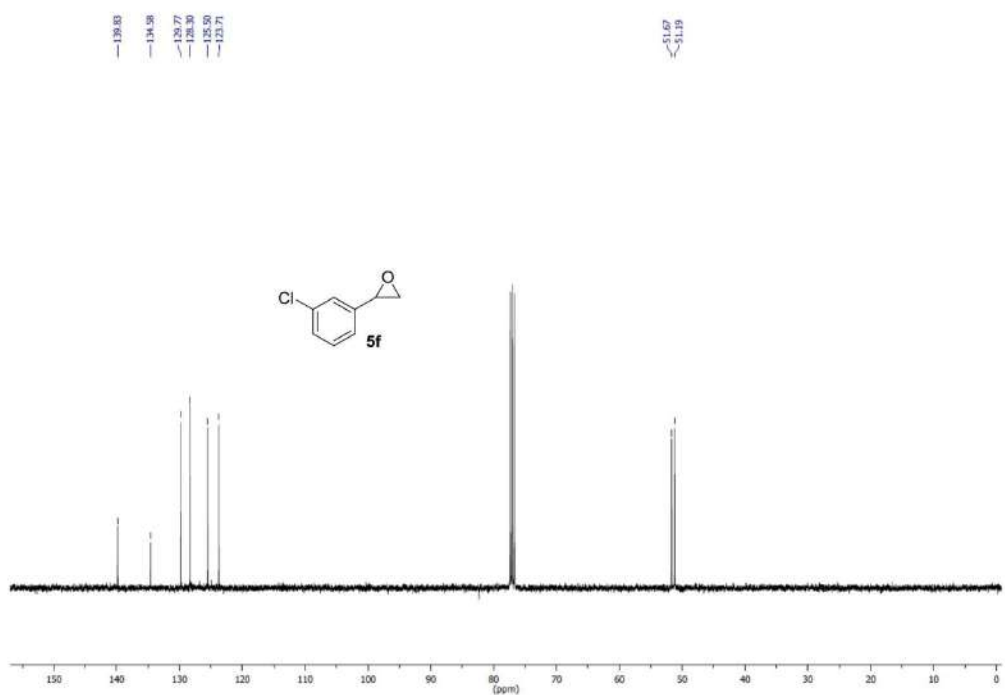


Figure S49. <sup>13</sup>C NMR (CDCl<sub>3</sub>, 101 MHz) spectrum: compound **5f**.

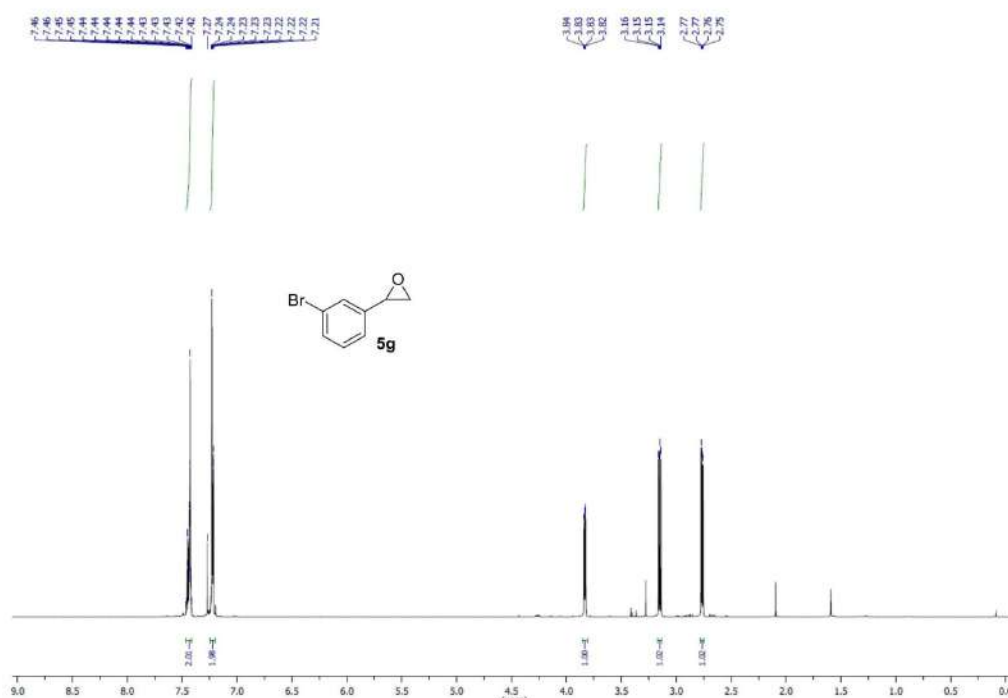


Figure S50. <sup>1</sup>H NMR (CDCl<sub>3</sub>, 400 MHz) spectrum: compound 5g.

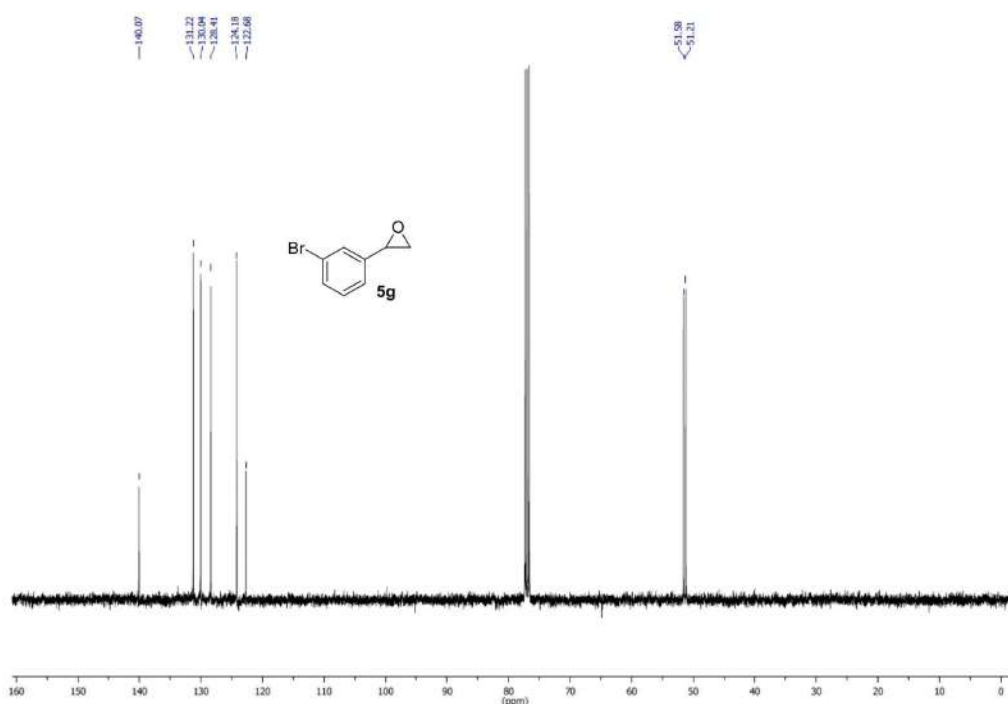


Figure S51. <sup>13</sup>C NMR (CDCl<sub>3</sub>, 101 MHz) spectrum: compound 5g.

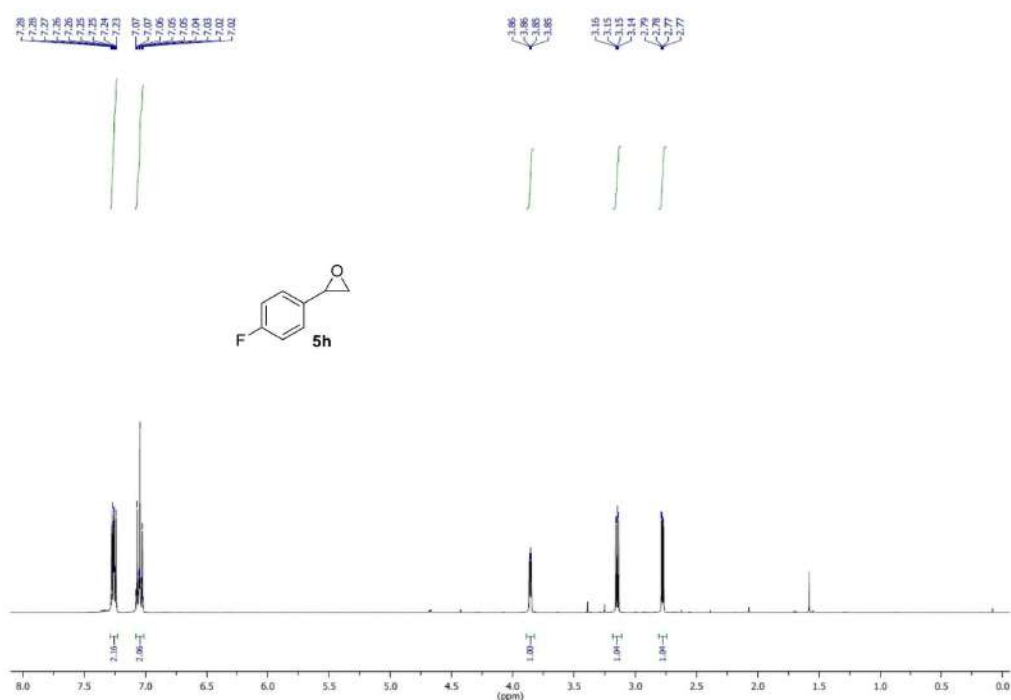


Figure S52. <sup>1</sup>H NMR (CDCl<sub>3</sub>, 400 MHz) spectrum: compound 5h.

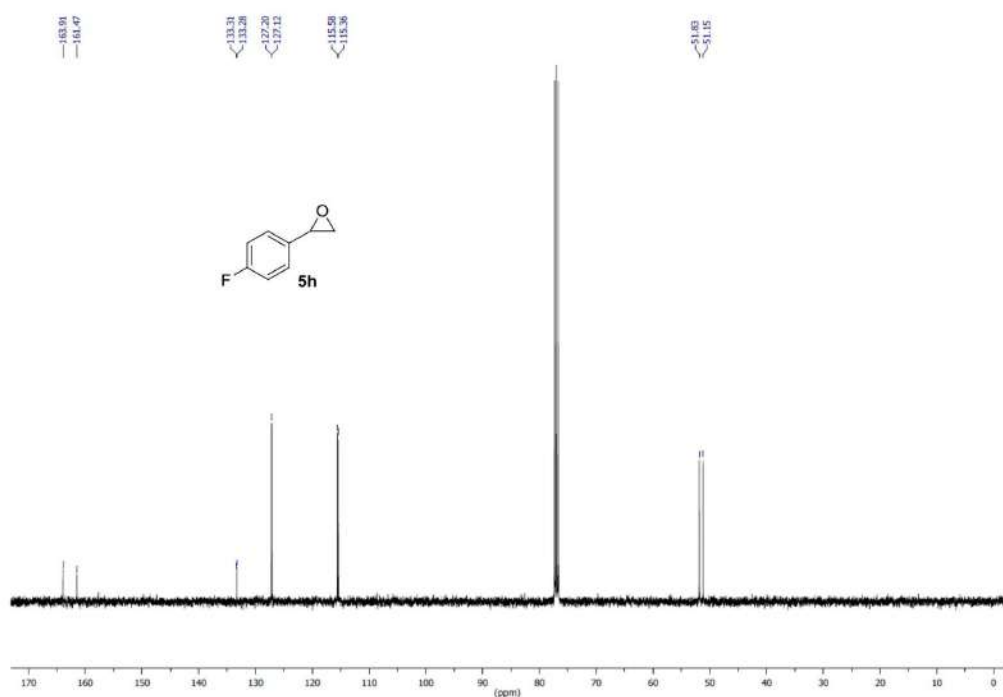


Figure S53. <sup>13</sup>C NMR (CDCl<sub>3</sub>, 101 MHz) spectrum: compound 5h.

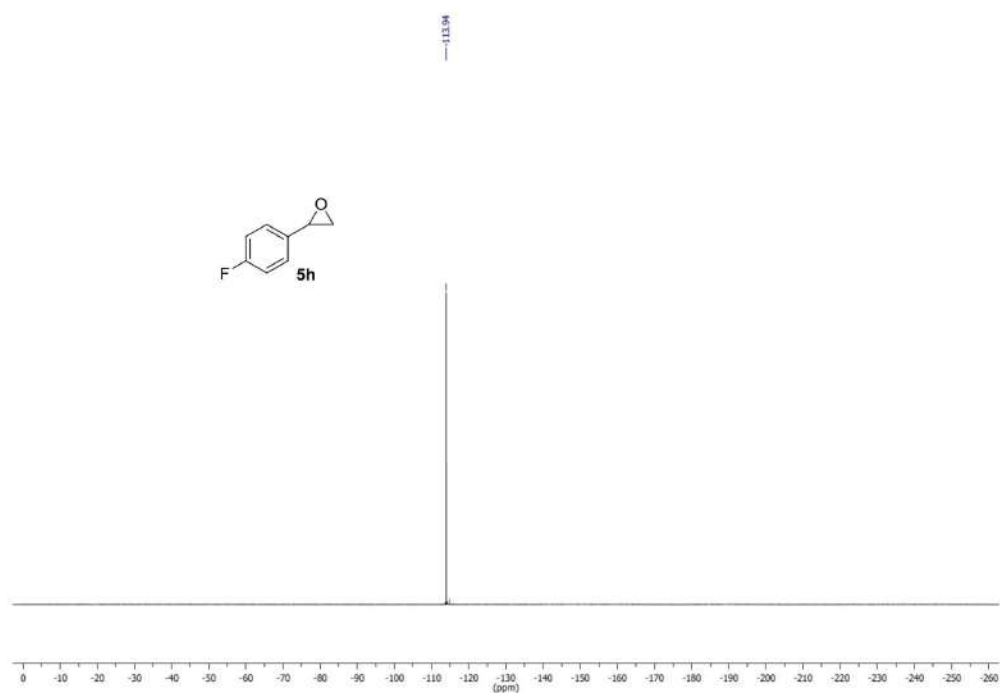


Figure S54.  $^{19}\text{F}$  NMR ( $\text{CDCl}_3$ , 376 MHz) spectrum: compound **5h**.

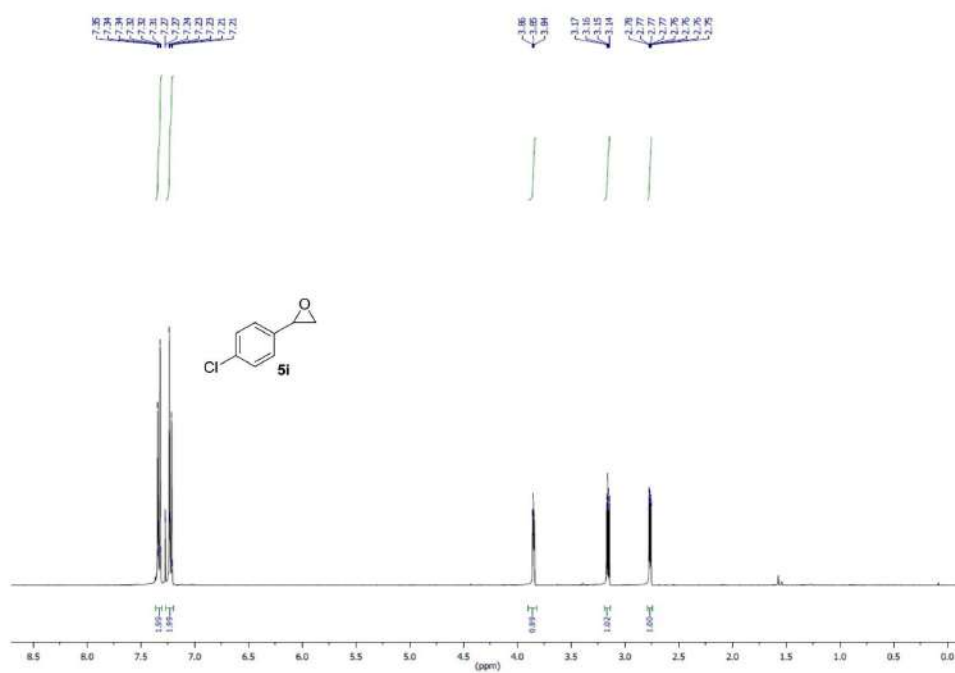


Figure S55. <sup>1</sup>H NMR (CDCl<sub>3</sub>, 400 MHz) spectrum: compound 5i.

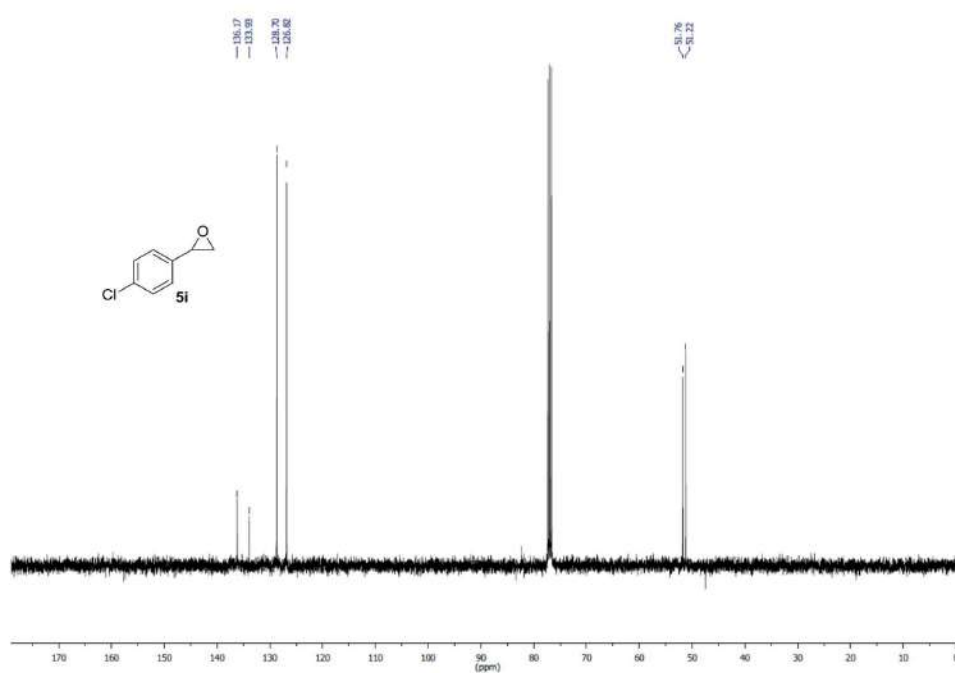


Figure S56. <sup>13</sup>C NMR (CDCl<sub>3</sub>, 101 MHz) spectrum: compound 5i.

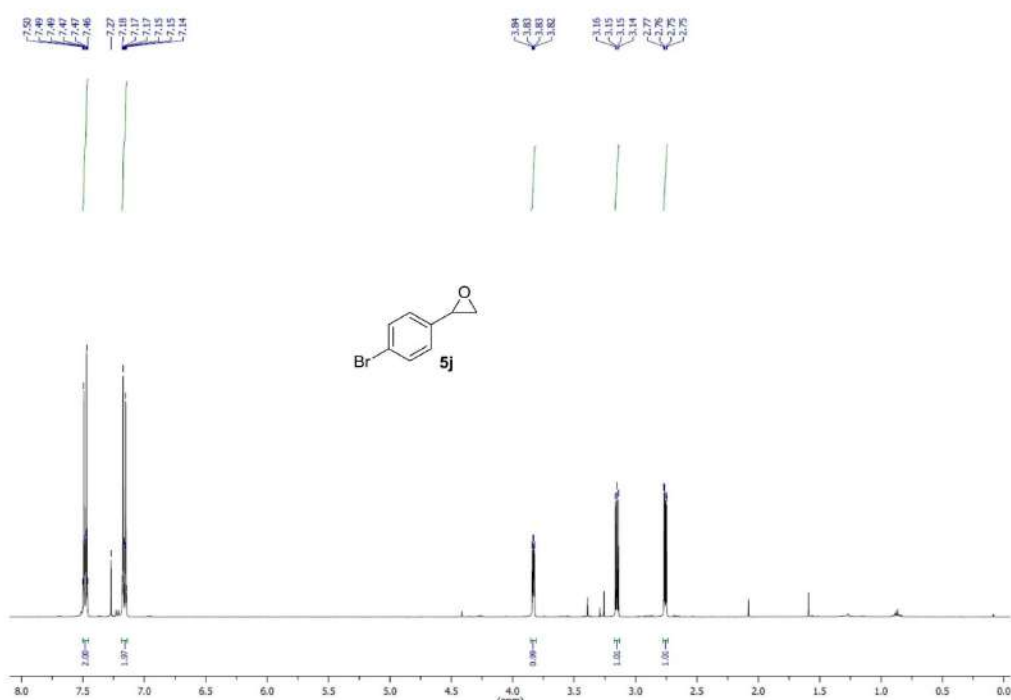


Figure S57. <sup>1</sup>H NMR (CDCl<sub>3</sub>, 400 MHz) spectrum: compound **5j**.

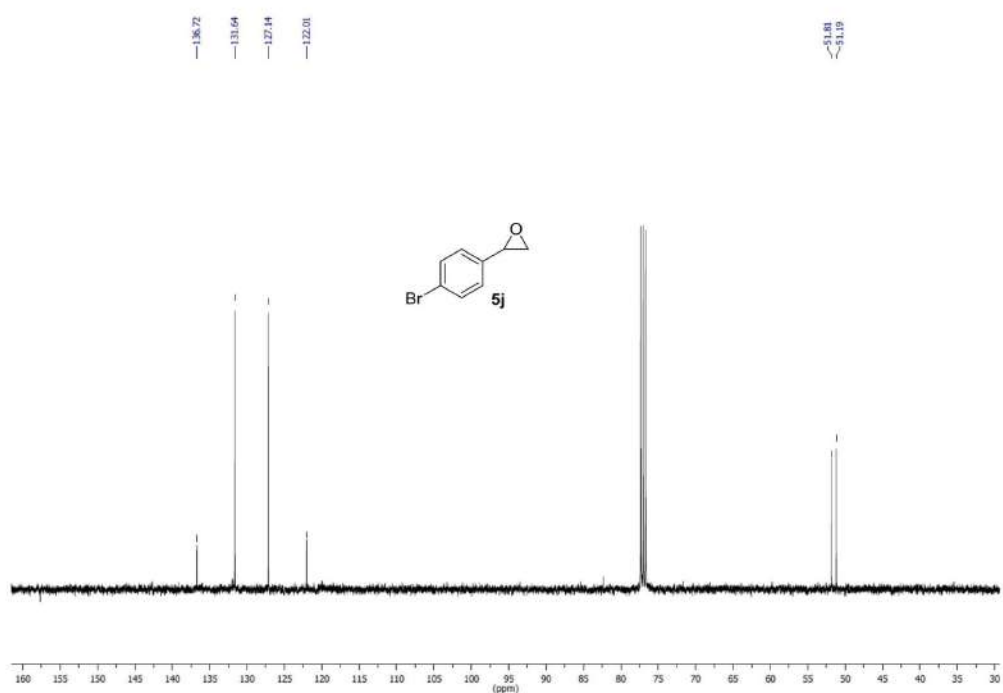


Figure S58. <sup>13</sup>C NMR (CDCl<sub>3</sub>, 101 MHz) spectrum: compound **5j**.



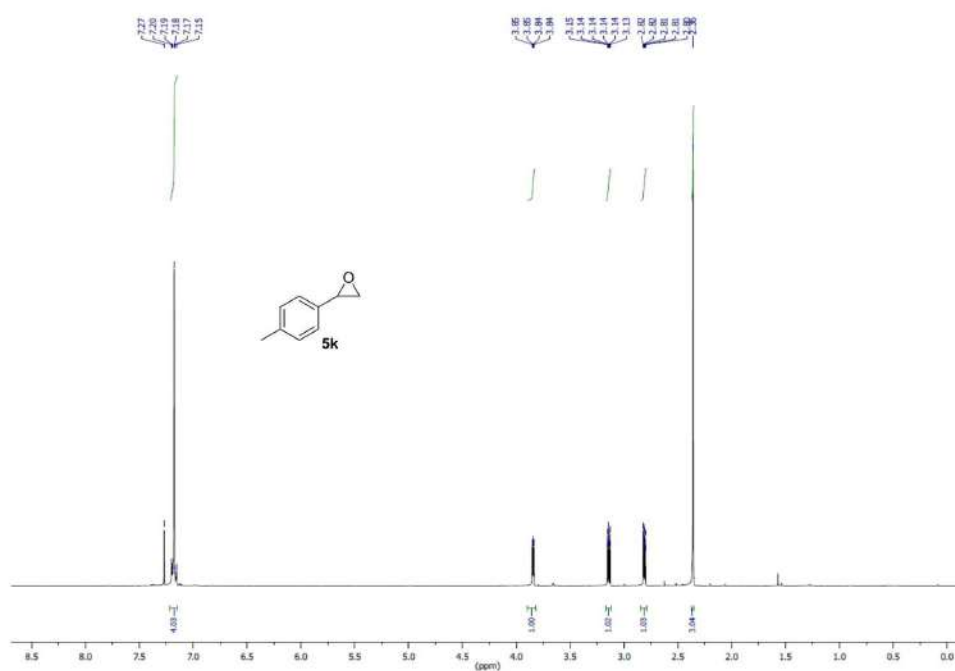


Figure S59.  $^1\text{H}$  NMR ( $\text{CDCl}_3$ , 400 MHz) spectrum: compound 5k.

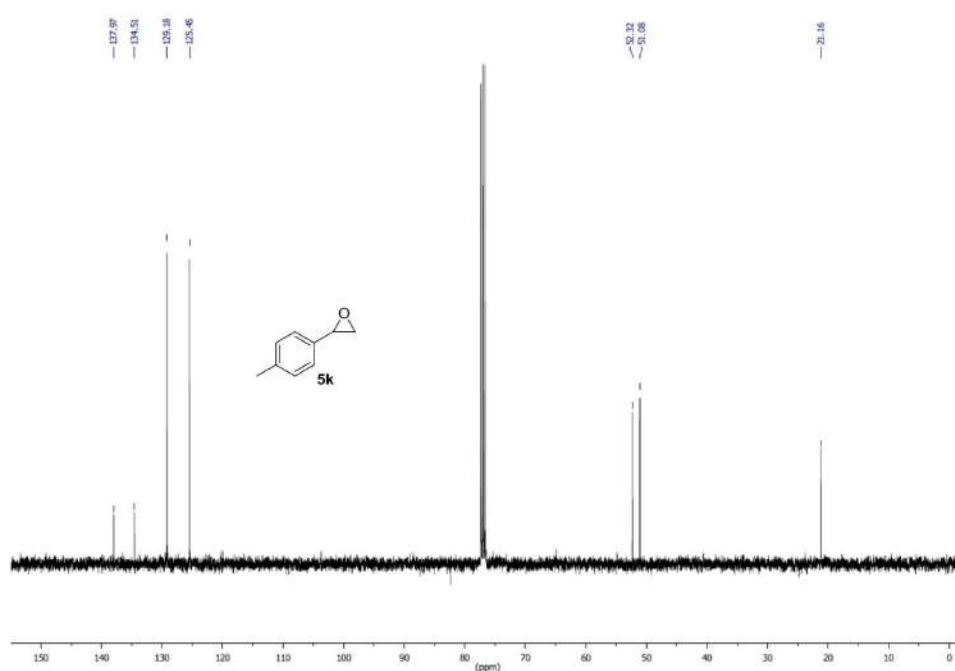


Figure S60.  $^{13}\text{C}$  NMR ( $\text{CDCl}_3$ , 101 MHz) spectrum: compound 5k.

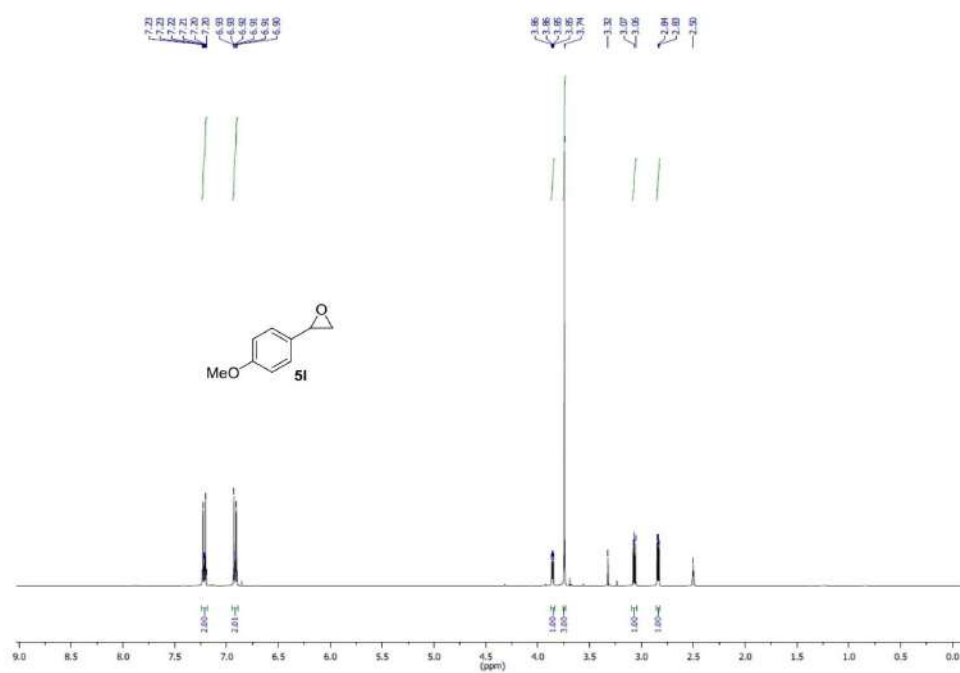


Figure S61. <sup>1</sup>H NMR (CDCl<sub>3</sub>, 400 MHz) spectrum: compound 5I.

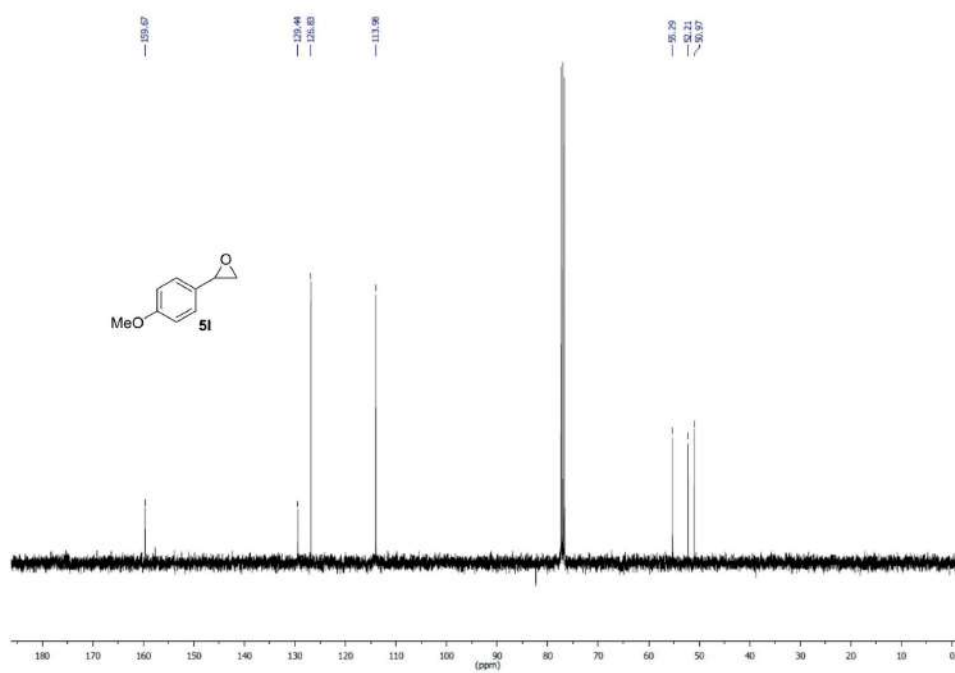
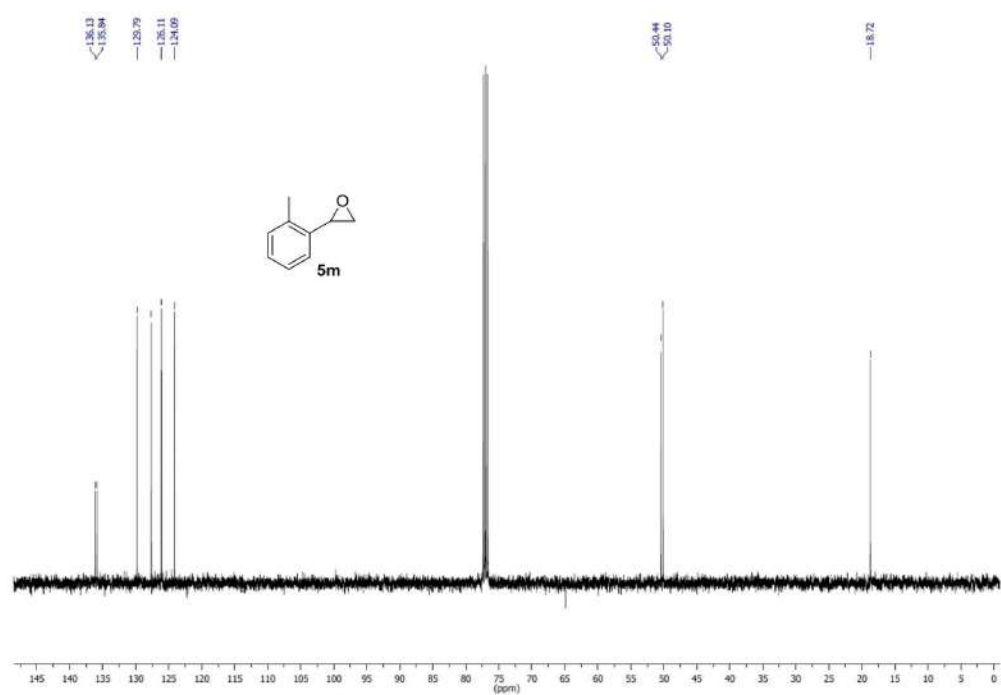
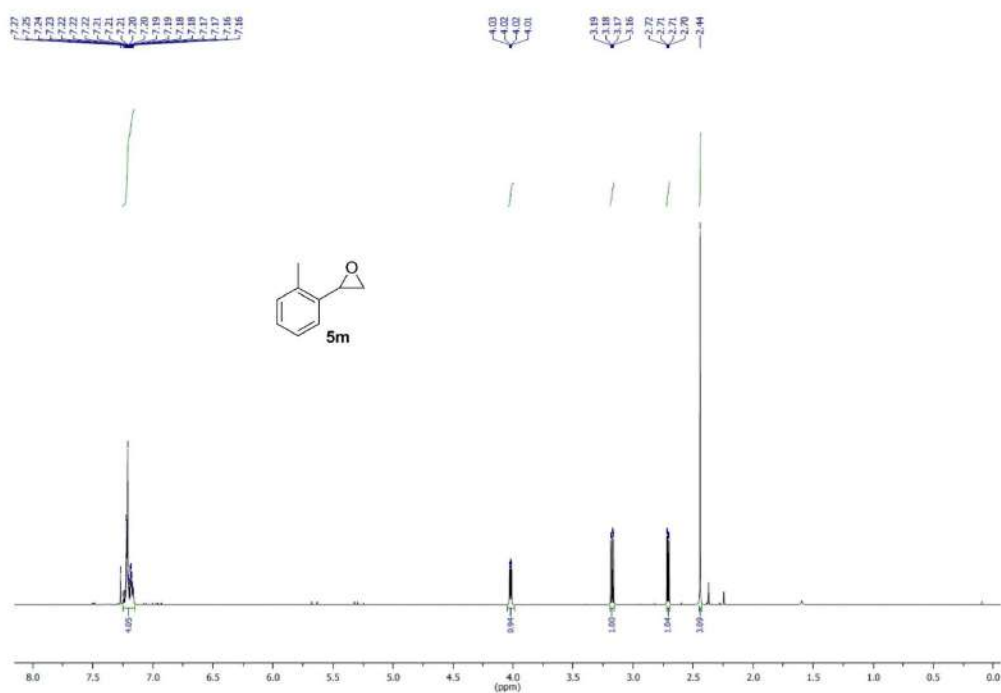


Figure S62. <sup>13</sup>C NMR (CDCl<sub>3</sub>, 101 MHz) spectrum: compound 5I.



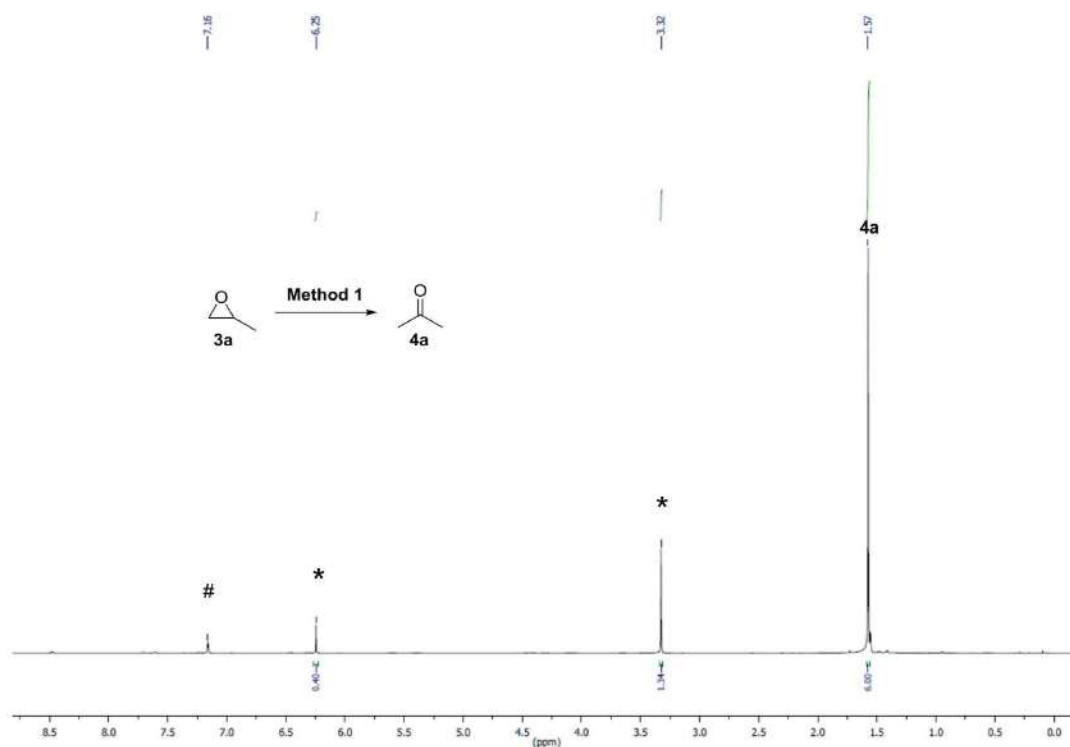


Figure S65. <sup>1</sup>H NMR (C<sub>6</sub>D<sub>6</sub> (#), 400 MHz) spectrum: isomerisation of **3a** into **4a** with **Method 1** including the internal standard (\*).

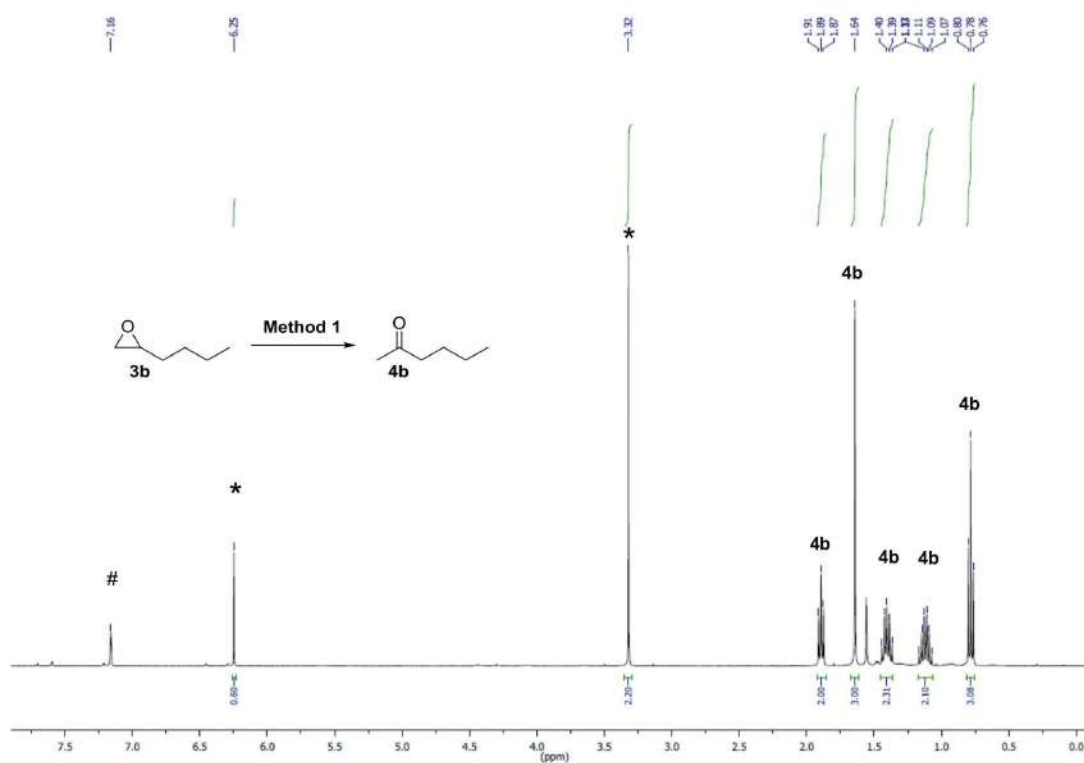


Figure S66. <sup>1</sup>H NMR (C<sub>6</sub>D<sub>6</sub> (#), 400 MHz) spectrum: isomerisation of **3b** into **4b** with **Method 1** including the internal standard (\*).

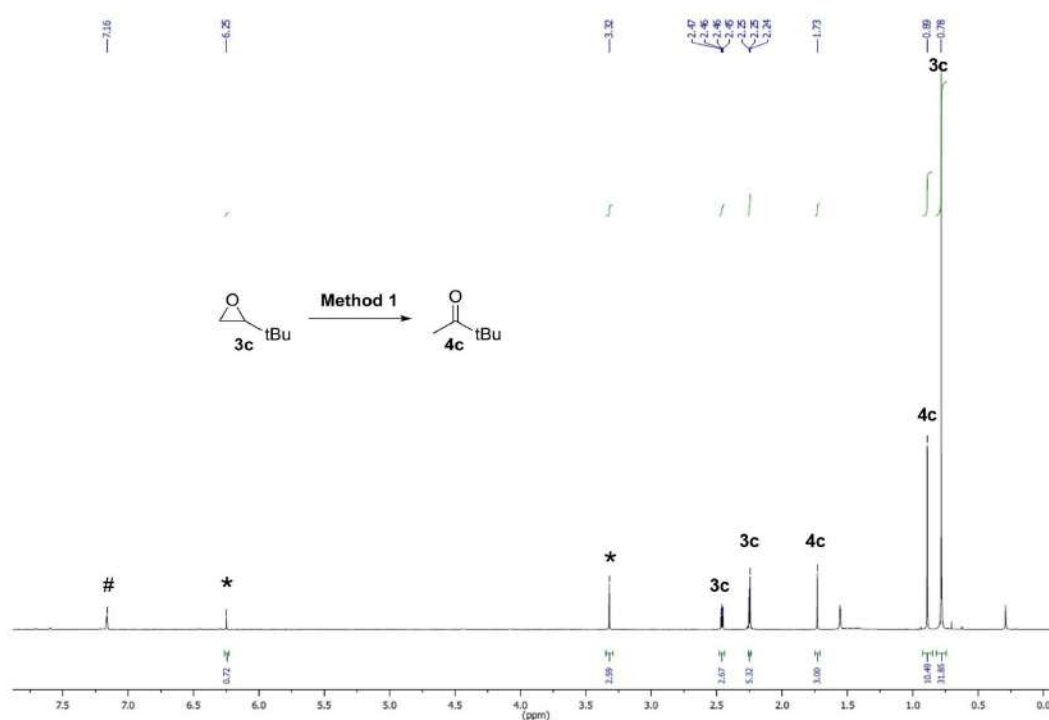


Figure S67. <sup>1</sup>H NMR (C<sub>6</sub>D<sub>6</sub> (#), 400 MHz) spectrum: isomerisation of 3c into 4c with Method 1 including the internal standard (\*).

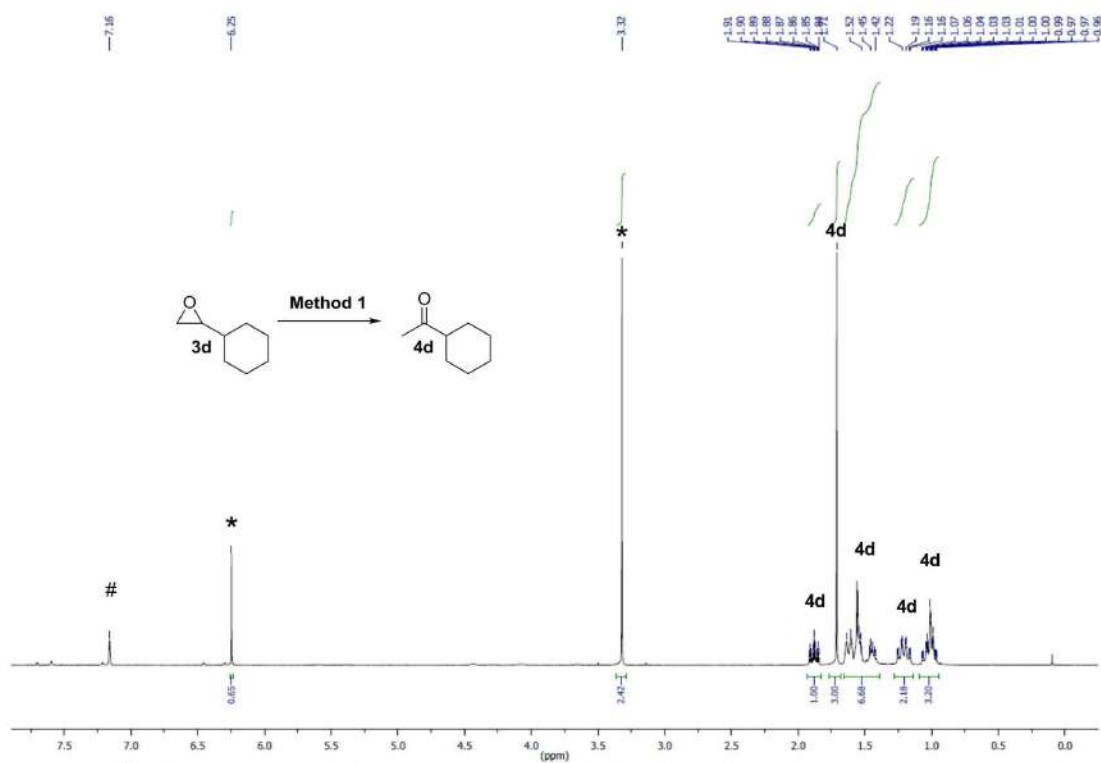


Figure S68. <sup>1</sup>H NMR (C<sub>6</sub>D<sub>6</sub> (#), 400 MHz) spectrum: isomerisation of 3d into 4d with Method 1 including the internal standard (\*).

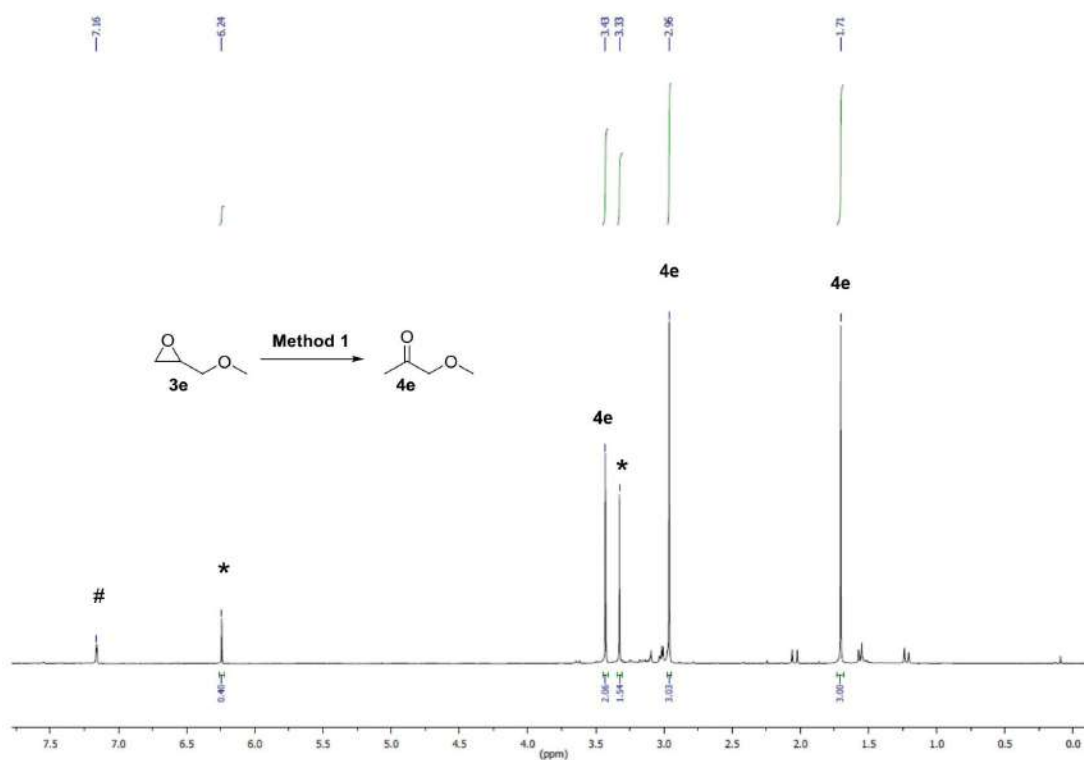


Figure S69. <sup>1</sup>H NMR (C<sub>6</sub>D<sub>6</sub> (#), 400 MHz) spectrum: isomerisation of **3e** into **4e** with **Method 1** including the internal standard (\*).

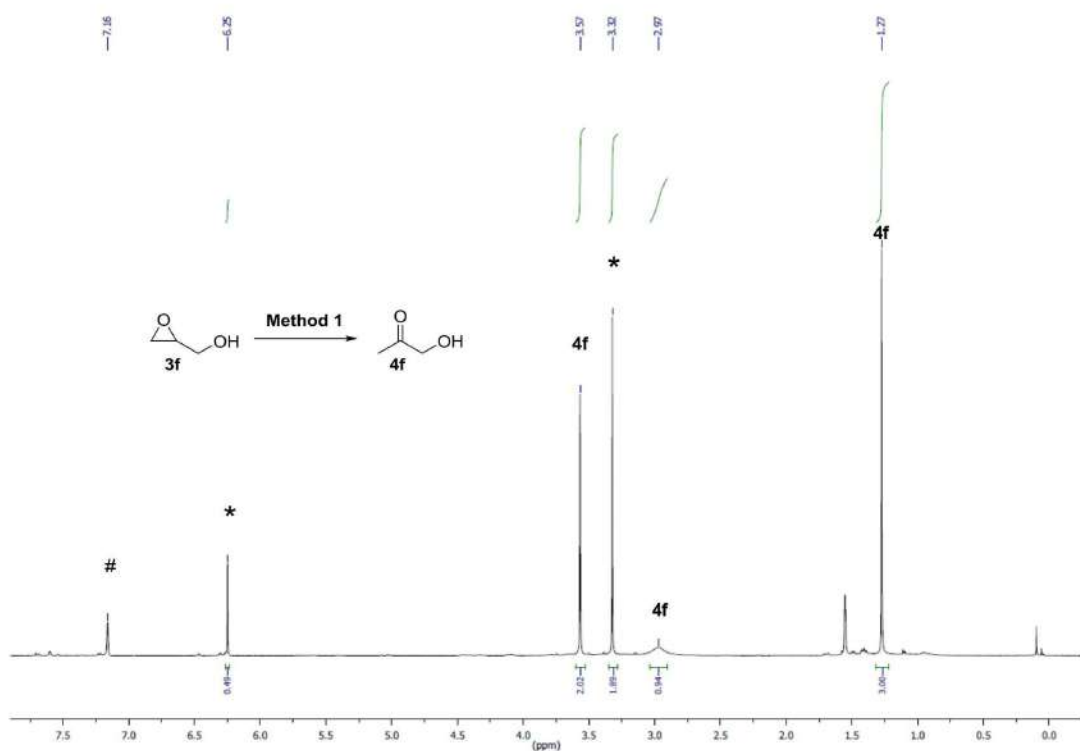


Figure S70. <sup>1</sup>H NMR (C<sub>6</sub>D<sub>6</sub> (#), 400 MHz) spectrum: isomerisation of **3f** into **4f** with **Method 1** including the internal standard (\*).

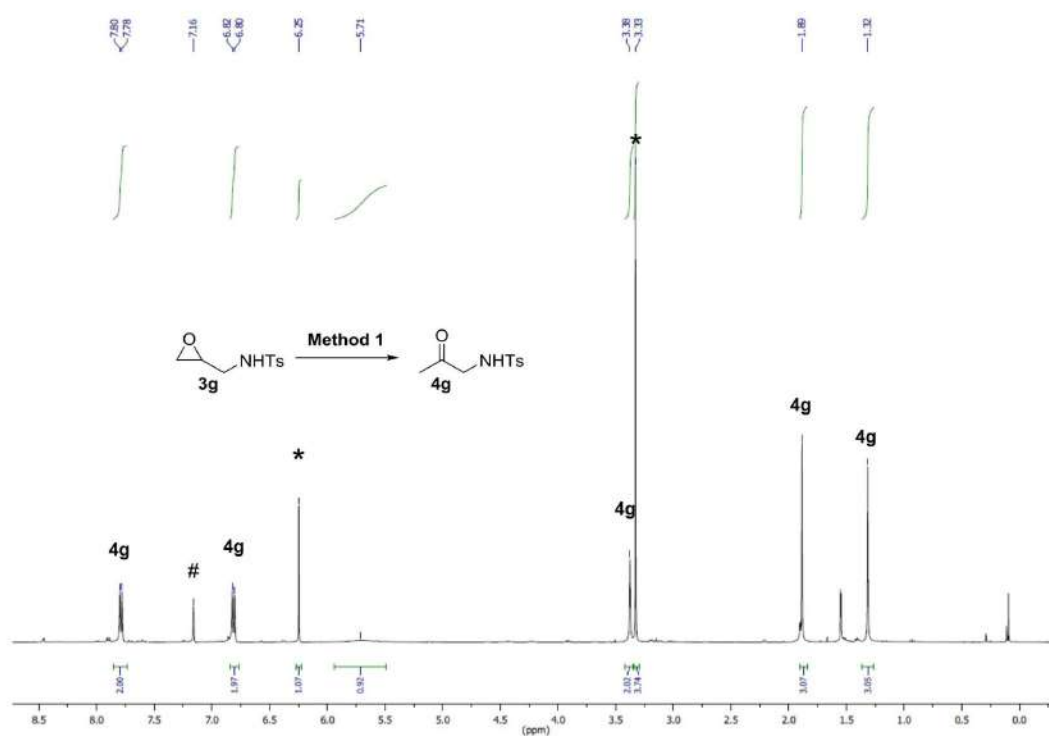


Figure S71.  $^1\text{H}$  NMR ( $\text{C}_6\text{D}_6$  (#), 400 MHz) spectrum: isomerisation of **3g** into **4g** with **Method 1** including the internal standard (\*).

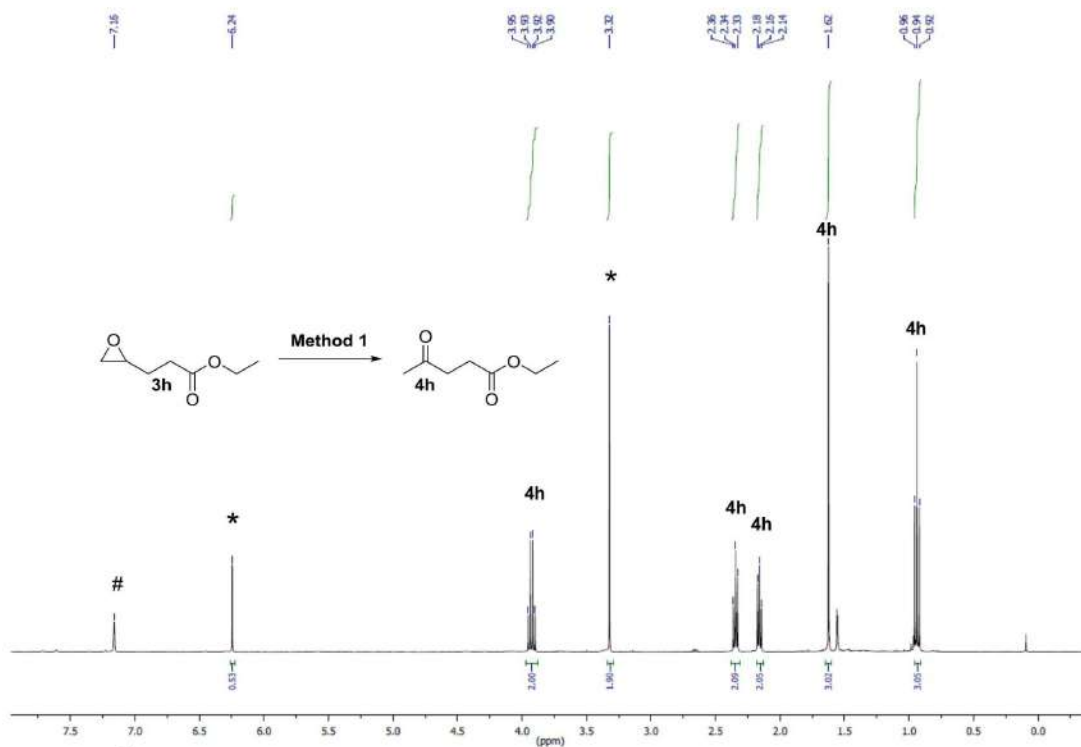


Figure S72.  $^1\text{H}$  NMR ( $\text{C}_6\text{D}_6$  (#), 400 MHz) spectrum: isomerisation of **3h** into **4h** with **Method 1** including the internal standard (\*).

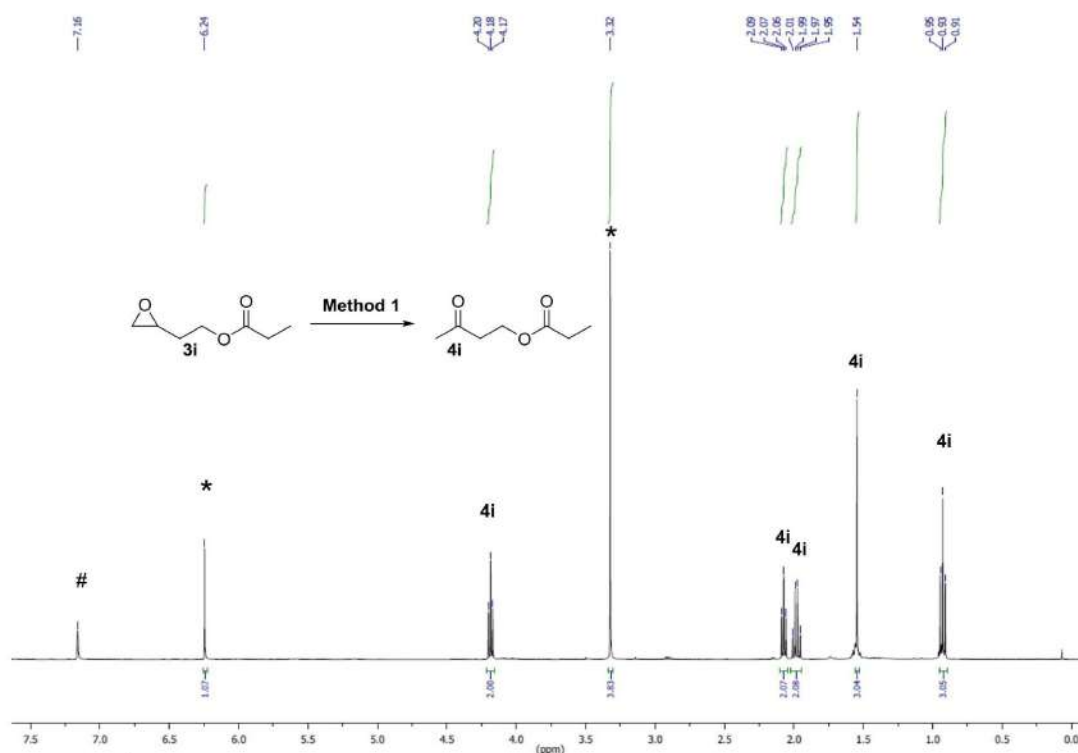


Figure S73. <sup>1</sup>H NMR (C<sub>6</sub>D<sub>6</sub> (#), 400 MHz) spectrum: isomerisation of 3i into 4i with Method 1 including the internal standard (\*).

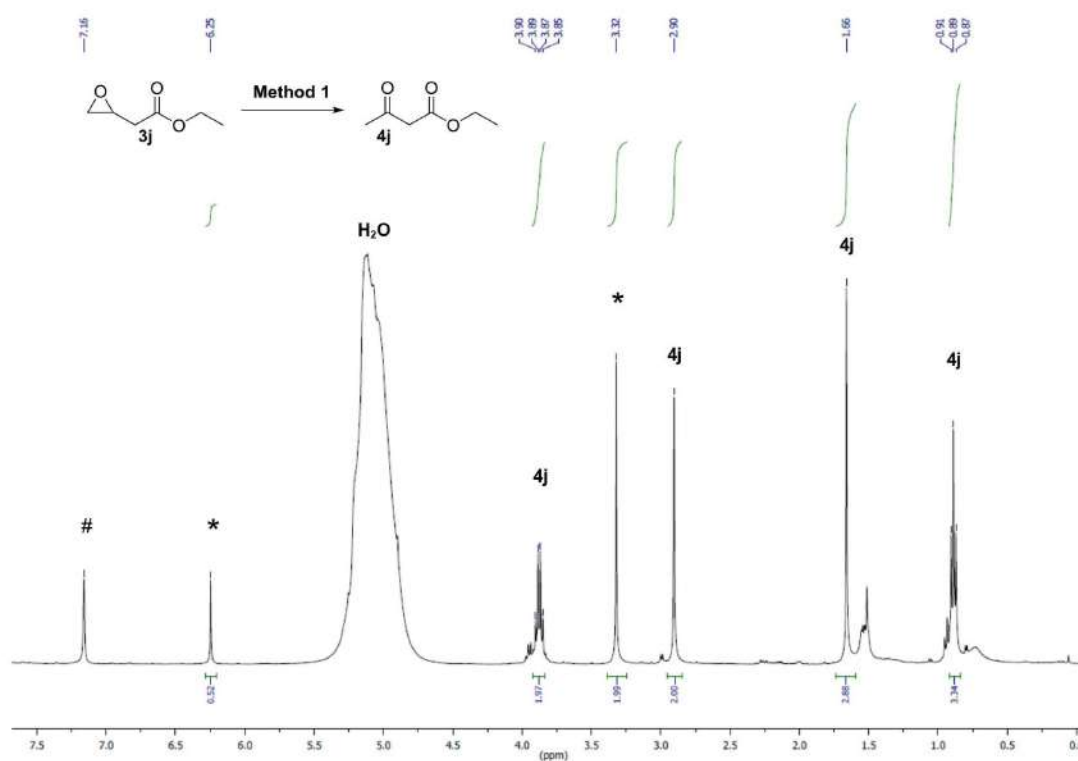


Figure S74. <sup>1</sup>H NMR (C<sub>6</sub>D<sub>6</sub> (#), 400 MHz) spectrum: isomerisation of 3j into 4j with Method 1 including the internal standard (\*). Notably, this reaction should be quenched with a drop of water otherwise there were all broad peaks in the spectrum.



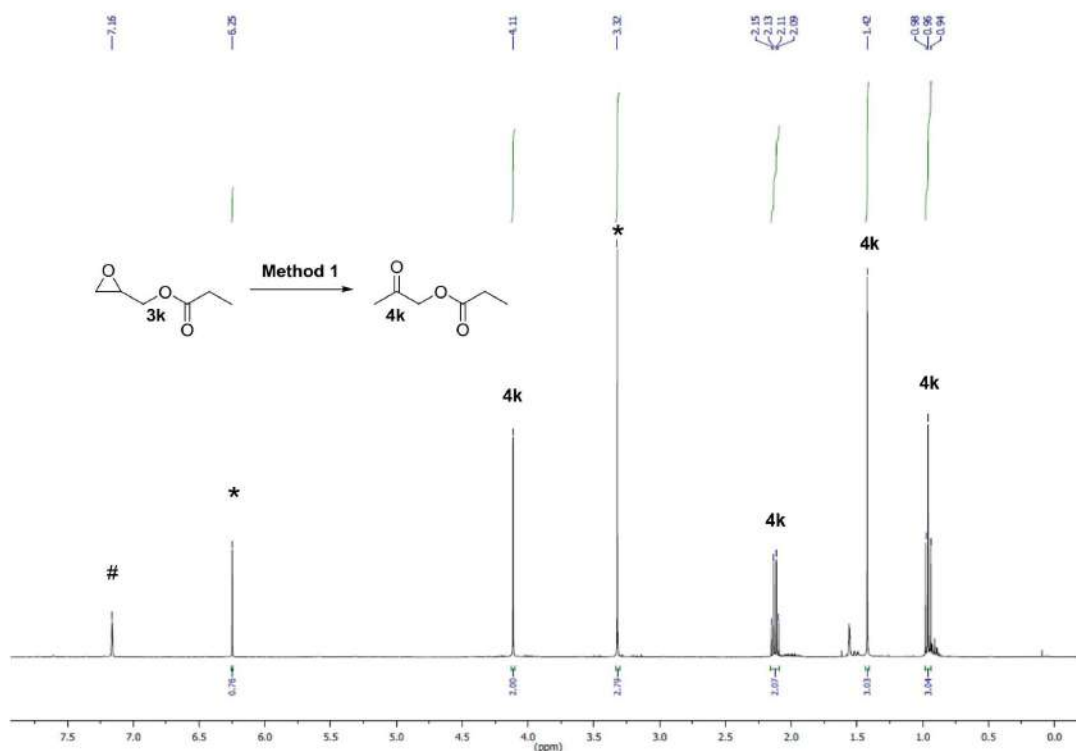


Figure S75. <sup>1</sup>H NMR (C<sub>6</sub>D<sub>6</sub> (#), 400 MHz) spectrum: isomerisation of 3k into 4k with Method 1 including the internal standard (\*).

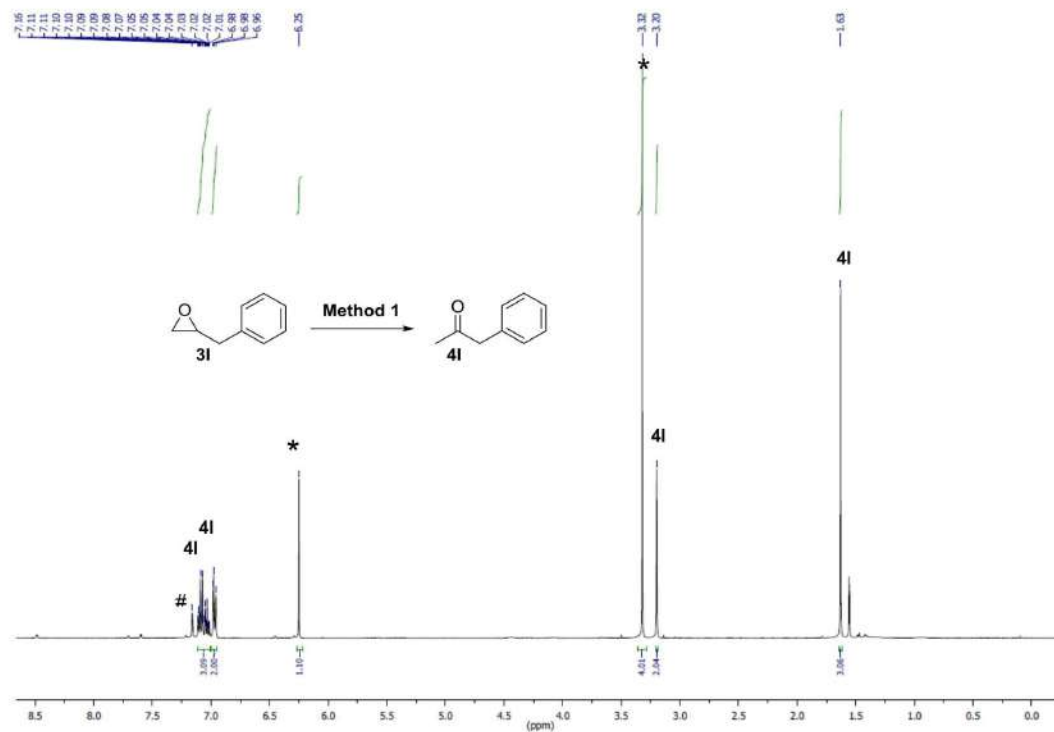
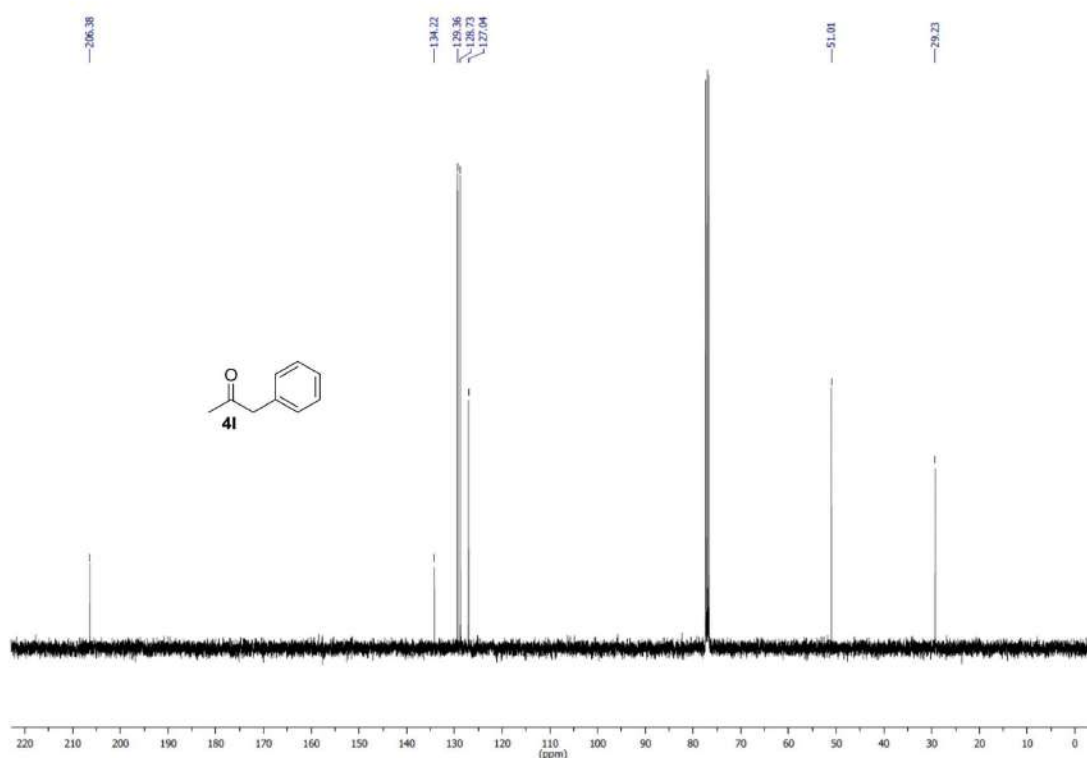
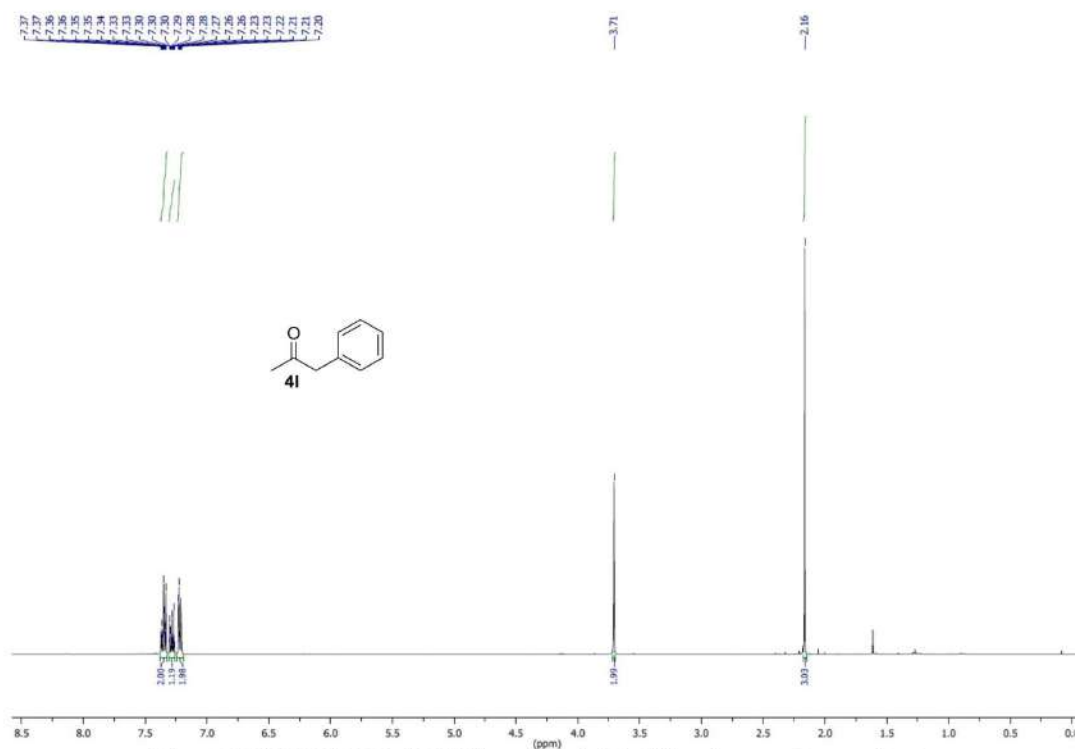


Figure S76. <sup>1</sup>H NMR (C<sub>6</sub>D<sub>6</sub> (#), 400 MHz) spectrum: isomerisation of 3l into 4l with Method 1 including the internal standard (\*).



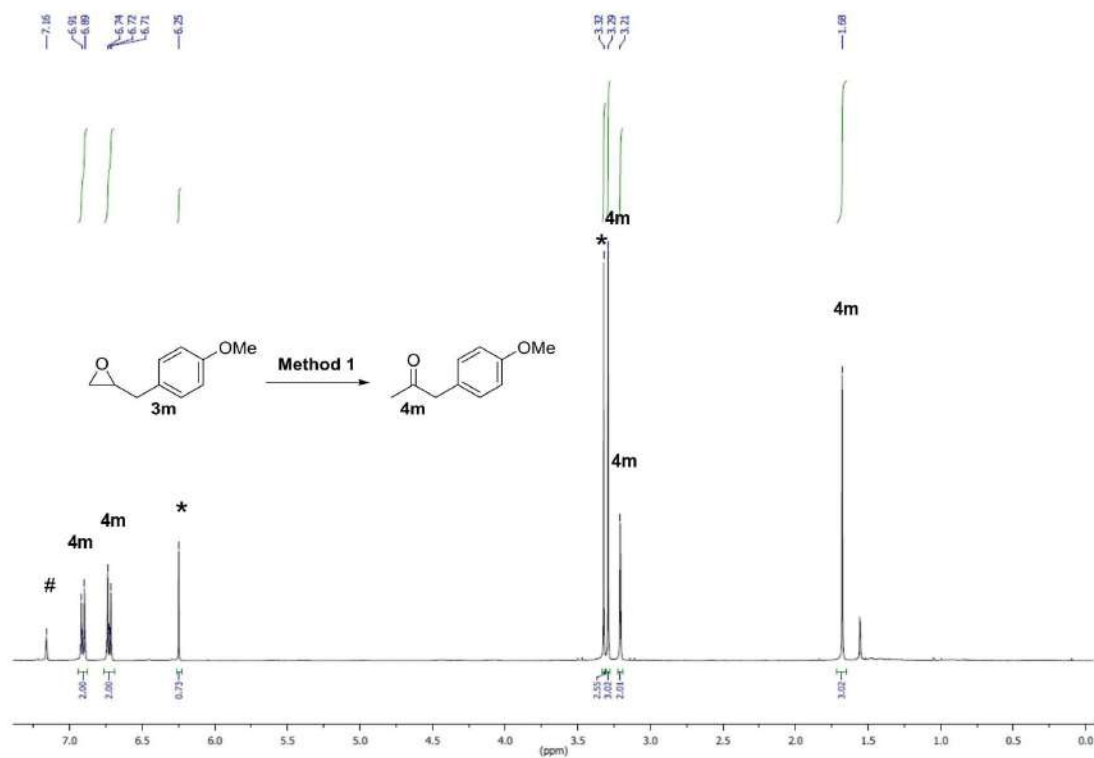


Figure S79. <sup>1</sup>H NMR (C<sub>6</sub>D<sub>6</sub> #), 400 MHz) spectrum: isomerisation of 3m into 4m with Method 1 including the internal standard (\*).

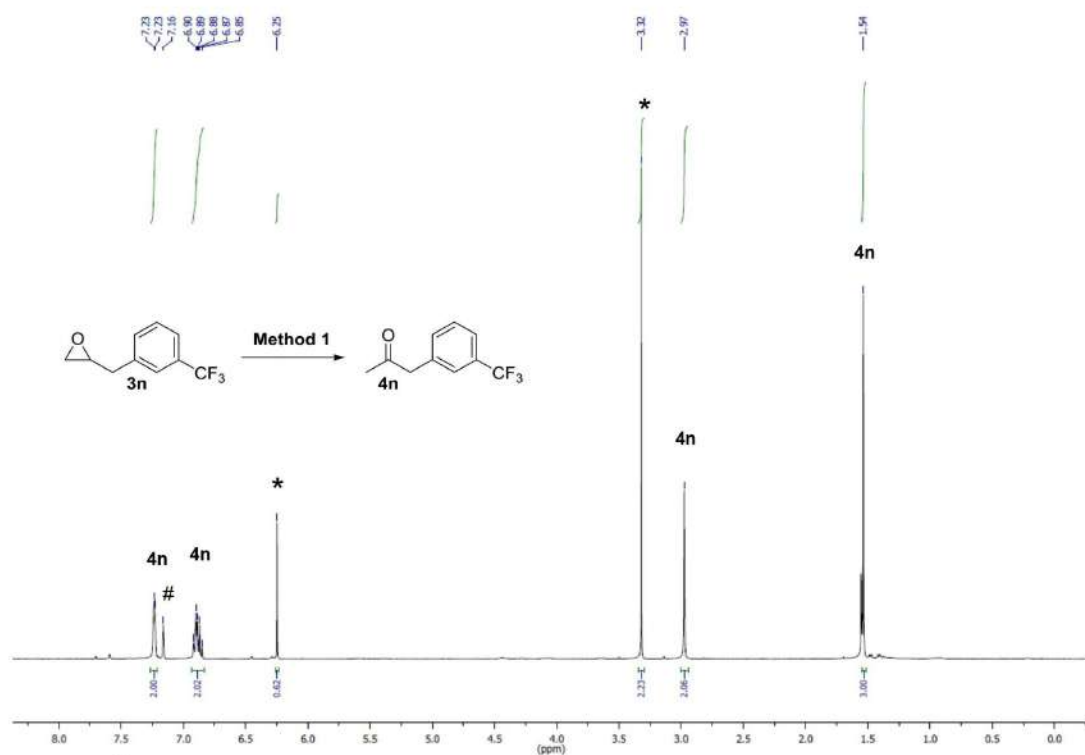
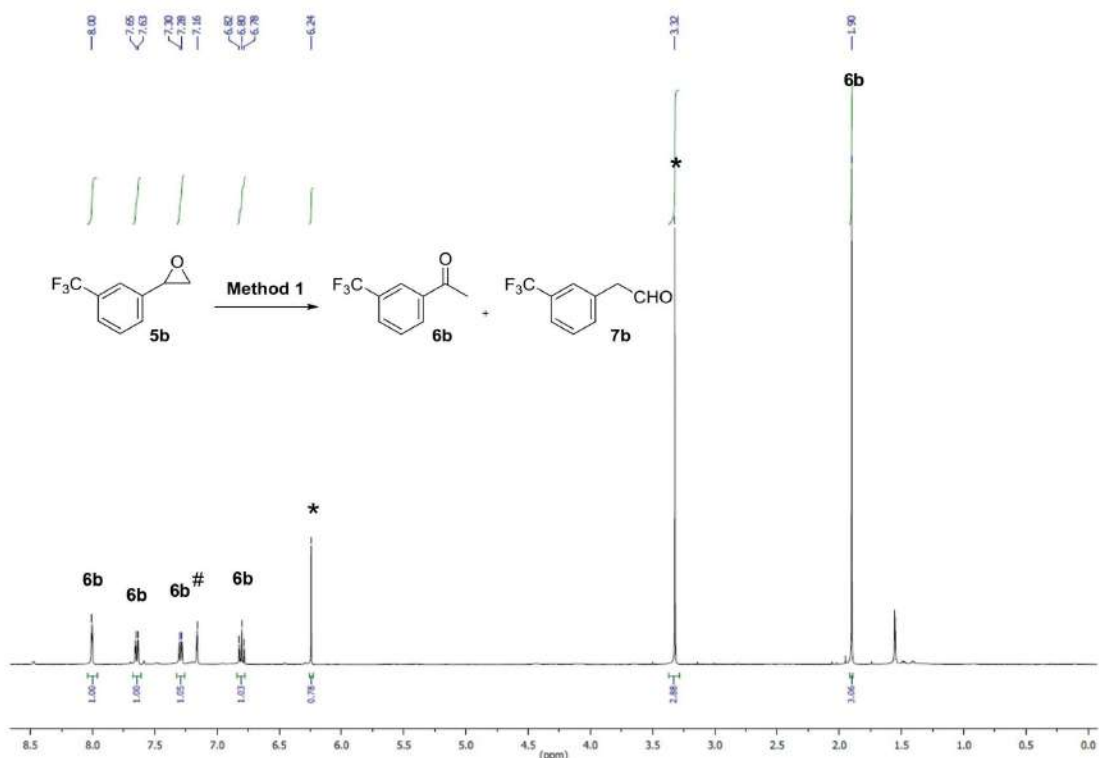
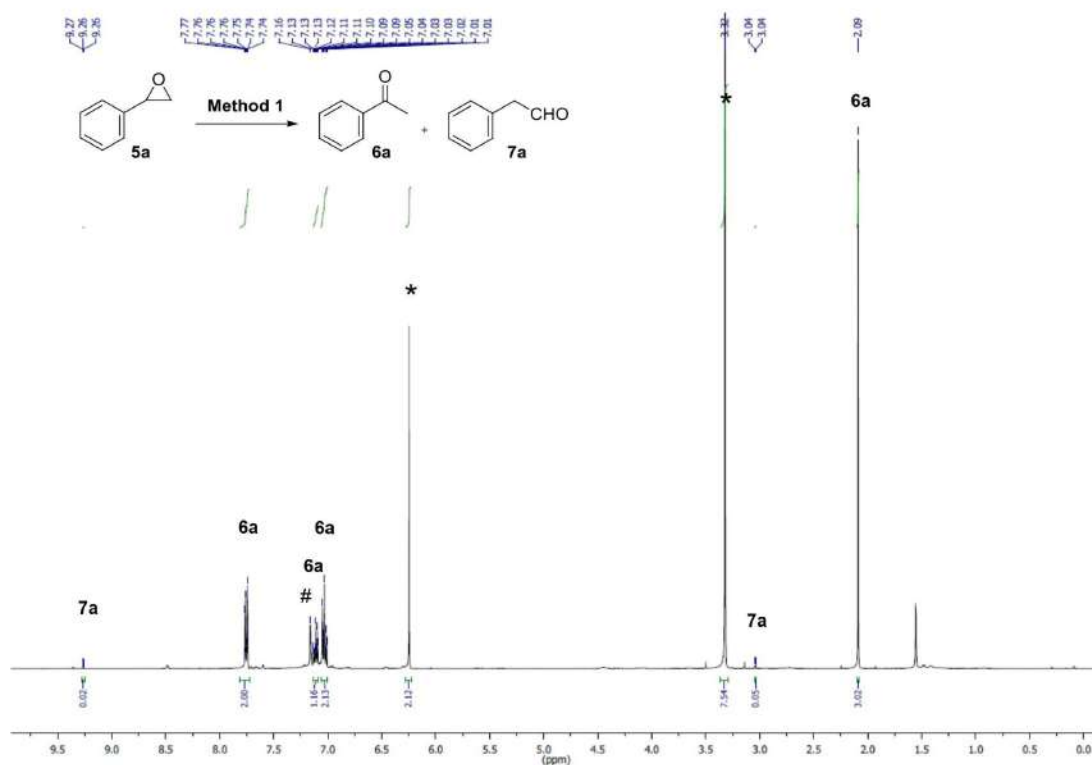


Figure S80. <sup>1</sup>H NMR (C<sub>6</sub>D<sub>6</sub> #), 400 MHz) spectrum: isomerisation of 3n into 4n with Method 1 including the internal standard (\*).



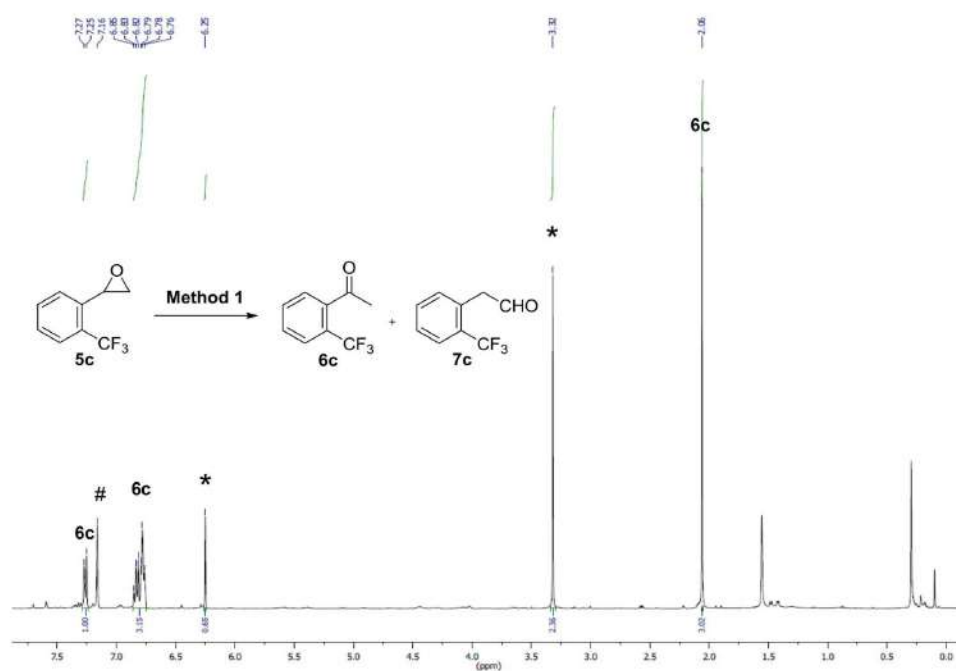


Figure S83.  $^1\text{H}$  NMR ( $\text{C}_6\text{D}_6$  (#), 400 MHz) spectrum: isomerisation of **5c** into **6c** with **Method 1** including the internal standard (\*).

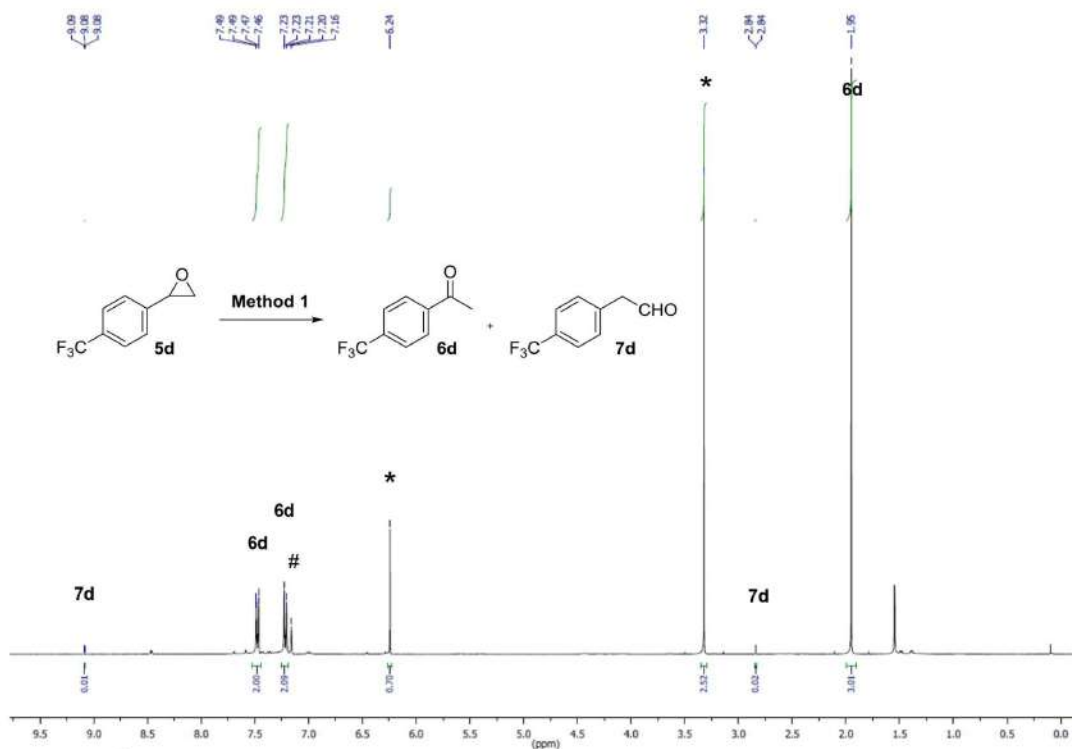


Figure S84.  $^1\text{H}$  NMR ( $\text{C}_6\text{D}_6$  (#), 400 MHz) spectrum: isomerisation of **5d** into **6d** with **Method 1** including the internal standard (\*).

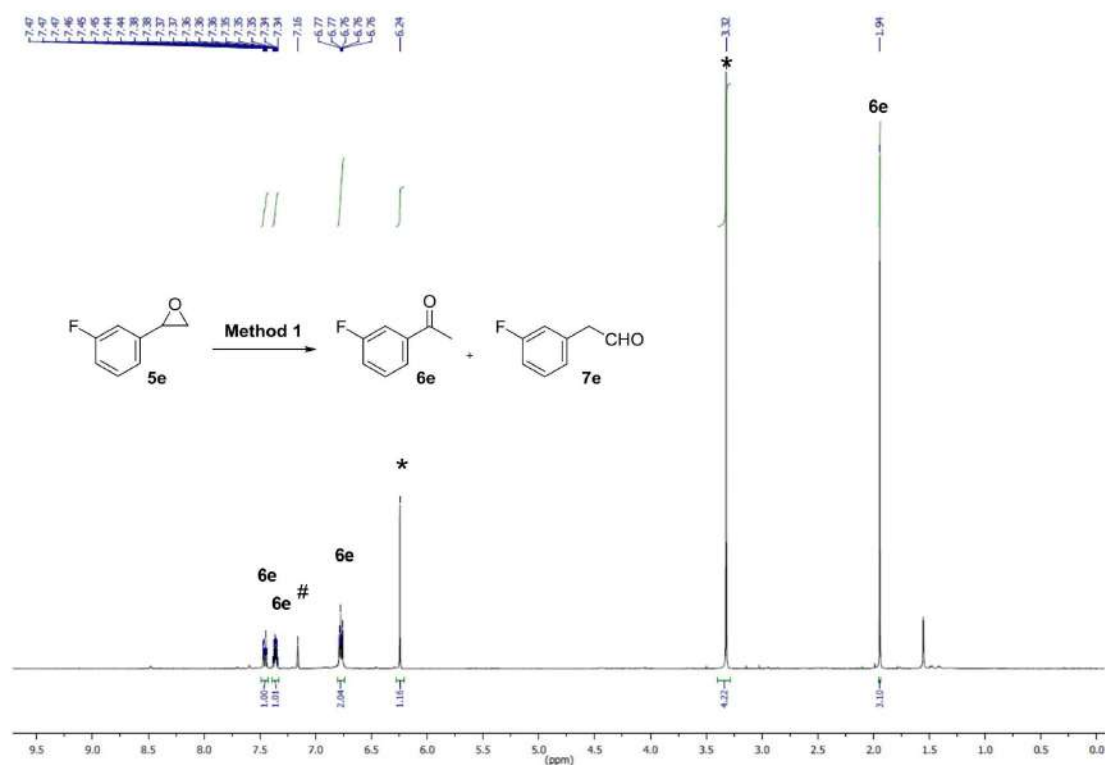


Figure S85. <sup>1</sup>H NMR (C<sub>6</sub>D<sub>6</sub> (#), 400 MHz) spectrum: isomerisation of **5e** into **6e** with **Method 1** including the internal standard (\*).

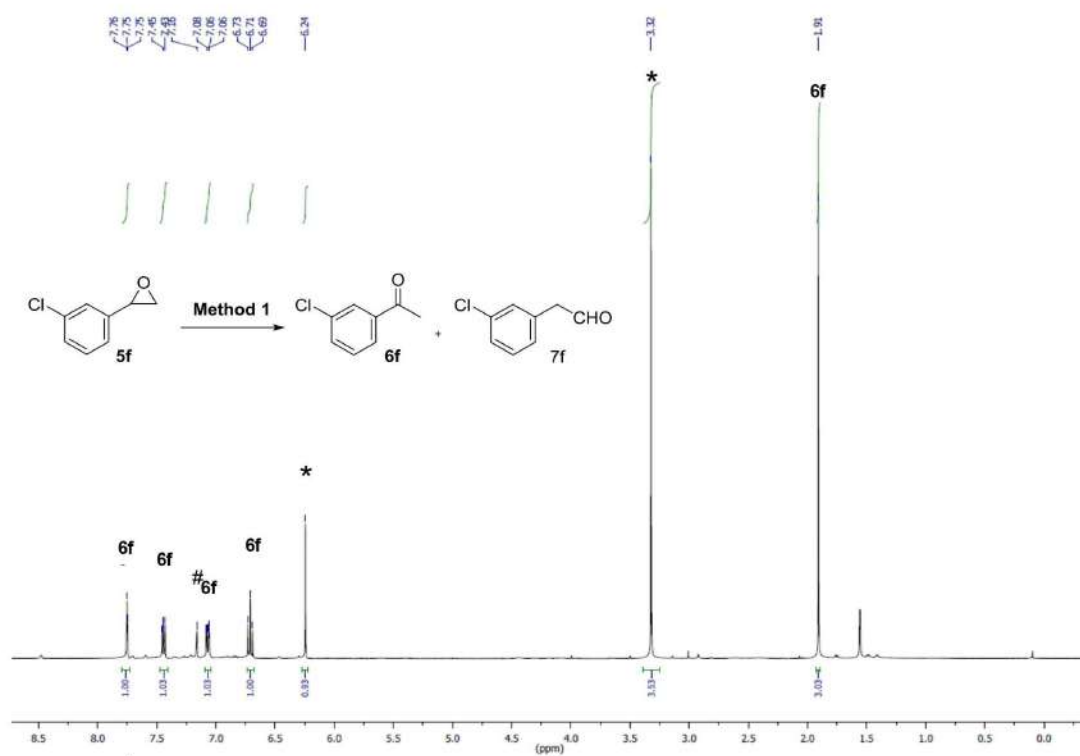


Figure S86. <sup>1</sup>H NMR (C<sub>6</sub>D<sub>6</sub> (#), 400 MHz) spectrum: isomerisation of **5f** into **6f** with **Method 1** including the internal standard (\*).

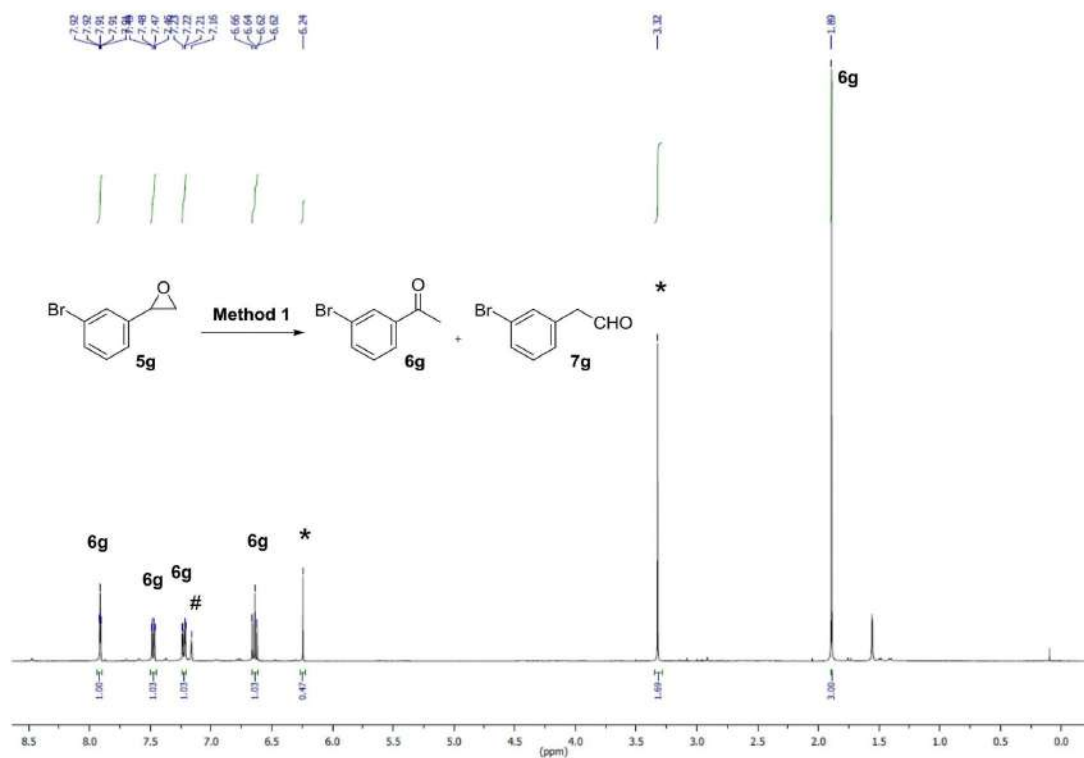


Figure S87.  $^1\text{H NMR}$  ( $\text{C}_6\text{D}_6$  (#), 400 MHz) spectrum: isomerisation of **5g** into **6g** with **Method 1** including the internal standard (\*).

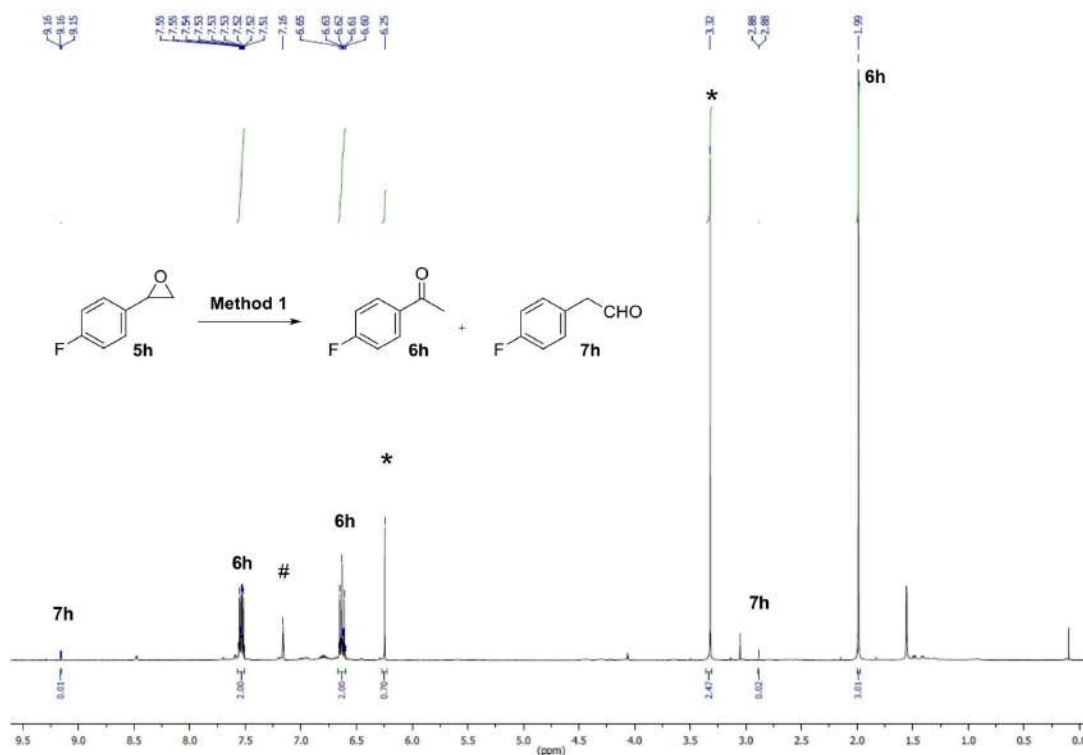


Figure S88.  $^1\text{H NMR}$  ( $\text{C}_6\text{D}_6$  (#), 400 MHz) spectrum: isomerisation of **5h** into **6h** with **Method 1** including the internal standard (\*).

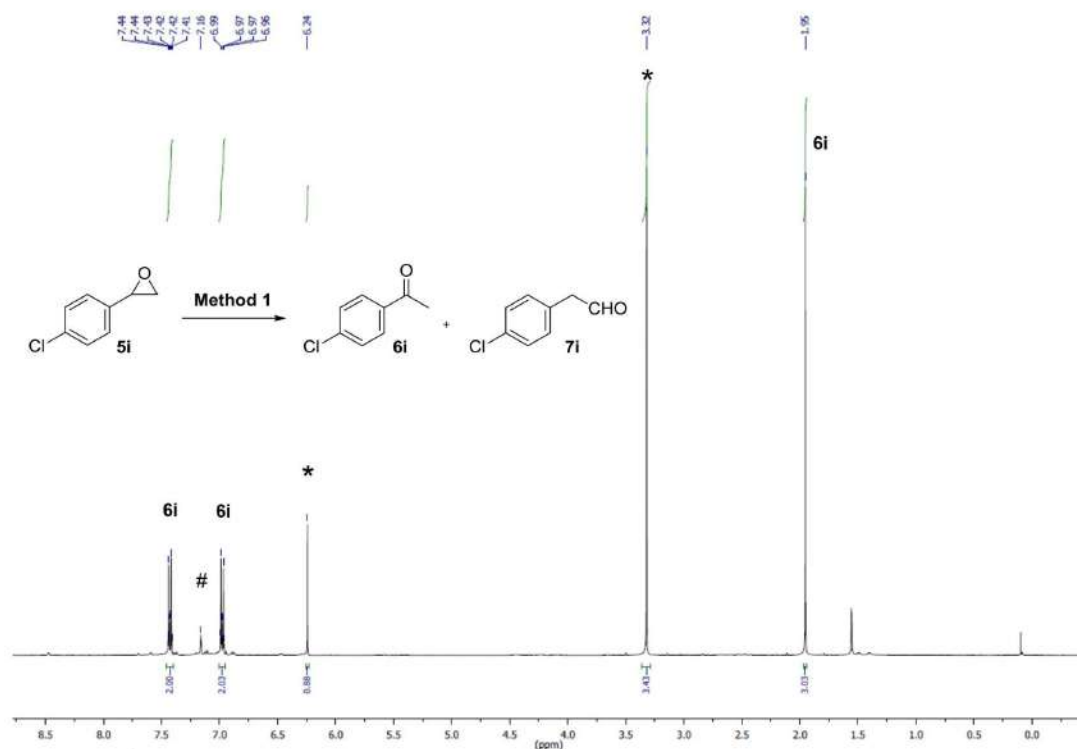


Figure S89. <sup>1</sup>H NMR (C<sub>6</sub>D<sub>6</sub> (#), 400 MHz) spectrum: isomerisation of **5i** into **6i** with Method 1 including the internal standard (\*).

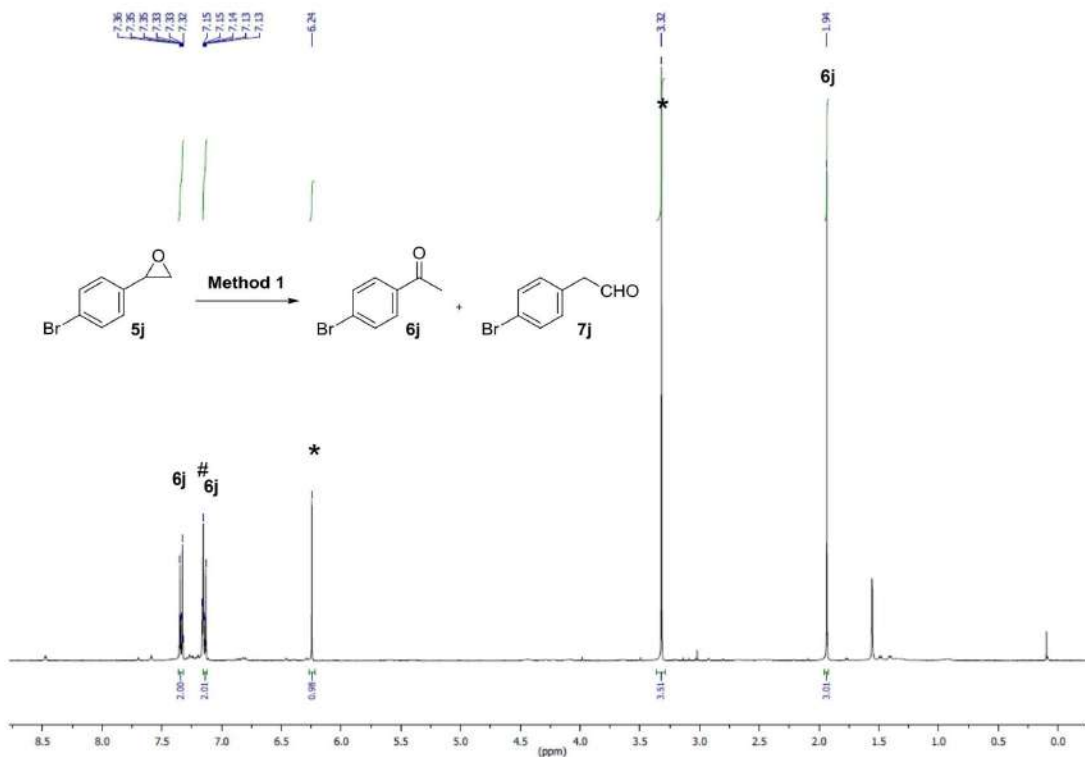
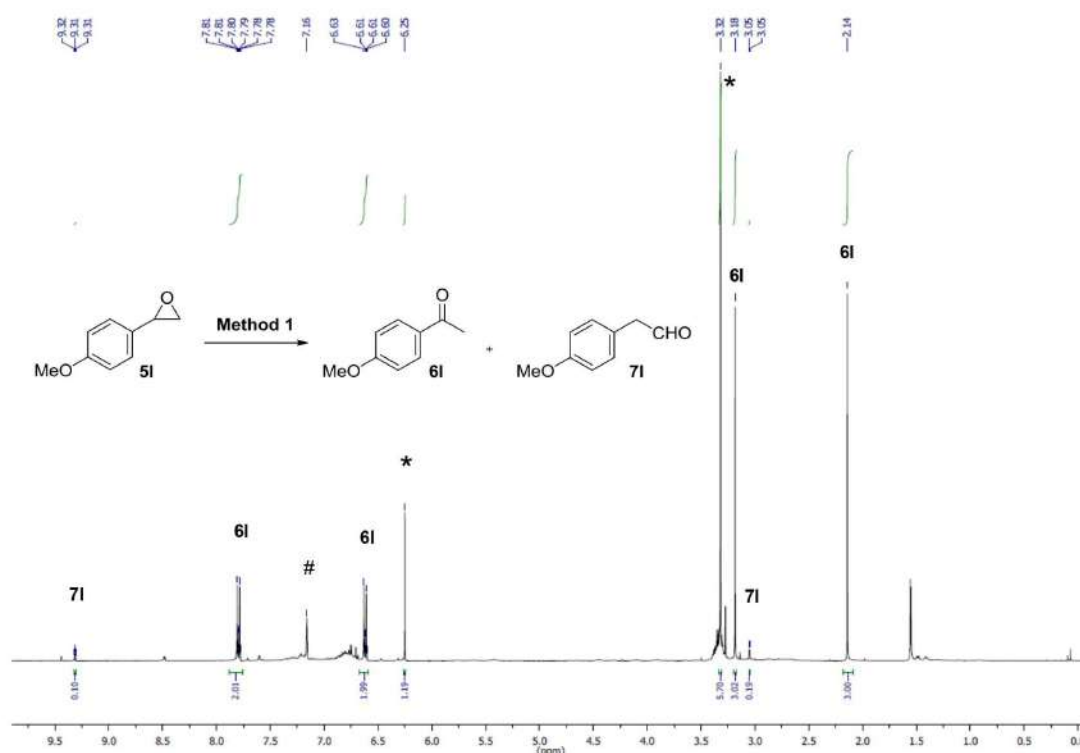
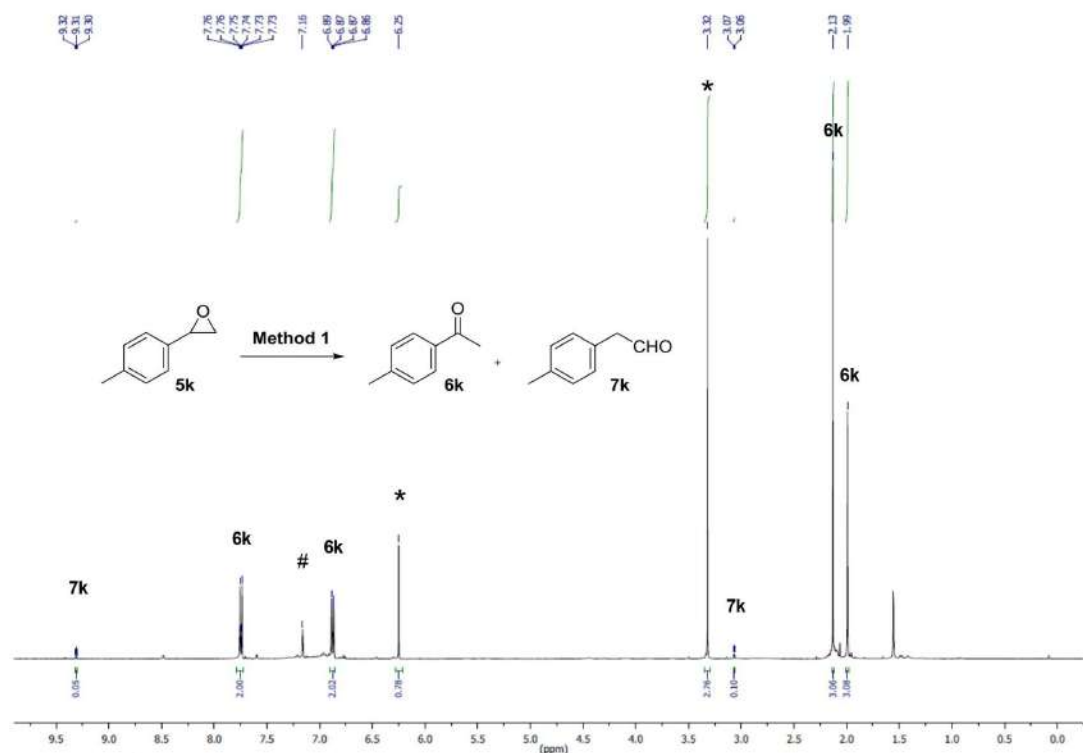


Figure S90. <sup>1</sup>H NMR (C<sub>6</sub>D<sub>6</sub> (#), 400 MHz) spectrum: isomerisation of **5j** into **6j** with Method 1 including the internal standard (\*).





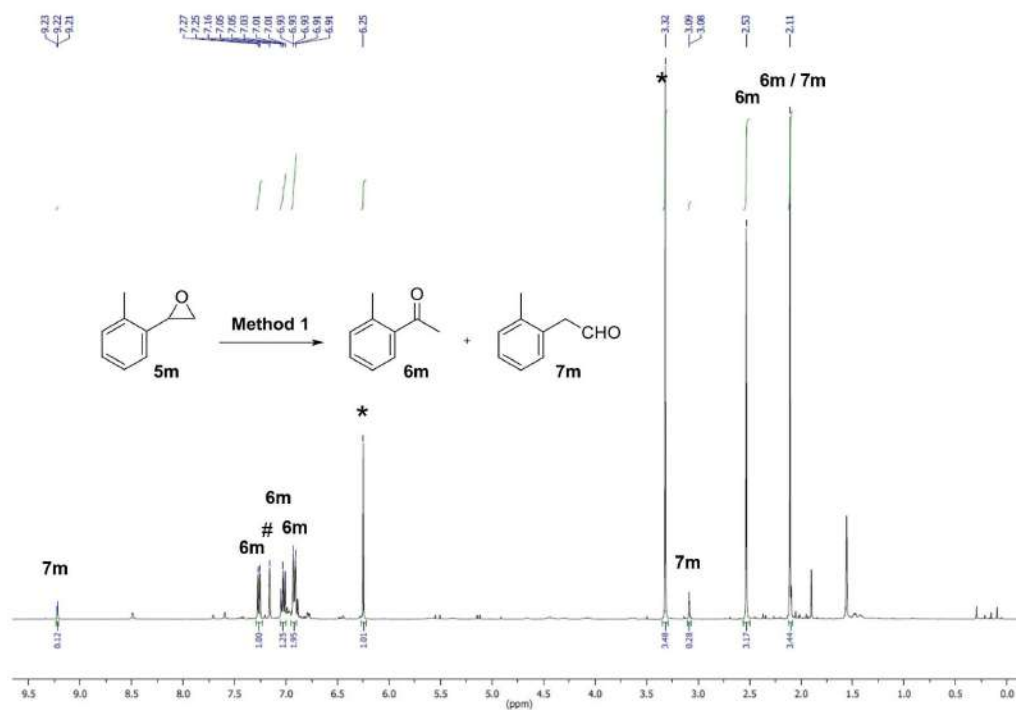
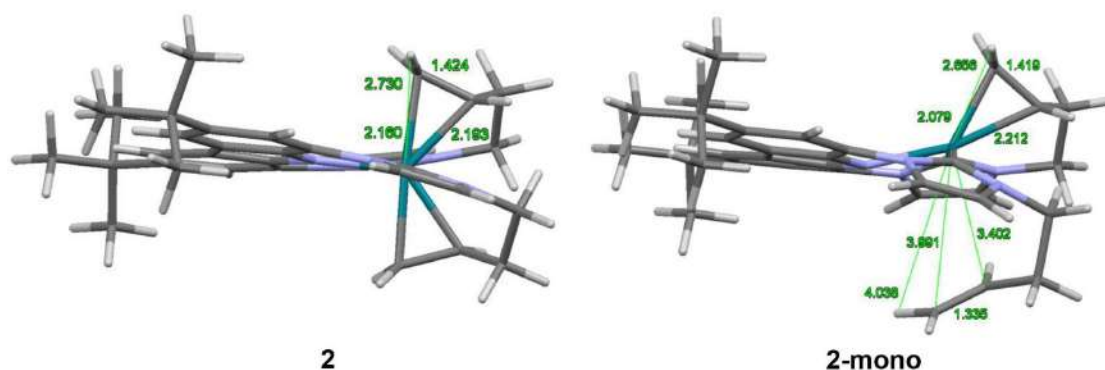


Figure S93.  $^1\text{H}$  NMR ( $\text{C}_6\text{D}_6$  (#), 400 MHz) spectrum: isomerisation of **5m** into **6m** with Method 1 including the internal standard (\*).

## 9. DFT calculations

**General information.** Calculations were performed based on density functional theory at the BP86/def2-SVP and/or BP86/def2-TZVP<sup>[12-17]</sup> level implemented in Turbomole<sup>[18-26]</sup>. The RI-approximation<sup>[27-32]</sup> was used all over and the Grimme dispersion correction D3-BJ<sup>[33-34]</sup>. Several structures were optimised differing in the conformation of the rings formed by the coordination of the double bonds. The two conformers **2** and **2-mono** were verified to be minimum structures at the BP86/def2-SVP level by calculating the Hessian matrix and ensuring that it has no imaginary frequency. The Cartesian coordinates are provided as a separate xyz-file.



### Thermodynamics of the two conformers of **2**

No. in Manuscript	<b>2</b>	<b>2-mono</b>
SCF	-1705,0810914	-1705,0601104
SCF+E <sub>vib</sub> 0	-1704,4236066	-1704,4052447
H (298K, 1 bar)	0,6950860	0,6941540
SCF+H (298K, 1 bar)	-1704,3860054	-1704,3659564
G (298K, 1 bar)	0,5922243	0,5838385
SCF+G (298K, 1 bar)	-1704,4888671	-1704,4762719
$\Delta$ (SCF) a.u.	0,0209810	55,09 kJ/mol
$\Delta$ (SCF+E <sub>vib</sub> 0) a.u.	0,0183619	48,21 kJ/mol
$\Delta H_{(298\text{ K}, 1\text{ bar})}$ a.u.	0,0200490	52,64 kJ/mol
$\Delta G_{(298\text{ K}, 1\text{ bar})}$ a.u.	0,0125952	33,07 kJ/mol

The unsymmetric complex **2-mono** is about 53 kJ/mol higher in energy ( $\Delta H^\ominus$ ) ( $\Delta G^\ominus = 33$  kJ/mol) than complex **2** and is also not supported by the experimental NMR data for symmetry reasons.

## 10. References

- 1 E. Jürgens, D. Kunz, *Eur. J. Inorg. Chem.*, 2017, **2017**, 233.
- 2 E. Jürgens, K. N. Buys, A.-T. Schmidt, S. K. Furfari, M. L. Cole, M. Moser, F. Rominger, D. Kunz, *New J. Chem.*, 2016, **40**, 9160.
- 3 M. Moser, B. Wucher, D. Kunz, F. Rominger, *Organometallics*, 2007, **26**, 1024.
- 4 S. V. Mulay, R. A. Fernandes, *Chem. -Eur. J.*, 2015, **21**, 4842.
- 5 J. Rintjema, R. Epping, G. Fiorani, E. Martín, E. C. Escudero-Adán, A. W. Kleij, *Angew. Chem. Int. Ed.*, 2016, **55**, 3972.
- 6 J. A. R. Schmidt, E. B. Lobkovsky, G. W. Coates, *J. Am. Chem. Soc.*, 2005, **127**, 11426.
- 7 C. Cook, F. Liron, X. Guinchard, E. Roulland, *J. Org. Chem.*, 2012, **77**, 6728.
- 8 K. L. Jensen, E. A. Standley, T. F. Jamison, *J. Am. Chem. Soc.*, 2014, **136**, 11145.
- 9 S. Baader, D. M. Ohlmann, L. J. Gooßen, *Chem. -Eur. J.*, 2013, **19**, 9807.
- 10 D. Zhao, X.-H. Liu, Z.-Z. Shi, C.-D. Zhu, Y. Zhao, P. Wang, W.-Y. Sun, *Dalton Trans.*, 2016, **45**, 14184.
- 11 S. A. Murray, E. C. M. Luc, S. J. Meek, *Org. Lett.*, 2018, **20**, 469.
- 12 A. Becke, *Phys. Rev. A*, 1988, **38**, 3098.
- 13 J. P. Perdew, *Phys. Rev. B*, 1986, **33**, 8822.
- 14 A. Schäfer, H. Horn, R. Ahlrichs, *J. Chem. Phys.*, 1992, **97**, 2571.
- 15 A. Schäfer, C. Huber, R. Ahlrichs, *J. Chem. Phys.*, 1994, **100**, 5829.
- 16 F. Weigend, R. Ahlrichs, *Phys. Chem. Chem. Phys.*, 2005, **7**, 3297.
- 17 F. Weigend, *Phys. Chem. Chem. Phys.*, 2006, **8**, 1057.
- 18 TURBOMOLE V6.3.1 2011, a development of University of Karlsruhe and Forschungszentrum Karlsruhe GmbH, 1989–2007, TURBOMOLE GmbH, since 2007; available from <http://www.turbomole.com>.
- 19 O. Treutler, R. Ahlrichs, *J. Chem. Phys.*, 1995, **102**, 346.
- 20 M. von Arnim, R. Ahlrichs, *J. Comp. Chem.*, 1998, **19**, 1746.
- 21 C. van Wüllen, *J. Comp. Chem.*, 2011, **32**, 1195.
- 22 P. Deglmann, F. Furche, R. Ahlrichs, *Chem. Phys. Lett.*, 2002, **362**, 511.
- 23 P. Deglmann, F. Furche, *J. Chem. Phys.*, 2002, **117**, 9535.
- 24 R. Ahlrichs, M. Bär, M. Häser, H. Horn, C. Kölmel, *Chem. Phys. Lett.*, 1989, **162**, 165.
- 25 M. K. Armbruster, F. Weigend, C. van Wüllen, W. Klopper, *Phys. Chem. Chem. Phys.*, 2008, **10**, 1748.
- 26 D. Peng, N. Middendorf, F. Weigend, M. Reiher, *J. Chem. Phys.*, 2013, **138**, 184105.
- 27 K. Eichkorn, O. Treutler, H. Öhm, M. Häser, R. Ahlrichs, *Chem. Phys. Lett.*, 1995, **240**, 283.
- 28 K. Eichkorn, O. Treutler, H. Öhm, M. Häser, R. Ahlrichs, *Chem. Phys. Lett.*, 1995, **242**, 652.
- 29 K. Eichkorn, F. Weigend, O. Treutler, R. Ahlrichs, *Theor. Chem. Acc.*, 1997, **97**, 119.
- 30 P. Deglmann, K. May, F. Furche, R. Ahlrichs, *Chem. Phys. Lett.*, 2004, **384**, 103.
- 31 F. Weigend, *Phys. Chem. Chem. Phys.*, 2002, **4**, 4285.
- 32 M. Sierka, A. Hogekamp, R. Ahlrichs, *J. Chem. Phys.*, 2003, **118**, 9136.
- 33 S. Grimme, J. Antony, S. Ehrlich, H. Krieg, *J. Chem. Phys.*, 2010, **132**, 154104.
- 34 S. Grimme, S. Ehrlich, L. Goerigk, *J. Comput. Chem.*, 2011, **32**, 1456.

# Nucleophilic Isomerization of Epoxides by Pincer-Rhodium Catalysts: Activity Increase and Mechanistic Insights

Yingying Tian,<sup>[a]</sup> Eva Jürgens,<sup>[a]</sup> Katharina Mill,<sup>[a]</sup> Ronja Jordan,<sup>[a]</sup> Theo Maulbetsch,<sup>[a]</sup> and Doris Kunz<sup>\*[a]</sup>

Herein, we present the efficient isomerization of epoxides into methyl ketones with a novel pincer-rhodium complex under very mild conditions. The catalyst system has an excellent functional group tolerance and a wide array of epoxides was tested. The corresponding methyl ketones were obtained in very high yields with excellent chemo- and regioselectivity. In

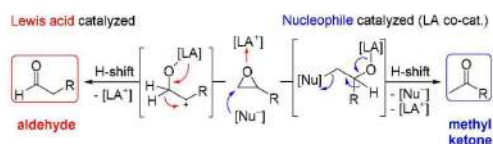
addition, we investigated mechanistic details like the isomerization of the catalyst, and we obtained evidence that the catalytic cycle follows a  $\beta$ -hydride elimination-reductive elimination pathway after the nucleophilic ring opening of the epoxide.

## Introduction

In contrast to the common Lewis acid catalyzed isomerization of terminal epoxides (Meinwald reaction),<sup>[1]</sup> which leads to the formation of aldehydes via generation of the more stable carbenium intermediate,<sup>[2]</sup> the isomerization by nucleophilic catalysts is rare and results in the formation of methyl ketones (Scheme 1).<sup>[3]</sup> This pathway is very attractive because, in combination with the Corey-Chaykovsky reaction, it provides an oxidation-free route for the synthesis of methyl ketones from aldehydes or, together with the epoxidation of olefins, an alternative to the Wacker oxidation. Since the discovery of this opposite regioselectivity in 1962 by Eisenmann,<sup>[3a]</sup> it was evident that the catalysis is not only achieved by a nucleophilic catalyst on its own, but typically requires a Lewis acid co-catalyst [LA<sup>+</sup>] which pre-activates the epoxide by coordination, but does not lead to ring opening under carbocation formation.

In case of the results of Eisenmann, the catalytic system **A** (Figure 1) most likely consists of the [Co(CO)<sub>4</sub>]<sup>-</sup> nucleophile and the Lewis acid [Co(CH<sub>3</sub>OH)<sub>6</sub>]<sup>2+</sup> formed *in situ* by disproportiona-

tion of [Co<sub>2</sub>(CO)<sub>8</sub>] in methanol that is required as a solvent. In 2015 we have reported on a selective ring opening using the nucleophilic Rh-catalyst **B** (5 mol%) along with 20 mol% of the Lewis acid co-catalyst LiNTf<sub>2</sub> at 60 °C.<sup>[3b]</sup> A more active system was reported by Coates using [Al(salen)]<sup>+</sup>[Co(CO)<sub>4</sub>]<sup>-</sup>.<sup>[3c]</sup> While both systems were highly selective with terminal alkyl epoxides, the isomerization of phenyl oxirane led to a mixture of the aldehyde and the ketone in almost equal amounts. This prompted us to develop the more nucleophilic CO-free rhodium catalyst **D**, in which the highly reactive metal center is intramolecularly stabilized by coordination of both *N*-homoallyl substituents of the so-called bimca<sup>homo</sup> (1,8-bis(imidazolylidene)-3,6-di(*tert*-butyl)carbazolide) carbene-pincer-ligand.<sup>[3d]</sup> Due to its higher nucleophilicity, a mixture of the weak Lewis acids LiBr and LiCl (2:1), which are present from the synthesis of **D** in THF, is sufficient to act as a co-catalyst in benzene. With

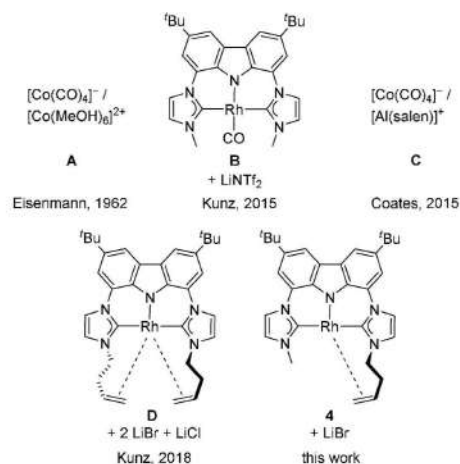


**Scheme 1.** Lewis acid- (left) and nucleophile- (right) catalyzed Meinwald reaction of terminal epoxides: formation of aldehydes versus methyl ketones.

[a] Y. Tian, E. Jürgens, K. Mill, R. Jordan, T. Maulbetsch, Prof. Dr. D. Kunz  
Institut für Anorganische Chemie  
Eberhard Karls Universität Tübingen  
Auf der Morgenstelle 18, 72076 Tübingen (Germany)  
E-mail: Doris.Kunz@uni-tuebingen.de

Supporting information for this article is available on the WWW under  
<https://doi.org/10.1002/cctc.201900594>

This manuscript is part of the Special Issue dedicated to the Women of Catalysis.



**Figure 1.** Rhodium pincer complexes and suitable Lewis acid co-catalysts for the nucleophilic Meinwald rearrangement.



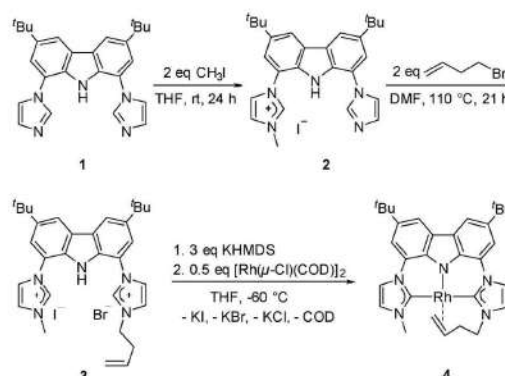
this system it was not only possible to achieve a selectivity of methyl ketone vs. aldehyde of 40:1 and 95% yield in the isomerization of phenyl oxirane after 2 h at room temperature (5 mol% **D**), but also to isomerize the highly sensitive *p*-methoxyphenyl oxirane to the corresponding ketone with a ratio of 10:1 and in 57% yield.

The functional group tolerance of catalyst **D** is very high, but sterically demanding substrates such as *tert*-butyloxirane,  $-\text{NH}_2$ , or  $-\text{OH}$  containing substrates, some *ortho*-substituted aryl oxiranes or internal epoxides required very long reaction times and/or elevated temperatures, which in some cases still led to low yields. Therefore, we were interested in developing our catalyst system further along with gaining more insight into the reaction mechanism.

As the 18  $e^-$  rhodium complex **D** requires the dissociation of one olefin moiety to react as a nucleophile, we envisaged the 16  $e^-$  complex **4** being an interesting target to fulfill our purpose: The complex would still be stabilized intramolecularly by one olefin moiety during catalysis but in addition exhibit a higher nucleophilicity and thus catalytic activity. However, an unsymmetrically *N*-substituted bimca ligand or related systems have hitherto not yet been reported. In the following, we will report on the synthesis of the unsymmetrical bimca ligand **bimca**<sup>Me,Homo</sup> and its Rh complex **4** as well as the catalytic activity of **4** in the regioselective epoxide isomerization. In addition, more insight into the reaction mechanism and deactivation pathways will be provided.

## Results and Discussion

The synthesis of an unsymmetrically substituted bimca ligand requires the selective monoalkylation of bisimidazol **1**. Based on the observation that the monoalkylated product **2** was formed as a byproduct when reacting bisimidazol **1** with an excess methyl iodide in THF,<sup>[4]</sup> we investigated the monoalkylation further. In acetonitrile the reaction of equimolar amounts of bisimidazol **1** and methyl iodide or Meerwein's salt ( $\text{Me}_3\text{OBF}_4$ ) leads to a 1:1 mixture of the dialkylated product and the starting material **1**. However, if the reaction is carried out with even a twofold excess of methyl iodide in THF at room temperature the desired product **2** is formed due to its precipitation under these conditions, which prevents further alkylation (Scheme 2). After workup by filtration, the imidazolium salt **2** was obtained in 90% yield as a yellow solid. The reduced symmetry leads to four signals for the carbazole moiety and six signals for the imidazolium moieties. The presence of only one NH signal with the same integral as the other aromatic peaks excludes a potential 1:1 mixture of **1** and the dimethylated product. The introduction of the *N*-homoallyl substituent was carried out with a twofold excess of 4-bromo-1-butene at 110 °C in dimethylformamide and the desired bisimidazolium salt **3** was isolated after workup in 95% yield. The 10 signals for the aromatic imidazolium and carbazole protons can be clearly assigned with the help of 2D NMR experiments including an NOE experiment to assign the peaks to the relative sides of the carbazole backbone.

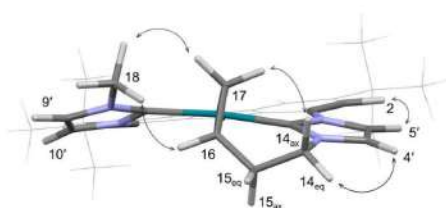


Scheme 2. Synthesis of the unsymmetrical rhodium catalyst **4**.

The preparation of **4**<sup>LIX</sup> was achieved by deprotonation of **3** with LiHMDS and subsequent addition of  $[\text{Rh}(\mu\text{-Cl})(\text{COD})_2]$ . However, the generated COD and HMDS during the reaction cannot be removed *in vacuo* without decomposition of the complex, possibly due to the presence of the lithium salts. To obtain the pure complex **4**, we transmetalated the ligand from the potassium complex  $[\text{K}(\text{bimca}^{\text{Me,Homo}})]$  generated *in situ* by deprotonation of **3** with KHMDS. The potassium halides formed could be readily removed by filtration and complex **4** isolated by removal of all volatiles *in vacuo*.

The structure of complex **4** could be identified by NMR experiments. Bonding of the terminal double bond to the rhodium centre is proven by the  $^1J_{\text{RhC}}$  coupling constants of 13.2 Hz (C16) and 13.7 Hz (C17) in the  $^{13}\text{C}$  NMR spectrum and the 4 signals for the diastereotopic hydrogen atoms at the two methylene groups of the homoallyl substituent. The *cis/trans* assignment of the olefinic signals at 3.50 ppm ( $^3J = 7.7$  Hz, H-17<sub>cis</sub>) and 2.94 ppm ( $^3J = 11.5$  Hz, H-17<sub>trans</sub>) is based on the vicinal coupling constants, which are smaller than those typically observed in non-coordinated olefins (e.g. in compound **3**:  $^3J_{\text{HH}} = 17.2$  Hz (*trans*) and 10.3 Hz (*cis*)), and can be explained with the lower *s*-character due to a rehybridization upon coordination of the metal ion. The relative assignment of axial and equatorial methylene signals is based on the Karplus equation. Finally, information on the relative conformation of the metallacycle were obtained with an NOE experiment, which confirmed the aforementioned assignments. Out of several minimum conformations of similar energy obtained by DFT-calculations, the NOE data is in accordance with the structure that is second lowest in energy ( $\Delta = 1.5$  kJ/mol; Figure 2 and Supporting Information).

With the new rhodium complex **4** in hand, we were able to investigate the isomerization of phenyl oxirane (**5a**) as the model substrate. To our satisfaction, an initial test using 5 mol% of complex **4** together with 10 mol% LiBr (pre-activated with 5  $\mu\text{L}$  THF- $d_6$ ) in  $\text{C}_6\text{D}_6$  revealed full conversion at room temperature in a short time and demonstrated that the catalyst was more active than the previous catalyst **D** (Table 1, entry 1).



**Figure 2.** Minimum conformation of complex **4** based on DFT-D3 calculations (TurboMole: BP86/def2-TZVP) and observed NOE cross peaks (indicated with arrows). For clarity reasons, part of the carbazole backbone is depicted in wireframe style.

**Table 1.** Optimization of the reaction conditions for the isomerization of phenyl oxirane in presence of rhodium catalyst **4**.<sup>[d]</sup>

Entry	<b>5a</b> Catalyst [mol %]	Conc. <b>5a</b> [mol/L]	<i>t</i>	Yield [%] <sup>[b]</sup>	Ratio ( <b>6a</b> : <b>7a</b> )
1	5	0.1	40 min	84	>99:1
2	3	0.1	70 min	89	>99:1
3	1	0.1	120 min	>99	>99:1
4 <sup>[c]</sup>	1	0.1	24 h	7	5:1
5 <sup>[d]</sup>	1	0.1	24 h	6	10:1
6	1	0.2	60 min	99	>99:1
7	1	0.4	50 min	95	>99:1
8	1	0.8	40 min	92	>99:1
9	–	0.8	60 min	<5	–

[a] Carried out in *J. Young* NMR tubes and with 10 mol% LiBr and 5  $\mu$ L THF-*d*<sub>6</sub>. [b] Yield (<sup>1</sup>H NMR) of **6a** calibrated to 1,3,5-trimethoxybenzene (internal standard). [c] Without LiBr. [d] THF-*d*<sub>6</sub> as the solvent.

Encouraged by this result, we tried to reduce the catalyst loading: 1 mol% of the catalyst was sufficient for a fast and quantitative rearrangement without influencing the excellent regioselectivity (Table 1, entries 2 and 3). To test whether lithium bromide was still necessary as a co-catalyst we applied the isolated catalyst **4** without adding any Lewis acids. The catalytic activity was reduced dramatically under these conditions (Table 1, entry 4). This indicates that a Lewis acid is essential for the pre-activation of the substrates. Low conversion was also obtained using THF-*d*<sub>6</sub> as the solvent which most likely stems from competitive binding between THF and the substrate to the Lewis acid co-catalyst (Table 1, entry 5). Afterward, the concentration of phenyl oxirane was studied. Epoxide concentrations of 0.2 mol/L (Table 1, entry 6) shortened the reaction time substantially and the reaction was 10 times faster compared to catalyst **D**. Further increase of the concentration led to a reduced reaction time whereas the yields decreased slightly (Table 1, entries 7 and 8). In addition, the need for catalyst **4** was also tested. Without rhodium catalyst **4** the yield remained below 5% (Table 1, entry 9). Thus, the optimized reaction conditions (1 mol% catalyst **4**, 0.2 M epoxide, C<sub>6</sub>D<sub>6</sub>, room temperature) were applied to investigate the generality of this protocol.

Using complex **4** as the catalyst, various functionalized epoxides were converted successfully into the desired methyl ketones (Table 2). Phenyl oxirane (**5a**) and aryl oxirane **5b** bearing the strong electron-withdrawing trifluoromethyl substituent were transformed regioselectively in excellent yield. To our delight, epoxides **5c** and **5d** possessing electron-donating groups (methyl or methoxy) were converted into **6c** and **6d** with still very good regioselectivities of 50:1 and 22:1 favoring the methyl ketones (**6c**, **6d**) over the aldehydes (**7c**, **7d**) in good to moderate yields. Even the *ortho*-substituted methyl ketone **6e** was obtained from **5e** in high yield and with excellent regioselectivity. Besides aryl ketones, epoxides bearing NH or OH groups like sulfonamide (**5f**) and hydroxyl groups (**5g**) were rearranged to the desired methyl ketones with 1 mol% catalyst loading in 83% (**6f**) and 90% (**6g**) yield, albeit at longer reaction time (24 h). The high nucleophilicity of complex **4** is also compatible with an ester group. The isomerization of epoxide **5h** afforded **6h** in moderate yield after 24 h at 60 °C and 5 mol% catalyst loading. As the extended reaction times may derive from competing coordination of LiBr at the Lewis basic centers of functional groups, we have increased the amount of LiBr to 50 mol% and achieved full conversion already after 1 h reaction time at moderate to excellent yield (entries 6–8) at room temperature. In the case of **5g**, the moderate yield resulted from unknown side products which will be studied further. Furthermore, the sterically demanding 2-(*tert*-butyl) oxirane (**5i**) can be also converted to the desired product **6i**, albeit with higher catalyst loading (5 mol%) and reaction temperature.

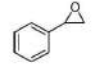
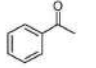
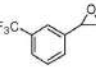
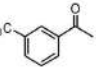
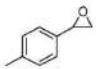
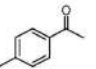
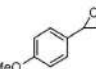
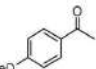
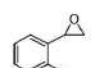
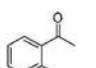
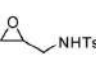
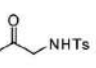
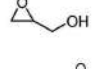
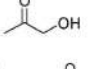
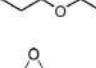
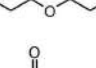

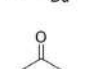
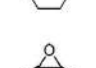
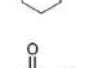

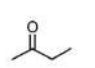
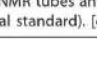
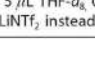
The internal epoxides **5j–l** react considerably faster compared with rhodium catalyst **D**. At 80 °C, 7-oxabicyclo[4.1.0]heptane (**5j**) was isomerized into cyclohexanone in almost quantitative yield. Furthermore, *cis*-2,3-epoxybutane (**5k**) was also compatible with the catalyst system and yielded 99% butan-2-one. In contrast, the conversion of *trans*-2,3-epoxybutane (**5l**) under otherwise identical conditions yielded only 7% of butan-2-one. This outcome is of considerable interest as it is contrary to the results from Coates and coworkers, who obtained less than 40% conversion with *cis*-2-hexene oxide but 98% yield with *trans*-2-hexene oxide applying [(salcy)Al(THF)<sub>2</sub>]<sup>+</sup>[Co(CO)<sub>4</sub>]<sup>−</sup> as the catalyst.<sup>[5]</sup>

**Mechanistic considerations.** When we tried to isolate catalyst **4** by chromatography at silica gel under argon, we isolated the isomerized complex **8** (Figure 3, top) as indicated by the characteristic substitution pattern in the NMR spectra. The signal at 1.17 ppm with an integral of 3H shows a <sup>3</sup>*J* (6.3 Hz) and a <sup>4</sup>*J* coupling to the olefinic signals at 4.56 (H-15) and 4.09 ppm (H-16). The *cis*-conformation of the double bond is not only confirmed by the <sup>3</sup>*J* coupling constant of 6.3 Hz, but also by the NOE between methyl signal H-17 and the signal H-14b of the methylene group. In addition, an NOE cross-peak is observed between the signals of both olefinic protons and the *N*-methyl signal. The assignment of the peaks of the imidazole moieties and carbazole backbone are based on the observed NOE cross peaks (Figure 3, bottom).

Complex **8** is of importance as it is also formed under the conditions applied for the catalysis. While the *in situ* prepared



**Table 2.** Substrate scope in the isomerization of epoxide catalysed by rhodium complex **4**.<sup>[a]</sup>

Entry	Substrate	Product	t	Yield [%] <sup>[b]</sup>	Ratio (6:7)
1			1 h	99	> 99:1
2			1 h	98	> 99:1
3			1 h	77	50:1
4			1 h	42	22:1
5			24 h	92	33:1
6			24 h 1 h	83 94 <sup>[c,d]</sup>	–
7			24 h 1 h	90 42 <sup>[e,f]</sup>	–
8			24 h 1 h	67 <sup>[c,e]</sup> 80 <sup>[e,f]</sup>	–
9 <sup>[d-f]</sup>			24 h	99	–
10 <sup>[d-f]</sup>			24 h	99	–
11 <sup>[d-f]</sup>			24 h	99	–
12 <sup>[d-f]</sup>			24 h	7	–

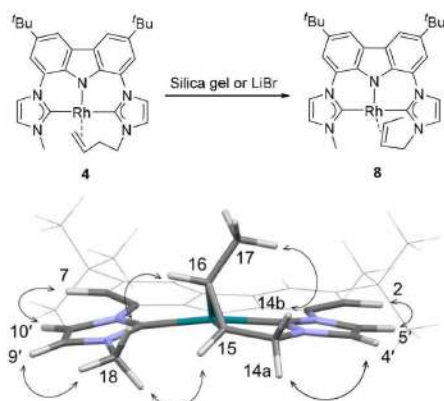
[a] Carried out in *J. Young* NMR tubes and with 10 mol% LiBr and 5  $\mu$ L THF-*d*<sub>6</sub>, 0.2 M concentration of epoxides. [b] Yield (<sup>1</sup>H NMR) of **6a** calibrated to 1,3,5-trimethoxybenzene (internal standard). [c] At 60 °C. [d] 20 mol% LiNTf<sub>2</sub> instead of LiBr. [e] 5 mol% catalyst **4**. [f] At 80 °C. [g] 50 mol% LiBr.

complex **4**<sup>LiX</sup> is stable in THF-*d*<sub>6</sub>, isomerization takes place within one hour at room temperature when 2 eq of LiBr are added to a solution of the isolated complex **4** in benzene-*d*<sub>6</sub> without the presence of any amount of epoxide. Obviously, the Lewis acidity of the lithium cation in benzene is enhanced to such an extent that the isomerization of the double bond can occur.

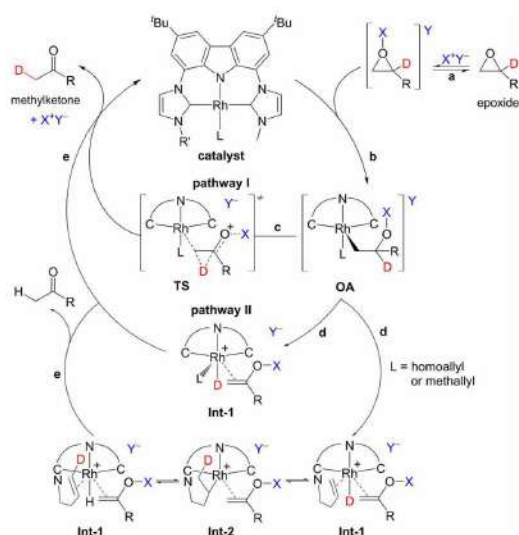
To prove that complex **8** is an active catalyst itself, we have carried out the Meinwald reaction of phenyl oxirane with the isolated complex **8** under the general conditions (1 mol% **8**,

10 mol% LiBr, 5  $\mu$ L THF-*d*<sub>6</sub>, room temperature). The reaction rate is comparable to that when starting from complex **4**. We assume that the isomerization of complex **4** to **8** as well as the Meinwald reaction of phenyl oxirane catalyzed by complex **4** or **8** occurs at comparable reaction rates. Isomerizations of the double bond can also be observed using catalyst **D**. However, due to the two *N*-homoallyl moieties, mixtures are obtained, and the NMR spectra become very complex.



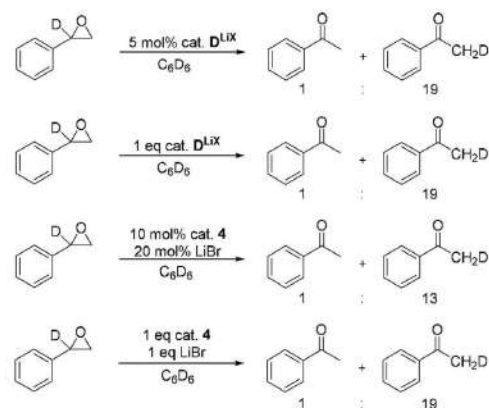


**Figure 3.** Top: Isomerization of the terminal double bond of complex **4** to an internal *cis*-double bond in complex **8** by Lewis acids. Bottom: Minimum conformation of the isomerized complex **8** based on DFT calculations (TurboMole: BP86/def2-TZVP) and observed NOE cross peaks (indicated with arrows). For clarity reasons, part of the carbazole moiety is depicted in wireframe style.



**Scheme 3.** Initially proposed catalytic cycle (pathway I and pathway II) for complex **B** ( $L=CO$ ) and evidence for pathway II following the observed H/D exchange in the case of the homoallyl complexes **D** and **4** (*vide infra*).

Earlier, we had proposed a catalytic cycle for catalyst **B**, in which the oxidative addition product **OA** was confirmed by NMR spectroscopy (Scheme 3).<sup>[3h]</sup> From this intermediate two possible pathways can lead to the product: a concerted 1,2-H shift under reductive elimination of the catalyst (**c**) or  $\beta$ -hydride elimination (**d**) to form the Rh-hydride intermediate (**Int-1**), which subsequently undergoes reductive elimination (**e**) to release the product and the catalyst.



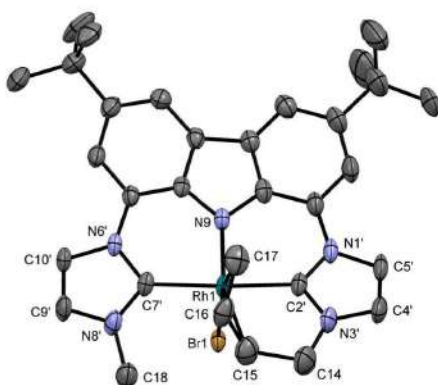
**Scheme 4.** D/H exchange during the isomerization of 1-D-phenyl oxirane with the *N*-homoallyl substituted catalysts **D** and **4** indicate a hydrido-Rh(III) intermediate **Int-1** in the catalytic cycle.

As the hydride intermediate (**Int-1**) was not observed during the catalysis with complex **B** ( $L=CO$ ), we envisaged that the *N*-homoallyl moiety of catalyst **D** or **4** could insert into the Rh–H intermediate **Int-1** to give the rhodium alkyl intermediate **Int-2**, which could undergo a D/H exchange in case deuterated phenyl oxirane was used. To prove this hypothesis, we carried out catalytic experiments with 1-D-phenyl oxirane as substrate with both *N*-homoallyl-substituted catalysts **D** and **4** under catalytic as well as stoichiometric conditions (Scheme 4). In all cases, we found an exchange of the deuterium by hydrogen in the methylphenyl ketone of 5–7%. (deuteration degree of the phenyl oxirane: 98%).

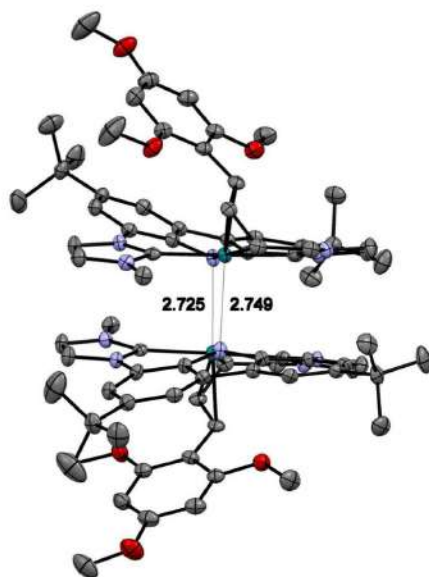
Based on these observations, we favor pathway II for the catalytic cycle of the nucleophilic Meinwald reaction with our rhodium catalysts. This pathway is also supported by the observations by Milstein, who isolated hydrido-2-oxoalkyl complexes when reacting  $RhCl(PMe_3)_3$  with neat methyl or phenyl oxirane.<sup>[3g]</sup> In this case, the reductive elimination to acetone or acetophenone is the rate limiting step.<sup>[6]</sup>

**Catalyst deactivation pathways.** In addition, we observed two deactivation products of the catalyst. We recognized the formation of red crystals after finishing a VT NMR experiment of catalyst **4** with 1.0 equiv. of phenyl oxirane at room temperature. The X-ray structure analysis reveals the formation of a bromido–Rh(III) complex, in which the *N*-homoallyl substituent is coordinated in a  $\eta^3$ -allyl coordination mode to the oxidized metal center (Figure 4). The allyl–Rh bonds measure 2.137 (Rh–C17), 2.114 (Rh–C16) and 2.220 Å (Rh–C15). As the isomerization of phenyl oxide **5a** is very fast, it is likely that the formation of complex **9** occurs after the catalysis. C–H activation at the allylic position to form an allylhydrido complex and subsequent substitution of the hydrido by a bromido ligand can explain its formation.

From the testing of *cis*-1,2-(diethoxycarboxyl)oxirane (5 mol% **4** (2.3 mg), 20 mol%  $LiNTf_2$  (4.6 mg), *cis*-1,2-(diethoxycarboxyl)oxirane (15.1 mg) and 1,3,5-trimethoxybenzene



**Figure 4.** Molecular structure of the catalyst deactivation product **9**. Atoms are shown with anisotropic atomic displacement parameters at the 50% probability level. Hydrogen atoms as well as 3.5 co-crystallized benzene molecules are omitted for clarity.



**Figure 5.** Molecular structure of the side product **10**. Atoms are shown with anisotropic atomic displacement parameters at the 50% probability level. Hydrogen atoms as well as the two  $\text{NTf}_2^-$  counter ions and two co-crystallized benzene molecules are omitted for clarity.

(4.3 mg), 24 h at 80 °C and 24 h at 100 °C) we obtained red single crystals in the NMR tube after several days at room temperature. The X-ray structure analysis reveals that under the elevated temperature the internal standard 1,3,5-trimethoxybenzene has reacted with the *N*-homoallyl moiety of complex **4** in a formal dehydrogenation and C–C bond formation to the Rh(III)( $\eta^3$ -allyl) complex **10** (Figure 5). In the solid state the  $16e^-$  Rh-d<sup>6</sup> complex forms a Lewis-pair dimer between the rhodium

and the carbazole nitrogen atoms with a mean distance of 2.74 Å. The allyl rhodium bonds measure 2.143 (Rh–C17), 2.124 (Rh–C16) and 2.243 Å (Rh–C15) (mean).

To avoid erroneous catalytic results in the NMR experiments, catalytic tests with substrates of low reactivity should be carried out either with an inert or without an internal standard.

## Conclusions

Herein, we have presented the most active and selective catalyst system for the nucleophilic Meinwald reaction of terminal epoxides so far. The reactivity enhancement of catalyst **4** was achieved by providing only one coordinating *N*-homoallyl substituent at the ligand scaffold. The isolated complex **4** can undergo isomerization of the double bond in the presence of weak Lewis acids and benzene as solvent to yield the *N*-methallyl complex **8**, which is itself a comparably active catalyst in the Meinwald reaction. D/H exchange experiments provide strong evidence for a  $\beta$ -hydride elimination/reductive elimination pathway via a hydrido–Rh intermediate for the Rh-catalyzed nucleophilic Meinwald reaction.

## Experimental Section

**General information.** Unless otherwise noted, all reactions were carried out under an argon atmosphere in dried and degassed solvents using Schlenk technique. Toluene, pentane, dichloromethane and tetrahydrofuran were purchased from Sigma Aldrich and dried using an MBraun SPS-800 solvent purification system. All lithium salts used were obtained from commercial suppliers, dried in vacuum and used without further purification. Chemicals from commercial suppliers were degassed through freeze-pump-thaw cycles prior to use. Rhodium complex **D** was synthesized according to the literature procedure.<sup>[31]</sup> <sup>1</sup>H and <sup>13</sup>C NMR spectra were recorded using a Bruker ARX 250 or AVANCE II + 400 spectrometer. Chemical shifts  $\delta$  (ppm) are given relative to the solvent's residual proton and carbon signal respectively: THF-*d*<sub>6</sub>: 3.58 ppm (<sup>1</sup>H NMR) and 67.57 ppm (<sup>13</sup>C{H} NMR); C<sub>6</sub>D<sub>6</sub>: 7.16 ppm (<sup>1</sup>H NMR) and 128.39 ppm (<sup>13</sup>C{H} NMR); DMSO-*d*<sub>6</sub>: 2.50 ppm (<sup>1</sup>H NMR) and 39.51 ppm (<sup>13</sup>C{H} NMR). Coupling constants (*J*) are expressed in Hz. Signals were assigned as s (singlet), d (doublet), t (triplet), q (quartet), quint (quintet), m (multiplet) and variations thereof; (br) refers to a broad signal. The assignment of peaks is based on 2D NMR correlation and NOE spectra.

**Synthesis of Hbimca<sup>Me,Homo</sup> HI·HBr (3).** *a) Synthesis of 2:* To a suspension of **1** (0.74 g, 1.8 mmol) in 10 mL THF was added Mel (0.51 g, 3.6 mmol) dropwise. The reaction was stirred at room temperature for 24 h to form a pale precipitate. The mixture was filtered and dissolved in dichloromethane. After removal of solvent, product **2** was obtained as a light yellow solid (0.89 g, 1.6 mmol, yield: 90%). <sup>1</sup>H NMR (250.13 MHz, DMSO-*d*<sub>6</sub>)  $\delta$  = 11.24 (s (br), 1H, NH), 9.69 (s (br), 1H, H-7'), 8.57 (d, <sup>4</sup>*J*<sub>HH</sub> = 1.7 Hz, 1H, H-5), 8.42 (d, <sup>4</sup>*J*<sub>HH</sub> = 1.7 Hz, 1H, H-4), 8.21 (s (br), 1H, H-2), 8.19 (ps t, <sup>3</sup>*J*<sub>HH</sub> = 1.8 Hz, 1H, H-10'), 7.98 (ps t, <sup>3</sup>*J*<sub>HH</sub> = 1.7 Hz, 1H, H-9'), 7.73 (ps t, <sup>3</sup>*J*<sub>HH</sub> = 1.3 Hz, 1H, H-5'), 7.66 (d, <sup>4</sup>*J*<sub>HH</sub> = 1.7 Hz, 1H, H-7), 7.50 (d, <sup>4</sup>*J*<sub>HH</sub> = 1.7 Hz, 1H, H-2), 7.22 (ps t, <sup>3</sup>*J*<sub>HH</sub> = 1.0 Hz, 1H, H-4'), 3.99 (s, 3H, H-18), 1.45 (s, 18H, H-11 and H-13). <sup>13</sup>C{H} NMR (62.90 MHz, DMSO-*d*<sub>6</sub>)  $\delta$  = 143.6 and 143.2 (C3 and C6), 138.0 (C7'), 137.2 (C2'), 132.7 (C8a), 132.1 (C1a), 129.1 (C4'), 125.7 (C4a), 125.0 (C5a), 123.7 (2x) (C10' and C9'), 121.7 (C1), 121.0 (C7), 120.2 (C5'), 120.0 (C2), 119.1 (C5), 118.9 (C8), 116.7 (C4),



36.0 (C18), 34.78 and 34.70 (C10 and C12), 31.65 and 31.62 (C11 and C13).  $C_{27}H_{33}N_3I$  (553.50): calcd C 58.59, H 5.83, N 12.65; found C 58.38, H 6.29, N 12.30. m.p.: 287 °C (dec.).

**b) Synthesis of 3:** To a solution of the monomethylated product **2** (0.89 g, 1.6 mmol) in 10 mL DMF was added 4-bromobutene (0.43 g, 3.2 mmol) in one portion. The reaction was stirred at 110 °C for 21 h. The solvent was removed via oil pump and a good precipitate was achieved after adding a bit of ethanol and diethyl ether. The mixture was filtered, and the residue was resolved in dichloromethane. After removal of the solvent, the product **3** was obtained as a light yellow solid (1.0 g, 1.5 mmol, yield: 95%).  $^1H$  NMR (250.13 MHz, DMSO- $d_6$ )  $\delta$  = 11.63 (s (br), 1H, NH), 10.06 (s (br), 1H, H-2'), 10.01 (s (br), 1H, H-7'), 8.65 (s (br), 2H, H-4 and H-5), 8.32 (s (br), 1H, H-5'), 8.29 (s (br), 1H, H-10'), 8.17 (s (br), 1H, H-4'), 8.06 (s (br), 1H, H-9'), 7.76 (d,  $^4J_{HH}$  = 1.3 Hz) and 7.75 (d,  $^4J_{HH}$  = 1.4 Hz) (2H, H-2 and H-7), 5.92 (ddt,  $^3J_{HH}$  = 17.2 Hz,  $^3J_{HH}$  = 10.3 Hz,  $^2J_{HH}$  = 6.8 Hz, 1H, H-16), 5.23 (dd,  $^3J_{HH}$  = 17.2 Hz,  $^2J_{HH}$  = 1.0 Hz, 1H, H-17<sub>trans</sub>), 5.16 (d (br),  $^3J_{HH}$  = 10.3 Hz, 1H, H-17<sub>cis</sub>), 4.44 (t,  $^3J_{HH}$  = 7.2 Hz, 2H, H-14), 4.03 (s, 3H, H-18), 2.78 (dt,  $^3J_{HH}$  = 6.8 Hz,  $^3J_{HH}$  = 7.2 Hz, 2H, H-15), 1.47 (s, 18H, H-11 and H-13).  $^{13}C$  NMR (62.90 MHz, DMSO- $d_6$ )  $\delta$  = 143.7 (C3 and C6), 137.9 (C7'), 137.3 (C2'), 133.7 (C16), 132.3 and 132.2 (C1a and C8a), 125.5 and 125.4 (C4a and C5a), 123.9 (C9'), 123.3 (C5'), 123.2 (C10'), 122.9 (C4'), 120.92 and 120.89 (C2 and C7), 119.42 and 119.37 (C4 and C5), 119.0 (C1 and C8), 118.3 (C17), 48.4 (C14), 36.1 (C18), 34.9 (C10 and C12), 33.2 (C15), 31.6 (C11 and C13). m.p.: 263 °C.

**Preparation of catalysts 4<sup>LiX</sup>.** *a) In situ generation of [Li(bimca<sup>Me,Homo</sup>)]:* Lithium bis(trimethylsilyl)amide (7.3 mg, 44  $\mu$ mol) was added to the suspension of **3** (10.0 mg, 14.5  $\mu$ mol) in 0.5 mL of THF- $d_6$  at room temperature and a light yellow solution with blue fluorescence was formed. After 10 min, the quantitative formation of [Li(bimca<sup>Me,Homo</sup>)] was confirmed by  $^1H$  NMR spectroscopy.  $^1H$  NMR (400 MHz, THF- $d_6$ )  $\delta$  = 7.99 (s (br), 2H, H-4 and H-5), 7.73 (s (br), 2H, H-5' and H10'), 7.39 (s (br), 2H, H-2 and H-7), 7.21 and 7.15 (each s (br), each 1H, H-4' and H-9'), 5.80–6.05 (m, 1H, H-16), 5.15 (d,  $^3J_{HH}$  = 16.5 Hz, 1H, H-17<sub>trans</sub>), 5.04 (d,  $^3J_{HH}$  = 10.5 Hz, 1H, H-17<sub>cis</sub>), 4.26–4.35 (m, 2H, H-14), 3.93 (s (br), 3H, H-18), 2.70–2.80 (m, 2H, H-15), 1.50 (s, 18H, H-11 and H-13).

*b) In situ generation of 4<sup>LiX</sup>:* [Rh( $\mu$ -Cl)(COD)]<sub>2</sub> (0.5 eq) was added to the previous prepared solution of [Li(bimca<sup>Me,Homo</sup>)] (1.0 eq) at room temperature. The solution was stirred for 10 min. Catalyst 4<sup>LiX</sup> was obtained as an orange solution in quantitative yield as determined by NMR spectroscopy.  $^1H$  NMR (400 MHz, THF- $d_6$ )  $\delta$  = 8.17 (d,  $^3J_{HH}$  = 2.2 Hz, 1H, H-10'), 8.10 (d,  $^3J_{HH}$  = 2.3 Hz, 1H, H-5'), 8.08–0.09 (m, 2H, H-4 and H-5), 7.73 (d,  $^4J_{HH}$  = 1.5 Hz, 1H, H-2), 7.70 (d,  $^4J_{HH}$  = 1.5 Hz, 1H, H-7), 7.17 (d,  $^3J_{HH}$  = 2.3 Hz, 1H, H-4'), 7.16 (d,  $^3J_{HH}$  = 2.2 Hz, 1H, H-9'), 4.65–4.58 (m, 1H, H-16), 4.28 (ps td,  $^{2/3}J_{HH}$  = 12.4 Hz,  $^3J_{HH}$  = 2.2 Hz, 1H, H-14<sub>ax</sub>), 4.09 (d ps t,  $^2J_{HH}$  = 13.0 Hz,  $^3J_{HH}$  = 3.6 Hz, 1H, H-14<sub>eq</sub>), 3.92 (s, 3H, H-18), 3.50 (d,  $^3J$  = 7.7 Hz, 1H, H-17<sub>cis</sub>), 2.94 (d,  $^3J$  = 11.5 Hz, 1H, H-17<sub>trans</sub>), 2.67 (br dd,  $^2J_{HH}$  = 15.1 Hz,  $^3J_{HH}$  = 12.4 Hz, 1H, H-15<sub>ax</sub>), 2.33–2.25 (m, 1H, H-15<sub>eq</sub>) (overlap with COD signal), 1.53 and 1.52 (each s, 18H, H-11 and H13).  $^{13}C$  NMR (101 MHz, THF- $d_6$ )  $\delta$  = 184.8 (d,  $^1J_{RhC}$  = 43.3 Hz, C7'), 179.0 (d,  $^1J_{RhC}$  = 45.7 Hz, C2'), 139.2 (C3), 139.1 (C6), 137.1 (C1a), 136.8 (C8a), 127.3 and 127.2 (C4a and C5a), 126.6 (C9'), 126.0 (C8), 125.7 (C1), 123.9 (C4'), 116.1 (C10'), 116.5 (C5'), 113.6 (C5), 113.4 (C4), 111.3 (C7), 110.2 (C2), 51.3 (d,  $^1J_{RhC}$  = 13.2 Hz, C16), 47.5 (C14), 38.9 (C18), 37.0 (d,  $^1J_{RhC}$  = 13.7 Hz, C17), 35.6 (C10 and C12), 32.8 (C11 and C13), 31.9 (C15).

**Preparation of catalyst 4.** Imidazolium salt **3** (100 mg, 145  $\mu$ mol), potassium bis(trimethylsilyl)amide (86.9 mg, 436  $\mu$ mol) and [Rh( $\mu$ -Cl)(COD)]<sub>2</sub> (35.8 mg, 72.6  $\mu$ mol) were added to a dry flask at room temperature. The flask was cooled down to –60 °C for 30 min. Cold THF was injected into the flask and the reaction was stirred for another 30 min at –60 °C. After completion, the reaction was

filtered to remove potassium halides. The collected filtrate was dried under vacuum and the residue was washed with pentane (3  $\times$  5 mL). Pure catalyst **4** was obtained after removal of solvent as a yellow solid (43.6 mg, 75.0  $\mu$ mol, yield: 52%). The NMR data (THF- $d_6$ ) correspond to the results obtained from using [Li(bimca<sup>Me,Homo</sup>)].  $C_{31}H_{36}N_3Rh$  (581.56): calcd C 64.02, H 6.24, N 12.04; found C 61.70, H 6.02, N 11.36. Possibly contains residual KBr:  $C_{31}H_{36}N_3Rh \cdot 0.2$  KBr: calcd C 61.51, H 5.99, N 11.57.

**Synthesis of the isomerized rhodium complex 8.** To a *J. Young* NMR tube containing LiBr (6.9 mg, 80  $\mu$ mol) and 20  $\mu$ L of THF- $d_6$ , was added catalyst **4** (23.2 mg, 40.0  $\mu$ mol) with  $C_6D_6$  (0.8 mL). Catalyst **8** was generated at room temperature after 1 h in quantitative yield as determined by NMR spectroscopy. Another method for achieving complex **8** was to run a chromatography on silica gel with complex **4**.  $^1H$  NMR (400 MHz, THF- $d_6$ )  $\delta$  = 8.19 (d,  $^3J_{HH}$  = 2.2 Hz, 1H, H-10'), 8.14 and 8.13 (each d, each  $^4J_{HH}$  = 1.6 Hz, each 1H, H-5 and H-4), 8.02 (d,  $^3J_{HH}$  = 2.2 Hz, 1H, H-5'), 7.81 (d,  $^4J_{HH}$  = 1.6 Hz, 1H, H-7), 7.73 (d,  $^4J_{HH}$  = 1.6 Hz, 1H, H-2), 7.27 (d,  $^3J_{HH}$  = 2.0 Hz, 1H, H-4'), 7.17 (d,  $^3J_{HH}$  = 2.0 Hz, 1H, H-9'), 4.56 (br ps t, 1H,  $^3J_{HH}$  = 7.2 Hz, H-15), 4.45 (dd,  $^2J_{HH}$  = 11.7 Hz,  $^3J_{HH}$  = 6.8 Hz, 1H, H-14<sub>a</sub>), 4.09 (d ps quint,  $^2J_{HH}$  = 6.2 Hz,  $^4J_{HH}$  = 2.3 Hz, 1H, H-16), 3.97 (br d,  $^2J$  = 11.7 Hz, 1H, H-14<sub>b</sub>), 3.71 (s, 3H, H-18), 1.55 and 1.54 (each s, 18H, H-11 and H-13), 1.17 (dd,  $^3J_{HH}$  = 6.3 Hz,  $^4J_{HH}$  = 0.6 Hz, 3H, H-17).  $^{13}C$  NMR (101 MHz, THF- $d_6$ )  $\delta$  = 187.9 (d,  $^1J_{RhC}$  = 42.4 Hz, C7'), 187.2 (d,  $^1J_{RhC}$  = 44.3 Hz, C2'), 139.5 and 139.2 (C3 and C6), 137.5 (C1a), 136.3 (C8a), 127.9 and 127.6 (C4a and C5a), 126.4 (C1), 126.2 (C8), 124.6 (C9'), 118.3 (C4'), 116.5 (C10'), 114.8 (C5'), 114.1 (C5), 113.8 (C4), 111.4 (C7), 109.7 (C2), 57.3 (d,  $^1J_{RhC}$  = 14.1 Hz, C16), 53.8 (d,  $^1J_{RhC}$  = 12.7 Hz, C15), 50.0 (C14), 37.6 (C18), 35.72 and 35.65 (C10 and C12), 32.93 and 32.90 (C11 and C13), 20.9 (C17).  $^1H$  NMR (400 MHz,  $C_6D_6$ )  $\delta$  = 8.46 (s, 2H), 7.67 (s, 1H), 7.59 (s, 1H), 7.49 (s, 1H), 7.23 (s, 1H), 6.36 (s, 1H), 6.14 (s, 1H), 4.48–4.40 (m, 1H, H-15), 4.31 (ps quint,  $^3J_{HH}$  = 6.0 Hz, 1H, H-16), 4.09 (dd,  $^2J_{HH}$  = 11.2 Hz,  $^3J_{HH}$  = 6.8 Hz, 1H, H-14<sub>a</sub>), 3.66 (br d,  $^2J_{HH}$  = 11.7 Hz, 1H, H-14<sub>b</sub>), 3.12 (s, 3H, H-18), 1.55 (br s, 18H, H-11 and H-13), 1.37 (br d,  $^3J_{HH}$  = 6.0 Hz, 3H, H-17).

**DFT calculations.** Performed based on density functional theory at the BP86/def2-SVP and/or BP86/def2-TZVP<sup>71</sup> level implemented in Turbomole.<sup>80</sup> The RI-approximation<sup>60</sup> and the Grimme dispersion correction D3-BJ<sup>10</sup> were used all over. Several structures were optimized differing in the conformation of the rings formed by the coordination of the double bond. Minimum structures were verified at the BP86/def2-SVP level by calculating the Hessian matrix and ensuring that it has no imaginary frequency.

**X-ray structure analysis.** CCDC 1907047 (9) and 1907048 (10) contain the supplementary crystallographic data. These data can be obtained free of charge from the Cambridge Crystallographic Data Centre at [www.ccdc.cam.ac.uk/data\\_request/cif](http://www.ccdc.cam.ac.uk/data_request/cif).

## Acknowledgements

Yingying Tian thanks the China Scholarship Council (CSC) for a predoctoral fellowship and Eva Jürgens the MWK-BW for funding (Landesgraduierföderung). We are grateful to Prof. Karl W. Törnroos for assistance in the X-ray structure analyses and thank Mario R. Rapp for helpful discussions as well as Nina F. Liska for help with the substrate synthesis.

## Conflict of Interest

The authors declare no conflict of interest.

**Keywords:** Rhodium • Homogenous catalysis • Epoxides • Isomerization • Carbene ligands

- [1] J. Meinwald, S. S. Labana, M. S. Chadha, *J. Am. Chem. Soc.* **1963**, *85*, 582–585.
- [2] Ni<sup>2+</sup>: a) A. Miyashita, T. Shimada, A. Sugawara, H. Nohiya, *Chem. Lett.* **1986**, *15*, 1323–1326; In<sup>+</sup>: b) B. C. Ranu, U. Jana, *J. Org. Chem.* **1998**, *63*, 8212–8216; Fe<sup>3+</sup>: c) K. Suda, K. Baba, S.-I. Nakajima, T. Takanami, *Tetrahedron Lett.* **1999**, *40*, 7243–7246; Bi<sup>3+</sup>: d) A. M. Anderson, J. M. Blazek, P. Garg, B. J. Payne, R. S. Mohan, *Tetrahedron Lett.* **2000**, *41*, 1527–1530; Er<sup>3+</sup>: e) A. Procopio, R. Dalpozzo, A. De Nino, M. Nardi, G. Sindona, A. Tagarelli, *Synlett* **2004**, *2004*, 2633–2635; Sn: f) M. Banerjee, U. K. Roy, P. Sinha, S. Roy, *J. Organomet. Chem.* **2005**, *690*, 1422–1428; Cu<sup>2+</sup>: g) M. W. C. Robinson, K. S. Pillinger, I. Mabbett, D. A. Timms, A. E. Graham, *Tetrahedron* **2010**, *66*, 8377–8382; [ReBr(CO)]<sub>2</sub>: h) R. Umeda, M. Muraki, Y. Nakamura, T. Tanaka, K. Kamiguchi, Y. Nishiyama, *Tetrahedron Lett.* **2017**, *58*, 2393–2395; Ru<sup>2+</sup>: i) C.-L. Chang, M. P. Kumar, R.-S. Liu, *J. Org. Chem.* **2004**, *69*, 2793–2796 (although Lewis-acid catalyzed, methyl ketones from  $\alpha$ -keto oxiranes possibly due to chelation effects); Pd<sup>2+</sup>: j) D. J. Vyas, E. Larionov, C. Besnard, L. Guéneé, C. Mazet, *J. Am. Chem. Soc.* **2013**, *135*, 6177–6183; k) N. Humbert, D. J. Vyas, C. Besnard, C. Mazet, *Chem. Commun.* **2014**, *50*, 10592–10595; l) S. Kulasegaram, R. J. Kulawiec, *J. Org. Chem.* **1997**, *62*, 6547–6561; m) S. Kulasegaram, R. J. Kulawiec, *Tetrahedron* **1998**, *54*, 1361–1374; Ni in a reaction sequence: n) A. N. Desnoyer, J. L. Geng, M. W. Drover, B. O. Patrick, J. A. Love, *Chem. Eur. J.* **2017**, *23*, 11509–11512.
- [3] a) J. L. Eisenmann, *J. Org. Chem.* **1962**, *27*, 2706; b) B. Rickborn, R. M. Gerkin, *J. Am. Chem. Soc.* **1968**, *90*, 4193–4194; c) B. Rickborn, R. M. Gerkin, *J. Am. Chem. Soc.* **1971**, *93*, 1693–1700; d) Z.-W. An, R. D'Aloisio, C. Venturello, *Synthesis* **1992**, *1992*, 1229–1231; e) S. Kulasegaram, R. J. Kulawiec, *J. Org. Chem.* **1994**, *59*, 7195–7196; f) J. Prandi, J. L. Namy, G. Menoret, H. B. Kagan, *J. Organomet. Chem.* **1985**, *285*, 449–460; g) D. Milstein, *J. Am. Chem. Soc.* **1982**, *104*, 5227–5228; h) E. Jürgens, B. Wucher, F. Rominger, K. W. Törnroos, D. Kunz, *Chem. Commun.* **2015**, *51*, 1897–1900; i) J. R. Lamb, Y. Jung, G. W. Coates, *Org. Chem. Front.* **2015**, *2*, 346–349; j) Y. Tian, E. Jürgens, D. Kunz, *Chem. Commun.* **2018**, *54*, 11340–11344.
- [4] M. Moser, *Dissertation*, Heidelberg University, Heidelberg, **2007**.
- [5] J. R. Lamb, M. Mulzer, A. M. LaPointe, G. W. Coates, *J. Am. Chem. Soc.* **2015**, *137*, 15049–15054.
- [6] D. Milstein, *Acc. Chem. Res.* **1984**, *17*, 221–226.
- [7] a) A. Becke, *Phys. Rev. A* **1988**, *38*, 3098–3100; b) J. P. Perdew, *Phys. Rev. B* **1986**, *33*, 8822–8824; c) A. Schäfer, H. Horn, R. Ahlrichs, *J. Chem. Phys.* **1992**, *97*, 2571–2577; d) A. Schäfer, C. Huber, R. Ahlrichs, *J. Chem. Phys.* **1994**, *100*, 5829–5835; e) F. Weigend, R. Ahlrichs, *Phys. Chem. Chem. Phys.* **2005**, *7*, 3297–3305; f) F. Weigend, *Phys. Chem. Chem. Phys.* **2006**, *8*, 1057–1065.
- [8] a) TURBOMOLE V6.3.1 2011, a development of University of Karlsruhe and Forschungszentrum Karlsruhe GmbH, 1989–2007, TURBOMOLE GmbH, since 2007; available from <http://www.turbomole.com>; b) O. Treutler, R. Ahlrichs, *J. Chem. Phys.* **1995**, *102*, 346–354; c) M. von Arnim, R. Ahlrichs, *J. Comp. Chem.* **1998**, *19*, 1746–1757; d) C. van Wüllen, *J. Comp. Chem.* **2011**, *32*, 1195–1201; e) P. Deglmann, F. Furche, R. Ahlrichs, *Chem. Phys. Lett.* **2002**, *362*, 511–518; f) P. Deglmann, F. Furche, *J. Chem. Phys.* **2002**, *117*, 9535–9538; g) R. Ahlrichs, M. Bär, M. Häser, H. Horn, C. Kölmel, *Chem. Phys. Lett.* **1989**, *162*, 165–169; h) M. K. Ambruster, F. Weigend, C. van Wüllen, W. Klopper, *Phys. Chem. Chem. Phys.* **2008**, *10*, 1748–1756; i) D. Peng, N. Middendorf, F. Weigend, M. Reiher, *J. Chem. Phys.* **2013**, *138*, 184105.
- [9] a) K. Eichkorn, O. Treutler, H. Öhm, M. Häser, R. Ahlrichs, *Chem. Phys. Lett.* **1995**, *240*, 283–290; b) K. Eichkorn, O. Treutler, H. Öhm, M. Häser, R. Ahlrichs, *Chem. Phys. Lett.* **1995**, *242*, 652–660; c) K. Eichkorn, F. Weigend, O. Treutler, R. Ahlrichs, *Theor. Chem. Acc.* **1997**, *97*, 119–124; d) P. Deglmann, K. May, F. Furche, R. Ahlrichs, *Chem. Phys. Lett.* **2004**, *384*, 103–107; e) F. Weigend, *Phys. Chem. Chem. Phys.* **2002**, *4*, 4285–4291; f) M. Sierka, A. Hogekamp, R. Ahlrichs, *J. Chem. Phys.* **2003**, *118*, 9136–9148.
- [10] a) S. Grimme, J. Antony, S. Ehrlich, H. Krieg, *J. Chem. Phys.* **2010**, *132*, 154104; b) S. Grimme, S. Ehrlich, L. Goerigk, *J. Comput. Chem.* **2011**, *32*, 1456–1465.

Manuscript received: April 1, 2019  
Revised manuscript received: May 20, 2019  
Version of record online: June 14, 2019

# CHEM**CAT**CHEM

## Supporting Information

© Copyright Wiley-VCH Verlag GmbH & Co. KGaA, 69451 Weinheim, 2019

### **Nucleophilic Isomerization of Epoxides by Pincer-Rhodium Catalysts: Activity Increase and Mechanistic Insights**

Yingying Tian, Eva Jürgens, Katharina Mill, Ronja Jordan, Theo Maulbetsch, and Doris Kunz\*  
\*This manuscript is part of the Special Issue dedicated to the Women of Catalysis.



## Supporting Information

### Nucleophilic Isomerization of Epoxides by Pincer-Rhodium

#### Catalysts: Activity Increase and Mechanistic Insights

Yingying Tian, Eva Jürgens, Katharina Mill, Ronja Jordan, Theo Maulbetsch and Doris Kunz\*

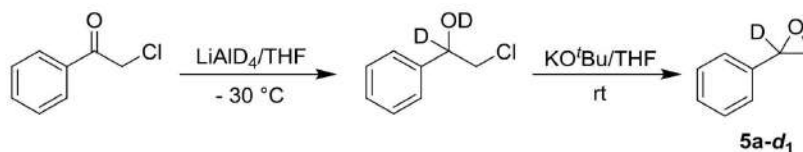
*Institut für Anorganische Chemie, Auf der Morgenstelle 18, 72076 Tübingen, Germany*

#### Table of Contents

1. General information .....	S2
2. Synthesis of Phenylloxirane-1- $d_1$ (5a- $d_1$ ) .....	S3
3. Experimental procedures for the Meinwald reaction of epoxides with catalyst 4 .....	S4
4. NMR spectra.....	S7
5. DFT calculations.....	S38
6. Reference .....	S39

## **1. General information**

Unless otherwise noted, all reactions were carried out under an argon atmosphere in dried and degassed solvents using Schlenk technique. Toluene, Pentane, dichloromethane and tetrahydrofuran were purchased from Sigma Aldrich and dried using an MBraun SPS-800 solvent purification system. All lithium salts used were obtained from commercial suppliers, dried in vacuum and used without further purification. Chemicals from commercial suppliers were degassed through freeze-pump-thaw cycles prior to use.  $^1\text{H}$  and  $^{13}\text{C}\{^1\text{H}\}$  NMR spectra were recorded using a Bruker AVANCE II+ 400 spectrometer. Chemical shifts  $\delta$  (ppm) are given relative to the solvent's residual proton and carbon signal respectively: THF- $d_8$ : 3.58 ppm ( $^1\text{H}$  NMR) and 67.57 ppm ( $^{13}\text{C}$  NMR);  $\text{C}_6\text{D}_6$ : 7.16 ppm ( $^1\text{H}$  NMR) and 128.39 ppm ( $^{13}\text{C}$  NMR); DMSO- $d_6$ : 2.50 ppm ( $^1\text{H}$  NMR) and 39.51 ppm ( $^{13}\text{C}$  NMR),  $\text{CDCl}_3$ : 7.27 ppm ( $^1\text{H}$  NMR) and 77.0 ppm ( $^{13}\text{C}$  NMR). Coupling constants ( $J$ ) are expressed in Hz. Signals were assigned as s (singlet), d (doublet), t (triplet), q (quartet), m (multiplet) and variations thereof.

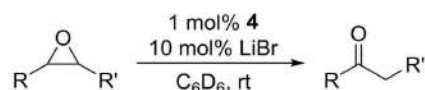
**2. Synthesis of Phenylloxirane-1-*d*<sub>1</sub> (5a-*d*<sub>1</sub>)**<sup>[1]</sup>

To a stirred solution of LiAlD<sub>4</sub> (109 mg, 2.59 mmol) in THF (3mL) at -30 °C, 2-chloro-1-phenylethan-1-one (400 mg, 2.59 mmol) in THF (2mL) was added dropwise. After reaction completed, the mixture was poured into 10% H<sub>2</sub>SO<sub>4</sub> aqueous, extracted with THF (3 × 5 mL) and then dried over Na<sub>2</sub>SO<sub>4</sub>. After removal of the solvent by rotary evaporation, the crude product was used directly without further purification. KO<sup>t</sup>Bu (290 mg, 2.59 mmol) was dissolved in THF and the raw product was added dropwise at room temperature. After completion, dilute HCl (5 mL) was slowly added and the mixture was stirred vigorously until bubbling ceased. The organic layer was separated and washed with brine and then dried over Na<sub>2</sub>SO<sub>4</sub>. After removal of the solvent by rotary evaporation, the crude product was purified by chromatography on silica gel (EtOAc/hexane, ratio 1:20) to afford the desired product **5a-*d*<sub>1</sub>** (53%) as a colorless liquid.

<sup>1</sup>H NMR (400 MHz, CDCl<sub>3</sub>) δ = 7.39–7.27 (m, 5H), 3.16 (d, <sup>2</sup>J<sub>HH</sub> = 5.4 Hz, 1H), 2.82 (d, <sup>2</sup>J<sub>HH</sub> = 5.4 Hz, 1H). <sup>13</sup>C{<sup>1</sup>H} NMR (101 MHz, CDCl<sub>3</sub>) δ = 137.5, 128.5, 128.2, 125.5, 52.0, 51.1.

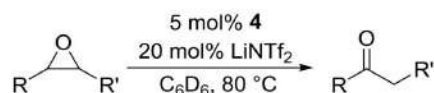


### 3. Experimental procedures for the Meinwald reaction of epoxides with catalyst **4**



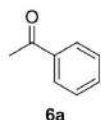
#### Method 1

To a *J. Young* NMR tube containing LiBr (0.7 mg, 8.0  $\mu\text{mol}$ ) and 5  $\mu\text{L}$  of THF, was added catalyst **4** (0.5 mg, 0.8  $\mu\text{mol}$ ) and a defined amount of the internal standard 1,3,5-trimethoxybenzene with  $\text{C}_6\text{D}_6$  (0.4 mL). Afterwards, epoxide **5** (80  $\mu\text{mol}$ ) was added. The reaction at mentioned temperature was monitored by  $^1\text{H}$  NMR spectroscopy. All yields were determined by 1,3,5-trimethoxybenzene (certain amount) as the internal standard. The NMR signals of the obtained ketones were confirmed with literature data.

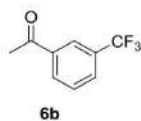


#### Method 2

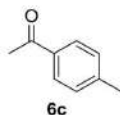
To a *J. Young* NMR tube containing LiNTf<sub>2</sub> (4.6 mg, 16  $\mu\text{mol}$ ) and 5  $\mu\text{L}$  of THF, was added catalyst **4** (2.3 mg, 4.0  $\mu\text{mol}$ ) and a defined amount of the internal standard 1,3,5-trimethoxybenzene with  $\text{C}_6\text{D}_6$  (0.4 mL). Afterwards, epoxide **5** (80  $\mu\text{mol}$ ) was added. The reaction at room temperature was monitored by  $^1\text{H}$  NMR spectroscopy. All yields were determined by 1,3,5-trimethoxybenzene (certain amount) as the internal standard. The NMR signals of the obtained ketones **6** were confirmed with literature data.



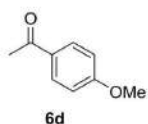
Acetophenone (**6a**).  $^1\text{H}$  NMR (400 MHz,  $\text{C}_6\text{D}_6$ )  $\delta$  = 7.77–7.74 (m, 2H), 7.13–7.09 (m, 1H), 7.06–7.00 (m, 2H), 2.09 (s, 3H).



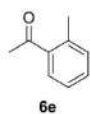
1-(3-(Trifluoromethyl)phenyl)ethan-1-one (**6b**).  $^1\text{H NMR}$  (400 MHz,  $\text{C}_6\text{D}_6$ )  $\delta$  = 8.00 (s, 1H), 7.64 (d,  $J$  = 7.8 Hz, 1H), 7.29 (d,  $J$  = 7.8 Hz, 1H), 6.80 (t,  $J$  = 7.8 Hz, 1H), 1.90 (s, 3H).



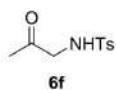
1-(*p*-Tolyl)ethan-1-one (**6c**).  $^1\text{H NMR}$  (400 MHz,  $\text{C}_6\text{D}_6$ )  $\delta$  = 7.76-7.73 (m, 2H), 6.89-6.86 (m, 2H), 2.13 (s, 3H), 1.99 (s, 3H).



1-(4-Methoxyphenyl)ethan-1-one (**6d**).  $^1\text{H NMR}$  (400 MHz,  $\text{C}_6\text{D}_6$ )  $\delta$  = 7.80 (dt,  $J$  = 8.9, 2.9 Hz, 2H), 6.62 (dt,  $J$  = 8.9, 2.9 Hz, 2H), 3.18 (s, 3H), 2.14 (s, 3H).



1-(*o*-Tolyl)ethan-1-one (**6e**).  $^1\text{H NMR}$  (400 MHz,  $\text{C}_6\text{D}_6$ )  $\delta$  = 7.26 (d,  $J$  = 7.5 Hz, 1H), 7.05-7.01 (m, 1H), 6.93-6.91 (m, 2H), 2.53 (s, 3H), 2.11 (s, 3H).

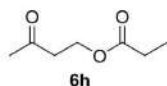


After full conversion within 1 h with 50 mol% LiBr as the co-catalyst, 12-crown-4 (2.0 eq to the epoxide) was added into the *J. Young* tube to sequester  $\text{Li}^+$  from a product-Li complex.

4-Methyl-*N*-(2-oxopropyl)benzenesulfonamide (**6f**).  $^1\text{H NMR}$  (400 MHz,  $\text{C}_6\text{D}_6$ )  $\delta$  = 7.79 (d,  $J$  = 8.1 Hz, 2H), 6.81 (d,  $J$  = 8.1 Hz, 2H), 5.71 (s, 1H), 3.38 (s, 2H), 1.87 (s, 3H), 1.32 (s, 3H).



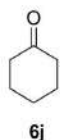
1-Hydroxypropan-2-one (**6g**).  $^1\text{H NMR}$  (400 MHz,  $\text{C}_6\text{D}_6$ )  $\delta$  = 3.57 (s, 2H), 2.97 (br s, 1H), 1.27 (s, 3H).



3-Oxobutyl-propionate (**6h**).  $^1\text{H NMR}$  (400 MHz,  $\text{C}_6\text{D}_6$ )  $\delta$  = 4.18 (t,  $J$  = 6.3 Hz, 2H), 2.07 (t,  $J$  = 6.3 Hz, 2H), 1.98 (q,  $J$  = 7.6 Hz, 2H), 1.55 (s, 3H), 0.93 (t,  $J$  = 7.6 Hz, 3H).



3,3-Dimethylbutan-2-one (**6i**).  $^1\text{H NMR}$  (400 MHz,  $\text{C}_6\text{D}_6$ )  $\delta$  = 1.73 (s, 3H), 0.89 (s, 9H).



Cyclohexanone (**6j**).  $^1\text{H NMR}$  (400 MHz,  $\text{C}_6\text{D}_6$ )  $\delta$  = 1.99 (t,  $J$  = 6.8 Hz, 4H), 1.32-1.38 (m, 4H), 1.11-1.17 (m, 2H).



1-Methoxypropan-2-one (**6k**).  $^1\text{H NMR}$  (400 MHz,  $\text{C}_6\text{D}_6$ )  $\delta$  = 1.84 (q,  $J$  = 7.2 Hz, 2H), 1.61 (s, 3H), 0.83 (t,  $J$  = 7.2 Hz, 3H).

#### 4. NMR spectra

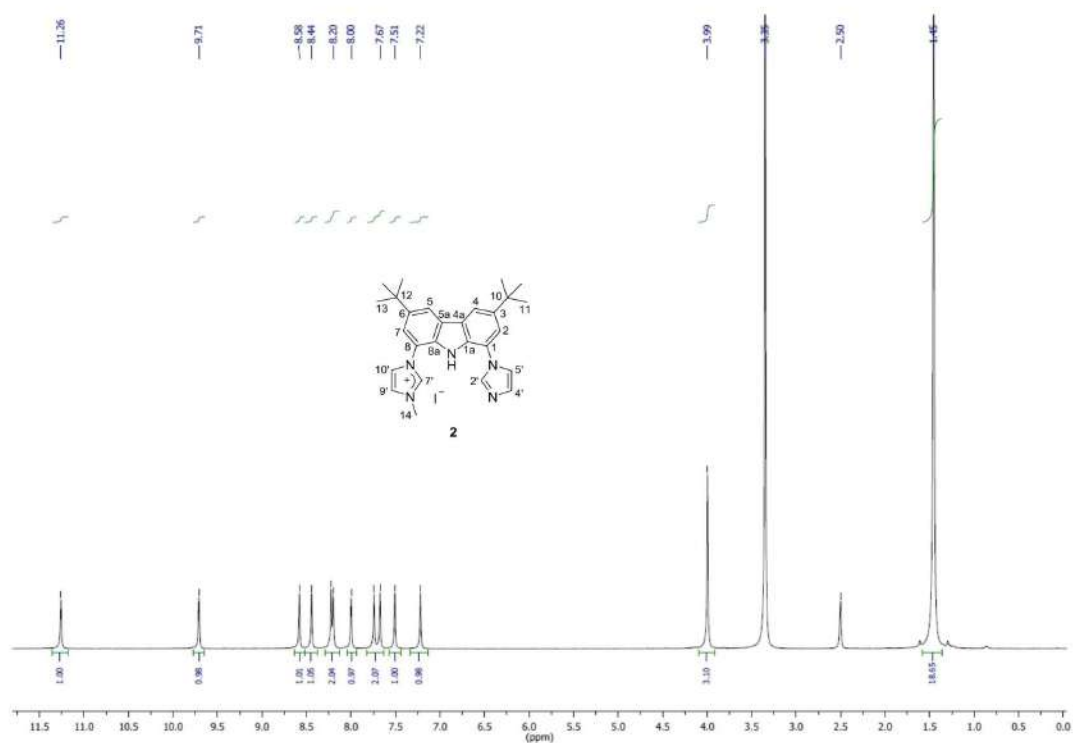


Figure S1.  $^1\text{H}$  NMR (DMSO- $d_6$ , 400 MHz) spectrum: synthesis of **2**.

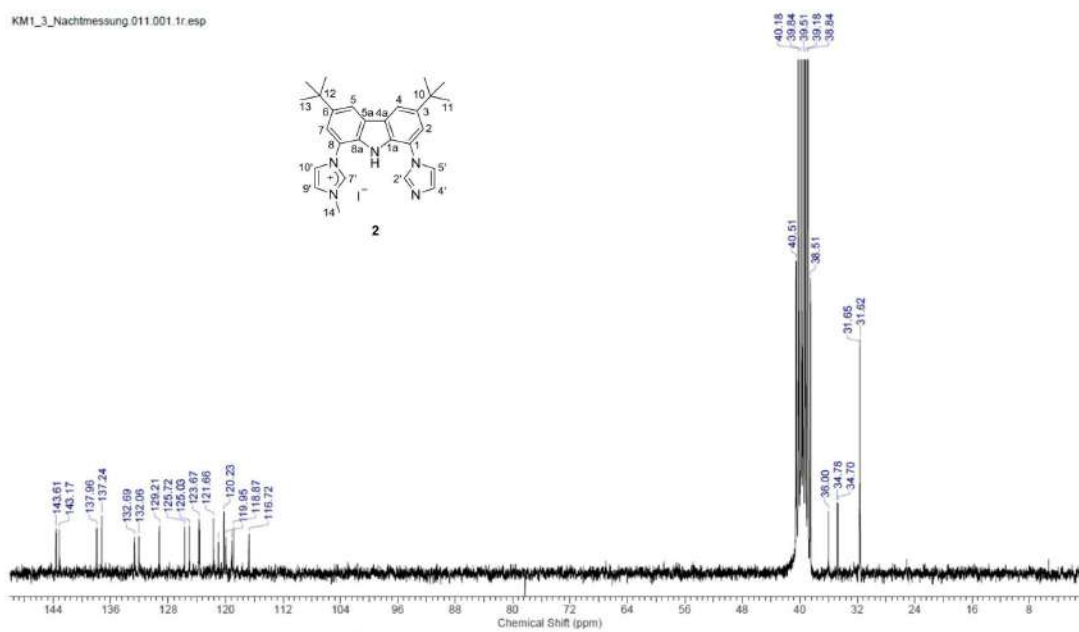


Figure S2.  $^{13}\text{C}\{^1\text{H}\}$  NMR (DMSO- $d_6$ , 101 MHz) spectrum: synthesis of **2**.

$^1\text{H}, ^{13}\text{C}$ -HSQC

KM1\_3\_Nachmessung.012.001.2rr.esp

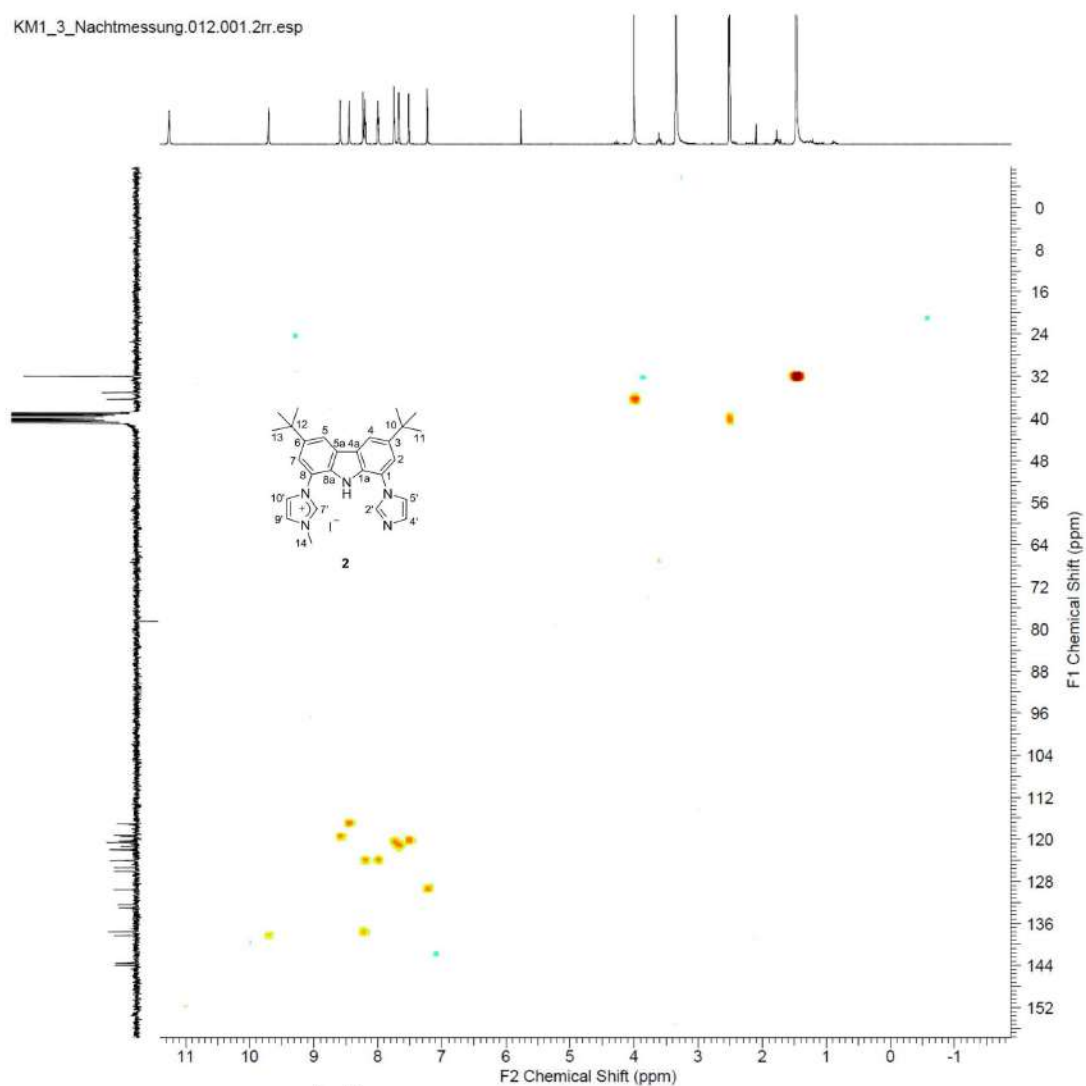


Figure S3.  $^1\text{H}, ^{13}\text{C}$ -HSQC NMR ( $\text{DMSO}-d_6$ , 400 MHz) spectrum: synthesis of **2**.

$^1\text{H}$ ,  $^{13}\text{C}$ -HMBC

KM1\_3\_Nachmessung.013.001.2rr.esp

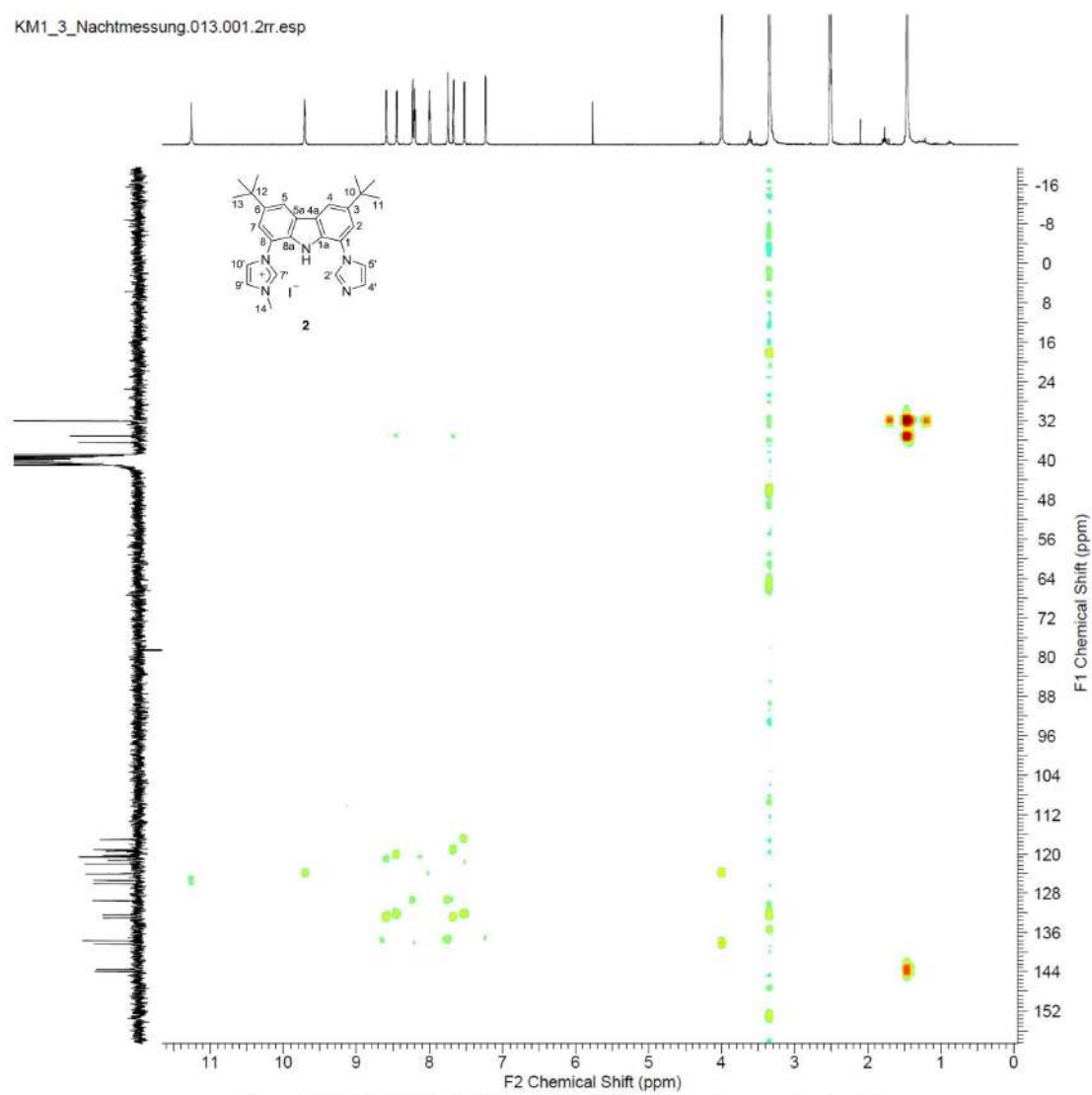


Figure S4.  $^1\text{H}$ ,  $^{13}\text{C}$ -HMBC NMR ( $\text{DMSO}-d_6$ , 400 MHz) spectrum: synthesis of **2**.

$^1\text{H}, ^1\text{H}$ -COSY

KM1\_3\_Nachtmessung.014.001.2rr.esp

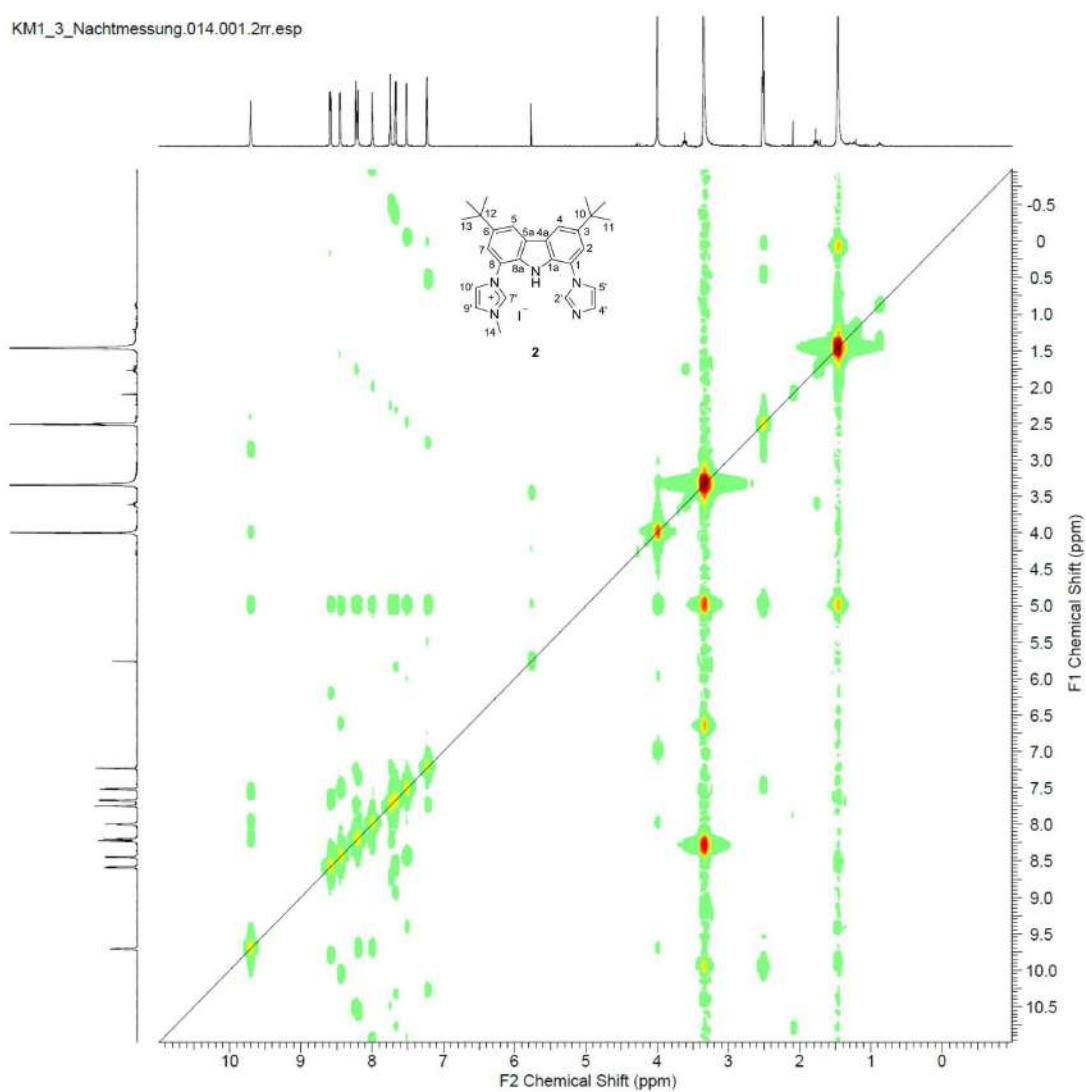


Figure S5.  $^1\text{H}, ^1\text{H}$ -COSY NMR ( $\text{DMSO}-d_6$ , 400 MHz) spectrum: synthesis of **2**.

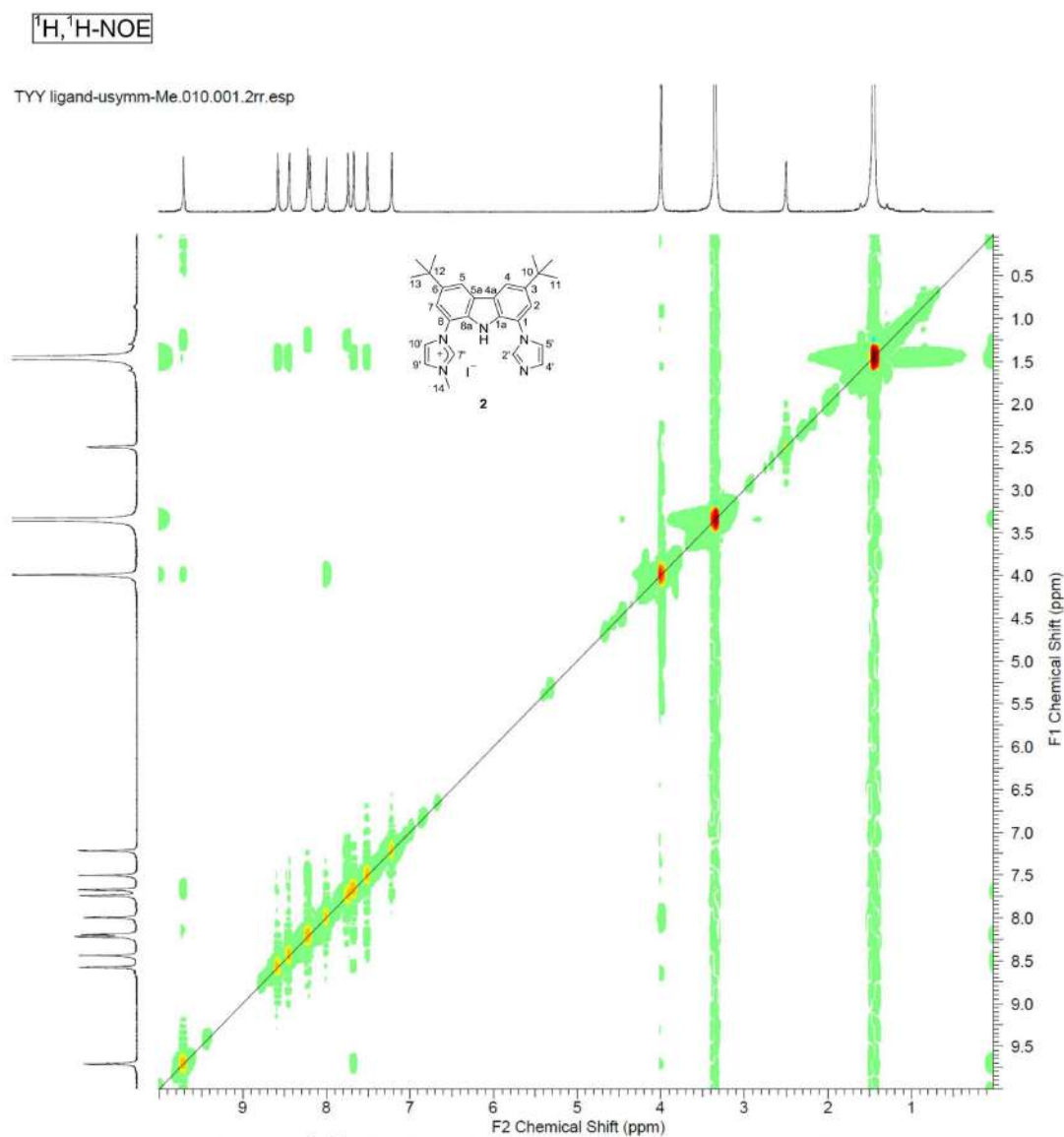


Figure S6.  $^1\text{H}, ^1\text{H}$ -NOE NMR ( $\text{DMSO}-d_6$ , 400 MHz) spectrum: synthesis of **2**.



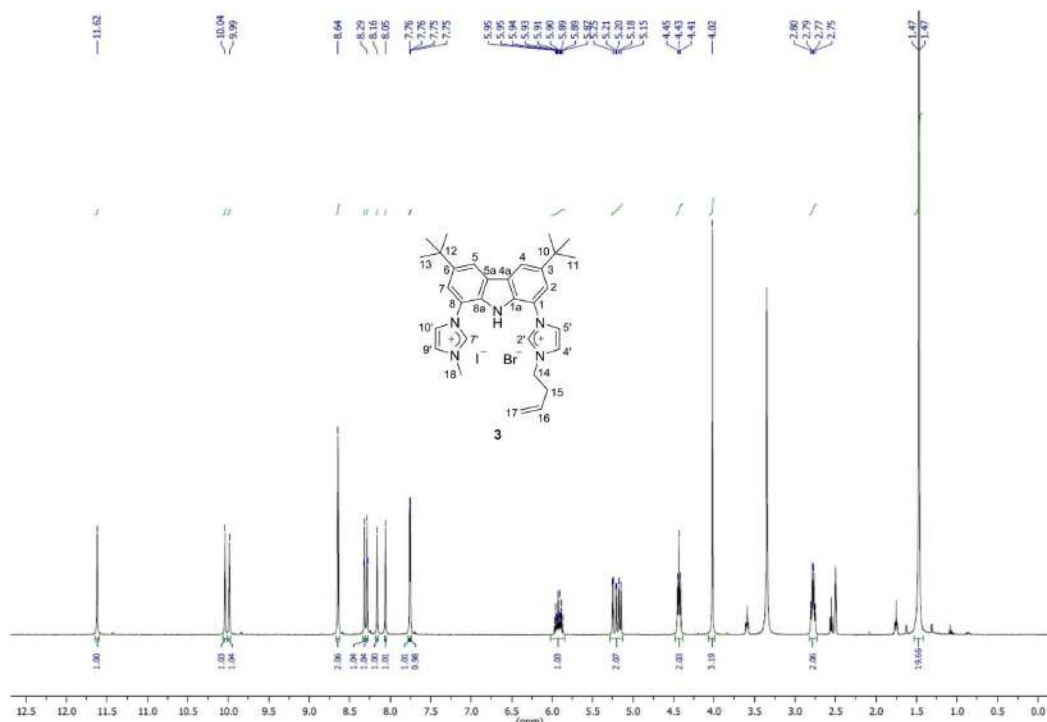


Figure S7.  $^1\text{H}$  NMR (DMSO- $d_6$ , 400 MHz) spectrum: synthesis of 3 from 2.

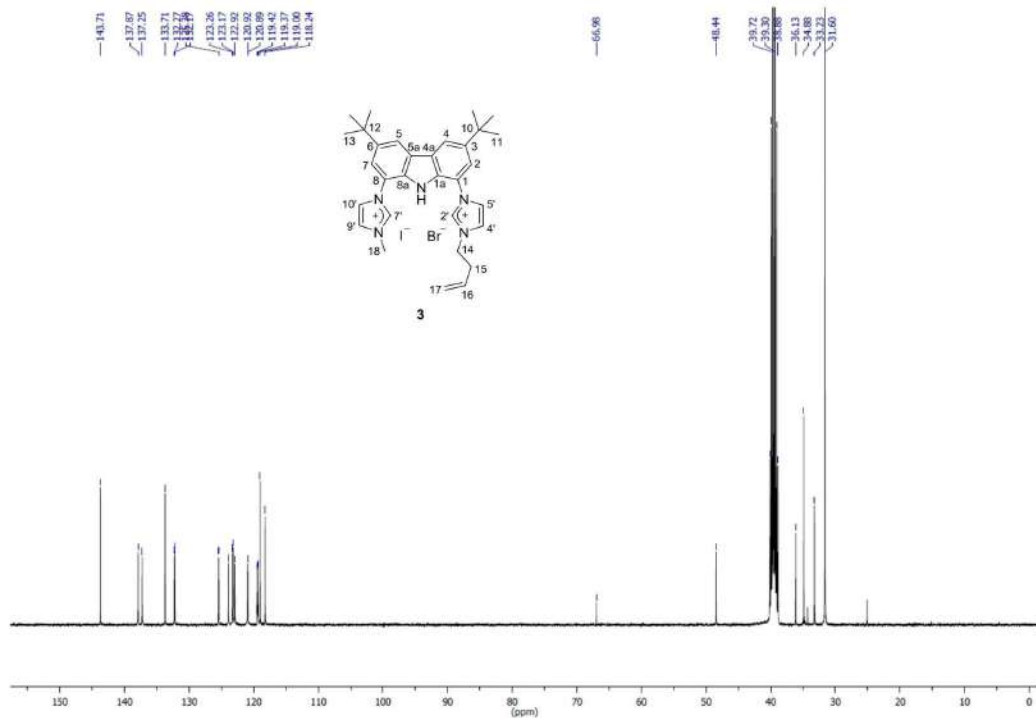
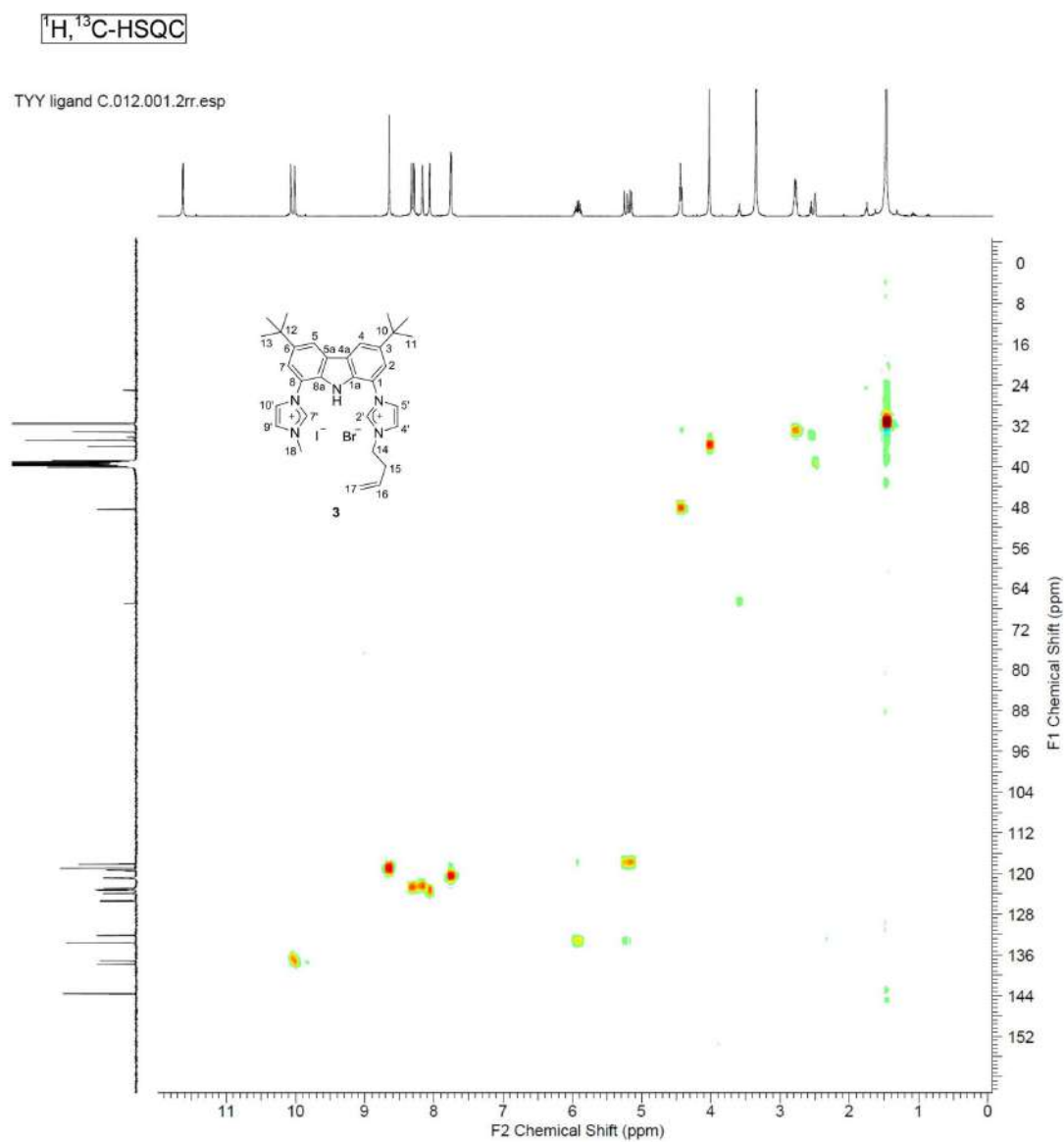
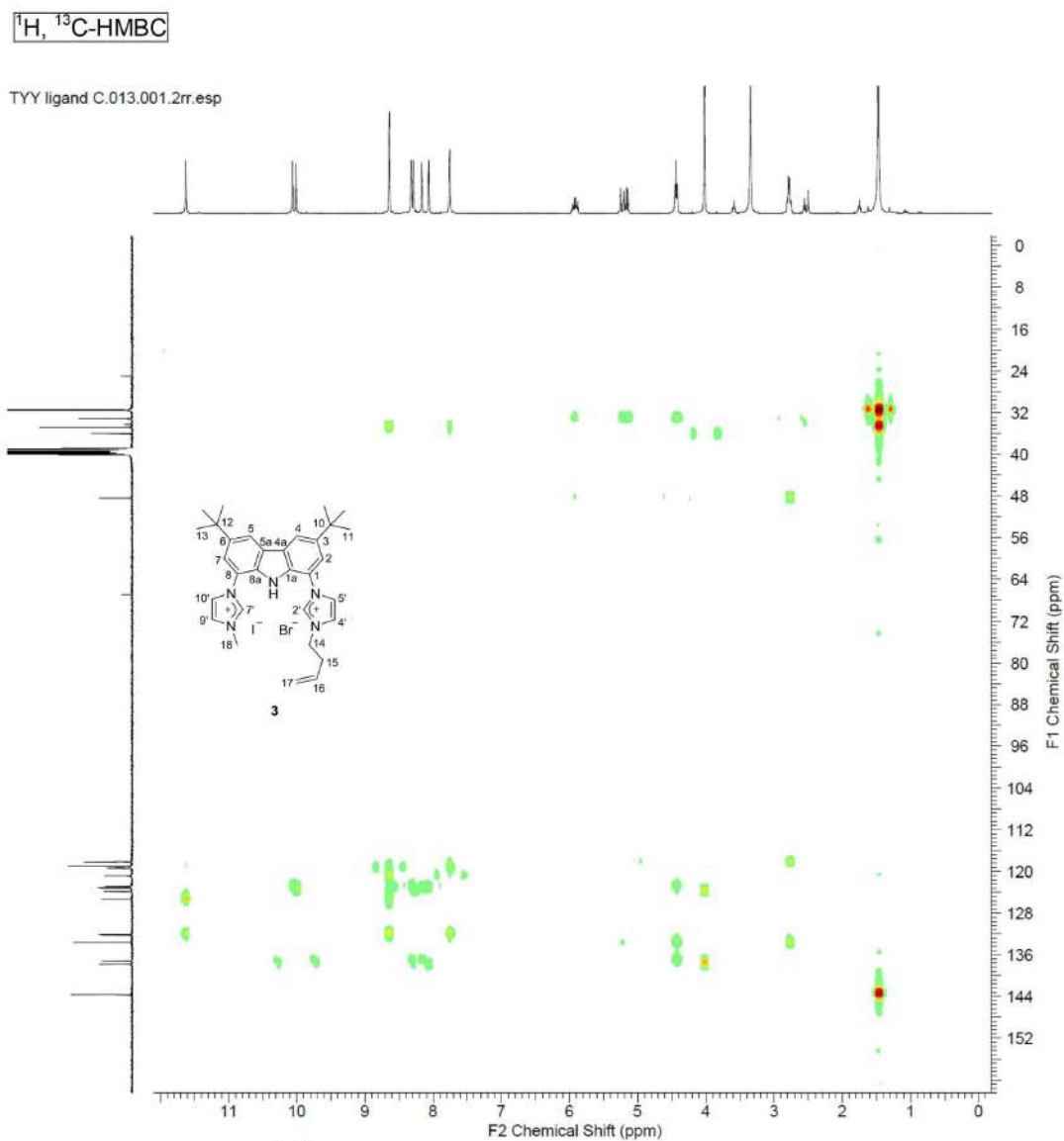


Figure S8.  $^{13}\text{C}$  NMR (DMSO- $d_6$ , 101 MHz) spectrum: synthesis of 3 from 2.





$^1\text{H}, ^1\text{H}$ -COSY

TTY ligand C.014.001.2rr.esp

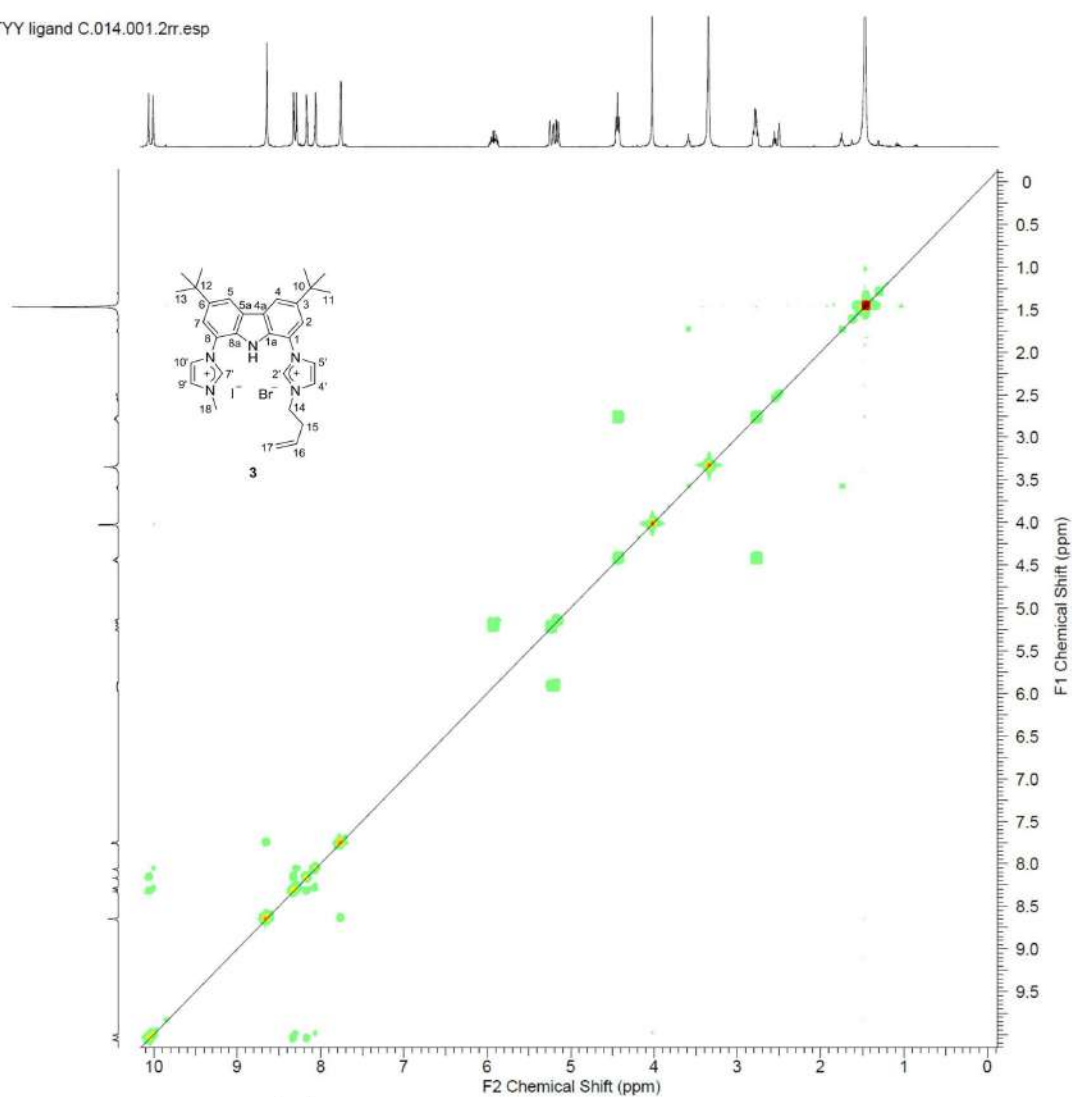


Figure S11.  $^1\text{H}, ^1\text{H}$ -COSY NMR (DMSO- $d_6$ , 400 MHz) spectrum: synthesis of **3** from **2**.

$^1\text{H}, ^1\text{H}$ -NOE

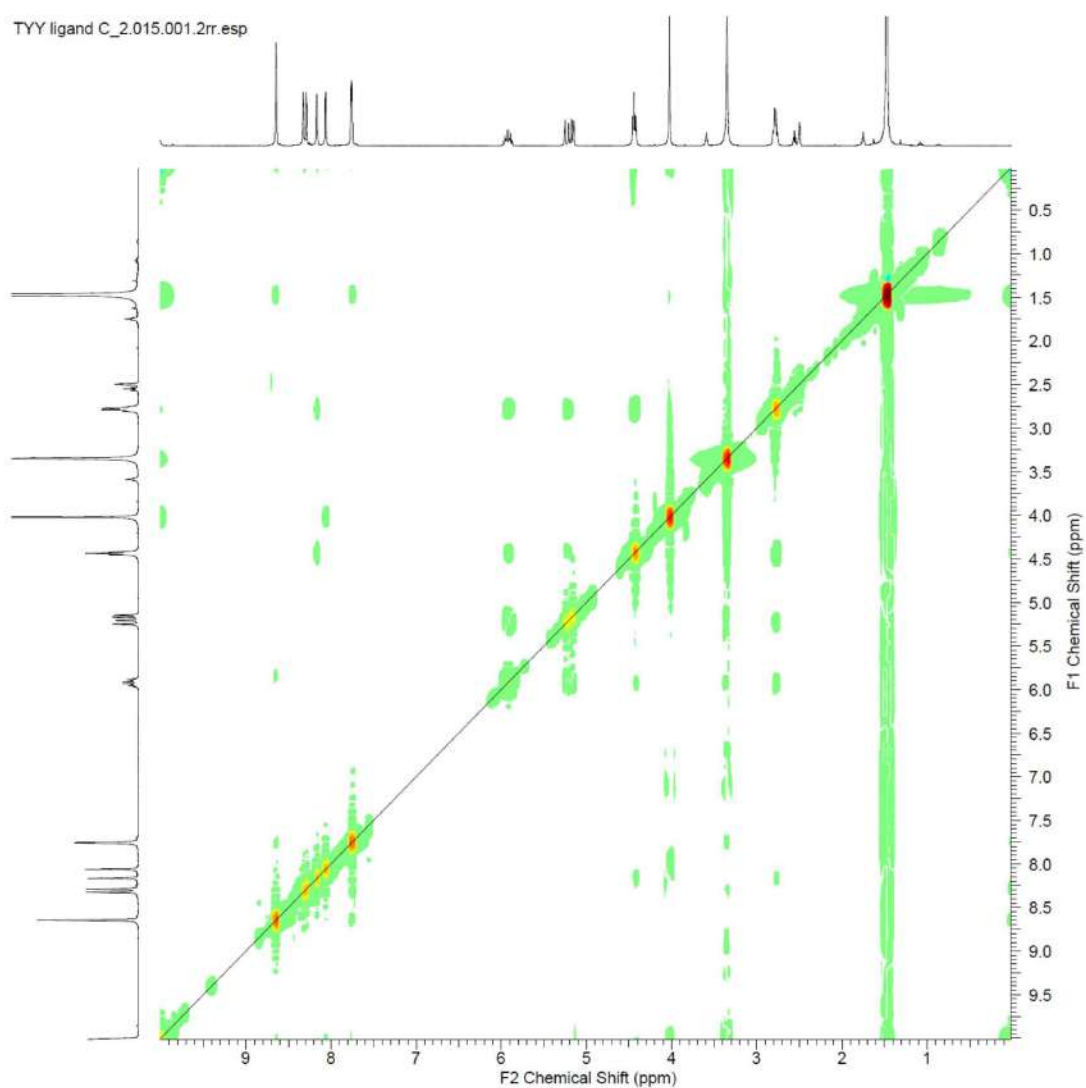
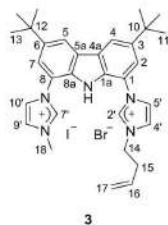


Figure S12.  $^1\text{H}, ^1\text{H}$ -NOE NMR (DMSO- $d_6$ , 400 MHz) spectrum: synthesis of 3 from 2.

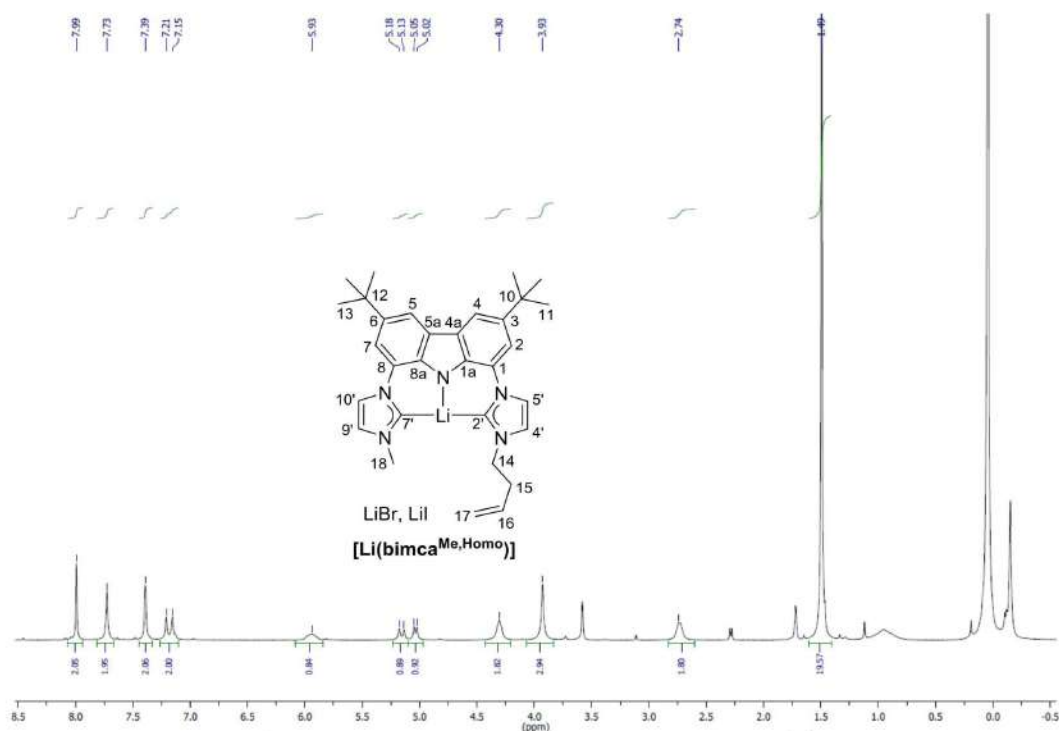


Figure S13. <sup>1</sup>H NMR (THF-d<sub>6</sub>, 400 MHz) spectrum: generation of **[Li(bimca<sup>Me,Homo</sup>)]** from **3**.

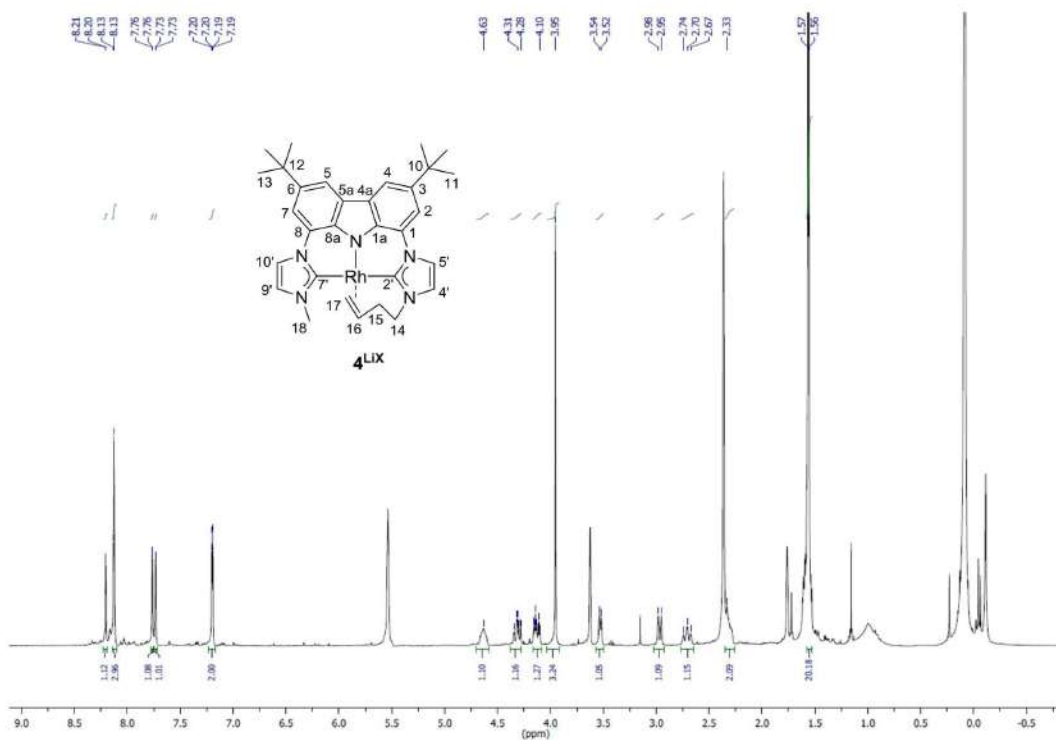


Figure S14. <sup>1</sup>H NMR (THF-d<sub>6</sub>, 400 MHz) spectrum: generation of catalyst **4<sup>LIX</sup>** from **[Li(bimca<sup>Me,Homo</sup>)]**.

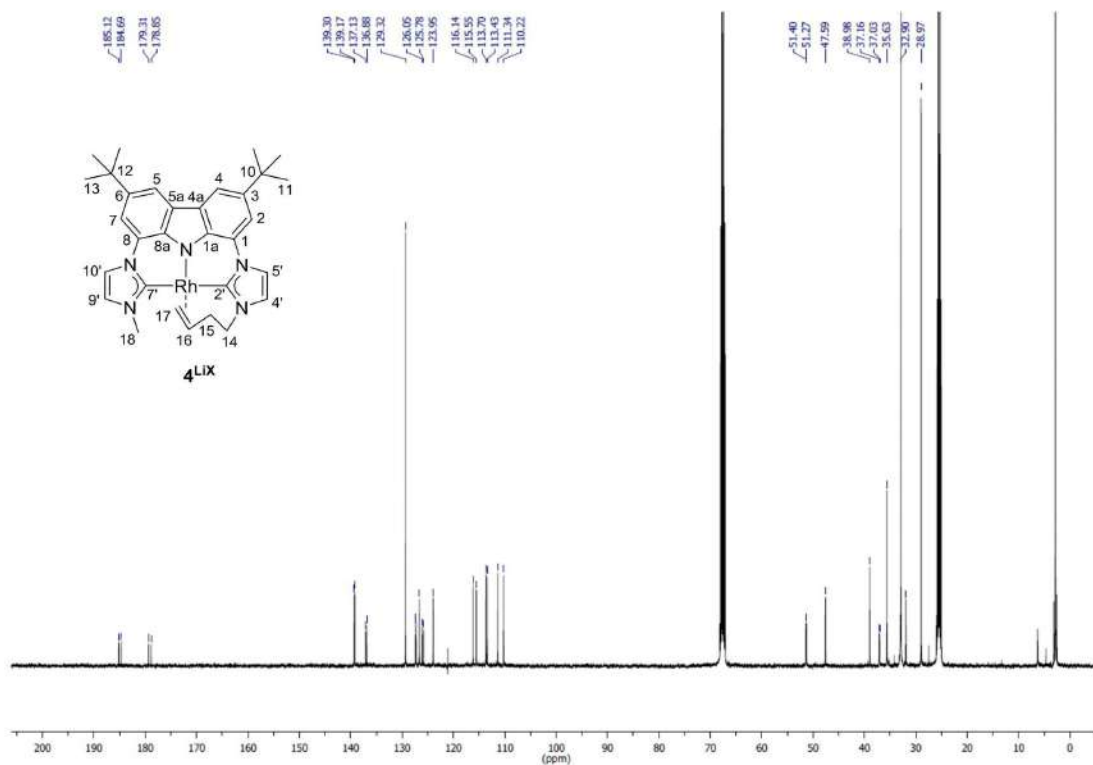


Figure S15.  $^{13}\text{C}\{^1\text{H}\}$  NMR ( $\text{THF-}d_6$ , 101 MHz) spectrum: generation of catalyst  $4^{\text{LiX}}$  from  $[\text{Li}(\text{bimca}^{\text{Me,Homo}})]$ .

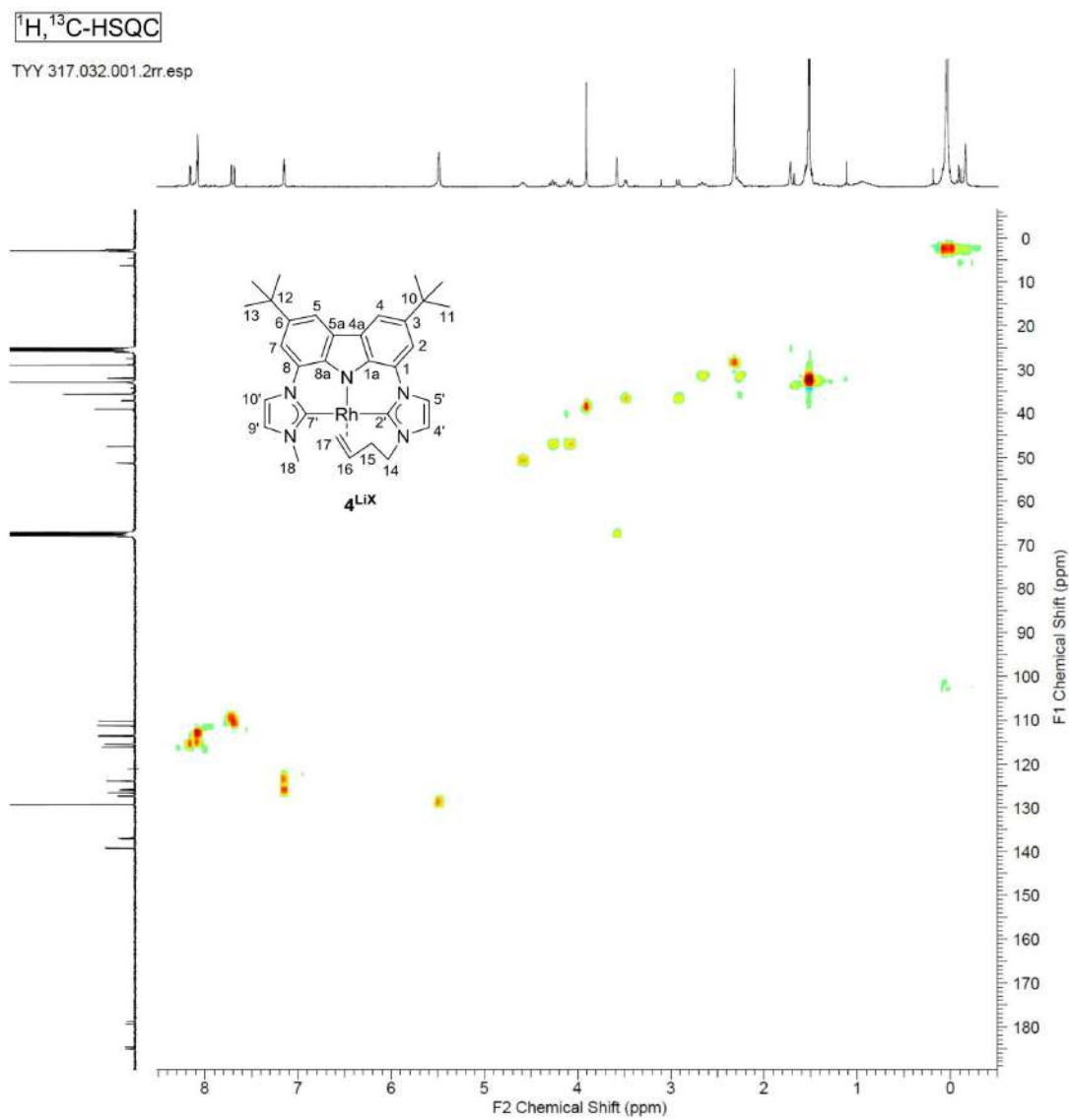


Figure S16.  $^1\text{H}, ^{13}\text{C}$ -HSQC NMR ( $\text{THF}-d_6$ , 400 MHz) spectrum: generation of catalyst  $4^{\text{LiX}}$  from  $[\text{Li}(\text{bimca}^{\text{Me,Homo}})]$ .



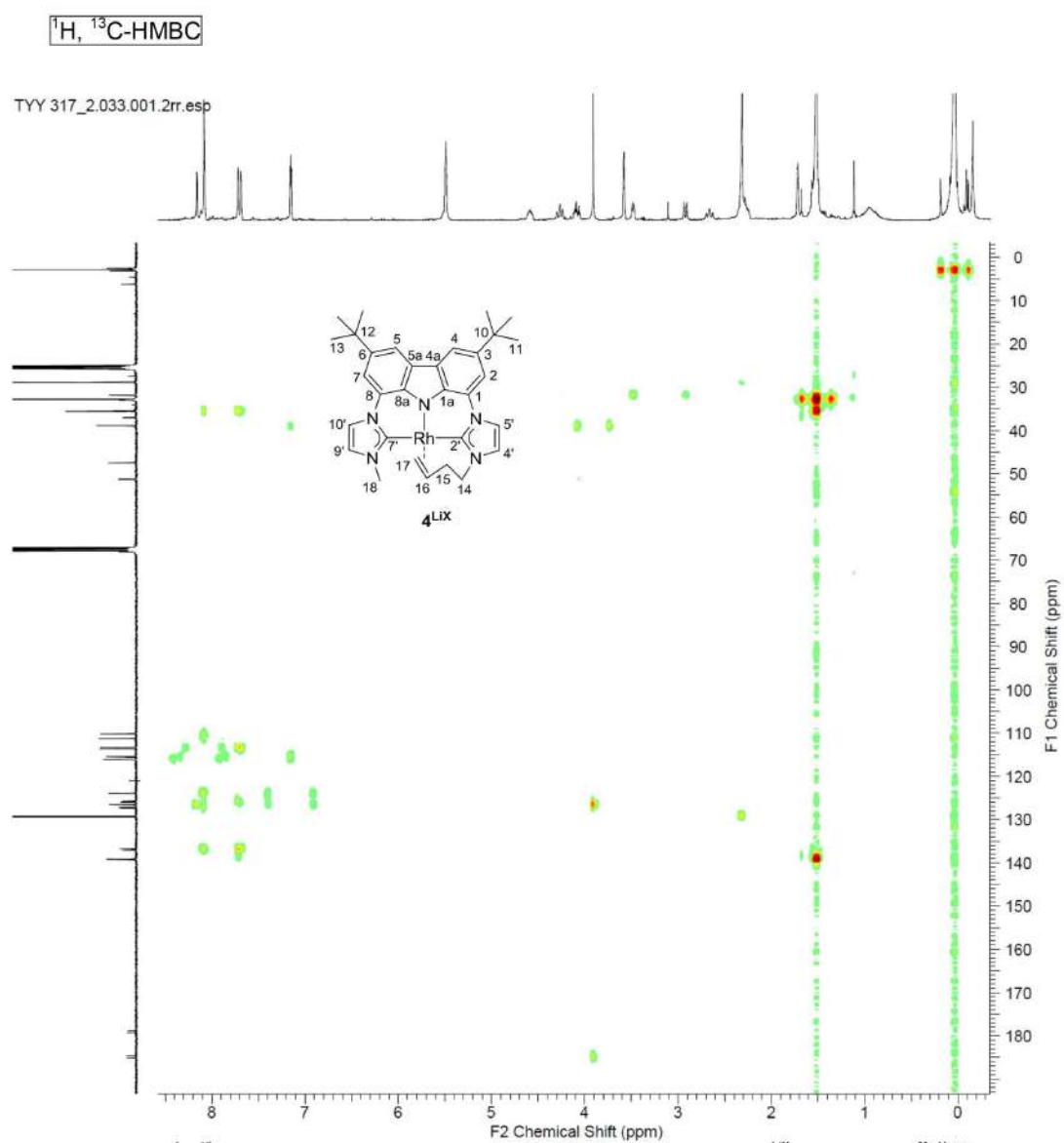


Figure S17.  $^1\text{H}, ^{13}\text{C}$ -HMBC NMR (THF- $d_6$ , 400 MHz) spectrum: generation of catalyst  $4^{\text{LiX}}$  from  $[\text{Li}(\text{bimca}^{\text{Me,Homo}})]$ .

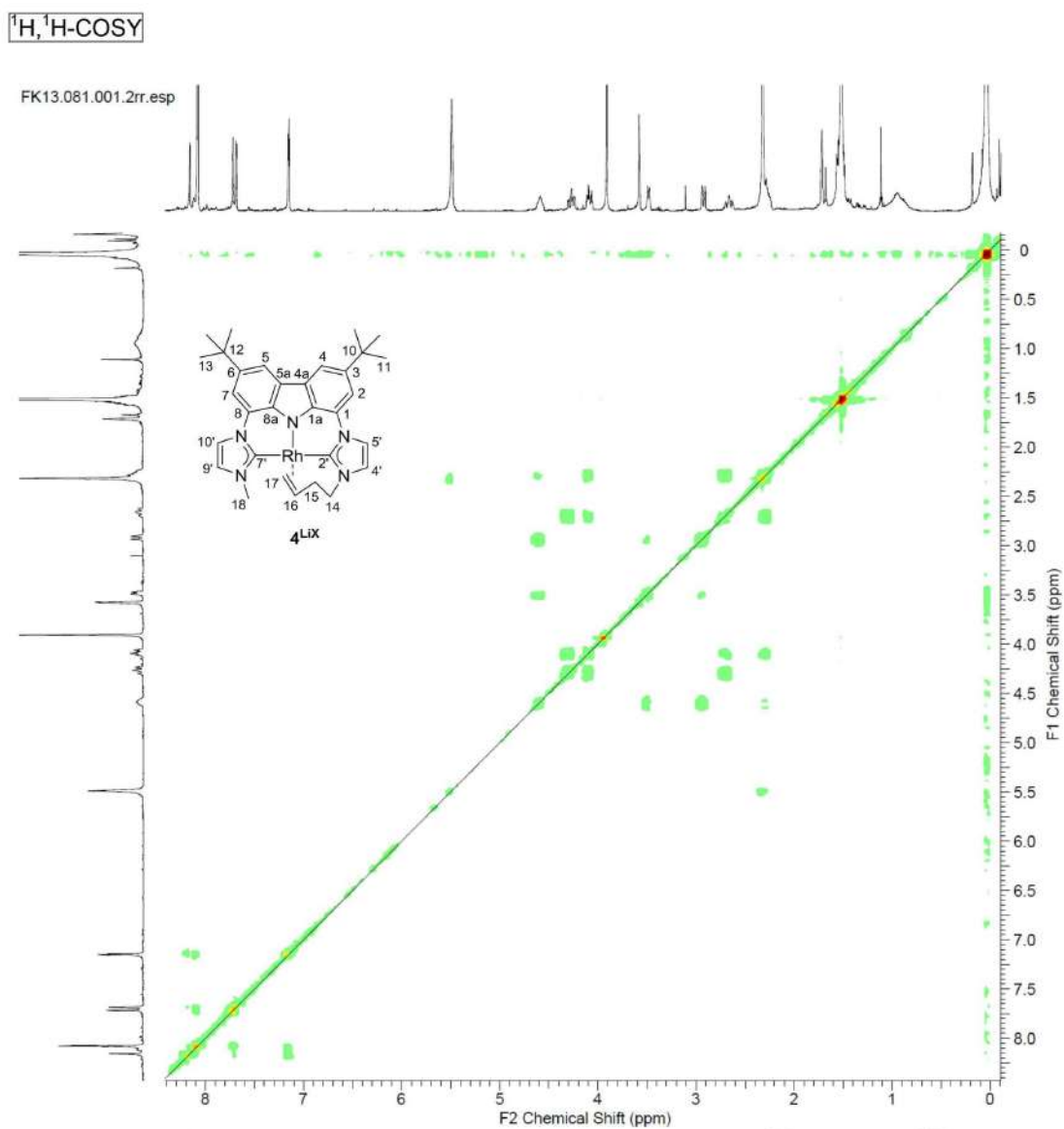


Figure S18.  $^1\text{H}, ^1\text{H}$ -COSY NMR ( $\text{THF-d}_6$ , 400 MHz) spectrum: generation of catalyst  $4^{\text{LiX}}$  from  $[\text{Li}(\text{bimca}^{\text{Me,Homo}})]$ .

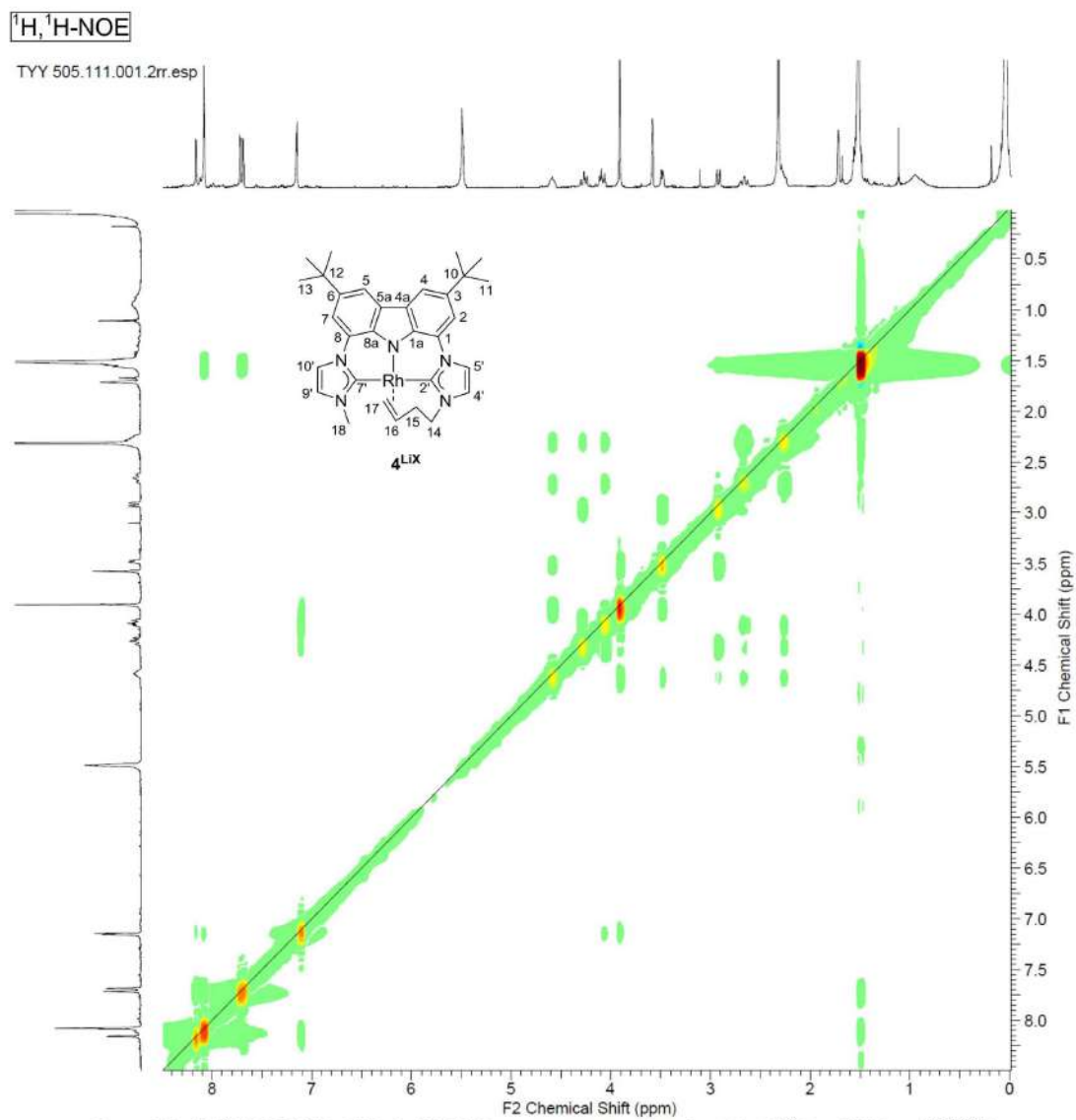
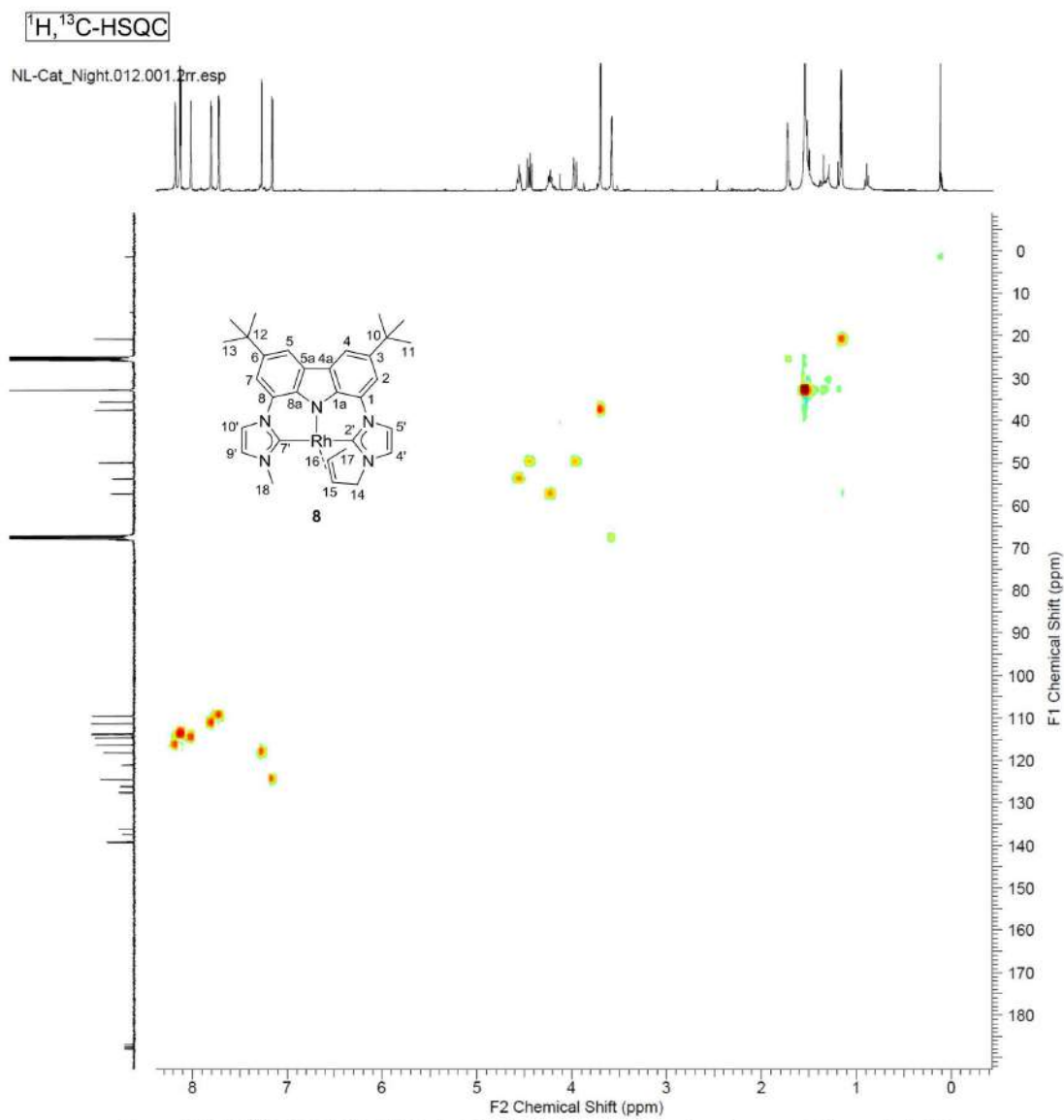


Figure S19.  $^1\text{H}, ^1\text{H}$ -NOE NMR ( $\text{THF-d}_6$ , 400 MHz) spectrum: generation of catalyst  $4^{\text{LiX}}$  from  $[\text{Li}(\text{bimca}^{\text{Me,Homo}})]$ .





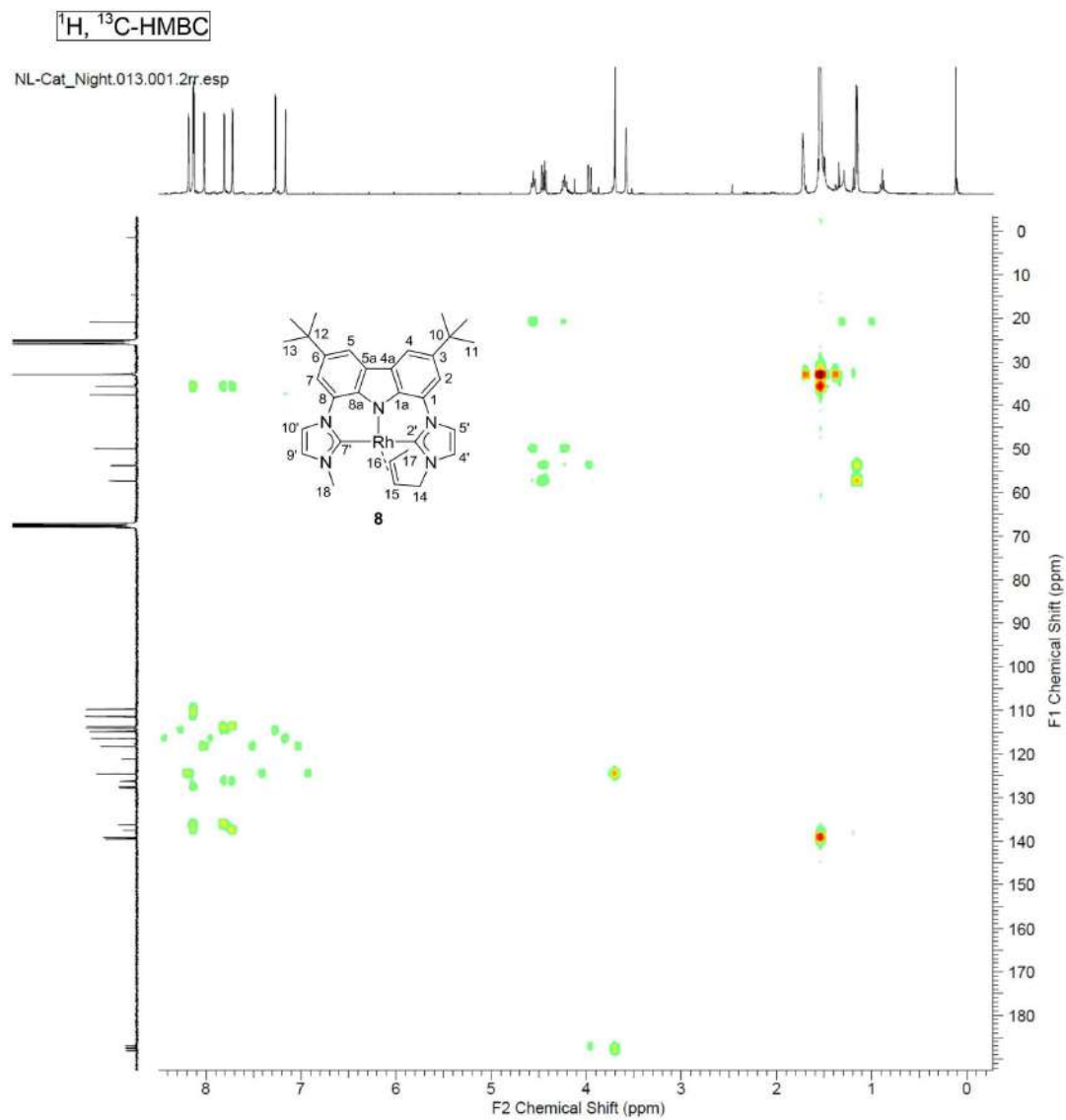


Figure S23.  $^1\text{H}, ^{13}\text{C}$ -HMBC NMR (THF- $d_6$ , 400 MHz) spectrum: generation of complex **8** from catalyst **4**.

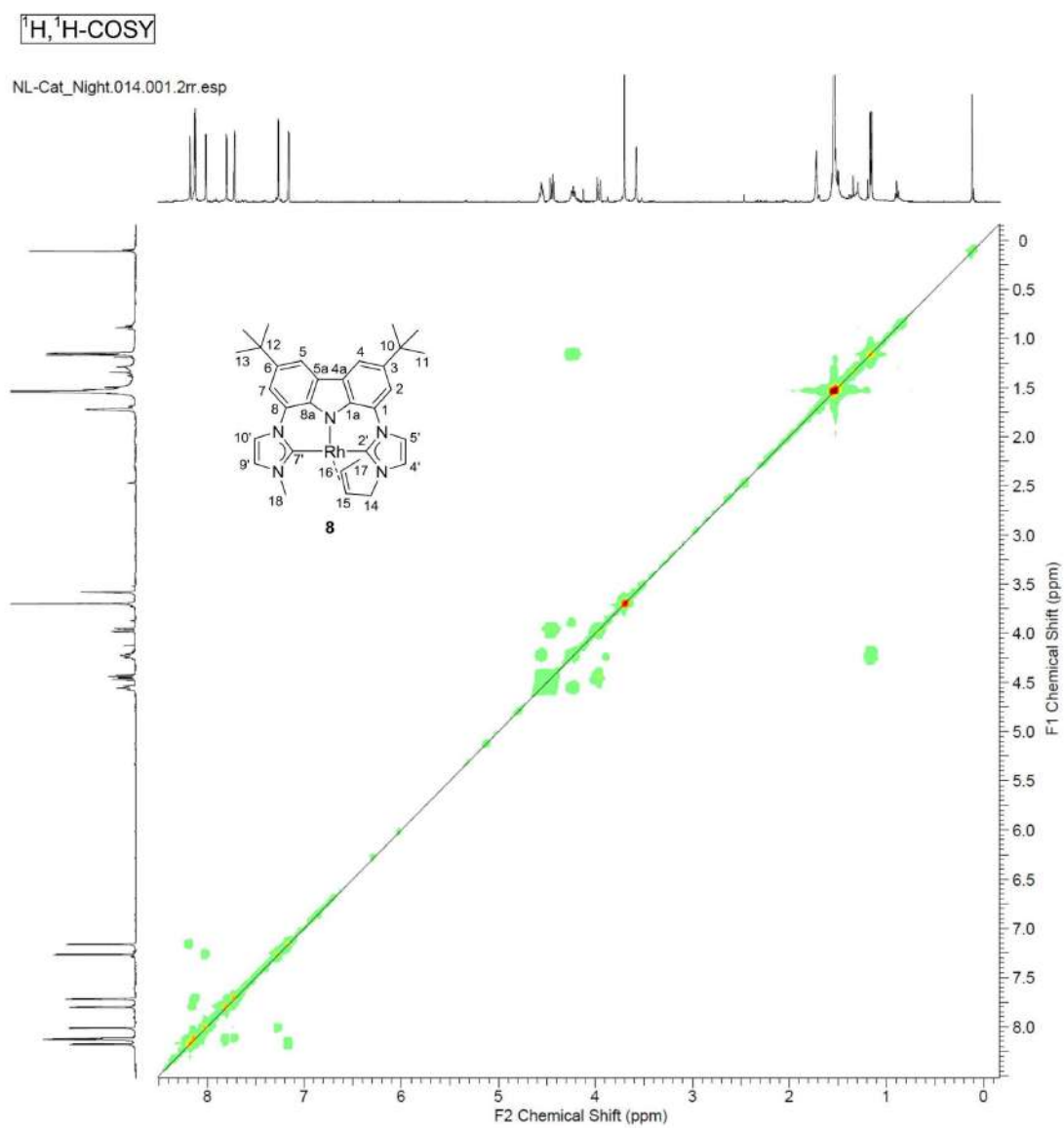


Figure S24.  $^1\text{H}, ^1\text{H}$ -COSY NMR ( $\text{THF-d}_8$ , 400 MHz) spectrum: generation of complex **8** from catalyst **4**.

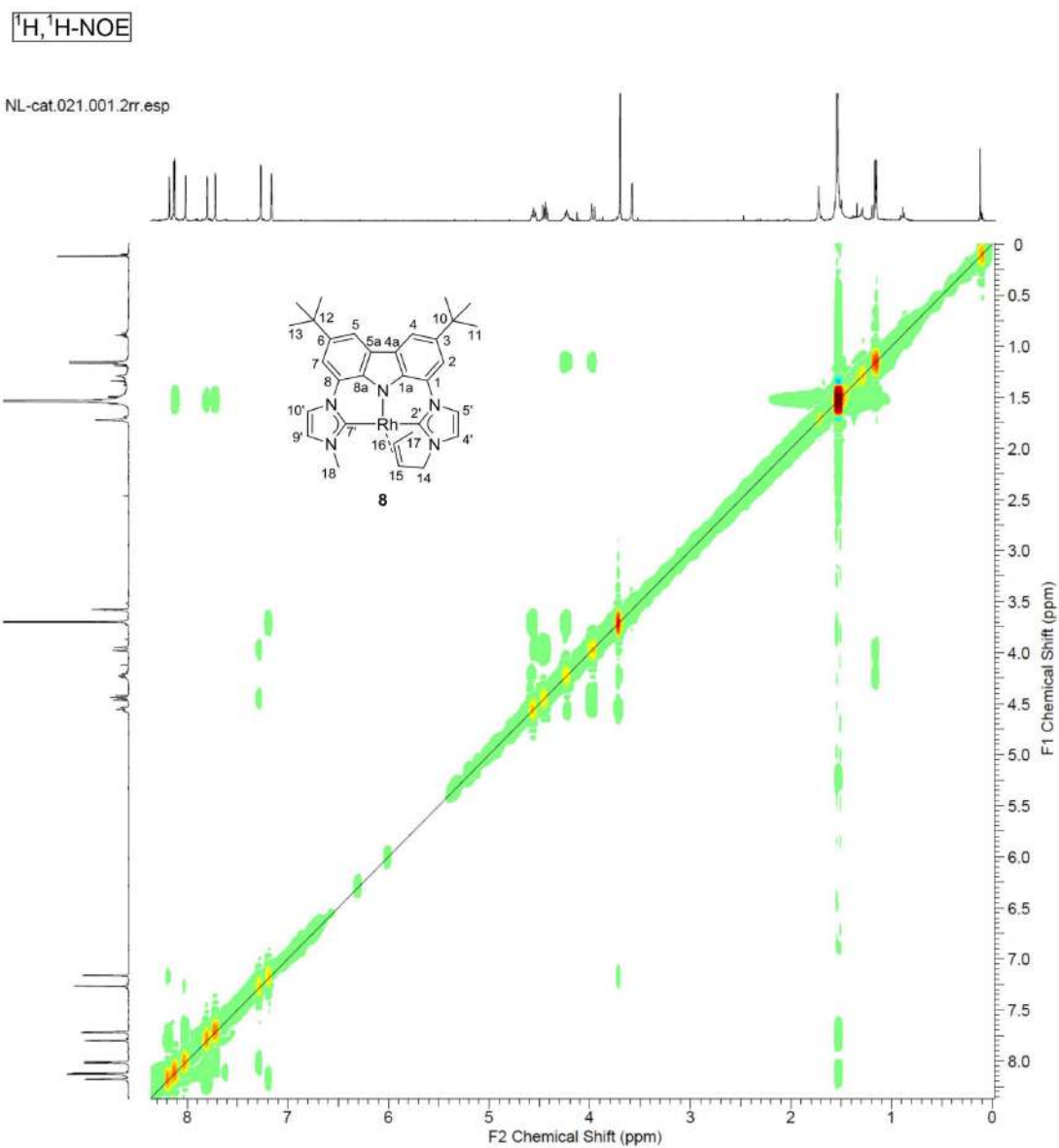


Figure S25.  $^1\text{H}, ^1\text{H}$ -NOE NMR ( $\text{THF-}d_6$ , 400 MHz) spectrum: generation of complex **8** from catalyst **4**.



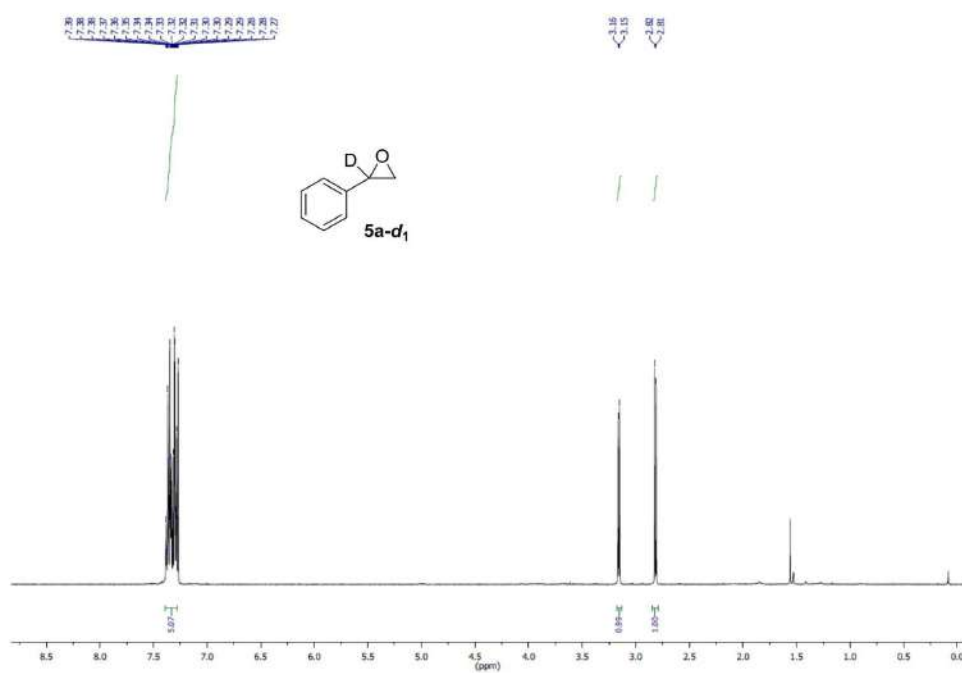


Figure S26. <sup>1</sup>H NMR (CDCl<sub>3</sub>, 400 MHz) spectrum: synthesis of **5a-d<sub>1</sub>**.

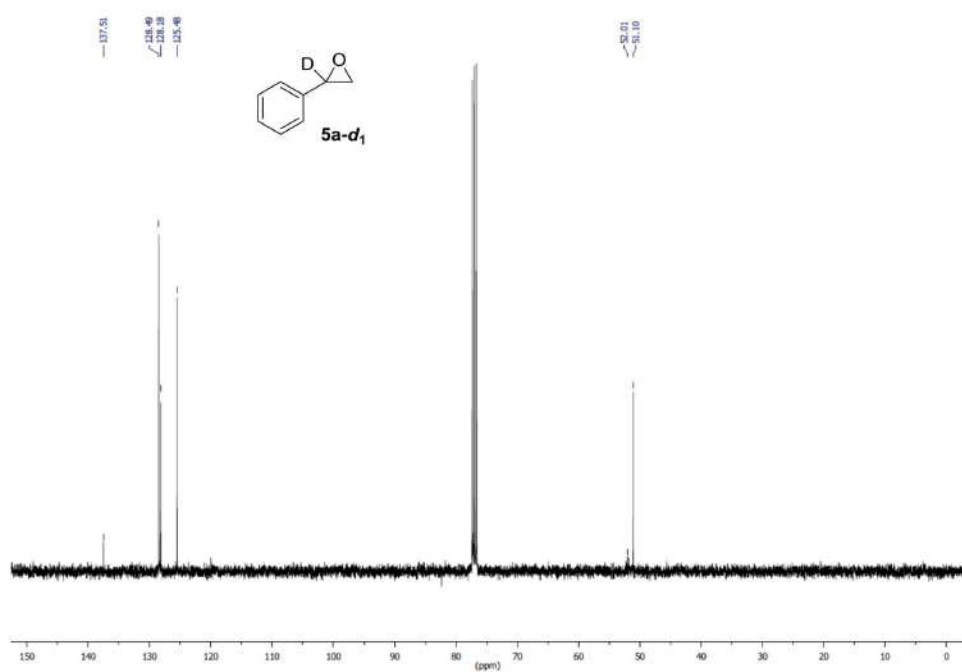


Figure S27. <sup>13</sup>C{<sup>1</sup>H} NMR (CDCl<sub>3</sub>, 101 MHz) spectrum: synthesis of **5a-d<sub>1</sub>**.

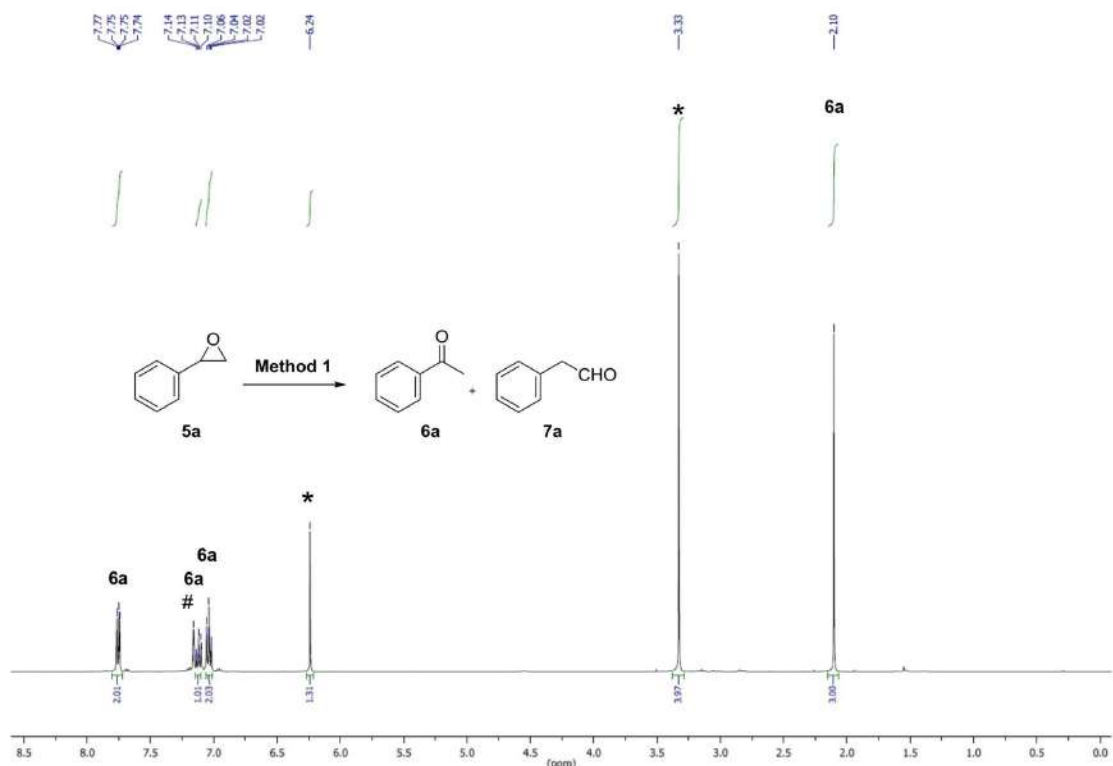


Figure S28. <sup>1</sup>H NMR (C<sub>6</sub>D<sub>6</sub> (#), 400 MHz) spectrum: isomerization of **5a** into **6a** with **Method 1** including the internal standard (\*).

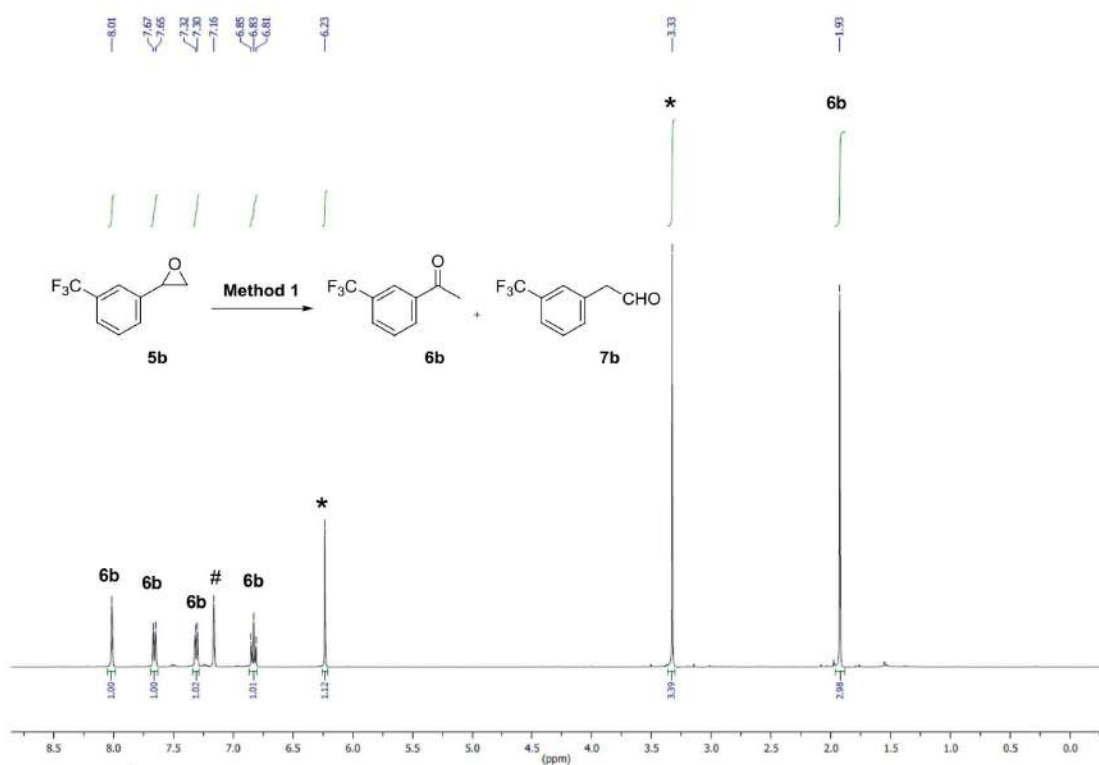
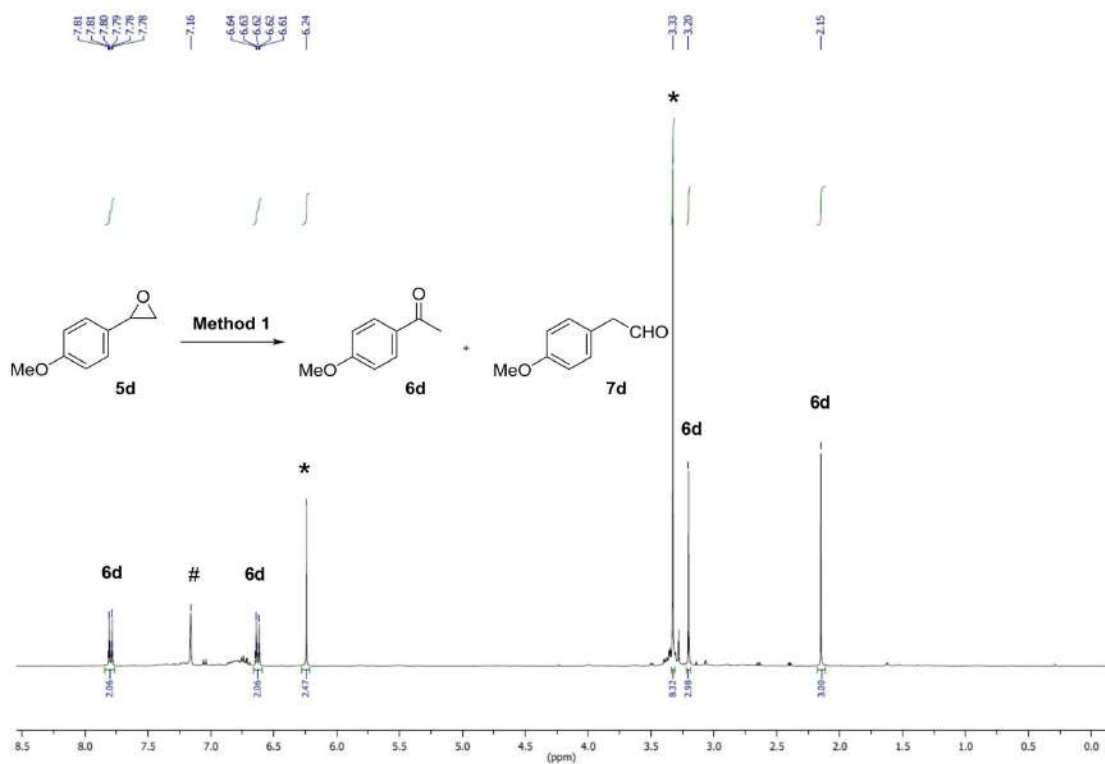
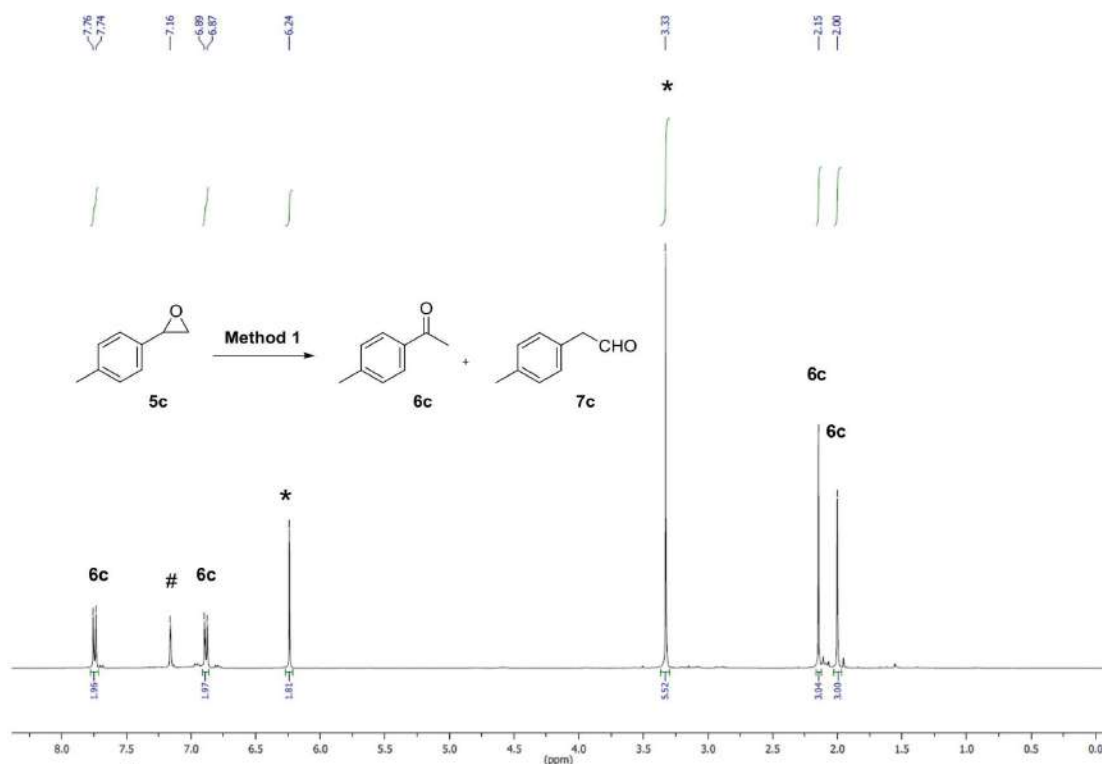


Figure S29. <sup>1</sup>H NMR (C<sub>6</sub>D<sub>6</sub> (#), 400 MHz) spectrum: isomerization of **5b** into **6b** with **Method 1** including the internal standard (\*).



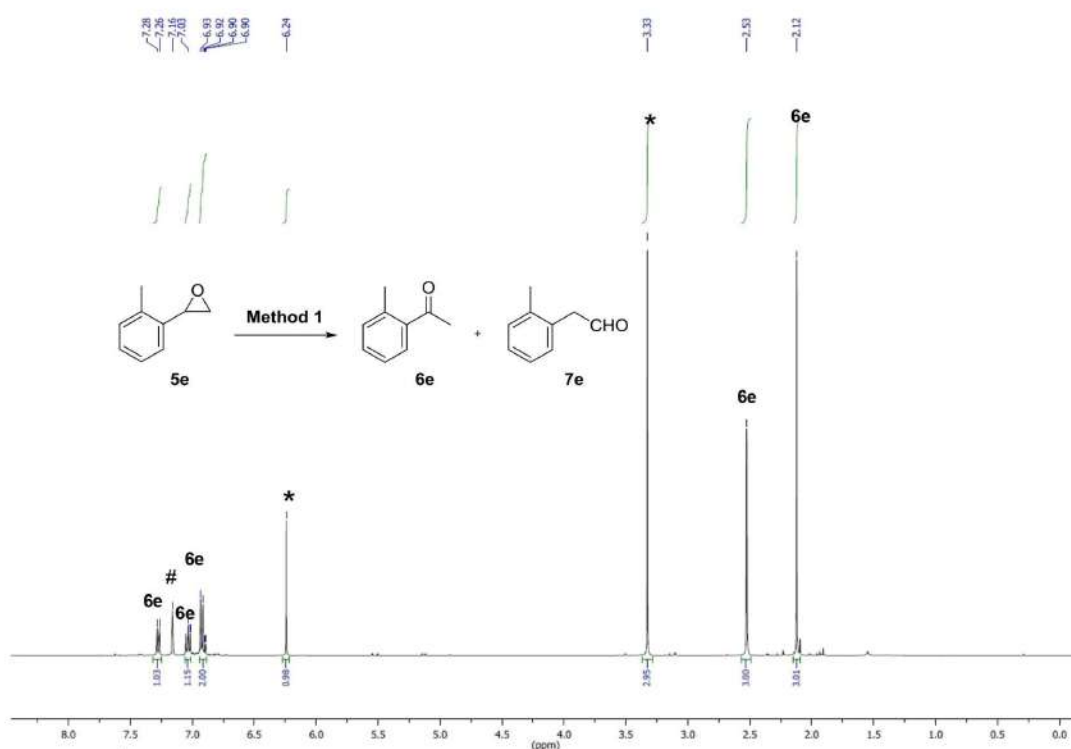


Figure S32. <sup>1</sup>H NMR (C<sub>6</sub>D<sub>6</sub> (#), 400 MHz) spectrum: isomerization of 5e into 6e with Method 1 including the internal standard (\*).

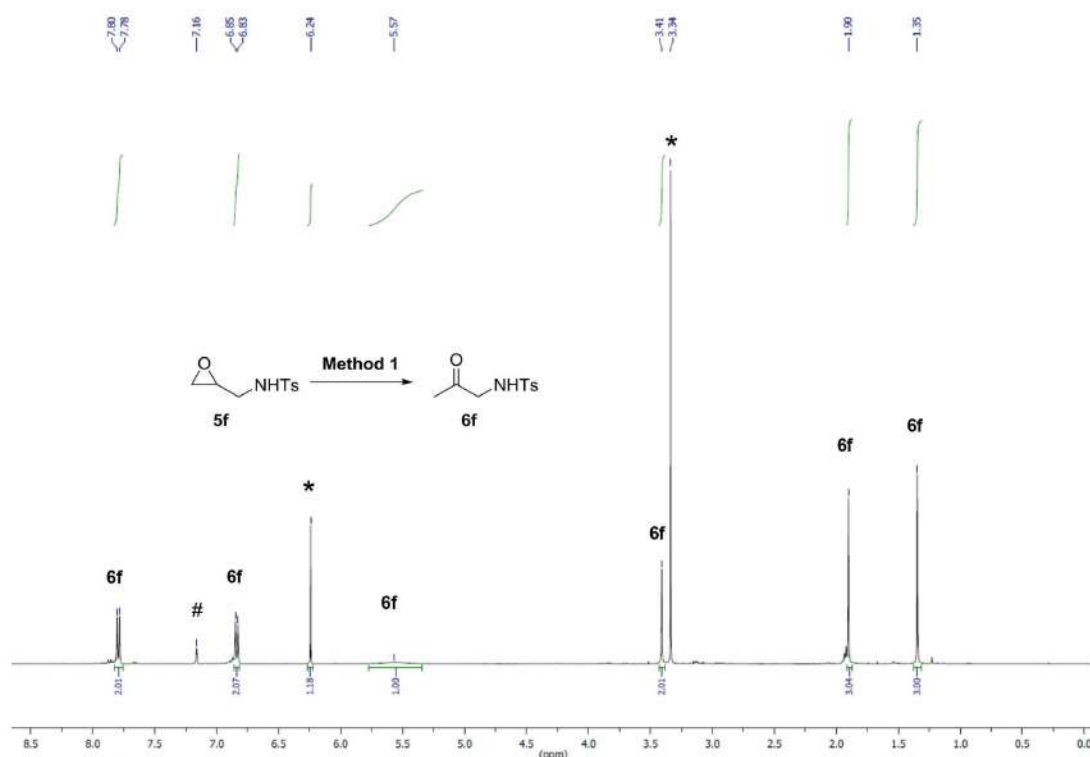


Figure S33-1. <sup>1</sup>H NMR (C<sub>6</sub>D<sub>6</sub> (#), 400 MHz) spectrum: isomerization of 5f into 6f with Method 1 using 10 mol% LiBr including the internal standard (\*).

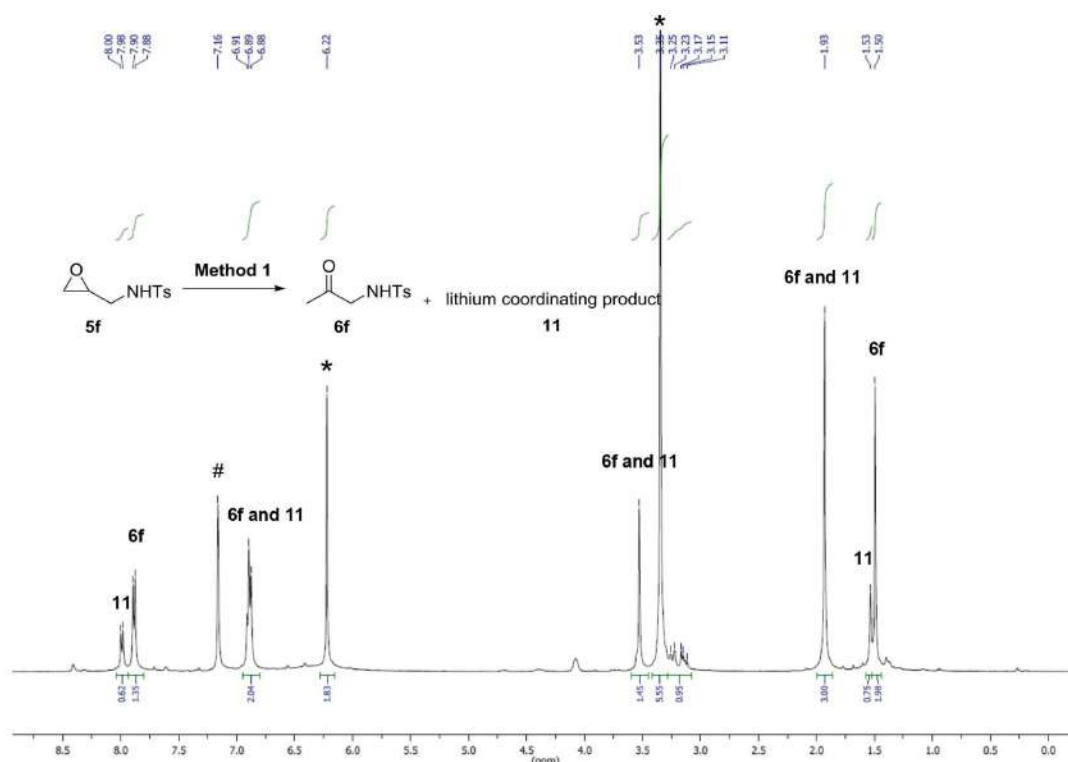


Figure S33-2. <sup>1</sup>H NMR (C<sub>6</sub>D<sub>6</sub> (#), 400 MHz) spectrum: isomerization of **5f** into **6f** and the lithium coordination product **11** with Method 1 using 50 mol% LiBr; internal standard (\*).

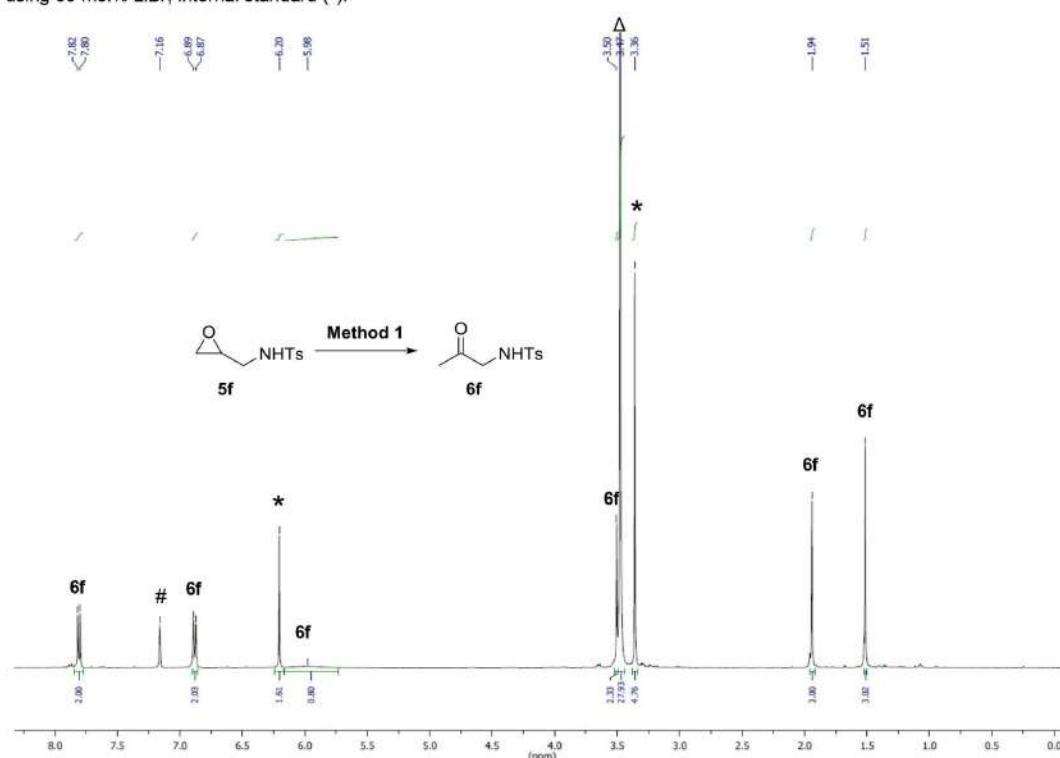


Figure S33-3. <sup>1</sup>H NMR (C<sub>6</sub>D<sub>6</sub> (#), 400 MHz) spectrum after adding 12-crown-4 (Δ) to the completed isomerization of **5f** into **6f** and **11** with Method 1 using 50 mol% LiBr; internal standard (\*).

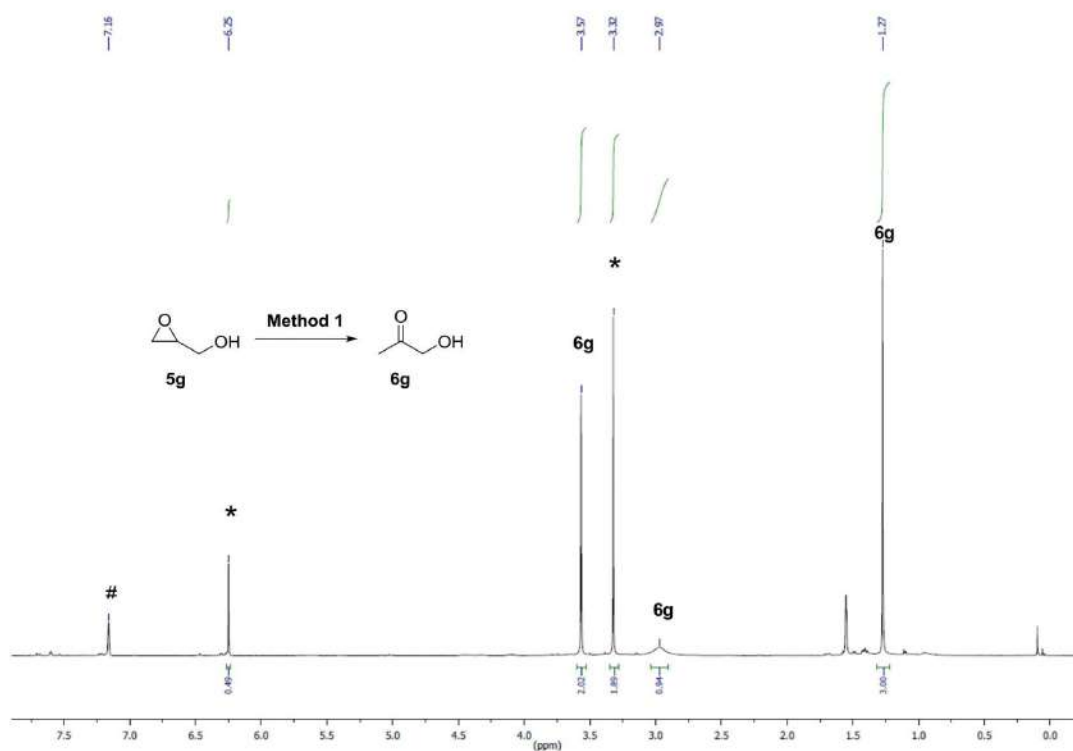


Figure S34-1.  $^1\text{H}$  NMR ( $\text{C}_6\text{D}_6$  (#), 400 MHz) spectrum: isomerization of **5g** into **6g** with **Method 1** using 10 mol% LiBr including the internal standard (\*).

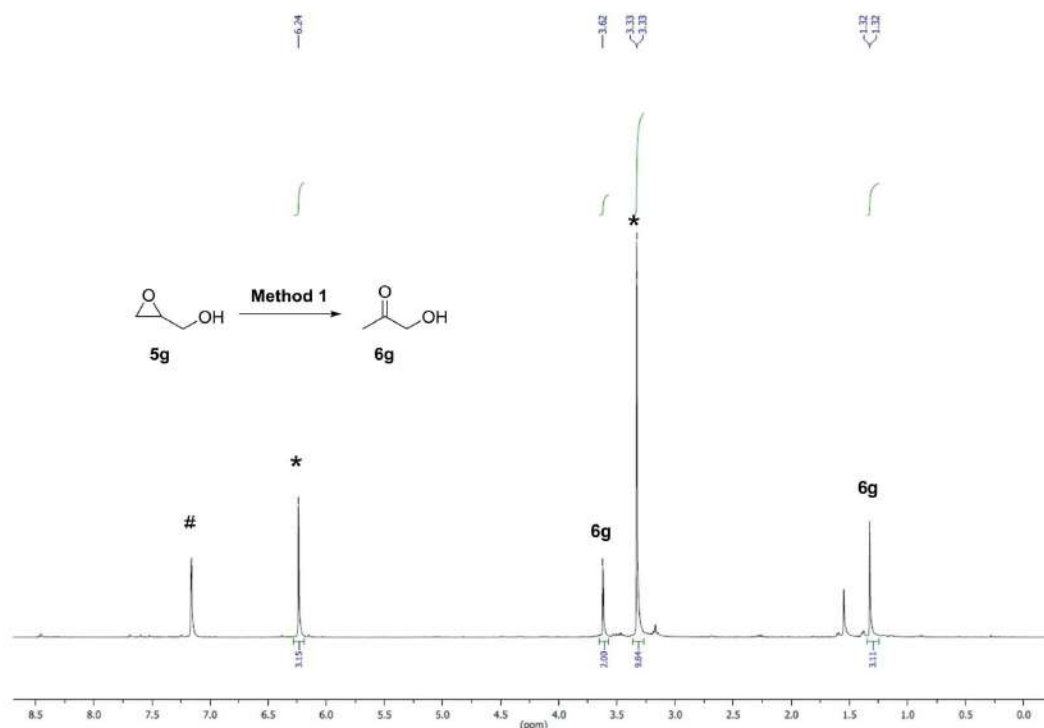


Figure S34-2.  $^1\text{H}$  NMR ( $\text{C}_6\text{D}_6$  (#), 400 MHz) spectrum: isomerization of **5g** into **6g** with **Method 1** using 50 mol% LiBr including the internal standard (\*).

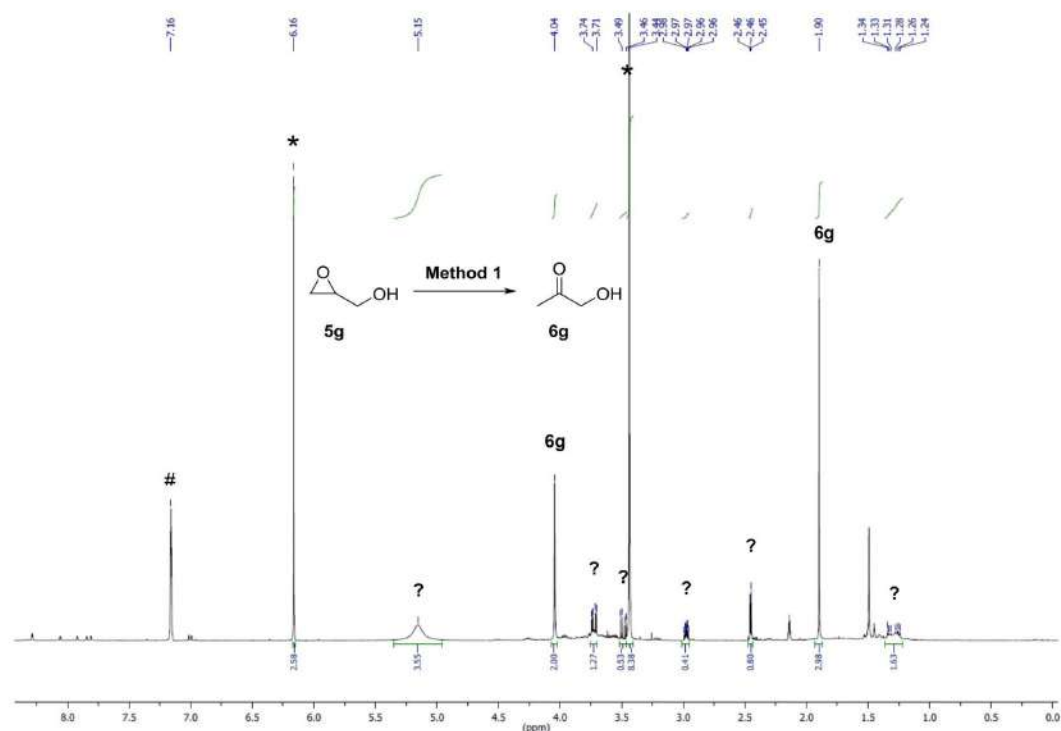


Figure S34-3.  $^1\text{H}$  NMR ( $\text{C}_6\text{D}_6$  (#), 400 MHz) spectrum: addition of  $\text{DMSO-}d_6$  after full conversion of **5g** into **6g** and unknown side products (?) with **Method 1** using 50 mol%  $\text{LiBr}$ , including the internal standard (\*).

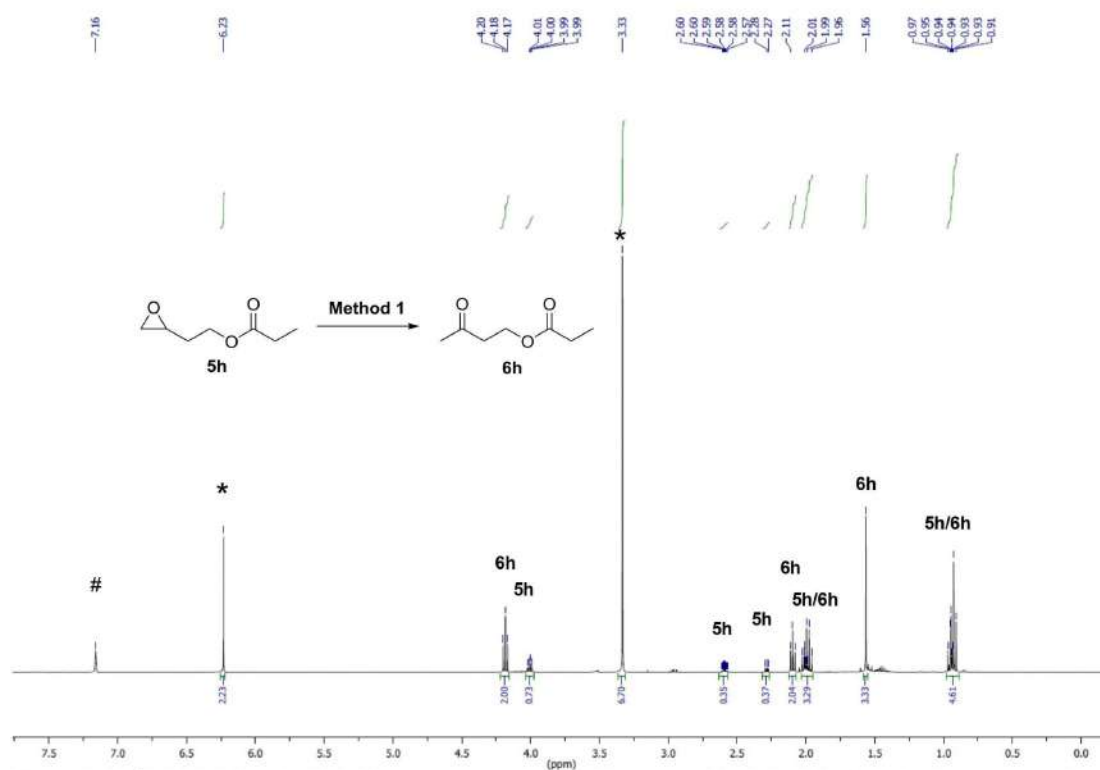


Figure S35-1.  $^1\text{H}$  NMR ( $\text{C}_6\text{D}_6$  (#), 400 MHz) spectrum: isomerization of **5h** into **6h** with **Method 1** including the internal standard (\*).

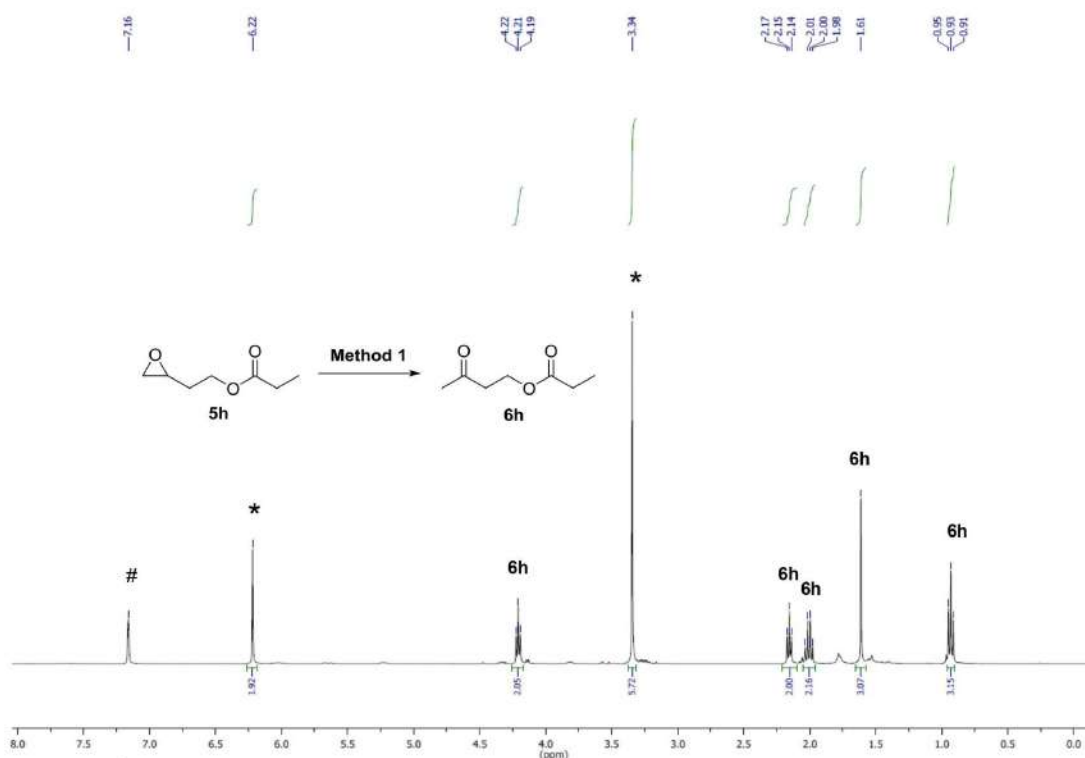


Figure S35-2. <sup>1</sup>H NMR (C<sub>6</sub>D<sub>6</sub> (#), 400 MHz) spectrum: isomerization of 5h into 6h with Method 1 using 50 mol% LiBr; including the internal standard (\*).

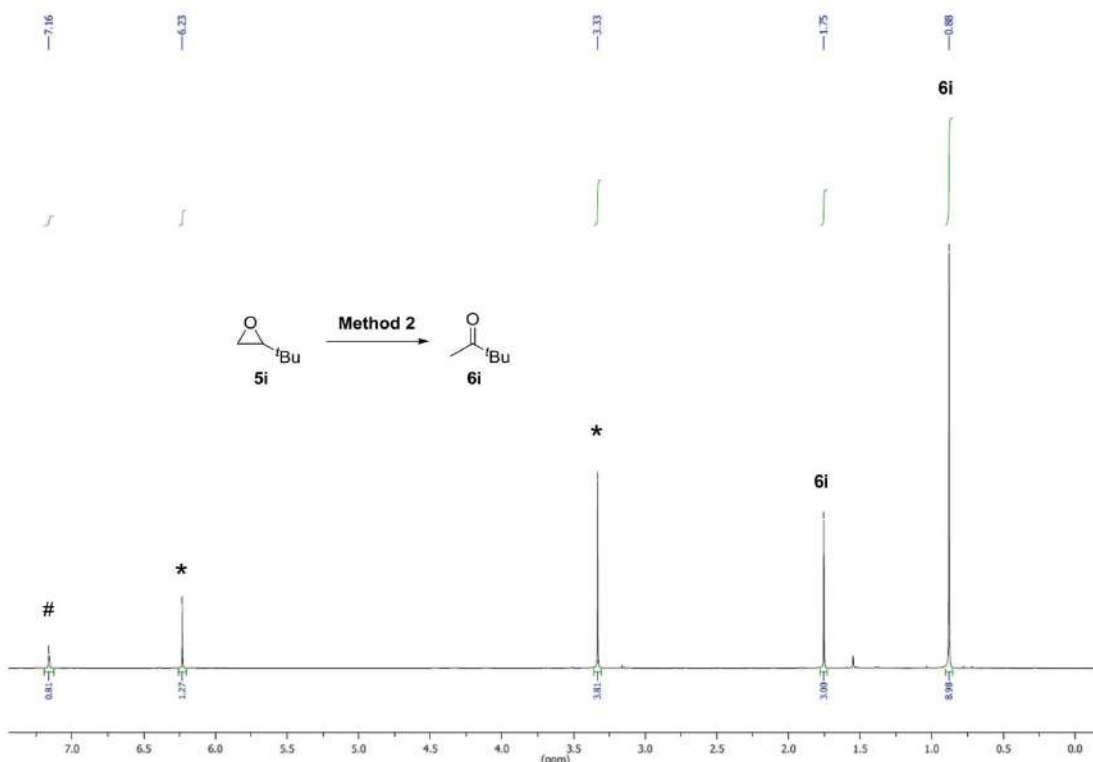


Figure S36. <sup>1</sup>H NMR (C<sub>6</sub>D<sub>6</sub> (#), 400 MHz) spectrum: isomerization of 5i into 6i with Method 2 including the internal standard (\*).



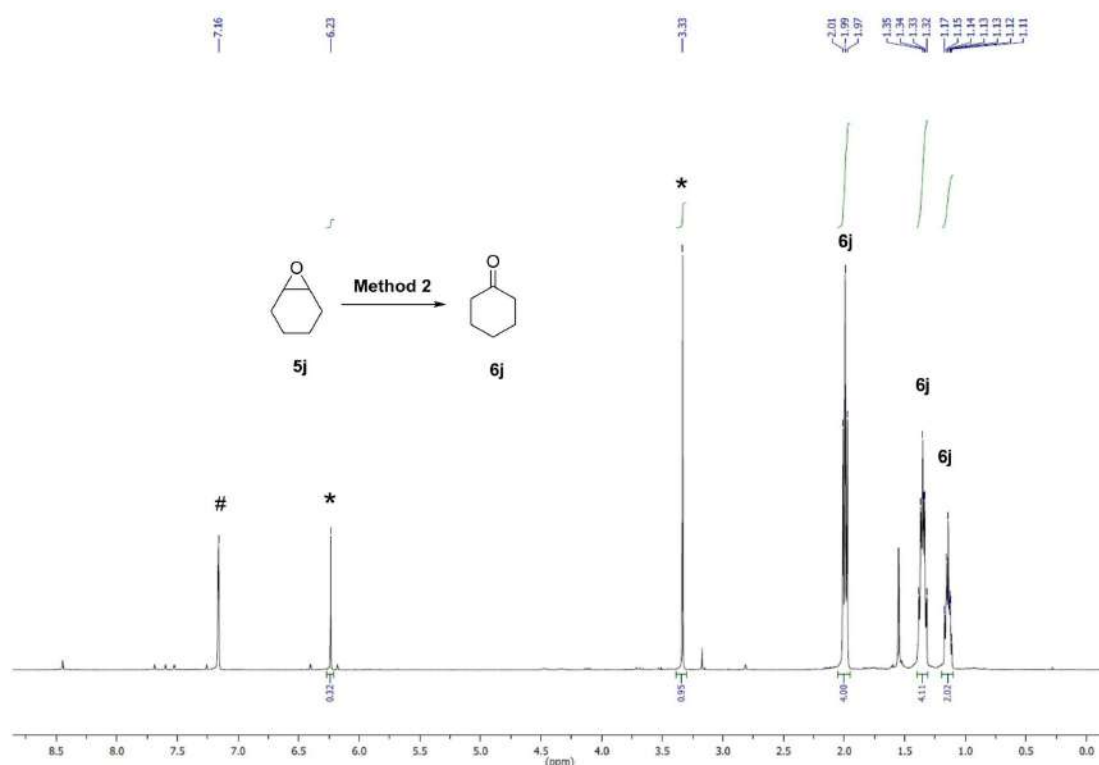


Figure S37. <sup>1</sup>H NMR (C<sub>6</sub>D<sub>6</sub> (#), 400 MHz) spectrum: isomerization of 5j into 6j with Method 2 including the internal standard (\*).

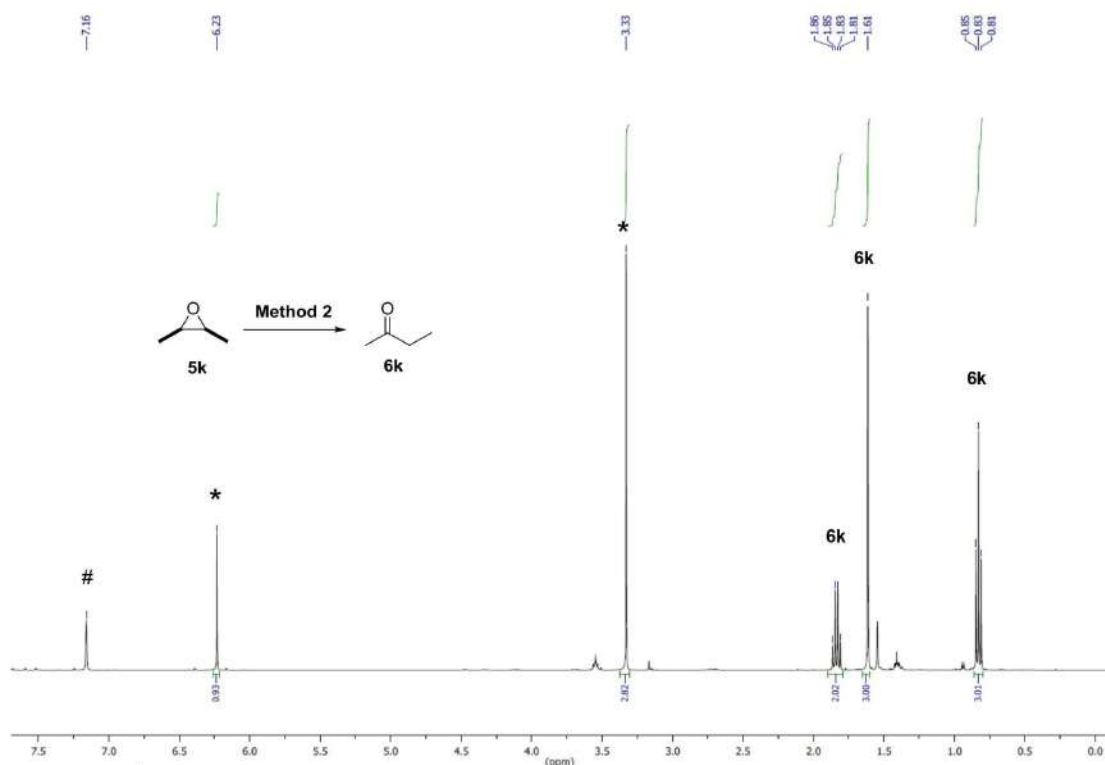


Figure S38. <sup>1</sup>H NMR (C<sub>6</sub>D<sub>6</sub> (#), 400 MHz) spectrum: isomerization of 5k into 6k with Method 2 including the internal standard (\*).

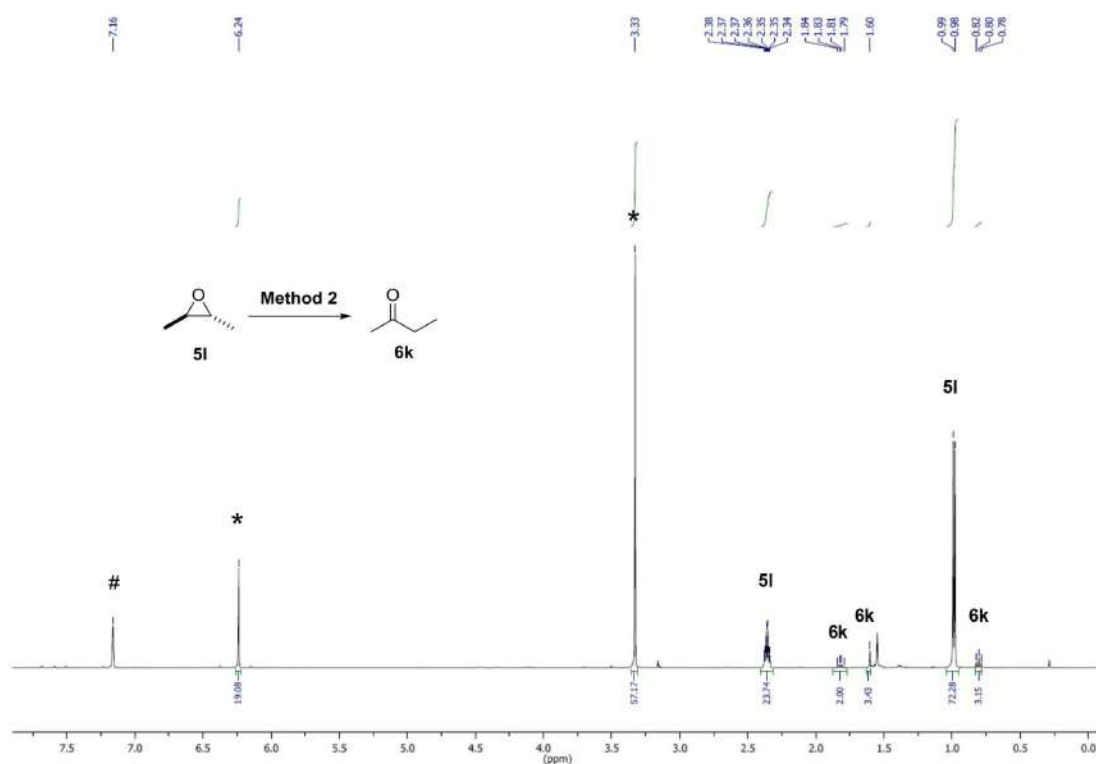
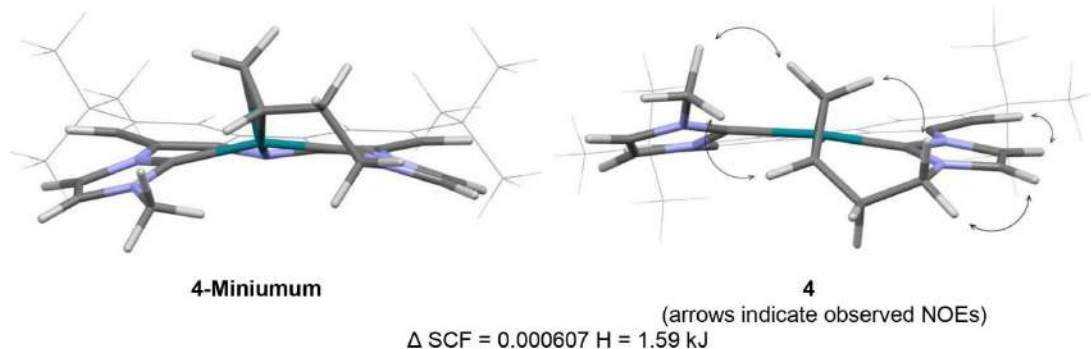


Figure S39. <sup>1</sup>H NMR (C<sub>6</sub>D<sub>6</sub> (#), 400 MHz) spectrum: isomerization of 5I into 6k with Method 2 including the internal standard (\*).

## 5. DFT calculations

Cartesian coordinates of the calculated structures:

73

**4-Minimum** (DFT BP-86/def2-TZVP), CHARGE=0; total energy = -1588.29320866827

C -3.092270 -2.860357 0.565816  
 C -1.734638 -3.244646 0.503824  
 C -0.708759 -2.338139 0.237148  
 C -1.036623 -0.987455 0.056007  
 C -2.404565 -0.580837 0.123619  
 C -3.417217 -1.514860 0.365291  
 H -1.477540 -4.287546 0.685578  
 H -4.452971 -1.181794 0.414000  
 C -1.001369 1.195251 -0.181512  
 C -0.631643 2.543942 -0.288879  
 C -1.635215 3.513639 -0.280237  
 C -3.005504 3.190121 -0.176162  
 C -3.369242 1.844601 -0.054888  
 C -2.382727 0.853782 -0.046125  
 H -1.346391 4.563210 -0.321790  
 H -4.415236 1.560943 0.050038  
 N -0.193067 0.083013 -0.134206  
 C 0.983748 -4.069570 -0.244289  
 H 0.253556 -4.858712 -0.351993  
 C 2.322580 -4.074701 -0.455182  
 H 2.985590 -4.875190 -0.759023  
 N 0.635905 -2.762809 0.089326  
 N 2.770733 -2.778964 -0.250877  
 C 1.745105 -1.924234 0.101951  
 C 1.794100 2.083896 -0.000167  
 C 2.543736 4.087812 -0.815632  
 H 3.281172 4.824031 -1.111103  
 N 0.735178 2.896640 -0.390604  
 N 2.893275 2.865020 -0.272981  
 C 1.187498 4.112610 -0.895695  
 H 0.520426 4.865397 -1.291161  
 C 4.126827 -2.373411 -0.582803  
 H 4.493475 -3.003472 -1.402996  
 H 4.802339 -2.476579 0.277421  
 C 4.269290 2.443666 -0.040054  
 C 4.378636 1.696095 1.285565  
 H 4.597312 1.797885 -0.870554  
 H 4.888757 3.351762 -0.043315  
 Rh 1.773929 0.088799 0.362791  
 C -4.033925 4.329622 -0.174129  
 C -4.149024 -3.934424 0.856578  
 C 3.793410 0.303485 1.242276  
 H 3.877644 2.297811 2.060378  
 H 5.446089 1.645047 1.560856  
 C 2.805505 -0.103832 2.169639  
 H 4.503163 -0.445815 0.892874  
 H 2.767749 -1.138576 2.515256  
 H 2.407435 0.622800 2.885406  
 C -5.570789 -3.353141 0.885351  
 C -3.865437 -4.580959 2.229188

73

**4** (DFT BP-86/def2-TZVP), CHARGE=0; total energy = -1588.29260152806

Rh 6.559518 -0.843112 16.199520  
 N 8.259891 1.676576 16.777092  
 C 10.338120 -1.106171 18.203384  
 C 9.337016 0.962582 17.365307  
 N 8.333599 -1.301346 17.047220  
 C 11.907833 -6.376239 18.646261  
 H 12.357224 -7.273891 19.097734  
 H 12.558463 -5.521421 18.874638  
 H 11.895268 -6.506444 17.554682  
 N 6.267810 2.324528 16.219059  
 N 5.482634 -3.419843 14.888869  
 N 7.034565 -3.889310 16.321320  
 C 8.314640 3.056512 16.590366  
 H 9.222575 3.630924 16.690470  
 C 9.960567 -2.502364 18.191826  
 C 6.344553 -2.810191 15.776623  
 C 11.425398 -0.406209 18.718557  
 H 12.216882 -0.943988 19.242884  
 C 6.987722 1.165045 16.497591  
 C 8.741909 -2.555028 17.444300  
 C 9.290668 -0.427240 17.502127  
 C 10.443639 1.640810 17.898479  
 H 10.478840 2.723139 17.832888  
 C 7.067954 3.455356 16.256205  
 H 6.679731 4.443387 16.042027  
 C 11.495014 0.985978 18.561319  
 C 10.518045 -3.657654 18.734644  
 H 11.443338 -3.593003 19.309183  
 C 8.142643 -3.794645 17.198362  
 C 12.696940 1.756989 19.125662  
 C 9.881406 -4.894355 18.552074  
 C 6.586160 -5.098524 15.793051  
 H 7.017267 -6.052583 16.057070  
 C 5.098143 -0.396844 14.732664  
 H 5.261980 0.627549 14.390647  
 C 4.817760 2.485733 16.193686  
 H 4.603199 3.541106 15.991874  
 H 4.390115 2.224249 17.170084  
 H 4.344776 1.879914 15.418797  
 C 8.707774 -4.937033 17.779905  
 H 8.218852 -5.895607 17.632359  
 C 10.530256 -5.985065 20.718225  
 C 5.022412 -1.360874 13.573872  
 C 12.595924 3.270141 18.878582  
 H 13.481004 3.771152 19.296030  
 H 11.709187 3.704176 19.363440  
 H 12.556315 3.504922 17.804771  
 C 9.653980 -7.418178 18.874992  
 H 8.626396 -7.336498 19.258083  
 H 10.119649 -8.290675 19.355175

C -4.096189 -5.019724 -0.240039  
 C -5.473623 3.807641 -0.055180  
 C -3.919431 5.129718 -1.489220  
 C -3.762439 5.268556 1.021093  
 H -6.175104 4.654490 -0.064811  
 H -5.629309 3.255937 0.882966  
 H -5.735579 3.145767 -0.892991  
 H -2.918111 5.565358 -1.610442  
 H -4.649347 5.953693 -1.504737  
 H -4.110556 4.481024 -2.355703  
 H -4.491898 6.092964 1.037236  
 H -3.839416 4.719227 1.970029  
 H -2.757537 5.709614 0.969803  
 H -4.849168 -5.798944 -0.047446  
 H -4.295149 -4.582382 -1.228809  
 H -3.111680 -5.506107 -0.280264  
 H -3.902022 -3.826611 3.028095  
 H -2.872908 -5.051418 2.258441  
 H -4.613543 -5.356950 2.451087  
 H -6.293551 -4.155782 1.090616  
 H -5.682782 -2.593213 1.671828  
 H -5.841557 -2.896276 -0.077251  
 H 4.095678 -1.327775 -0.905700

H 9.608089 -7.618767 17.794626  
 C 13.988382 1.245859 18.451441  
 H 14.867122 1.776297 18.849249  
 H 13.948781 1.407125 17.364611  
 H 14.133817 0.171035 18.625298  
 C 10.478086 -6.159202 19.185347  
 C 12.788319 1.523612 20.648653  
 H 13.651937 2.060736 21.069809  
 H 12.905082 0.457674 20.885626  
 H 11.878647 1.881736 21.151558  
 C 5.615183 -4.797827 14.898013  
 H 5.023385 -5.440269 14.257515  
 C 4.465689 -0.629074 15.980597  
 H 3.955024 -1.575223 16.167458  
 H 4.072351 0.181673 16.587204  
 C 4.566353 -2.753707 13.961360  
 H 3.561276 -2.714130 14.409667  
 H 4.503807 -3.390379 13.067776  
 H 11.140317 -5.117236 21.002537  
 H 10.965988 -6.877515 21.192842  
 H 9.520659 -5.833843 21.126438  
 H 4.298481 -0.985880 12.826789  
 H 5.998370 -1.415717 13.064847

73

8 (DFT BP-86/def2-TZVP), CHARGE=0; total energy = -  
 1588.30336656444

C -3.063578 -2.787404 0.585704  
 C -1.702383 -3.153865 0.527489  
 C -0.676876 -2.238017 0.278107  
 C -1.026452 -0.888533 0.117414  
 C -2.400406 -0.500413 0.173039  
 C -3.405510 -1.444667 0.395606  
 H -1.446432 -4.197310 0.701349  
 H -4.445674 -1.124606 0.433950  
 C -1.025540 1.303359 -0.124797  
 C -0.692629 2.665931 -0.254330  
 C -1.723217 3.605148 -0.289857  
 C -3.085241 3.248371 -0.193415  
 C -3.413107 1.897524 -0.042485  
 C -2.400143 0.934315 -0.002340  
 H -1.466066 4.660025 -0.375990  
 H -4.452155 1.586035 0.051566  
 N -0.202559 0.194904 -0.064322  
 C 1.022480 -4.003235 -0.000718  
 H 0.297276 -4.802404 -0.031718  
 C 2.368204 -4.042843 -0.147584  
 H 3.034578 -4.880782 -0.310480  
 N 0.673061 -2.662937 0.156538  
 N 2.821592 -2.736447 -0.078058  
 C 1.793251 -1.833577 0.105879  
 C 1.703168 2.172297 -0.122948  
 C 2.525434 4.251686 -0.537592  
 H 3.279178 5.015020 -0.687181  
 N 0.666771 3.055806 -0.323460  
 N 2.829668 2.931591 -0.256448  
 C 1.164656 4.336496 -0.582450  
 H 0.527424 5.184930 -0.787770  
 C 4.206568 -2.390688 -0.350740  
 H 4.763717 -3.316578 -0.532939  
 H 4.661707 -1.867544 0.497156  
 C 4.119194 2.251251 -0.163713

C 3.894270 0.785896 0.193551  
 H 4.630479 2.329205 -1.134997  
 H 4.741569 2.769278 0.586845  
 Rh 1.800378 0.226325 0.140845  
 C -4.144188 4.358190 -0.244112  
 C -4.108028 -3.878362 0.858839  
 C 3.430148 0.387686 1.477826  
 H 3.705878 -0.618401 1.809016  
 C -5.536962 -3.314836 0.886056  
 C -3.823982 -4.535478 2.226286  
 C -4.036031 -4.951073 -0.248762  
 C -5.570198 3.800925 -0.121448  
 C -4.035342 5.112139 -1.586677  
 C -3.912927 5.347480 0.918237  
 H -6.294448 4.627279 -0.165353  
 H -5.720080 3.275712 0.832711  
 H -5.805702 3.105536 -0.939527  
 H -3.044831 5.570401 -1.713545  
 H -4.787302 5.914308 -1.640787  
 H -4.198330 4.427157 -2.430586  
 H -4.664616 6.151591 0.895386  
 H -3.986585 4.832234 1.886355  
 H -2.920090 5.814579 0.861901  
 H -4.780228 -5.741603 -0.068339  
 H -4.235400 -4.505899 -1.233919  
 H -3.045480 -5.424899 -0.289644  
 H -3.873733 -3.790064 3.032803  
 H -2.826175 -4.994672 2.256332  
 H -4.563954 -5.322495 2.436227  
 H -6.250905 -4.128142 1.079995  
 H -5.662178 -2.563881 1.679062  
 H -5.808855 -2.852296 -0.073527  
 H 4.262408 -1.753772 -1.241449  
 C 3.191316 1.326900 2.634333  
 H 4.554473 0.120994 -0.360247  
 H 4.096812 1.402866 3.264532  
 H 2.377094 0.955940 3.272720  
 H 2.916711 2.337295 2.308072

## 6. Reference

[1] N. Oguni, S. Watanabe, M. Maki, H. Tani, *Macromolecules*, **1973**, *6*, 195-199.



# Synthesis and Reactivity of Cobalt(I) and Iridium(I) Complexes Bearing a Pentadentate *N*-Homoallyl-Substituted Bis(NHC) Pincer Ligand

Yingying Tian, Theo Maulbetsch, Ronja Jordan, Karl W. Törnroos, and Doris Kunz\*



Cite This: *Organometallics* 2020, 39, 1221–1229



Read Online

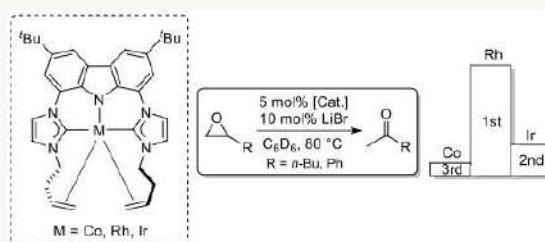
ACCESS |

Metrics & More

Article Recommendations

Supporting Information

**ABSTRACT:** Two methods for the synthesis of the bis-(imidazolin-2-ylidene)carbazolide cobalt(I) complex [Co(bimca<sup>Homo</sup>)] (**2**) have been developed. The first route relies on the direct transmetalation of the *in situ* generated lithium complex [Li(bimca<sup>Homo</sup>)] with CoCl(PPh<sub>3</sub>)<sub>3</sub>. The second route is a two-step synthesis that consists of the transmetalation of [Li(bimca<sup>Homo</sup>)] with CoCl<sub>2</sub> followed by reduction of the Co(II) complex to yield the desired Co(I) complex **2**. The analogous iridium complex [Ir(bimca<sup>Homo</sup>)] (**4**) was prepared by transmetalation of [Li(bimca<sup>Homo</sup>)] or [K(bimca<sup>Homo</sup>)] with [Ir(μ-Cl)(COD)]<sub>2</sub>. The catalytic activity of complexes **2** and **4** in the epoxide isomerization was tested in the absence and presence of H<sub>2</sub>. When [M(bimca<sup>Homo</sup>)] (M = Ir (**4**), Rh (**3**)) was exposed to 1 bar of H<sub>2</sub> at 80 °C, single crystals formed whose X-ray structure analyses revealed the hydrogenation of the *N*-homoallyl moieties and formation of the dimeric hydrido complexes [Ir(bimca<sup>n-Bu</sup>)(H)<sub>2</sub>]<sub>2</sub> (**7**) and [Rh(bimca<sup>n-Bu</sup>)(H)<sub>2</sub>]<sub>2</sub> (**8**).



## INTRODUCTION

*N*-heterocyclic carbenes (NHCs) have experienced huge success in the last few decades due to their use as ligands for metal catalysts or as organocatalysts in various kinds of catalytic reactions.<sup>1</sup> Electronically, NHCs usually possess strong  $\sigma$ -donor and weak  $\pi$ -acceptor properties. This leads to strong metal–ligand bonds and electron-rich metal centers and imparts nucleophilic character to these complexes.<sup>2</sup> Incorporation of more than one NHC unit in one ligand increases the stability of the complex due to the chelate effect. In addition, it stabilizes metal centers in high oxidation states and activates metal centers in low oxidation states.

Well-defined bis(NHC)-pincer transition-metal complexes have been widely applied as catalysts in versatile homogeneous catalytic reactions: for example, Chirik's cobalt catalyst with a (C<sub>NHC</sub>NC<sub>NHC</sub>)-pincer ligand represents one of the most active base-metal catalysts for the hydrogenation of unactivated, sterically hindered olefins and (C<sub>NHC</sub>C<sub>aryl</sub>C<sub>NHC</sub>)-pincer cobalt complexes from the Fout group are used for the hydrogenation of unsaturated bonds.<sup>3,4</sup> We reported on several highly reactive nucleophilic Rh(I) complexes bearing the electron-rich bis(NHC)-pincer ligand called bimca, such as bimca<sup>Me</sup>, bimca<sup>Homo</sup>, and bimca<sup>MeHomo</sup> (bimca = 1,8-bis(imidazolin-2-ylidene)-3,6-di(*tert*-butyl)carbazolide; the superscript denotes the *N* substituent methyl or homoallyl). They are, for example, efficient catalysts for the regio- and chemoselective isomerization of diversely functionalized epoxides to yield methyl ketones and are the only regioselective catalysts for the

isomerization of aryl oxiranes to acetophenone derivatives to date. This selectivity is very attractive, as it could substitute the Wacker oxidation by a two-step epoxidation–isomerization sequence for temperature and Lewis acid sensitive substrates.<sup>5</sup> Rh complexes with the neutral, macrocyclic C<sub>NHC</sub>N<sub>aryl</sub>C<sub>NHC</sub> ligands from the Chaplin group were found to be active in the selective en-yne dimerization.<sup>6</sup> (C<sub>NHC</sub>C<sub>aryl</sub>C<sub>NHC</sub>)-pincer complexes of iridium have been well studied by Chianese and co-workers and are active in acceptorless alkane dehydrogenation and in alkene isomerization.<sup>7</sup>

As a continuation of our interest in low-valent, nucleophilic transition-metal catalysts, we report herein the synthesis and characterization of both [Co(bimca<sup>Homo</sup>)] (**2**) and [Ir(bimca<sup>Homo</sup>)] (**4**) and their catalytic activity together with that of the previously reported Rh complex [Rh(bimca<sup>Homo</sup>)] (**3**)<sup>5b</sup> in nucleophilic epoxide isomerization is discussed.

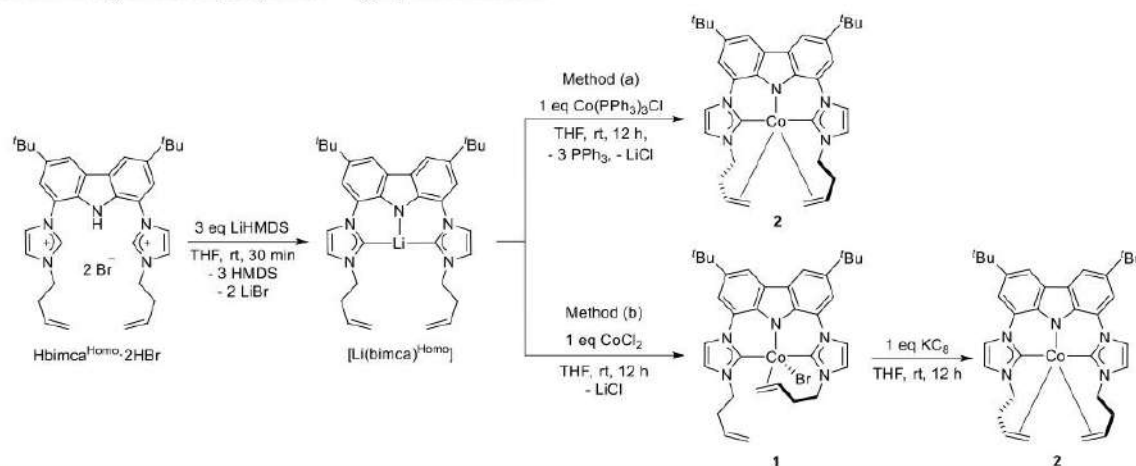
## RESULTS AND DISCUSSION

Our studies commenced with the preparation of complex **2** (Scheme 1). One challenge associated with the synthesis of

Received: January 10, 2020

Published: April 13, 2020

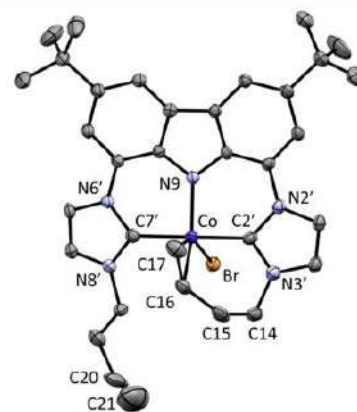


Scheme 1. Synthesis of  $[\text{Co}(\text{bimca}^{\text{Homo}})]$  by Two Methods

cobalt(I) complexes is their extreme air and moisture sensitivity. The ligand precursor  $\text{Hbimca}^{\text{Homo}}\cdot 2\text{HBr}$  and its lithium complex were generated according to previously reported methods.<sup>5b</sup> The transmetalation of  $[\text{Li}(\text{bimca}^{\text{Homo}})]$  was initially explored with the addition of 1.0 equiv of  $\text{CoCl}(\text{PPh}_3)_3$  in THF at room temperature. A color change from light yellow to red was observed immediately, and the single signal set in the  $^1\text{H}$  NMR spectrum of the *in situ* generated compound **2** confirmed a symmetrical coordination mode of the ligand. However, the complex obtained by this method always contained residual  $\text{PPh}_3$ , even after chromatography on silica in the glovebox.

An alternative route was inspired by the work of Braunstein<sup>8</sup> and Nishibayashi,<sup>9</sup> who demonstrated that addition of alkali-metal complexes to a solution of the Co(II) precursor resulted in the formation of four-coordinate cobalt halogen complexes. Reduction with  $\text{KC}_8$  at room temperature afforded the corresponding diamagnetic Co(I) complexes. To explore the analogous chemistry with our own ligand, paramagnetic  $[\text{Co}(\text{bimca}^{\text{Homo}})\text{Br}]$  (**1**) was prepared by treatment of freshly generated  $[\text{Li}(\text{bimca}^{\text{Homo}})]$  in THF with solid  $\text{CoCl}_2$ . We suppose that  $[\text{Co}(\text{bimca}^{\text{Homo}})\text{Cl}]$  is generated first, but instant halogen exchange occurs with the bromide anion still present in the solution from the ligand precursor  $\text{Hbimca}^{\text{Homo}}\cdot 2\text{HBr}$ . Brown single crystals of **1** suitable for X-ray diffraction were grown by slow evaporation from benzene at room temperature. Crystallographic characterization of the complex (Figure 1) reveals a distorted-trigonal-bipyramidal geometry at the cobalt center with one coordinated homoallyl moiety, the bromide ligand, and the carbazole nitrogen atom in the equatorial positions ( $\text{Br1}-\text{Co}-\text{c}(\text{C16,C17}) = 129.0^\circ$ ;  $c = \text{midpoint of bond}$ ). The NHC moieties take apical positions with a  $\text{C2}'-\text{Co}-\text{C7}'$  angle of  $174.0(2)^\circ$ . Both  $\text{Co}-\text{C}_{\text{NHC}}$  bond lengths are within the range reported for Co(II)- $\text{C}_{\text{NHC}}$  bonds of 1.791–2.152 Å.<sup>10</sup>

Due to the coordinating homoallyl substituent, one  $\text{Co}-\text{C}_{\text{NHC}}$  bond ( $\text{Co}-\text{C2}' = 1.917(4)$  Å) is shorter than the other ( $\text{Co}-\text{C7}' = 1.978(4)$  Å). Danopoulos<sup>11</sup> reported an intermediate bond length for the symmetric complex  $\text{Co}(\text{C}_{\text{NHC}}\text{NC}_{\text{NHC}})\text{Br}_2$  ( $\text{CNC} = 2,6\text{-bis}(\text{arylimidazolin-2-ylidene})\text{-pyridine}$ ) of 1.942(6) Å. In the coordinated homoallyl moiety, the  $\text{C}=\text{C}$  bond is elongated ( $\text{C16}-\text{C17} = 1.384(6)$  Å) due to



**Figure 1.** Solid-state molecular structure of **1**. Atoms are shown with anisotropic atomic displacement parameters at the 50% probability level. Hydrogen atoms are omitted for clarity. Selected bond lengths (Å) and angles (deg):  $\text{Co}-\text{N9} = 1.915(3)$ ,  $\text{Co}-\text{C2}' = 1.917(4)$ ,  $\text{Co}-\text{C7}' = 1.978(4)$ ,  $\text{Co}-\text{c}(\text{C16,C17}) = 1.950$ ,  $\text{Co}-\text{Br} = 2.515(1)$ ,  $\text{C16}-\text{C17} = 1.384(6)$ ,  $\text{C20}-\text{C21} = 1.274(10)$ ,  $\text{N9}-\text{Co}-\text{c}(\text{C16,C17}) = 119.3$ ,  $\text{N9}-\text{Co}-\text{Br} = 111.45(9)$ ,  $\text{C2}'-\text{Co}-\text{C7}' = 173.95(15)$ ,  $\text{Br}-\text{Co}-\text{c}(\text{C16,C17}) = 129.0$  ( $c = \text{midpoint of bond}$ ).

a good  $\pi$ -back-bonding ability of the cobalt center. This is the first structural report of a cobalt(II) NHC complex with a coordinated olefin.

DFT optimized structures fit very well with a low-spin state ( $S = 1/2$ ) at the cobalt center, which is reasonable, as the five donor atoms require at least one empty  $d$  orbital for this  $d^7$  electron configuration. Attempts to calculate a high-spin complex ( $S = 3/2$ ) resulted in dissociation of the olefin moiety and larger deviations from the experimentally determined bond lengths of the obtained structure (see the Supporting Information).

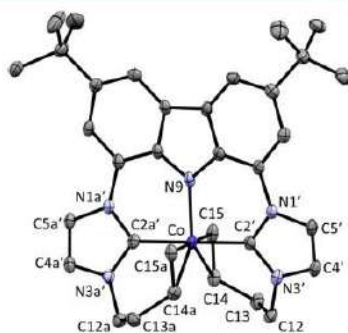
In addition, single crystals of the cobalt(III) complex  $[\text{Co}(\text{bimca}^{\text{Homo}})_2]\text{Br}$  with two coordinated  $\text{bimca}^{\text{Homo}}$  ligands in an octahedral fashion were generated as a side product in one of the experiments (see p S39 in the Supporting Information for a further description). Very few cobalt complexes bearing two bis(NHC)pincer ligands are known,



all of them in the oxidation state +III.<sup>12</sup> Starting from Co(II), they are presumably formed with traces of oxygen.

Complex **1** was successfully reduced with  $\text{KC}_8$  in THF at room temperature, and a red solution was obtained after completion. The raw product was purified by chromatography to yield the desired complex **2** as a red solid. Complex **2** is extremely air sensitive, and an obvious color change was observed with traces of oxygen. The  $^1\text{H}$  NMR spectrum of **2** in  $\text{THF-}d_8$  is consistent with a  $\text{C}_2$ -symmetric ligand environment with both *N*-homoallyl substituents coordinated to the cobalt(I) center. The signals of the olefinic protons are strongly shifted upfield (4.09–4.02 (H-14), 3.21 (H-15<sub>cis</sub>), 2.54 ppm (H-15<sub>trans</sub>)). The  $^{13}\text{C}$  NMR signal of the carbene carbon atoms at 191.1 ppm lie about 26 ppm at higher field than the signal of a comparable unsaturated free NHC (217.1 ppm<sup>13</sup>). About the same difference ( $\Delta \approx 22$  ppm) is found when the reported  $\text{Co}(\text{C}_{\text{NHC}}\text{C}_{\text{aryl}}\text{C}_{\text{NHC}})\text{N}_2$  complex<sup>14</sup> is compared.

Single crystals of **2** suitable for X-ray diffraction were grown from a concentrated solution of toluene and pentane at  $-30$  °C. The molecular structure confirms the structure derived from the NMR spectra in solution (Figure 2). The



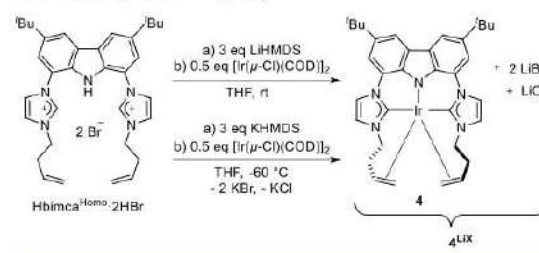
**Figure 2.** Solid-state molecular structure of **2**. Atoms are shown with anisotropic atomic displacement parameters at the 50% probability level. One cocrystallized toluene and the hydrogen atoms are omitted for clarity. Selected bond lengths (Å) and angles (deg) (mean of the two independent enantiomers in the unit cell): Co–N9 = 1.947(4), Co–C2' = 1.911(5), Co–C2a' = 1.913(5), Co–C15 = 2.043(5), Co–C14 = 2.092(5), Co–C15a = 2.037(5), Co–C14a = 2.084(5), C14–C15 = 1.401(8), C14a–C15a = 1.400(7); N9–Co–c(C15,C14) = 110.0, N9–Co–c(C15a,C14a) = 110.8(5), c(C15,C14)–Co–c(C15a,C14a) = 139.2, C2'–Co–C2a' = 179.0(3) (c = midpoint of bond).

coordination geometry at the Co(I) center is trigonal bipyramidal with both olefin moieties and the carbazole nitrogen taking the equatorial positions and both NHC moieties the axial positions ( $\text{C2}'\text{--Co--C2a}' = 179.0(3)^\circ$ ,  $\text{c}(\text{C15},\text{C14})\text{--Co--c}(\text{C15}',\text{C14}') = 139.2^\circ$ ; c = midpoint of bond). The Co– $\text{C}_{\text{NHC}}$  bond lengths (Co–C2' = 1.911(5) Å, Co–C2a' = 1.913(5) Å) are comparable to those of reported  $(\text{C}_{\text{NHC}}\text{NC}_{\text{NHC}})$ -pincer cobalt(I) complexes,<sup>3,9</sup> while the Co–N bond (1.947(4) Å) in **2** is substantially longer than the pyridine Co–N bond (e.g., 1.839(4) Å<sup>9</sup>), possibly due to steric reasons. The C14–C15 (1.401(8) Å) and C14'–C15' bond lengths (1.400(7) Å) are pronouncedly elongated in comparison to the noncoordinated olefinic bond in the Co(II) complex **1** or in the respective imidazolium salt<sup>15</sup> (1.28–1.32

Å), which confirms a certain amount of metallacyclopropane character in **2**.

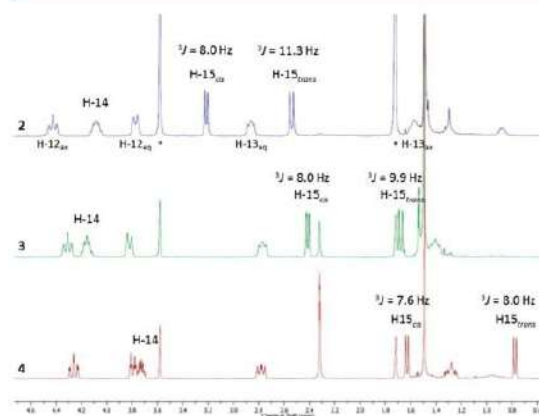
*In situ* generation of the iridium complex **4**<sup>LIX</sup> was achieved by applying the same route as for  $[\text{Rh}(\text{bimca}^{\text{Homo}})]$  (**3**),<sup>5b</sup> which is deprotonation of  $\text{Hbimca}^{\text{Homo}}\cdot 2\text{HBr}$  with LiHMDS and subsequent transmetalation with  $[\text{Ir}(\mu\text{-Cl})(\text{COD})]_2$  (Scheme 2). To obtain the pure complex **4**, the trans-

### Scheme 2. Synthesis of both *In Situ* Generated **4**<sup>LIX</sup> and Isolated $[\text{Ir}(\text{bimca}^{\text{Homo}})]$ (**4**)



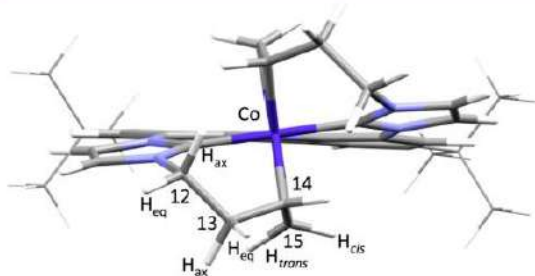
metalation step was conducted at low temperature using the potassium complex  $[\text{K}(\text{bimca}^{\text{Homo}})]$  generated *in situ* by deprotonation of  $\text{Hbimca}^{\text{Homo}}\cdot 2\text{HBr}$  with KHMDS at  $-60$  °C. In contrast to lithium halides, the potassium halides that formed could be readily removed by filtration.

The molecular structure of **4** is isostructural with **2**, as revealed by NMR spectroscopy, showing a symmetrical coordination mode of the ligand. All signals could be assigned by means of 2D and NOE experiments. The coordination of both double bonds and both carbene moieties to the Ir center is confirmed by the upfield shift of the respective signals in the  $^1\text{H}$  NMR spectrum (3.77–3.69 (H-14), 1.63 (H-15<sub>cis</sub>), 0.78 ppm (H-15<sub>trans</sub>)) as well as in the  $^{13}\text{C}$  NMR spectrum (39.7 (C15) and 27.7 ppm (C14)). The carbene signal is found at the typical 164.5 ppm. In comparison with the  $^1\text{H}$  NMR spectra of complexes **2** (Co) and **3** (Rh) (Figure 3) the stronger metallacyclopropane character of complex **4** can be derived from the stronger high-field shift of the olefinic proton signals from **2** to **4** as well as the decreasing  $^3J_{\text{HH}}$  coupling constant of the olefinic protons from 8.0 (*cis*) and 11.3 Hz



**Figure 3.**  $^1\text{H}$  NMR spectra (section) of the *N*-homoallyl signals of **2** (Co), **3** (Rh), and **4** (Ir) and the  $^3J_{\text{HH}}$  coupling constants in comparison (the asterisk denotes  $\text{THF-}d_7$ ).

(*trans*) in **2** to only 7.6 (*cis*) and 8.0 Hz (*trans*) in **4** due to the reduced *s* character of the olefinic carbon atoms (from  $sp^2$  to partial  $sp^3$  hybridization). This reflects the tendency of 5d metals to form stronger metal–C bonds and the increased stability of the higher oxidation state. DFT calculations of complexes **2–4** confirm the experimental results of the bond lengths and angles from the X-ray structure analysis of **2** (Figure 4). The increasing metallacyclopropane character from

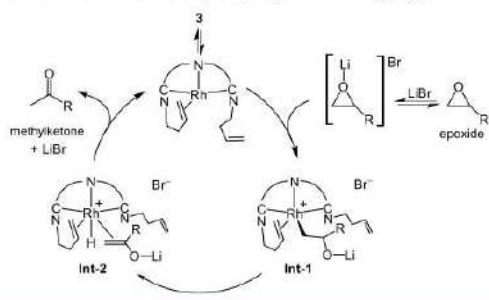


**Figure 4.** Calculated structure (DFT-D3) of **2** with *t*-Bu groups depicted in wireframe for clarity. The geometry optimized structures of **3** and **4** are isostructural. The olefinic bond length C14–C15 (mean) is increasing from **2** (1.413 Å) to **3** (1.424 Å) and **4** (1.446 Å).

the cobalt to the iridium complex is also displayed in the increasing C=C bond lengths of the coordinated homoallyl moieties from 1.413 (**2**) to 1.446 Å (**4**).

**Reactivity of [M(bimca<sup>Homo</sup>)] (M = Co (**2**), Rh (**3**), Ir (**4**)) toward Epoxide Isomerization.** As the rhodium complex **3** was found to be a highly reactive nucleophilic catalyst for rearrangement of terminal epoxides into methyl ketones already at room temperature, we were eager to test the catalytic reactivity of its analogues **2** and **4** in the same reaction. The general mechanism for the nucleophilic isomerization of terminal epoxides catalyzed by **3** requires the dissociation of one homoallyl moiety from the rhodium center to generate the nucleophilic, catalytically active species (Scheme 3).<sup>5b</sup> This is followed by nucleophilic ring opening

**Scheme 3.** Mechanism of the Nucleophilic Epoxide Isomerization with Catalyst [Rh(bimca<sup>Homo</sup>)] (**3**)



of the epoxide preactivated by the Lewis acid cocatalyst to generate the Rh(III) intermediate **Int-1**.<sup>5c</sup> After  $\beta$ -hydride elimination to **Int-2**,<sup>5a</sup> the desired methyl ketone is obtained by a formal reductive elimination and release of the catalytically active species, which can be stabilized by recoordination of the *N*-homoallyl moiety.

As initial catalytic attempts with complexes **2** and **4** and 1,2-epoxyhexane (**5a**) at room temperature did not lead to any conversion after 6 days, further catalytic experiments were conducted at 80 °C with 5 mol % of the catalyst and 10 mol % of LiBr in  $C_6D_6$ . The results of the epoxide isomerizations with catalysts **2** and **4** are summarized in Table 1. When **2** was

**Table 1.** Regioselective Isomerization of Terminal Epoxides with [M(bimca<sup>Homo</sup>)]<sup>a</sup>

Entry	Epoxide	[Cat.]	H <sub>2</sub> (bar)	Time	Conversion (%)	Yield (%)
1	5a	2	-	6 days	32	18
2		3	-	30 min	100	92
3		4	-	6 days	100	92
4		2	1	24 h	19	11
5		4	1	24 h	81	52
6	5b	2	-	6 days	0	0
7		3	-	30 min	100	88
8 <sup>b</sup>		4	-	6 days <sup>b</sup>	100	26
9		2	1	24 h	11	5
10		4	1	24 h	75	38

<sup>a</sup>Reactions were carried out in J. Young NMR tubes with 10  $\mu$ L of THF-*d*<sub>6</sub>, and the yield of **6** was calibrated to 1,3,5-trimethoxybenzene (internal standard). <sup>b</sup>After 24 h: 20% conversion and 13% yield.

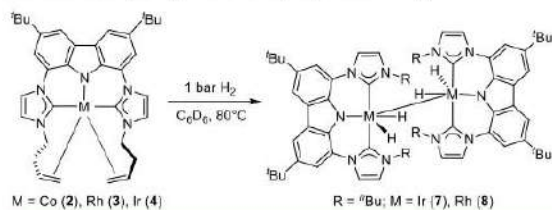
applied using 1,2-epoxyhexane (**5a**) as the substrate, the isomerization was surprisingly slow and only an 18% yield was obtained after 6 days (entry 1). No conversion was obtained with the more challenging styrene oxide **5b**, which contains a less electrophilic  $\beta$ -C atom and can be easily isomerized by Lewis acids to the aldehyde (entry 6). Under identical conditions (80 °C), the reactions with catalyst **3** were completed already within 30 min (entries 2 and 7) and high yields of 2-hexanone (**6a**) and acetophenone (**6b**) were obtained.<sup>16</sup> We suppose that the low reactivity of the Co(I) complex **2** results from a higher energy barrier of **2** in the nucleophilic ring opening to form the Co(III) intermediate. In reports from Eisenman and Coates on the nucleophilic epoxide isomerization, the active species is  $[Co(CO)_4]^-$  (Co(-I)), which explains the higher reactivity apart from using a stronger Lewis acid.<sup>17</sup> Iridium(I) complexes, which have a considerably lower redox potential, should react much more easily, as the oxidative addition of the epoxide (e.g., by a nucleophilic ring-opening mechanism) is the rate-limiting step in the Rh catalysis. Therefore, we tested **4** in the isomerization of **5a** to yield 2-hexanone in 92% yield (entry 3), but surprisingly, the reaction proceeded much more slowly (6 days) than with **3** ( $\leq 30$  min). With substrate **5b**, only a 26% yield was achieved despite full conversion (entry 8). This can be explained by a higher degree of side reactions: a polymerization might arise from more stable Ir(III) intermediates analogous to **Int-1** or



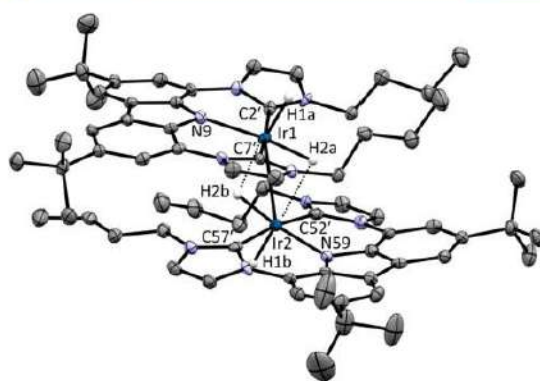
**Int-2** (Scheme 3) that in addition slow down the  $\beta$ -hydride elimination step. The lower activity of complex **4** (6 days for full conversion) can be rationalized by the higher stability of the coordinated *N*-homoallyl moieties (stronger metallocyclopropane character), one of which has to dissociate to form the nucleophilic active species. Therefore, we tried to run the reactions in the presence of 1 bar of hydrogen, so that the homoallyl moieties could be hydrogenated *in situ* and a highly reactive nucleophilic metal complex could form. On the other hand, the formation of hydrido complexes could reduce the activity or lead to side reactions. Indeed, when the reactions with **2** or **4** were conducted in the presence of 1 bar of hydrogen, we observed an enhanced reactivity at the beginning with 11% and 52% yields for substrate **5a** (entries 4 and 5) and 5% and 38% for the less electrophilic substrate **5b** (entries 9 and 10) after 24 h. However, the reaction stops and cannot be completed by extending the reaction time. The higher conversion with catalyst **4** can be attributed to the formation of 2-phenylethanol (confirmed by  $^1\text{H}$  NMR spectroscopy) as well as some degree of polymerization. Unfortunately, neither complex **2** nor **4** was able to compete with our previously reported rhodium catalyst **3**.<sup>5b</sup>

**Reactivity of [M(bimca<sup>Homo</sup>)] (M = Co, Rh, Ir) with H<sub>2</sub>.** To elucidate whether the *N*-homoallyl moieties of complexes **2–4** can indeed be hydrogenated in the presence of hydrogen under the catalytic conditions, we exposed a solution of **4** in benzene-*d*<sub>6</sub> to 1 bar of H<sub>2</sub> at 80 °C (Scheme 4), which resulted in a color change from yellow to dark red after 24 h and the formation of red crystals upon cooling to ambient temperature.

#### Scheme 4. Hydrogenation of [M(bimca<sup>Homo</sup>)]



The X-ray structure analysis reveals a dimeric structure in which the former *N*-homoallyl moieties are fully hydrogenated and residual electron density at the metal indicates the formation of the iridium(III) hydrido complex **7** (Figure 5). As it can be expected that the hydrido ligands cannot be identified with certainty from X-ray data, the Ir–H bond lengths were fixed at the value obtained from DFT calculations on the basis of the X-ray structure (with all bonds and angles fixed, except of those of the hydrido ligands; see the Supporting Information). The structural motif [Ir(H)( $\mu$ -H)]<sub>2</sub> has been found before, for example, in phosphine complexes,<sup>18,19</sup> and the Ir–Ir distance of 2.784 Å in **7** is comparable to the distance in those complexes (2.73 and 2.77 Å), but in contrast, the hydride atoms in **7** are less symmetrically bridged, possibly for steric reasons. It is also noteworthy that the more flexible bis(phosphinomethyl)carbazolide ligand (PNP) in an analogous complex by Yamashita and co-workers led to a bridging instead of a pincer-type ligand coordination.<sup>18</sup> The hydrogen bridges in **7** measure 2.50 Å (Ir1–H2b) and 2.53 Å (Ir2–H2a), which was also confirmed by DFT geometry optimizations without constraints. In addition, London dispersion<sup>20</sup> seems to play an important role for the dimer



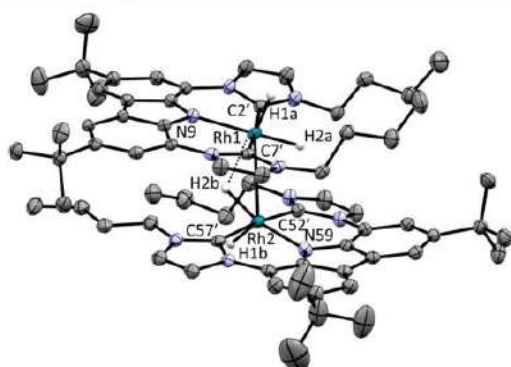
**Figure 5.** Solid-state molecular structure of **7**. Atoms are shown with anisotropic atomic displacement parameters at the 50% probability level. The co-crystallized benzene molecule and the hydrogen atoms (except for the hydrido ligands) are omitted for clarity. Selected bond lengths (Å) and angles (deg): Ir1–N9 = 2.059(3), Ir1–C2' = 2.035(4), Ir1–C7' = 2.027(4), Ir2–N59 = 2.059(3), Ir2–C52' = 2.035(4), Ir2–C57' = 2.027(4), Ir1–Ir2 = 2.7836(2); N9–Ir1–Ir2 = 115.21(9), N59–Ir2–Ir1 = 114.10(9). The metal–hydrogen bond lengths and angles were fixed (Ir1–H1a = 1.58, Ir1–H2a = 1.63, Ir2–H1b = 1.58, Ir2–H2b = 1.63) on the basis of DFT calculations. Hydrogen bridges: 2.50 Å (Ir1–H2b) and 2.53 Å (Ir2–H2a).

formation, as the energy difference between the monomers and the dimer strongly favors the dimer (see the Supporting Information). The intramolecular distances of the carbazolide planes at Ir1 and Ir2 are between 3.71 and 4.15 Å (measured from the respective pyrrolide centers). However, intermolecular London dispersion is pronounced in the crystal. The distance between the coplanar carbazolide planes at Ir2 and Ir2# measures only 2.63 Å. The metal–carbene bond lengths Ir–C<sub>NHC</sub> (2.03 Å, mean) are comparable with those of a C<sub>NHC</sub>CC<sub>NHC</sub>–Ir complex from Braunschweig.<sup>21</sup>

Also with bis(NHC)Rh<sup>I</sup> complexes, the formation of hydrido Rh(III) complexes is to be expected.<sup>22</sup> Under analogous conditions, the reaction with rhodium complex **3** leads to the formation of red single crystals as well. An X-ray structure analysis confirms the successful hydrogenation of the *N*-homoallyl moieties and formation of the dimer **8** that is isostructural with complex **7** (Figure 6). All intra (3.64 and 4.10 Å)- and intermolecular (2.63 Å) distances of the carbazolide planes are comparable with those of the iridium complex **7**. The only striking difference from complex **7** is the longer metal–metal distance of 2.934 Å that also comes with 6° more acute N–Rh–Rh angles of 107.5° (N9–Rh1–Rh2) and 109.0° (N59–Rh2–Rh1). As already performed in the X-ray data refinement of complex **7**, the Rh–H bond lengths and angles were calculated by DFT methods by fixing all bonds and angles on the basis of the X-ray structure analysis except for the hydrido ligands. At Rh1, a square-pyramidal arrangement and at Rh2 a Y-shaped distorted-trigonal-bipyramidal coordination geometry was found (the latter is also obtained by DFT calculations for a monomeric species). Thus, only one intramolecular hydrogen bridge is found (Rh1–H2b = 2.54 Å; Rh2–H2a = 2.79 Å), which explains the longer Rh1–Rh2 distance in comparison to complex **7**.

Hydrogenation of the cobalt complex **2** under identical conditions led to formation of a dark green solution whose  $^1\text{H}$  NMR spectrum shows broad peaks between 16 and –9 ppm





**Figure 6.** Solid-state molecular structure of **8**. Atoms are shown with anisotropic atomic displacement parameters at the 50% probability level. The cocrystallized benzene molecule and the hydrogen atoms (except for the hydrido ligands) are omitted for clarity. The crystal structures of **7** and **8** are isomorphous. Selected bond lengths (Å) and angles (deg): Rh1–N9 = 2.062(2), Rh1–C2' = 2.037(2), Rh1–C7' = 2.029(2), Rh2–N59 = 2.035(2), Rh2–C52' = 2.036(2), Rh2–C57' = 2.029(2), Rh1–Rh2 = 2.9335(3); N9–Rh1–Rh2 = 107.53(5), N59–Rh2–Rh1 = 108.97(5). The metal–hydrogen bond lengths and angles were fixed at Rh1–H1a = 1.54, Rh1–H2a = 1.58, Rh2–H1b = 1.54, Rh2–H2b = 1.58 on the basis of DFT calculations. Hydrogen bridges: 2.54 Å (Rh1–H2b) and 2.79 Å (Rh2–H2a).

possibly due to a paramagnetic influence. More detailed analyses are beyond the scope of this investigation.

## CONCLUSIONS

On the basis of the pentadentate pincer bis-NHC ligand  $\text{bimca}^{\text{Homo}}$ , the corresponding cobalt complex **2** was successfully synthesized by a deprotonation–transmetalation–reduction sequence starting from  $\text{CoCl}_2$  which involves  $[\text{Co}(\text{bimca}^{\text{Homo}})\text{Br}]$  (**1**), in which the  $\text{bimca}^{\text{Homo}}$  ligand shows a tetradentate coordination mode. The iridium catalyst **4** was synthesized straightforwardly by transmetalation of  $[\text{Li}(\text{bimca}^{\text{Homo}})]$  with  $[\text{Ir}(\mu\text{-Cl})(\text{COD})]_2$ . In contrast to the highly reactive rhodium analogue **3**, complexes **2** and **4** were much less active in the nucleophilic epoxide isomerization. This can be ascribed to the lower oxidation potential of **2** in comparison to **3** and in the case of **4** to a higher oxidation potential, which is also displayed in the increasing metalacyclopropane character of the coordinated *N*-homoallyl moieties. When the reaction was carried out in the presence of 1 bar of  $\text{H}_2$ , an increased activity was observed; however, this was at the cost of side reactions. The successful hydrogenation of the *N*-homoallyl to *N*-*n*-butyl substituents and the formation of hydrido pincer complexes under these conditions was confirmed by the X-ray structure analyses of **7** (Ir) and **8** (Rh). Further investigations of these interesting complexes will be the subject of future work in our group.

## EXPERIMENTAL SECTION

**General Information.** Unless otherwise noted, all reactions were carried out under an argon atmosphere in dried and degassed solvents using Schlenk techniques. All glassware was stored in a preheated oven prior to use. Toluene, pentane, benzene, and tetrahydrofuran were purchased from Sigma-Aldrich and dried using an MBraun SPS-800 solvent purification system. The lithium and potassium bases used were obtained from commercial suppliers, dried under vacuum, and used without further purification.  $\text{KC}_8^{23}$  and  $\text{Rh}(\text{bimca}^{\text{Homo}})^{\text{Sb}}$

were synthesized, and  $[\text{Li}(\text{bimca}^{\text{Homo}})]^{\text{Sb}}$  and  $[\text{K}(\text{bimca}^{\text{Homo}})]^{\text{Sb}}$  were generated *in situ* according to the literature. Liquid chemicals from commercial suppliers were degassed through freeze–pump–thaw cycles prior to use.  $^1\text{H}$  and  $^{13}\text{C}$  NMR spectra were recorded using a Bruker AVANCE II+ 400 spectrometer. Chemical shifts  $\delta$  (ppm) are given relative to the solvent's residual proton and carbon signals, respectively: THF- $d_6$ , 3.58 ppm ( $^1\text{H}$  NMR) and 67.57 ppm ( $^{13}\text{C}$  NMR);  $\text{C}_6\text{D}_6$ , 7.16 ppm ( $^1\text{H}$  NMR) and 128.39 ppm ( $^{13}\text{C}$  NMR).  $^1\text{H}$  NMR data for diamagnetic compounds are reported as follows: chemical shift, multiplicity (s = singlet, d = doublet, t = triplet, q = quartet, br = broad, m = multiplet), coupling constants (Hz), integration, assignment. The assignment of peaks is based on 2D NMR correlation and NOE spectra.

**X-ray Data Collection and Structure Analysis.** Suitable crystals for the X-ray analysis were obtained as described below. Data collection (except for  $[\text{Co}(\text{bimca}^{\text{Homo}})_2]\text{Br}$ ; see p S39 in the Supporting Information) was carried out on a Bruker APEX Duo CCD with an Incoatec  $\mu\text{S}$  Microsource with a Quazar MX mirror using Mo  $K\alpha$  radiation ( $\lambda = 0.71073$  Å) and a graphite monochromator. Corrections for absorption effects were applied using SADABS.<sup>24a</sup> All structures were solved by direct methods using SHELXT and refined using SHELXL.<sup>24</sup> In the case of structure **1** and  $[\text{Co}(\text{bimca}^{\text{Homo}})_2]\text{Br}$  the SQUEEZE routine<sup>25</sup> was applied for disordered solvent.

**Synthesis of  $[\text{Co}(\text{bimca}^{\text{Homo}})\text{Br}]$  (**1**).**  $\text{CoCl}_2$  (9.5 mg, 73  $\mu\text{mol}$ , 1 equiv) was added to a previously prepared solution of  $[\text{Li}(\text{bimca}^{\text{Homo}})]$  (73.4  $\mu\text{mol}$ ) at room temperature. The solution was shaken for 2 min. After 12 h, the brown crystals that appeared were filtered, washed with THF (0.5 mL  $\times$  3), and dried *in vacuo*. Single crystals suitable for X-ray diffraction were obtained (39.1 mg). Although C, H, N analysis reveals residual impurities, most probably LiBr and THF, the material can be used directly in the next step. Anal. Calcd for  $\text{C}_{34}\text{H}_{40}\text{BrCoN}_5$ : 0.25LiBr·1.25 $\text{C}_6\text{H}_6\text{O}$ : C, 60.88; H, 6.55; N, 9.10. Found: C, 61.02; H, 6.30; N, 8.95.

**Synthesis of  $[\text{Co}(\text{bimca}^{\text{Homo}})_2]$  (**2**) from  $[\text{Co}(\text{bimca}^{\text{Homo}})\text{Br}]$  (**1**).** To a suspension of  $[\text{Co}(\text{bimca}^{\text{Homo}})\text{Br}]$  (**1**) (39.1 mg from the material obtained above) in THF (2.0 mL) was added  $\text{KC}_8$  (8.0 mg, 59  $\mu\text{mol}$ ). The suspension was stirred at room temperature for 12 h in an argon-filled glovebox. After completion of the reaction, the mixture was filtered with a syringe filter and purified by column chromatography using THF as eluent in the glovebox.  $[\text{Co}(\text{bimca}^{\text{Homo}})_2]$  (**2**) containing 0.75 mol of THF (13.0 mg, 21  $\mu\text{mol}$ , 28% yield over two steps) was obtained as a red solid after removal of the solvent. Single crystals suitable for X-ray diffraction were grown from a concentrated solution of **2** in toluene and pentane at  $-30$  °C.  $^1\text{H}$  NMR (400 MHz, THF- $d_6$ ):  $\delta$  8.00 (d,  $^3J_{\text{HH}} = 1.3$  Hz, 2H, H-4/5), 7.79 (d,  $^3J_{\text{HH}} = 1.0$  Hz, 2H, H-5'), 7.37 (d,  $^3J_{\text{HH}} = 1.3$  Hz, 2H, H-2/7), 6.91 (d,  $^3J_{\text{HH}} = 1.0$  Hz, 2H, H-4'), 4.38 (br ps  $t_{2/3}^2/3J_{\text{HH}} = 12.6$  Hz, 2H, H-12 $_{\text{ax}}$ ), 4.11–4.02 (m, 2H, H-14), 3.72 (br d,  $^3J_{\text{HH}} = 12.3$  Hz, 2H, H-12 $_{\text{eq}}$ ), 3.21 (d,  $^3J_{\text{HH}} = 8.0$  Hz, 2H, H-15 $_{\text{ax}}$ ), 2.86–2.80 (m, 2H, H-13 $_{\text{eq}}$ ), 2.54 (br d,  $^3J_{\text{HH}} = 11.3$  Hz, 2H, H-15 $_{\text{trans}}$ ), 1.59–1.50 (m, 2H, H-13 $_{\text{ax}}$ ), 1.50 (s, 18H, H-11).  $^{13}\text{C}$  NMR (101 MHz, THF- $d_6$ ):  $\delta$  191.1 (C2'), 138.6 (C3/6), 136.5 (C1a/8a), 128.5 (C4a/5a), 125.4 (C1/8), 122.4 (C4'), 115.9 (C5'), 115.0 (C4/5), 107.6 (C2/7), 66.1 (C15), 57.5 (C14), 50.8 (C12), 35.6 (C13 and C10), 33.0 (C11). Anal. Calcd for  $\text{C}_{34}\text{H}_{40}\text{N}_5\text{Co}\cdot 0.75\text{C}_6\text{H}_6\text{O}$ : C, 70.35; H, 7.34; N, 11.09. Found: C, 70.49; H, 7.47; N, 11.08.

**Synthesis of  $[\text{Co}(\text{bimca}^{\text{Homo}})_2]$  (**2**) from  $[\text{Co}(\text{PPh}_3)_3\text{Cl}]$ .** To a freshly generated solution of  $[\text{Li}(\text{bimca}^{\text{Homo}})]$  (29.3  $\mu\text{mol}$ ) in THF (0.6 mL) was added  $[\text{Co}(\text{PPh}_3)_3\text{Cl}]$  (25.6 mg, 29.3  $\mu\text{mol}$ ). The mixture was shaken until the cobalt precursor was fully dissolved. After completion of the reaction, the mixture was purified by column chromatography using THF as eluent in an argon-filled glovebox.  $[\text{Co}(\text{bimca}^{\text{Homo}})_2]$  (**2**) was obtained as a red solid after removal of the solvent; however, it contained residual  $\text{PPh}_3$ . The NMR data correspond to the results obtained by starting with **1**.

**In Situ Generation of LiX Containing  $[\text{Ir}(\text{bimca}^{\text{Homo}})]$  ( $4^{\text{LiX}}$ ).**  $[\text{Ir}(\mu\text{-Cl})(\text{COD})]_2$  (9.7 mg, 15  $\mu\text{mol}$ ) was added to a previously prepared solution of  $[\text{Li}(\text{bimca}^{\text{Homo}})]$  (29  $\mu\text{mol}$ ) in THF (0.6 mL) at room temperature. The solution was stirred for 30 min. *In situ*



generated  $[\text{Ir}(\text{bimca}^{\text{Homo}})]$  (**4**<sup>LX</sup>) was obtained as an orange solution in quantitative yield as determined by NMR spectroscopy. <sup>1</sup>H NMR (400 MHz, THF-*d*<sub>6</sub>): δ 8.02 (d, <sup>3</sup>J<sub>HH</sub> = 1.5 Hz, 2H, H-4/5), 7.94 (d, <sup>3</sup>J<sub>HH</sub> = 2.3 Hz, 2H, H-5'), 7.53 (d, <sup>3</sup>J<sub>HH</sub> = 1.5 Hz, 2H, H-2/7), 7.11 (d, <sup>3</sup>J<sub>HH</sub> = 2.3 Hz, 2H, H-4'), 4.26 (dt, <sup>2</sup>J<sub>HH</sub> = 12.6 Hz, <sup>3</sup>J<sub>HH</sub> = 2.7 Hz, 2H, H-12<sub>ax</sub>), 3.80 (dt, <sup>2</sup>J<sub>HH</sub> = 12.6 Hz, <sup>3</sup>J<sub>HH</sub> = 3.2 Hz, 2H, H-12<sub>eq</sub>), 3.77–3.69 (m, 2H, H-14), 2.82–2.75 (m, 2H, H-13<sub>eq</sub>), 1.63 (d, <sup>3</sup>J<sub>HH</sub> = 7.6 Hz, 2H, H-15<sub>ax</sub>), 1.49 (s, 18H, H-11), 1.33–1.24 (m, 2H, H-13<sub>ax</sub>), 0.78 (br d, <sup>3</sup>J<sub>HH</sub> = 8.0 Hz, 2H, H-15<sub>ax</sub>). <sup>13</sup>C NMR (101 MHz, THF-*d*<sub>6</sub>): δ 164.5 (C2'), 137.3 (C1a/8a), 136.1 (C3/6), 128.1 (C4a/5a), 126.4 (C1/8), 121.1 (C4'), 115.7 (C5'), 115.2 (C4/5), 109.6 (C2/7), 53.8 (C12), 39.7 (C15), 35.6 (C10), 35.3 (C13), 32.9 (C11), 27.7 (C14).

**Synthesis of Salt-Free  $[\text{Ir}(\text{bimca}^{\text{Homo}})]$  (**4**).**  $[\text{Ir}(\mu\text{-Cl})(\text{COD})]_2$  (9.8 mg, 15 μmol) was added to an *in situ* generated solution of  $[\text{K}(\text{bimca}^{\text{Homo}})]$  (29.3 μmol) at –60 °C. The solution was stirred for 30 min. The potassium salts that formed were filtered off, and the filtrate was dried *in vacuo*. The residue was washed with pentane (2 mL × 3) and dried again *in vacuo* to give complex **4** as a yellow solid (5.7 mg, 8.1 μmol, 55% yield). The NMR data correspond to the results obtained by using  $[\text{Li}(\text{bimca}^{\text{Homo}})]$ . Anal. Calcd for C<sub>34</sub>H<sub>40</sub>IrN<sub>3</sub>·0.85C<sub>6</sub>H<sub>8</sub>O: C, 58.17; H, 6.11; N, 9.07. Found: C, 58.04; H, 6.26; N, 9.24.

**General Procedure for Epoxide Isomerization with  $[\text{M}(\text{bimca}^{\text{Homo}})]$ .** In an argon-filled glovebox a J. Young NMR tube was charged with a solution of the epoxide (40 μmol), LiBr (4.0 μmol with 10 μL of THF-*d*<sub>6</sub>),  $[\text{M}(\text{bimca}^{\text{Homo}})]$  (2.0 μmol), and a certain amount of 1,3,5-trimethoxybenzene as internal standard in C<sub>6</sub>D<sub>6</sub> (0.4 mL). The reaction mixture was heated at 80 °C for the given reaction time and analyzed by <sup>1</sup>H NMR spectroscopy.

**General Procedure for Epoxide Isomerization with  $[\text{M}(\text{bimca}^{\text{Homo}})]$  in the Presence of 1 bar of H<sub>2</sub>.** In an argon-filled glovebox a J. Young NMR tube was charged with a solution of the epoxide (40 μmol), LiBr (4.0 μmol with 10 μL of THF-*d*<sub>6</sub>),  $[\text{M}(\text{bimca}^{\text{Homo}})]$  (2.0 μmol), and a certain amount of the internal standard (1,3,5-trimethoxybenzene) in C<sub>6</sub>D<sub>6</sub> (0.4 mL). The tube was sealed, brought outside of the glovebox, and attached to a Schlenk line. After a freeze–pump–thaw cycle with liquid nitrogen, the tube was charged with 1 bar of H<sub>2</sub> at room temperature. The reaction mixture was heated at 80 °C for 24 h and analyzed by <sup>1</sup>H NMR spectroscopy.

**Formation of  $[\text{Ir}(\text{bimca}^{\text{n-Bu}})(\text{H})_2]_2$  (**7**).** In an argon-filled glovebox a J. Young NMR tube was charged with a solution of  $[\text{Ir}(\text{bimca}^{\text{Homo}})]$  (5.7 mg, 8.0 μmol) in C<sub>6</sub>D<sub>6</sub> (0.5 mL). The tube was sealed, brought outside of the glovebox, and attached to a Schlenk line. After a freeze–pump–thaw cycle with liquid nitrogen, the tube was charged with 1 bar of H<sub>2</sub> at room temperature and heated at 80 °C for 24 h. Red single crystals suitable for X-ray diffraction were obtained upon cooling to room temperature that confirm full hydrogenation of the homoallyl chain under the reaction conditions of the epoxide isomerization as a preliminary result. Further characterization was hampered by their slow solubility.

**Formation of  $[\text{Rh}(\text{bimca}^{\text{n-Bu}})(\text{H})_2]_2$  (**8**).** In an argon-filled glovebox a J. Young NMR tube was charged with a solution of  $[\text{Rh}(\text{bimca}^{\text{Homo}})]$  (5.0 mg, 8.0 μmol) in C<sub>6</sub>D<sub>6</sub> (0.5 mL). The tube was sealed, brought outside of the glovebox, and attached to a Schlenk line. After a freeze–pump–thaw cycle with liquid nitrogen, the tube was charged with 1 bar of H<sub>2</sub> at room temperature and heated at 80 °C for 24 h. Red single crystals suitable for X-ray diffraction were obtained upon cooling to room temperature that confirm full hydrogenation of the homoallyl chain under the reaction conditions of the epoxide isomerization as a preliminary result. Further characterization was hampered by their slow solubility.

An identical procedure using the cobalt complex **2** resulted in a green solution, whose <sup>1</sup>H NMR spectrum showed broad peaks between 16 and –9 ppm indicating paramagnetic character.

**DFT Calculations.** The calculations were performed on the basis of density functional theory at the BP86/def2-SVP and/or BP86/def2-TZVP<sup>26</sup> level implemented in Turbomole.<sup>27</sup> The RI approximation<sup>28</sup> was used all over, and the Grimme dispersion correction

D3-BJ<sup>29</sup> was used where indicated. Minimum structures (except for the dimeric structures) were verified at the BP86/def2-SVP level by calculating the Hessian matrix and ensuring that it had no imaginary frequency.

## ■ ASSOCIATED CONTENT

### Supporting Information

The Supporting Information is available free of charge at <https://pubs.acs.org/doi/10.1021/acs.organomet.0c00018>.

NMR spectra of all new diamagnetic compounds, catalysis results, X-ray crystal data for complexes **1**, **2**, **7**, **8** and  $[\text{Co}(\text{bimca}^{\text{Homo}})_2]\text{Br}$  and details of all calculated structures (PDF)

Cartesian coordinates of the calculated structures (XYZ)

## Accession Codes

CCDC 1976073–1976076 contain the supplementary crystallographic data for this paper. These data can be obtained free of charge via [www.ccdc.cam.ac.uk/data\\_request/cif](http://www.ccdc.cam.ac.uk/data_request/cif), or by emailing [data\\_request@ccdc.cam.ac.uk](mailto:data_request@ccdc.cam.ac.uk), or by contacting The Cambridge Crystallographic Data Centre, 12 Union Road, Cambridge CB2 1EZ, UK; fax: +44 1223 336033.

## ■ AUTHOR INFORMATION

### Corresponding Author

**Doris Kunz** – Institut für Anorganische Chemie, Eberhard Karls Universität Tübingen, 72076 Tübingen, Germany; [orcid.org/0000-0002-4388-6804](https://orcid.org/0000-0002-4388-6804); Email: [Doris.Kunz@uni-tuebingen.de](mailto:Doris.Kunz@uni-tuebingen.de)

### Authors

**Yingying Tian** – Institut für Anorganische Chemie, Eberhard Karls Universität Tübingen, 72076 Tübingen, Germany; [orcid.org/0000-0001-8894-576X](https://orcid.org/0000-0001-8894-576X)

**Theo Maulbetsch** – Institut für Anorganische Chemie, Eberhard Karls Universität Tübingen, 72076 Tübingen, Germany

**Ronja Jordan** – Institut für Anorganische Chemie, Eberhard Karls Universität Tübingen, 72076 Tübingen, Germany

**Karl W. Törnroos** – Department of Chemistry, University of Bergen, 5007 Bergen, Norway; [orcid.org/0000-0001-6140-5915](https://orcid.org/0000-0001-6140-5915)

Complete contact information is available at:

<https://pubs.acs.org/10.1021/acs.organomet.0c00018>

### Notes

The authors declare no competing financial interest.

## ■ ACKNOWLEDGMENTS

Y.T. thanks the China Scholarship Council (CSC) for a predoctoral fellowship. T.M. thanks the MWK-BW for a fellowship (Landesgradurierterförderung). We are grateful to the Swiss-Norwegian beamlines at the ESRF, Grenoble, France and to Dr. D. Chernyshov for assistance on beamline BM01A and thank Prof. Kazushi Mashima for a helpful discussion.

## ■ REFERENCES

- (a) Arduengo, A. J., III; Harlow, R. L.; Kline, M. A. Stable Crystalline Carbene. *J. Am. Chem. Soc.* **1991**, *113*, 361–363. (b) Díez-González, S.; Marion, N.; Nolan, S. P. N-Heterocyclic Carbenes in Late Transition Metal Catalysis. *Chem. Rev.* **2009**, *109*, 3612–3676. (c) Bourissou, D.; Guerret, O.; Gabbai, F. P.; Bertrand, G. Stable Carbenes. *Chem. Rev.* **2000**, *100*, 39–91. (d) Herrmann, W. A. N-Heterocyclic Carbenes: A New Concept in Organometallic Catalysis. *Angew. Chem., Int. Ed.* **2002**, *41*, 1290–1309. (e) Hahn, F. E.; Jahnke,



- M. C. Heterocyclic Carbenes: Synthesis and Coordination Chemistry. *Angew. Chem., Int. Ed.* **2008**, *47*, 3122–3172. (f) Enders, D.; Niemeier, O.; Henseler, A. Organocatalysis by N-Heterocyclic Carbenes. *Chem. Rev.* **2007**, *107*, S606–S655. (g) Hopkinson, M. N.; Richter, C.; Schedler, M.; Glorius, F. An overview of N-heterocyclic carbenes. *Nature* **2014**, *510*, 485–496.
- (2) (a) Danopoulos, A. A.; Simler, T.; Braunstein, P. N-Heterocyclic Carbene Complexes of Copper, Nickel, and Cobalt. *Chem. Rev.* **2019**, *119*, 3730–3961. (b) Iglesias, M.; Oro, L. A. A leap forward in iridium-NHC catalysis: new horizons and mechanistic insights. *Chem. Soc. Rev.* **2018**, *47*, 2772–2808.
- (3) Yu, R. P.; Darmon, J. M.; Milsmann, C.; Margulieux, G. W.; Stieber, S. C. E.; DeBeer, S.; Chirik, P. J. Catalytic Hydrogenation Activity and Electronic Structure Determination of Bis(arylimidazol-2-ylidene)pyridine Cobalt Alkyl and Hydride Complexes. *J. Am. Chem. Soc.* **2013**, *135*, 13168–13184.
- (4) (a) Ibrahim, A. D.; Entsminger, S. W.; Zhu, L.; Fout, A. R. A Highly Chemoselective Cobalt Catalyst for the Hydrosilylation of Alkenes using Tertiary Silanes and Hydrosiloxanes. *ACS Catal.* **2016**, *6*, 3589–3593. (b) Tokmic, K.; Markus, C. R.; Zhu, L.; Fout, A. R. Well-Defined Cobalt(I) Dihydrogen Catalyst: Experimental Evidence for a Co(I)/Co(III) Redox Process in Olefin Hydrogenation. *J. Am. Chem. Soc.* **2016**, *138*, 11907–11913. (c) Ibrahim, A. D.; Entsminger, S. W.; Fout, A. R. Insights into a Chemoselective Cobalt Catalyst for the Hydroboration of Alkenes and Nitriles. *ACS Catal.* **2017**, *7*, 3730–3734. (d) Tokmic, K.; Jackson, B. J.; Salazar, A.; Woods, T. J.; Fout, A. R. Cobalt-Catalyzed and Lewis Acid-Assisted Nitrile Hydrogenation to Primary Amines: A Combined Effort. *J. Am. Chem. Soc.* **2017**, *139*, 13554–13561.
- (5) (a) Tian, Y.; Jürgens, E.; Mill, K.; Jordan, R.; Maulbetsch, T.; Kunz, D. Nucleophilic Isomerization of Epoxides by Pincer-Rhodium Catalysts: Activity Increase and Mechanistic Insights. *ChemCatChem* **2019**, *11*, 4028–4035. (b) Tian, Y.; Jürgens, E.; Kunz, D. Regio- and chemoselective rearrangement of terminal epoxides into methyl alkyl and aryl ketones. *Chem. Commun.* **2018**, *54*, 11340–11343. (c) Jürgens, E.; Wucher, B.; Rominger, F.; Törnroos, K. W.; Kunz, D. Selective rearrangement of terminal epoxides into methylketones catalyzed by a nucleophilic rhodium-NHC-pincer complex. *Chem. Commun.* **2015**, *51*, 1897–1900.
- (6) Storey, C. M.; Gyton, M. R.; Andrew, R. E.; Chaplin, A. B. Terminal Alkyne Coupling Reactions through a Ring: Mechanistic Insights and Regiochemical Switching. *Angew. Chem., Int. Ed.* **2018**, *57*, 12003–12006.
- (7) (a) Chianese, A. R.; Mo, A.; Lampland, N. L.; Swartz, R. L.; Bremer, P. T. Iridium Complexes of CCC-Pincer N-Heterocyclic Carbene Ligands: Synthesis and Catalytic C-H Functionalization. *Organometallics* **2010**, *29*, 3019–3026. (b) Chianese, A. R.; Shaner, S. E.; Tendler, J. A.; Pudalov, D. M.; Shopov, D. Y.; Kim, D.; Rogers, S. L.; Mo, A. Iridium Complexes of Bulky CCC-Pincer N-Heterocyclic Carbene Ligands: Steric Control of Coordination Number and Catalytic Alkene Isomerization. *Organometallics* **2012**, *31*, 7359–7367. (c) Chianese, A. R.; Drance, M. J.; Jensen, K. H.; McCollom, S. P.; Yusufova, N.; Shaner, S. E.; Shopov, D. Y.; Tendler, J. A. Acceptorless Alkene Dehydrogenation Catalyzed by Iridium CCC-Pincer Complexes. *Organometallics* **2014**, *33*, 457–464. (d) Knapp, S. M. M.; Shaner, S. E.; Kim, D.; Shopov, D. Y.; Tendler, J. A.; Pudalov, D. M.; Chianese, A. R. Mechanistic Studies of Alkene Isomerization Catalyzed by CCC-Pincer Complexes of Iridium. *Organometallics* **2014**, *33*, 473–484.
- (8) Simler, T.; Choua, S.; Danopoulos, A. A.; Braunstein, P. Reactivity of a dearomatized pincer Co<sup>II</sup>Br complex with PNC-NHC donors: alkylation and Si–H bond activation via metal–ligand cooperation. *Dalton Trans.* **2018**, *47*, 7888–7895.
- (9) Kuriyama, S.; Arashiba, K.; Tanaka, H.; Matsuo, Y.; Nakajima, K.; Yoshizawa, K.; Nishibayashi, Y. Direct Transformation of Molecular Dinitrogen into Ammonia Catalyzed by Cobalt Dinitrogen Complexes Bearing Anionic PNP Pincer Ligands. *Angew. Chem., Int. Ed.* **2016**, *55*, 14291–14295.
- (10) Allen, F. H. The Cambridge Structural Database: a quarter of a million crystal structures and rising. *Acta Crystallogr., Sect. B: Struct. Sci.* **2002**, *B58*, 380–388.
- (11) Danopoulos, A. A.; Wright, J. A.; Motherwell, W. B.; Ellwood, S. N-Heterocyclic “Pincer” Dicarbene Complexes of Cobalt(I), Cobalt(II), and Cobalt(III). *Organometallics* **2004**, *23*, 4807–4810.
- (12) (a) Reilly, S. W.; Webster, C. E.; Hollis, T. K.; Valle, H. U. Transmetalation from CCC-NHC pincer Zr complexes in the synthesis of air-stable CCC-NHC pincer Co(III) complexes and initial hydroboration trials. *Dalton Trans.* **2016**, *45*, 2823–2828. (b) Denny, J. A.; Lamb, R. W.; Reilly, S. W.; Donnadiou, B.; Webster, C. E.; Hollis, T. K. Investigation of metallation/transmetalation reactions to synthesize a series of CCC–NHC Co pincer complexes and their X-ray structures. *Polyhedron* **2018**, *151*, 568–574. (c) Xi, Z.; Liu, B.; Lu, C.; Chen, W. Cobalt(III) complexes bearing bidentate, tridentate, and tetradentate N-heterocyclic carbenes: synthesis, X-ray structures and catalytic activities. *Dalton Trans.* **2009**, 7008–7014.
- (13) Fürstner, A.; Krause, H.; Ackermann, L.; Lehmann, C. W. N-Heterocyclic carbenes can coexist with alkenes and C–H acidic sites. *Chem. Commun.* **2001**, 2240–2241.
- (14) Ibrahim, A. D.; Tokmic, K.; Brennan, M. R.; Kim, D.; Matson, E. M.; Nilges, M. J.; Bertke, J. A.; Fout, A. R. Monoanionic bis(carbene) pincer complexes featuring cobalt(I–III) oxidation states. *Dalton Trans.* **2016**, *45*, 9805–9811.
- (15) Jürgens, E.; Kunz, D. A Rigid CNC Pincer Ligand Acting as a Tripodal Cp Analogue. *Eur. J. Inorg. Chem.* **2017**, *2017*, 233–236.
- (16) In earlier results we showed that catalyst **3** is already very active at room temperature and full conversion is achieved within 2 h with substrate **5a** (99% yield) and substrate **5b** (95% yield) (under comparable conditions). Due to this high activity at room temperature catalytic reactions with **3** under H<sub>2</sub> have not been carried out, as the reaction would already proceed before H<sub>2</sub> could be added in our setup.
- (17) (a) Eisenmann, J. L. Isomerization of Epoxides by Dicobalt Octacarbonyl. *J. Org. Chem.* **1962**, *27*, 2706. (b) Lamb, J. R.; Jung, Y.; Coates, G. W. Meinwald-type rearrangement of monosubstituted epoxides to methyl ketones using an [Al porphyrin]<sup>+</sup>[Co(CO)<sub>4</sub>]<sup>−</sup> catalyst. *Org. Chem. Front.* **2015**, *2*, 346–349.
- (18) Nakayama, S.; Morisako, S.; Yamashita, M. Synthesis and Application of Pyrrole-Based PNP–Ir Complexes to Catalytic Transfer Dehydrogenation of Cyclooctane. *Organometallics* **2018**, *37*, 1304–1313.
- (19) (a) Choualeb, A.; Lough, A. J.; Gusev, D. G. Hemilabile Pincer-Type Hydride Complexes of Iridium. *Organometallics* **2007**, *26*, S224–S229. (b) Peloso, R.; Pattacini, R.; Cazin, C. S. J.; Braunstein, P. Structure and Reactivity of New Iridium Complexes with Bis(Oxazoline)-Phosphonito Ligands. *Inorg. Chem.* **2009**, *48*, 11415–11424. (c) Chadwick, F. M.; Olliff, N.; Weller, A. S. A convenient route to a norbornadiene adduct of iridium with chelating phosphines, [Ir(R<sub>2</sub>PCH<sub>2</sub>CH<sub>2</sub>PR<sub>2</sub>)(NBD)]<sup>+</sup>[BAR<sup>F</sup><sub>4</sub>]<sup>−</sup> and a comparison of reactivity with H<sub>2</sub> in solution and the solid-state. *J. Organomet. Chem.* **2016**, *812*, 268–271. (d) Cano, I.; Martínez-Prieto, L. M.; Vendier, L.; van Leeuwen, P. W. N. M. An iridium–SPO complex as bifunctional catalyst for the highly selective hydrogenation of aldehydes. *Catal. Sci. Technol.* **2018**, *8*, 221–228.
- (20) (a) Grimme, S.; Huenerbein, R.; Ehrlich, S. On the Importance of the Dispersion Energy for the Thermodynamic Stability of Molecules. *ChemPhysChem* **2011**, *12*, 1258–1261. (b) Wagner, J. P.; Schreiner, P. R. London Dispersion Decisively Contributes to the Thermodynamic Stability of Bulky NHC-Coordinated Main Group Compounds. *J. Chem. Theory Comput.* **2016**, *12*, 231–237. (c) Liptrot, D. J.; Power, P. P. London dispersion forces in sterically crowded inorganic and organometallic molecules. *Nat. Rev. Chem.* **2017**, *1*, 0004.
- (21) Raynal, M.; Pattacini, R.; Cazin, C. S. J.; Vallée, C.; Olivier-Bourbigou, H.; Braunstein, P. Reaction Intermediates in the Synthesis of New Hydrido, N-Heterocyclic Dicarbene Iridium(III) Pincer Complexes. *Organometallics* **2009**, *28*, 4028–4047.



- (22) (a) Huang, J.; Stevens, E. D.; Nolan, S. P. Intramolecular C-H Activation Involving a Rhodium-Imidazol-2-ylidene Complex and Its Reaction with H<sub>2</sub> and CO. *Organometallics* **2000**, *19*, 1194–1197. (b) Praetorius, J. M.; Wang, R.; Crudden, C. M. Structure and Reactivity of Dinitrogen Rhodium Complexes Containing N-Heterocyclic Carbene Ligands. *Eur. J. Inorg. Chem.* **2009**, *2009*, 1746–1751.
- (23) Chakraborty, S.; Chattopadhyay, J.; Guo, W.; Billups, W. E. Functionalization of Potassium Graphite. *Angew. Chem., Int. Ed.* **2007**, *46*, 4486–4488.
- (24) (a) Sheldrick, G. M. *SADABS 2012/1*; University of Göttingen: Göttingen, Germany, 2012. (b) Sheldrick, G. M. A short history of SHELX. *Acta Crystallogr., Sect. A: Found. Crystallogr.* **2008**, *A64*, 112–122. (c) Sheldrick, G. M. Crystal structure refinement with SHELXL. *Acta Crystallogr., Sect. C: Struct. Chem.* **2015**, *C71*, 3–8. (d) Hübschle, C. B.; Sheldrick, G. M.; Dittrich, B. ShelXle: a Qt graphical user interface for SHELXL. *J. Appl. Crystallogr.* **2011**, *44*, 1281–1284. (e) Sheldrick, G. M. SHELXT – Integrated space-group and crystal-structure determination. *Acta Crystallogr., Sect. A: Found. Adv.* **2015**, *A71*, 3–8.
- (25) Spek, A. L. PLATON SQUEEZE: a tool for the calculation of the disordered solvent contribution to the calculated structure factors. *Acta Crystallogr., Sect. C: Struct. Chem.* **2015**, *C71*, 9–18.
- (26) (a) Becke, A. Density-functional exchange-energy approximation with correct asymptotic behavior. *Phys. Rev. A: At., Mol., Opt. Phys.* **1988**, *38*, 3098–3100. (b) Perdew, J. P. Density-functional approximation for the correlation energy of the inhomogeneous electron gas. *Phys. Rev. B: Condens. Matter Mater. Phys.* **1986**, *33*, 8822–8824. (c) Schäfer, A.; Horn, H.; Ahlrichs, R. Fully optimized contracted Gaussian basis sets for atoms Li to Kr. *J. Chem. Phys.* **1992**, *97*, 2571–2577. (d) Weigend, F.; Ahlrichs, R. Balanced basis sets of split valence, triple zeta valence and quadruple zeta valence quality for H to Rn: Design and assessment of accuracy. *Phys. Chem. Chem. Phys.* **2005**, *7*, 3297–3305. (e) Weigend, F. Accurate Coulomb-fitting basis sets for H to Rn. *Phys. Chem. Chem. Phys.* **2006**, *8*, 1057–1065.
- (27) (a) TURBOMOLE V6.3.1, a development of the University of Karlsruhe and Forschungszentrum Karlsruhe GmbH, 1989–2007; TURBOMOLE GmbH, since 2007; available from <http://www.turbomole.com>. (b) Treutler, O.; Ahlrichs, R. Efficient molecular numerical integration schemes. *J. Chem. Phys.* **1995**, *102*, 346–354. (c) von Arnim, M.; Ahlrichs, R. Performance of Parallel TURBOMOLE for Density Functional Calculations. *J. Comput. Chem.* **1998**, *19*, 1746–1757. (d) van Wüllen, C. Shared-memory parallelization of the TURBOMOLE programs AOFORCE, ESCF, and EGRAD: How to quickly parallelize legacy code. *J. Comput. Chem.* **2011**, *32*, 1195–1201. (e) Deglmann, P.; Furche, F.; Ahlrichs, R. An efficient implementation of second analytical derivatives for density functional methods. *Chem. Phys. Lett.* **2002**, *362*, 511–518. (f) Deglmann, P.; Furche, F. Efficient characterization of stationary points on potential energy surfaces. *J. Chem. Phys.* **2002**, *117*, 9535–9538. (g) Ahlrichs, R.; Bär, M.; Häser, M.; Horn, H.; Kölmel, C. Electronic structure calculations on workstation computers: The program system turbomole. *Chem. Phys. Lett.* **1989**, *162*, 165–169. (h) Armbruster, M. K.; Weigend, F.; van Wüllen, C.; Klopper, W. Self-consistent treatment of spin-orbit interactions with efficient Hartree-Fock and density functional methods. *Phys. Chem. Chem. Phys.* **2008**, *10*, 1748–1756. (i) Peng, D.; Middenorf, N.; Weigend, F.; Reiher, M. An efficient implementation of two-component relativistic exact-decoupling methods for large molecules. *J. Chem. Phys.* **2013**, *138*, 184105–184114.
- (28) (a) Eichkorn, K.; Treutler, O.; Öhm, H.; Häser, M.; Ahlrichs, R. Auxiliary basis sets to approximate Coulomb potentials. *Chem. Phys. Lett.* **1995**, *240*, 283–290. (b) Eichkorn, K.; Weigend, F.; Treutler, O.; Ahlrichs, R. Auxiliary basis sets for main row atoms and transition metals and their use to approximate Coulomb potentials. *Theor. Chem. Acc.* **1997**, *97*, 119–124. (c) Deglmann, P.; May, K.; Furche, F.; Ahlrichs, R. *Chem. Phys. Lett.* **2004**, *384*, 103–107. (d) Weigend, F. A fully direct RI-HF algorithm: Implementation, optimized auxiliary basis sets, demonstration of accuracy and efficiency. *Phys. Chem. Chem. Phys.* **2002**, *4*, 4285–4291. (e) Sierka, M.; Hogeckamp, A.; Ahlrichs, R. Fast evaluation of the Coulomb potential for electron densities using multipole accelerated resolution of identity approximation. *J. Chem. Phys.* **2003**, *118*, 9136–9148.
- (29) (a) Grimme, S.; Antony, J.; Ehrlich, S.; Krieg, H. A consistent and accurate ab initio parametrization of density functional dispersion correction (DFT-D) for the 94 elements H-Pu. *J. Chem. Phys.* **2010**, *132*, 154104. (b) Grimme, S.; Ehrlich, S.; Goerigk, L. Effect of the Damping Function in Dispersion Corrected Density Functional Theory. *J. Comput. Chem.* **2011**, *32*, 1456–1465.

**Supporting Information**

**Synthesis and Reactivity of Cobalt(I) and Iridium(I) Complexes  
Bearing a Pentadentate *N*-Homoallyl Substituted Bis(NHC) Pincer-  
Ligand**

Yingying Tian,<sup>†</sup> Theo Maulbetsch,<sup>†</sup> Ronja Jordan,<sup>†</sup> Karl W. Törnroos,<sup>‡</sup> and Doris Kunz<sup>\*\*†</sup>

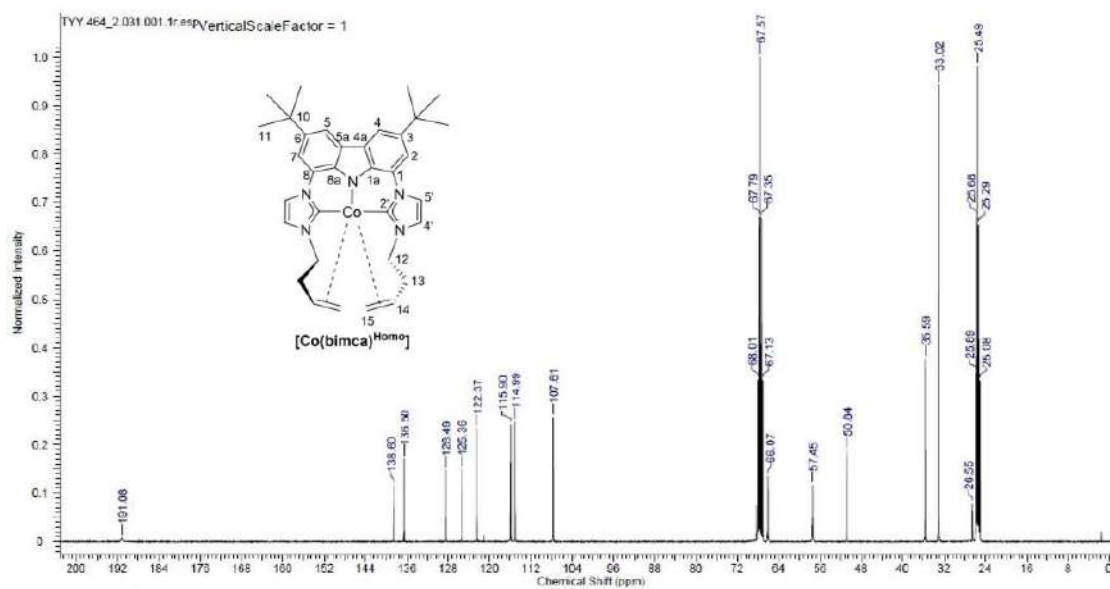
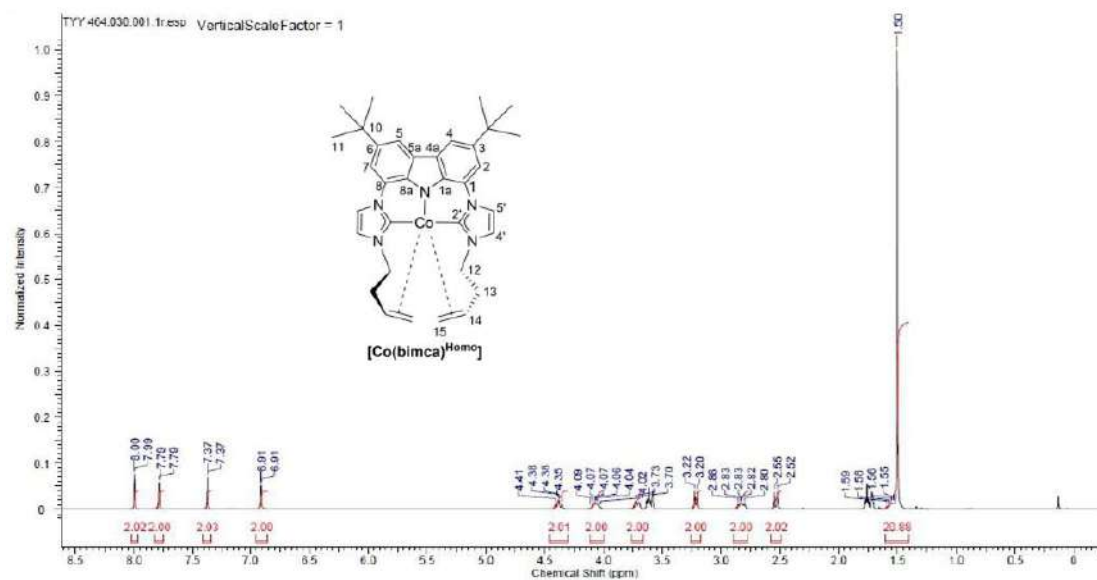
<sup>†</sup> Institut für Anorganische Chemie, Eberhard Karls Universität Tübingen, Auf der Morgenstelle 18,  
D72076 Tübingen, Germany

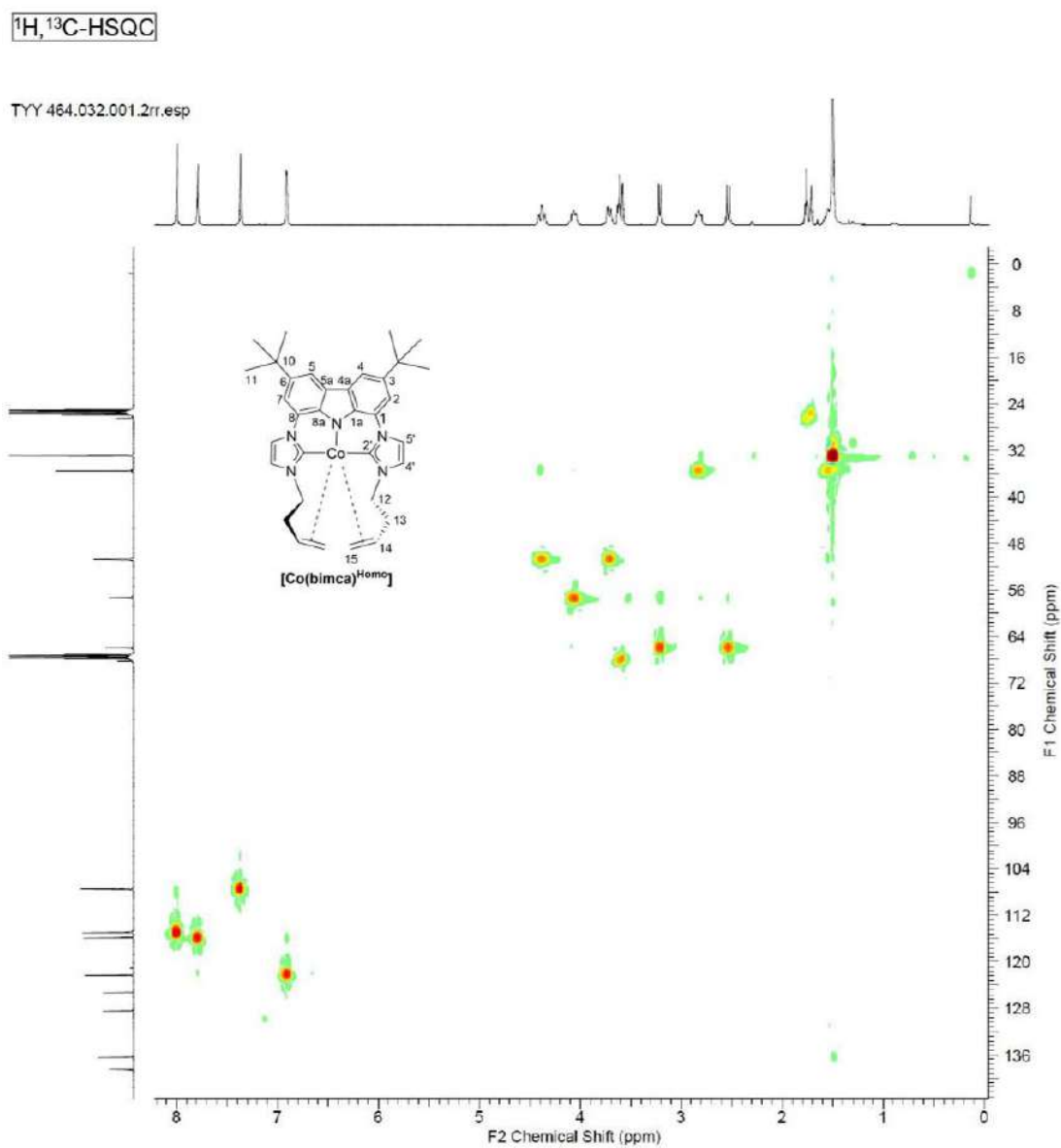
<sup>‡</sup> Department of Chemistry, University of Bergen, Allégaten 41, 5007 Bergen, Norway

**Table of Contents**

1. NMR spectra.....	S2
2. X-ray crystal structure analysis.....	S16
3. DFT calculations.....	S47
4. References.....	S51

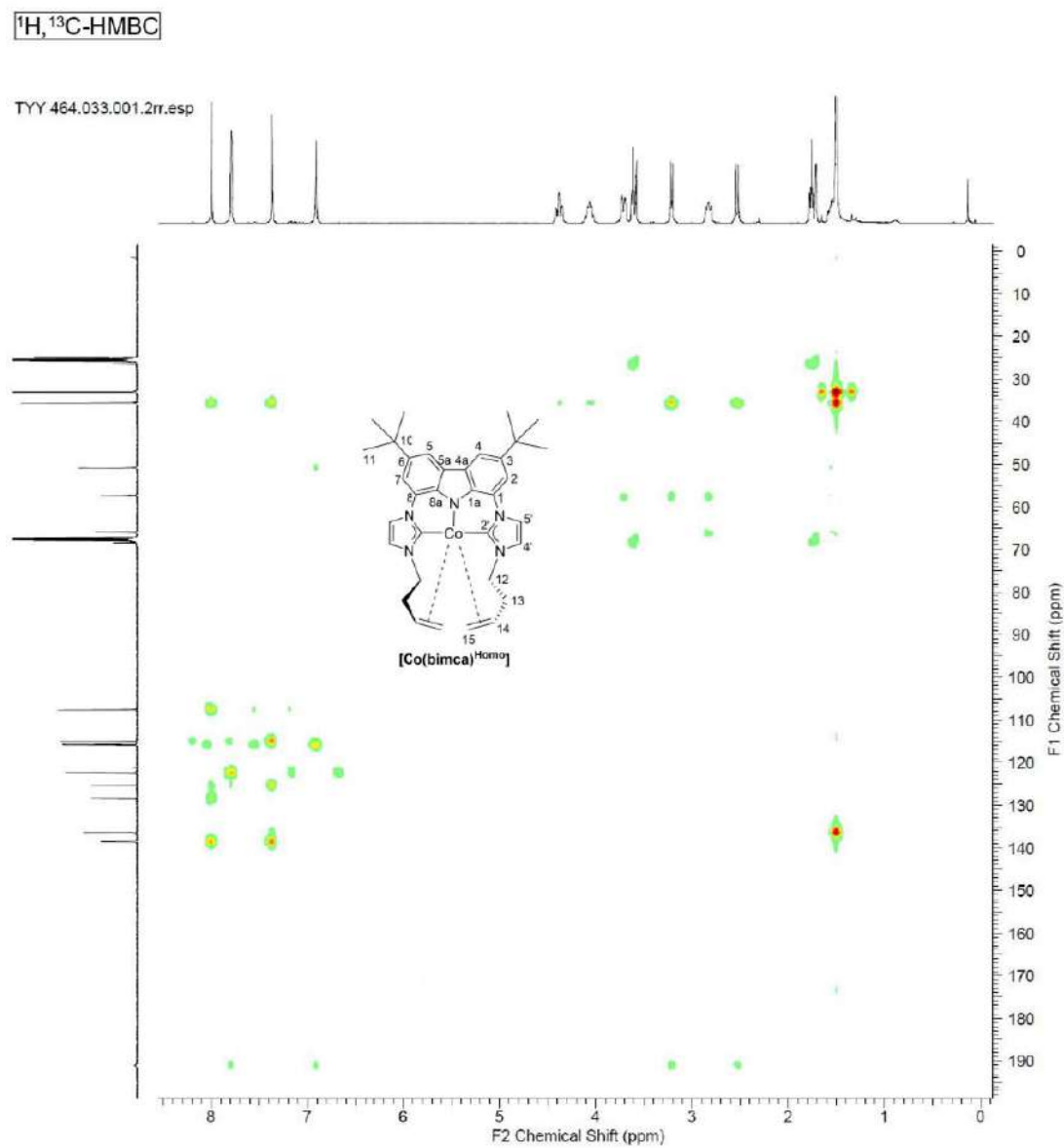
### 1. NMR spectra



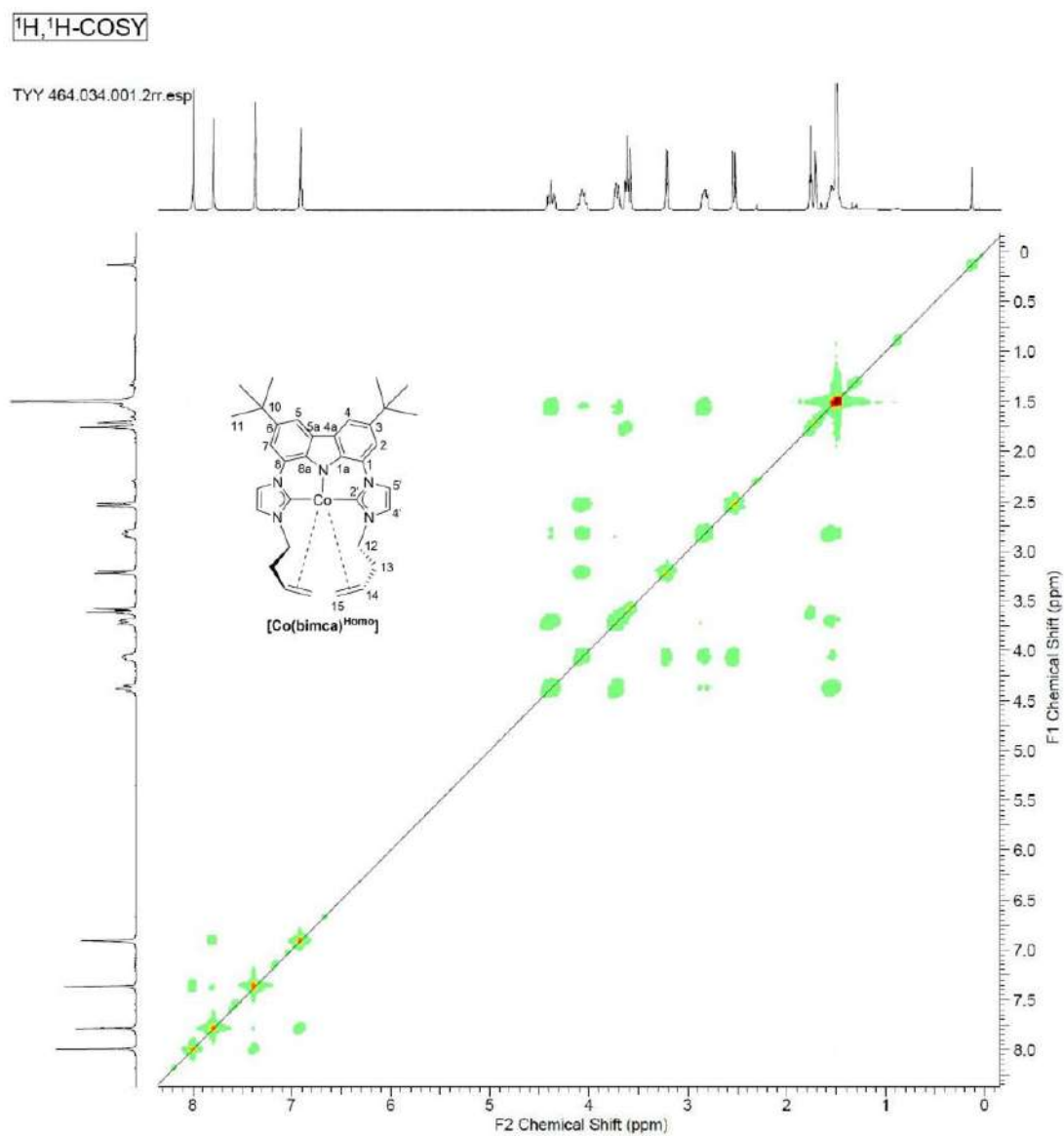


**Figure S3.**  $^1\text{H}, ^{13}\text{C}$ -HSQC (THF- $d_6$ , 400 MHz) spectrum: **[Co(bimca)<sup>Homo</sup>]** (2) from the reduction of **[Co(bimca)<sup>Homo</sup>Br]** (1) with  $\text{KCs}$ .

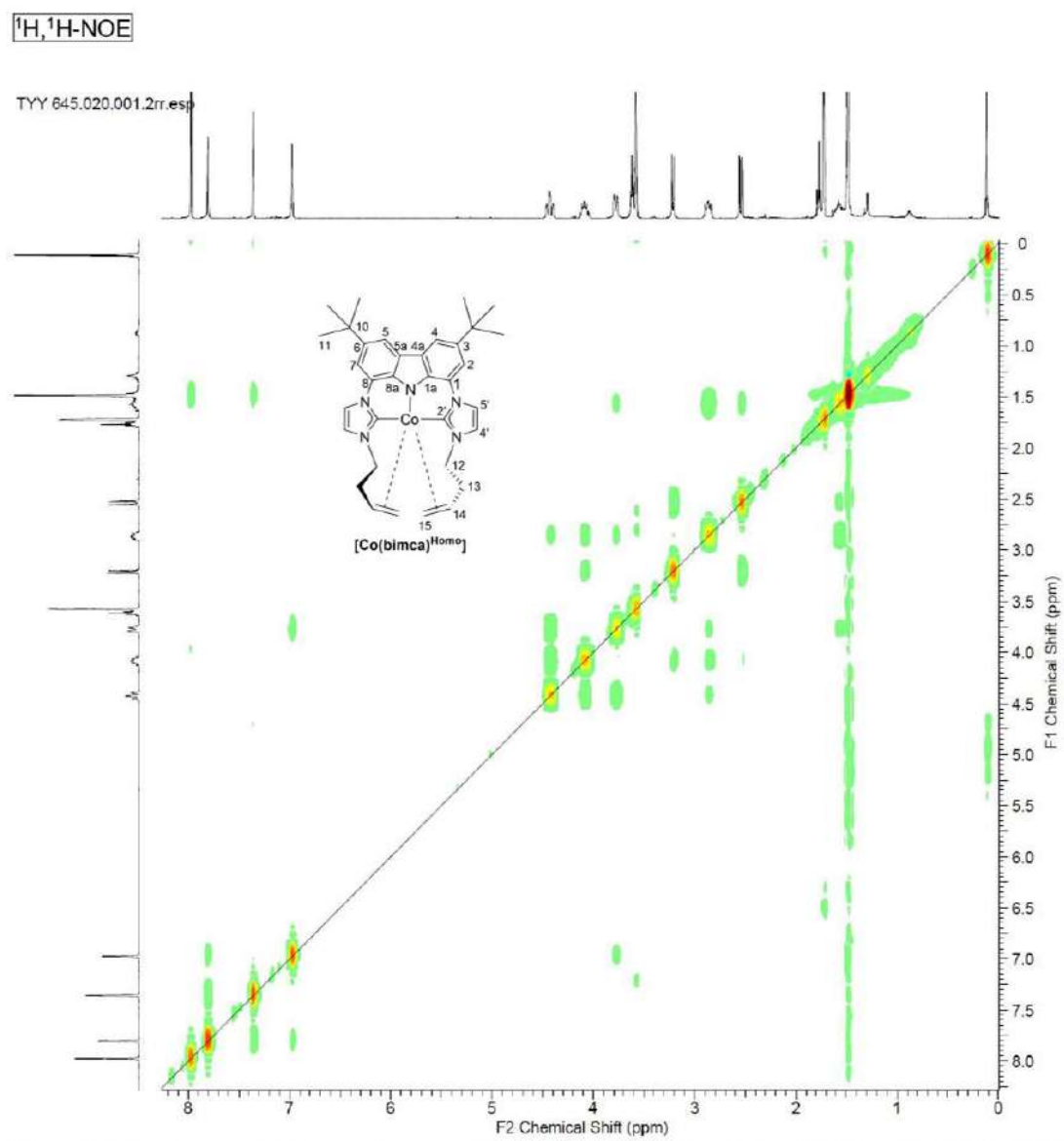




**Figure S4.**  $^1\text{H}, ^{13}\text{C}$ -HMBC (THF- $d_6$ , 400 MHz) spectrum: **[Co(bimca)<sup>Homoc</sup>]** (2) from the reduction of **[Co(bimca)<sup>Homoc</sup>Br]** (1) with KC<sub>8</sub>.



**Figure S5.** <sup>1</sup>H, <sup>1</sup>H-COSY NMR (THF-d<sub>8</sub>, 400 MHz) spectrum: **[Co(bimca)<sup>Homo</sup>]** (**2**) from the reduction of **[Co(bimca)<sup>Homo</sup>Br]** (**1**) with K<sup>+</sup>C<sub>8</sub>.



**Figure S6.**  $^1\text{H}, ^1\text{H}$ -NOE NMR ( $\text{THF-d}_8$ , 400 MHz) spectrum: **[Co(bimca)<sup>Homo</sup>]** (2) from the reduction of **[Co(bimca)<sup>Homo</sup>Br]** (1) with  $\text{K}^+\text{C}_6\text{H}_6^-$ .

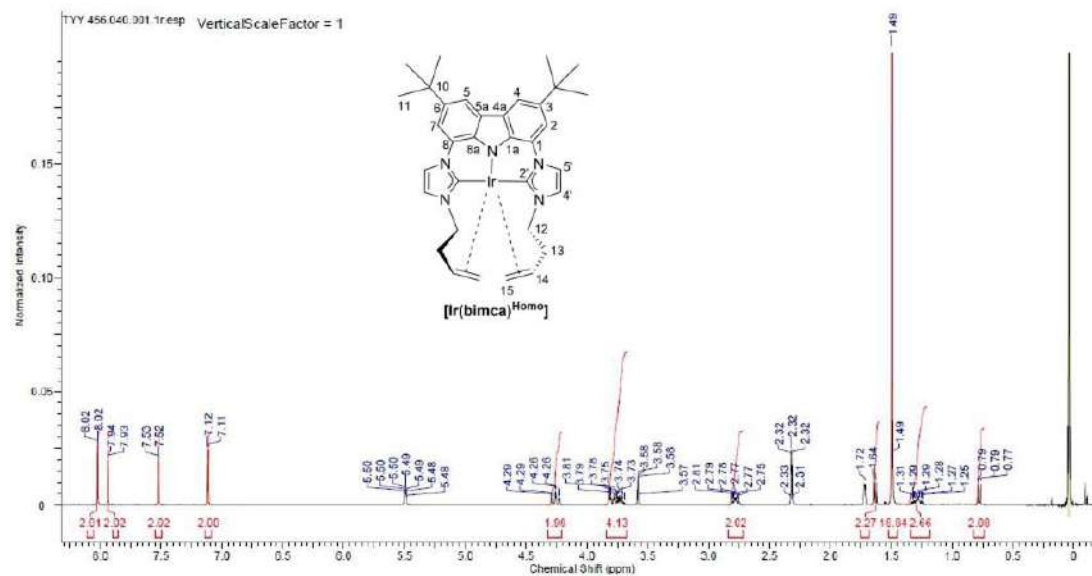


Figure S7.  $^1\text{H}$  NMR (THF- $d_8$ , 400 MHz) spectrum:  $[\text{Ir}(\text{bimca})^{\text{HomO}}]$  (**4**) from the transmetalation of  $[\text{Li}(\text{bimca})^{\text{HomO}}]$  containing COD.

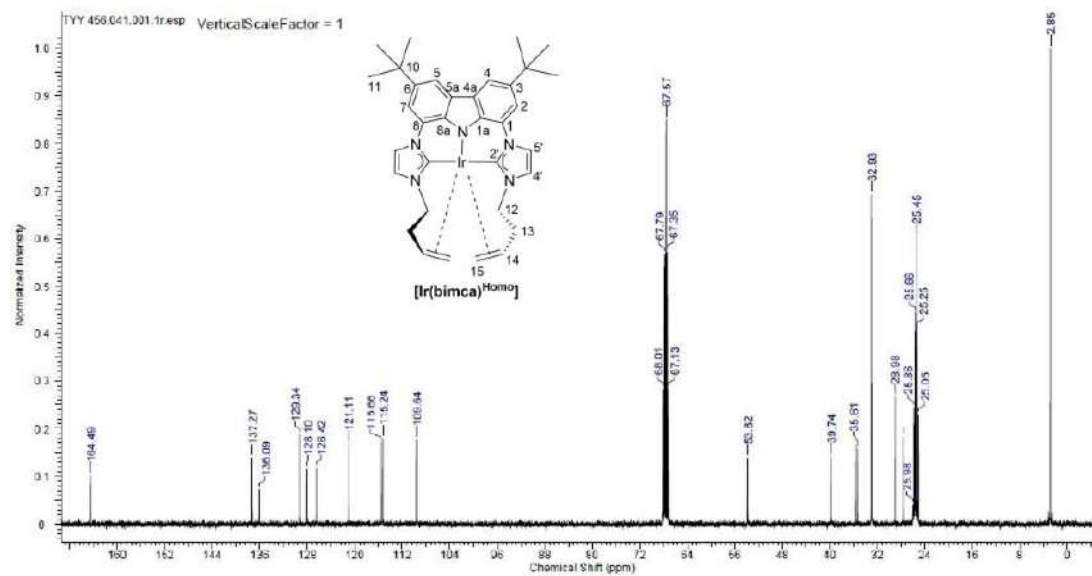
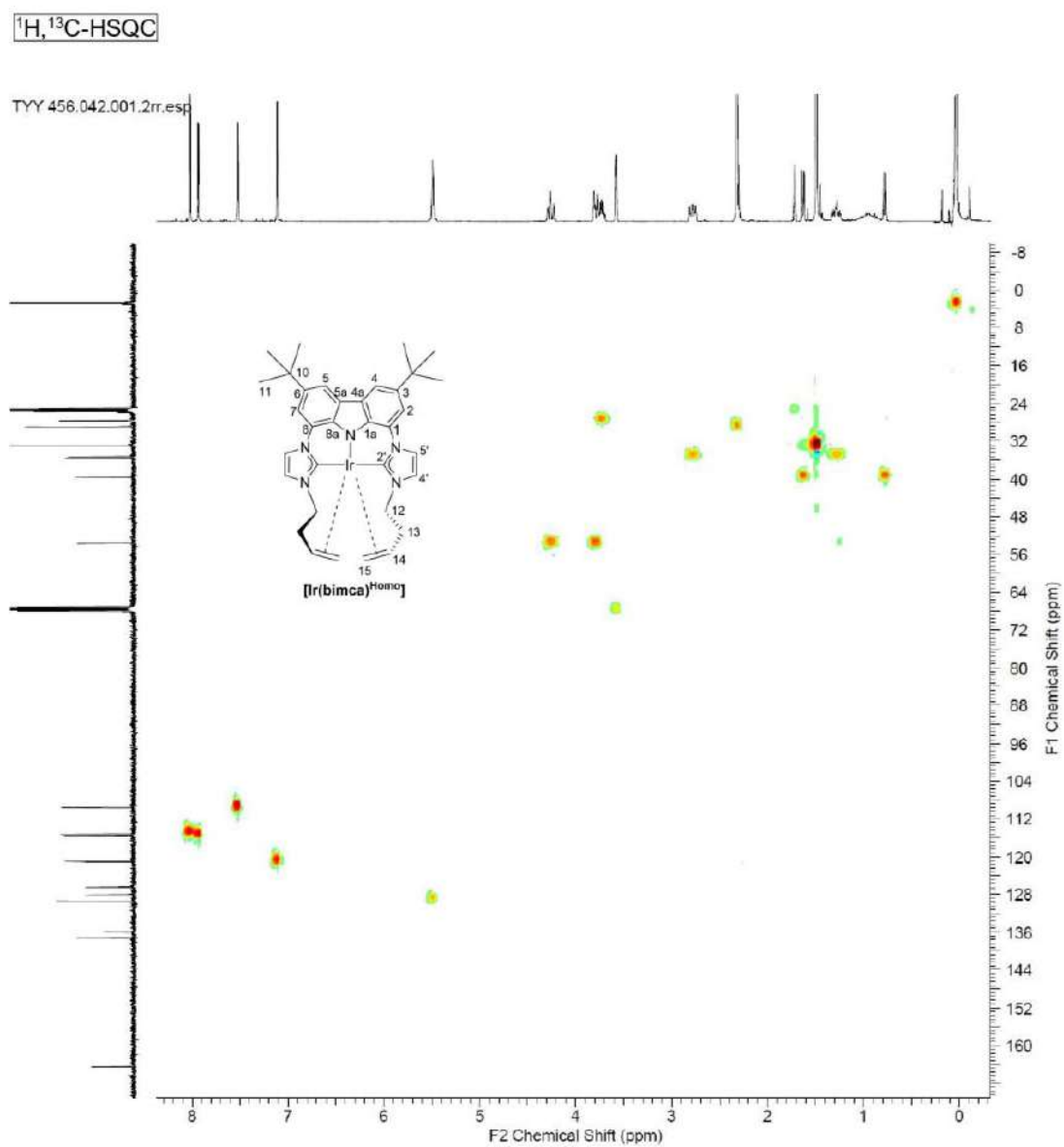
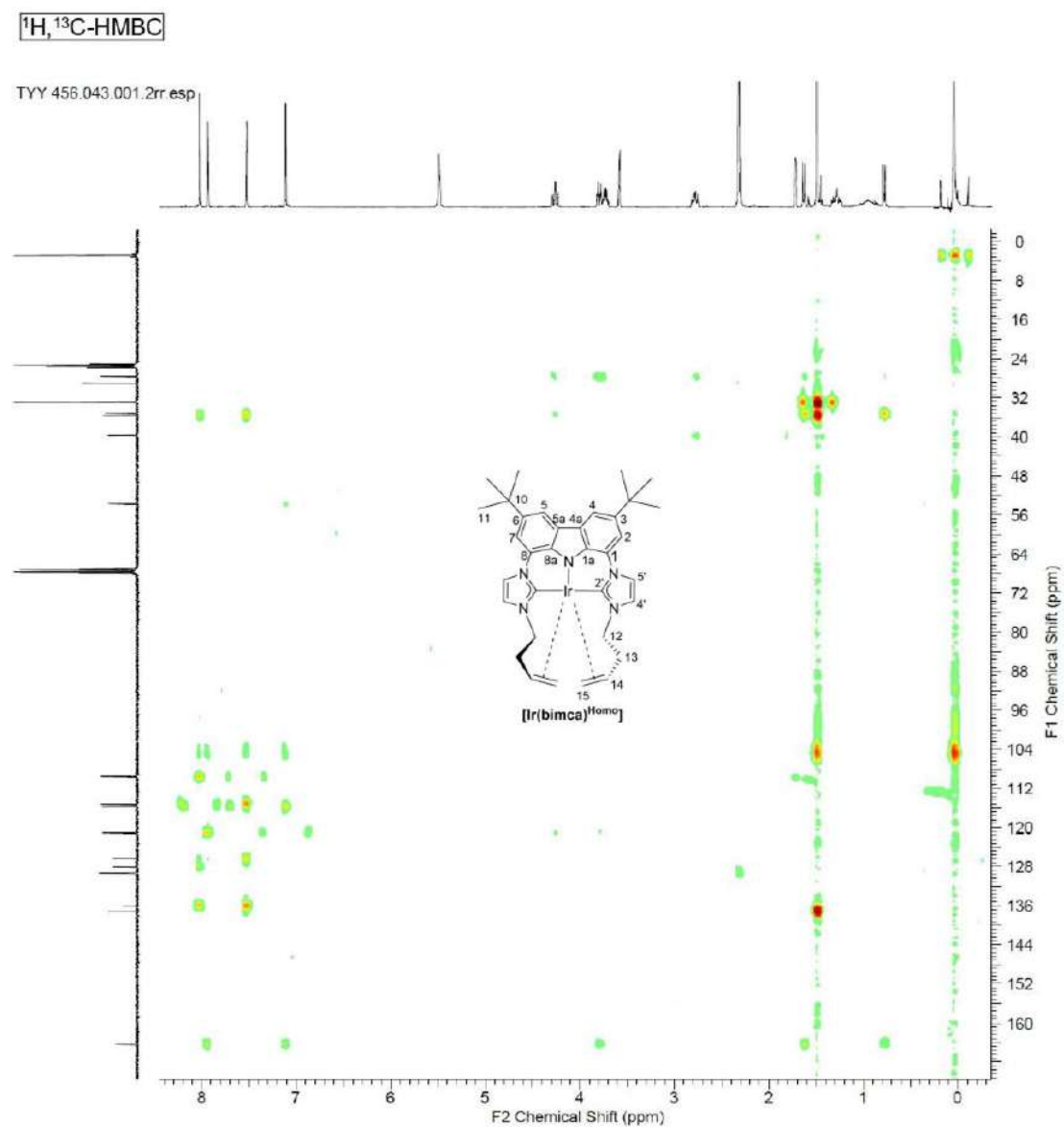


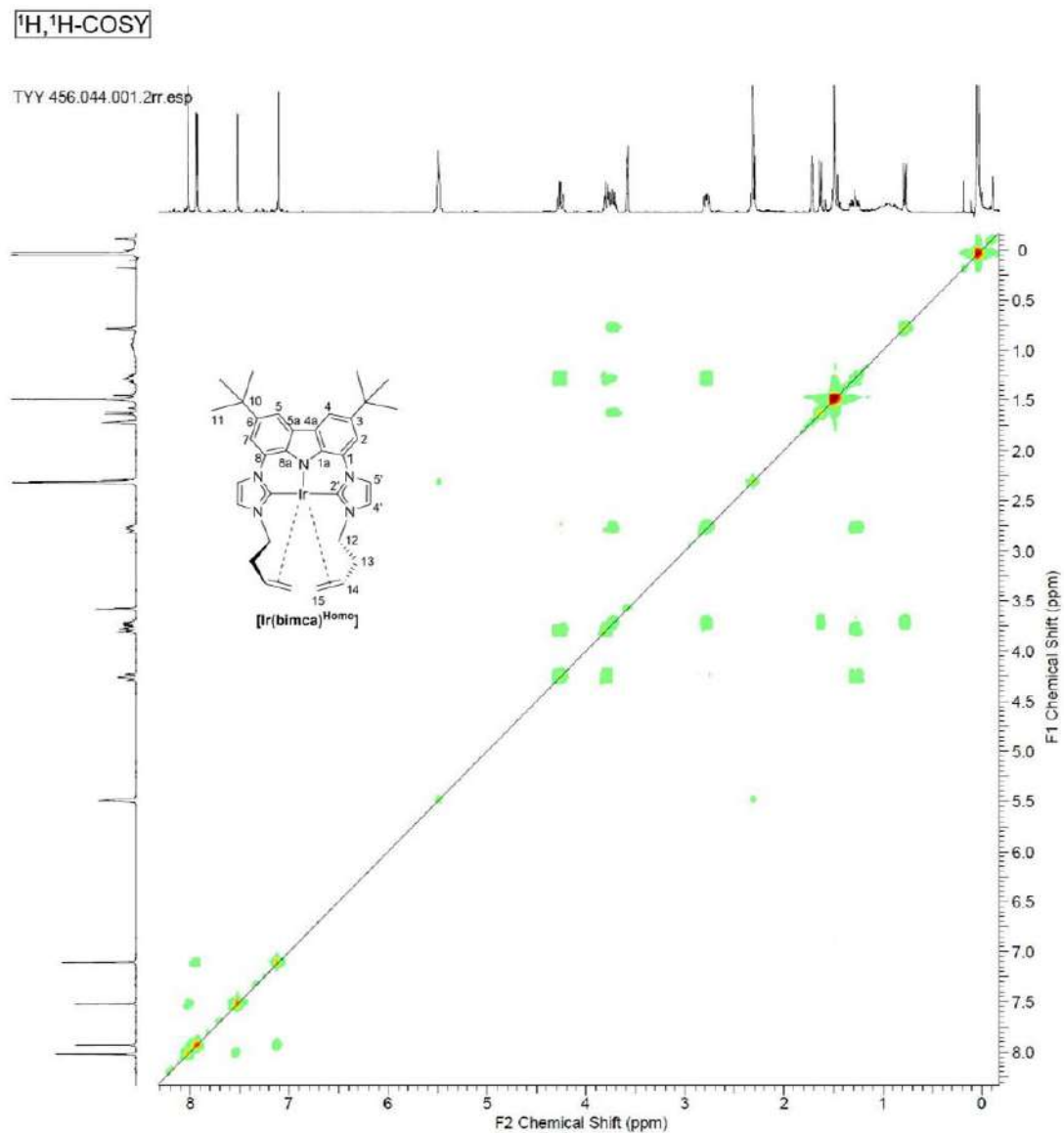
Figure S8.  $^{13}\text{C}$  NMR (THF- $d_8$ , 101 MHz) spectrum:  $[\text{Ir}(\text{bimca})^{\text{HomO}}]$  (**4**) from the transmetalation of  $[\text{Li}(\text{bimca})^{\text{HomO}}]$  containing COD.



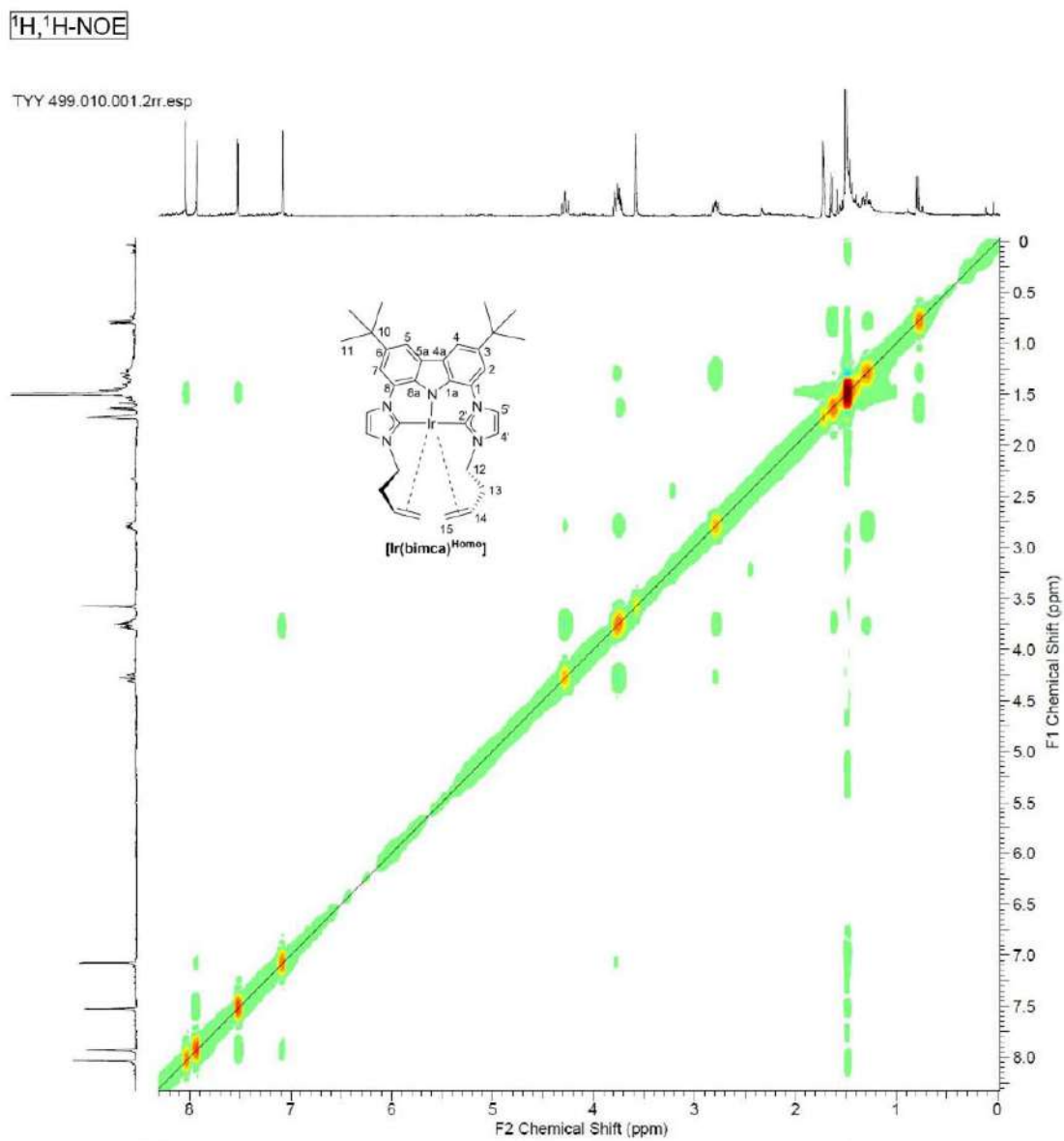
**Figure S9.**  $^1\text{H}, ^{13}\text{C}$ -HSQC (THF- $d_6$ , 400 MHz) spectrum: **[Ir(bimca)<sup>HOMO</sup>]** (**4**) from the transmetalation of **[Li(bimca)<sup>HOMO</sup>]** containing COD.



**Figure S10.**  $^1\text{H}, ^{13}\text{C}$ -HMBC (THF- $d_6$ , 400 MHz) spectrum: **[Ir(bimca)<sup>Homoc</sup>]** from the transmetalation of **[Li(bimca)<sup>Homoc</sup>]** (**4**) containing COD.



**Figure S11.** <sup>1</sup>H, <sup>1</sup>H-COSY NMR (THF-d<sub>8</sub>, 400 MHz) spectrum: **[Ir(bimca)<sup>Homo</sup>]** (**4**) from the transmetalation of **[Li(bimca)<sup>Homo</sup>]** containing COD.



**Figure S12.**  $^1\text{H}, ^1\text{H}$ -NOE NMR (THF- $d_6$ , 400 MHz) spectrum: **[Ir(bimca)<sup>Homo</sup>]** (4) from the transmetalation of **[K(bimca)<sup>Homo</sup>]**.



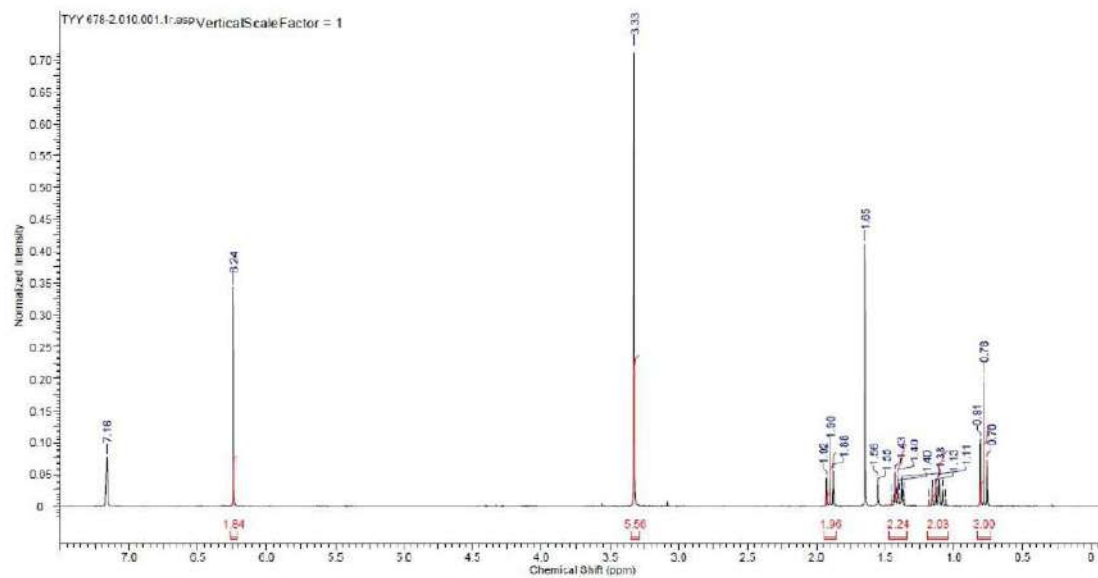


Figure S13. <sup>1</sup>H NMR (C<sub>6</sub>D<sub>6</sub>, 400 MHz) spectrum: The isomerization of 1,2-epoxyhexane with [Rh(bimca)<sup>Homo</sup>] (3).

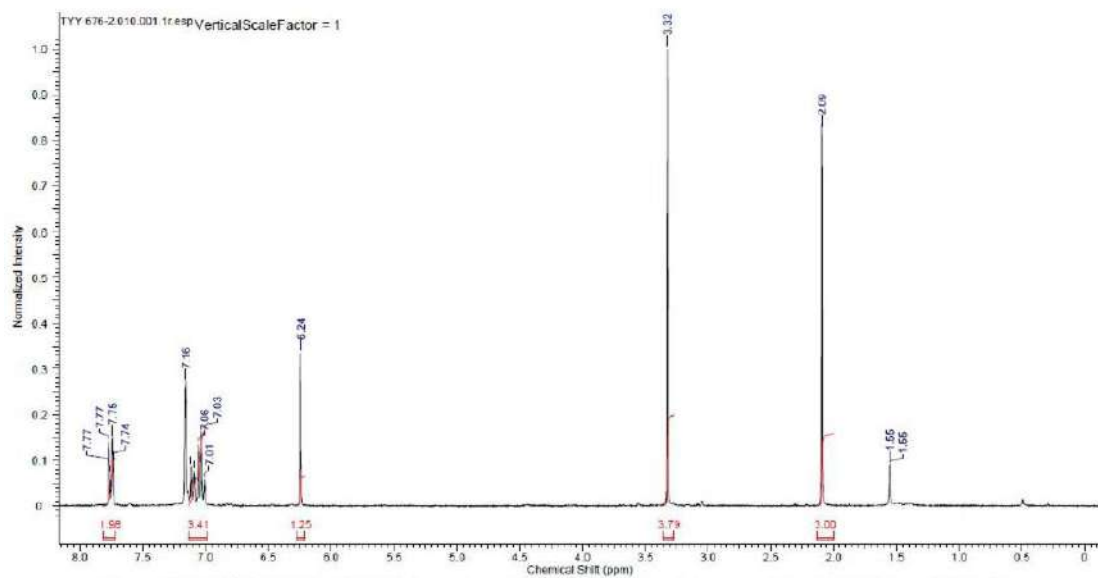


Figure S14. <sup>1</sup>H NMR (C<sub>6</sub>D<sub>6</sub>, 400 MHz) spectrum: The isomerization of styrene oxide with [Rh(bimca)<sup>Homo</sup>] (3).

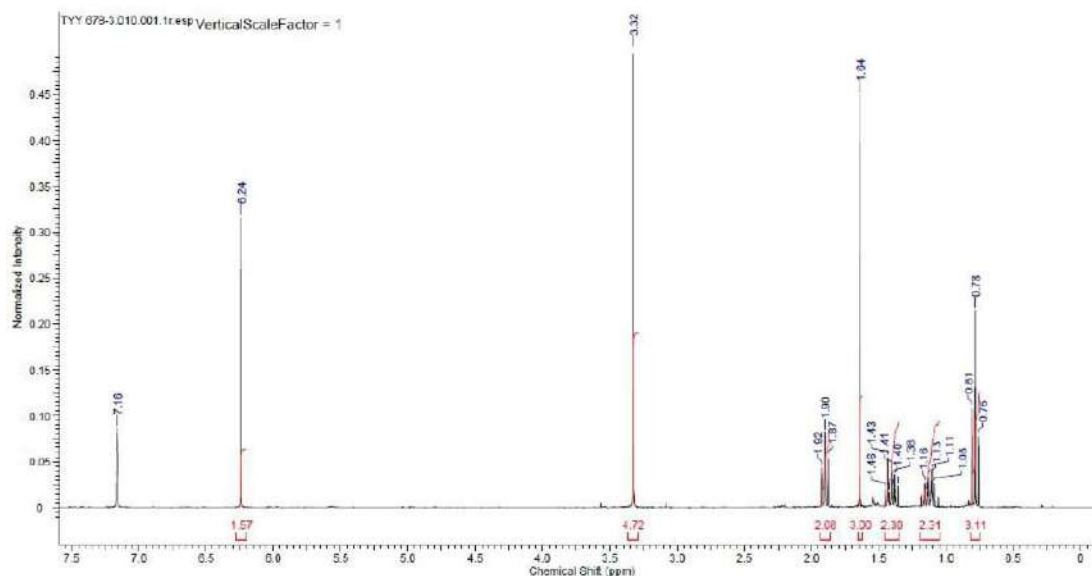


Figure S15. <sup>1</sup>H NMR (C<sub>6</sub>D<sub>6</sub>, 400 MHz) spectrum: The isomerization of 1,2-epoxyhexane with [Ir(bimca)<sup>HomO</sup>] (4).

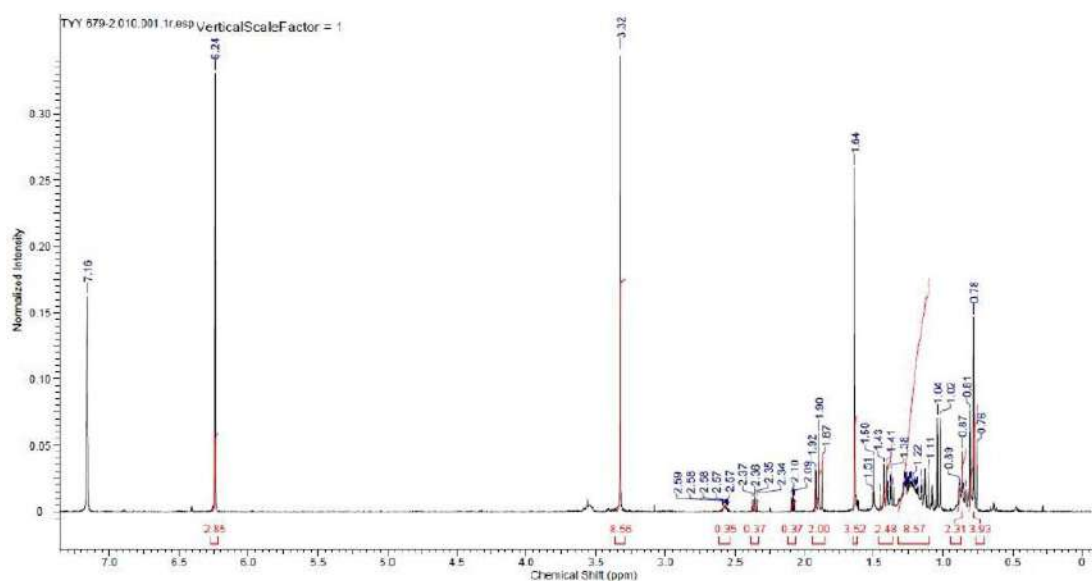


Figure S16. <sup>1</sup>H NMR (C<sub>6</sub>D<sub>6</sub>, 400 MHz) spectrum: The isomerization of 1,2-epoxyhexane with [Ir(bimca)<sup>HomO</sup>] (4) in presence of H<sub>2</sub>.

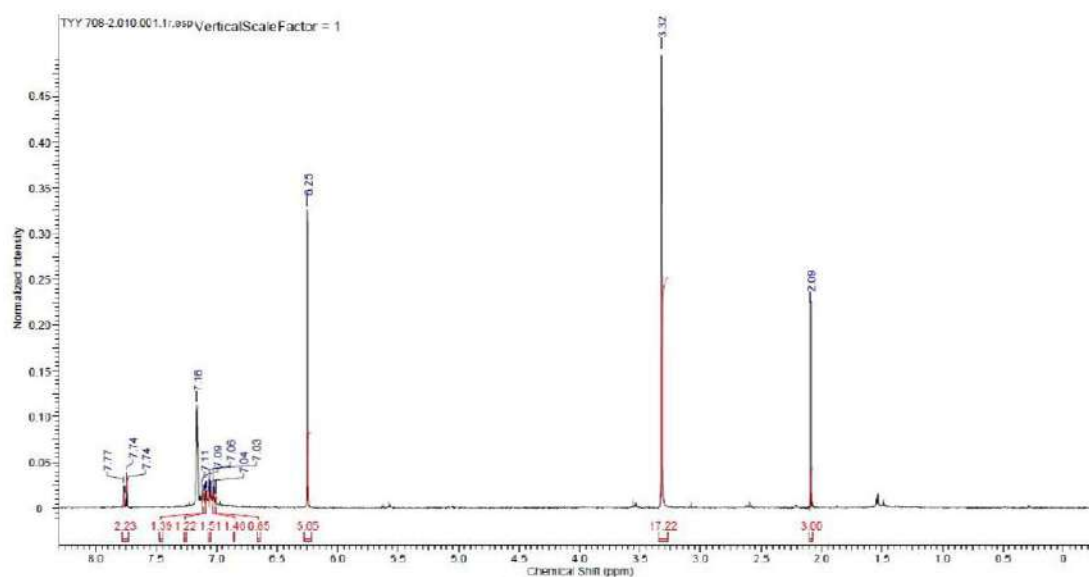


Figure S17. <sup>1</sup>H NMR (C<sub>6</sub>D<sub>6</sub>, 400 MHz) spectrum: The isomerization of styrene oxide with **[Ir(bimca)<sup>hom</sup>]** (**4**).

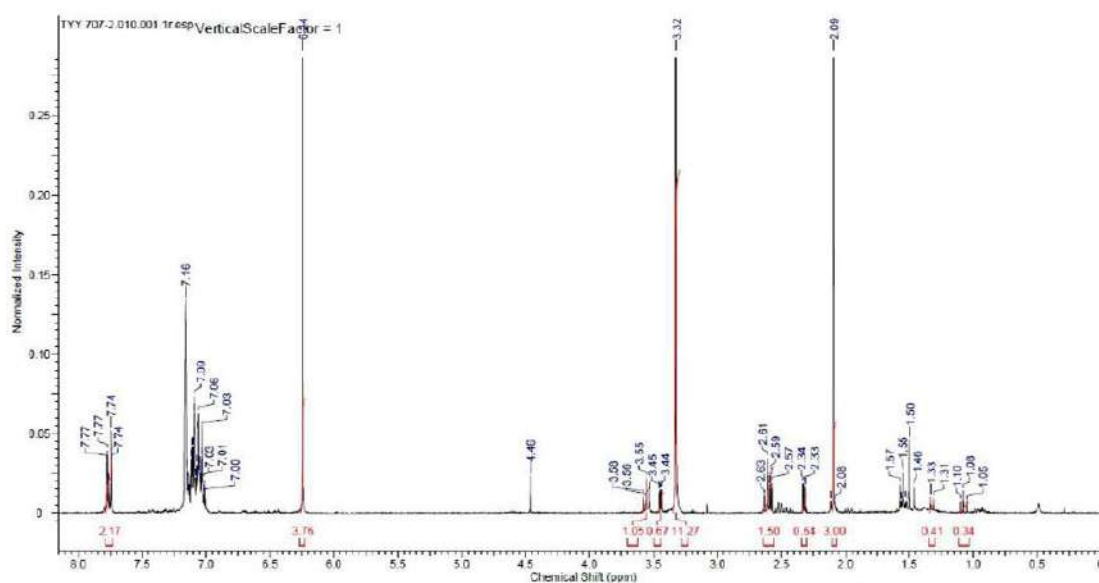


Figure S18. <sup>1</sup>H NMR (C<sub>6</sub>D<sub>6</sub>, 400 MHz) spectrum: The isomerization of styrene oxide with **[Ir(bimca)<sup>hom</sup>]** (**4**) in presence of H<sub>2</sub>.

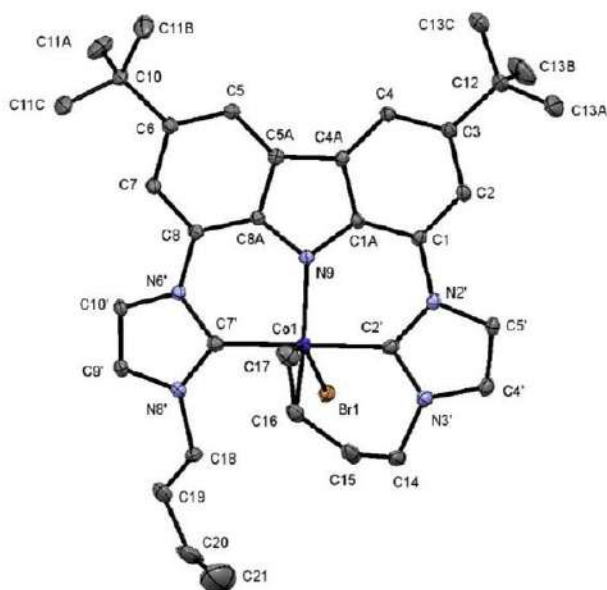


## 2. X-ray crystal structure analysis

### *X-ray Data Collection and Structure Analysis.*

Suitable crystals for the X-ray analysis were obtained as described below. Data collection was carried out on a Bruker APEX Duo CCD with an Incoatec  $\mu$ S Microsource with a Quazar MX mirror using Mo  $K_{\alpha}$  radiation ( $\lambda = 0.71073 \text{ \AA}$ ) and a graphite monochromator. Corrections for absorption effects were applied using SADABS.<sup>1a</sup> All structures were solved by direct methods using SHELXS and refined using SHELXL.<sup>1b,c</sup> In the case of structure **1** the SQUEEZE routine<sup>2</sup> was applied for disordered solvent.

### 2.1. Compound **1**



**Figure S20.** Solid-state molecular structure of **1**. Atoms are shown with anisotropic atomic displacement parameters at the 30% probability level. A strongly disordered molecule of THF was removed using the SQUEEZE routine. Hydrogen atoms are omitted for clarity.

**Table S1.** Crystal data and structure refinement for compound **1**.

Identification code	Compound <b>1</b>	
Empirical formula	$C_{34} H_{40} Br Co N_5$	
Formula weight	657.55	
Temperature	100(2) K	
Wavelength	0.71073 $\text{\AA}$	
Crystal system	Tetragonal	
Space group	$I4_1/a$	
Unit cell dimensions	$a = 28.7917(9) \text{ \AA}$ $b = 28.7917(9) \text{ \AA}$ $c = 15.7744(5) \text{ \AA}$	$\alpha = 90^\circ$ $\beta = 90^\circ$ $\gamma = 90^\circ$
Volume	13076.4(9) $\text{\AA}^3$	
Z	16	
Density (calculated)	1.336 $\text{Mg/m}^3$	
Absorption coefficient	1.777 $\text{mm}^{-1}$	
F(000)	5456	
Crystal size	0.338 x 0.082 x 0.066 $\text{mm}^3$	
Theta range for data collection	1.415 to 25.362 $^\circ$ .	

Index ranges	-34<=h<=34, -34<=k<=34, -18<=l<=19
Reflections collected	95047
Independent reflections	5994 [R(int) = 0.1191]
Completeness to theta = 25.242°	99.9 %
Absorption correction	Semi-empirical from equivalents
Refinement method	Full-matrix least-squares on F <sup>2</sup>
Data / restraints / parameters	5994 / 86 / 396
Goodness-of-fit on F <sup>2</sup>	1.031
Final R indices [I>2sigma(I)]	R1 = 0.0436, wR2 = 0.1074
R indices (all data)	R1 = 0.0617, wR2 = 0.1181
Extinction coefficient	n/a
Largest diff. peak and hole	1.628 and -0.555 e.Å <sup>-3</sup>

**Table S2.** Bond lengths [Å] and angles [°] for compound **1**.

Co(1)-N(9)	1.915(3)	C(9')-H(9')	0.9500	C(15)-H(15B)	0.9900
Co(1)-C(2')	1.917(4)	C(10)-C(11B)	1.516(6)	C(16)-C(17)	1.384(6)
Co(1)-C(7')	1.978(4)	C(10)-C(11C)	1.517(6)	C(16)-H(16)	0.98(2)
Co(1)-C(17)	2.052(4)	C(10)-C(11A)	1.547(6)	C(17)-H(17A)	0.98(2)
Co(1)-C(16)	2.087(4)	C(10')-H(10')	0.9500	C(17)-H(17B)	0.98(2)
Co(1)-Br(1)	2.5148(6)	C(11A)-H(11A)	0.9800	C(18)-C(19)	1.539(6)
N(2')-C(2')	1.372(5)	C(11A)-H(11B)	0.9800	C(18)-H(18A)	0.9900
N(2')-C(5')	1.400(5)	C(11A)-H(11C)	0.9800	C(18)-H(18B)	0.9900
N(2')-C(1)	1.423(4)	C(11B)-H(11D)	0.9800	C(19)-C(20)	1.4905(10)
N(3')-C(2')	1.351(5)	C(11B)-H(11E)	0.9800	C(19)-H(19A)	0.9900
N(3')-C(4')	1.387(5)	C(11B)-H(11F)	0.9800	C(19)-H(19B)	0.9900
N(3')-C(14)	1.453(5)	C(11C)-H(11G)	0.9800	C(20)-C(21)	1.274(7)
N(6')-C(7')	1.376(5)	C(11C)-H(11H)	0.9800	C(20)-H(20)	0.9500
N(6')-C(10')	1.398(4)	C(11C)-H(11I)	0.9800	C(21)-H(21A)	0.9500
N(6')-C(8)	1.429(4)	C(12)-C(13B)	1.519(4)	C(21)-H(21B)	0.9500
N(8')-C(7')	1.359(5)	C(12)-C(13F)	1.527(5)		
N(8')-C(9')	1.384(5)	C(12)-C(13C)	1.527(4)	N(9)-Co(1)-C(2')	89.69(14)
N(8')-C(18)	1.461(5)	C(12)-C(13E)	1.528(5)	N(9)-Co(1)-C(7')	90.29(13)
N(9)-C(8A)	1.376(4)	C(12)-C(13A)	1.530(4)	C(2')-Co(1)-C(7')	173.95(15)
N(9)-C(1A)	1.380(4)	C(12)-C(13D)	1.531(5)	N(9)-Co(1)-C(17)	99.64(15)
C(1)-C(2)	1.385(5)	C(13A)-H(13A)	0.9800	C(2')-Co(1)-C(17)	93.51(18)
C(1)-C(1A)	1.403(5)	C(13A)-H(13B)	0.9800	C(7')-Co(1)-C(17)	92.46(17)
C(2)-C(3)	1.412(5)	C(13A)-H(13C)	0.9800	N(9)-Co(1)-C(16)	138.55(15)
C(2)-H(2)	0.9500	C(13B)-H(13D)	0.9800	C(2')-Co(1)-C(16)	89.79(16)
C(1A)-C(4A)	1.415(5)	C(13B)-H(13E)	0.9800	C(7')-Co(1)-C(16)	94.22(15)
C(3)-C(4)	1.387(5)	C(13B)-H(13F)	0.9800	C(17)-Co(1)-C(16)	39.06(17)
C(3)-C(12)	1.530(5)	C(13C)-H(13G)	0.9800	N(9)-Co(1)-Br(1)	111.45(9)
C(4)-C(4A)	1.398(5)	C(13C)-H(13H)	0.9800	C(2')-Co(1)-Br(1)	83.50(11)
C(4)-H(4)	0.9500	C(13C)-H(13I)	0.9800	C(7')-Co(1)-Br(1)	90.88(11)
C(4')-C(5')	1.338(5)	C(13D)-H(13J)	0.9800	C(17)-Co(1)-Br(1)	148.71(13)
C(4')-H(4')	0.9500	C(13D)-H(13K)	0.9800	C(16)-Co(1)-Br(1)	109.66(12)
C(5)-C(6)	1.392(5)	C(13D)-H(13L)	0.9800	C(2')-N(2')-C(5')	110.4(3)
C(5)-C(5A)	1.399(5)	C(13E)-H(13M)	0.9800	C(2')-N(2')-C(1)	123.5(3)
C(5)-H(5)	0.9500	C(13E)-H(13N)	0.9800	C(5')-N(2')-C(1)	125.6(3)
C(4A)-C(5A)	1.443(5)	C(13E)-H(13O)	0.9800	C(2')-N(3')-C(4')	111.4(3)
C(5')-H(5')	0.9500	C(13F)-H(13P)	0.9800	C(2')-N(3')-C(14)	122.6(3)
C(6)-C(7)	1.414(5)	C(13F)-H(13Q)	0.9800	C(4')-N(3')-C(14)	126.0(3)
C(6)-C(10)	1.541(5)	C(13F)-H(13R)	0.9800	C(7')-N(6')-C(10')	111.0(3)
C(5A)-C(8A)	1.420(5)	C(14)-C(15)	1.516(7)	C(7')-N(6')-C(8)	125.6(3)
C(7)-C(8)	1.380(5)	C(14)-H(14A)	0.9900	C(10')-N(6')-C(8)	123.3(3)
C(7)-H(7)	0.9500	C(14)-H(14B)	0.9900	C(7')-N(8')-C(9')	111.2(3)
C(8)-C(8A)	1.394(5)	C(15)-C(16)	1.518(6)	C(7')-N(8')-C(18)	127.0(3)
C(9')-C(10')	1.333(5)	C(15)-H(15A)	0.9900	C(9')-N(8')-C(18)	121.8(3)

C(8A)-N(9)-C(1A)	104.4(3)	C(11B)-C(10)-C(11A)	108.7(4)	C(12)-C(13D)-H(13L)	109.5
C(8A)-N(9)-Co(1)	126.7(2)	C(11C)-C(10)-C(11A)	106.9(4)	H(13J)-C(13D)-H(13L)	109.5
C(1A)-N(9)-Co(1)	127.0(2)	C(6)-C(10)-C(11A)	109.3(3)	H(13K)-C(13D)-H(13L)	109.5
C(2)-C(1)-C(1A)	118.8(3)	C(9')-C(10')-N(6')	106.1(3)	C(12)-C(13E)-H(13M)	109.5
C(2)-C(1)-N(2')	122.6(3)	C(9'')-C(10'')-H(10'')	126.9	C(12)-C(13E)-H(13N)	109.5
C(1A)-C(1)-N(2')	118.4(3)	N(6'')-C(10'')-H(10'')	126.9	H(13M)-C(13E)-H(13N)	109.5
C(1)-C(2)-C(3)	122.3(3)	C(10)-C(11A)-H(11A)	109.5	C(12)-C(13E)-H(13O)	109.5
C(1)-C(2)-H(2)	118.9	C(10)-C(11A)-H(11B)	109.5	H(13M)-C(13E)-H(13O)	109.5
C(3)-C(2)-H(2)	118.9	H(11A)-C(11A)-H(11B)	109.5	H(13N)-C(13E)-H(13O)	109.5
N(9)-C(1A)-C(1)	128.0(3)	C(10)-C(11A)-H(11C)	109.5	C(12)-C(13F)-H(13P)	109.5
N(9)-C(1A)-C(4A)	112.7(3)	H(11A)-C(11A)-H(11C)	109.5	C(12)-C(13F)-H(13Q)	109.5
C(1)-C(1A)-C(4A)	119.3(3)	H(11B)-C(11A)-H(11C)	109.5	H(13P)-C(13F)-H(13Q)	109.5
N(3')-C(2')-N(2')	104.3(3)	C(10)-C(11B)-H(11D)	109.5	C(12)-C(13F)-H(13R)	109.5
N(3')-C(2')-Co(1)	124.7(3)	C(10)-C(11B)-H(11E)	109.5	H(13P)-C(13F)-H(13R)	109.5
N(2')-C(2')-Co(1)	130.2(3)	H(11D)-C(11B)-H(11E)	109.5	H(13Q)-C(13F)-H(13R)	109.5
C(4)-C(3)-C(2)	118.6(3)	C(10)-C(11B)-H(11F)	109.5	N(3'')-C(14)-C(15)	110.0(3)
C(4)-C(3)-C(12)	121.9(3)	H(11D)-C(11B)-H(11F)	109.5	N(3'')-C(14)-H(14A)	109.7
C(2)-C(3)-C(12)	119.5(3)	H(11E)-C(11B)-H(11F)	109.5	C(15)-C(14)-H(14A)	109.7
C(3)-C(4)-C(4A)	120.2(3)	C(10)-C(11C)-H(11G)	109.5	N(3'')-C(14)-H(14B)	109.7
C(3)-C(4)-H(4)	119.9	C(10)-C(11C)-H(11H)	109.5	C(15)-C(14)-H(14B)	109.7
C(4A)-C(4)-H(4)	119.9	H(11G)-C(11C)-H(11H)	109.5	H(14A)-C(14)-H(14B)	108.2
C(5')-C(4')-N(3')	107.2(3)	C(10)-C(11C)-H(11I)	109.5	C(14)-C(15)-C(16)	116.2(3)
C(5')-C(4')-H(4')	126.4	H(11G)-C(11C)-H(11I)	109.5	C(14)-C(15)-H(15A)	108.2
N(3'')-C(4')-H(4')	126.4	H(11H)-C(11C)-H(11I)	109.5	C(16)-C(15)-H(15A)	108.2
C(6)-C(5)-C(5A)	120.5(3)	C(13B)-C(12)-C(13C)	109.1(3)	C(14)-C(15)-H(15B)	108.2
C(6)-C(5)-H(5)	119.8	C(13F)-C(12)-C(13E)	108.4(4)	C(16)-C(15)-H(15B)	108.2
C(5A)-C(5)-H(5)	119.8	C(13B)-C(12)-C(3)	108.5(4)	H(15A)-C(15)-H(15B)	107.4
C(4)-C(4A)-C(1A)	120.7(3)	C(13F)-C(12)-C(3)	115.3(13)	C(17)-C(16)-C(15)	123.7(4)
C(4)-C(4A)-C(5A)	134.1(3)	C(13C)-C(12)-C(3)	112.0(3)	C(17)-C(16)-Co(1)	69.1(2)
C(1A)-C(4A)-C(5A)	105.2(3)	C(13E)-C(12)-C(3)	115.6(13)	C(15)-C(16)-Co(1)	117.7(3)
C(4'')-C(5'')-N(2'')	106.7(3)	C(13B)-C(12)-C(13A)	109.1(3)	C(17)-C(16)-H(16)	117(2)
C(4'')-C(5'')-H(5'')	126.6	C(13C)-C(12)-C(13A)	107.7(3)	C(15)-C(16)-H(16)	114(2)
N(2'')-C(5'')-H(5'')	126.6	C(3)-C(12)-C(13A)	110.4(3)	Co(1)-C(16)-H(16)	105(2)
C(5)-C(6)-C(7)	118.0(3)	C(13F)-C(12)-C(13D)	108.1(4)	C(16)-C(17)-Co(1)	71.8(2)
C(5)-C(6)-C(10)	121.9(3)	C(13E)-C(12)-C(13D)	108.1(4)	C(16)-C(17)-H(17A)	119(2)
C(7)-C(6)-C(10)	120.2(3)	C(3)-C(12)-C(13D)	100.7(12)	Co(1)-C(17)-H(17A)	109(2)
C(5)-C(5A)-C(8A)	120.1(3)	C(12)-C(13A)-H(13A)	109.5	C(16)-C(17)-H(17B)	123(2)
C(5)-C(5A)-C(4A)	135.1(3)	C(12)-C(13A)-H(13B)	109.5	Co(1)-C(17)-H(17B)	108(3)
C(8A)-C(5A)-C(4A)	104.8(3)	H(13A)-C(13A)-H(13B)	109.5	H(17A)-C(17)-H(17B)	115(4)
C(8)-C(7)-C(6)	122.7(3)	C(12)-C(13A)-H(13C)	109.5	N(8'')-C(18)-C(19)	112.1(3)
C(8)-C(7)-H(7)	118.7	H(13A)-C(13A)-H(13C)	109.5	N(8'')-C(18)-H(18A)	109.2
N(8'')-C(7)-N(6'')	103.6(3)	H(13B)-C(13A)-H(13C)	109.5	C(19)-C(18)-H(18A)	109.2
N(8'')-C(7)-Co(1)	129.4(3)	C(12)-C(13B)-H(13D)	109.5	N(8'')-C(18)-H(18B)	109.2
N(6'')-C(7)-Co(1)	126.7(3)	C(12)-C(13B)-H(13E)	109.5	C(19)-C(18)-H(18B)	109.2
C(7)-C(8)-C(8A)	119.0(3)	H(13D)-C(13B)-H(13E)	109.5	H(18A)-C(18)-H(18B)	107.9
C(7)-C(8)-N(6'')	122.0(3)	C(12)-C(13B)-H(13F)	109.5	C(20)-C(19)-C(18)	111.3(4)
C(8A)-C(8)-N(6'')	119.1(3)	H(13D)-C(13B)-H(13F)	109.5	C(20)-C(19)-H(19A)	109.4
N(9)-C(8A)-C(8)	127.5(3)	H(13E)-C(13B)-H(13F)	109.5	C(18)-C(19)-H(19A)	109.4
N(9)-C(8A)-C(5A)	112.8(3)	C(12)-C(13C)-H(13G)	109.5	C(20)-C(19)-H(19B)	109.4
C(8)-C(8A)-C(5A)	119.7(3)	C(12)-C(13C)-H(13H)	109.5	C(18)-C(19)-H(19B)	109.4
C(10')-C(9')-N(8')	108.0(3)	H(13G)-C(13C)-H(13H)	109.5	H(19A)-C(19)-H(19B)	108.0
C(10')-C(9')-H(9')	126.0	C(12)-C(13C)-H(13I)	109.5	C(21)-C(20)-C(19)	129.4(7)
N(8'')-C(9')-H(9')	126.0	H(13G)-C(13C)-H(13I)	109.5	C(21)-C(20)-H(20)	115.3
C(11B)-C(10)-C(11C)	109.4(4)	H(13H)-C(13C)-H(13I)	109.5	C(19)-C(20)-H(20)	115.3
C(11B)-C(10)-C(6)	110.9(3)	C(12)-C(13D)-H(13J)	109.5	C(20)-C(21)-H(21A)	120.0
C(11C)-C(10)-C(6)	111.5(3)	C(12)-C(13D)-H(13K)	109.5	C(20)-C(21)-H(21B)	120.0
		H(13J)-C(13D)-H(13K)	109.5	H(21A)-C(21)-H(21B)	120.0

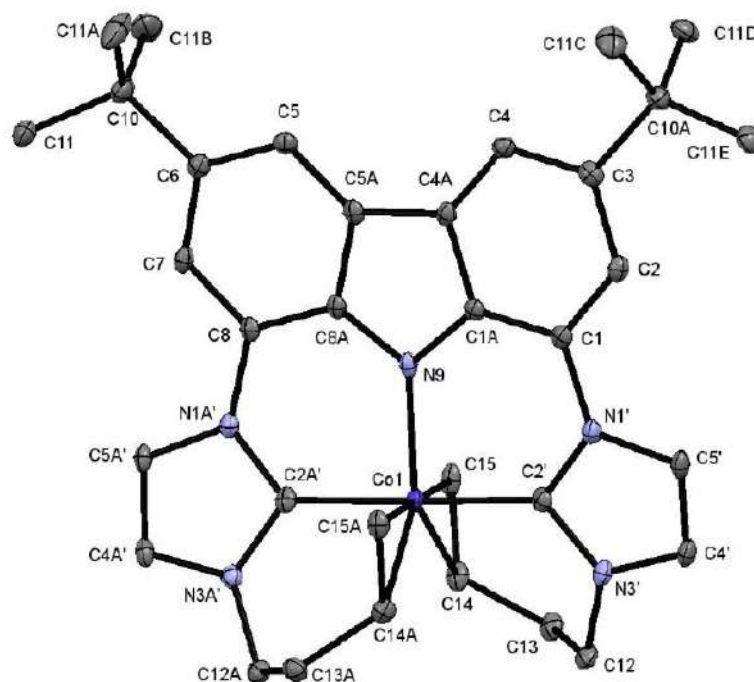


**Table S3.** Torsion angles [°] for compound 1.

C(2')-N(2')-C(1)-C(2)	-166.3(3)	C(10')-N(6')-C(7')-Co(1)	-171.4(3)
C(5')-N(2')-C(1)-C(2)	4.3(5)	C(8)-N(6')-C(7')-Co(1)	7.1(5)
C(2')-N(2')-C(1)-C(1A)	9.6(5)	C(6)-C(7)-C(8)-C(8A)	-0.3(6)
C(5')-N(2')-C(1)-C(1A)	-179.8(3)	C(6)-C(7)-C(8)-N(6')	178.8(3)
C(1A)-C(1)-C(2)-C(3)	-1.8(5)	C(7')-N(6')-C(8)-C(7)	164.9(3)
N(2')-C(1)-C(2)-C(3)	174.1(3)	C(10')-N(6')-C(8)-C(7)	-16.9(5)
C(8A)-N(9)-C(1A)-C(1)	180.0(3)	C(7')-N(6')-C(8)-C(8A)	-16.1(5)
Co(1)-N(9)-C(1A)-C(1)	-15.0(5)	C(10')-N(6')-C(8)-C(8A)	162.1(3)
C(8A)-N(9)-C(1A)-C(4A)	0.7(4)	C(1A)-N(9)-C(8A)-C(8)	-177.6(3)
Co(1)-N(9)-C(1A)-C(4A)	165.7(2)	Co(1)-N(9)-C(8A)-C(8)	17.4(5)
C(2)-C(1)-C(1A)-N(9)	-175.4(3)	C(1A)-N(9)-C(8A)-C(5A)	1.4(4)
N(2')-C(1)-C(1A)-N(9)	8.5(5)	Co(1)-N(9)-C(8A)-C(5A)	-163.7(2)
C(2)-C(1)-C(1A)-C(4A)	3.8(5)	C(7)-C(8)-C(8A)-N(9)	-177.3(3)
N(2')-C(1)-C(1A)-C(4A)	-172.2(3)	N(6')-C(8)-C(8A)-N(9)	3.7(5)
C(4')-N(3')-C(2')-N(2')	2.1(4)	C(7)-C(8)-C(8A)-C(5A)	3.8(5)
C(14)-N(3')-C(2')-N(2')	-179.0(3)	N(6')-C(8)-C(8A)-C(5A)	-175.2(3)
C(4')-N(3')-C(2')-Co(1)	-167.9(3)	C(5)-C(5A)-C(8A)-N(9)	176.7(3)
C(14)-N(3')-C(2')-Co(1)	11.0(5)	C(4A)-C(5A)-C(8A)-N(9)	-2.8(4)
C(5')-N(2')-C(2')-N(3')	-2.4(4)	C(5)-C(5A)-C(8A)-C(8)	-4.2(5)
C(1)-N(2')-C(2')-N(3')	169.5(3)	C(4A)-C(5A)-C(8A)-C(8)	176.2(3)
C(5')-N(2')-C(2')-Co(1)	166.8(3)	C(7')-N(8')-C(9')-C(10')	0.8(4)
C(1)-N(2')-C(2')-Co(1)	-21.3(5)	C(18)-N(8')-C(9')-C(10')	-178.5(3)
C(1)-C(2)-C(3)-C(4)	-1.4(6)	C(5)-C(6)-C(10)-C(11B)	26.3(6)
C(1)-C(2)-C(3)-C(12)	177.7(3)	C(7)-C(6)-C(10)-C(11B)	-153.9(4)
C(2)-C(3)-C(4)-C(4A)	2.5(5)	C(5)-C(6)-C(10)-C(11C)	148.5(4)
C(12)-C(3)-C(4)-C(4A)	-176.6(3)	C(7)-C(6)-C(10)-C(11C)	-31.8(5)
C(2')-N(3')-C(4')-C(5')	-1.1(4)	C(5)-C(6)-C(10)-C(11A)	-93.5(5)
C(14)-N(3')-C(4')-C(5')	-179.9(4)	C(7)-C(6)-C(10)-C(11A)	86.3(4)
C(3)-C(4)-C(4A)-C(1A)	-0.4(5)	N(8')-C(9')-C(10')-N(6')	0.5(4)
C(3)-C(4)-C(4A)-C(5A)	178.2(4)	C(7')-N(6')-C(10')-C(9')	-1.8(4)
N(9)-C(1A)-C(4A)-C(4)	176.6(3)	C(8)-N(6')-C(10')-C(9')	179.8(3)
C(1)-C(1A)-C(4A)-C(4)	-2.8(5)	C(4)-C(3)-C(12)-C(13B)	100.5(5)
N(9)-C(1A)-C(4A)-C(5A)	-2.4(4)	C(2)-C(3)-C(12)-C(13B)	-78.5(5)
C(1)-C(1A)-C(4A)-C(5A)	178.2(3)	C(4)-C(3)-C(12)-C(13F)	-47.0(15)
N(3')-C(4')-C(5')-N(2')	-0.5(4)	C(2)-C(3)-C(12)-C(13F)	134.0(15)
C(2')-N(2')-C(5')-C(4')	1.9(4)	C(4)-C(3)-C(12)-C(13C)	-20.0(5)
C(1)-N(2')-C(5')-C(4')	-169.8(3)	C(2)-C(3)-C(12)-C(13C)	161.0(4)
C(5A)-C(5)-C(6)-C(7)	2.6(5)	C(4)-C(3)-C(12)-C(13E)	-174.7(16)
C(5A)-C(5)-C(6)-C(10)	-177.7(3)	C(2)-C(3)-C(12)-C(13E)	6.3(17)
C(6)-C(5)-C(5A)-C(8A)	1.0(5)	C(4)-C(3)-C(12)-C(13A)	-140.0(4)
C(6)-C(5)-C(5A)-C(4A)	-179.7(4)	C(2)-C(3)-C(12)-C(13A)	41.0(5)
C(4)-C(4A)-C(5A)-C(5)	4.8(7)	C(4)-C(3)-C(12)-C(13D)	69.1(15)
C(1A)-C(4A)-C(5A)-C(5)	-176.4(4)	C(2)-C(3)-C(12)-C(13D)	-109.9(14)
C(4)-C(4A)-C(5A)-C(8A)	-175.8(4)	C(2')-N(3')-C(14)-C(15)	48.7(5)
C(1A)-C(4A)-C(5A)-C(8A)	3.0(4)	C(4')-N(3')-C(14)-C(15)	-132.7(4)
C(5)-C(6)-C(7)-C(8)	-3.0(6)	N(3')-C(14)-C(15)-C(16)	-63.9(5)
C(10)-C(6)-C(7)-C(8)	177.2(4)	C(14)-C(15)-C(16)-C(17)	104.9(5)
C(9')-N(8')-C(7')-N(6')	-1.8(4)	C(14)-C(15)-C(16)-Co(1)	22.6(5)
C(18)-N(8')-C(7')-N(6')	177.4(3)	C(15)-C(16)-C(17)-Co(1)	-110.1(4)
C(9')-N(8')-C(7')-Co(1)	171.5(3)	C(7')-N(8')-C(18)-C(19)	-106.5(4)
C(18)-N(8')-C(7')-Co(1)	-9.3(6)	C(9')-N(8')-C(18)-C(19)	72.7(5)
C(10')-N(6')-C(7')-N(8')	2.2(4)	N(8')-C(18)-C(19)-C(20)	165.8(4)
C(8)-N(6')-C(7')-N(8')	-179.4(3)	C(18)-C(19)-C(20)-C(21)	-116.1(8)



## 2.2. Compound 2



**Figure S21.** Solid-state molecular structure of **2** ( $\Delta$ -enantiomer). Atoms are shown with anisotropic atomic displacement parameters at the 30% probability level. The  $\Lambda$ -enantiomer, one co-crystallized toluene and the hydrogen atoms are omitted for clarity.

**Table S4.** Crystal data and structure refinement for compound **2**.

Identification code	Compound <b>2</b>	
Empirical formula	$C_{75} H_{88} Co_2 N_{10}$	
Formula weight	1247.41	
Temperature	100(2) K	
Wavelength	0.71073 Å	
Crystal system	Orthorhombic	
Space group	$Pca2_1$	
Unit cell dimensions	$a = 29.2752(8)$ Å	$\alpha = 90^\circ$ .
	$b = 12.3930(4)$ Å	$\beta = 90^\circ$ .
	$c = 17.4867(5)$ Å	$\gamma = 90^\circ$ .
Volume	6344.3(3) Å <sup>3</sup>	
Z	4	
Density (calculated)	1.306 Mg/m <sup>3</sup>	
Absorption coefficient	0.576 mm <sup>-1</sup>	
F(000)	2648	
Crystal size	0.284 x 0.269 x 0.183 mm <sup>3</sup>	
Theta range for data collection	1.814 to 27.620°.	
Index ranges	-38 ≤ h ≤ 38, -16 ≤ k ≤ 15, -21 ≤ l ≤ 22	
Reflections collected	105972	
Independent reflections	13536 [R(int) = 0.0623]	
Completeness to theta = 25.242°	99.9 %	
Absorption correction	Semi-empirical from equivalents	
Refinement method	Full-matrix least-squares on F <sup>2</sup>	
Data / restraints / parameters	13536 / 1 / 798	
Goodness-of-fit on F <sup>2</sup>	1.021	
Final R indices [I > 2σ(I)]	R1 = 0.0363, wR2 = 0.0798	

R indices (all data)	R1 = 0.0492, wR2 = 0.0855
Absolute structure parameter	0.363(12)
Extinction coefficient	n/a
Largest diff. peak and hole	0.520 and -0.275 e.Å <sup>-3</sup>

**Table S5.** Bond lengths [Å] and angles [°] for compound 2.

Co(1)-C(2A')	1.912(4)	C(4')-C(5')	1.340(5)	C(15)-H(16A)	0.9900
Co(1)-C(2')	1.913(3)	C(4')-H(4')	0.9500	C(15)-H(15A)	0.9900
Co(1)-N(9)	1.945(3)	C(5)-C(6)	1.388(5)	C(14A)-C(15A)	1.400(4)
Co(1)-C(15)	2.037(3)	C(5)-C(5A)	1.392(5)	C(14A)-H(14A)	1.0000
Co(1)-C(15A)	2.041(3)	C(5)-H(5)	0.9500	C(15A)-H(15B)	0.9900
Co(1)-C(14A)	2.079(3)	C(4A)-C(5A)	1.448(5)	C(15A)-H(15)	0.9900
Co(1)-C(14)	2.097(3)	C(5')-H(5')	0.9500	C(51)-C(52)	1.382(5)
Co(2)-C(52')	1.904(3)	C(6)-C(7)	1.413(5)	C(51)-C(51A)	1.402(5)
Co(2)-C(52A)	1.914(3)	C(6)-C(10)	1.541(4)	C(52)-C(53)	1.410(5)
Co(2)-N(59)	1.948(2)	C(5A)-C(8A)	1.424(4)	C(52)-H(52)	0.9500
Co(2)-C(65A)	2.033(3)	C(7)-C(8)	1.379(5)	C(51A)-C(54A)	1.422(4)
Co(2)-C(65)	2.049(3)	C(7)-H(7)	0.9500	C(53)-C(54)	1.393(5)
Co(2)-C(64)	2.086(3)	C(8)-C(8A)	1.407(5)	C(53)-C(60A)	1.540(5)
Co(2)-C(64A)	2.088(3)	C(10)-C(11B)	1.529(5)	C(54)-C(54A)	1.397(4)
N(1')-C(2')	1.376(4)	C(10)-C(11A)	1.535(5)	C(54)-H(54)	0.9500
N(1')-C(5')	1.392(4)	C(10)-C(11)	1.541(5)	C(54')-C(55')	1.342(5)
N(1')-C(1)	1.428(4)	C(11)-H(11M)	0.9800	C(54')-H(54')	0.9500
N(3')-C(2')	1.354(4)	C(11)-H(11N)	0.9800	C(55)-C(56)	1.385(5)
N(3')-C(4')	1.385(4)	C(11)-H(11O)	0.9800	C(55)-C(55A)	1.403(4)
N(3')-C(12)	1.465(4)	C(10A)-C(11E)	1.525(5)	C(55)-H(55)	0.9500
N(9)-C(8A)	1.360(4)	C(10A)-C(11C)	1.533(5)	C(54A)-C(55A)	1.437(5)
N(9)-C(1A)	1.371(4)	C(10A)-C(11D)	1.540(5)	C(54B)-C(55B)	1.336(5)
N(51')-C(52')	1.373(4)	C(12)-C(13)	1.517(5)	C(54B)-H(54B)	0.9500
N(51')-C(55')	1.394(4)	C(12)-H(12A)	0.9900	C(55')-H(55')	0.9500
N(51')-C(51)	1.427(4)	C(12)-H(12B)	0.9900	C(56)-C(57)	1.413(4)
N(51A)-C(52A)	1.375(4)	C(11A)-H(11A)	0.9800	C(56)-C(60)	1.532(5)
N(51A)-C(55B)	1.400(4)	C(11A)-H(11B)	0.9800	C(55A)-C(58A)	1.424(4)
N(51A)-C(58)	1.428(4)	C(11A)-H(11C)	0.9800	C(55B)-H(55B)	0.9500
N(53')-C(52')	1.359(4)	C(11B)-H(11D)	0.9800	C(57)-C(58)	1.381(5)
N(53')-C(54')	1.390(4)	C(11B)-H(11E)	0.9800	C(57)-H(57)	0.9500
N(53')-C(62)	1.465(4)	C(11B)-H(11F)	0.9800	C(58)-C(58A)	1.412(5)
N(53A)-C(52A)	1.352(4)	C(11C)-H(11P)	0.9800	C(60)-C(61A)	1.524(5)
N(53A)-C(54B)	1.386(4)	C(11C)-H(11Q)	0.9800	C(60)-C(61)	1.531(5)
N(53A)-C(62A)	1.470(4)	C(11C)-H(11R)	0.9800	C(60)-C(61B)	1.536(5)
N(59)-C(58A)	1.345(4)	C(11D)-H(11G)	0.9800	C(61)-H(61P)	0.9800
N(59)-C(51A)	1.359(4)	C(11D)-H(11H)	0.9800	C(61)-H(61Q)	0.9800
N(1A')-C(2A')	1.381(4)	C(11D)-H(11I)	0.9800	C(61)-H(61R)	0.9800
N(1A')-C(5A')	1.390(4)	C(11E)-H(11J)	0.9800	C(60A)-C(61E)	1.522(5)
N(1A')-C(8)	1.433(4)	C(11E)-H(11K)	0.9800	C(60A)-C(61D)	1.530(5)
N(3A')-C(2A')	1.358(4)	C(11E)-H(11L)	0.9800	C(60A)-C(61C)	1.535(5)
N(3A')-C(4A')	1.380(4)	C(13)-C(14)	1.527(5)	C(62)-C(63)	1.521(5)
N(3A')-C(12A)	1.470(4)	C(13)-H(13A)	0.9900	C(62)-H(62C)	0.9900
C(1)-C(2)	1.379(5)	C(13)-H(13B)	0.9900	C(62)-H(62D)	0.9900
C(1)-C(1A)	1.404(5)	C(12A)-C(13A)	1.520(5)	C(61A)-H(61A)	0.9800
C(2)-C(3)	1.410(5)	C(12A)-H(12C)	0.9900	C(61A)-H(61B)	0.9800
C(2)-H(2)	0.9500	C(12A)-H(12D)	0.9900	C(61A)-H(61C)	0.9800
C(1A)-C(4A)	1.424(4)	C(14)-C(15)	1.396(5)	C(61B)-H(61D)	0.9800
C(3)-C(4)	1.389(5)	C(14)-H(14)	1.0000	C(61B)-H(61E)	0.9800
C(3)-C(10A)	1.542(5)	C(13A)-C(14A)	1.526(5)	C(61B)-H(61F)	0.9800
C(4)-C(4A)	1.388(5)	C(13A)-H(13C)	0.9900	C(61C)-H(61M)	0.9800
C(4)-H(4)	0.9500	C(13A)-H(13D)	0.9900	C(61C)-H(61N)	0.9800

C(61C)-H(61O)	0.9800	N(9)-Co(1)-C(14)	129.34(13)	C(3)-C(2)-H(2)	118.9
C(61D)-H(61G)	0.9800	C(15)-Co(1)-C(14)	39.45(13)	N(9)-C(1A)-C(1)	127.9(3)
C(61D)-H(61H)	0.9800	C(15A)-Co(1)-C(14)	139.13(13)	N(9)-C(1A)-C(4A)	112.5(3)
C(61D)-H(61I)	0.9800	C(14A)-Co(1)-C(14)	99.84(13)	C(1)-C(1A)-C(4A)	119.6(3)
C(61E)-H(61J)	0.9800	C(52)-Co(2)-C(52A)	178.72(14)	N(3')-C(2')-N(1')	103.7(3)
C(61E)-H(61K)	0.9800	C(52)-Co(2)-N(59)	89.97(12)	N(3')-C(2')-Co(1)	126.2(2)
C(61E)-H(61L)	0.9800	C(52A)-Co(2)-N(59)	89.57(12)	N(1')-C(2')-Co(1)	129.8(2)
C(63)-C(64)	1.516(5)	C(52)-Co(2)-C(65A)	88.16(14)	C(4)-C(3)-C(2)	119.1(3)
C(63)-H(63C)	0.9900	C(52A)-Co(2)-C(65A)	93.04(14)	C(4)-C(3)-C(10A)	119.6(3)
C(63)-H(63D)	0.9900	N(59)-Co(2)-C(65A)	90.33(12)	C(2)-C(3)-C(10A)	121.2(3)
C(62A)-C(63A)	1.521(5)	C(52)-Co(2)-C(65)	91.00(14)	C(4A)-C(4)-C(3)	120.1(3)
C(62A)-H(62A)	0.9900	C(52A)-Co(2)-C(65)	87.80(14)	C(4A)-C(4)-H(4)	120.0
C(62A)-H(62B)	0.9900	N(59)-Co(2)-C(65)	89.90(12)	C(3)-C(4)-H(4)	120.0
C(64)-C(65)	1.406(5)	C(65A)-Co(2)-C(65)	179.13(15)	C(5')-C(4')-N(3')	106.9(3)
C(64)-H(64)	1.0000	C(52)-Co(2)-C(64)	89.19(14)	C(5')-C(4')-H(4')	126.6
C(63A)-C(64A)	1.524(5)	C(52A)-Co(2)-C(64)	90.18(14)	N(3')-C(4')-H(4')	126.6
C(63A)-H(63A)	0.9900	N(59)-Co(2)-C(64)	129.61(12)	C(6)-C(5)-C(5A)	120.3(3)
C(63A)-H(63B)	0.9900	C(65A)-Co(2)-C(64)	139.98(13)	C(6)-C(5)-H(5)	119.8
C(65)-H(65B)	0.9900	C(65)-Co(2)-C(64)	39.75(13)	C(5A)-C(5)-H(5)	119.8
C(65)-H(65A)	0.9900	C(52)-Co(2)-C(64A)	92.65(13)	C(4)-C(4A)-C(1A)	120.4(3)
C(64A)-C(65A)	1.400(5)	C(52A)-Co(2)-C(64A)	88.57(13)	C(4)-C(4A)-C(5A)	134.8(3)
C(64A)-H(64A)	1.0000	N(59)-Co(2)-C(64A)	129.73(12)	C(1A)-C(4A)-C(5A)	104.8(3)
C(65A)-H(66')	0.9900	C(65A)-Co(2)-C(64A)	39.70(13)	C(4')-C(5')-N(1')	106.9(3)
C(65A)-H(65')	0.9900	C(65)-Co(2)-C(64A)	140.16(13)	C(4')-C(5')-H(5')	126.6
C(70)-C(71)	1.511(8)	C(64)-Co(2)-C(64A)	100.63(13)	N(1')-C(5')-H(5')	126.6
C(70)-H(70A)	0.9800	C(2')-N(1')-C(5')	110.7(3)	C(5)-C(6)-C(7)	118.6(3)
C(70)-H(70B)	0.9800	C(2')-N(1')-C(1)	124.3(3)	C(5)-C(6)-C(10)	120.1(3)
C(70)-H(70C)	0.9800	C(5')-N(1')-C(1)	124.5(3)	C(7)-C(6)-C(10)	121.2(3)
C(71)-C(72)	1.380(7)	C(2')-N(3')-C(4')	111.8(3)	C(5)-C(5A)-C(8A)	120.6(3)
C(71)-C(76)	1.380(7)	C(2')-N(3')-C(12)	123.3(3)	C(5)-C(5A)-C(4A)	134.6(3)
C(72)-C(73)	1.386(8)	C(4')-N(3')-C(12)	124.0(3)	C(8A)-C(5A)-C(4A)	104.6(3)
C(72)-H(72)	0.9500	C(8A)-N(9)-C(1A)	105.2(3)	C(8)-C(7)-C(6)	122.2(3)
C(73)-C(74)	1.376(8)	C(8A)-N(9)-Co(1)	127.8(2)	C(8)-C(7)-H(7)	118.9
C(73)-H(73)	0.9500	C(1A)-N(9)-Co(1)	127.0(2)	C(6)-C(7)-H(7)	118.9
C(74)-C(75)	1.386(7)	C(52)-N(51')-C(55')	110.9(3)	C(7)-C(8)-C(8A)	119.2(3)
C(74)-H(74)	0.9500	C(52)-N(51')-C(51)	124.4(3)	C(7)-C(8)-N(1A')	121.7(3)
C(75)-C(76)	1.377(7)	C(55)-N(51')-C(51)	123.9(3)	C(8A)-C(8)-N(1A')	118.7(3)
C(75)-H(75)	0.9500	C(52A)-N(51A)-C(55B)	110.7(3)	N(9)-C(8A)-C(8)	128.1(3)
C(76)-H(76)	0.9500	C(52A)-N(51A)-C(58)	124.3(3)	N(9)-C(8A)-C(5A)	112.9(3)
C(4A)-C(5A)	1.343(5)	C(55B)-N(51A)-C(58)	124.7(3)	C(8)-C(8A)-C(5A)	118.9(3)
C(4A)-H(4A)	0.9500	C(52)-N(53')-C(54')	111.6(3)	C(11B)-C(10)-C(11A)	110.3(3)
C(5A)-H(5A)	0.9500	C(52)-N(53')-C(62)	122.7(3)	C(11B)-C(10)-C(11)	108.7(3)
		C(54')-N(53')-C(62)	125.3(3)	C(11A)-C(10)-C(11)	106.3(3)
C(2A)-Co(1)-C(2')	179.20(15)	C(52A)-N(53A)-C(54B)	111.7(3)	C(11B)-C(10)-C(6)	109.2(3)
C(2A)-Co(1)-N(9)	89.56(13)	C(52A)-N(53A)-C(62A)	123.1(3)	C(11A)-C(10)-C(6)	110.1(3)
C(2)-Co(1)-N(9)	89.89(13)	C(54B)-N(53A)-C(62A)	124.5(3)	C(11)-C(10)-C(6)	112.3(3)
C(2A)-Co(1)-C(15)	88.04(14)	C(58A)-N(59)-C(51A)	106.0(3)	C(10)-C(11)-H(11M)	109.5
C(2)-Co(1)-C(15)	92.55(14)	C(58A)-N(59)-Co(2)	127.4(2)	C(10)-C(11)-H(11N)	109.5
N(9)-Co(1)-C(15)	90.17(13)	C(51A)-N(59)-Co(2)	126.5(2)	H(11M)-C(11)-H(11N)	109.5
C(2A)-Co(1)-C(15A)	91.85(14)	C(2A)-N(1A)-C(5A')	110.4(3)	C(10)-C(11)-H(11O)	109.5
C(2)-Co(1)-C(15A)	87.57(14)	C(2A)-N(1A)-C(8)	124.5(3)	H(11M)-C(11)-H(11O)	109.5
N(9)-Co(1)-C(15A)	91.27(12)	C(5A)-N(1A)-C(8)	124.4(3)	H(11N)-C(11)-H(11O)	109.5
C(15)-Co(1)-C(15A)	178.55(14)	C(2A)-N(3A)-C(4A')	111.8(3)	C(11E)-C(10A)-C(11C)	108.1(3)
C(2A)-Co(1)-C(14A)	88.59(14)	C(2A)-N(3A)-C(12A)	122.7(3)	C(11E)-C(10A)-C(11D)	107.8(3)
C(2)-Co(1)-C(14A)	91.32(14)	C(4A)-N(3A)-C(12A)	124.9(3)	C(11C)-C(10A)-C(11D)	109.2(3)
N(9)-Co(1)-C(14A)	130.81(12)	C(2)-C(1)-C(1A)	118.7(3)	C(11E)-C(10A)-C(3)	112.7(3)
C(15)-Co(1)-C(14A)	138.84(14)	C(2)-C(1)-N(1')	121.8(3)	C(11C)-C(10A)-C(3)	110.2(3)
C(15A)-Co(1)-C(14A)	39.71(12)	C(1A)-C(1)-N(1')	119.3(3)	C(11D)-C(10A)-C(3)	108.8(3)
C(2A)-Co(1)-C(14)	92.73(14)	C(1)-C(2)-C(3)	122.2(3)	N(3')-C(12)-C(13)	109.2(3)
C(2)-Co(1)-C(14)	88.07(14)	C(1)-C(2)-H(2)	118.9	N(3')-C(12)-H(12A)	109.8

C(13)-C(12)-H(12A)	109.8	Co(1)-C(15)-H(16A)	116.3	N(51A)-C(55B)-H(55B)	126.7
N(3')-C(12)-H(12B)	109.8	C(14)-C(15)-H(15A)	116.3	C(58)-C(57)-C(56)	123.1(3)
C(13)-C(12)-H(12B)	109.8	Co(1)-C(15)-H(15A)	116.3	C(58)-C(57)-H(57)	118.4
H(12A)-C(12)-H(12B)	108.3	H(16A)-C(15)-H(15A)	113.3	C(56)-C(57)-H(57)	118.4
C(10)-C(11A)-H(11A)	109.5	C(15A)-C(14A)-C(13A)	120.3(3)	C(57)-C(58)-C(58A)	118.4(3)
C(10)-C(11A)-H(11B)	109.5	C(15A)-C(14A)-Co(1)	68.67(19)	C(57)-C(58)-N(51A)	122.5(3)
H(11A)-C(11A)-H(11B)	109.5	C(13A)-C(14A)-Co(1)	120.5(2)	C(58A)-C(58)-N(51A)	119.0(3)
C(10)-C(11A)-H(11C)	109.5	C(15A)-C(14A)-H(14A)	113.4	N(59)-C(58A)-C(58)	128.1(3)
H(11A)-C(11A)-H(11C)	109.5	C(13A)-C(14A)-H(14A)	113.4	N(59)-C(58A)-C(55A)	112.7(3)
H(11B)-C(11A)-H(11C)	109.5	Co(1)-C(14A)-H(14A)	113.4	C(58)-C(58A)-C(55A)	119.2(3)
C(10)-C(11B)-H(11D)	109.5	C(14A)-C(15A)-Co(1)	71.6(2)	C(61A)-C(60)-C(61)	108.6(3)
C(10)-C(11B)-H(11E)	109.5	C(14A)-C(15A)-H(15B)	116.4	C(61A)-C(60)-C(56)	112.3(3)
H(11D)-C(11B)-H(11E)	109.5	Co(1)-C(15A)-H(15B)	116.4	C(61)-C(60)-C(56)	109.2(3)
C(10)-C(11B)-H(11F)	109.5	C(14A)-C(15A)-H(15)	116.4	C(61A)-C(60)-C(61B)	107.6(3)
H(11D)-C(11B)-H(11F)	109.5	Co(1)-C(15A)-H(15)	116.4	C(61)-C(60)-C(61B)	108.9(3)
H(11E)-C(11B)-H(11F)	109.5	H(15B)-C(15A)-H(15)	113.4	C(56)-C(60)-C(61B)	110.2(3)
C(10A)-C(11C)-H(11P)	109.5	C(52)-C(51)-C(51)	118.4(3)	C(60)-C(61)-H(61P)	109.5
C(10A)-C(11C)-H(11Q)	109.5	C(52)-C(51)-N(51')	122.2(3)	C(60)-C(61)-H(61Q)	109.5
H(11P)-C(11C)-H(11Q)	109.5	C(51A)-C(51)-N(51')	119.0(3)	H(61P)-C(61)-H(61Q)	109.5
C(10A)-C(11C)-H(11R)	109.5	C(51)-C(52)-C(53)	122.6(3)	C(60)-C(61)-H(61R)	109.5
H(11P)-C(11C)-H(11R)	109.5	C(51)-C(52)-H(52)	118.7	H(61P)-C(61)-H(61R)	109.5
H(11Q)-C(11C)-H(11R)	109.5	C(53)-C(52)-H(52)	118.7	H(61Q)-C(61)-H(61R)	109.5
C(10A)-C(11D)-H(11G)	109.5	N(59)-C(51A)-C(51)	128.3(3)	C(61E)-C(60A)-C(61D)	109.2(3)
C(10A)-C(11D)-H(11H)	109.5	N(59)-C(51A)-C(54A)	111.8(3)	C(61E)-C(60A)-C(61C)	109.3(3)
H(11G)-C(11D)-H(11H)	109.5	C(51)-C(51A)-C(54A)	119.8(3)	C(61D)-C(60A)-C(61C)	107.1(3)
C(10A)-C(11D)-H(11I)	109.5	N(53')-C(52')-N(51')	103.8(3)	C(61E)-C(60A)-C(53)	111.1(3)
H(11G)-C(11D)-H(11I)	109.5	N(53')-C(52')-Co(2)	126.4(3)	C(61D)-C(60A)-C(53)	108.5(3)
H(11H)-C(11D)-H(11I)	109.5	N(51')-C(52')-Co(2)	129.8(2)	C(61C)-C(60A)-C(53)	111.5(3)
C(10A)-C(11E)-H(11J)	109.5	C(54)-C(53)-C(52)	118.7(3)	N(53')-C(62)-C(63)	111.2(3)
C(10A)-C(11E)-H(11K)	109.5	C(54)-C(53)-C(60A)	122.6(3)	N(53')-C(62)-H(62C)	109.4
H(11J)-C(11E)-H(11K)	109.5	C(52)-C(53)-C(60A)	118.7(3)	C(63)-C(62)-H(62C)	109.4
C(10A)-C(11E)-H(11L)	109.5	N(53A)-C(52A)-N(51A)	103.8(3)	N(53')-C(62)-H(62D)	109.4
H(11J)-C(11E)-H(11L)	109.5	N(53A)-C(52A)-Co(2)	126.2(2)	C(63)-C(62)-H(62D)	109.4
H(11K)-C(11E)-H(11L)	109.5	N(51A)-C(52A)-Co(2)	129.5(2)	H(62C)-C(62)-H(62D)	108.0
C(12)-C(13)-C(14)	115.7(3)	C(53)-C(54)-C(54A)	120.0(3)	C(60)-C(61A)-H(61A)	109.5
C(12)-C(13)-H(13A)	108.4	C(53)-C(54)-H(54)	120.0	C(60)-C(61A)-H(61B)	109.5
C(14)-C(13)-H(13A)	108.4	C(54A)-C(54)-H(54)	120.0	H(61A)-C(61A)-H(61B)	109.5
C(12)-C(13)-H(13B)	108.4	C(55')-C(54')-N(53')	106.8(3)	C(60)-C(61A)-H(61C)	109.5
C(14)-C(13)-H(13B)	108.4	C(55')-C(54')-H(54')	126.6	H(61A)-C(61A)-H(61C)	109.5
H(13A)-C(13)-H(13B)	107.4	N(53')-C(54')-H(54')	126.6	H(61B)-C(61A)-H(61C)	109.5
N(3A')-C(12A)-C(13A)	110.2(3)	C(56)-C(55)-C(55A)	120.1(3)	C(60)-C(61B)-H(61D)	109.5
N(3A')-C(12A)-H(12C)	109.6	C(56)-C(55)-H(55)	120.0	C(60)-C(61B)-H(61E)	109.5
C(13A)-C(12A)-H(12C)	109.6	C(55A)-C(55)-H(55)	120.0	H(61D)-C(61B)-H(61E)	109.5
N(3A')-C(12A)-H(12D)	109.6	C(54)-C(54A)-C(51A)	120.3(3)	C(60)-C(61B)-H(61F)	109.5
C(13A)-C(12A)-H(12D)	109.6	C(54)-C(54A)-C(55A)	134.6(3)	H(61D)-C(61B)-H(61F)	109.5
H(12C)-C(12A)-H(12D)	108.1	C(51A)-C(54A)-C(55A)	105.1(3)	H(61E)-C(61B)-H(61F)	109.5
C(15)-C(14)-C(13)	121.3(3)	C(55B)-C(54B)-N(53A)	107.2(3)	C(60A)-C(61C)-H(61M)	109.5
C(15)-C(14)-Co(1)	67.94(19)	C(55B)-C(54B)-H(54B)	126.4	C(60A)-C(61C)-H(61N)	109.5
C(13)-C(14)-Co(1)	119.3(2)	N(53A)-C(54B)-H(54B)	126.4	H(61M)-C(61C)-H(61N)	109.5
C(15)-C(14)-H(14)	113.6	C(54')-C(55')-N(51')	106.9(3)	C(60A)-C(61C)-H(61O)	109.5
C(13)-C(14)-H(14)	113.6	C(54')-C(55')-H(55')	126.5	H(61M)-C(61C)-H(61O)	109.5
Co(1)-C(14)-H(14)	113.6	N(51')-C(55')-H(55')	126.5	H(61N)-C(61C)-H(61O)	109.5
C(12A)-C(13A)-C(14A)	114.7(3)	C(55)-C(56)-C(57)	118.5(3)	C(60A)-C(61D)-H(61G)	109.5
C(12A)-C(13A)-H(13C)	108.6	C(55)-C(56)-C(60)	123.0(3)	C(60A)-C(61D)-H(61H)	109.5
C(14A)-C(13A)-H(13C)	108.6	C(57)-C(56)-C(60)	118.6(3)	H(61G)-C(61D)-H(61H)	109.5
C(12A)-C(13A)-H(13D)	108.6	C(55)-C(55A)-C(58A)	120.7(3)	C(60A)-C(61D)-H(61I)	109.5
C(14A)-C(13A)-H(13D)	108.6	C(55)-C(55A)-C(54A)	135.0(3)	H(61G)-C(61D)-H(61I)	109.5
H(13C)-C(13A)-H(13D)	107.6	C(58A)-C(55A)-C(54A)	104.3(3)	H(61H)-C(61D)-H(61I)	109.5
C(14)-C(15)-Co(1)	72.61(19)	C(54B)-C(55B)-N(51A)	106.5(3)	C(60A)-C(61E)-H(61J)	109.5
C(14)-C(15)-H(16A)	116.3	C(54B)-C(55B)-H(55B)	126.7	C(60A)-C(61E)-H(61K)	109.5



H(61J)-C(61E)-H(61K)	109.5	H(63A)-C(63A)-H(63B)	107.4	C(76)-C(71)-C(70)	120.7(5)
C(60A)-C(61E)-H(61L)	109.5	C(64)-C(65)-Co(2)	71.53(19)	C(71)-C(72)-C(73)	120.7(5)
H(61J)-C(61E)-H(61L)	109.5	C(64)-C(65)-H(65B)	116.4	C(71)-C(72)-H(72)	119.7
H(61K)-C(61E)-H(61L)	109.5	Co(2)-C(65)-H(65B)	116.4	C(73)-C(72)-H(72)	119.7
C(64)-C(63)-C(62)	115.5(3)	C(64)-C(65)-H(65A)	116.4	C(74)-C(73)-C(72)	122.1(5)
C(64)-C(63)-H(63C)	108.4	Co(2)-C(65)-H(65A)	116.4	C(74)-C(73)-H(73)	118.9
C(62)-C(63)-H(63C)	108.4	H(65B)-C(65)-H(65A)	113.4	C(72)-C(73)-H(73)	118.9
C(64)-C(63)-H(63D)	108.4	C(65A)-C(64A)-C(63A)	121.1(3)	C(73)-C(74)-C(75)	116.7(5)
C(62)-C(63)-H(63D)	108.4	C(65A)-C(64A)-Co(2)	68.05(18)	C(73)-C(74)-H(74)	121.7
H(63C)-C(63)-H(63D)	107.5	C(63A)-C(64A)-Co(2)	119.2(2)	C(75)-C(74)-H(74)	121.7
N(53A)-C(62A)-C(63A)	109.7(3)	C(65A)-C(64A)-H(64A)	113.7	C(76)-C(75)-C(74)	121.6(5)
N(53A)-C(62A)-H(62A)	109.7	C(63A)-C(64A)-H(64A)	113.7	C(76)-C(75)-H(75)	119.2
C(63A)-C(62A)-H(62A)	109.7	Co(2)-C(64A)-H(64A)	113.7	C(74)-C(75)-H(75)	119.2
N(53A)-C(62A)-H(62B)	109.7	C(64A)-C(65A)-Co(2)	72.26(19)	C(75)-C(76)-C(71)	121.3(5)
C(63A)-C(62A)-H(62B)	109.7	C(64A)-C(65A)-H(66')	116.3	C(75)-C(76)-H(76)	119.4
H(62A)-C(62A)-H(62B)	108.2	Co(2)-C(65A)-H(66')	116.3	C(71)-C(76)-H(76)	119.4
C(65)-C(64)-C(63)	121.2(3)	C(64A)-C(65A)-H(65')	116.3	N(3A')-C(2A')-N(1A')	103.8(3)
C(65)-C(64)-Co(2)	68.72(19)	Co(2)-C(65A)-H(65')	116.3	N(3A')-C(2A')-Co(1)	126.3(3)
C(63)-C(64)-Co(2)	120.5(2)	H(66')-C(65A)-H(65')	113.3	N(1A')-C(2A')-Co(1)	129.7(2)
C(65)-C(64)-H(64)	113.2	C(71)-C(70)-H(70A)	109.5	C(5A')-C(4A')-N(3A')	106.9(3)
C(63)-C(64)-H(64)	113.2	C(71)-C(70)-H(70B)	109.5	C(5A')-C(4A')-H(4A')	126.6
Co(2)-C(64)-H(64)	113.2	H(70A)-C(70)-H(70B)	109.5	N(3A')-C(4A')-H(4A')	126.6
C(62A)-C(63A)-C(64A)	116.0(3)	C(71)-C(70)-H(70C)	109.5	C(4A')-C(5A')-N(1A')	107.2(3)
C(62A)-C(63A)-H(63A)	108.3	H(70A)-C(70)-H(70C)	109.5	C(4A')-C(5A')-H(5A')	126.4
C(64A)-C(63A)-H(63A)	108.3	H(70B)-C(70)-H(70C)	109.5	N(1A')-C(5A')-H(5A')	126.4
C(62A)-C(63A)-H(63B)	108.3	C(72)-C(71)-C(76)	117.7(5)		
C(64A)-C(63A)-H(63B)	108.3	C(72)-C(71)-C(70)	121.7(5)		

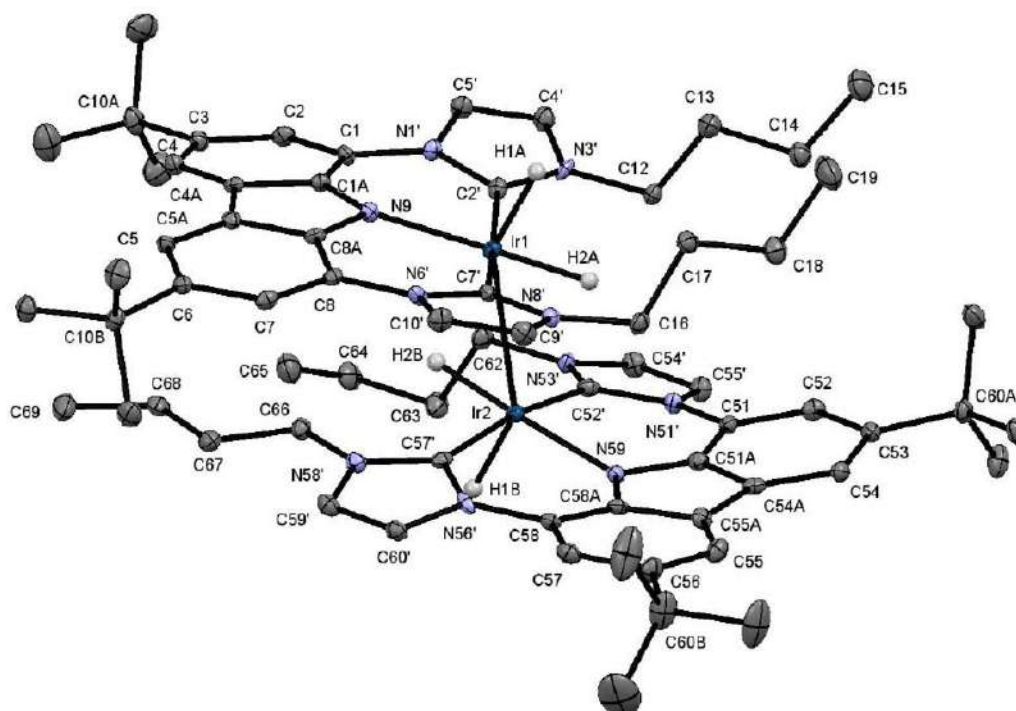
Table S6. Torsion angles [°] for compound 2.

C(2')-N(1')-C(1)-C(2)	-173.6(3)	C(3)-C(4)-C(4A)-C(1A)	-0.2(5)
C(5')-N(1')-C(1)-C(2)	-2.2(5)	C(3)-C(4)-C(4A)-C(5A)	-179.9(3)
C(2')-N(1')-C(1)-C(1A)	2.7(5)	N(9)-C(1A)-C(4A)-C(4)	-179.4(3)
C(5')-N(1')-C(1)-C(1A)	174.0(3)	C(1)-C(1A)-C(4A)-C(4)	0.3(5)
C(1A)-C(1)-C(2)-C(3)	-0.3(5)	N(9)-C(1A)-C(4A)-C(5A)	0.4(3)
N(1')-C(1)-C(2)-C(3)	176.0(3)	C(1)-C(1A)-C(4A)-C(5A)	-179.9(3)
C(8A)-N(9)-C(1A)-C(1)	-179.9(3)	N(3')-C(4')-C(5')-N(1')	-0.1(4)
Co(1)-N(9)-C(1A)-C(1)	2.5(5)	C(2')-N(1')-C(5')-C(4')	0.7(4)
C(8A)-N(9)-C(1A)-C(4A)	-0.3(3)	C(1)-N(1')-C(5')-C(4')	-171.6(3)
Co(1)-N(9)-C(1A)-C(4A)	-177.9(2)	C(5A)-C(5)-C(6)-C(7)	-2.2(5)
C(2)-C(1)-C(1A)-N(9)	179.5(3)	C(5A)-C(5)-C(6)-C(10)	178.2(3)
N(1')-C(1)-C(1A)-N(9)	3.2(5)	C(6)-C(5)-C(5A)-C(8A)	-0.2(5)
C(2)-C(1)-C(1A)-C(4A)	-0.1(4)	C(6)-C(5)-C(5A)-C(4A)	-175.2(3)
N(1')-C(1)-C(1A)-C(4A)	-176.4(3)	C(4)-C(4A)-C(5A)-C(5)	-5.0(7)
C(4')-N(3')-C(2')-N(1')	1.0(4)	C(1A)-C(4A)-C(5A)-C(5)	175.3(4)
C(12)-N(3')-C(2')-N(1')	-168.8(3)	C(4)-C(4A)-C(5A)-C(8A)	179.4(4)
C(4')-N(3')-C(2')-Co(1)	-173.4(2)	C(1A)-C(4A)-C(5A)-C(8A)	-0.3(3)
C(12)-N(3')-C(2')-Co(1)	16.9(5)	C(5)-C(6)-C(7)-C(8)	3.0(5)
C(5')-N(1')-C(2')-N(3')	-1.0(4)	C(10)-C(6)-C(7)-C(8)	-177.5(3)
C(1)-N(1')-C(2')-N(3')	171.4(3)	C(6)-C(7)-C(8)-C(8A)	-1.2(5)
C(5')-N(1')-C(2')-Co(1)	173.1(2)	C(6)-C(7)-C(8)-N(1A')	171.6(3)
C(1)-N(1')-C(2')-Co(1)	-14.6(5)	C(2A')-N(1A')-C(8)-C(7)	-168.3(3)
C(1)-C(2)-C(3)-C(4)	0.4(5)	C(5A')-N(1A')-C(8)-C(7)	0.5(5)
C(1)-C(2)-C(3)-C(10A)	-175.6(3)	C(2A')-N(1A')-C(8)-C(8A)	4.5(4)
C(2)-C(3)-C(4)-C(4A)	-0.2(5)	C(5A')-N(1A')-C(8)-C(8A)	173.3(3)
C(10A)-C(3)-C(4)-C(4A)	175.9(3)	C(1A)-N(9)-C(8A)-C(8)	-177.9(3)
C(2')-N(3')-C(4')-C(5')	-0.5(4)	Co(1)-N(9)-C(8A)-C(8)	-0.3(5)
C(12)-N(3')-C(4')-C(5')	169.1(3)	C(1A)-N(9)-C(8A)-C(5A)	0.1(3)

Co(1)-N(9)-C(8A)-C(5A)	177.6(2)	C(62A)-N(53A)-C(52A)-Co(2)	-17.5(4)
C(7)-C(8)-C(8A)-N(9)	176.6(3)	C(55B)-N(51A)-C(52A)-N(53A)	1.1(3)
N(1A')-C(8)-C(8A)-N(9)	3.6(5)	C(58)-N(51A)-C(52A)-N(53A)	-172.7(3)
C(7)-C(8)-C(8A)-C(5A)	-1.3(5)	C(55B)-N(51A)-C(52A)-Co(2)	-171.6(2)
N(1A')-C(8)-C(8A)-C(5A)	-174.3(3)	C(58)-N(51A)-C(52A)-Co(2)	14.6(5)
C(5)-C(5A)-C(8A)-N(9)	-176.2(3)	C(52)-C(53)-C(54)-C(54A)	-0.5(5)
C(4A)-C(5A)-C(8A)-N(9)	0.2(4)	C(60A)-C(53)-C(54)-C(54A)	177.8(3)
C(5)-C(5A)-C(8A)-C(8)	2.0(5)	C(52')-N(53')-C(54')-C(55')	-0.6(4)
C(4A)-C(5A)-C(8A)-C(8)	178.3(3)	C(62)-N(53')-C(54')-C(55')	-173.9(3)
C(5)-C(6)-C(10)-C(11B)	76.9(4)	C(53)-C(54)-C(54A)-C(51A)	1.1(5)
C(7)-C(6)-C(10)-C(11B)	-102.6(4)	C(53)-C(54)-C(54A)-C(55A)	178.8(3)
C(5)-C(6)-C(10)-C(11A)	-44.3(4)	N(59)-C(51A)-C(54A)-C(54)	179.1(3)
C(7)-C(6)-C(10)-C(11A)	136.2(4)	C(51)-C(51A)-C(54A)-C(54)	0.7(5)
C(5)-C(6)-C(10)-C(11)	-162.5(3)	N(59)-C(51A)-C(54A)-C(55A)	0.8(4)
C(7)-C(6)-C(10)-C(11)	18.0(5)	C(51)-C(51A)-C(54A)-C(55A)	-177.6(3)
C(4)-C(3)-C(10A)-C(11E)	178.5(3)	C(52A)-N(53A)-C(54B)-C(55B)	0.7(4)
C(2)-C(3)-C(10A)-C(11E)	-5.6(5)	C(62A)-N(53A)-C(54B)-C(55B)	-169.7(3)
C(4)-C(3)-C(10A)-C(11C)	57.7(4)	N(53')-C(54')-C(55')-N(51')	0.5(4)
C(2)-C(3)-C(10A)-C(11C)	-126.4(3)	C(52')-N(51')-C(55')-C(54')	-0.3(4)
C(4)-C(3)-C(10A)-C(11D)	-62.0(4)	C(51)-N(51')-C(55')-C(54')	169.9(3)
C(2)-C(3)-C(10A)-C(11D)	113.9(3)	C(55A)-C(55)-C(56)-C(57)	-1.0(5)
C(2')-N(3')-C(12)-C(13)	43.5(4)	C(55A)-C(55)-C(56)-C(60)	178.9(3)
C(4')-N(3')-C(12)-C(13)	-125.0(3)	C(56)-C(55)-C(55A)-C(58A)	1.2(5)
N(3')-C(12)-C(13)-C(14)	-63.6(4)	C(56)-C(55)-C(55A)-C(54A)	-179.1(3)
C(2A')-N(3A')-C(12A)-C(13A)	45.4(4)	C(54)-C(54A)-C(55A)-C(55)	1.3(7)
C(4A')-N(3A')-C(12A)-C(13A)	-125.3(3)	C(51A)-C(54A)-C(55A)-C(55)	179.3(4)
C(12)-C(13)-C(14)-C(15)	108.3(4)	C(54)-C(54A)-C(55A)-C(58A)	-178.9(4)
C(12)-C(13)-C(14)-Co(1)	27.6(4)	C(51A)-C(54A)-C(55A)-C(58A)	-0.9(3)
N(3A')-C(12A)-C(13A)-C(14A)	-62.6(4)	N(53A)-C(54B)-C(55B)-N(51A)	0.0(4)
C(13)-C(14)-C(15)-Co(1)	-111.7(3)	C(52A)-N(51A)-C(55B)-C(54B)	-0.7(4)
C(12A)-C(13A)-C(14A)-C(15A)	107.1(4)	C(58)-N(51A)-C(55B)-C(54B)	173.0(3)
C(12A)-C(13A)-C(14A)-Co(1)	25.5(4)	C(55)-C(56)-C(57)-C(58)	-0.6(5)
C(13A)-C(14A)-C(15A)-Co(1)	-113.7(3)	C(60)-C(56)-C(57)-C(58)	179.5(3)
C(52')-N(51')-C(51)-C(52)	175.2(3)	C(56)-C(57)-C(58)-C(58A)	1.9(5)
C(55')-N(51')-C(51)-C(52)	6.3(5)	C(56)-C(57)-C(58)-N(51A)	-174.1(3)
C(52')-N(51')-C(51)-C(51A)	1.3(4)	C(52A)-N(51A)-C(58)-C(57)	175.5(3)
C(55')-N(51')-C(51)-C(51A)	-167.5(3)	C(55B)-N(51A)-C(58)-C(57)	2.5(5)
C(51A)-C(51)-C(52)-C(53)	3.8(5)	C(52A)-N(51A)-C(58)-C(58A)	-0.5(4)
N(51')-C(51)-C(52)-C(53)	-170.1(3)	C(55B)-N(51A)-C(58)-C(58A)	-173.5(3)
C(58A)-N(59)-C(51A)-C(51)	177.9(3)	C(51A)-N(59)-C(58A)-C(58)	-179.9(3)
Co(2)-N(59)-C(51A)-C(51)	-0.7(5)	Co(2)-N(59)-C(58A)-C(58)	-1.2(5)
C(58A)-N(59)-C(51A)-C(54A)	-0.3(4)	C(51A)-N(59)-C(58A)-C(55A)	-0.4(4)
Co(2)-N(59)-C(51A)-C(54A)	-178.9(2)	Co(2)-N(59)-C(58A)-C(55A)	178.3(2)
C(52)-C(51)-C(51A)-N(59)	178.8(3)	C(57)-C(58)-C(58A)-N(59)	177.8(3)
N(51')-C(51)-C(51A)-N(59)	-7.1(5)	N(51A)-C(58)-C(58A)-N(59)	-6.1(5)
C(52)-C(51)-C(51A)-C(54A)	-3.1(5)	C(57)-C(58)-C(58A)-C(55A)	-1.7(4)
N(51')-C(51)-C(51A)-C(54A)	171.0(3)	N(51A)-C(58)-C(58A)-C(55A)	174.4(3)
C(54')-N(53')-C(52')-N(51')	0.4(4)	C(55)-C(55A)-C(58A)-N(59)	-179.3(3)
C(62)-N(53')-C(52')-N(51')	173.9(3)	C(54A)-C(55A)-C(58A)-N(59)	0.8(4)
C(54')-N(53')-C(52')-Co(2)	177.8(2)	C(55)-C(55A)-C(58A)-C(58)	0.2(5)
C(62)-N(53')-C(52')-Co(2)	-8.7(4)	C(54A)-C(55A)-C(58A)-C(58)	-179.6(3)
C(55')-N(51')-C(52')-N(53')	-0.1(4)	C(55)-C(56)-C(60)-C(61A)	4.9(5)
C(51)-N(51')-C(52')-N(53')	-170.2(3)	C(57)-C(56)-C(60)-C(61A)	-175.2(3)
C(55')-N(51')-C(52')-Co(2)	-177.4(2)	C(55)-C(56)-C(60)-C(61)	-115.6(4)
C(51)-N(51')-C(52')-Co(2)	12.5(5)	C(57)-C(56)-C(60)-C(61)	64.3(4)
C(51)-C(52)-C(53)-C(54)	-2.0(5)	C(55)-C(56)-C(60)-C(61B)	124.9(4)
C(51)-C(52)-C(53)-C(60A)	179.7(3)	C(57)-C(56)-C(60)-C(61B)	-55.2(4)
C(54B)-N(53A)-C(52A)-N(51A)	-1.1(4)	C(54)-C(53)-C(60A)-C(61E)	133.3(4)
C(62A)-N(53A)-C(52A)-N(51A)	169.4(3)	C(52)-C(53)-C(60A)-C(61E)	-48.4(4)
C(54B)-N(53A)-C(52A)-Co(2)	171.9(2)	C(54)-C(53)-C(60A)-C(61D)	-106.7(4)

C(52)-C(53)-C(60A)-C(61D)	71.6(4)	C(72)-C(73)-C(74)-C(75)	-0.8(7)
C(54)-C(53)-C(60A)-C(61C)	11.1(5)	C(73)-C(74)-C(75)-C(76)	1.0(7)
C(52)-C(53)-C(60A)-C(61C)	-170.6(3)	C(74)-C(75)-C(76)-C(71)	-1.0(7)
C(52)-N(53)-C(62)-C(63)	-48.0(4)	C(72)-C(71)-C(76)-C(75)	0.8(7)
C(54)-N(53)-C(62)-C(63)	124.5(3)	C(70)-C(71)-C(76)-C(75)	180.0(5)
N(53)-C(62)-C(63)-C(64)	59.5(4)	C(4A)-N(3A)-C(2A)-N(1A)	0.6(4)
C(52A)-N(53A)-C(62A)-C(63A)	-42.1(4)	C(12A)-N(3A)-C(2A)-N(1A)	-171.1(3)
C(54B)-N(53A)-C(62A)-C(63A)	127.2(3)	C(4A)-N(3A)-C(2A)-Co(1)	-174.4(2)
C(62)-C(63)-C(64)-C(65)	-101.9(4)	C(12A)-N(3A)-C(2A)-Co(1)	13.9(4)
C(62)-C(63)-C(64)-Co(2)	-19.8(4)	C(5A)-N(1A)-C(2A)-N(3A)	-1.0(4)
N(53A)-C(62A)-C(63A)-C(64A)	62.9(4)	C(8)-N(1A)-C(2A)-N(3A)	169.2(3)
C(63)-C(64)-C(65)-Co(2)	113.6(3)	C(5A)-N(1A)-C(2A)-Co(1)	173.8(2)
C(62A)-C(63A)-C(64A)-C(65A)	-108.1(4)	C(8)-N(1A)-C(2A)-Co(1)	-16.1(5)
C(62A)-C(63A)-C(64A)-Co(2)	-27.5(4)	C(2A)-N(3A)-C(4A)-C(5A)	-0.1(4)
C(63A)-C(64A)-C(65A)-Co(2)	111.7(3)	C(12A)-N(3A)-C(4A)-C(5A)	171.5(3)
C(76)-C(71)-C(72)-C(73)	-0.6(7)	N(3A)-C(4A)-C(5A)-N(1A)	-0.5(4)
C(70)-C(71)-C(72)-C(73)	-179.8(5)	C(2A)-N(1A)-C(5A)-C(4A)	0.9(4)
C(71)-C(72)-C(73)-C(74)	0.6(7)	C(8)-N(1A)-C(5A)-C(4A)	-169.2(3)

## 2.3. Compound 7



**Figure S22.** Molecular structure of **7**. Atoms are shown with anisotropic atomic displacement parameters at the 30% probability level. The co-crystallized benzene molecule and the hydrogen atoms (except Ir-H) are omitted for clarity. Based on DFT calculations (see 3.2) the metal-hydrogen bond lengths and angles were fixed (Ir1-H1a = 1.58, Ir1-H2a = 1.63, Ir2-H1b = 1.58, Ir2-H2b = 1.63).

**Table S7.** Crystal data and structure refinement for compound **7**.

Identification code	Compound <b>7</b>	
Empirical formula	C <sub>74</sub> H <sub>98</sub> Ir <sub>2</sub> N <sub>10</sub>	
Formula weight	1512.02	
Temperature	100(2) K	
Wavelength	0.71073 Å	
Crystal system	Monoclinic	
Space group	P2 <sub>1</sub> /c	
Unit cell dimensions	a = 18.3538(11) Å	α = 90°.
	b = 28.7745(16) Å	β = 110.2920(10)°.
	c = 13.3926(8) Å	γ = 90°.
Volume	6634.0(7) Å <sup>3</sup>	
Z	4	
Density (calculated)	1.514 Mg/m <sup>3</sup>	
Absorption coefficient	4.058 mm <sup>-1</sup>	
F(000)	3064	
Crystal size	0.273 x 0.120 x 0.056 mm <sup>3</sup>	
Theta range for data collection	1.415 to 28.283°.	
Index ranges	-24 ≤ h ≤ 24, -38 ≤ k ≤ 38, -17 ≤ l ≤ 17	
Reflections collected	120608	
Independent reflections	16467 [R(int) = 0.0955]	
Completeness to theta = 25.242°	99.9 %	
Absorption correction	Numerical	
Max. and min. transmission	0.7461 and 0.5443	
Refinement method	Full-matrix least-squares on F <sup>2</sup>	
Data / restraints / parameters	16467 / 44 / 800	
Goodness-of-fit on F <sup>2</sup>	1.029	
Final R indices [I > 2σ(I)]	R1 = 0.0350, wR2 = 0.0692	
R indices (all data)	R1 = 0.0545, wR2 = 0.0771	
Extinction coefficient	n/a	
Largest diff. peak and hole	2.200 and -0.886 e.Å <sup>-3</sup>	

**Table S8.** Bond lengths [Å] and angles [°] for compound **7**.

Ir(1)-C(7')	2.027(4)	C(5)-C(6)	1.389(5)	C(11I)-C(10B)	1.524(6)
Ir(1)-C(2')	2.035(4)	C(5)-C(5A)	1.397(5)	C(11I)-H(11A)	0.9800
Ir(1)-N(9)	2.059(3)	C(5)-H(5)	0.9500	C(11I)-H(11B)	0.9800
Ir(1)-Ir(2)	2.7836(2)	C(6)-C(7)	1.419(5)	C(11I)-H(11C)	0.9800
Ir(1)-H(1A)	1.5797(10)	C(6)-C(10B)	1.527(5)	C(11H)-C(10B)	1.541(6)
Ir(1)-H(2A)	1.6299(10)	N(6')-C(7')	1.373(5)	C(11H)-H(11D)	0.9800
C(2')-N(3')	1.350(5)	N(6')-C(10')	1.401(5)	C(11H)-H(11E)	0.9800
C(2')-N(1')	1.381(5)	N(6')-C(8)	1.441(5)	C(11H)-H(11F)	0.9800
C(2)-C(1)	1.389(5)	C(7')-N(8')	1.358(5)	C(11G)-C(10B)	1.542(5)
C(2)-C(3)	1.400(5)	C(7)-C(8)	1.377(5)	C(11G)-H(11G)	0.9800
C(2)-H(2)	0.9500	C(7)-H(7)	0.9500	C(11G)-H(11H)	0.9800
Ir(2)-C(57')	2.027(4)	N(8')-C(9')	1.389(5)	C(11G)-H(11I)	0.9800
Ir(2)-C(52')	2.035(4)	N(8')-C(16)	1.466(5)	C(10A)-C(11E)	1.410(17)
Ir(2)-N(59)	2.059(3)	C(8)-C(8A)	1.403(5)	C(10A)-C(11B)	1.477(8)
Ir(2)-H(1B)	1.5798(10)	N(9)-C(8A)	1.367(5)	C(10A)-C(11A)	1.534(9)
Ir(2)-H(2B)	1.6299(10)	N(9)-C(1A)	1.368(5)	C(10A)-C(11F)	1.565(15)
N(3')-C(4')	1.400(5)	C(9')-C(10')	1.342(6)	C(10A)-C(11C)	1.570(8)
N(3')-C(12)	1.478(5)	C(9')-H(9')	0.9500	C(10A)-C(11D)	1.601(16)
C(3)-C(4)	1.394(5)	C(13)-C(12)	1.506(6)	C(8A)-C(5A)	1.418(5)
C(3)-C(10A)	1.542(5)	C(13)-C(14)	1.519(6)	C(17)-C(18)	1.530(6)
N(1')-C(5')	1.395(5)	C(13)-H(13A)	0.9900	C(17)-H(17A)	0.9900
N(1')-C(1)	1.430(5)	C(13)-H(13B)	0.9900	C(17)-H(17B)	0.9900
C(4')-C(5')	1.330(5)	C(1)-C(1A)	1.402(5)	C(18)-C(19)	1.515(6)
C(4')-H(4')	0.9500	C(10'')-H(10'')	0.9500	C(18)-H(18A)	0.9900
C(4)-C(4A)	1.387(5)	C(16)-C(17)	1.506(6)	C(18)-H(18B)	0.9900
C(4)-H(4)	0.9500	C(16)-H(16A)	0.9900	C(1A)-C(4A)	1.422(5)
C(5')-H(5')	0.9500	C(16)-H(16B)	0.9900	C(19)-H(19A)	0.9800



C(19)-H(19B)	0.9800	C(61D)-H(61N)	0.9800	C(111)-H(111)	0.9500
C(19)-H(19C)	0.9800	C(61D)-H(61O)	0.9800	C(112)-H(112)	0.9500
C(12)-H(12A)	0.9900	C(57')-N(58')	1.370(5)	C(7')-Ir(1)-C(2')	171.36(15)
C(12)-H(12B)	0.9900	C(57)-C(58)	1.387(5)	C(7')-Ir(1)-N(9)	89.05(13)
C(14)-C(15)	1.522(6)	C(57)-H(57)	0.9500	C(2')-Ir(1)-N(9)	88.50(13)
C(14)-H(14A)	0.9900	C(58)-C(58A)	1.412(5)	C(7')-Ir(1)-Ir(2)	88.73(10)
C(14)-H(14B)	0.9900	N(58')-C(59')	1.384(5)	C(2')-Ir(1)-Ir(2)	99.80(11)
C(15)-H(15A)	0.9800	N(58')-C(66)	1.468(5)	N(9)-Ir(1)-Ir(2)	115.21(9)
C(15)-H(15B)	0.9800	C(59')-C(60')	1.334(6)	C(7')-Ir(1)-H(1A)	83.6(11)
C(15)-H(15C)	0.9800	C(59')-H(59')	0.9500	C(2')-Ir(1)-H(1A)	88.7(11)
C(60A)-C(61C)	1.524(6)	N(59)-C(58A)	1.366(5)	N(9)-Ir(1)-H(1A)	99.27(14)
C(60A)-C(53)	1.533(5)	C(66)-H(66A)	0.9900	Ir(2)-Ir(1)-H(1A)	144.5(3)
C(60A)-C(61A)	1.538(6)	C(66)-H(66B)	0.9900	C(7')-Ir(1)-H(2A)	91.7(12)
C(60A)-C(61B)	1.544(6)	C(60')-H(60')	0.9500	C(2')-Ir(1)-H(2A)	90.9(12)
C(61B)-H(61A)	0.9800	C(64)-C(65)	1.517(6)	N(9)-Ir(1)-H(2A)	178.7(5)
C(61B)-H(61B)	0.9800	C(64)-C(63)	1.527(6)	Ir(2)-Ir(1)-H(2A)	63.8(3)
C(61B)-H(61C)	0.9800	C(64)-H(64A)	0.9900	H(1A)-Ir(1)-H(2A)	81.86(7)
C(61A)-H(61D)	0.9800	C(64)-H(64B)	0.9900	N(3')-C(2')-N(1')	103.0(3)
C(61A)-H(61E)	0.9800	C(62)-C(63)	1.510(6)	N(3')-C(2')-Ir(1)	129.4(3)
C(61A)-H(61F)	0.9800	C(62)-H(62A)	0.9900	N(1')-C(2')-Ir(1)	127.5(3)
C(67)-C(66)	1.521(5)	C(62)-H(62B)	0.9900	C(1)-C(2)-C(3)	123.1(4)
C(67)-C(68)	1.522(6)	C(61C)-H(61P)	0.9800	C(1)-C(2)-H(2)	118.5
C(67)-H(67A)	0.9900	C(61C)-H(61Q)	0.9800	C(3)-C(2)-H(2)	170.19(15)
C(67)-H(67B)	0.9900	C(61C)-H(61R)	0.9800	C(57')-Ir(2)-C(52')	88.45(14)
N(51')-C(52')	1.382(5)	C(65)-H(65A)	0.9800	C(57')-Ir(2)-N(59)	88.94(14)
N(51')-C(55')	1.391(5)	C(65)-H(65B)	0.9800	C(52')-Ir(2)-N(59)	92.05(10)
N(51')-C(51)	1.428(5)	C(65)-H(65C)	0.9800	C(57')-Ir(2)-Ir(1)	97.65(11)
C(51A)-N(59)	1.375(5)	C(63)-H(63A)	0.9900	N(59)-Ir(2)-Ir(1)	114.10(9)
C(51A)-C(54A)	1.399(5)	C(63)-H(63B)	0.9900	C(57')-Ir(2)-H(1B)	81.6(12)
C(51A)-C(51)	1.401(5)	C(11A)-H(11J)	0.9800	C(52')-Ir(2)-H(1B)	89.6(12)
C(51)-C(52)	1.384(5)	C(11A)-H(11K)	0.9800	N(59)-Ir(2)-H(1B)	100.84(14)
C(4A)-C(5A)	1.447(5)	C(11A)-H(11L)	0.9800	Ir(1)-Ir(2)-H(1B)	144.3(3)
C(68)-C(69)	1.527(6)	C(11B)-H(11M)	0.9800	C(57')-Ir(2)-H(2B)	91.2(12)
C(68)-H(68A)	0.9900	C(11B)-H(11N)	0.9800	C(52')-Ir(2)-H(2B)	91.9(12)
C(68)-H(68B)	0.9900	C(11B)-H(11O)	0.9800	N(59)-Ir(2)-H(2B)	176.9(4)
C(52')-N(53')	1.353(5)	C(11C)-H(11P)	0.9800	Ir(1)-Ir(2)-H(2B)	62.8(2)
C(52)-C(53)	1.416(5)	C(11C)-H(11Q)	0.9800	H(1B)-Ir(2)-H(2B)	82.14(7)
C(52)-H(52)	0.9500	C(11C)-H(11R)	0.9800	C(2')-N(3')-C(4')	112.4(3)
C(69)-H(69A)	0.9800	C(11D)-H(11S)	0.9800	C(2')-N(3')-C(12)	128.3(3)
C(69)-H(69B)	0.9800	C(11D)-H(11T)	0.9800	C(4')-N(3')-C(12)	119.3(3)
C(69)-H(69C)	0.9800	C(11D)-H(11U)	0.9800	C(4)-C(3)-C(2)	118.7(4)
N(53')-C(54')	1.387(5)	C(11E)-H(11V)	0.9800	C(4)-C(3)-C(10A)	121.5(4)
N(53')-C(62)	1.479(5)	C(11E)-H(11W)	0.9800	C(2)-C(3)-C(10A)	119.8(4)
C(53)-C(54)	1.389(5)	C(11E)-H(11WW)	0.9800	C(2')-N(1')-C(5')	111.1(3)
C(60B)-C(61E)	1.524(7)	C(11F)-H(11X)	0.9800	C(2')-N(1')-C(1)	126.0(3)
C(60B)-C(61F)	1.526(8)	C(11F)-H(11Y)	0.9800	C(5')-N(1')-C(1)	122.9(3)
C(60B)-C(61D)	1.536(7)	C(11F)-H(11Z)	0.9800	C(5')-C(4')-N(3')	106.3(3)
C(60B)-C(56)	1.538(6)	C(101)-C(102)	1.3900	C(5')-C(4')-H(4')	126.8
C(54')-C(55')	1.339(6)	C(101)-C(106)	1.3900	N(3')-C(4')-H(4')	126.8
C(54')-H(54')	0.9500	C(101)-H(101)	0.9500	C(4A)-C(4)-C(3)	119.7(4)
C(54)-C(54A)	1.405(5)	C(102)-C(103)	1.3900	C(4A)-C(4)-H(4)	120.2
C(54)-H(54)	0.9500	C(102)-H(102)	0.9500	C(3)-C(4)-H(4)	120.2
C(61E)-H(61G)	0.9800	C(103)-C(104)	1.3900	C(4')-C(5')-N(1')	107.2(4)
C(61E)-H(61H)	0.9800	C(103)-H(103)	0.9500	C(4')-C(5')-H(5')	126.4
C(61E)-H(61I)	0.9800	C(104)-C(105)	1.3900	N(1')-C(5')-H(5')	126.4
C(55')-H(55')	0.9500	C(104)-H(104)	0.9500	C(6)-C(5)-C(5A)	120.2(4)
C(55A)-C(55)	1.394(5)	C(105)-C(106)	1.3900	C(6)-C(5)-H(5)	119.9
C(55A)-C(58A)	1.425(5)	C(105)-H(105)	0.9500	C(5A)-C(5)-H(5)	119.9
C(55A)-C(54A)	1.447(5)	C(106)-H(106)	0.9500	C(5)-C(6)-C(7)	117.7(4)
C(55)-C(56)	1.380(6)	C(107)-C(108)	1.3900	C(5)-C(6)-C(10B)	123.9(3)
C(55)-H(55)	0.9500	C(107)-C(112)	1.3900	C(7)-C(6)-C(10B)	118.3(3)
C(61F)-H(61J)	0.9800	C(107)-H(107)	0.9500	C(7')-N(6')-C(10')	111.0(3)
C(61F)-H(61K)	0.9800	C(108)-C(109)	1.3900	C(7')-N(6')-C(8)	127.5(3)
C(61F)-H(61L)	0.9800	C(108)-H(108)	0.9500	C(10')-N(6')-C(8)	121.5(3)
N(56')-C(57')	1.366(5)	C(109)-C(110)	1.3900	N(8')-C(7')-N(6')	103.6(3)
N(56')-C(60')	1.397(5)	C(109)-H(109)	0.9500	N(8')-C(7')-Ir(1)	129.2(3)
N(56')-C(58)	1.440(5)	C(110)-C(111)	1.3900	N(6')-C(7')-Ir(1)	126.9(3)
C(56)-C(57)	1.414(6)	C(110)-H(110)	0.9500		
C(61D)-H(61M)	0.9800	C(111)-C(112)	1.3900		

C(8)-C(7)-C(6)	123.3(4)	N(9)-C(8A)-C(8)	128.6(3)	N(59)-C(51A)-C(54A)	112.6(3)
C(8)-C(7)-H(7)	118.4	N(9)-C(8A)-C(5A)	112.1(3)	N(59)-C(51A)-C(51)	127.2(4)
C(6)-C(7)-H(7)	118.4	C(8)-C(8A)-C(5A)	119.1(3)	C(54A)-C(51A)-C(51)	120.2(4)
C(7)-N(8)-C(9')	111.9(3)	C(16)-C(17)-C(18)	109.9(3)	C(52)-C(51)-C(51A)	118.1(4)
C(7)-N(8)-C(16)	125.8(3)	C(16)-C(17)-H(17A)	109.7	C(52)-C(51)-N(51')	120.6(3)
C(9)-N(8)-C(16)	122.2(3)	C(18)-C(17)-H(17A)	109.7	C(51A)-C(51)-N(51')	121.3(3)
C(7)-C(8)-C(8A)	118.6(3)	C(16)-C(17)-H(17B)	109.7	C(4)-C(4A)-C(1A)	121.0(3)
C(7)-C(8)-N(6')	121.5(3)	C(18)-C(17)-H(17B)	109.7	C(4)-C(4A)-C(5A)	134.0(4)
C(8A)-C(8)-N(6')	119.9(3)	H(17A)-C(17)-H(17B)	108.2	C(1A)-C(4A)-C(5A)	104.7(3)
C(8A)-N(9)-C(1A)	105.7(3)	C(19)-C(18)-C(17)	112.6(4)	C(67)-C(68)-C(69)	112.7(4)
C(8A)-N(9)-Ir(1)	125.7(2)	C(19)-C(18)-H(18A)	109.1	C(67)-C(68)-H(68A)	109.0
C(1A)-N(9)-Ir(1)	125.6(2)	C(17)-C(18)-H(18A)	109.1	C(69)-C(68)-H(68A)	109.0
C(10)-C(9)-N(8')	106.9(4)	C(19)-C(18)-H(18B)	109.1	C(67)-C(68)-H(68B)	109.0
C(10)-C(9)-H(9')	126.5	C(17)-C(18)-H(18B)	109.1	C(69)-C(68)-H(68B)	109.0
N(8)-C(9)-H(9')	126.5	H(18A)-C(18)-H(18B)	107.8	H(68A)-C(68)-H(68B)	107.8
C(12)-C(13)-C(14)	111.5(3)	N(9)-C(1A)-C(1)	128.2(3)	N(53')-C(52')-N(51')	102.9(3)
C(12)-C(13)-H(13A)	109.3	N(9)-C(1A)-C(4A)	112.2(3)	N(53')-C(52')-Ir(2)	130.2(3)
C(14)-C(13)-H(13A)	109.3	C(1)-C(1A)-C(4A)	119.6(3)	N(51')-C(52')-Ir(2)	126.4(3)
C(12)-C(13)-H(13B)	109.3	C(18)-C(19)-H(19A)	109.5	C(51)-C(52)-C(53)	122.6(4)
C(14)-C(13)-H(13B)	109.3	C(18)-C(19)-H(19B)	109.5	C(51)-C(52)-H(52)	118.7
H(13A)-C(13)-H(13B)	108.0	H(19A)-C(19)-H(19B)	109.5	C(53)-C(52)-H(52)	118.7
C(2)-C(1)-C(1A)	117.9(3)	C(18)-C(19)-H(19C)	109.5	C(68)-C(69)-H(69A)	109.5
C(2)-C(1)-N(1')	121.3(3)	H(19A)-C(19)-H(19C)	109.5	C(68)-C(69)-H(69B)	109.5
C(1A)-C(1)-N(1')	120.8(3)	H(19B)-C(19)-H(19C)	109.5	H(69A)-C(69)-H(69B)	109.5
C(9)-C(10)-N(6')	106.6(4)	N(3)-C(12)-C(13)	115.0(3)	C(68)-C(69)-H(69C)	109.5
C(9)-C(10)-H(10')	126.7	N(3)-C(12)-H(12A)	108.5	H(69A)-C(69)-H(69C)	109.5
N(6)-C(10)-H(10')	126.7	C(13)-C(12)-H(12A)	108.5	H(69B)-C(69)-H(69C)	109.5
N(8)-C(16)-C(17)	114.0(3)	N(3)-C(12)-H(12B)	108.5	C(52')-N(53')-C(54')	112.5(3)
N(8)-C(16)-H(16A)	108.8	C(13)-C(12)-H(12B)	108.5	C(52')-N(53')-C(62)	126.5(3)
C(17)-C(16)-H(16A)	108.8	H(12A)-C(12)-H(12B)	107.5	C(54')-N(53')-C(62)	121.0(3)
N(8)-C(16)-H(16B)	108.8	C(13)-C(14)-C(15)	113.7(4)	C(54)-C(53)-C(52)	118.6(4)
C(17)-C(16)-H(16B)	108.8	C(13)-C(14)-H(14A)	108.8	C(54)-C(53)-C(60A)	123.0(4)
H(16A)-C(16)-H(16B)	107.7	C(15)-C(14)-H(14A)	108.8	C(52)-C(53)-C(60A)	118.4(3)
C(10B)-C(11)-H(11A)	109.5	C(13)-C(14)-H(14B)	108.8	C(61E)-C(60B)-C(61F)	109.8(5)
C(10B)-C(11)-H(11B)	109.5	C(15)-C(14)-H(14B)	108.8	C(61E)-C(60B)-C(61D)	107.2(5)
H(11A)-C(11)-H(11B)	109.5	H(14A)-C(14)-H(14B)	107.7	C(61F)-C(60B)-C(61D)	108.2(5)
C(10B)-C(11)-H(11C)	109.5	C(14)-C(15)-H(15A)	109.5	C(61E)-C(60B)-C(56)	110.4(4)
H(11A)-C(11)-H(11C)	109.5	C(14)-C(15)-H(15B)	109.5	C(61F)-C(60B)-C(56)	109.1(4)
H(11B)-C(11)-H(11C)	109.5	H(15A)-C(15)-H(15B)	109.5	C(61D)-C(60B)-C(56)	112.1(4)
C(10B)-C(11H)-H(11D)	109.5	C(14)-C(15)-H(15C)	109.5	C(55')-C(54')-N(53')	106.5(3)
C(10B)-C(11H)-H(11E)	109.5	H(15A)-C(15)-H(15C)	109.5	C(55')-C(54')-H(54')	126.7
C(10B)-C(11H)-H(11F)	109.5	H(15B)-C(15)-H(15C)	109.5	N(53')-C(54')-H(54')	126.7
H(11D)-C(11H)-H(11E)	109.5	C(61C)-C(60A)-C(53)	112.7(3)	C(53)-C(54)-C(54A)	119.5(4)
C(10B)-C(11H)-H(11F)	109.5	C(61C)-C(60A)-C(61A)	108.6(3)	C(53)-C(54)-H(54)	120.3
H(11D)-C(11H)-H(11F)	109.5	C(53)-C(60A)-C(61A)	109.5(3)	C(54A)-C(54)-H(54)	120.3
C(10B)-C(11G)-H(11G)	109.5	C(61C)-C(60A)-C(61B)	107.5(3)	C(60B)-C(61E)-H(61G)	109.5
C(10B)-C(11G)-H(11H)	109.5	C(53)-C(60A)-C(61B)	109.7(3)	C(60B)-C(61E)-H(61H)	109.5
H(11G)-C(11G)-H(11H)	109.5	C(61A)-C(60A)-C(61B)	108.8(4)	H(61G)-C(61E)-H(61H)	109.5
C(10B)-C(11G)-H(11I)	109.5	C(60A)-C(61B)-H(61A)	109.5	C(60B)-C(61E)-H(61I)	109.5
H(11H)-C(11G)-H(11I)	109.5	C(60A)-C(61B)-H(61B)	109.5	H(61G)-C(61E)-H(61I)	109.5
C(11I)-C(10B)-C(6)	110.6(3)	C(60A)-C(61B)-H(61C)	109.5	C(54')-C(55')-N(51')	106.9(4)
C(11I)-C(10B)-C(11H)	110.1(4)	H(61A)-C(61B)-H(61C)	109.5	C(54')-C(55')-H(55')	126.5
C(6)-C(10B)-C(11H)	108.9(3)	H(61B)-C(61B)-H(61C)	109.5	N(51')-C(55')-H(55')	126.5
C(11I)-C(10B)-C(11G)	108.4(3)	C(60A)-C(61A)-H(61D)	109.5	C(55)-C(55A)-C(58A)	120.8(4)
C(6)-C(10B)-C(11G)	112.0(3)	C(60A)-C(61A)-H(61E)	109.5	C(55)-C(55A)-C(54A)	134.6(4)
C(11H)-C(10B)-C(11G)	106.7(3)	H(61D)-C(61A)-H(61E)	109.5	C(58A)-C(55A)-C(54A)	104.5(3)
C(11B)-C(10A)-C(11A)	111.1(6)	C(60A)-C(61A)-H(61F)	109.5	C(51A)-C(54A)-C(54)	120.9(4)
C(11E)-C(10A)-C(3)	116.1(8)	H(61D)-C(61A)-H(61F)	109.5	C(51A)-C(54A)-C(55A)	105.5(3)
C(11B)-C(10A)-C(3)	114.0(4)	H(61E)-C(61A)-H(61F)	109.5	C(54)-C(54A)-C(55A)	133.4(4)
C(11A)-C(10A)-C(3)	108.7(4)	C(66)-C(67)-C(68)	109.9(3)	C(56)-C(55)-C(55A)	120.0(4)
C(11E)-C(10A)-C(11F)	111.9(10)	C(66)-C(67)-H(67A)	109.7	C(56)-C(55)-H(55)	120.0
C(3)-C(10A)-C(11F)	109.1(6)	C(68)-C(67)-H(67A)	109.7	C(55A)-C(55)-H(55)	120.0
C(11B)-C(10A)-C(11C)	108.7(5)	C(66)-C(67)-H(67B)	109.7	C(60B)-C(61F)-H(61J)	109.5
C(11A)-C(10A)-C(11C)	104.8(5)	C(68)-C(67)-H(67B)	109.7	C(60B)-C(61F)-H(61K)	109.5
C(3)-C(10A)-C(11C)	109.1(4)	H(67A)-C(67)-H(67B)	108.2	H(61J)-C(61F)-H(61K)	109.5
C(11E)-C(10A)-C(11D)	109.8(11)	C(52')-N(51')-C(55')	111.1(3)	C(60B)-C(61F)-H(61L)	109.5
C(3)-C(10A)-C(11D)	105.8(7)	C(52')-N(51')-C(51)	125.7(3)	H(61J)-C(61F)-H(61L)	109.5
C(11F)-C(10A)-C(11D)	103.3(10)	C(55')-N(51')-C(51)	123.1(3)	H(61K)-C(61F)-H(61L)	109.5

C(57')-N(56')-C(60')	111.3(3)	C(63)-C(64)-H(64B)	108.8	H(11T)-C(11D)-H(11U)	109.5
C(57')-N(56')-C(58)	126.5(3)	H(64A)-C(64)-H(64B)	107.7	C(10A)-C(11E)-H(11V)	109.5
C(60')-N(56')-C(58)	122.2(3)	N(53')-C(62)-C(63)	113.4(3)	C(10A)-C(11E)-H(11W)	109.5
C(55)-C(56)-C(57)	118.8(4)	N(53')-C(62)-H(62A)	108.9	H(11V)-C(11E)-H(11W)	109.5
C(55)-C(56)-C(60B)	123.2(4)	C(63)-C(62)-H(62A)	108.9	C(10A)-C(11E)-H(11WW)	109.5
C(57)-C(56)-C(60B)	118.0(4)	N(53')-C(62)-H(62B)	108.9	H(11V)-C(11E)-H(11WW)	109.5
C(60B)-C(61D)-H(61M)	109.5	C(63)-C(62)-H(62B)	108.9	H(11W)-C(11E)-H(11WW)	109.5
C(60B)-C(61D)-H(61N)	109.5	H(62A)-C(62)-H(62B)	107.7	C(10A)-C(11F)-H(11X)	109.5
H(61M)-C(61D)-H(61N)	109.5	C(60A)-C(61C)-H(61P)	109.5	C(10A)-C(11F)-H(11Y)	109.5
C(60B)-C(61D)-H(61O)	109.5	C(60A)-C(61C)-H(61Q)	109.5	H(11X)-C(11F)-H(11Y)	109.5
H(61M)-C(61D)-H(61O)	109.5	H(61P)-C(61C)-H(61Q)	109.5	C(10A)-C(11F)-H(11Z)	109.5
H(61N)-C(61D)-H(61O)	109.5	C(60A)-C(61C)-H(61R)	109.5	H(11X)-C(11F)-H(11Z)	109.5
N(56')-C(57')-N(58')	103.5(3)	H(61P)-C(61C)-H(61R)	109.5	H(11Y)-C(11F)-H(11Z)	109.5
N(56')-C(57')-Ir(2)	128.3(3)	H(61Q)-C(61C)-H(61R)	109.5	C(102)-C(101)-C(106)	120.0
N(58')-C(57')-Ir(2)	128.0(3)	C(64)-C(65)-H(65A)	109.5	C(102)-C(101)-H(101)	120.0
C(58)-C(57)-C(56)	123.0(4)	C(64)-C(65)-H(65B)	109.5	C(106)-C(101)-H(101)	120.0
C(58)-C(57)-H(57)	118.5	H(65A)-C(65)-H(65B)	109.5	C(103)-C(102)-C(101)	120.0
C(56)-C(57)-H(57)	118.5	C(64)-C(65)-H(65C)	109.5	C(103)-C(102)-H(102)	120.0
C(57)-C(58)-C(58A)	117.6(4)	H(65A)-C(65)-H(65C)	109.5	C(101)-C(102)-H(102)	120.0
C(57)-C(58)-N(56')	121.7(3)	H(65B)-C(65)-H(65C)	109.5	C(102)-C(103)-C(104)	120.0
C(58A)-C(58)-N(56')	120.6(3)	C(62)-C(63)-C(64)	111.2(4)	C(102)-C(103)-H(103)	120.0
C(57')-N(58')-C(59')	111.3(3)	C(62)-C(63)-H(63A)	109.4	C(104)-C(103)-H(103)	120.0
C(57')-N(58')-C(66)	123.7(3)	C(64)-C(63)-H(63A)	109.4	C(105)-C(104)-C(103)	120.0
C(59')-N(58')-C(66)	124.9(3)	C(62)-C(63)-H(63B)	109.4	C(105)-C(104)-H(104)	120.0
C(60')-C(59')-N(58')	107.5(4)	C(64)-C(63)-H(63B)	109.4	C(103)-C(104)-H(104)	120.0
C(60')-C(59')-H(59')	126.3	H(63A)-C(63)-H(63B)	108.0	C(106)-C(105)-C(104)	120.0
N(58')-C(59')-H(59')	126.3	C(10A)-C(11A)-H(11J)	109.5	C(106)-C(105)-H(105)	120.0
C(58A)-N(59)-C(51A)	105.2(3)	C(10A)-C(11A)-H(11K)	109.5	C(104)-C(105)-H(105)	120.0
C(58A)-N(59)-Ir(2)	126.2(3)	H(11J)-C(11A)-H(11K)	109.5	C(105)-C(106)-C(101)	120.0
C(51A)-N(59)-Ir(2)	124.7(3)	C(10A)-C(11A)-H(11L)	109.5	C(105)-C(106)-H(106)	120.0
N(58')-C(66)-C(67)	113.8(3)	H(11J)-C(11A)-H(11L)	109.5	C(101)-C(106)-H(106)	120.0
N(58')-C(66)-H(66A)	108.8	H(11K)-C(11A)-H(11L)	109.5	C(108)-C(107)-C(112)	120.0
C(67)-C(66)-H(66A)	108.8	C(10A)-C(11B)-H(11M)	109.5	C(108)-C(107)-H(107)	120.0
N(58')-C(66)-H(66B)	108.8	C(10A)-C(11B)-H(11N)	109.5	C(112)-C(107)-H(107)	120.0
C(67)-C(66)-H(66B)	108.8	H(11M)-C(11B)-H(11N)	109.5	C(109)-C(108)-C(107)	120.0
H(66A)-C(66)-H(66B)	107.7	C(10A)-C(11B)-H(11O)	109.5	C(109)-C(108)-H(108)	120.0
C(59')-C(60')-N(56')	106.6(4)	H(11M)-C(11B)-H(11O)	109.5	C(107)-C(108)-H(108)	120.0
C(59')-C(60')-H(60')	126.7	H(11N)-C(11B)-H(11O)	109.5	C(108)-C(109)-C(110)	120.0
N(56')-C(60')-H(60')	126.7	C(10A)-C(11C)-H(11P)	109.5	C(108)-C(109)-H(109)	120.0
N(59)-C(58A)-C(58)	128.0(4)	C(10A)-C(11C)-H(11Q)	109.5	C(110)-C(109)-H(109)	120.0
N(59)-C(58A)-C(55A)	112.2(3)	H(11P)-C(11C)-H(11Q)	109.5	C(111)-C(110)-C(109)	120.0
C(58)-C(58A)-C(55A)	119.5(3)	C(10A)-C(11C)-H(11R)	109.5	C(111)-C(110)-H(110)	120.0
C(5)-C(5A)-C(8A)	121.1(4)	H(11P)-C(11C)-H(11R)	109.5	C(109)-C(110)-H(110)	120.0
C(5)-C(5A)-C(4A)	133.5(4)	H(11Q)-C(11C)-H(11R)	109.5	C(112)-C(111)-C(110)	120.0
C(8A)-C(5A)-C(4A)	105.2(3)	C(10A)-C(11D)-H(11S)	109.5	C(112)-C(111)-H(111)	120.0
C(65)-C(64)-C(63)	113.7(4)	C(10A)-C(11D)-H(11T)	109.5	C(110)-C(111)-H(111)	120.0
C(65)-C(64)-H(64A)	108.8	H(11S)-C(11D)-H(11T)	109.5	C(111)-C(112)-C(107)	120.0
C(63)-C(64)-H(64A)	108.8	C(10A)-C(11D)-H(11U)	109.5	C(111)-C(112)-H(112)	120.0
C(65)-C(64)-H(64B)	108.8	H(11S)-C(11D)-H(11U)	109.5	C(107)-C(112)-H(112)	120.0

**Table S9.** Torsion angles [°] for compound 7.

N(1')-C(2')-N(3')-C(4')	1.5(4)	C(10A)-C(3)-C(4)-C(4A)	177.4(4)
Ir(1)-C(2')-N(3')-C(4')	-173.6(3)	N(3')-C(4)-C(5')-N(1')	0.5(4)
N(1')-C(2')-N(3')-C(12)	-179.6(3)	C(2')-N(1')-C(5')-C(4')	0.5(5)
Ir(1)-C(2')-N(3')-C(12)	5.3(6)	C(1)-N(1')-C(5')-C(4')	-176.3(4)
C(1)-C(2)-C(3)-C(4)	1.2(6)	C(5A)-C(5)-C(6)-C(7)	0.2(6)
C(1)-C(2)-C(3)-C(10A)	-178.6(4)	C(5A)-C(5)-C(6)-C(10B)	-175.6(4)
N(3')-C(2')-N(1')-C(5')	-1.2(4)	C(10')-N(6')-C(7')-N(8')	1.6(4)
Ir(1)-C(2')-N(1')-C(5')	174.0(3)	C(8)-N(6')-C(7')-N(8')	-179.5(3)
N(3')-C(2')-N(1')-C(1)	175.4(3)	C(10')-N(6')-C(7')-Ir(1)	-172.2(3)
Ir(1)-C(2')-N(1')-C(1)	-9.4(5)	C(8)-N(6')-C(7')-Ir(1)	6.7(5)
C(2')-N(3')-C(4')-C(5')	-1.3(5)	C(5)-C(6)-C(7)-C(8)	-0.6(6)
C(12)-N(3')-C(4')-C(5')	179.7(3)	C(10B)-C(6)-C(7)-C(8)	175.5(4)
C(2)-C(3)-C(4)-C(4A)	-2.3(6)	N(6')-C(7')-N(8')-C(9')	-1.2(4)

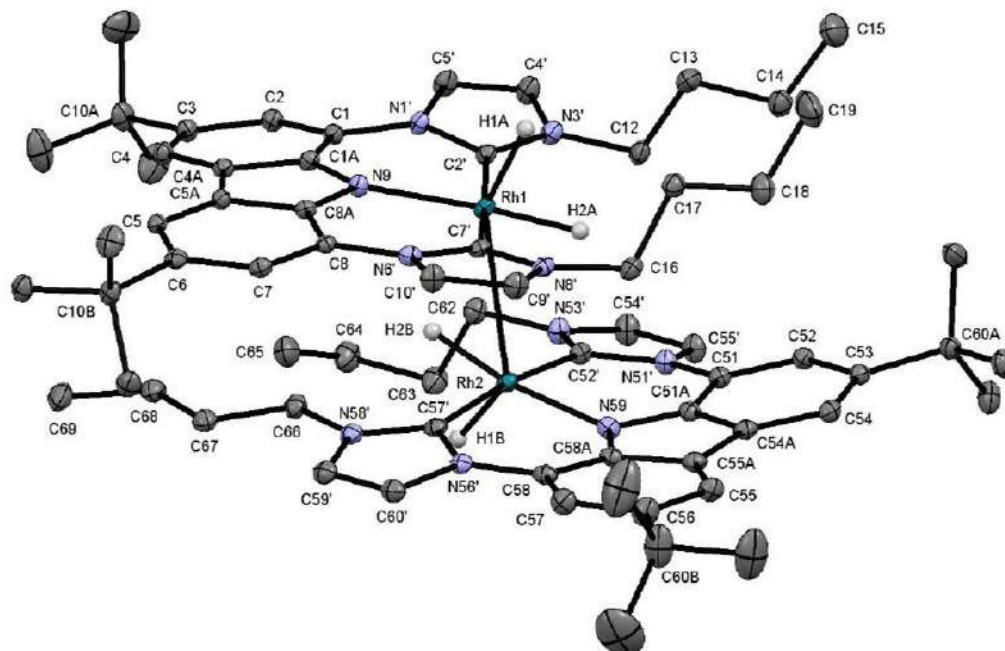
Ir(1)-C(7 <sup>+</sup> )-N(8 <sup>+</sup> )-C(9 <sup>+</sup> )	172.4(3)	C(14)-C(13)-C(12)-N(3 <sup>+</sup> )	-176.0(3)
N(6 <sup>+</sup> )-C(7 <sup>+</sup> )-N(8 <sup>+</sup> )-C(16)	-178.5(3)	C(12)-C(13)-C(14)-C(15)	175.0(4)
Ir(1)-C(7 <sup>+</sup> )-N(8 <sup>+</sup> )-C(16)	-4.9(6)	N(59)-C(51A)-C(51)-C(52)	173.8(4)
C(6)-C(7)-C(8)-C(8A)	0.7(6)	C(54A)-C(51A)-C(51)-C(52)	-3.7(6)
C(6)-C(7)-C(8)-N(6 <sup>+</sup> )	-177.9(3)	N(59)-C(51A)-C(51)-N(51 <sup>+</sup> )	-5.8(6)
C(7 <sup>+</sup> )-N(6 <sup>+</sup> )-C(8)-C(7)	165.4(4)	C(54A)-C(51A)-C(51)-N(51 <sup>+</sup> )	176.6(3)
C(10 <sup>+</sup> )-N(6 <sup>+</sup> )-C(8)-C(7)	-15.8(5)	C(52 <sup>+</sup> )-N(51 <sup>+</sup> )-C(51)-C(52)	-157.1(4)
C(7 <sup>+</sup> )-N(6 <sup>+</sup> )-C(8)-C(8A)	-13.1(6)	C(55 <sup>+</sup> )-N(51 <sup>+</sup> )-C(51)-C(52)	18.8(6)
C(10 <sup>+</sup> )-N(6 <sup>+</sup> )-C(8)-C(8A)	165.7(4)	C(52 <sup>+</sup> )-N(51 <sup>+</sup> )-C(51)-C(51A)	22.5(6)
C(7 <sup>+</sup> )-N(8 <sup>+</sup> )-C(9 <sup>+</sup> )-C(10 <sup>+</sup> )	0.4(5)	C(55 <sup>+</sup> )-N(51 <sup>+</sup> )-C(51)-C(51A)	-161.6(4)
C(16)-N(8 <sup>+</sup> )-C(9 <sup>+</sup> )-C(10 <sup>+</sup> )	177.8(4)	C(3)-C(4)-C(4A)-C(1A)	0.6(6)
C(3)-C(2)-C(1)-C(1A)	1.7(6)	C(3)-C(4)-C(4A)-C(5A)	-172.0(4)
C(3)-C(2)-C(1)-N(1 <sup>+</sup> )	179.7(4)	N(9)-C(1A)-C(4A)-C(4)	-174.7(3)
C(2 <sup>+</sup> )-N(1 <sup>+</sup> )-C(1)-C(2)	-160.4(4)	C(1)-C(1A)-C(4A)-C(4)	2.4(6)
C(5 <sup>+</sup> )-N(1 <sup>+</sup> )-C(1)-C(2)	15.8(6)	N(9)-C(1A)-C(4A)-C(5A)	-0.3(4)
C(2 <sup>+</sup> )-N(1 <sup>+</sup> )-C(1)-C(1A)	17.5(6)	C(1)-C(1A)-C(4A)-C(5A)	176.9(3)
C(5 <sup>+</sup> )-N(1 <sup>+</sup> )-C(1)-C(1A)	-166.2(4)	C(66)-C(67)-C(68)-C(69)	-173.8(3)
N(8 <sup>+</sup> )-C(9 <sup>+</sup> )-C(10 <sup>+</sup> )-N(6 <sup>+</sup> )	0.6(5)	C(55 <sup>+</sup> )-N(51 <sup>+</sup> )-C(52 <sup>+</sup> )-N(53 <sup>+</sup> )	-1.3(4)
C(7 <sup>+</sup> )-N(6 <sup>+</sup> )-C(10 <sup>+</sup> )-C(9 <sup>+</sup> )	-1.4(5)	C(51)-N(51 <sup>+</sup> )-C(52 <sup>+</sup> )-N(53 <sup>+</sup> )	174.9(3)
C(8)-N(6 <sup>+</sup> )-C(10 <sup>+</sup> )-C(9 <sup>+</sup> )	179.6(3)	C(55 <sup>+</sup> )-N(51 <sup>+</sup> )-C(52 <sup>+</sup> )-Ir(2)	171.2(3)
C(7 <sup>+</sup> )-N(8 <sup>+</sup> )-C(16)-C(17)	87.2(5)	C(51)-N(51 <sup>+</sup> )-C(52 <sup>+</sup> )-Ir(2)	-12.5(5)
C(9 <sup>+</sup> )-N(8 <sup>+</sup> )-C(16)-C(17)	-89.9(4)	C(51A)-C(51)-C(52)-C(53)	1.7(6)
C(5)-C(6)-C(10B)-C(11I)	-117.0(4)	N(51 <sup>+</sup> )-C(51)-C(52)-C(53)	-178.6(3)
C(7)-C(6)-C(10B)-C(11I)	67.2(5)	N(51 <sup>+</sup> )-C(52 <sup>+</sup> )-N(53 <sup>+</sup> )-C(54 <sup>+</sup> )	1.7(4)
C(5)-C(6)-C(10B)-C(11H)	121.9(4)	Ir(2)-C(52 <sup>+</sup> )-N(53 <sup>+</sup> )-C(54 <sup>+</sup> )	-170.4(3)
C(7)-C(6)-C(10B)-C(11H)	-53.9(5)	N(51 <sup>+</sup> )-C(52 <sup>+</sup> )-N(53 <sup>+</sup> )-C(62)	-179.1(4)
C(5)-C(6)-C(10B)-C(11G)	4.1(5)	Ir(2)-C(52 <sup>+</sup> )-N(53 <sup>+</sup> )-C(62)	8.7(6)
C(7)-C(6)-C(10B)-C(11G)	-171.7(4)	C(51)-C(52)-C(53)-C(54)	1.0(6)
C(4)-C(3)-C(10A)-C(11E)	-178.8(10)	C(51)-C(52)-C(53)-C(60A)	-178.7(4)
C(2)-C(3)-C(10A)-C(11E)	1.0(11)	C(61C)-C(60A)-C(53)-C(54)	-4.6(6)
C(4)-C(3)-C(10A)-C(11B)	-10.1(7)	C(61A)-C(60A)-C(53)-C(54)	116.4(4)
C(2)-C(3)-C(10A)-C(11B)	169.7(6)	C(61B)-C(60A)-C(53)-C(54)	-124.3(4)
C(4)-C(3)-C(10A)-C(11A)	114.5(5)	C(61C)-C(60A)-C(53)-C(52)	175.1(4)
C(2)-C(3)-C(10A)-C(11A)	-65.8(6)	C(61A)-C(60A)-C(53)-C(52)	-63.9(5)
C(4)-C(3)-C(10A)-C(11F)	-51.2(9)	C(61B)-C(60A)-C(53)-C(52)	55.4(5)
C(2)-C(3)-C(10A)-C(11F)	128.5(8)	C(52 <sup>+</sup> )-N(53 <sup>+</sup> )-C(54 <sup>+</sup> )-C(55 <sup>+</sup> )	-1.5(5)
C(4)-C(3)-C(10A)-C(11C)	-131.8(5)	C(62)-N(53 <sup>+</sup> )-C(54 <sup>+</sup> )-C(55 <sup>+</sup> )	179.2(4)
C(2)-C(3)-C(10A)-C(11C)	47.9(6)	C(52)-C(53)-C(54)-C(54A)	-1.7(6)
C(4)-C(3)-C(10A)-C(11D)	59.3(9)	C(60A)-C(53)-C(54)-C(54A)	178.0(4)
C(2)-C(3)-C(10A)-C(11D)	-121.0(8)	N(53 <sup>+</sup> )-C(54 <sup>+</sup> )-C(55 <sup>+</sup> )-N(51 <sup>+</sup> )	0.6(5)
C(1A)-N(9)-C(8A)-C(8)	174.0(4)	C(52 <sup>+</sup> )-N(51 <sup>+</sup> )-C(55 <sup>+</sup> )-C(54 <sup>+</sup> )	0.5(5)
Ir(1)-N(9)-C(8A)-C(8)	12.8(6)	C(51)-N(51 <sup>+</sup> )-C(55 <sup>+</sup> )-C(54 <sup>+</sup> )	-175.9(4)
C(1A)-N(9)-C(8A)-C(5A)	-1.7(4)	N(59)-C(51A)-C(54A)-C(54)	-174.7(3)
Ir(1)-N(9)-C(8A)-C(5A)	-162.9(3)	C(51)-C(51A)-C(54A)-C(54)	3.1(6)
C(7)-C(8)-C(8A)-N(9)	-176.0(4)	N(59)-C(51A)-C(54A)-C(55A)	1.0(4)
N(6 <sup>+</sup> )-C(8)-C(8A)-N(9)	2.6(6)	C(51)-C(51A)-C(54A)-C(55A)	178.9(3)
C(7)-C(8)-C(8A)-C(5A)	-0.5(5)	C(53)-C(54)-C(54A)-C(51A)	-0.3(6)
N(6 <sup>+</sup> )-C(8)-C(8A)-C(5A)	178.1(3)	C(53)-C(54)-C(54A)-C(55A)	-174.7(4)
N(8 <sup>+</sup> )-C(16)-C(17)-C(18)	-171.8(3)	C(55)-C(55A)-C(54A)-C(51A)	-178.0(4)
C(16)-C(17)-C(18)-C(19)	-176.8(4)	C(58A)-C(55A)-C(54A)-C(51A)	-1.9(4)
C(8A)-N(9)-C(1A)-C(1)	-175.6(4)	C(55)-C(55A)-C(54A)-C(54)	-3.0(8)
Ir(1)-N(9)-C(1A)-C(1)	-14.4(6)	C(58A)-C(55A)-C(54A)-C(54)	173.1(4)
C(8A)-N(9)-C(1A)-C(4A)	1.2(4)	C(58A)-C(55A)-C(55)-C(56)	-1.7(6)
Ir(1)-N(9)-C(1A)-C(4A)	162.4(2)	C(54A)-C(55A)-C(55)-C(56)	173.8(4)
C(2)-C(1)-C(1A)-N(9)	173.2(4)	C(55A)-C(55)-C(56)-C(57)	-2.4(6)
N(1 <sup>+</sup> )-C(1)-C(1A)-N(9)	-4.9(6)	C(55A)-C(55)-C(56)-C(60B)	176.5(4)
C(2)-C(1)-C(1A)-C(4A)	-3.4(6)	C(61E)-C(60B)-C(56)-C(55)	120.8(5)
N(1 <sup>+</sup> )-C(1)-C(1A)-C(4A)	178.5(3)	C(61F)-C(60B)-C(56)-C(55)	-118.4(5)
C(2 <sup>+</sup> )-N(3 <sup>+</sup> )-C(12)-C(13)	-104.6(5)	C(61D)-C(60B)-C(56)-C(55)	1.4(7)
C(4 <sup>+</sup> )-N(3 <sup>+</sup> )-C(12)-C(13)	74.2(5)	C(61E)-C(60B)-C(56)-C(57)	-60.3(6)

C(61F)-C(60B)-C(56)-C(57)	60.5(6)	C(57)-C(58)-C(58A)-N(59)	-177.5(4)
C(61D)-C(60B)-C(56)-C(57)	-179.7(5)	N(56')-C(58)-C(58A)-N(59)	1.8(6)
C(60')-N(56')-C(57')-N(58')	-0.5(4)	C(57)-C(58)-C(58A)-C(55A)	-5.3(6)
C(58)-N(56')-C(57')-N(58')	177.5(3)	N(56')-C(58)-C(58A)-C(55A)	174.0(3)
C(60')-N(56')-C(57')-Ir(2)	-174.6(3)	C(55)-C(55A)-C(58A)-N(59)	179.0(4)
C(58)-N(56')-C(57')-Ir(2)	3.5(5)	C(54A)-C(55A)-C(58A)-N(59)	2.3(4)
C(55)-C(56)-C(57)-C(58)	2.6(6)	C(55)-C(55A)-C(58A)-C(58)	5.7(6)
C(60B)-C(56)-C(57)-C(58)	-176.3(4)	C(54A)-C(55A)-C(58A)-C(58)	-171.1(3)
C(56)-C(57)-C(58)-C(58A)	1.2(6)	C(6)-C(5)-C(5A)-C(8A)	-0.1(6)
C(56)-C(57)-C(58)-N(56')	-178.0(4)	C(6)-C(5)-C(5A)-C(4A)	173.1(4)
C(57')-N(56')-C(58)-C(57)	168.9(4)	N(9)-C(8A)-C(5A)-C(5)	176.4(3)
C(60')-N(56')-C(58)-C(57)	-13.3(5)	C(8)-C(8A)-C(5A)-C(5)	0.2(6)
C(57')-N(56')-C(58)-C(58A)	-10.4(6)	N(9)-C(8A)-C(5A)-C(4A)	1.6(4)
C(60')-N(56')-C(58)-C(58A)	167.5(3)	C(8)-C(8A)-C(5A)-C(4A)	-174.6(3)
N(56')-C(57')-N(58')-C(59')	0.6(4)	C(4)-C(4A)-C(5A)-C(5)	-1.3(8)
Ir(2)-C(57')-N(58')-C(59')	174.6(3)	C(1A)-C(4A)-C(5A)-C(5)	-174.7(4)
N(56')-C(57')-N(58')-C(66)	-175.5(3)	C(4)-C(4A)-C(5A)-C(8A)	172.7(4)
Ir(2)-C(57')-N(58')-C(66)	-1.5(5)	C(1A)-C(4A)-C(5A)-C(8A)	-0.8(4)
C(57')-N(58')-C(59')-C(60')	-0.4(4)	C(52')-N(53')-C(62)-C(63)	-101.9(5)
C(66)-N(58')-C(59')-C(60')	175.7(4)	C(54')-N(53')-C(62)-C(63)	77.3(5)
C(54A)-C(51A)-N(59)-C(58A)	0.4(4)	N(53')-C(62)-C(63)-C(64)	178.5(4)
C(51)-C(51A)-N(59)-C(58A)	-177.3(4)	C(65)-C(64)-C(63)-C(62)	-70.0(5)
C(54A)-C(51A)-N(59)-Ir(2)	159.3(3)	C(106)-C(101)-C(102)-C(103)	0.0
C(51)-C(51A)-N(59)-Ir(2)	-18.4(5)	C(101)-C(102)-C(103)-C(104)	0.0
C(57')-N(58')-C(66)-C(67)	179.1(3)	C(102)-C(103)-C(104)-C(105)	0.0
C(59')-N(58')-C(66)-C(67)	3.5(5)	C(103)-C(104)-C(105)-C(106)	0.0
C(68)-C(67)-C(66)-N(58')	-178.8(3)	C(104)-C(105)-C(106)-C(101)	0.0
N(58')-C(59')-C(60')-N(56')	0.0(4)	C(102)-C(101)-C(106)-C(105)	0.0
C(57')-N(56')-C(60')-C(59')	0.3(4)	C(112)-C(107)-C(108)-C(109)	0.0
C(58)-N(56')-C(60')-C(59')	-177.8(3)	C(107)-C(108)-C(109)-C(110)	0.0
C(51A)-N(59)-C(58A)-C(58)	171.0(4)	C(108)-C(109)-C(110)-C(111)	0.0
Ir(2)-N(59)-C(58A)-C(58)	12.5(6)	C(109)-C(110)-C(111)-C(112)	0.0
C(51A)-N(59)-C(58A)-C(55A)	-1.7(4)	C(110)-C(111)-C(112)-C(107)	0.0
Ir(2)-N(59)-C(58A)-C(55A)	-160.2(3)	C(108)-C(107)-C(112)-C(111)	0.0

---



## 2.4. Compound 8



**Figure S23.** Solid-state molecular structure of **8**. Atoms are shown with anisotropic atomic displacement parameters at the 30% probability level. The co-crystallized benzene molecule and the hydrogen atoms (except Rh-H) are omitted for clarity. Based on DFT calculations (see 3.2), the metal-hydrogen bond lengths and angles were fixed at Rh1-H1a = 1.54, Rh1-H2a = 1.58, Rh2-H1b = 1.54, Rh2-H2b = 1.58 Å. The structures of **7** and **8** are isomorphous.

**Table S10.** Crystal data and structure refinement for compound **8**.

Identification code	Compound <b>8</b>	
Empirical formula	C <sub>74</sub> H <sub>98</sub> N <sub>10</sub> Rh <sub>2</sub>	
Formula weight	1333.44	
Temperature	100(2) K	
Wavelength	0.71073 Å	
Crystal system	Monoclinic	
Space group	<i>P</i> 2 <sub>1</sub> / <i>c</i>	
Unit cell dimensions	a = 18.2960(12) Å	α = 90°.
	b = 28.9467(17) Å	β = 110.393(2)°.
	c = 13.3801(8) Å	γ = 90°.
Volume	6642.1(7) Å <sup>3</sup>	
Z	4	
Density (calculated)	1.333 Mg/m <sup>3</sup>	
Absorption coefficient	0.547 mm <sup>-1</sup>	
F(000)	2808	
Crystal size	0.226 x 0.191 x 0.130 mm <sup>3</sup>	
Theta range for data collection	1.407 to 30.408°.	
Index ranges	-26 ≤ h ≤ 26, -41 ≤ k ≤ 41, -19 ≤ l ≤ 18	
Reflections collected	134132	
Independent reflections	20068 [R(int) = 0.0757]	
Completeness to theta = 25.242°	100.0 %	
Absorption correction	Semi-empirical from equivalents	
Refinement method	Full-matrix least-squares on F <sup>2</sup>	
Data / restraints / parameters	20068 / 134 / 867	

Goodness-of-fit on $F^2$	1.026
Final R indices [ $I > 2\sigma(I)$ ]	R1 = 0.0393, wR2 = 0.0856
R indices (all data)	R1 = 0.0589, wR2 = 0.0960
Extinction coefficient	n/a
Largest diff. peak and hole	0.845 and -0.680 e.Å <sup>-3</sup>

**Table S11.** Bond lengths [Å] and angles [°] for compound **8**.

Rh(1)-C(7')	2.029(2)	C(16)-C(17)	1.514(3)	C(61A)-C(60A)	1.540(3)
Rh(1)-C(2')	2.037(2)	C(16)-H(16A)	0.9900	C(61A)-H(61A)	0.9800
Rh(1)-N(9)	2.0624(16)	C(16)-H(16B)	0.9900	C(61A)-H(61B)	0.9800
Rh(1)-Rh(2)	2.9335(3)	C(17)-C(18)	1.528(3)	C(61A)-H(61C)	0.9800
Rh(1)-H(1A)	1.541(2)	C(17)-H(17A)	0.9900	C(60B)-C(61F)	1.514(5)
Rh(1)-H(2A)	1.580(2)	C(17)-H(17B)	0.9900	C(60B)-C(61E)	1.527(6)
Rh(2)-C(57')	2.029(2)	C(1A)-N(9)	1.362(2)	C(60B)-C(61D)	1.534(4)
Rh(2)-N(59)	2.0348(17)	C(19)-C(18)	1.511(4)	C(60A)-C(61B)	1.530(3)
Rh(2)-C(52')	2.036(2)	C(19)-H(19A)	0.9800	C(60A)-C(61C)	1.530(3)
Rh(2)-H(1B)	1.538(2)	C(19)-H(19B)	0.9800	C(61B)-H(61D)	0.9800
Rh(2)-H(2B)	1.579(2)	C(19)-H(19C)	0.9800	C(61B)-H(61E)	0.9800
C(1)-C(2)	1.385(3)	C(18)-H(18A)	0.9900	C(61B)-H(61F)	0.9800
C(1)-C(1A)	1.407(3)	C(18)-H(18B)	0.9900	C(61C)-H(61G)	0.9800
C(1)-N(1')	1.431(2)	C(51)-C(52)	1.384(3)	C(61C)-H(61H)	0.9800
N(1')-C(2')	1.383(3)	C(51)-C(51A)	1.401(3)	C(61C)-H(61I)	0.9800
N(1')-C(5')	1.397(3)	C(51)-N(51')	1.420(3)	C(60')-H(60')	0.9500
C(12)-N(3')	1.476(3)	N(51')-C(52')	1.383(3)	C(61F)-H(61J)	0.9800
C(12)-C(13)	1.496(3)	N(51')-C(55')	1.390(3)	C(61F)-H(61K)	0.9800
C(12)-H(12A)	0.9900	C(52)-C(53)	1.415(3)	C(61F)-H(61L)	0.9800
C(12)-H(12B)	0.9900	C(52)-H(52)	0.9500	C(11G)-C(10B)	1.537(3)
C(2)-C(3)	1.411(3)	C(52)-N(53')	1.361(3)	C(11G)-H(11A)	0.9800
C(2)-H(2)	0.9500	N(53')-C(54')	1.386(3)	C(11G)-H(11B)	0.9800
C(2')-N(3')	1.353(3)	N(53')-C(62)	1.466(3)	C(11G)-H(11C)	0.9800
C(13)-C(14)	1.530(3)	C(53)-C(54)	1.385(3)	C(10B)-C(11I)	1.532(3)
C(13)-H(13A)	0.9900	C(53)-C(60A)	1.534(3)	C(10B)-C(11H)	1.533(3)
C(13)-H(13B)	0.9900	C(54')-C(55')	1.342(3)	C(10A)-C(11F)	1.431(9)
C(3)-C(4)	1.385(3)	C(54')-H(54')	0.9500	C(10A)-C(11A)	1.476(5)
C(3)-C(10A)	1.540(3)	C(54A)-C(54)	1.399(3)	C(10A)-C(11C)	1.495(5)
N(3')-C(4')	1.380(3)	C(54A)-C(51A)	1.416(3)	C(10A)-C(11E)	1.524(8)
C(14)-C(15)	1.515(4)	C(54A)-C(55A)	1.444(3)	C(10A)-C(11B)	1.596(5)
C(14)-H(14A)	0.9900	C(51A)-N(59)	1.378(3)	C(10A)-C(11D)	1.646(9)
C(14)-H(14B)	0.9900	C(54)-H(54)	0.9500	C(8A)-N(9)	1.363(3)
C(4A)-C(4)	1.396(3)	C(55')-H(55')	0.9500	C(8A)-C(8)	1.402(3)
C(4A)-C(1A)	1.420(3)	C(55A)-C(55)	1.390(3)	C(69)-C(68)	1.522(3)
C(4A)-C(5A)	1.441(3)	C(55A)-C(58A)	1.422(3)	C(69)-H(69A)	0.9800
C(4)-H(4)	0.9500	C(55)-C(56)	1.391(3)	C(69)-H(69B)	0.9800
C(4')-C(5')	1.338(3)	C(55)-H(55)	0.9500	C(69)-H(69C)	0.9800
C(4')-H(4')	0.9500	N(56')-C(57')	1.378(3)	C(68)-C(67)	1.524(3)
C(15)-H(15A)	0.9800	N(56')-C(60')	1.397(3)	C(68)-H(68A)	0.9900
C(15)-H(15B)	0.9800	N(56')-C(58)	1.429(3)	C(68)-H(68B)	0.9900
C(15)-H(15C)	0.9800	C(56)-C(57)	1.412(3)	C(67)-C(66)	1.508(3)
C(5A)-C(5)	1.399(3)	C(56)-C(60B)	1.534(3)	C(67)-H(67A)	0.9900
C(5A)-C(8A)	1.424(3)	C(57')-N(58')	1.363(3)	C(67)-H(67B)	0.9900
C(5)-C(6)	1.385(3)	C(57)-C(58)	1.389(3)	C(66)-H(66A)	0.9900
C(5)-H(5)	0.9500	C(57)-H(57)	0.9500	C(66)-H(66B)	0.9900
C(5')-H(5')	0.9500	N(58')-C(59')	1.382(3)	C(65)-C(64)	1.510(4)
C(6)-C(7)	1.413(3)	N(58')-C(66)	1.472(3)	C(65)-H(65A)	0.9800
C(6)-C(10B)	1.537(3)	C(58)-C(58A)	1.402(3)	C(65)-H(65B)	0.9800
C(7)-C(8)	1.391(3)	C(59')-C(60')	1.341(3)	C(65)-H(65C)	0.9800
C(7)-H(7)	0.9500	C(59')-H(59')	0.9500	C(64)-C(63)	1.531(3)
C(16)-N(8')	1.462(3)	N(59)-C(58A)	1.371(3)	C(64)-H(64A)	0.9900

C(64)-H(64B)	0.9900	C(109)-C(110)	1.3900	C(12)-C(13)-H(13B)	109.4
C(63)-C(62)	1.509(3)	C(109)-H(109)	0.9500	C(14)-C(13)-H(13B)	109.4
C(63)-H(63A)	0.9900	C(110)-C(111)	1.3900	H(13A)-C(13)-H(13B)	108.0
C(63)-H(63B)	0.9900	C(110)-H(111)	0.9500	C(4)-C(3)-C(2)	119.03(19)
C(62)-H(62A)	0.9900	C(111)-C(112)	1.3900	C(4)-C(3)-C(10A)	121.41(19)
C(62)-H(62B)	0.9900	C(111)-H(112)	0.9500	C(2)-C(3)-C(10A)	119.56(19)
C(61D)-H(61M)	0.9800	C(112)-H(113)	0.9500	C(2)-N(3)-C(4)	112.82(17)
C(61D)-H(61N)	0.9800	N(6)-C(7)	1.383(3)	C(2)-N(3)-C(12)	126.70(18)
C(61D)-H(61O)	0.9800			C(4)-N(3)-C(12)	120.47(18)
C(11H)-H(11D)	0.9800	C(7)-Rh(1)-C(2')	173.30(8)	C(15)-C(14)-C(13)	113.5(2)
C(11H)-H(11E)	0.9800	C(7)-Rh(1)-N(9)	88.73(7)	C(15)-C(14)-H(14A)	108.9
C(11H)-H(11F)	0.9800	C(2)-Rh(1)-N(9)	88.73(7)	C(13)-C(14)-H(14A)	108.9
C(61E)-H(61P)	0.9800	C(7)-Rh(1)-Rh(2)	86.55(6)	C(15)-C(14)-H(14B)	108.9
C(61E)-H(61Q)	0.9800	C(2)-Rh(1)-Rh(2)	100.13(6)	C(13)-C(14)-H(14B)	108.9
C(61E)-H(61R)	0.9800	N(9)-Rh(1)-Rh(2)	107.53(5)	H(14A)-C(14)-H(14B)	107.7
C(11I)-H(11G)	0.9800	C(7)-Rh(1)-H(1A)	86.4(13)	C(4)-C(4A)-C(1A)	120.98(18)
C(11I)-H(11H)	0.9800	C(2)-Rh(1)-H(1A)	88.3(13)	C(4)-C(4A)-C(5A)	133.87(19)
C(11I)-H(11I)	0.9800	N(9)-Rh(1)-H(1A)	105.18(12)	C(1A)-C(4A)-C(5A)	104.91(16)
C(8)-N(6')	1.433(2)	Rh(2)-Rh(1)-H(1A)	146.3(3)	C(3)-C(4)-C(4A)	119.58(19)
N(8)-C(7')	1.363(2)	C(7)-Rh(1)-H(2A)	90.9(13)	C(3)-C(4)-H(4)	120.2
N(8)-C(9')	1.377(3)	C(2)-Rh(1)-H(2A)	92.0(13)	C(4A)-C(4)-H(4)	120.2
C(9)-C(10')	1.345(3)	N(9)-Rh(1)-H(2A)	176.6(5)	C(5)-C(4)-N(3)	106.86(19)
C(9)-H(9')	0.9500	Rh(2)-Rh(1)-H(2A)	69.0(5)	C(5)-C(4)-H(4')	126.6
C(10)-N(6')	1.390(3)	H(1A)-Rh(1)-H(2A)	78.2(5)	N(3)-C(4)-H(4')	126.6
C(10)-H(10')	0.9500	C(57)-Rh(2)-N(59)	88.62(8)	C(14)-C(15)-H(15A)	109.5
C(11A)-H(11J)	0.9800	C(57)-Rh(2)-C(52')	172.28(8)	C(14)-C(15)-H(15B)	109.5
C(11A)-H(11K)	0.9800	N(59)-Rh(2)-C(52')	89.37(7)	H(15A)-C(15)-H(15B)	109.5
C(11A)-H(11L)	0.9800	C(57)-Rh(2)-Rh(1)	94.68(6)	C(14)-C(15)-H(15C)	109.5
C(11B)-H(11M)	0.9800	N(59)-Rh(2)-Rh(1)	108.97(5)	H(15A)-C(15)-H(15C)	109.5
C(11B)-H(11N)	0.9800	C(52)-Rh(2)-Rh(1)	93.02(6)	H(15B)-C(15)-H(15C)	109.5
C(11B)-H(11O)	0.9800	C(57)-Rh(2)-H(1B)	87.4(11)	C(5)-C(5A)-C(8A)	120.82(18)
C(11C)-H(11P)	0.9800	N(59)-Rh(2)-H(1B)	119.63(16)	C(5)-C(5A)-C(4A)	134.10(18)
C(11C)-H(11Q)	0.9800	C(52)-Rh(2)-H(1B)	87.1(11)	C(8A)-C(5A)-C(4A)	104.93(17)
C(11C)-H(11R)	0.9800	Rh(1)-Rh(2)-H(1B)	131.40(17)	C(6)-C(5)-C(5A)	119.86(18)
C(11D)-H(11S)	0.9800	C(57)-Rh(2)-H(2B)	91.9(11)	C(6)-C(5)-H(5)	120.1
C(11D)-H(11T)	0.9800	N(59)-Rh(2)-H(2B)	169.2(2)	C(5A)-C(5)-H(5)	120.1
C(11D)-H(11U)	0.9800	C(52)-Rh(2)-H(2B)	91.5(11)	C(4)-C(5)-N(1')	106.57(19)
C(11E)-H(11V)	0.9800	Rh(1)-Rh(2)-H(2B)	60.2(2)	C(4)-C(5)-H(5')	126.7
C(11E)-H(11W)	0.9800	H(1B)-Rh(2)-H(2B)	71.21(9)	N(1)-C(5)-H(5')	126.7
C(11E)-H(11X)	0.9800	C(2)-C(1)-C(1A)	118.11(18)	C(5)-C(6)-C(7)	118.57(18)
C(11F)-H(11Y)	0.9800	C(2)-C(1)-N(1')	120.94(18)	C(5)-C(6)-C(10B)	123.24(18)
C(11F)-H(11Z)	0.9800	C(1A)-C(1)-N(1')	120.94(17)	C(7)-C(6)-C(10B)	118.13(18)
C(11F)-H(110)	0.9800	C(2)-N(1)-C(5')	111.08(17)	C(8)-C(7)-C(6)	123.19(19)
C(101)-C(102)	1.3900	C(2)-N(1)-C(1)	126.25(17)	C(8)-C(7)-H(7)	118.4
C(101)-C(106)	1.3900	C(5)-N(1)-C(1)	122.51(17)	C(6)-C(7)-H(7)	118.4
C(101)-H(101)	0.9500	N(3)-C(12)-C(13)	113.67(19)	N(8)-C(16)-C(17)	113.52(17)
C(102)-C(103)	1.3900	N(3)-C(12)-H(12A)	108.8	N(8)-C(16)-H(16A)	108.9
C(102)-H(102)	0.9500	C(13)-C(12)-H(12A)	108.8	C(17)-C(16)-H(16A)	108.9
C(103)-C(104)	1.3900	N(3)-C(12)-H(12B)	108.8	N(8)-C(16)-H(16B)	108.9
C(103)-H(103)	0.9500	C(13)-C(12)-H(12B)	108.8	C(17)-C(16)-H(16B)	108.9
C(104)-C(105)	1.3900	H(12A)-C(12)-H(12B)	107.7	H(16A)-C(16)-H(16B)	107.7
C(104)-H(104)	0.9500	C(1)-C(2)-C(3)	122.69(19)	C(16)-C(17)-C(18)	110.13(19)
C(105)-C(106)	1.3900	C(1)-C(2)-H(2)	118.7	C(16)-C(17)-H(17A)	109.6
C(105)-H(105)	0.9500	C(3)-C(2)-H(2)	118.7	C(18)-C(17)-H(17A)	109.6
C(106)-H(106)	0.9500	N(3)-C(2)-N(1')	102.67(17)	C(16)-C(17)-H(17B)	109.6
C(107)-C(108)	1.3900	N(3)-C(2)-Rh(1)	129.80(15)	C(18)-C(17)-H(17B)	109.6
C(107)-C(112)	1.3900	N(1)-C(2)-Rh(1)	127.31(14)	H(17A)-C(17)-H(17B)	108.1
C(107)-H(107)	0.9500	C(12)-C(13)-C(14)	111.3(2)	N(9)-C(1A)-C(1)	128.13(18)
C(108)-C(109)	1.3900	C(12)-C(13)-H(13A)	109.4	N(9)-C(1A)-C(4A)	112.30(17)
C(108)-H(108)	0.9500	C(14)-C(13)-H(13A)	109.4	C(1)-C(1A)-C(4A)	119.49(17)



C(18)-C(19)-H(19A)	109.5	C(58)-C(57)-C(56)	123.0(2)	C(10B)-C(11G)-H(11C)	109.5
C(18)-C(19)-H(19B)	109.5	C(58)-C(57)-H(57)	118.5	H(11A)-C(11G)-H(11C)	109.5
H(19A)-C(19)-H(19B)	109.5	C(56)-C(57)-H(57)	118.5	H(11B)-C(11G)-H(11C)	109.5
C(18)-C(19)-H(19C)	109.5	C(57)-N(58)-C(59)	111.54(18)	C(11I)-C(10B)-C(11H)	110.2(2)
H(19A)-C(19)-H(19C)	109.5	C(57)-N(58)-C(66)	123.95(18)	C(11I)-C(10B)-C(11G)	108.38(18)
H(19B)-C(19)-H(19C)	109.5	C(59)-N(58)-C(66)	124.48(18)	C(11H)-C(10B)-C(11G)	107.40(19)
C(19)-C(18)-C(17)	112.6(2)	C(57)-C(58)-C(58A)	117.8(2)	C(11I)-C(10B)-C(6)	110.02(19)
C(19)-C(18)-H(18A)	109.1	C(57)-C(58)-N(56')	121.25(19)	C(11H)-C(10B)-C(6)	109.05(17)
C(17)-C(18)-H(18A)	109.1	C(58A)-C(58)-N(56')	120.93(19)	C(11G)-C(10B)-C(6)	111.77(17)
C(19)-C(18)-H(18B)	109.1	C(60)-C(59)-N(58')	107.40(19)	C(11A)-C(10A)-C(11C)	112.9(4)
C(17)-C(18)-H(18B)	109.1	C(60)-C(59)-H(59')	126.3	C(11F)-C(10A)-C(11E)	114.3(6)
H(18A)-C(18)-H(18B)	107.8	N(58')-C(59)-H(59')	126.3	C(11F)-C(10A)-C(3)	115.9(4)
C(52)-C(51)-C(51A)	118.05(18)	C(58A)-N(59)-C(51A)	105.40(17)	C(11A)-C(10A)-C(3)	114.0(2)
C(52)-C(51)-N(51')	120.99(19)	C(58A)-N(59)-Rh(2)	126.69(14)	C(11C)-C(10A)-C(3)	109.8(2)
C(51A)-C(51)-N(51')	120.96(18)	C(51A)-N(59)-Rh(2)	124.95(14)	C(11E)-C(10A)-C(3)	110.3(4)
C(52)-N(51)-C(55)	111.21(17)	C(60A)-C(61A)-H(61A)	109.5	C(11A)-C(10A)-C(11B)	106.3(4)
C(52)-N(51)-C(51)	125.69(17)	C(60A)-C(61A)-H(61B)	109.5	C(11C)-C(10A)-C(11B)	104.6(4)
C(55)-N(51)-C(51)	122.98(17)	H(61A)-C(61A)-H(61B)	109.5	C(3)-C(10A)-C(11B)	108.6(2)
C(51)-C(52)-C(53)	122.8(2)	C(60A)-C(61A)-H(61C)	109.5	C(11F)-C(10A)-C(11D)	106.0(6)
C(51)-C(52)-H(52)	118.6	H(61A)-C(61A)-H(61C)	109.5	C(11E)-C(10A)-C(11D)	103.1(5)
C(53)-C(52)-H(52)	118.6	H(61B)-C(61A)-H(61C)	109.5	C(3)-C(10A)-C(11D)	105.8(3)
N(53)-C(52)-N(51')	103.12(17)	C(61F)-C(60B)-C(61E)	110.8(3)	N(9)-C(8A)-C(8)	128.09(18)
N(53)-C(52)-Rh(2)	129.92(15)	C(61F)-C(60B)-C(56)	110.3(3)	N(9)-C(8A)-C(5A)	112.06(17)
N(51)-C(52)-Rh(2)	126.55(15)	C(61E)-C(60B)-C(56)	109.1(3)	C(8)-C(8A)-C(5A)	119.77(18)
C(52)-N(53)-C(54')	111.78(18)	C(61F)-C(60B)-C(61D)	106.6(3)	C(68)-C(69)-H(69A)	109.5
C(52)-N(53)-C(62)	126.54(18)	C(61E)-C(60B)-C(61D)	107.8(3)	C(68)-C(69)-H(69B)	109.5
C(54)-N(53)-C(62)	121.68(18)	C(56)-C(60B)-C(61D)	112.2(2)	H(69A)-C(69)-H(69B)	109.5
C(54)-C(53)-C(52)	118.64(19)	C(61B)-C(60A)-C(61C)	108.14(19)	C(68)-C(69)-H(69C)	109.5
C(54)-C(53)-C(60A)	123.49(18)	C(61B)-C(60A)-C(53)	109.89(18)	H(69A)-C(69)-H(69C)	109.5
C(52)-C(53)-C(60A)	117.86(19)	C(61C)-C(60A)-C(53)	112.29(19)	H(69B)-C(69)-H(69C)	109.5
C(55)-C(54)-N(53')	107.18(19)	C(61B)-C(60A)-C(61A)	109.3(2)	C(69)-C(68)-C(67)	112.6(2)
C(55)-C(54)-H(54')	126.4	C(61C)-C(60A)-C(61A)	107.68(19)	C(69)-C(68)-H(68A)	109.1
N(53)-C(54)-H(54')	126.4	C(53)-C(60A)-C(61A)	109.52(18)	C(67)-C(68)-H(68A)	109.1
C(54)-C(54A)-C(51A)	120.84(19)	N(59)-C(58A)-C(58)	128.02(19)	C(69)-C(68)-H(68B)	109.1
C(54)-C(54A)-C(55A)	133.84(19)	N(59)-C(58A)-C(55A)	112.09(18)	C(67)-C(68)-H(68B)	109.1
C(51A)-C(54A)-C(55A)	105.21(18)	C(58)-C(58A)-C(55A)	119.74(19)	H(68A)-C(68)-H(68B)	107.8
N(59)-C(51A)-C(51)	128.01(18)	C(60A)-C(61B)-H(61D)	109.5	C(66)-C(67)-C(68)	110.2(2)
N(59)-C(51A)-C(54A)	112.13(18)	C(60A)-C(61B)-H(61E)	109.5	C(66)-C(67)-H(67A)	109.6
C(51)-C(51A)-C(54A)	119.82(18)	H(61D)-C(61B)-H(61E)	109.5	C(68)-C(67)-H(67A)	109.6
C(53)-C(54)-C(54A)	119.71(19)	C(60A)-C(61B)-H(61F)	109.5	C(66)-C(67)-H(67B)	109.6
C(53)-C(54)-H(54)	120.1	H(61D)-C(61B)-H(61F)	109.5	C(68)-C(67)-H(67B)	109.6
C(54A)-C(54)-H(54)	120.1	H(61E)-C(61B)-H(61F)	109.5	H(67A)-C(67)-H(67B)	108.1
C(54)-C(55)-N(51')	106.64(19)	C(60A)-C(61C)-H(61G)	109.5	N(58')-C(66)-C(67)	114.84(19)
C(54)-C(55)-H(55')	126.7	C(60A)-C(61C)-H(61H)	109.5	N(58')-C(66)-H(66A)	108.6
N(51)-C(55)-H(55')	126.7	H(61G)-C(61C)-H(61H)	109.5	C(67)-C(66)-H(66A)	108.6
C(55)-C(55A)-C(58A)	121.0(2)	C(60A)-C(61C)-H(61I)	109.5	N(58')-C(66)-H(66B)	108.6
C(55)-C(55A)-C(54A)	133.8(2)	H(61G)-C(61C)-H(61I)	109.5	C(67)-C(66)-H(66B)	108.6
C(58A)-C(55A)-C(54A)	105.09(18)	H(61H)-C(61C)-H(61I)	109.5	H(66A)-C(66)-H(66B)	107.5
C(55A)-C(55)-C(56)	119.7(2)	C(59)-C(60)-N(56')	106.7(2)	C(64)-C(65)-H(65A)	109.5
C(55A)-C(55)-H(55)	120.2	C(59)-C(60)-H(60')	126.7	C(64)-C(65)-H(65B)	109.5
C(56)-C(55)-H(55)	120.2	N(56')-C(60)-H(60')	126.7	H(65A)-C(65)-H(65B)	109.5
C(57)-N(56)-C(60')	110.69(17)	C(60B)-C(61F)-H(61J)	109.5	C(64)-C(65)-H(65C)	109.5
C(57)-N(56)-C(58)	126.42(17)	C(60B)-C(61F)-H(61K)	109.5	H(65A)-C(65)-H(65C)	109.5
C(60)-N(56)-C(58)	122.88(18)	H(61J)-C(61F)-H(61K)	109.5	H(65B)-C(65)-H(65C)	109.5
C(55)-C(56)-C(57)	118.6(2)	C(60B)-C(61F)-H(61L)	109.5	C(65)-C(64)-C(63)	112.9(2)
C(55)-C(56)-C(60B)	122.7(2)	H(61J)-C(61F)-H(61L)	109.5	C(65)-C(64)-H(64A)	109.0
C(57)-C(56)-C(60B)	118.7(2)	H(61K)-C(61F)-H(61L)	109.5	C(63)-C(64)-H(64A)	109.0
N(58)-C(57)-N(56')	103.68(18)	C(10B)-C(11G)-H(11A)	109.5	C(65)-C(64)-H(64B)	109.0
N(58)-C(57)-Rh(2)	128.33(16)	C(10B)-C(11G)-H(11B)	109.5	C(63)-C(64)-H(64B)	109.0
N(56)-C(57)-Rh(2)	127.85(15)	H(11A)-C(11G)-H(11B)	109.5	H(64A)-C(64)-H(64B)	107.8

C(62)-C(63)-C(64)	111.2(2)	C(7')-N(8')-C(16)	125.76(18)	H(11Z)-C(11F)-H(110)	109.5
C(62)-C(63)-H(63A)	109.4	C(9')-N(8')-C(16)	122.05(17)	C(102)-C(101)-C(106)	120.0
C(64)-C(63)-H(63A)	109.4	C(10')-C(9')-N(8')	106.93(19)	C(102)-C(101)-H(101)	120.0
C(62)-C(63)-H(63B)	109.4	C(10')-C(9')-H(9')	126.5	C(106)-C(101)-H(101)	120.0
C(64)-C(63)-H(63B)	109.4	N(8')-C(9')-H(9')	126.5	C(103)-C(102)-C(101)	120.0
H(63A)-C(63)-H(63B)	108.0	C(9')-C(10')-N(6')	106.92(19)	C(103)-C(102)-H(102)	120.0
N(53')-C(62)-C(63)	113.47(19)	C(9')-C(10')-H(10')	126.5	C(101)-C(102)-H(102)	120.0
N(53')-C(62)-H(62A)	108.9	N(6')-C(10')-H(10')	126.5	C(102)-C(103)-C(104)	120.0
C(63)-C(62)-H(62A)	108.9	C(10A)-C(11A)-H(11J)	109.5	C(102)-C(103)-H(103)	120.0
N(53')-C(62)-H(62B)	108.9	C(10A)-C(11A)-H(11K)	109.5	C(104)-C(103)-H(103)	120.0
C(63)-C(62)-H(62B)	108.9	H(11J)-C(11A)-H(11K)	109.5	C(105)-C(104)-C(103)	120.0
H(62A)-C(62)-H(62B)	107.7	C(10A)-C(11A)-H(11L)	109.5	C(105)-C(104)-H(104)	120.0
C(60B)-C(61D)-H(61M)	109.5	H(11J)-C(11A)-H(11L)	109.5	C(103)-C(104)-H(104)	120.0
C(60B)-C(61D)-H(61N)	109.5	H(11K)-C(11A)-H(11L)	109.5	C(104)-C(105)-C(106)	120.0
H(61M)-C(61D)-H(61N)	109.5	C(10A)-C(11B)-H(11M)	109.5	C(104)-C(105)-H(105)	120.0
C(60B)-C(61D)-H(61O)	109.5	C(10A)-C(11B)-H(11N)	109.5	C(106)-C(105)-H(105)	120.0
H(61M)-C(61D)-H(61O)	109.5	H(11M)-C(11B)-H(11N)	109.5	C(105)-C(106)-C(101)	120.0
H(61N)-C(61D)-H(61O)	109.5	C(10A)-C(11B)-H(11O)	109.5	C(105)-C(106)-H(106)	120.0
C(10B)-C(11H)-H(11D)	109.5	H(11M)-C(11B)-H(11O)	109.5	C(101)-C(106)-H(106)	120.0
C(10B)-C(11H)-H(11E)	109.5	H(11N)-C(11B)-H(11O)	109.5	C(108)-C(107)-C(112)	120.0
H(11D)-C(11H)-H(11E)	109.5	C(10A)-C(11C)-H(11P)	109.5	C(108)-C(107)-H(107)	120.0
C(10B)-C(11H)-H(11F)	109.5	C(10A)-C(11C)-H(11Q)	109.5	C(112)-C(107)-H(107)	120.0
H(11D)-C(11H)-H(11F)	109.5	H(11P)-C(11C)-H(11Q)	109.5	C(109)-C(108)-C(107)	120.0
H(11E)-C(11H)-H(11F)	109.5	C(10A)-C(11C)-H(11R)	109.5	C(109)-C(108)-H(108)	120.0
C(60B)-C(61E)-H(61P)	109.5	H(11P)-C(11C)-H(11R)	109.5	C(107)-C(108)-H(108)	120.0
C(60B)-C(61E)-H(61Q)	109.5	H(11Q)-C(11C)-H(11R)	109.5	C(108)-C(109)-C(110)	120.0
H(61P)-C(61E)-H(61Q)	109.5	C(10A)-C(11D)-H(11S)	109.5	C(108)-C(109)-H(109)	120.0
C(60B)-C(61E)-H(61R)	109.5	C(10A)-C(11D)-H(11T)	109.5	C(110)-C(109)-H(109)	120.0
H(61P)-C(61E)-H(61R)	109.5	H(11S)-C(11D)-H(11T)	109.5	C(111)-C(110)-C(109)	120.0
H(61Q)-C(61E)-H(61R)	109.5	C(10A)-C(11D)-H(11U)	109.5	C(111)-C(110)-H(111)	120.0
C(10B)-C(11I)-H(11G)	109.5	H(11S)-C(11D)-H(11U)	109.5	C(109)-C(110)-H(111)	120.0
C(10B)-C(11I)-H(11H)	109.5	H(11T)-C(11D)-H(11U)	109.5	C(112)-C(111)-C(110)	120.0
H(11G)-C(11I)-H(11H)	109.5	C(10A)-C(11E)-H(11V)	109.5	C(112)-C(111)-H(112)	120.0
C(10B)-C(11I)-H(11I)	109.5	C(10A)-C(11E)-H(11W)	109.5	C(110)-C(111)-H(112)	120.0
H(11G)-C(11I)-H(11I)	109.5	H(11V)-C(11E)-H(11W)	109.5	C(111)-C(112)-C(107)	120.0
H(11H)-C(11I)-H(11I)	109.5	C(10A)-C(11E)-H(11X)	109.5	C(111)-C(112)-H(113)	120.0
C(1A)-N(9)-C(8A)	105.79(16)	H(11V)-C(11E)-H(11X)	109.5	C(107)-C(112)-H(113)	120.0
C(1A)-N(9)-Rh(1)	126.32(13)	H(11W)-C(11E)-H(11X)	109.5	C(7')-N(6')-C(10')	110.87(17)
C(8A)-N(9)-Rh(1)	126.52(13)	C(10A)-C(11F)-H(11Y)	109.5	C(7')-N(6')-C(8)	126.34(17)
C(7)-C(8)-C(8A)	117.78(18)	C(10A)-C(11F)-H(11Z)	109.5	C(10')-N(6')-C(8)	122.80(17)
C(7)-C(8)-N(6')	120.90(18)	H(11Y)-C(11F)-H(11Z)	109.5	N(8')-C(7')-N(6')	103.10(17)
C(8A)-C(8)-N(6')	121.31(17)	C(10A)-C(11F)-H(110)	109.5	N(8')-C(7')-Rh(1)	128.92(15)
C(7')-N(8')-C(9')	112.18(17)	H(11Y)-C(11F)-H(110)	109.5	N(6')-C(7')-Rh(1)	127.76(14)

Table S12. Torsion angles [°] for compound 8.

C(2)-C(1)-N(1)-C(2)	-162.6(2)	N(51)-C(52)-N(53)-C(54)	2.8(2)
C(1A)-C(1)-N(1)-C(2)	16.2(3)	Rh(2)-C(52)-N(53)-C(54)	-170.06(17)
C(2)-C(1)-N(1)-C(5)	12.4(3)	N(51)-C(52)-N(53)-C(62)	-177.7(2)
C(1A)-C(1)-N(1)-C(5)	-168.8(2)	Rh(2)-C(52)-N(53)-C(62)	9.5(3)
C(1A)-C(1)-C(2)-C(3)	1.1(3)	C(51)-C(52)-C(53)-C(54)	1.0(3)
N(1)-C(1)-C(2)-C(3)	179.9(2)	C(51)-C(52)-C(53)-C(60A)	-177.8(2)
C(5)-N(1)-C(2)-N(3)	-0.8(2)	C(52)-N(53)-C(54)-C(55)	-2.2(3)
C(1)-N(1)-C(2)-N(3)	174.67(19)	C(62)-N(53)-C(54)-C(55)	178.3(2)
C(5)-N(1)-C(2)-Rh(1)	174.20(16)	C(52)-C(51)-C(51A)-N(59)	174.0(2)
C(1)-N(1)-C(2)-Rh(1)	-10.3(3)	N(51)-C(51)-C(51A)-N(59)	-5.6(3)
N(3)-C(12)-C(13)-C(14)	-176.9(2)	C(52)-C(51)-C(51A)-C(54A)	-3.5(3)
C(1)-C(2)-C(3)-C(4)	1.7(3)	N(51)-C(51)-C(51A)-C(54A)	176.87(19)
C(1)-C(2)-C(3)-C(10A)	-177.9(2)	C(54)-C(54A)-C(51A)-N(59)	-175.31(19)
N(1)-C(2)-N(3)-C(4)	0.6(2)	C(55A)-C(54A)-C(51A)-N(59)	1.3(2)
Rh(1)-C(2)-N(3)-C(4)	-174.26(17)	C(54)-C(54A)-C(51A)-C(51)	2.6(3)
N(1)-C(2)-N(3)-C(12)	-178.19(19)	C(55A)-C(54A)-C(51A)-C(51)	179.13(19)
Rh(1)-C(2)-N(3)-C(12)	7.0(3)	C(52)-C(53)-C(54)-C(54A)	-2.0(3)
C(13)-C(12)-N(3)-C(2)	-102.8(3)	C(60A)-C(53)-C(54)-C(54A)	176.74(19)
C(13)-C(12)-N(3)-C(4)	78.5(3)	C(51A)-C(54A)-C(54)-C(53)	0.2(3)
C(12)-C(13)-C(14)-C(15)	174.9(2)	C(55A)-C(54A)-C(54)-C(53)	-175.2(2)
C(2)-C(3)-C(4)-C(4A)	-2.3(3)	N(53)-C(54)-C(55)-N(51)	0.5(3)
C(10A)-C(3)-C(4)-C(4A)	177.4(2)	C(52)-N(51)-C(55)-C(54)	1.2(3)
C(1A)-C(4A)-C(4)-C(3)	0.0(3)	C(51)-N(51)-C(55)-C(54)	-175.0(2)
C(5A)-C(4A)-C(4)-C(3)	-173.4(2)	C(54)-C(54A)-C(55A)-C(55)	-2.9(4)
C(2)-N(3)-C(4)-C(5)	-0.1(3)	C(51A)-C(54A)-C(55A)-C(55)	-178.8(2)
C(12)-N(3)-C(4)-C(5)	178.7(2)	C(54)-C(54A)-C(55A)-C(58A)	173.5(2)
C(4)-C(4A)-C(5A)-C(5)	-2.3(4)	C(51A)-C(54A)-C(55A)-C(58A)	-2.5(2)
C(1A)-C(4A)-C(5A)-C(5)	-176.4(2)	C(58A)-C(55A)-C(55)-C(56)	-0.6(3)
C(4)-C(4A)-C(5A)-C(8A)	173.1(2)	C(54A)-C(55A)-C(55)-C(56)	175.2(2)
C(1A)-C(4A)-C(5A)-C(8A)	-1.0(2)	C(55A)-C(55)-C(56)-C(57)	-2.9(4)
C(8A)-C(5A)-C(5)-C(6)	-0.7(3)	C(55A)-C(55)-C(56)-C(60B)	177.5(3)
C(4A)-C(5A)-C(5)-C(6)	174.2(2)	C(60)-N(56)-C(57)-N(58)	-0.5(2)
N(3)-C(4)-C(5)-N(1)	-0.4(3)	C(58)-N(56)-C(57)-N(58)	178.30(18)
C(2)-N(1)-C(5)-C(4)	0.8(3)	C(60)-N(56)-C(57)-Rh(2)	-176.46(15)
C(1)-N(1)-C(5)-C(4)	-174.9(2)	C(58)-N(56)-C(57)-Rh(2)	2.3(3)
C(5A)-C(5)-C(6)-C(7)	1.1(3)	C(55)-C(56)-C(57)-C(58)	3.2(4)
C(5A)-C(5)-C(6)-C(10B)	-176.01(19)	C(60B)-C(56)-C(57)-C(58)	-177.1(3)
C(5)-C(6)-C(7)-C(8)	-1.1(3)	N(56)-C(57)-N(58)-C(59)	0.4(2)
C(10B)-C(6)-C(7)-C(8)	176.09(19)	Rh(2)-C(57)-N(58)-C(59)	176.33(15)
N(8)-C(16)-C(17)-C(18)	-172.88(19)	N(56)-C(57)-N(58)-C(66)	-177.57(18)
C(2)-C(1)-C(1A)-N(9)	173.3(2)	Rh(2)-C(57)-N(58)-C(66)	-1.6(3)
N(1)-C(1)-C(1A)-N(9)	-5.5(3)	C(56)-C(57)-C(58)-C(58A)	0.1(4)
C(2)-C(1)-C(1A)-C(4A)	-3.4(3)	C(56)-C(57)-C(58)-N(56)	-178.6(2)
N(1)-C(1)-C(1A)-C(4A)	177.80(19)	C(57)-N(56)-C(58)-C(57)	171.2(2)
C(4)-C(4A)-C(1A)-N(9)	-174.25(19)	C(60)-N(56)-C(58)-C(57)	-10.2(3)
C(5A)-C(4A)-C(1A)-N(9)	0.8(2)	C(57)-N(56)-C(58)-C(58A)	-7.6(3)
C(4)-C(4A)-C(1A)-C(1)	2.9(3)	C(60)-N(56)-C(58)-C(58A)	171.1(2)
C(5A)-C(4A)-C(1A)-C(1)	177.95(19)	C(57)-N(58)-C(59)-C(60)	-0.2(2)
C(16)-C(17)-C(18)-C(19)	-177.5(2)	C(66)-N(58)-C(59)-C(60)	177.81(19)
C(52)-C(51)-N(51)-C(52)	-158.7(2)	C(51)-C(51A)-N(59)-C(58A)	-177.1(2)
C(51A)-C(51)-N(51)-C(52)	21.0(3)	C(54A)-C(51A)-N(59)-C(58A)	0.6(2)
C(52)-C(51)-N(51)-C(55)	17.0(3)	C(51)-C(51A)-N(59)-Rh(2)	-15.6(3)
C(51A)-C(51)-N(51)-C(55)	-163.4(2)	C(54A)-C(51A)-N(59)-Rh(2)	162.09(14)
C(51A)-C(51)-C(52)-C(53)	1.7(3)	C(55)-C(56)-C(60B)-C(61F)	117.4(3)
N(51)-C(51)-C(52)-C(53)	-178.59(19)	C(57)-C(56)-C(60B)-C(61F)	-62.2(4)
C(55)-N(51)-C(52)-N(53)	-2.4(2)	C(55)-C(56)-C(60B)-C(61E)	-120.6(3)
C(51)-N(51)-C(52)-N(53)	173.64(19)	C(57)-C(56)-C(60B)-C(61E)	59.7(4)
C(55)-N(51)-C(52)-Rh(2)	170.74(16)	C(55)-C(56)-C(60B)-C(61D)	-1.3(4)
C(51)-N(51)-C(52)-Rh(2)	-13.2(3)	C(57)-C(56)-C(60B)-C(61D)	179.1(3)

C(54)-C(53)-C(60A)-C(61B)	-122.6(2)	C(52')-N(53')-C(62)-C(63)	-101.4(3)
C(52)-C(53)-C(60A)-C(61B)	56.1(3)	C(54')-N(53')-C(62)-C(63)	78.0(3)
C(54)-C(53)-C(60A)-C(61C)	-2.2(3)	C(64)-C(63)-C(62)-N(53')	178.6(2)
C(52)-C(53)-C(60A)-C(61C)	176.5(2)	C(1)-C(1A)-N(9)-C(8A)	-177.1(2)
C(54)-C(53)-C(60A)-C(61A)	117.4(2)	C(4A)-C(1A)-N(9)-C(8A)	-0.2(2)
C(52)-C(53)-C(60A)-C(61A)	-63.9(3)	C(1)-C(1A)-N(9)-Rh(1)	-9.8(3)
C(51A)-N(59)-C(58A)-C(58)	173.2(2)	C(4A)-C(1A)-N(9)-Rh(1)	167.08(14)
Rh(2)-N(59)-C(58A)-C(58)	12.1(3)	C(8)-C(8A)-N(9)-C(1A)	176.1(2)
C(51A)-N(59)-C(58A)-C(55A)	-2.2(2)	C(5A)-C(8A)-N(9)-C(1A)	-0.5(2)
Rh(2)-N(59)-C(58A)-C(55A)	-163.36(14)	C(8)-C(8A)-N(9)-Rh(1)	8.8(3)
C(57)-C(58)-C(58A)-N(59)	-178.8(2)	C(5A)-C(8A)-N(9)-Rh(1)	-167.74(14)
N(56')-C(58)-C(58A)-N(59)	-0.1(3)	C(6)-C(7)-C(8)-C(8A)	0.7(3)
C(57)-C(58)-C(58A)-C(55A)	-3.7(3)	C(6)-C(7)-C(8)-N(6')	-178.50(19)
N(56')-C(58)-C(58A)-C(55A)	175.06(19)	N(9)-C(8A)-C(8)-C(7)	-176.6(2)
C(55)-C(55A)-C(58A)-N(59)	179.9(2)	C(5A)-C(8A)-C(8)-C(7)	-0.3(3)
C(54A)-C(55A)-C(58A)-N(59)	3.0(2)	N(9)-C(8A)-C(8)-N(6')	2.6(3)
C(55)-C(55A)-C(58A)-C(58)	4.0(3)	C(5A)-C(8A)-C(8)-N(6')	178.94(18)
C(54A)-C(55A)-C(58A)-C(58)	-172.85(19)	C(17)-C(16)-N(8')-C(7')	88.7(2)
N(58')-C(59)-C(60')-N(56')	-0.2(2)	C(17)-C(16)-N(8')-C(9')	-90.9(2)
C(57')-N(56')-C(60')-C(59')	0.4(2)	C(7')-N(8')-C(9')-C(10')	-0.2(3)
C(58)-N(56')-C(60')-C(59')	-178.42(19)	C(16)-N(8')-C(9')-C(10')	179.5(2)
C(5)-C(6)-C(10B)-C(11I)	-116.2(2)	N(8')-C(9')-C(10')-N(6')	0.6(3)
C(7)-C(6)-C(10B)-C(11I)	66.7(2)	C(106)-C(101)-C(102)-C(103)	0.0
C(5)-C(6)-C(10B)-C(11H)	122.9(2)	C(101)-C(102)-C(103)-C(104)	0.0
C(7)-C(6)-C(10B)-C(11H)	-54.2(3)	C(102)-C(103)-C(104)-C(105)	0.0
C(5)-C(6)-C(10B)-C(11G)	4.3(3)	C(103)-C(104)-C(105)-C(106)	0.0
C(7)-C(6)-C(10B)-C(11G)	-172.82(19)	C(104)-C(105)-C(106)-C(101)	0.0
C(4)-C(3)-C(10A)-C(11F)	178.0(6)	C(102)-C(101)-C(106)-C(105)	0.0
C(2)-C(3)-C(10A)-C(11F)	-2.4(7)	C(112)-C(107)-C(108)-C(109)	0.0
C(4)-C(3)-C(10A)-C(11A)	-15.2(5)	C(107)-C(108)-C(109)-C(110)	0.0
C(2)-C(3)-C(10A)-C(11A)	164.5(4)	C(108)-C(109)-C(110)-C(111)	0.0
C(4)-C(3)-C(10A)-C(11C)	112.7(3)	C(109)-C(110)-C(111)-C(112)	0.0
C(2)-C(3)-C(10A)-C(11C)	-67.7(4)	C(110)-C(111)-C(112)-C(107)	0.0
C(4)-C(3)-C(10A)-C(11E)	-50.1(5)	C(108)-C(107)-C(112)-C(111)	0.0
C(2)-C(3)-C(10A)-C(11E)	129.5(5)	C(9')-C(10')-N(6')-C(7')	-0.8(3)
C(4)-C(3)-C(10A)-C(11B)	-133.5(3)	C(9')-C(10')-N(6')-C(8)	178.92(19)
C(2)-C(3)-C(10A)-C(11B)	46.2(4)	C(7)-C(8)-N(6')-C(7')	168.69(19)
C(4)-C(3)-C(10A)-C(11D)	60.8(5)	C(8A)-C(8)-N(6')-C(7')	-10.5(3)
C(2)-C(3)-C(10A)-C(11D)	-119.6(5)	C(7)-C(8)-N(6')-C(10')	-11.0(3)
C(5)-C(5A)-C(8A)-N(9)	177.14(18)	C(8A)-C(8)-N(6')-C(10')	169.8(2)
C(4A)-C(5A)-C(8A)-N(9)	1.0(2)	C(9')-N(8')-C(7')-N(6')	-0.3(2)
C(5)-C(5A)-C(8A)-C(8)	0.3(3)	C(16)-N(8')-C(7')-N(6')	-179.96(18)
C(4A)-C(5A)-C(8A)-C(8)	-175.92(18)	C(9')-N(8')-C(7')-Rh(1)	174.53(16)
C(69)-C(68)-C(67)-C(66)	-175.3(2)	C(16)-N(8')-C(7')-Rh(1)	-5.1(3)
C(57')-N(58')-C(66)-C(67)	179.54(19)	C(10')-N(6')-C(7')-N(8')	0.7(2)
C(59')-N(58')-C(66)-C(67)	1.8(3)	C(8)-N(6')-C(7')-N(8')	-179.02(18)
C(68)-C(67)-C(66)-N(58')	-179.44(18)	C(10')-N(6')-C(7')-Rh(1)	-174.26(16)
C(65)-C(64)-C(63)-C(62)	-70.4(3)	C(8)-N(6')-C(7')-Rh(1)	6.0(3)

## 2.5. Compound $[\text{Co}(\text{bimca}^{\text{Homo}})_2]\text{Br}$

### *X-ray Experimental Information and Comments for $[\text{Co}(\text{bimcaHomo})_2]\text{Br}$ :*

A gold colored thin plate crystal specimen was mounted inside a MiTiGen MicroLoop and single crystal Bragg diffraction data were collected at 103 K using an Oxford Cryosystems, Cryostream 700 Plus N<sub>2</sub> open flow blower, on the PILATUS@SNBL diffractometer<sup>3</sup> at the BM01A station of the Swiss–Norwegian Beamlines at the ESRF (Grenoble, France). The energy (wavelength) of the synchrotron

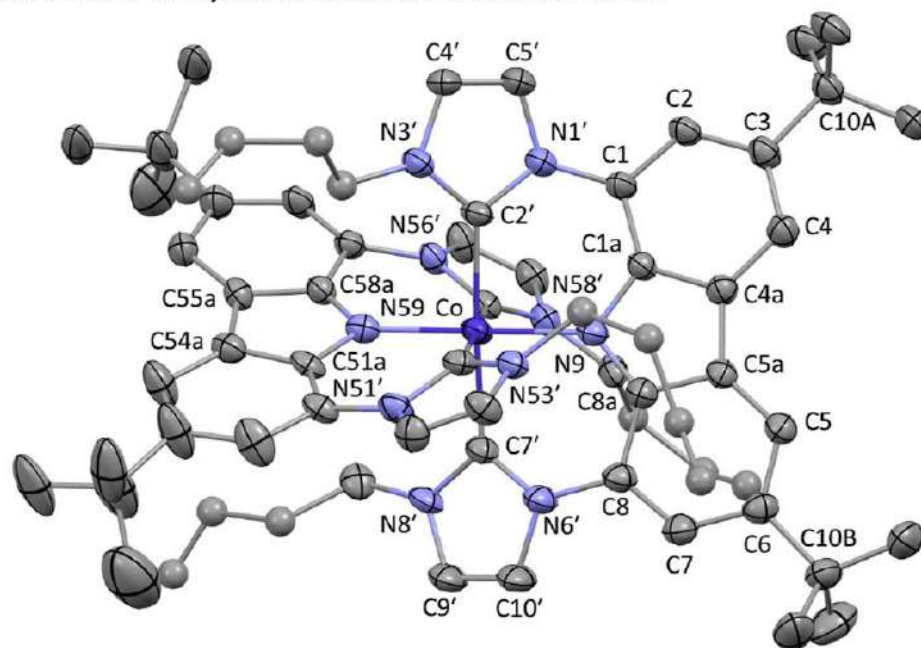


radiation was set to  $E = 15.813$  keV ( $0.78405$  Å) using 200 mA Top-Up Full Bunch electron storage ring mode. The crystals scatter very weakly and the Bragg profiles are wide (streaky) and lamellar twinning is present. The data were collected by way of four  $\phi$  360-degree scans of 3600 0.5 second images, with an angular step of  $0.1^\circ$  in a shutter-free mode using the Dectris PILATUS2M detector. The resulting 14400 raw frames were binned to finally produce 360, 1.0 degree frames.

The raw data were processed with the *SNBL Toolbox*;<sup>3</sup> the integrated intensities were extracted from the frames, scaled and corrected for absorption with the *CrysAlisPro* software;<sup>4</sup> the crystal structure was solved with *SHELXT*<sup>1e</sup> and refined with *SHELXL* version 2017/4<sup>1c</sup>.

The structural raw data suffer from wide Bragg profiles and overlaps due to twinning and the final experimental resolution is  $0.90$  Å despite the use of synchrotron light. Hence the structure presented suffers from low precision in terms of geometric and displacement parameters. The peripheral allyl groups all display disorder, and some are also split into two discrete conformers. All homoallyl groups were refined isotropically and with idealized distances. The structure also contains one disordered solvent site which was suppressed using the SQUEEZE routine in PLATON.<sup>2</sup> Therefore, this structure is not to be discussed in detail nor deposited in the Cambridge Structural Database. However, the integrity of the structural model is beyond doubt.

**Acknowledgement:** We are grateful to the Swiss-Norwegian beamlines at the ESRF, Grenoble, France and to Dr. D. Chernyshov for assistance on beamline BM01A.



**Table S13.** Crystal data and structure refinement for **[Co(bimca<sup>Hom</sup>)<sub>2</sub>Br]**.

Identification code	<b>[Co(bimca<sup>Hom</sup>)<sub>2</sub>Br]</b>		
Empirical formula	C <sub>68</sub> H <sub>80</sub> Br Co N <sub>10</sub>		
Formula weight	1176.26		
Temperature	103(2) K		
Wavelength	0.78405 Å		
Crystal system	Orthorhombic		
Space group	<i>Pccn</i>		
Unit cell dimensions	a = 29.106(2) Å	α = 90°.	
	b = 15.1466(5) Å	β = 90°.	
	c = 30.843(3) Å	γ = 90°.	
Volume	13597.3(15) Å <sup>3</sup>		
Z	8		
Density (calculated)	1.149 Mg/m <sup>3</sup>		
Absorption coefficient	1.129 mm <sup>-1</sup>		
F(000)	4960		
Crystal size	0.140 x 0.120 x 0.010 mm <sup>3</sup>		
Theta range for data collection	1.457 to 25.812°.		
Index ranges	-19 ≤ h ≤ 19, -16 ≤ k ≤ 16, -32 ≤ l ≤ 32		
Reflections collected	38052		
Independent reflections	7046 [R(int) = 0.1201]		
Completeness to theta = 25.812°	72.3 % [One axis Phi-scan]		
Absorption correction	Semi-empirical from equivalents		
Max. and min. transmission	1.785 and 0.548		
Refinement method	Full-matrix least-squares on F <sup>2</sup>		
Data / restraints / parameters	7046 / 732 / 689		
Goodness-of-fit on F <sup>2</sup>	1.316		
Final R indices [I > 2σ(I)]	R1 = 0.1367, wR2 = 0.3550		
R indices (all data)	R1 = 0.1886, wR2 = 0.3873		
Extinction coefficient	n/a		
Largest diff. peak and hole	1.139 and -0.574 e.Å <sup>-3</sup>		

**Table S14.** Bond lengths [Å] and angles [°] for **[Co(bimca<sup>Hom</sup>)<sub>2</sub>Br]**.

Co(1)-N(9')	1.910(10)	N(51')-C(52')	1.370(16)	C(3)-C(10A)	1.520(9)
Co(1)-N(59)	1.939(10)	N(51')-C(55')	1.394(14)	C(4)-C(4A)	1.431(18)
Co(1)-C(2')	1.976(15)	N(51')-C(51)	1.416(16)	C(4)-H(4)	0.9500
Co(1)-C(57')	2.008(11)	N(53')-C(54')	1.364(17)	C(4')-C(5')	1.314(19)
Co(1)-C(7')	2.013(14)	N(53')-C(52')	1.380(14)	C(4')-H(4')	0.9500
Co(1)-C(52')	2.017(12)	N(53')-C(62A)	1.467(9)	C(5)-C(6)	1.34(2)
N(1')-C(2')	1.365(15)	N(53')-C(62)	1.467(9)	C(5)-C(5A)	1.459(19)
N(1')-C(5')	1.423(17)	N(56')-C(58)	1.406(15)	C(5)-H(5)	0.9500
N(1')-C(1)	1.450(9)	N(56')-C(57')	1.412(15)	C(5')-H(5')	0.9500
N(3')-C(2')	1.361(16)	N(56')-C(60')	1.413(16)	C(4A)-C(5A)	1.478(17)
N(3')-C(4')	1.411(18)	N(58')-C(57')	1.350(15)	C(6)-C(7)	1.41(2)
N(3')-C(12)	1.436(16)	N(58')-C(59')	1.416(14)	C(6)-C(10B)	1.523(10)
N(6')-C(10')	1.360(17)	N(58')-C(66)	1.466(9)	C(5A)-C(8A)	1.411(18)
N(6')-C(8)	1.378(16)	N(59)-C(51A)	1.334(15)	C(7)-C(8)	1.380(18)
N(6')-C(7')	1.384(15)	N(59)-C(58A)	1.384(14)	C(7)-H(7)	0.9500
N(8')-C(9')	1.338(15)	C(1)-C(2)	1.328(16)	C(8)-C(8A)	1.400(17)
N(8')-C(7')	1.361(15)	C(1)-C(1A)	1.435(17)	C(9')-C(10')	1.312(18)
N(8')-C(16A)	1.475(9)	C(2)-C(3)	1.377(18)	C(9')-H(9')	0.9500
N(8')-C(16)	1.475(9)	C(2)-H(2)	0.9500	C(10')-H(10')	0.9500
N(9')-C(1A)	1.343(15)	C(1A)-C(4A)	1.399(17)	C(11C)-C(10A)	1.541(10)
N(9')-C(8A)	1.357(15)	C(3)-C(4)	1.417(19)	C(11C)-H(11A)	0.9800

C(11C)-H(11B)	0.9800	C(54)-H(54)	0.9500	C(65A)-H(65D)	0.9500
C(11C)-H(11C)	0.9800	C(54')-C(55')	1.31(2)	C(66)-C(67)	1.521(10)
C(10A)-C(11A)	1.525(10)	C(54')-H(54')	0.9500	C(66)-H(66A)	0.9900
C(10A)-C(11B)	1.533(10)	C(55)-C(56)	1.363(17)	C(66)-H(66B)	0.9900
C(10B)-C(11F)	1.514(10)	C(55)-C(55A)	1.433(17)	C(67)-C(68)	1.4900(11)
C(10B)-C(11E)	1.523(10)	C(55)-H(55)	0.9500	C(67)-H(67A)	0.9900
C(10B)-C(11D)	1.539(10)	C(55')-H(55')	0.9500	C(67)-H(67B)	0.9900
C(12)-C(13)	1.516(9)	C(54A)-C(55A)	1.427(17)	C(68)-C(69)	1.3000(11)
C(12)-H(12A)	0.9900	C(56)-C(57)	1.384(17)	C(68)-H(68)	0.9500
C(12)-H(12B)	0.9900	C(56)-C(60B)	1.543(9)	C(69)-H(69A)	0.9500
C(11A)-H(11D)	0.9800	C(55A)-C(58A)	1.398(16)	C(69)-H(69B)	0.9500
C(11A)-H(11E)	0.9800	C(57)-C(58)	1.417(16)		
C(11A)-H(11F)	0.9800	C(57)-H(57)	0.9500	N(9')-Co(1)-N(59)	178.8(5)
C(11B)-H(11G)	0.9800	C(58)-C(58A)	1.395(16)	N(9')-Co(1)-C(2')	89.2(5)
C(11B)-H(11H)	0.9800	C(59')-C(60')	1.313(18)	N(59)-Co(1)-C(2')	89.7(5)
C(11B)-H(11I)	0.9800	C(59')-H(59')	0.9500	N(9')-Co(1)-C(57')	90.2(5)
C(11D)-H(11J)	0.9800	C(60')-H(60')	0.9500	N(59)-Co(1)-C(57')	89.4(5)
C(11D)-H(11K)	0.9800	C(60A)-C(61B)	1.528(10)	C(2')-Co(1)-C(57')	88.9(5)
C(11D)-H(11L)	0.9800	C(60A)-C(61A)	1.532(9)	N(9')-Co(1)-C(7')	88.0(5)
C(11E)-H(11M)	0.9800	C(60A)-C(61C)	1.545(10)	N(59)-Co(1)-C(7')	93.2(5)
C(11E)-H(11N)	0.9800	C(60B)-C(61F)	1.523(9)	C(2')-Co(1)-C(7')	176.4(5)
C(11E)-H(11O)	0.9800	C(60B)-C(61D)	1.527(9)	C(57')-Co(1)-C(7')	93.3(5)
C(11F)-H(11P)	0.9800	C(60B)-C(61E)	1.529(9)	N(9')-Co(1)-C(52')	92.8(5)
C(11F)-H(11Q)	0.9800	C(61A)-H(61A)	0.9800	N(59)-Co(1)-C(52')	87.7(5)
C(11F)-H(11R)	0.9800	C(61A)-H(61B)	0.9800	C(2')-Co(1)-C(52')	92.9(5)
C(13)-C(14)	1.4900(11)	C(61A)-H(61C)	0.9800	C(57')-Co(1)-C(52')	176.5(5)
C(13)-H(13A)	0.9900	C(61B)-H(61D)	0.9800	C(7')-Co(1)-C(52')	85.0(5)
C(13)-H(13B)	0.9900	C(61B)-H(61E)	0.9800	C(2')-N(1')-C(5')	110.2(11)
C(14)-C(15)	1.2998(11)	C(61B)-H(61F)	0.9800	C(2')-N(1')-C(1)	127.6(11)
C(14)-H(14A)	0.9500	C(61C)-H(61G)	0.9800	C(5')-N(1')-C(1)	120.2(11)
C(15)-H(15A)	0.9500	C(61C)-H(61H)	0.9800	C(2')-N(3')-C(4')	111.7(13)
C(15)-H(15B)	0.9500	C(61C)-H(61I)	0.9800	C(2')-N(3')-C(12)	125.6(12)
C(16)-C(17)	1.526(10)	C(61D)-H(61J)	0.9800	C(4')-N(3')-C(12)	122.7(13)
C(16)-H(16A)	0.9900	C(61D)-H(61K)	0.9800	C(10')-N(6')-C(8)	124.5(12)
C(16)-H(16B)	0.9900	C(61D)-H(61L)	0.9800	C(10')-N(6')-C(7')	107.6(12)
C(17)-C(18)	1.4900(11)	C(61E)-H(61M)	0.9800	C(8)-N(6')-C(7')	125.2(11)
C(17)-H(17A)	0.9900	C(61E)-H(61N)	0.9800	C(9')-N(8')-C(7')	111.4(11)
C(17)-H(17B)	0.9900	C(61E)-H(61O)	0.9800	C(9')-N(8')-C(16A)	120.2(11)
C(18)-C(19)	1.3000(11)	C(61F)-H(61P)	0.9800	C(7')-N(8')-C(16A)	126.7(11)
C(18)-H(18A)	0.9500	C(61F)-H(61Q)	0.9800	C(9')-N(8')-C(16)	120.2(11)
C(19)-H(19A)	0.9500	C(61F)-H(61R)	0.9800	C(7')-N(8')-C(16)	126.7(11)
C(19)-H(19B)	0.9500	C(62)-C(63)	1.525(10)	C(1A)-N(9')-C(8A)	106.2(11)
C(16A)-C(17A)	1.51(3)	C(62)-H(62A)	0.9900	C(1A)-N(9')-Co(1)	126.5(9)
C(16A)-H(16C)	0.9900	C(62)-H(62B)	0.9900	C(8A)-N(9')-Co(1)	127.3(9)
C(16A)-H(16D)	0.9900	C(63)-C(64)	1.4900(11)	C(52')-N(51')-C(55')	108.2(11)
C(17A)-C(18A)	1.4900(11)	C(63)-H(63A)	0.9900	C(52')-N(51')-C(51)	126.5(10)
C(17A)-H(17C)	0.9900	C(63)-H(63B)	0.9900	C(55')-N(51')-C(51)	123.0(12)
C(17A)-H(17D)	0.9900	C(64)-C(65)	1.3001(11)	C(54')-N(53')-C(52')	109.9(11)
C(18A)-C(19A)	1.3000(11)	C(64)-H(64)	0.9500	C(54')-N(53')-C(62A)	119.9(10)
C(18A)-H(18C)	0.9500	C(65)-H(65A)	0.9500	C(52')-N(53')-C(62A)	129.7(10)
C(19A)-H(19D)	0.9500	C(65)-H(65B)	0.9500	C(54')-N(53')-C(62)	119.9(10)
C(19A)-H(19E)	0.9500	C(62A)-C(63A)	1.34(3)	C(52')-N(53')-C(62)	129.7(10)
C(51)-C(52)	1.354(18)	C(62A)-H(62C)	0.9900	C(58)-N(56')-C(57')	125.5(10)
C(51)-C(51A)	1.461(17)	C(62A)-H(62D)	0.9900	C(58)-N(56')-C(60')	122.8(10)
C(52)-C(53)	1.396(18)	C(63A)-C(64A)	1.4901(11)	C(57')-N(56')-C(60')	109.7(11)
C(52)-H(52)	0.9500	C(63A)-H(63C)	0.9900	C(57')-N(58')-C(59')	110.8(10)
C(51A)-C(54A)	1.376(17)	C(63A)-H(63D)	0.9900	C(57')-N(58')-C(66)	126.2(10)
C(53)-C(54)	1.396(16)	C(64A)-C(65A)	1.3001(11)	C(59')-N(58')-C(66)	122.0(12)
C(53)-C(60A)	1.535(9)	C(64A)-H(64A)	0.9500	C(51A)-N(59)-C(58A)	104.9(10)
C(54)-C(54A)	1.366(17)	C(65A)-H(65C)	0.9500	C(51A)-N(59)-Co(1)	129.6(8)

C(58A)-N(59)-Co(1)	125.5(8)	H(11B)-C(11C)-H(11C)	109.5	H(15A)-C(15)-H(15B)	120.0
C(2)-C(1)-C(1A)	119.8(11)	C(3)-C(10A)-C(11A)	112.8(13)	N(8')-C(16)-C(17)	119.1(17)
C(2)-C(1)-N(1')	125.4(12)	C(3)-C(10A)-C(11B)	108.9(13)	N(8')-C(16)-H(16A)	107.5
C(1A)-C(1)-N(1')	114.4(11)	C(11A)-C(10A)-C(11B)	106.8(16)	C(17)-C(16)-H(16A)	107.5
C(1)-C(2)-C(3)	124.7(13)	C(3)-C(10A)-C(11C)	108.6(12)	N(8')-C(16)-H(16B)	107.5
C(1)-C(2)-H(2)	117.7	C(11A)-C(10A)-C(11C)	105.6(12)	C(17)-C(16)-H(16B)	107.5
C(3)-C(2)-H(2)	117.7	C(11B)-C(10A)-C(11C)	114.3(16)	H(16A)-C(16)-H(16B)	107.0
N(9')-C(1A)-C(4A)	114.0(12)	C(11F)-C(10B)-C(6)	113.2(15)	C(18)-C(17)-C(16)	121(2)
N(9')-C(1A)-C(1)	129.6(12)	C(11F)-C(10B)-C(11E)	112.5(18)	C(18)-C(17)-H(17A)	107.2
C(4A)-C(1A)-C(1)	116.4(12)	C(6)-C(10B)-C(11E)	110.5(16)	C(16)-C(17)-H(17A)	107.2
N(3')-C(2')-N(1')	103.7(12)	C(11F)-C(10B)-C(11D)	100.3(19)	C(18)-C(17)-H(17B)	107.2
N(3')-C(2')-Co(1)	132.7(10)	C(6)-C(10B)-C(11D)	119(2)	C(16)-C(17)-H(17B)	107.2
N(1')-C(2')-Co(1)	123.5(10)	C(11E)-C(10B)-C(11D)	101(2)	H(17A)-C(17)-H(17B)	106.8
C(2)-C(3)-C(4)	119.2(12)	N(3')-C(12)-C(13)	111.6(11)	C(19)-C(18)-C(17)	142(5)
C(2)-C(3)-C(10A)	121.9(13)	N(3')-C(12)-H(12A)	109.3	C(19)-C(18)-H(18A)	109.0
C(4)-C(3)-C(10A)	118.9(13)	C(13)-C(12)-H(12A)	109.3	C(17)-C(18)-H(18A)	109.0
C(3)-C(4)-C(4A)	116.2(12)	N(3')-C(12)-H(12B)	109.3	C(18)-C(19)-H(19A)	120.0
C(3)-C(4)-H(4)	121.9	C(13)-C(12)-H(12B)	109.3	C(18)-C(19)-H(19B)	120.0
C(4A)-C(4)-H(4)	121.9	H(12A)-C(12)-H(12B)	108.0	H(19A)-C(19)-H(19B)	120.0
C(5')-C(4')-N(3')	106.3(15)	C(10A)-C(11A)-H(11D)	109.5	N(8')-C(16A)-C(17A)	110.4(13)
C(5')-C(4')-H(4')	126.8	C(10A)-C(11A)-H(11E)	109.5	N(8')-C(16A)-H(16C)	109.6
N(3')-C(4')-H(4')	126.8	H(11D)-C(11A)-H(11E)	109.5	C(17A)-C(16A)-H(16C)	109.6
C(6)-C(5)-C(5A)	117.2(16)	C(10A)-C(11A)-H(11F)	109.5	N(8')-C(16A)-H(16D)	109.6
C(6)-C(5)-H(5)	121.4	H(11D)-C(11A)-H(11F)	109.5	C(17A)-C(16A)-H(16D)	109.6
C(5A)-C(5)-H(5)	121.4	H(11E)-C(11A)-H(11F)	109.5	H(16C)-C(16A)-H(16D)	108.1
C(4')-C(5')-N(1')	107.7(14)	C(10A)-C(11B)-H(11G)	109.5	C(18A)-C(17A)-C(16A)	110.1(16)
C(4')-C(5')-H(5')	126.2	C(10A)-C(11B)-H(11H)	109.5	C(18A)-C(17A)-H(17C)	109.6
N(1')-C(5')-H(5')	126.2	H(11G)-C(11B)-H(11H)	109.5	C(16A)-C(17A)-H(17C)	109.6
C(1A)-C(4A)-C(4)	123.3(13)	C(10A)-C(11B)-H(11I)	109.5	C(18A)-C(17A)-H(17D)	109.6
C(1A)-C(4A)-C(5A)	102.9(12)	H(11G)-C(11B)-H(11I)	109.5	C(16A)-C(17A)-H(17D)	109.6
C(4)-C(4A)-C(5A)	133.6(12)	H(11H)-C(11B)-H(11I)	109.5	H(17C)-C(17A)-H(17D)	108.2
C(5)-C(6)-C(7)	121.4(14)	C(10B)-C(11D)-H(11J)	109.5	C(19A)-C(18A)-C(17A)	124(2)
C(5)-C(6)-C(10B)	124.3(17)	C(10B)-C(11D)-H(11K)	109.5	C(19A)-C(18A)-H(18C)	117.8
C(7)-C(6)-C(10B)	113.5(17)	H(11J)-C(11D)-H(11K)	109.5	C(17A)-C(18A)-H(18C)	117.8
C(8A)-C(5A)-C(5)	120.6(13)	C(10B)-C(11D)-H(11L)	109.5	C(18A)-C(19A)-H(19D)	120.0
C(8A)-C(5A)-C(4A)	105.1(11)	H(11J)-C(11D)-H(11L)	109.5	C(18A)-C(19A)-H(19E)	120.0
C(5)-C(5A)-C(4A)	134.3(14)	H(11K)-C(11D)-H(11L)	109.5	H(19D)-C(19A)-H(19E)	120.0
C(8)-C(7)-C(6)	122.8(15)	C(10B)-C(11E)-H(11M)	109.5	C(52)-C(51)-N(51')	125.5(12)
C(8)-C(7)-H(7)	118.6	C(10B)-C(11E)-H(11N)	109.5	C(52)-C(51)-C(51A)	116.1(13)
C(6)-C(7)-H(7)	118.6	H(11M)-C(11E)-H(11N)	109.5	N(51')-C(51)-C(51A)	118.0(12)
N(8')-C(7')-N(8')	104.1(11)	C(10B)-C(11E)-H(11O)	109.5	C(51)-C(52)-C(53)	125.2(13)
N(8')-C(7')-Co(1)	130.7(10)	H(11M)-C(11E)-H(11O)	109.5	C(51)-C(52)-H(52)	117.4
N(6')-C(7')-Co(1)	123.1(10)	H(11N)-C(11E)-H(11O)	109.5	C(53)-C(52)-H(52)	117.4
N(6')-C(8)-C(7)	122.9(13)	C(10B)-C(11F)-H(11P)	109.5	N(51')-C(52')-N(53')	105.0(10)
N(6')-C(8)-C(8A)	119.3(12)	C(10B)-C(11F)-H(11Q)	109.5	N(51')-C(52')-Co(1)	124.4(8)
C(7)-C(8)-C(8A)	117.5(14)	H(11P)-C(11F)-H(11Q)	109.5	N(53')-C(52')-Co(1)	129.8(10)
C(10')-C(9')-N(8')	106.8(14)	C(10B)-C(11F)-H(11R)	109.5	N(59)-C(51A)-C(54A)	114.9(11)
C(10')-C(9')-H(9')	126.6	H(11P)-C(11F)-H(11R)	109.5	N(59)-C(51A)-C(51)	126.5(12)
N(8')-C(9')-H(9')	126.6	H(11Q)-C(11F)-H(11R)	109.5	C(54A)-C(51A)-C(51)	118.2(12)
N(9')-C(8A)-C(8)	128.2(13)	C(14)-C(13)-C(12)	121.6(14)	C(54)-C(53)-C(52)	117.2(11)
N(9')-C(8A)-C(5A)	111.5(12)	C(14)-C(13)-H(13A)	106.9	C(54)-C(53)-C(60A)	122.7(12)
C(8)-C(8A)-C(5A)	120.0(12)	C(12)-C(13)-H(13A)	106.9	C(52)-C(53)-C(60A)	119.5(12)
C(9')-C(10')-N(6')	110.0(14)	C(14)-C(13)-H(13B)	106.9	C(54A)-C(54)-C(53)	119.5(12)
C(9')-C(10')-H(10')	125.0	C(12)-C(13)-H(13B)	106.9	C(54A)-C(54)-H(54)	120.2
N(6')-C(10')-H(10')	125.0	H(13A)-C(13)-H(13B)	106.7	C(53)-C(54)-H(54)	120.2
C(10A)-C(11C)-H(11A)	109.5	C(15)-C(14)-C(13)	120(2)	C(55')-C(54')-N(53')	108.0(12)
C(10A)-C(11C)-H(11B)	109.5	C(15)-C(14)-H(14A)	119.9	C(55')-C(54')-H(54')	126.0
H(11A)-C(11C)-H(11B)	109.5	C(13)-C(14)-H(14A)	119.9	N(53')-C(54')-H(54')	126.0
C(10A)-C(11C)-H(11C)	109.5	C(14)-C(15)-H(15A)	120.0	C(56)-C(55)-C(55A)	122.0(13)
H(11A)-C(11C)-H(11C)	109.5	C(14)-C(15)-H(15B)	120.0	C(56)-C(55)-H(55)	119.0



C(55A)-C(55)-H(55)	119.0	H(61A)-C(61A)-H(61B)	109.5	H(63A)-C(63)-H(63B)	107.6
C(54)-C(55)-N(51')	108.8(14)	C(60A)-C(61A)-H(61C)	109.5	C(65)-C(64)-C(63)	120(4)
C(54)-C(55)-H(55')	125.6	H(81A)-C(61A)-H(61C)	109.5	C(65)-C(64)-H(64)	119.9
N(51')-C(55)-H(55')	125.6	H(61B)-C(61A)-H(61C)	109.5	C(63)-C(64)-H(64)	119.9
C(54)-C(54A)-C(51A)	123.2(12)	C(60A)-C(61B)-H(61D)	109.5	C(64)-C(65)-H(65A)	120.0
C(54)-C(54A)-C(55A)	133.4(12)	C(60A)-C(61B)-H(61E)	109.5	C(64)-C(65)-H(65B)	120.0
C(51A)-C(54A)-C(55A)	103.4(11)	H(61D)-C(61B)-H(61E)	109.5	H(65A)-C(65)-H(65B)	120.0
C(55)-C(56)-C(57)	117.7(10)	C(60A)-C(61B)-H(61F)	109.5	C(63A)-C(62A)-N(53')	115.7(13)
C(55)-C(56)-C(60B)	123.9(12)	H(61D)-C(61B)-H(61F)	109.5	C(63A)-C(62A)-H(62C)	108.4
C(57)-C(56)-C(60B)	118.4(11)	H(61E)-C(61B)-H(61F)	109.5	N(53')-C(62A)-H(62C)	108.4
C(58A)-C(55A)-C(54A)	107.0(10)	C(60A)-C(61C)-H(61G)	109.5	C(63A)-C(62A)-H(62D)	108.4
C(58A)-C(55A)-C(55)	117.9(11)	C(60A)-C(61C)-H(61H)	109.5	N(53')-C(62A)-H(62D)	108.4
C(54A)-C(55A)-C(55)	135.1(12)	H(61G)-C(61C)-H(61H)	109.5	H(62C)-C(62A)-H(62D)	107.4
C(56)-C(57)-C(58)	123.6(11)	C(60A)-C(61C)-H(61I)	109.5	C(62A)-C(63A)-C(64A)	111(2)
C(56)-C(57)-H(57)	118.2	H(61G)-C(61C)-H(61I)	109.5	C(62A)-C(63A)-H(63C)	109.4
C(58)-C(57)-H(57)	118.2	H(61H)-C(61C)-H(61I)	109.5	C(64A)-C(63A)-H(63C)	109.4
N(58')-C(57)-N(56')	103.9(9)	C(60B)-C(61D)-H(61J)	109.5	C(62A)-C(63A)-H(63D)	109.4
N(58')-C(57)-Co(1)	131.8(9)	C(60B)-C(61D)-H(61K)	109.5	C(64A)-C(63A)-H(63D)	109.4
N(56')-C(57)-Co(1)	123.0(9)	H(61J)-C(61D)-H(61K)	109.5	H(63C)-C(63A)-H(63D)	108.0
C(58A)-C(58)-N(56')	119.6(10)	C(60B)-C(61D)-H(61L)	109.5	C(65A)-C(64A)-C(63A)	125.1(17)
C(58A)-C(58)-C(57)	116.8(12)	H(61J)-C(61D)-H(61L)	109.5	C(65A)-C(64A)-H(64A)	117.4
N(56')-C(58)-C(57)	123.4(11)	H(61K)-C(61D)-H(61L)	109.5	C(63A)-C(64A)-H(64A)	117.4
N(59)-C(58A)-C(58)	128.8(11)	C(60B)-C(61E)-H(61M)	109.5	C(64A)-C(65A)-H(65C)	120.0
N(59)-C(58A)-C(55A)	109.7(10)	C(60B)-C(61E)-H(61N)	109.5	C(64A)-C(65A)-H(65D)	120.0
C(58)-C(58A)-C(55A)	121.4(11)	H(61M)-C(61E)-H(61N)	109.5	H(65C)-C(65A)-H(65D)	120.0
C(60')-C(59')-N(58')	108.4(12)	C(60B)-C(61E)-H(61O)	109.5	N(58')-C(66)-C(67)	117.6(15)
C(60')-C(59')-H(59')	125.8	H(61M)-C(61E)-H(61O)	109.5	N(58')-C(66)-H(66A)	107.9
N(58')-C(59')-H(59')	125.8	H(61N)-C(61E)-H(61O)	109.5	C(67)-C(66)-H(66A)	107.9
C(59')-C(60')-N(56')	107.1(11)	C(60B)-C(61F)-H(61P)	109.5	N(58')-C(66)-H(66B)	107.9
C(59')-C(60')-H(60')	126.4	C(60B)-C(61F)-H(61Q)	109.5	C(67)-C(66)-H(66B)	107.9
N(56')-C(60')-H(60')	126.4	H(61P)-C(61F)-H(61Q)	109.5	H(66A)-C(66)-H(66B)	107.2
C(61B)-C(60A)-C(61A)	110.6(14)	C(60B)-C(61F)-H(61R)	109.5	C(68)-C(67)-C(66)	111.9(14)
C(61B)-C(60A)-C(53)	109.8(11)	H(61P)-C(61F)-H(61R)	109.5	C(68)-C(67)-H(67A)	109.2
C(61A)-C(60A)-C(53)	112.3(11)	H(61Q)-C(61F)-H(61R)	109.5	C(66)-C(67)-H(67A)	109.2
C(61B)-C(60A)-C(61C)	107.0(15)	N(53')-C(62)-C(63)	113.1(12)	C(68)-C(67)-H(67B)	109.2
C(61A)-C(60A)-C(61C)	108.8(13)	N(53')-C(62)-H(62A)	109.0	C(66)-C(67)-H(67B)	109.2
C(53)-C(60A)-C(61C)	108.2(11)	C(63)-C(62)-H(62A)	109.0	H(67A)-C(67)-H(67B)	107.9
C(61F)-C(60B)-C(61D)	106.5(11)	N(53')-C(62)-H(62B)	109.0	C(69)-C(68)-C(67)	127.8(19)
C(61F)-C(60B)-C(61E)	108.8(12)	C(63)-C(62)-H(62B)	109.0	C(69)-C(68)-H(68)	116.1
C(61D)-C(60B)-C(61E)	108.7(12)	H(62A)-C(62)-H(62B)	107.8	C(67)-C(68)-H(68)	116.1
C(61F)-C(60B)-C(56)	112.7(10)	C(64)-C(63)-C(62)	114.4(18)	C(68)-C(69)-H(69A)	120.0
C(61D)-C(60B)-C(56)	108.9(10)	C(64)-C(63)-H(63A)	108.7	C(68)-C(69)-H(69B)	120.0
C(61E)-C(60B)-C(56)	111.1(10)	C(62)-C(63)-H(63A)	108.7	H(69A)-C(69)-H(69B)	120.0
C(60A)-C(61A)-H(61A)	109.5	C(64)-C(63)-H(63B)	108.7		
C(60A)-C(61A)-H(61B)	109.5	C(62)-C(63)-H(63B)	108.7		

**Table S15.** Torsion angles [°] for [Co(bimca<sup>Homop</sup>)<sub>2</sub>]Br.

C(2')-N(1')-C(1)-C(2)	-176.7(12)	Co(1)-N(9')-C(1A)-C(1)	2.7(19)
C(5')-N(1')-C(1)-C(2)	-14.7(18)	C(2)-C(1)-C(1A)-N(9')	-171.1(13)
C(2')-N(1')-C(1)-C(1A)	-5.0(17)	N(1')-C(1)-C(1A)-N(9')	16.7(18)
C(5')-N(1')-C(1)-C(1A)	157.0(11)	C(2)-C(1)-C(1A)-C(4A)	7.3(18)
C(1A)-C(1)-C(2)-C(3)	-4(2)	N(1')-C(1)-C(1A)-C(4A)	-165.0(11)
N(1')-C(1)-C(2)-C(3)	166.9(13)	C(4')-N(3')-C(2')-N(1')	6.0(12)
C(8A)-N(9')-C(1A)-C(4A)	4.0(14)	C(12)-N(3')-C(2')-N(1')	-174.8(10)
Co(1)-N(9')-C(1A)-C(4A)	-175.7(8)	C(4')-N(3')-C(2')-Co(1)	-170.0(9)
C(8A)-N(9')-C(1A)-C(1)	-177.6(12)	C(12)-N(3')-C(2')-Co(1)	9.1(17)

C(5')-N(1')-C(2')-N(3')	-3.3(12)	N(8')-C(9')-C(10')-N(6')	1.3(17)
C(1)-N(1')-C(2')-N(3')	160.1(11)	C(8)-N(6')-C(10')-C(9')	-163.8(13)
C(5')-N(1')-C(2')-Co(1)	173.2(8)	C(7')-N(6')-C(10')-C(9')	-1.6(17)
C(1)-N(1')-C(2')-Co(1)	-23.3(16)	C(2)-C(3)-C(10A)-C(11A)	-166.6(15)
C(1)-C(2)-C(3)-C(4)	0(2)	C(4)-C(3)-C(10A)-C(11A)	11(2)
C(1)-C(2)-C(3)-C(10A)	178.5(14)	C(2)-C(3)-C(10A)-C(11B)	75.1(19)
C(2)-C(3)-C(4)-C(4A)	0(2)	C(4)-C(3)-C(10A)-C(11B)	-106.8(18)
C(10A)-C(3)-C(4)-C(4A)	-177.7(13)	C(2)-C(3)-C(10A)-C(11C)	-50(2)
C(2')-N(3')-C(4')-C(5')	-6.7(15)	C(4)-C(3)-C(10A)-C(11C)	128.2(16)
C(12)-N(3')-C(4')-C(5')	174.2(11)	C(5)-C(6)-C(10B)-C(11F)	1(4)
N(3')-C(4')-C(5')-N(1')	4.2(15)	C(7)-C(6)-C(10B)-C(11F)	-169(2)
C(2')-N(1')-C(5')-C(4')	-0.7(15)	C(5)-C(6)-C(10B)-C(11E)	-126(2)
C(1)-N(1')-C(5')-C(4')	-165.5(11)	C(7)-C(6)-C(10B)-C(11E)	64(3)
N(9')-C(1A)-C(4A)-C(4)	171.9(11)	C(5)-C(6)-C(10B)-C(11D)	118(3)
C(1)-C(1A)-C(4A)-C(4)	-6.7(18)	C(7)-C(6)-C(10B)-C(11D)	-52(3)
N(9')-C(1A)-C(4A)-C(5A)	-4.6(14)	C(2')-N(3')-C(12)-C(13)	142.6(12)
C(1)-C(1A)-C(4A)-C(5A)	176.8(11)	C(4')-N(3')-C(12)-C(13)	-38.4(16)
C(3)-C(4)-C(4A)-C(1A)	3(2)	N(3')-C(12)-C(13)-C(14)	177.7(15)
C(3)-C(4)-C(4A)-C(5A)	178.3(14)	C(12)-C(13)-C(14)-C(15)	4(3)
C(5A)-C(5)-C(6)-C(7)	3(3)	C(9')-N(8')-C(16)-C(17)	36(3)
C(5A)-C(5)-C(6)-C(10B)	-167(2)	C(7')-N(8')-C(16)-C(17)	-160(2)
C(6)-C(5)-C(5A)-C(8A)	2(3)	N(8')-C(16)-C(17)-C(18)	44(5)
C(6)-C(5)-C(5A)-C(4A)	180.0(18)	C(16)-C(17)-C(18)-C(19)	-139(5)
C(1A)-C(4A)-C(5A)-C(8A)	3.3(13)	C(9')-N(8')-C(16A)-C(17A)	-55.8(17)
C(4)-C(4A)-C(5A)-C(8A)	-172.7(13)	C(7')-N(8')-C(16A)-C(17A)	107.9(15)
C(1A)-C(4A)-C(5A)-C(5)	-174.6(16)	N(8')-C(16A)-C(17A)-C(18A)	-61(2)
C(4)-C(4A)-C(5A)-C(5)	9(3)	C(16A)-C(17A)-C(18A)-C(19A)	-121(3)
C(5)-C(6)-C(7)-C(8)	-2(3)	C(52')-N(51')-C(51)-C(52)	-167.0(14)
C(10B)-C(6)-C(7)-C(8)	168.7(19)	C(55')-N(51')-C(51)-C(52)	-6(2)
C(9')-N(8')-C(7')-N(6')	-0.5(14)	C(52')-N(51')-C(51)-C(51A)	6(2)
C(16A)-N(8')-C(7')-N(6')	-165.4(12)	C(55')-N(51')-C(51)-C(51A)	166.5(14)
C(16)-N(8')-C(7')-N(6')	-165.4(12)	N(51')-C(51)-C(52)-C(53)	171.3(14)
C(9')-N(8')-C(7')-Co(1)	-164.0(10)	C(51A)-C(51)-C(52)-C(53)	-2(2)
C(16A)-N(8')-C(7')-Co(1)	31.1(18)	C(55')-N(51')-C(52')-N(53')	-2.1(15)
C(16)-N(8')-C(7')-Co(1)	31.1(18)	C(51)-N(51')-C(52')-N(53')	160.8(13)
C(10')-N(6')-C(7')-N(8')	1.3(14)	C(55')-N(51')-C(52')-Co(1)	168.9(11)
C(8)-N(6')-C(7')-N(8')	163.3(12)	C(51)-N(51')-C(52')-Co(1)	-28(2)
C(10')-N(6')-C(7')-Co(1)	166.4(10)	C(54')-N(53')-C(52')-N(51')	2.7(16)
C(8)-N(6')-C(7')-Co(1)	-31.5(18)	C(62A)-N(53')-C(52')-N(51')	-169.0(13)
C(10')-N(6')-C(8)-C(7)	-8(2)	C(62)-N(53')-C(52')-N(51')	-169.0(13)
C(7')-N(6')-C(8)-C(7)	-166.8(14)	C(54')-N(53')-C(52')-Co(1)	-167.6(11)
C(10')-N(6')-C(8)-C(8A)	165.5(13)	C(62A)-N(53')-C(52')-Co(1)	21(2)
C(7')-N(6')-C(8)-C(8A)	6(2)	C(62)-N(53')-C(52')-Co(1)	21(2)
C(6)-C(7)-C(8)-N(6')	169.3(17)	C(58A)-N(59)-C(51A)-C(54A)	-0.9(16)
C(6)-C(7)-C(8)-C(8A)	-4(3)	Co(1)-N(59)-C(51A)-C(54A)	179.3(9)
C(7')-N(8')-C(9')-C(10')	-0.4(16)	C(58A)-N(59)-C(51A)-C(51)	-173.4(14)
C(16A)-N(8')-C(9')-C(10')	165.5(12)	Co(1)-N(59)-C(51A)-C(51)	7(2)
C(16)-N(8')-C(9')-C(10')	165.5(12)	C(52)-C(51)-C(51A)-N(59)	179.5(14)
C(1A)-N(9')-C(8A)-C(8)	-175.8(12)	N(51')-C(51)-C(51A)-N(59)	6(2)
Co(1)-N(9')-C(8A)-C(8)	3.8(18)	C(52)-C(51)-C(51A)-C(54A)	7(2)
C(1A)-N(9')-C(8A)-C(5A)	-1.5(14)	N(51')-C(51)-C(51A)-C(54A)	-166.3(13)
Co(1)-N(9')-C(8A)-C(5A)	178.1(8)	C(51)-C(52)-C(53)-C(54)	-5(2)
N(6')-C(8)-C(8A)-N(9')	9(2)	C(51)-C(52)-C(53)-C(60A)	-176.2(13)
C(7)-C(8)-C(8A)-N(9')	-177.3(13)	C(52)-C(53)-C(54)-C(54A)	6(2)
N(6')-C(8)-C(8A)-C(5A)	-164.9(12)	C(60A)-C(53)-C(54)-C(54A)	177.1(13)
C(7)-C(8)-C(8A)-C(5A)	8.7(19)	C(52')-N(53')-C(54')-C(55')	-2.3(19)
C(5)-C(5A)-C(8A)-N(9')	177.0(13)	C(62A)-N(53')-C(54')-C(55')	170.3(14)
C(4A)-C(5A)-C(8A)-N(9')	-1.3(14)	C(62)-N(53')-C(54')-C(55')	170.3(14)
C(5)-C(5A)-C(8A)-C(8)	-8.1(19)	N(53')-C(54')-C(55')-N(51')	1(2)
C(4A)-C(5A)-C(8A)-C(8)	173.6(11)	C(52')-N(51')-C(55')-C(54')	0.8(19)

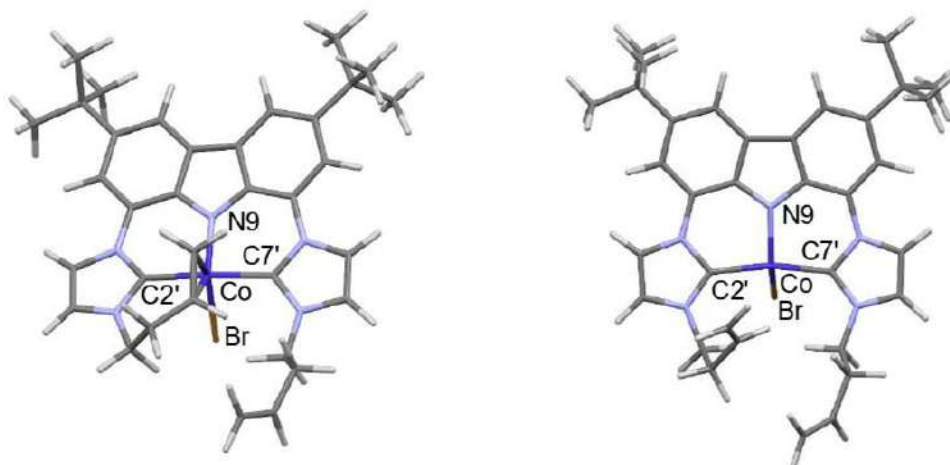
C(51)-N(51)-C(55)-C(54)	-162.9(15)	C(57)-C(58)-C(58A)-N(59)	-175.2(12)
C(53)-C(54)-C(54A)-C(51A)	-1(2)	N(56)-C(58)-C(58A)-C(55A)	-166.2(12)
C(53)-C(54)-C(54A)-C(55A)	-178.3(14)	C(57)-C(58)-C(58A)-C(55A)	8(2)
N(59)-C(51A)-C(54A)-C(54)	-179.4(13)	C(54A)-C(55A)-C(58A)-N(59)	-3.5(15)
C(51)-C(51A)-C(54A)-C(54)	-6(2)	C(55)-C(55A)-C(58A)-N(59)	174.4(12)
N(59)-C(51A)-C(54A)-C(55A)	-1.1(16)	C(54A)-C(55A)-C(58A)-C(58)	173.5(12)
C(51)-C(51A)-C(54A)-C(55A)	172.0(13)	C(55)-C(55A)-C(58A)-C(58)	-9(2)
C(55A)-C(55)-C(56)-C(57)	4(2)	C(57)-N(58)-C(59)-C(60)	2.0(18)
C(55A)-C(55)-C(56)-C(60B)	-176.7(13)	C(66)-N(58)-C(59)-C(60)	171.6(14)
C(54)-C(54A)-C(55A)-C(58A)	-179.3(15)	N(58)-C(59)-C(60)-N(56)	-1.1(17)
C(51A)-C(54A)-C(55A)-C(58A)	2.7(15)	C(58)-N(56)-C(60)-C(59)	-164.8(13)
C(54)-C(54A)-C(55A)-C(55)	3(3)	C(57)-N(56)-C(60)-C(59)	0.0(17)
C(51A)-C(54A)-C(55A)-C(55)	-174.6(16)	C(54)-C(53)-C(60A)-C(61B)	-103.0(17)
C(56)-C(55)-C(55A)-C(58A)	2(2)	C(52)-C(53)-C(60A)-C(61B)	67.6(18)
C(56)-C(55)-C(55A)-C(54A)	179.3(15)	C(54)-C(53)-C(60A)-C(61A)	20.5(19)
C(55)-C(56)-C(57)-C(58)	-4(2)	C(52)-C(53)-C(60A)-C(61A)	-169.0(14)
C(60B)-C(56)-C(57)-C(58)	176.6(12)	C(54)-C(53)-C(60A)-C(61C)	140.5(14)
C(59)-N(58)-C(57)-N(56)	-1.9(15)	C(52)-C(53)-C(60A)-C(61C)	-48.9(18)
C(66)-N(58)-C(57)-N(56)	-170.9(12)	C(55)-C(56)-C(60B)-C(61F)	6(2)
C(59)-N(58)-C(57)-Co(1)	-168.5(11)	C(57)-C(56)-C(60B)-C(61F)	-174.2(13)
C(66)-N(58)-C(57)-Co(1)	22(2)	C(55)-C(56)-C(60B)-C(61D)	-111.4(16)
C(58)-N(56)-C(57)-N(58)	165.5(12)	C(57)-C(56)-C(60B)-C(61D)	67.9(16)
C(60)-N(56)-C(57)-N(58)	1.2(15)	C(55)-C(56)-C(60B)-C(61E)	128.9(15)
C(58)-N(56)-C(57)-Co(1)	-26.4(18)	C(57)-C(56)-C(60B)-C(61E)	-51.8(17)
C(60)-N(56)-C(57)-Co(1)	169.4(10)	C(54)-N(53)-C(62)-C(63)	57(2)
C(57)-N(56)-C(58)-C(58A)	1(2)	C(52)-N(53)-C(62)-C(63)	-131.8(18)
C(60)-N(56)-C(58)-C(58A)	163.8(13)	N(53)-C(62)-C(63)-C(64)	-173.1(19)
C(57)-N(56)-C(58)-C(57)	-172.8(13)	C(62)-C(63)-C(64)-C(65)	127(4)
C(60)-N(56)-C(58)-C(57)	-11(2)	C(54)-N(53)-C(62A)-C(63A)	-66(2)
C(56)-C(57)-C(58)-C(58A)	-2(2)	C(52)-N(53)-C(62A)-C(63A)	105(2)
C(56)-C(57)-C(58)-N(56)	172.5(13)	N(53)-C(62A)-C(63A)-C(64A)	172(2)
C(51A)-N(59)-C(58A)-C(58)	-173.9(14)	C(62A)-C(63A)-C(64A)-C(65A)	29(6)
Co(1)-N(59)-C(58A)-C(58)	5.8(19)	C(57)-N(58)-C(66)-C(67)	128(2)
C(51A)-N(59)-C(58A)-C(55A)	2.7(14)	C(59)-N(58)-C(66)-C(67)	-40(2)
Co(1)-N(59)-C(58A)-C(55A)	-177.5(9)	N(58)-C(66)-C(67)-C(68)	155(2)
N(56)-C(58)-C(58A)-N(59)	10(2)	C(66)-C(67)-C(68)-C(69)	97(4)

---

### 3. DFT calculations

**General information.** Calculations were performed based on density functional theory at the BP86/def2-SVP and/or BP86/def2-TZVP<sup>[4-10]</sup> level implemented in Turbomole<sup>[11-19]</sup>. The RI-approximation<sup>[20-25]</sup> was used all over and the Grimme dispersion correction D3-BJ<sup>[26-27]</sup> where indicated. Several structures were optimized differing in the conformation of the rings formed by the coordination of the double bonds. The mononuclear complexes **1**, **2**, **3**, **4** and **7-mono**, **8-mono**, and **9-mono** were verified to be minimum structures at the BP86/def2-SVP level by calculating the Hessian matrix and ensuring that it has no imaginary frequency. The dimers **7**, **8** and **9** (Co) were too large for this purpose. The Cartesian coordinates are provided as a separate xyz-file.

#### 3.1. Geometry optimized structures of **1**.

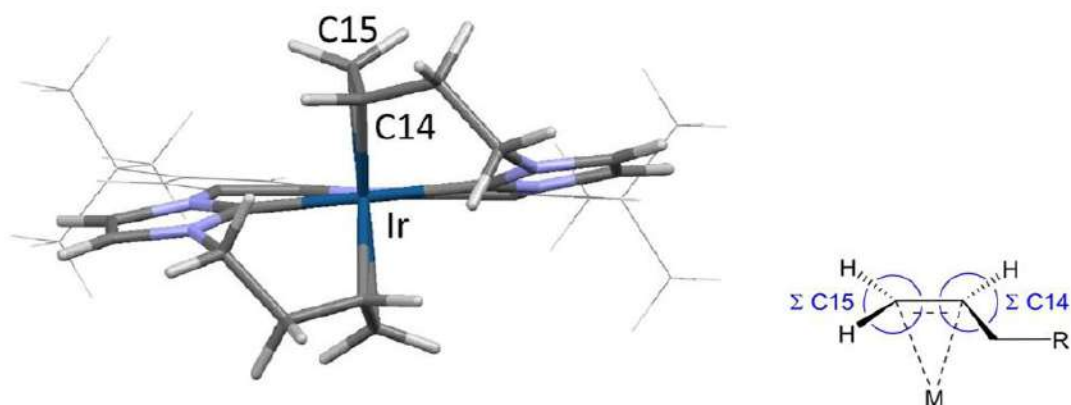


**Figure S25.** Geometry optimized structures of **1** in the low-spin ( $S = 1/2$ ) (left) and high-spin ( $S = 3/2$ ) state (right).

**Table S16.** Characteristic data from the geometry optimized complexes **1** in the low-spin and in the high-spin state and comparison of the bond lengths with the experimental values from X-ray diffraction analysis.

Complex	SCF energy / H	$\Delta(\text{HOMO-LUMO})$ (eV)	Co-Br (Å)	Co-C2' (Å)	Co-C7' (Å)	Co-N9 (Å)
<b>1-LS</b>	-5551.8822133961	0.981	2.485	1.909	1.950	1.918
<b>1-HS</b>	-5551.842741142	0.555	2.374	1.986	1.990	1.907
<b>1 (X-ray)</b>	--	--	2.515(1)	1.917(4)	1.978(4)	1.915(3)

## 3.2. Geometry optimized structures 2-4.



**Figure S26.** Exemplary representation of the geometry optimized structure of compound **4** and the angles described in Tabel S1.

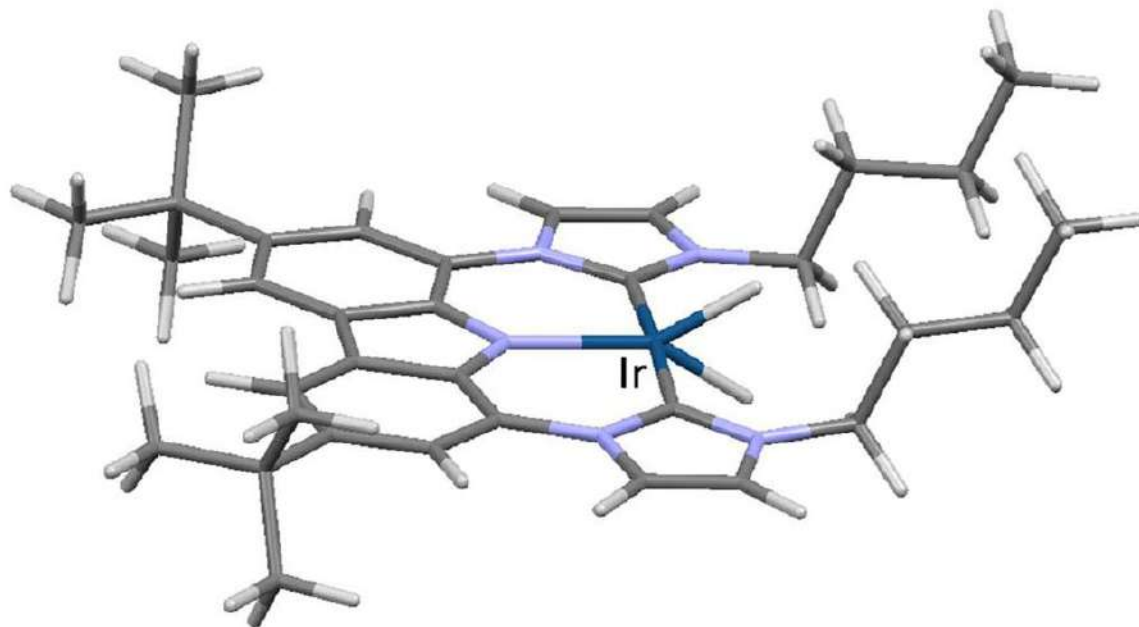
**Table S17.** Characteristic data from the geometry optimized complexes **2-4**.

Complex	SCF energy / H	$\Delta(\text{HOMO-LUMO})$ (eV)	C14=C15 (Å)	M-C15 (Å)	M-C14 (Å)	$\Sigma$ (angle C15)	$\Sigma$ (angle C15)
<b>2</b>	-2977.395912188	1.996	1.413	2.049	2.098	354.87	351.52
<b>3</b>	-1705.081043977	2.083	1.424	2.159	2.193	353.87	351.13
<b>4</b>	-1698.922919483	2.091	1.446	2.156	2.170	351.40	348.56

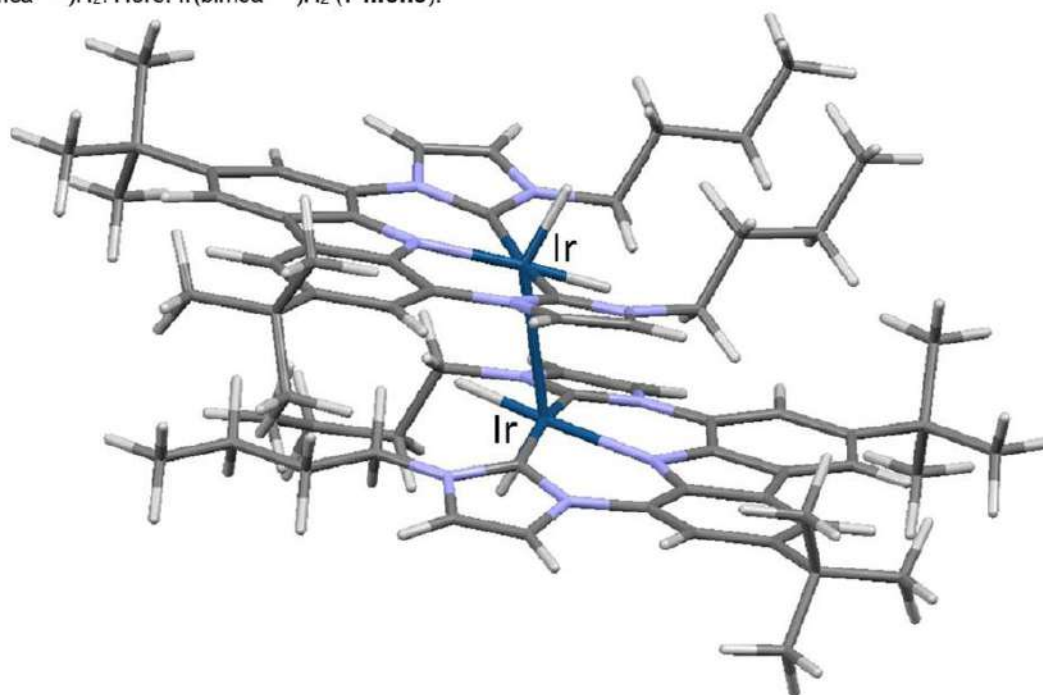
All optimizations with BP86/def2-TZVP and D3-BJ. The distances and angles are given as the mean value of the two olefin moieties.



3.3. Geometry optimized structures of the hydrogenated complexes **7** and **8**.



**Figure S27.** Exemplary representation of the geometry optimized structures of monomeric complexes  $M(\text{bimca}^{n\text{-Bu}})\text{H}_2$ . Here:  $\text{Ir}(\text{bimca}^{n\text{-Bu}})\text{H}_2$  (**7-mono**).



**Figure S28.** Exemplary representation of the geometry optimized structures of the dimeric complexes  $[\text{M}(\text{bimca}^{n\text{-Bu}})\text{H}_2]_2$ . Here:  $[\text{Ir}(\text{bimca}^{n\text{-Bu}})\text{H}_2]_2$  (**7**).

**Table S18.** Fixed geometry optimization to obtain the M-H distances for the X-ray structure refinement of **7** and **8**.

Complex	SCF energy / H	M-H distances
<b>7-fixed</b>	-3400.603229	1.579 / 1.577 (H <sub>ax</sub> ) 1.628 / 1.627 (H <sub>eq</sub> )
<b>8-fixed</b>	-3412.862656	1.541 / 1.538 (H <sub>ax</sub> ) 1.583 / 1.580 (H <sub>eq</sub> )

All coordinates except for the hydrido ligands were taken from the X-ray structure analysis and fixed, the hydrido ligands were added and then refined (BP86/def2-SVP, D3-BJ).

**Table S19.** Geometry optimization of **7** and **8** and their monomeric forms **7-mono** and **8-mono** with (DFT-D3) and without (DFT) taking into account intramolecular London dispersion.

Complex	SCF energy / H	$\Delta$ SCF (dimer – 2·monomer) / H	$\Delta$ SCF (dimer – 2·monomer) / kJ·mol <sup>-1</sup>
<b>7-mono</b>	-1700.639572	+0.001747	+4.6
<b>7</b>	-3401.277397		
<b>7-mono (D3)</b>	-1700.837913	-0.101942	-267.6
<b>7 (D3)</b>	-3401.777768		
<b>8-mono</b>	-1706.784014	-0.00093	-2.4
<b>8</b>	-3413.568958		
<b>8-mono (D3)</b>	-1706.979910	-0.098588	-258.8
<b>8 (D3)</b>	-3414.058408		

#### 4. References

- 1 (a) G. M. Sheldrick, SADABS 2012/1; University of Göttingen, Göttingen, Germany, 2012. (b) G. M. Sheldrick, *Acta Cryst.* **2008**, *A64*, 112–122. (c) G. M. Sheldrick, *Acta Cryst.* **2015**, *C71*, 3–8. (d) C. B. Hübschle, G. M. Sheldrick, B. Dittrich, *J. Appl. Cryst.* **2011**, *44*, 1281–1284. (e) G. M. Sheldrick, *Acta Cryst.* **2015**, *A71*, 3–8.
- 2 A. L. Spek, *Acta Cryst.* **2015**, *C71*, 9–18.
- 3 V. Dyadkin, P. Pattison, V. Dmitriev, D. Chernyshov, *J. Synchrotron Rad.* **2016**, *23*, 825.
- 4 Rigaku (2014). *Rigaku Oxford Diffraction, CrysAlisPro Software System*. Version 1.171.37.34. <http://www.rigaku.com/en>.
- 5 A. Becke, *Phys. Rev. A*, **1988**, *38*, 3098.
- 6 J. P. Perdew, *Phys. Rev. B*, **1986**, *33*, 8822.
- 7 A. Schäfer, H. Horn, R. Ahlrichs, *J. Chem. Phys.*, **1992**, *97*, 2571.
- 8 A. Schäfer, C. Huber, R. Ahlrichs, *J. Chem. Phys.*, **1994**, *100*, 5829.
- 9 F. Weigend, R. Ahlrichs, *Phys. Chem. Chem. Phys.*, **2005**, *7*, 3297.
- 10 F. Weigend, *Phys. Chem. Chem. Phys.*, **2006**, *8*, 1057.
- 11 TURBOMOLE V6.3.1 2011, a development of University of Karlsruhe and Forschungszentrum Karlsruhe GmbH, 1989–2007, TURBOMOLE GmbH, since 2007; available from <http://www.turbomole.com>.
- 12 O. Treutler, R. Ahlrichs, *J. Chem. Phys.*, **1995**, *102*, 346.
- 13 M. von Arnim, R. Ahlrichs, *J. Comp. Chem.*, **1998**, *19*, 1746.
- 14 C. van Wüllen, *J. Comp. Chem.*, **2011**, *32*, 1195.
- 15 P. Deglmann, F. Furche, R. Ahlrichs, *Chem. Phys. Lett.*, **2002**, *362*, 511.
- 16 P. Deglmann, F. Furche, *J. Chem. Phys.*, **2002**, *117*, 9535.
- 17 R. Ahlrichs, M. Bär, M. Häser, H. Horn, C. Kölmel, *Chem. Phys. Lett.*, **1989**, *162*, 165.
- 18 M. K. Armbruster, F. Weigend, C. van Wüllen, W. Klopper, *Phys. Chem. Chem. Phys.*, **2008**, *10*, 1748.
- 19 D. Peng, N. Middendorf, F. Weigend, M. Reiher, *J. Chem. Phys.*, **2013**, *138*, 184105.
- 20 K. Eichkorn, O. Treutler, H. Öhm, M. Häser, R. Ahlrichs, *Chem. Phys. Lett.*, **1995**, *240*, 283.
- 21 K. Eichkorn, O. Treutler, H. Öhm, M. Häser, R. Ahlrichs, *Chem. Phys. Lett.*, **1995**, *242*, 652.
- 22 K. Eichkorn, F. Weigend, O. Treutler, R. Ahlrichs, *Theor. Chem. Acc.*, **1997**, *97*, 119.
- 23 P. Deglmann, K. May, F. Furche, R. Ahlrichs, *Chem. Phys. Lett.*, **2004**, *384*, 103.
- 24 F. Weigend, *Phys. Chem. Chem. Phys.*, **2002**, *4*, 4285.
- 25 M. Sierka, A. Hogeckamp, R. Ahlrichs, *J. Chem. Phys.*, **2003**, *118*, 9136.
- 26 S. Grimme, J. Antony, S. Ehrlich, H. Krieg, *J. Chem. Phys.*, **2010**, *132*, 154104.
- 27 S. Grimme, S. Ehrlich, L. Goerigk, *J. Comput. Chem.*, **2011**, *32*, 1456.



# Nucleophilic Rh<sup>I</sup> Catalyzed Selective Isomerization of Terminal Aziridines to Enamides

Yingying Tian,<sup>[a]</sup> and Doris Kunz\*<sup>[a]</sup>

[a] Y. Tian, Prof. Dr. D. Kunz  
Institut für Anorganische Chemie  
Eberhard Karls Universität Tübingen  
Auf der Morgenstelle 18, 72076 Tübingen (Germany)  
E-mail: doris.kunz@uni-tuebingen.de

Supporting information for this article is given via a link at the end of the document.

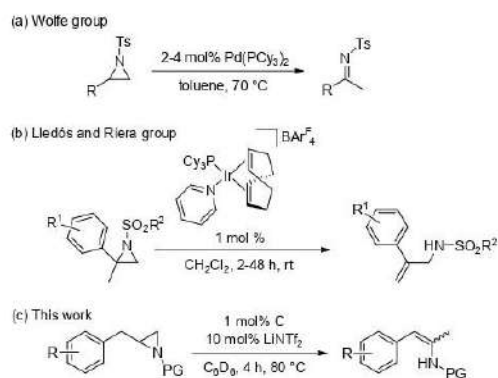
**Abstract:** The selective isomerization of various terminal *N*-Boc protected aziridines to enamides was realized using the highly reactive nucleophilic rhodium catalyst **C** with the Lewis acid LiNTf<sub>2</sub> as co-catalyst under moderate conditions. The reaction proceeds smoothly with only 1 mol% catalyst loading and excellent yields were achieved. An intermediate containing an enamide with a non-conjugated terminal C=C double bond was detected during the course of the reaction, which isomerizes to form the thermodynamically favored 2-amido styrene. Mechanistic insight is gained based on these observations.

Catalytic isomerizations of small molecules are of great importance for synthetic chemistry due to the ready availability of the substrates and the ideal atom economy of the transformation. The isomerization of epoxides, known as the Meinwald rearrangement, is an efficient method for the conversion of epoxides to carbonyl compounds, such as aldehydes and methyl ketones, which is catalyzed by Lewis acids to obtain aldehydes<sup>[1]</sup> and promoted by Lewis acids with nucleophilic catalysts to yield methyl ketones.<sup>[2]</sup> Recently, our group has realized the chemo- and regioselective isomerization of a diverse range of epoxides including the challenging  $\alpha$ -aryl oxiranes, with the highly nucleophilic rhodium bis(NHC) pincer catalysts **A-C** to obtain almost exclusively methyl ketones in excellent yields under very mild conditions.<sup>[2b,d,e]</sup> Aziridines, the analogue of epoxides, are quite useful building blocks in both organic and pharmaceutical chemistry.<sup>[3]</sup> The most popular reaction for an aziridine transformation is the generation of  $\beta$ -lactams catalyzed by transition-metal complexes under the exposure of carbon monoxide.<sup>[4]</sup> Most recently, the ring opening of aziridines was well-studied and it behaves as an effective pathway to gain  $\beta$ -functionalized amines which can easily be transformed further.<sup>[5]</sup>

However, the isomerization of aziridines has been rarely investigated. In 2002, the Nakayama group reported a Lewis acid catalyzed aza-pinacol rearrangement of various *N*-tosyl aziridines to *N*-tosyl imines with BF<sub>3</sub>.<sup>[6]</sup> One year later, the Wolfe group introduced the palladium-catalyzed isomerization of terminal *N*-tosyl aziridines to sulfonyl ketimines (Scheme 1, (a)).<sup>[7]</sup> Recently, Liedós, Riera and co-workers described an iridium-catalyzed

isomerization of geminal disubstituted *N*-sulfonyl aziridines to allyl amines (Scheme 1, (b)).<sup>[8]</sup>

The potential products of the aziridine isomerization are manifold, such as the mentioned *N*-tosyl imines and allyl amines. Another kind of products expected are enamides which are valuable substrates for the asymmetric hydrogenation to gain access to optically pure amides.<sup>[9]</sup> Common methods to generate enamides usually include reacting ketones with amides<sup>[10]</sup> or applying its derivatives such as vinyl halides, triflates and tosylates with amides through transition-metal catalyzed cross-coupling reactions.<sup>[11]</sup> Recently, the Beller group described the Pd-catalyzed carbonylation reaction of imines to enamides.<sup>[12]</sup> Herein, we provide an alternative synthetic strategy for the preparation of various enamides via the selective isomerization of terminal aziridines catalyzed by highly nucleophilic rhodium catalysts (Scheme 1, (c)).



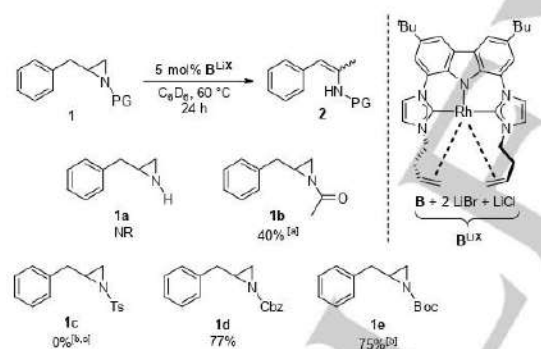
**Scheme 1.** Isomerization of terminal aziridines with transition-metal complexes.

The synthesis of the aziridine candidates usually started from commercially available phenylalanine derivatives. They were reduced firstly with NaBH<sub>4</sub> as the reducing agent and I<sub>2</sub> as the

## COMMUNICATION

catalyst to obtain the corresponding amino alcohols in almost quantitative yields.<sup>[13]</sup> Afterward, the amino substituent of the amino alcohols was protected with the respective protecting group.<sup>[14]</sup> The last step was a one pot reaction that consisted of converting the hydroxyl group into a better leaving group by tosylation and the ring closure with the strong base KOH in refluxing THF.<sup>[15]</sup> All desired terminal aziridines were generated in moderate to good yields.

With the successfully prepared terminal aziridines, different protecting groups on the nitrogen atom were tested at the beginning (Scheme 2). The initial reaction conditions were 5 mol% *in situ* generated  $B^{LiX}$ <sup>[2d]</sup> and aziridines in  $C_6D_6$  at 60 °C for 24 h. Non-protected aziridine **1a** was not reactive under these conditions. *N*-Acetyl aziridine **1b** was isomerized, but the desired product **2b** was only formed in 40% yield along with 28% of dihydrooxazole. The latter is formed in a Lewis acid catalyzed side reaction with LiBr, as confirmed in a blank reaction. When the *N*-tosyl protected substrate **1c** was applied, the reaction went quite fast even at room temperature and full conversion was achieved after 2 h. However, the desired enamides were not obtained due to polymerization as a side reaction. At 60 °C, **1d** possessing the *N*-Cbz group was converted smoothly to obtain the desired **2d** in 77% yield. To our delight, the *N*-Boc aziridine **1e** can be rearranged at room temperature to yield the corresponding enamides in 75% yield. Therefore, the *N*-Boc protecting group was chosen for all further aziridines.



**Scheme 2.** Isomerization of terminal aziridines with different protecting groups (PG). The yield of **2** was determined by <sup>1</sup>H NMR calibrated to 1,3,5-trimethoxybenzene (internal standard).<sup>[2d]</sup> Along with 28% of dihydrooxazole.<sup>[2f]</sup> rt. <sup>[2g]</sup> 2 h.

We tested the isomerization of *N*-Boc-2-benzylaziridine (**1e**) as the model substrate. A series of isolated rhodium catalysts efficient for epoxide rearrangement was applied. With the CO-containing catalyst **A**, only traces of the desired enamide were detected after 24 h (Table 1, entry 1). Under the identical conditions, a better yield (28%) was obtained with the more nucleophilic CO-free catalyst **B** and the best result was achieved using catalyst **C** to yield enamide **2e** in 57% yield (Table 1, entries 2 and 3). This can be rationalized with the enhanced nucleophilicity of the 16 *e*<sup>-</sup> complex **C** with a high-lying HOMO, while the 18 *e*<sup>-</sup> catalyst **B** requires the dissociation of one olefin moiety to react as a nucleophile. A stronger Lewis acid, necessary

for the pre-activation of the aziridine was beneficial for the catalytic reaction and the yield was increased to 66% when LiNTf<sub>2</sub> was used as the co-catalyst (Table 1, entry 4). Furthermore, the reaction proceeds considerably fast when it is carried out at elevated temperatures and the desired product **2e** is obtained in 96% after 4 h at 80 °C (Table 1, entries 5, 6 and 7). To check the role of the additive, LiNTf<sub>2</sub> was omitted and no reaction was observed after 4 h at 80 °C, which shows that the Lewis acid is essential for the catalytic reaction (Table 1, entry 8). This also explains why the reaction almost stands still when the solvent  $C_6D_6$  is replaced by THF-*d*<sub>8</sub> or CD<sub>3</sub>CN, which indicates competitive binding between THF-*d*<sub>8</sub> or CD<sub>3</sub>CN and the substrate to the Lewis acid co-catalyst (Table 1, entries 9 and 10). Surprisingly, full conversions were also obtained with lower catalyst loadings and 1 mol% catalyst **C** proved sufficient for a fast and selective isomerization (Table 1, entries 11 and 12).

**Table 1.** Rh-catalyzed isomerization of **1e**: Optimization of the reaction conditions.<sup>[2f]</sup>

Entry	Catalyst [mol%]	Additive [mol%]	T (°C)	Time	Yield	
					[%] <sup>[2f]</sup>	(Z:E)
1	5 (A)	10 (LiBr)	rt	24 h	< 5	-
2	5 (B)	10 (LiBr)	rt	24 h	28	50:50
3	5 (C)	10 (LiBr)	rt	24 h	57	50:50
4	5 (C)	10 (LiNTf <sub>2</sub> )	rt	24 h	66	47:53
5	5 (C)	10 (LiNTf <sub>2</sub> )	40	4 h	87	47:53
6	5 (C)	10 (LiNTf <sub>2</sub> )	60	4 h	87	45:55
7	5 (C)	10 (LiNTf <sub>2</sub> )	80	4 h	96	41:59
8	5 (C)	-	80	4 h	0	-
9 <sup>[2i]</sup>	5 (C)	10 (LiNTf <sub>2</sub> )	rt	24 h	< 5	-
10 <sup>[2j]</sup>	5 (C)	10 (LiNTf <sub>2</sub> )	rt	24 h	< 5	-
11	3 (C)	10 (LiNTf <sub>2</sub> )	80	4 h	91	40:60
12	1 (C)	10 (LiNTf <sub>2</sub> )	80	4 h	90	54:46
				24 h	90	33:67
13	1 (C)	20 (LiNTf <sub>2</sub> )	80	4 h	93	45:55
14	1 (C)	5 (LiNTf <sub>2</sub> )	80	7 h	86	28:72

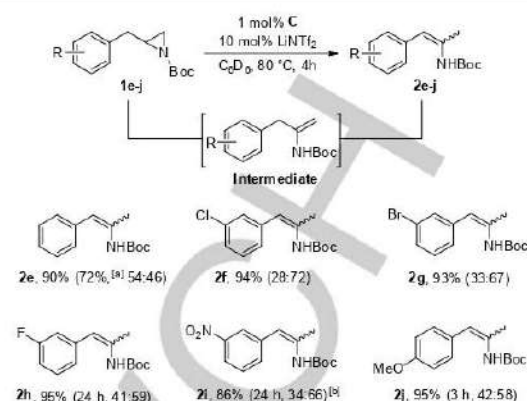
## COMMUNICATION

15	1 (C)	70 (B(C <sub>6</sub> F <sub>5</sub> ) <sub>3</sub> )	rt	2 h	23 <sup>[a]</sup>	57:43
16 <sup>[b]</sup>	1 (C)	10 (LiNTf <sub>2</sub> )	80	4 h	88	35:65
17 <sup>[b]</sup>	1 (C)	10 (LiNTf <sub>2</sub> )	80	4 h	88	36:64

[a] All reactions were carried out in *J. Young* NMR tubes and the additive was pre-activated with 10  $\mu$ L THF-*d*<sub>6</sub>. [b] The yield (<sup>1</sup>H NMR) of **2e** was determined using 1,3,5-trimethoxybenzene as internal standard. [c] THF-*d*<sub>6</sub> as the solvent. [d] CD<sub>3</sub>CN as the solvent. [e] along with 40 % *N*-Boc deprotected product; full conversion of **1e**. [f] 0.2 M of **1e**. [g] 0.4 M of **1e**.

When extending the reaction time from 4 h to 24 h the *Z/E* ratio changes from 54:46 to 33:67, without influencing the overall yield. This indicates an isomerization of the kinetically favored *Z*-(**2e**) isomer into the thermodynamically favored *E*-(**2e**) isomer. The loadings of the Lewis acid co-catalyst were examined as well. The yield of enamide **2e** improved slightly with 20 mol% LiNTf<sub>2</sub> and a longer reaction time was needed when only 5 mol% Lewis acid were used (Table 1, entries 13 and 14). Usually strong Lewis acids are not compatible with carbamate protecting groups.<sup>[15]</sup> Nevertheless, we used 70 mol% of B(C<sub>6</sub>F<sub>5</sub>)<sub>3</sub> and found full conversion after 2 h room temperature, but besides 23 % of the product, also 40 % of the deprotected product was obtained (entry 15). Higher aziridine concentrations (0.2 mol/L and 0.4 mol/L, respectively) rarely influence the reaction rate and the desired enamide was obtained in comparable yields (Table 1, entries 16 and 17). The *Z/E* selectivity varies between 54:46 and 28:72. Finally, a blank test without rhodium catalyst **C** showed no conversion (Table 1, entry 20). Thus, the optimized reaction conditions (1 mol% **C**, 0.1 M aziridine, C<sub>6</sub>D<sub>6</sub>, 80 °C) were applied to explore the generality of this protocol.

With the optimized conditions in hand, various *N*-Boc terminal aziridines were converted successfully into the desired enamides (Scheme 3). The terminal aziridines **1f** and **1g**, possessing weak electron-withdrawing chloro and bromo substituents on the phenyl ring, were isomerized smoothly to yield the corresponding enamides in excellent yield (94% and 93%, respectively). Interestingly, aziridine **1h** bearing a moderate electron-withdrawing fluoro group was rearranged much slower and full conversion was obtained after 24 h in 95% yield. To confirm this tendency, substrate **1i** bearing a strong electron-withdrawing nitro group was tested. Harsher reaction conditions were required and the reaction can only be completed with 5 mol% catalyst **C** in 24 h (86% yield for **1i**). Notably, the **Intermediate** bearing a terminal C=C double bond was observed, which is fully rearranged to the desired product after 24 h (see SI for details). In comparison, aziridine **1j** with a strongly electron-donating methoxy substituent was converted considerably fast finished within 3 h and no intermediate was detected. The corresponding enamides **2j** were obtained in 95% yield. A closer look at the <sup>1</sup>H NMR spectra monitoring the reaction of the other substrates **1e** and **1h** revealed the formation of the respective intermediates as well. While the isomerization is fast for the substrate with an electron donating substituent (**1j**), it becomes even rate limiting in the case of **1h** (14% left after 18 h) and **1i** bearing electron-withdrawing substituents. To check the feasibility of this novel method for synthetic chemistry, a scaled-up reaction using **1e** (1.3 mmol) and 1 mol% catalyst **C** was prepared and the desired enamide **2e** was isolated by column chromatography in 72% yield with a *Z/E* ratio of 54:46.

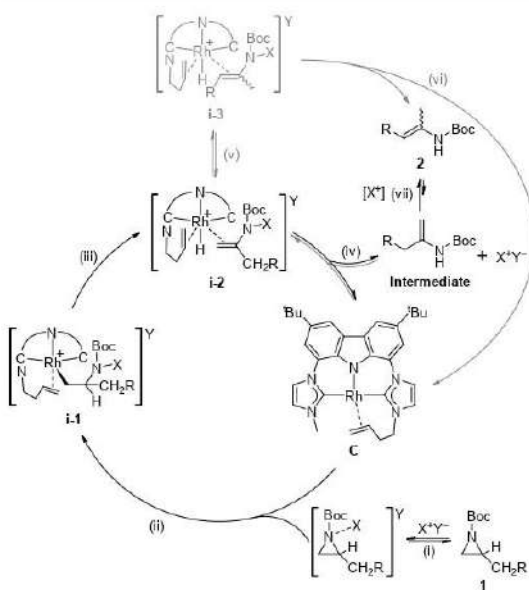


**Scheme 3.** Substrate scope of the rhodium-catalyzed isomerization of *N*-Boc terminal aziridines. The yield of **2** was determined by <sup>1</sup>H NMR against the internal standard 1,3,5-trimethoxybenzene and *Z/E* ratios are given in brackets. <sup>a</sup>0.3 g of **1e** (1.3 mmol) and 1 mol% catalyst **C** used; isolated yield of **2e** in brackets. <sup>b</sup>5 mol% catalyst **C**.

A nucleophilic mechanism for the aziridine isomerization by a palladium(0) catalyst was suggested by the Wolfe group.<sup>[7]</sup> Together with the nucleophilic dual-activation mechanism (substrate pre-activation by a Lewis acid) we have reported for the epoxide isomerization, an analogous mechanism for the aziridines was proposed.<sup>[20e]</sup> The fact that the Lewis acid additive and non-coordinating solvents are required indicates a pre-activation of the terminal aziridines (Scheme 4, step (i)). This is followed by a nucleophilic attack of the 16 e<sup>-</sup> Rh<sup>I</sup> catalyst **C** at the most electrophilic side of the aziridine, which is also the least hindered position in this case (ii) and formation of intermediate **i-1** which is likely stabilized by the Lewis acid as well. Subsequent  $\beta$ -hydride elimination (iii) could lead to the Rh<sup>III</sup> hydrido complex **i-2** which releases the **Intermediate** by reductive elimination (iv) under regeneration of complex **C**. In case of aziridines containing electron donating substituents, **i-2** could also isomerize directly to intermediate **i-3** (v) from which the thermodynamically favored product is released by reductive elimination under recovery of catalyst **C** (vi). As the isomerization rate of the **Intermediate** to the product **2** (step vi) is substrate depending and slows down in case of more electron-withdrawing substituents, we assume that this step is Lewis-acid catalyzed. [1,3]-H shifts are thermally forbidden and a resting state that requires the oxidative addition of the **Intermediate** to the nucleophilic catalyst **C** under reformation of the Rh<sup>III</sup> hydrido complex **i-2** would require the breaking of a strong NH bond and thus seems less likely.

Accepted Manuscript

## COMMUNICATION



**Scheme 4.** Proposed mechanism of the isomerization of terminal aziridines with the highly nucleophilic Rh-pincer complex **C**.

In conclusion, we have presented the selective isomerization of a series of terminal aziridines to yield the desired enamides using the highly reactive nucleophilic rhodium catalyst **C** under moderate conditions. Most of the tested aziridines were converted smoothly with only 1 mol% catalyst loading and excellent yields were obtained. Intermediates containing the terminal C=C double bond were detected during the course of the reaction with substrates containing an electron poor group. The double bond migrates to the internal C=C double bond to complete the reaction. Based on these observations, a dual-activation mechanism including the activation of the substrate by the Lewis acid and the nucleophilic opening by Rh catalyst is proposed. This novel transformation provides an alternative strategy for the synthesis of enamides.

### Acknowledgements

Yingying Tian thanks the China Scholarship Council (CSC) for a predoctoral fellowship. We are grateful to Xiaoli Su, Jan Grammel and Christina Breitenstein for their help with some substrate synthesis.

**Keywords:** enamides • isomerization • rhodium • terminal aziridines • thermodynamics

[1] a) J. Meinwald, S. S. Labana, M. S. Chadha, *J. Am. Chem. Soc.* **1963**, *85*, 582-585; b) A. Miyashita, T. Shimada, A. Sugawara, H. Nohira, *Chem. Lett.* **1986**, 1323-1326; c) S. Kulasegaram, R. J. Kulawiec, *J. Org. Chem.* **1997**, *62*, 6547-6561; d) C.-L. Chang, M. P. Kumar, R.-S. Liu, *J. Org. Chem.* **2004**, *69*, 2793-2796; e) M. W. C. Robinson, K. S. Pillinger, I. Mabbett, D. A. Timms, A. E.

Graham, *Tetrahedron* **2010**, *66*, 8377-8382; f) D. J. Vyas, E. Lanonov, C. Besnard, L. Guéneé, C. Mazet, *J. Am. Chem. Soc.* **2013**, *135*, 6177-6183; g) N. Humbert, D. J. Vyas, C. Besnard, C. Mazet, *Chem. Commun.* **2014**, *50*, 10592-10595.

[2] a) J. L. Eisenmann, *J. Org. Chem.* **1962**, *27*, 2704-2710; b) E. Jürgens, B. Wucher, F. Rominger, K. W. Tornroos, D. Kunz, *Chem. Commun.* **2015**, *51*, 1897-900; c) J. R. Lamb, Y. Jung, G. W. Coates, *Org. Chem. Front.* **2015**, *2*, 346-349; d) Y. Tian, E. Jürgens, D. Kunz, *Chem. Commun.* **2018**, *54*, 11340-11343; e) Y. Tian, E. Jürgens, K. Mill, R. Jordan, T. Maubetsch, D. Kunz, *ChemCatChem* **2019**, *11*, 4028-4035.

[3] a) J. B. Sweeney, *Chem. Soc. Rev.* **2002**, *31*, 247-258; b) C.-Y. Huang, A. G. Doyle, *Chem. Rev.* **2014**, *114*, 8153-8198.

[4] a) H. Alper, F. Urso, D. J. H. Smith, *J. Am. Chem. Soc.* **1983**, *105*, 6737-6738; b) W. Chamchaang, A. R. Pinhas, *J. Org. Chem.* **1990**, *55*, 2943-2950; c) M. E. Piotti, H. Alper, *J. Am. Chem. Soc.* **1996**, *118*, 111-116; d) D. Ardura, R. López, T. L. Sordo, *J. Org. Chem.* **2006**, *71*, 7315-7321; e) C. R. Pitts, T. Ledka, *Chem. Rev.* **2014**, *114*, 7930-7953.

[5] a) B. L. Lin, C. R. Clough, G. L. Hillhouse, *J. Am. Chem. Soc.* **2002**, *124*, 2890-2891; b) P. Lu, *Tetrahedron* **2010**, *66*, 2549-2560; c) C.-Y. Huang, A. G. Doyle, *J. Am. Chem. Soc.* **2012**, *134*, 9541-9544; d) Y. Takeda, A. Kuroda, W. M. C. Sameera, K. Morokuma, S. Minakata, *Chem. Sci.* **2016**, *7*, 6141-6152; e) H. Yi, M. Oestreich, *Chem.-Eur. J.* **2019**, *25*, 6505-6507.

[6] Y. Sugihara, S. Imura, J. Nakayama, *Chem. Commun.* **2002**, 134-135.

[7] J. P. Wolfe, J. E. Ney, *Org. Lett.* **2003**, *5*, 4607-4610.

[8] A. Cabré, G. Sciortino, G. Ujaque, X. Verdagué, A. Lledós, A. Riera, *Org. Lett.* **2018**, *20*, 5747-5751.

[9] a) M. J. Burk, G. Casey, N. B. Johnson, *J. Org. Chem.* **1998**, *63*, 6084-6085; b) Z. Zhang, G. Zhu, Q. Jiang, D. Xiao, X. Zhang, *J. Org. Chem.* **1999**, *64*, 1774-1775; c) J. Chen, W. Zhang, H. Geng, W. Li, G. Hou, A. Lei, X. Zhang, *Angew. Chem. Int. Ed.* **2009**, *48*, 800-802; *Angew. Chem.* **2009**, *121*, 814-816; d) T. C. Nugent, M. El-Shazly, *Adv. Synth. Catal.* **2010**, *352*, 753-819; e) S.-F. Zhu, T. Liu, S. Yang, S. Song, Q.-L. Zhou, *Tetrahedron* **2012**, *68*, 7685-7690; f) G. Liu, X. Liu, Z. Cai, G. Jiao, G. Xu, W. Tang, *Angew. Chem. Int. Ed.* **2013**, *52*, 4235-4238; *Angew. Chem.* **2013**, *125*, 4329-4332.

[10] a) D. M. Tschaen, L. Abramson, D. Cai, R. Desmond, U.-H. Dolling, L. Frey, S. Karady, Y.-J. Shi, T. R. Verhoeven, *J. Org. Chem.* **1995**, *60*, 4324-4330; b) P. Dupau, P. Le Gendre, C. Bruneau, P. H. Dixneuf, *Synlett* **1999**, 1832-1834.

[11] a) O. Takuji, K. Toshiyuki, H. Kazuo, S. Hitomi, *Chem. Lett.* **1991**, *20*, 1443-1446; b) R. Shen, J. Porco, *Org. Lett.* **2000**, *2*, 1333-1336; c) L. Jiang, G. E. Job, A. Klapars, S. L. Buchwald, *Org. Lett.* **2003**, *5*, 3667-3669; d) R. S. Coleman, P.-H. Liu, *Org. Lett.* **2004**, *6*, 577-580; e) D. J. Wallace, D. J. Klauer, C.-y. Chen, R. P. Volante, *Org. Lett.* **2003**, *5*, 4749-4752; f) A. Klapars, K. R. Campos, C.-y. Chen, R. P. Volante, *Org. Lett.* **2005**, *7*, 1185-1188.

[12] L. Wang, H. Neumann, A. Spännenberg, M. Beller, *Chem.-Eur. J.* **2018**, *24*, 2164-2172.

[13] R. Villa, A. L. Mandel, B. D. Jones, J. J. La Clair, M. D. Burkart, *Org. Lett.* **2012**, *14*, 5396-5399.

[14] H.-S. Chong, H. A. Song, M. Dadwal, X. Sun, I. Sin, Y. Chen, *J. Org. Chem.* **2010**, *75*, 219-221.

[15] P. Wessig, J. Schwarz, *Synlett* **1997**, 893-894.

[16] T. W. Greene, P. G. M. Wuts, *Protective Groups in Organic Synthesis*, 3<sup>rd</sup> Ed., Wiley, **1999**.

## Supporting Information

# Nucleophilic Rh<sup>I</sup> Catalyzed Selective Isomerization of Terminal Aziridines to Enamides

Yingying Tian, Doris Kunz\*

*Institut für Anorganische Chemie, Auf der Morgenstelle 18, 72076 Tübingen, Germany*

### Table of Contents

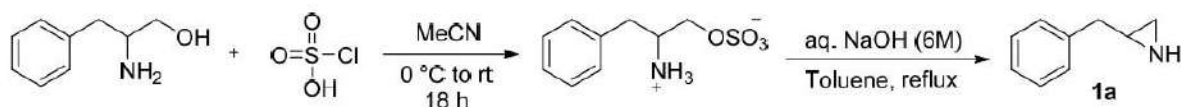
1. General information.....	2
2. Synthesis of aziridines with different protecting groups .....	3
3. General procedure for the synthesis of the <i>N</i> -Boc terminal aziridine derivatives <b>1f-j</b> .....	6
4. Process <sup>1</sup> H NMR spectra of <b>1e</b> , <b>1h</b> and <b>1i</b> .....	9
5. Isomerization of <b>1e</b> with BCF .....	12
6. Experimental procedures for the isomerization of terminal aziridines with catalyst <b>C</b> .....	13
7. NMR spectra .....	17
8. References .....	32

## 1. General information

Unless otherwise noted, all reactions were carried out under an argon atmosphere in dried and degassed solvents using Schlenk technique. Toluene, pentane, dichloromethane and tetrahydrofuran were purchased from Sigma Aldrich and dried using an MBraun SPS-800 solvent purification system. All liquid aziridines were degassed through freeze-pump-thaw cycles prior to use. Rhodium catalysts **A**, **B** and **C** were synthesized according to the literature procedures.<sup>[1-3]</sup> <sup>1</sup>H and <sup>13</sup>C NMR spectra were recorded using a Bruker ARX 300 and AVANCE II+ 400 spectrometer. Chemical shifts  $\delta$  (ppm) are given relative to the solvent's residual proton and carbon signal relative to tetramethyl silane: C<sub>6</sub>D<sub>6</sub>: 7.16 ppm (<sup>1</sup>H NMR) and 128.39 ppm (<sup>13</sup>C NMR); CDCl<sub>3</sub>: 7.27 ppm (<sup>1</sup>H NMR) and 77.00 ppm (<sup>13</sup>C NMR). Coupling constants (*J*) are reported in Hz. Multiplets were assigned as s (singlet), br s (broad singlet), d (doublet), dd (doublet of doublets), dt (doublet of triplets), dtd (doublet of triplet of doublets), t (triplet) and tt (triplet of triplets), m (multiplet). Silica gel was used for column chromatography.

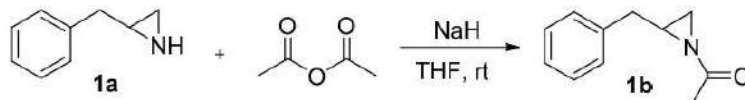


## 2. Synthesis of aziridines with different protecting groups

2-Benzylaziridine (**1a**)<sup>[4]</sup>

2-Amino-3-phenylpropan-1-ol (2.30 g, 15.2 mmol) was dissolved in acetonitrile (110 mL), and the reaction mixture was cooled to 0 °C followed by the dropwise addition of chlorosulfonic acid (1.77 g, 15.2 mmol). The reaction mixture was stirred for 18 h at room temperature. After completion, the reaction was filtered under vacuum, followed by washing with ethyl acetate (3 × 2 mL) and diethyl ether (3 × 5 mL). The residue was dried under reduced pressure. The product was obtained as a colorless solid (2.59 g, 11.1 mol, yield: 73%).

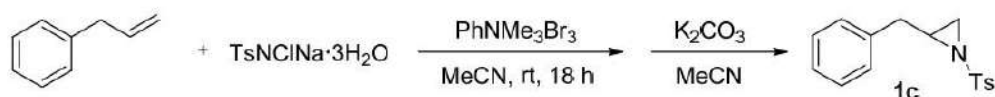
The generated aminosulfate salt (11.1 mmol) was dissolved in NaOH (80 mL, aq. 6 M) followed by the addition of toluene (80 mL). The resulting mixture was stirred and heated under reflux for 20 h. After completion, the organic phase was extracted with ethyl acetate, dried over MgSO<sub>4</sub>, and evaporated under reduced pressure to afford the aziridine **1a** (1.32 g, 9.88 mmol, yield: 89%) as a pale yellow oil. **1a** was used without further purification. The <sup>1</sup>H NMR was in accord with the literature.

N-Acetyl-2-benzylaziridine (**1b**)<sup>[5]</sup>

To a suspension of the sodium hydride (300 mg, 7.51 mmol, 60%) in THF (20 mL) was added the aziridine **1a** (1.00 g, 7.51 mmol) dissolved in THF (5 mL). The reaction mixture was stirred for 30 min at room temperature followed by the addition of acetic anhydride (767 mg, 7.51 mmol) and then stirred for another 2 h. The reaction mixture was poured into diethyl ether (30 mL) and washed with water (30 mL). The organic phase was evaporated to yield the raw product. The residue was purified by column chromatography (methanol/dichloromethane, 1 : 40) to yield the aziridine **1b** (1.01 g, 5.78 mmol, yield: 77%) as a white solid.

$^1\text{H}$  NMR (400 MHz,  $\text{CDCl}_3$ )  $\delta$  7.36 – 7.25 (m, 6H), 2.90 – 2.80 (m, 2H), 2.65 (dtd,  $J = 6.5, 5.8, 3.3$  Hz, 1H), 2.42 (d,  $J = 5.8$  Hz, 1H), 2.09 (d,  $J = 3.3$  Hz, 1H), 1.96 (s, 3H).  $^{13}\text{C}$  NMR (101 MHz,  $\text{CDCl}_3$ )  $\delta$  183.2, 137.8, 128.9, 128.6, 126.8, 38.7, 38.0, 30.8, 23.4.

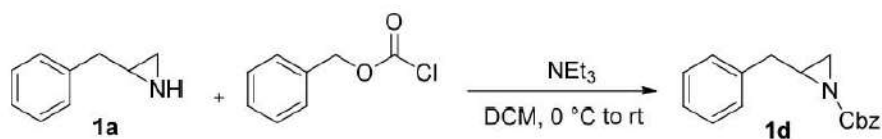
**N-Tosyl-2-benzylaziridine (1c)<sup>[6]</sup>**



To a solution of  $\text{TsNCINa}\cdot 3\text{H}_2\text{O}$  (5.24 g, 18.6 mmol) and allylbenzene (2.00 g, 16.9 mmol) in acetonitrile (40 mL) was added  $\text{PhNMe}_3\text{Br}_3$  (636 mg, 1.69 mmol). The reaction mixture was vigorously stirred for 18 h at room temperature. After completion, the reaction was concentrated, dissolved in dichloromethane (10 mL) and filtered through a short column with ethyl acetate and petrol ether as the eluent (1:10). The organic solution was dried and dissolved in acetonitrile (20 mL). To the solution was added  $\text{K}_2\text{CO}_3$  (9.34 g, 67.6 mmol) and the reaction was stirred for another 2 h at 45 °C. Afterward, the reaction mixture was diluted with diethyl ether (20 mL), filtered through a pad of Celite® and the filtrate was evaporated to yield the raw product. Pure product **1c** (1.89 g, 6.59 mmol, yield: 39%) was obtained by column chromatography (EtOAc/petrol ether, 1 : 10) as a white solid.

$^1\text{H}$  NMR (400 MHz,  $\text{CDCl}_3$ )  $\delta$  7.70 (d,  $J = 8.4$  Hz, 2H), 7.22 (d,  $J = 8.4$  Hz, 2H), 7.19 – 7.13 (m, 3H), 7.07 – 7.04 (m, 2H), 2.96 (tt,  $J = 7.1, 4.9$  Hz, 1H), 2.85 – 2.67 (m, 3H), 2.43 (s, 3H), 2.18 (d,  $J = 4.5$  Hz, 1H).  $^{13}\text{C}$  NMR (101 MHz,  $\text{CDCl}_3$ )  $\delta$  144.3, 137.0, 134.8, 129.5, 128.7, 128.4, 127.8, 126.5, 41.1, 37.4, 32.8, 21.6.

**N-Benzoyloxycarbonyl-2-benzylaziridine (1d)<sup>[7]</sup>**



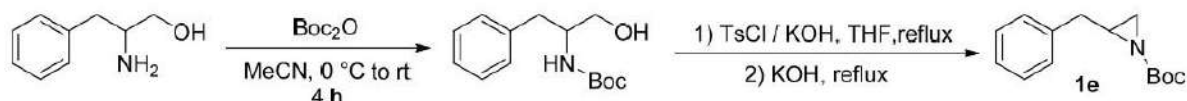
To a solution of the aziridine **1a** (200 mg, 1.50 mmol) and triethyl amine (228 mg, 2.25 mmol) in dichloromethane (25 mL) at 0 °C was added benzyl chloroformate (256 mg, 1.50 mmol). The mixture was warmed up to room temperature and stirred overnight. After completion, the reaction mixture was washed with water (5 mL) and brine (5 mL). The solvent was removed at reduced pressure and the residue was



purified by column chromatography (*n*-hexane/EtOAc, 12 : 1) to yield **1d** (361 mg, 1.35 mmol, yield: 90%) as a colorless oil.

<sup>1</sup>H NMR (400 MHz, C<sub>6</sub>D<sub>6</sub>) δ 7.15 – 7.02 (m, 10H), 4.98 (s, 2H), 2.69 – 2.63 (m, 1H), 2.34 – 2.31 (m, 2H), 1.98 (d, *J* = 5.7 Hz, 1H), 1.66 (d, *J* = 3.4 Hz, 1H). <sup>13</sup>C NMR (101 MHz, CDCl<sub>3</sub>) δ 163.2, 137.6, 135.7, 128.8, 128.5, 128.5, 128.2, 128.0, 126.6, 68.1, 38.5, 38.3, 31.6.

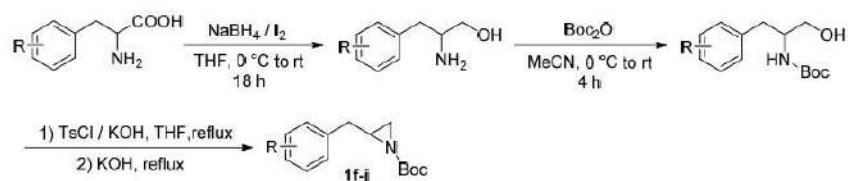
***N*-tert-Butyloxycarbonyl-2-benzylaziridine (**1e**)**<sup>[8]</sup>



To a solution of the 2-amino-3-phenylpropan-1-ol (2.00 g, 13.2 mmol) in acetonitrile (30 mL), Boc<sub>2</sub>O (2.89 g, 13.2 mmol) was added dropwise at 0 °C and the resulting mixture was stirred for 4 h at room temperature. The mixture was dried under reduced pressure to yield the raw Boc protected aminoalcohol which was used without purification.

Under argon atmosphere, KOH (2.96 g, 52.8 mmol) was added to a solution of the raw Boc protected aminoalcohol in THF (40 mL) and TsCl (3.02 g, 15.8 mmol) was added. The reaction was stirred under reflux for 4 h. A second portion of KOH (2.96 g, 52.8 mmol) was added and the reaction was refluxed for another 2 h. After completion, the reaction was cooled down to room temperature and washed with brine. The aqueous phase was extracted with dichloromethane (2 × 20 mL) and the organic layers were combined. After removal of solvent, the raw product was purified by column chromatography (*n*-hexane/EtOAc, 12 : 1) to yield the desired product **1e** (1.32 g, 5.68 mmol, yield: 43%) as a colorless liquid.

<sup>1</sup>H NMR (400 MHz, CDCl<sub>3</sub>) δ 7.35 – 7.22 (m, 5H), 2.97 (dd, *J* = 14.1, 5.5 Hz, 1H), 2.69 – 2.61 (m, 2H), 2.32 (d, *J* = 5.7 Hz, 1H), 2.04 (d, *J* = 3.6 Hz, 1H), 1.45 (s, 9H). <sup>13</sup>C NMR (101 MHz, CDCl<sub>3</sub>) δ 162.4, 138.0, 128.8, 128.4, 126.5, 81.1, 38.4, 38.3, 31.4, 27.9.

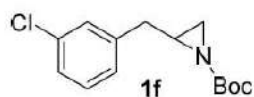
3. General procedure for the synthesis of the *N*-Boc terminal aziridine derivatives **1f-j**<sup>[8,9]</sup>

A suspension of the amino acid (12.0 mmol) in dry THF (40 mL) was cooled down to 0 °C and sodium borohydride (1.13 g, 30.0 mmol) was added in one portion. A solution of iodine (7.61 g, 30.0 mmol) in dry THF (10 mL) was added to this suspension over 10 min. Once the addition was completed, the cooling was removed and the reaction was warmed to reflux for 18 h. After completion, the reaction mixture was cooled to room temperature and methanol (10 mL) was added very slowly until the mixture became a clear solution. After 30 min stirring, the solution was concentrated and the residue was dissolved with an aqueous solution of KOH (3.5 M, 30 mL) and stirred for 30 min at room temperature. The aqueous layer was extracted with dichloromethane (3 x 30 mL) and the combined organic layers dried over anhydrous MgSO<sub>4</sub>, filtered and concentrated under reduced pressure to yield the corresponding amino alcohols which were used in the next step without further purification.

To a solution of the amino alcohol (12.0 mmol) in acetonitrile (30 mL), Boc<sub>2</sub>O (2.62 g, 12.0 mmol) was added dropwise at 0 °C and the resulting mixture was stirred for 4 h at room temperature. The mixture was dried under reduced pressure to yield the Boc protected aminoalcohol which was used without purification.

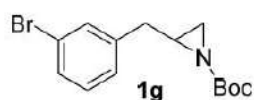
Under an argon atmosphere, KOH (2.69 g, 48.0 mmol) was added to a solution of the Boc protected aminoalcohol in THF (40 mL) and TsCl (2.75 g, 14.4 mmol) was added. The reaction was stirred under reflux for 4 h. A second portion of KOH (2.69 g, 48.0 mmol) was added and the reaction was refluxed for another 2 h. After completion, the reaction was cooled down to room temperature and washed with brine. The aqueous phase was extracted with dichloromethane (2 x 20 mL) and the organic layers were combined. After removal of the solvent, the raw product was purified by column chromatography (*n*-hexane/EtOAc = 12 : 1) to yield the desired products **1f-j**.

*N*-*tert*-Butyloxycarbonyl-2-(3-chlorobenzyl)aziridine (**1f**) was obtained as a white solid (36%).



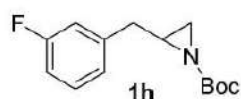
$^1\text{H}$  NMR (400 MHz,  $\text{CDCl}_3$ )  $\delta$  7.33 (d,  $J = 1.7$  Hz, 1H), 7.27 – 7.17 (m, 3H), 2.83 (dd,  $J = 14.8, 6.7$  Hz, 1H), 2.73 (dd,  $J = 14.8, 5.3$  Hz, 1H), 2.64 – 2.55 (m, 1H), 2.33 (d,  $J = 6.0$  Hz, 1H), 2.01 (d,  $J = 3.7$  Hz, 1H), 1.43 (s, 9H).  $^{13}\text{C}$  NMR (101 MHz,  $\text{CDCl}_3$ )  $\delta$  162.2, 140.1, 134.1, 129.6, 128.8, 127.0, 126.7, 81.2, 38.1, 37.8, 31.2, 27.8.

*N*-tert-Butyloxycarbonyl-2-(3-bromobenzyl)aziridine (**1g**) was obtained as a white solid (28%).



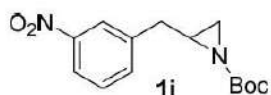
$^1\text{H}$  NMR (400 MHz,  $\text{CDCl}_3$ )  $\delta$  7.48 (s, 1H), 7.38 (d,  $J = 7.9$  Hz, 1H), 7.26 (d,  $J = 8.7$  Hz, 1H), 7.18 (d,  $J = 7.9$  Hz, 1H), 2.84 (dd,  $J = 14.8, 6.7$  Hz, 1H), 2.72 (dd,  $J = 14.8, 5.5$  Hz, 1H), 2.62 – 2.57 (m, 1H), 2.33 (d,  $J = 6.0$  Hz, 1H), 2.02 (d,  $J = 3.6$  Hz, 1H), 1.44 (s, 9H).  $^{13}\text{C}$  NMR (101 MHz,  $\text{CDCl}_3$ )  $\delta$  162.2, 140.4, 131.8, 130.0, 129.7, 127.4, 122.4, 81.2, 38.1, 37.9, 31.3, 27.9.

*N*-tert-Butyloxycarbonyl-2-(3-fluorobenzyl)aziridine (**1h**) was obtained as a colorless liquid (34%).



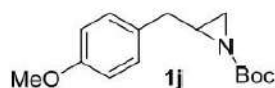
$^1\text{H}$  NMR (400 MHz,  $\text{CDCl}_3$ )  $\delta$  7.30 – 7.24 (m, 1H), 7.09 – 7.08 (m, 2H), 6.96 – 6.91 (m, 1H), 2.85 (dd,  $J = 14.8, 6.7$  Hz, 1H), 2.72 (dd,  $J = 14.8, 5.3$  Hz, 1H), 2.61 (m, 1H), 2.34 (d,  $J = 6.0$  Hz, 1H), 2.02 (d,  $J = 3.7$  Hz, 1H), 1.44 (s, 9H).  $^{13}\text{C}$  NMR (101 MHz,  $\text{CDCl}_3$ )  $\delta$  162.9 (d,  $^1J_{\text{CF}} = 245.4$  Hz), 162.2, 140.57 (d,  $^3J_{\text{CF}} = 7.5$  Hz), 129.8 (d,  $^3J_{\text{CF}} = 8.5$  Hz), 124.4 (d,  $^4J_{\text{CF}} = 2.8$  Hz), 115.7 (d,  $^2J_{\text{CF}} = 21.2$  Hz), 113.4 (d,  $^2J_{\text{CF}} = 21.2$  Hz), 81.2, 38.1 (d,  $J_{\text{CF}} = 1.9$  Hz), 37.9, 31.2, 27.8.  $^{19}\text{F}$  NMR (376 MHz,  $\text{CDCl}_3$ )  $\delta = -113.5$ .

*N*-*tert*-Butyloxycarbonyl-2-(3-nitrobenzyl)aziridine (**1i**) was obtained as a colorless liquid (30%).



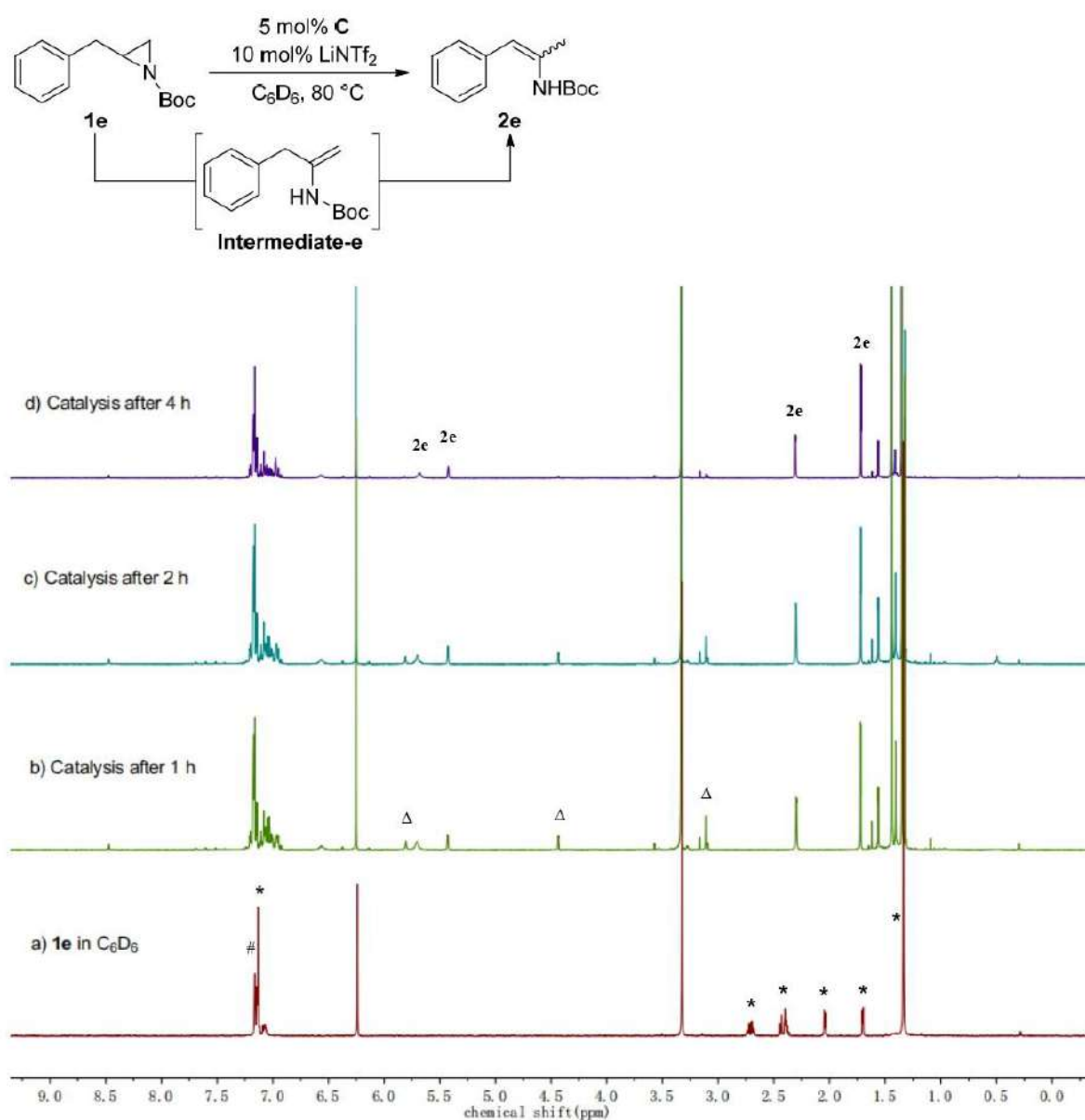
$^1\text{H}$  NMR (400 MHz,  $\text{CDCl}_3$ )  $\delta$  8.18 (s, 1H), 8.11 (d,  $J = 8.2$  Hz, 1H), 7.71 (d,  $J = 7.6$  Hz, 1H), 7.49 (t,  $J = 7.9$  Hz, 1H), 2.97 (dd,  $J = 14.8, 4.8$  Hz, 1H), 2.85 (dd,  $J = 14.8, 7.1$  Hz, 1H), 2.66 – 2.61 (m, 1H), 2.37 (d,  $J = 6.1$  Hz, 1H), 2.04 (d,  $J = 3.6$  Hz, 1H), 1.40 (s, 9H).  $^{13}\text{C}$  NMR (101 MHz,  $\text{CDCl}_3$ )  $\delta$  162.1, 148.3, 140.1, 135.1, 129.3, 123.7, 121.7, 81.4, 38.0, 37.5, 31.2, 27.8.

*N*-*tert*-Butyloxycarbonyl-2-(4-methoxybenzyl)aziridine (**1j**) was obtained as a white solid (28%).

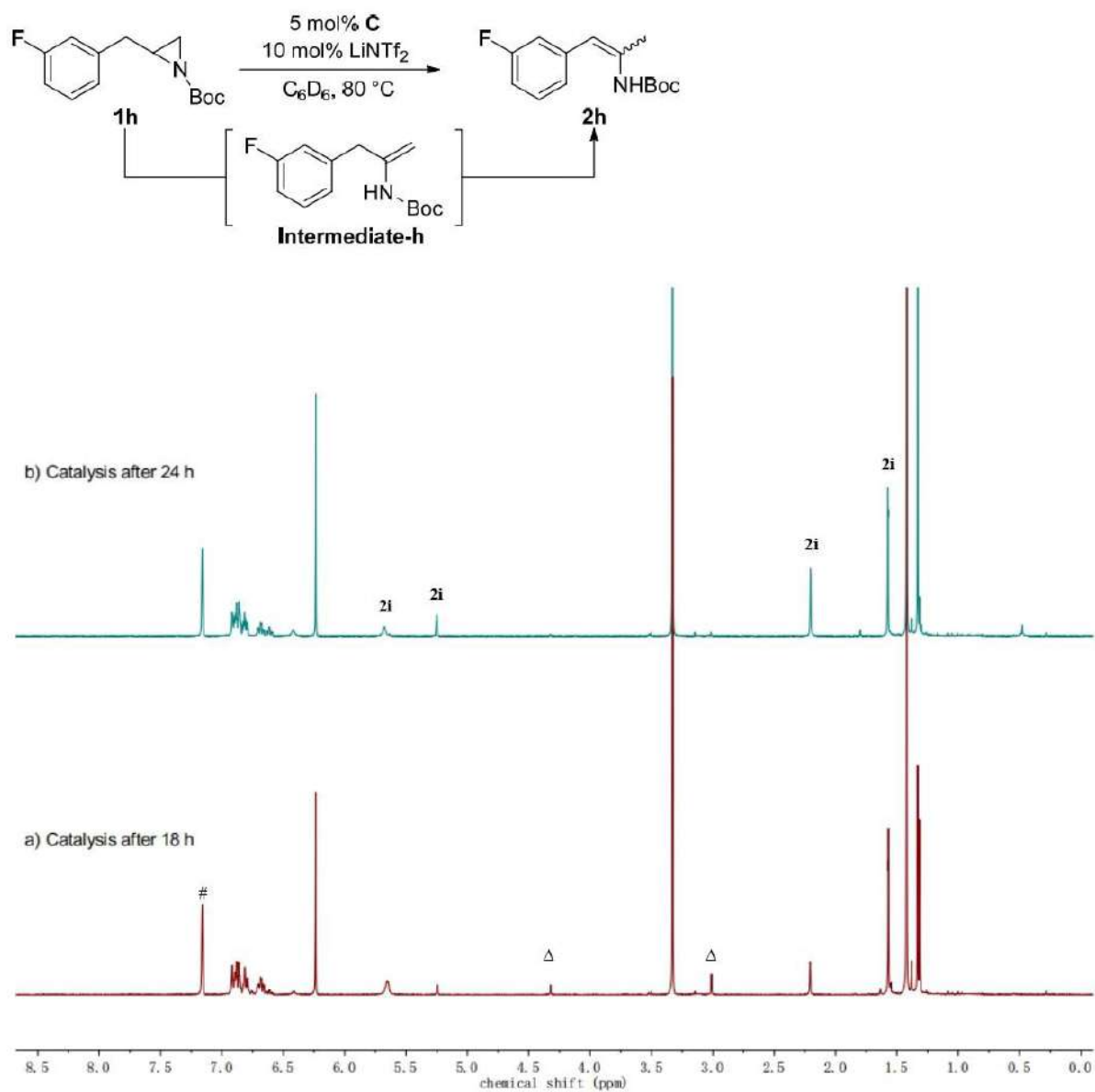


$^1\text{H}$  NMR (400 MHz,  $\text{CDCl}_3$ )  $\delta$  7.23 (d,  $J = 8.6$ , 2H), 6.86 (d,  $J = 8.6$  Hz, 2H), 3.80 (s, 3H), 2.94 – 2.88 (m, 1H), 2.64 – 2.56 (m, 2H), 2.30 (d,  $J = 5.8$  Hz, 1H), 2.01 (d,  $J = 3.4$  Hz, 1H), 1.45 (s, 9H).  $^{13}\text{C}$  NMR (101 MHz,  $\text{CDCl}_3$ )  $\delta$  162.4, 158.3, 130.0, 129.7, 113.8, 81.0, 55.2, 38.5, 37.5, 31.3, 27.9.

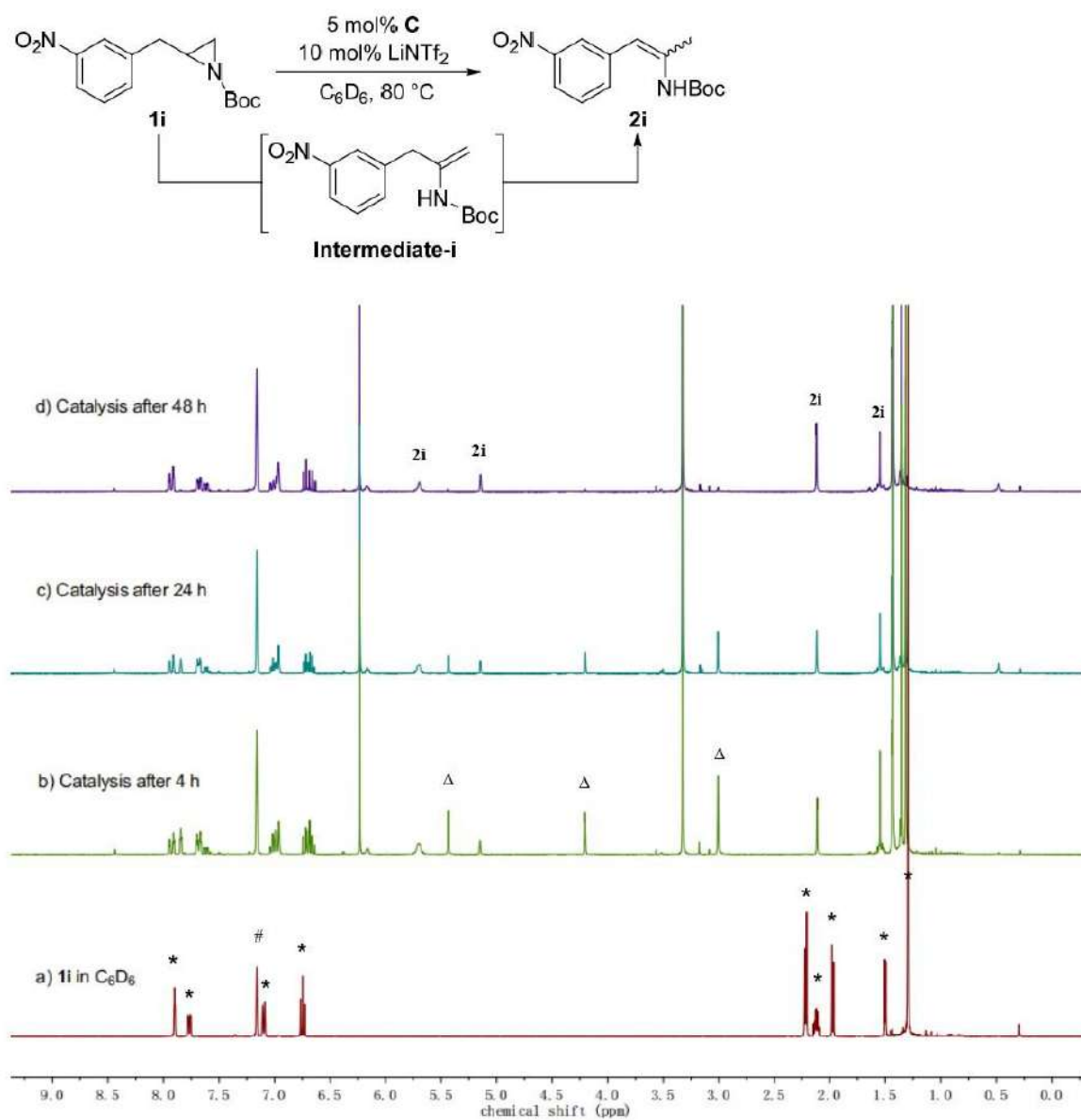
4. Process  $^1\text{H}$  NMR spectra of **1e**, **1h** and **1i**



**Figure S1.** a) **1e** (\*) in  $\text{C}_6\text{D}_6$  (#). b) The isomerization of **1e** using 5 mol% **C** and 10 mol%  $\text{LiNTf}_2$  in  $\text{C}_6\text{D}_6$  at  $80^\circ\text{C}$  for 1 h reveals the presence of the **Intermediate-e** ( $\Delta$ ). c) After 2 h: **Intermediate-e** still present. d) After 4 h only **2e** is observed.

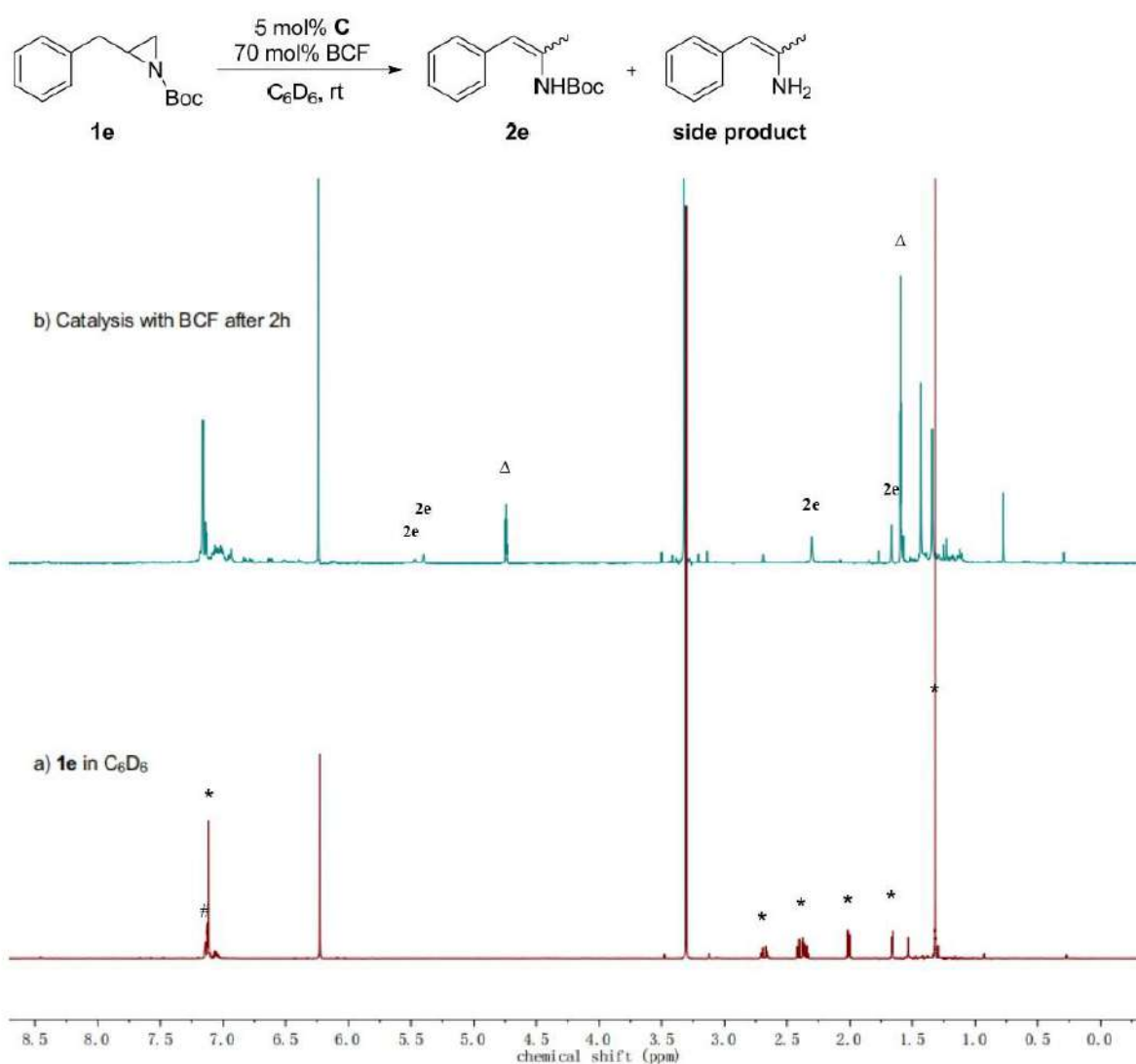


**Figure S2.** a) The isomerization of **1h** using 1 mol% **C** and 10 mol% LiINTf<sub>2</sub> in C<sub>6</sub>D<sub>6</sub> (#) at 80 °C for 18 h reveals the presence of the **Intermediate-h** (Δ). b) After 24 h only **2h** is observed.



**Figure S3.** a) **1i** (\*) in C<sub>6</sub>D<sub>6</sub> (#). b) The isomerization of **1i** using 5 mol% **C** and 10 mol% LiNTf<sub>2</sub> in C<sub>6</sub>D<sub>6</sub> at 80 °C for 4 h reveals the presence of the **Intermediate-i** (Δ). c) After 24 h: **Intermediate-i** is still present. d) After 48 h only **2i** is observed.

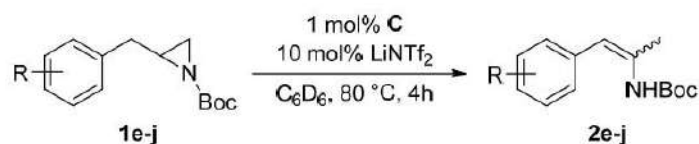
5. Isomerization of 1e with BCF



**Figure S4.** a) **1e** (\*) in  $C_6D_6$  (#). b) The isomerization of **1e** using 5 mol% **C** and 70 mol%  $B(C_6F_5)_3$  (BCF) in  $C_6D_6$  at rt for 2 h reveals full conversion and the deprotected side product (Δ) was generated along with **2e**.



## 6. Experimental procedures for the isomerization of terminal aziridines with catalyst C

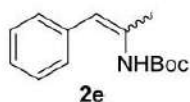
**Method 1 for 1e-h and 1j**

THF- $d_8$  (10  $\mu\text{L}$ ) was added into a *J. Young* NMR tube containing LiNTf<sub>2</sub> (1.2 mg, 4.0  $\mu\text{mol}$ ) to solubilize this salt. Catalyst **C** (0.3 mg, 0.4  $\mu\text{mol}$ ), the respective terminal aziridine (40  $\mu\text{mol}$ ) and a defined amount of the internal standard 1,3,5-trimethoxybenzene and C<sub>6</sub>D<sub>6</sub> (0.4 mL) were added successively. The reaction was heated at 80  $^\circ\text{C}$  for the given time. All yields were determined according to the internal standard 1,3,5-trimethoxybenzene (defined amount) by <sup>1</sup>H NMR spectroscopy. The NMR signals of the obtained enamides were confirmed by comparison with isolated **2e**.

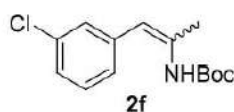
The up-scaling of this method was tested with **1e** (1.3 mmol). THF- $d_8$  (20  $\mu\text{L}$ ) was added into a round bottom flask containing LiNTf<sub>2</sub> (36.9 mg, 0.129  $\mu\text{mol}$ ) to solubilize it. Catalyst **C** (7.5 mg, 13  $\mu\text{mol}$ ), **1e** (300 mg, 1.29 mmol) and toluene (12.8 mL) were added successively. The reaction was heated at 80  $^\circ\text{C}$  for 4 h. After removal of the solvent by rotary evaporation, the crude product was purified by column chromatography at silica gel (EtOAc/hexane, 1 : 50) to afford the desired product **2e** (214 mg, 0.917 mmol, yield: 71%) as a colorless liquid [(**Z**)-**2e** (114 mg) and (**E**)-**2e** (100 mg)].

**Method 2 for 1i**

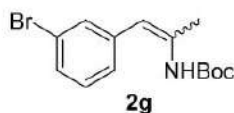
THF- $d_8$  (10  $\mu\text{L}$ ) was added into a *J. Young* NMR tube containing LiNTf<sub>2</sub> (1.2 mg, 4.0  $\mu\text{mol}$ ) to pre-activate the additive. Catalyst **C** (1.2 mg, 2.0  $\mu\text{mol}$ ), the aziridine **1i** (11.1 mg, 39.9  $\mu\text{mol}$ ) and a defined amount of the internal standard 1,3,5-trimethoxybenzene and C<sub>6</sub>D<sub>6</sub> (0.4 mL) were added successively. The reaction was heated at 80  $^\circ\text{C}$  for 24 h. The yield of **2i** was determined by 1,3,5-trimethoxybenzene (defined amount) as the internal standard by <sup>1</sup>H NMR spectroscopy. The NMR signals of the obtained enamide **2i** were assigned by comparison with isolated **2e**.



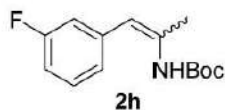
2-*N*-*tert*-Butyloxycarbonylamido-1-phenylprop-1-ene (**2e**, yield: 90%). <sup>1</sup>H NMR (400 MHz, C<sub>6</sub>D<sub>6</sub>) δ 7.21 – 6.92 (m, 4.5H), 6.57 (br s, 0.48H), 5.68 (br s, 0.43H), 5.42 (s, 0.53H), 2.31 (d, *J* = 1.1 Hz, 1.6H), 1.72 (d, *J* = 1.1 Hz, 1.38H), 1.44 (s, 4.18H), 1.35 (s, 4.82H). *Z*:*E* = 54:46. Broken integrals are given due to the mixture of the isomers.



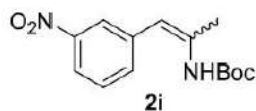
2-*N*-*tert*-Butyloxycarbonylamido-1-(3-chlorophenyl)prop-1-ene (**2f**, yield: 94%). <sup>1</sup>H NMR (400 MHz, C<sub>6</sub>D<sub>6</sub>) δ 7.06 – 6.71 (m, 4.2H), 6.33 (br s, 0.27H), 5.64 (br s, 0.75H), 5.20 (s, 0.28H), 2.19 (s, 0.84H), 1.53 (d, *J* = 0.9 Hz, 2.15H), 1.42 (s, 6.48H), 1.34 (s, 2.53H). *Z*:*E* = 28:72.



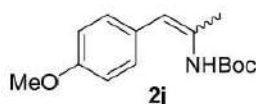
2-*N*-*tert*-Butyloxycarbonylamido-1-(3-bromophenyl)prop-1-ene (**2g**, yield: 93%). <sup>1</sup>H NMR (400 MHz, C<sub>6</sub>D<sub>6</sub>) δ 7.33 – 7.32 (m, 1.06H), 7.13 – 6.64 (m, 4.48H), 6.30 (br s, 0.36H), 5.63 (br s, 0.66H), 5.18 (s, 0.32H), 2.18 (s, 0.99H), 1.52 (d, *J* = 0.9 Hz, 2.01H), 1.42 (s, 6.01H), 1.34 (s, 2.98H). *Z*:*E* = 33:67.



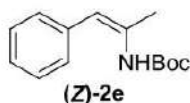
2-*N-tert*-Butyloxycarbonylamido-1-(3-fluorophenyl)prop-1-ene (**2h**, yield: 95%). <sup>1</sup>H NMR (400 MHz, C<sub>6</sub>D<sub>6</sub>) δ 6.88 – 6.80 (m, 3.70H), 6.71 – 6.59 (m, 1.13H), 6.42 (br s, 0.38H), 5.68 (br s, 0.52H), 5.25 (s, 0.41H), 2.20 (s, 1.22H), 1.57 (d, *J* = 0.9 Hz, 1.77H), 1.42 (s, 5.28H), 1.33 (s, 3.70H). *Z:E* = 41:59.



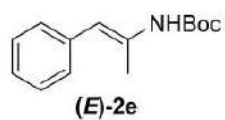
2-*N-tert*-Butyloxycarbonylamido-1-(3-nitrophenyl)prop-1-ene (**2i**, yield: 86%). <sup>1</sup>H NMR (400 MHz, C<sub>6</sub>D<sub>6</sub>) δ 7.95 – 7.91 (m, 1.04H), 7.69 – 7.60 (m, 1.15H), 7.04 – 6.96 (m, 1.68H), 6.74 – 6.63 (m, 1.09H), 6.17 (br s, 0.36H), 5.70 (br s, 0.57H), 5.14 (s, 0.40H), 2.12 (d, *J* = 1.1 Hz, 1.21H), 1.44 – 1.43 (m, 7.15H), 1.36 (s, 3.65H). *Z:E* = 34:66.



2-*N-tert*-Butyloxycarbonylamido-1-(4-methoxyphenyl)prop-1-ene (**2j**, yield: 95%). <sup>1</sup>H NMR (400 MHz, C<sub>6</sub>D<sub>6</sub>) δ 7.13 – 7.07 (m, 2.05H), 6.91 (br s, 0.56H), 6.76 (dt, *J* = 8.9, 2.7 Hz, 1.23H), 6.68 (dt, *J* = 8.7, 2.4 Hz, 0.96H), 6.52 (br s, 0.37H), 5.73 (br s, 0.55H), 5.44 (s, 0.42H), 3.32 (s, 1.72H), 3.27 (s, 1.31H), 2.32 (s, 1.27H), 1.77 (d, *J* = 0.5 Hz, 1.73H), 1.44 (s, 5.19H), 1.37 (s, 3.80H). *Z:E* = 42:58.



(*Z*)-2-*N-tert*-Butyloxycarbonylamido-1-phenylprop-1-ene [(*Z*)-**2e**]. <sup>1</sup>H NMR (300 MHz, CDCl<sub>3</sub>) δ 7.38 – 7.34 (m, 2H), 7.27 – 7.19 (m, 3H), 6.51 (br s, 1H), 5.55 (s, 1H), 2.27 (d, *J* = 1.1 Hz, 3H), 1.47 (s, 9H). <sup>13</sup>C NMR (75 MHz, CDCl<sub>3</sub>) δ 152.9, 136.2, 133.8, 128.8, 128.1, 126.3, 111.0, 80.2, 28.3, 21.3.



(*E*)-2-*N*-*tert*-Butyloxycarbonylamido-1-phenylprop-1-ene [(*E*)-2e].  $^1\text{H}$  NMR (300 MHz,  $\text{CDCl}_3$ )  $\delta$  7.32 – 7.13 (m, 5H), 6.78 (s, 1H), 5.87 (br s, 1H), 2.05 (d,  $J = 1.1$  Hz, 3H), 1.50 (s, 9H).  $^{13}\text{C}$  NMR (75 MHz,  $\text{CDCl}_3$ )  $\delta$  152.7, 137.5, 132.7, 128.0, 125.6, 112.5, 111.0, 80.2, 28.3, 17.8.



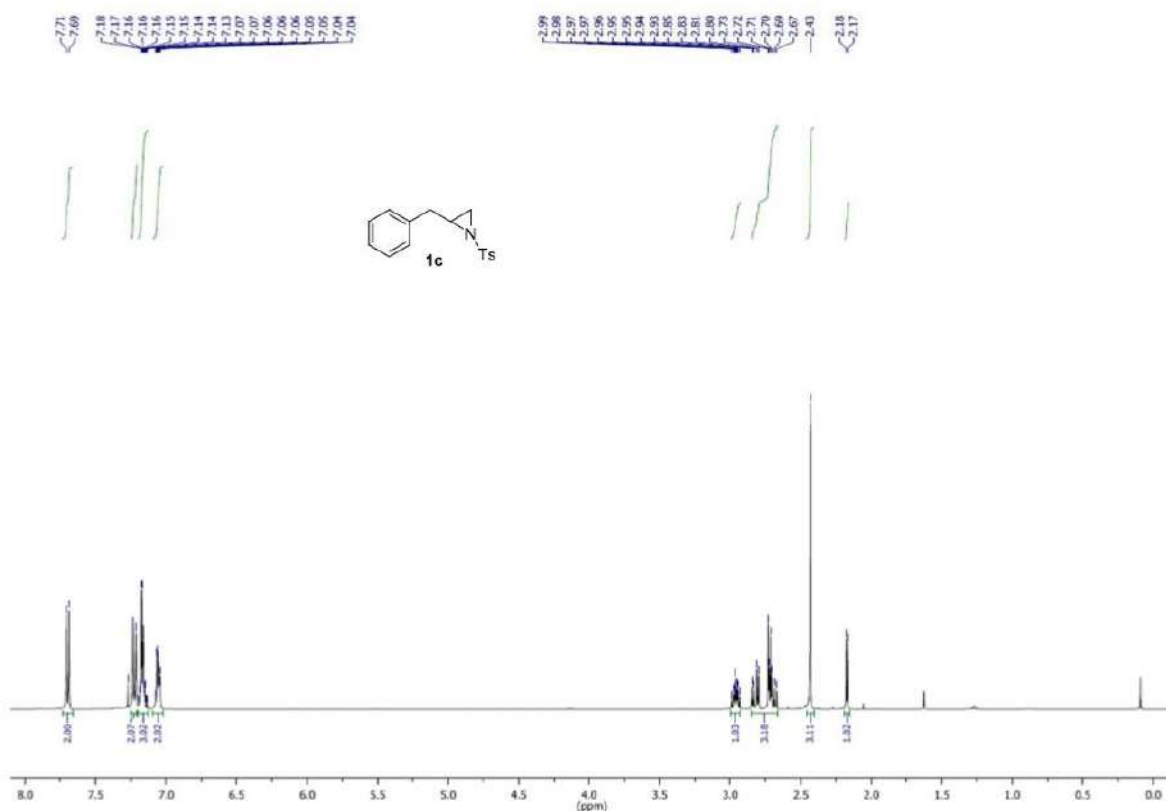


Figure S7. <sup>1</sup>H NMR (CDCl<sub>3</sub>, 400 MHz) spectrum of compound **1c**.

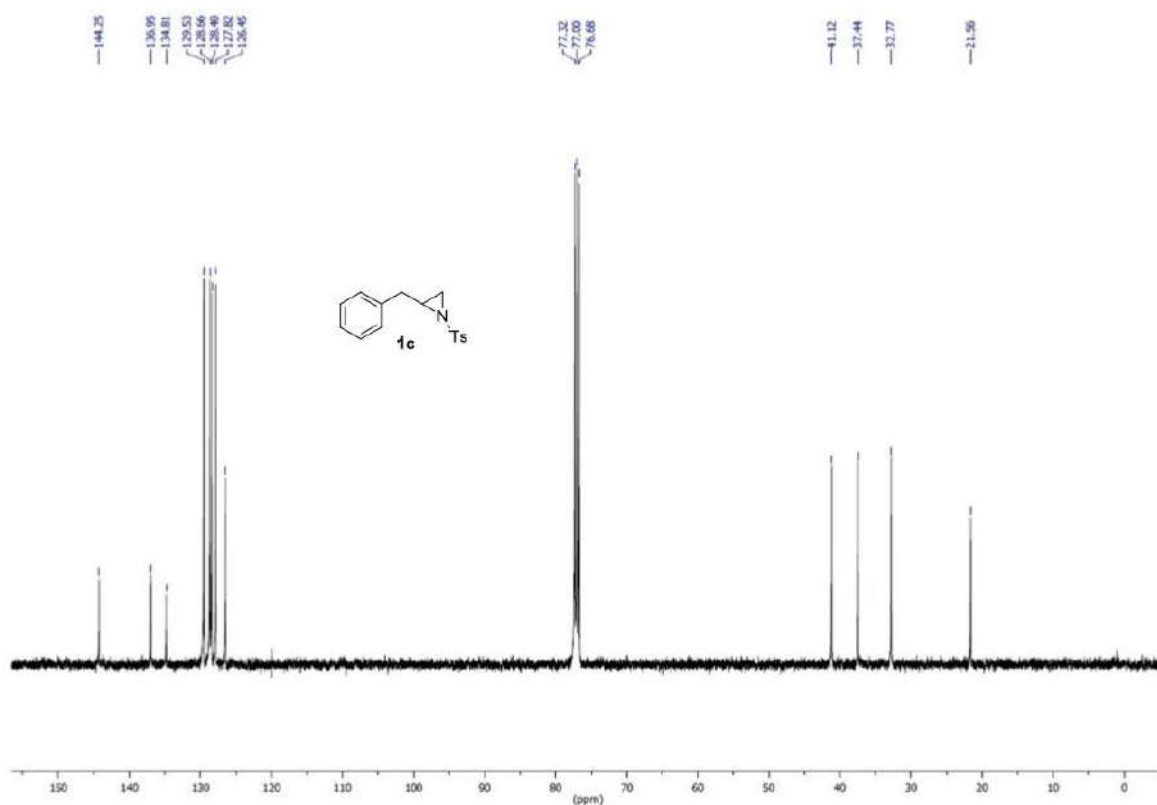


Figure S8. <sup>13</sup>C NMR (CDCl<sub>3</sub>, 101 MHz) spectrum of compound **1c**.

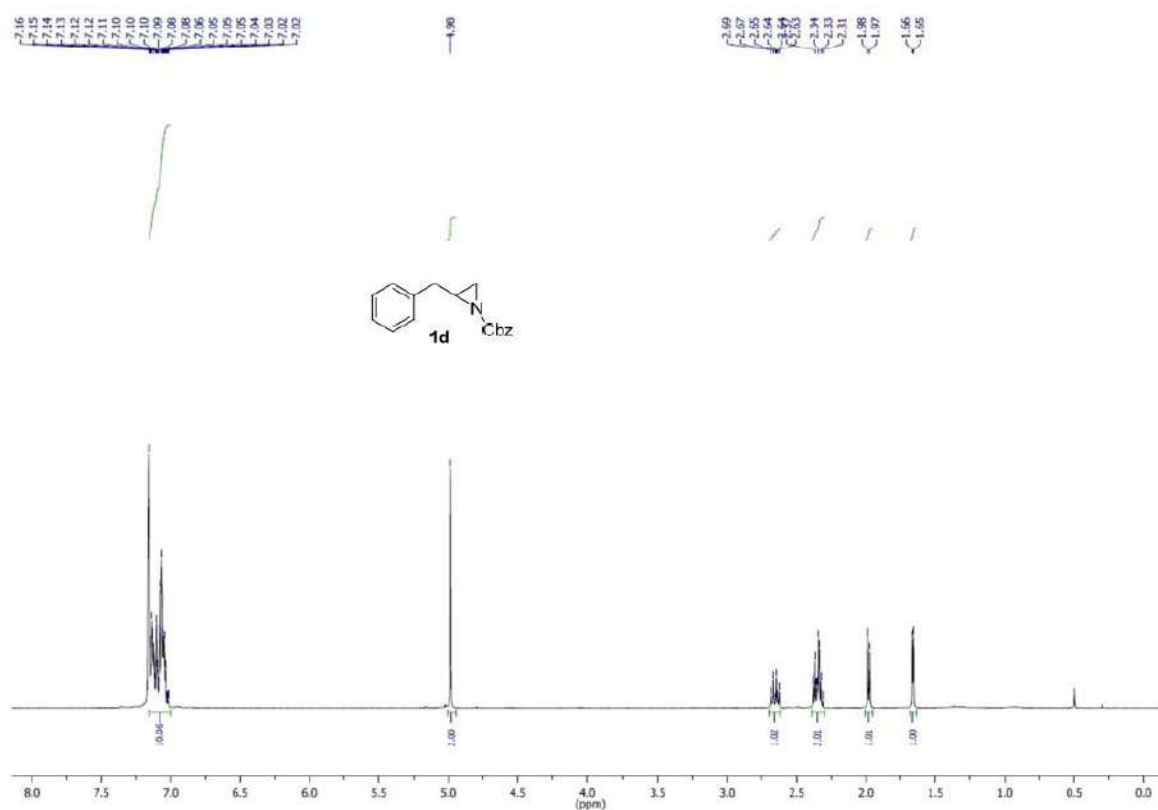


Figure S9. <sup>1</sup>H NMR (C<sub>6</sub>D<sub>6</sub>, 400 MHz) spectrum of compound **1d**.

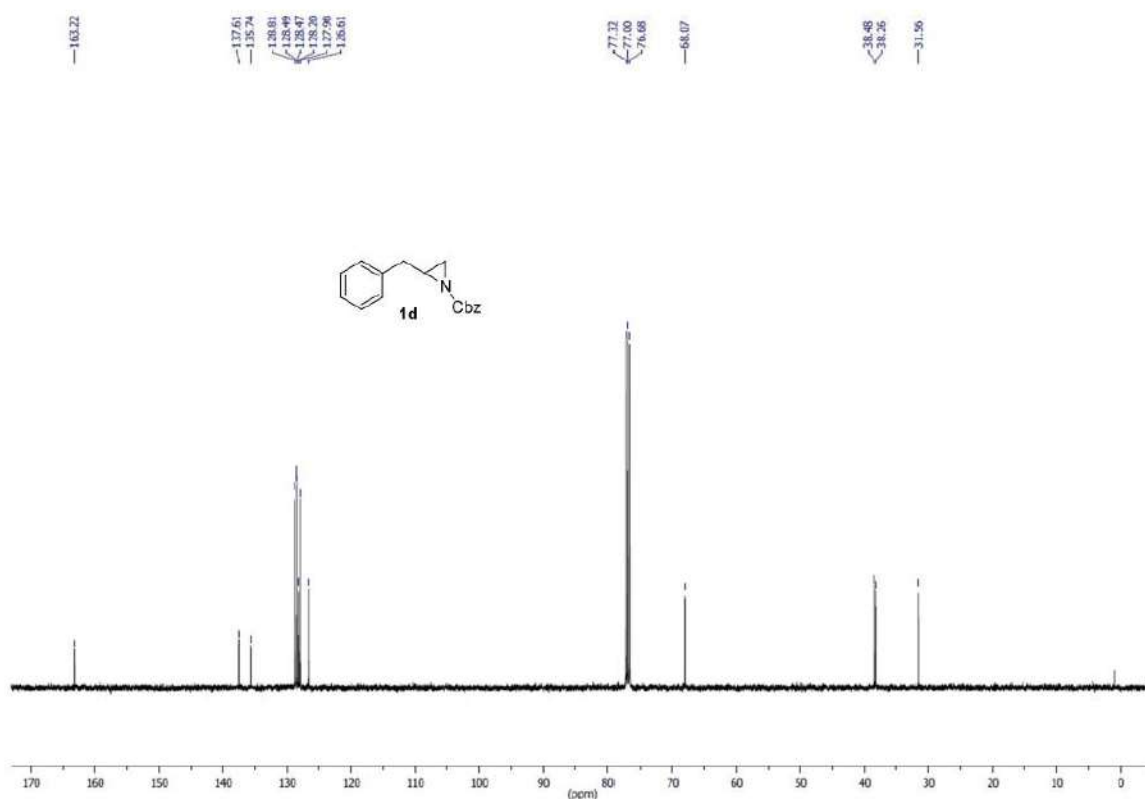
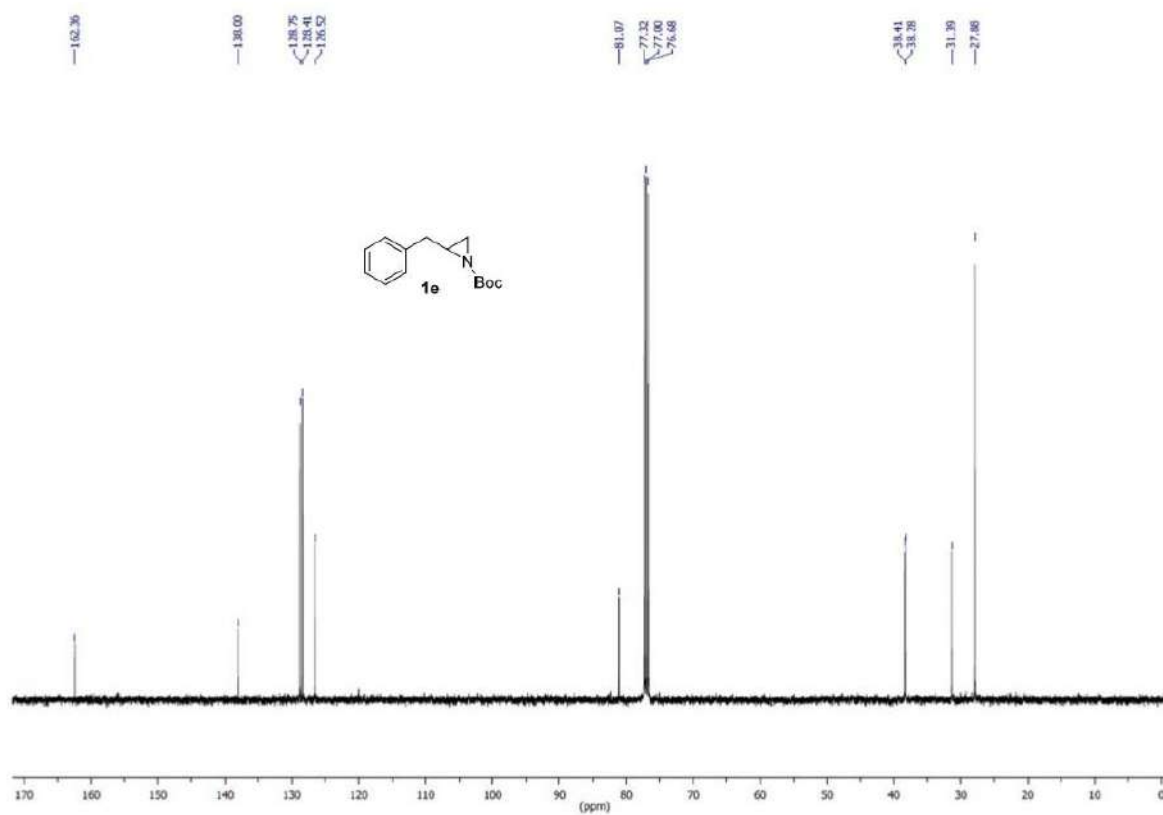
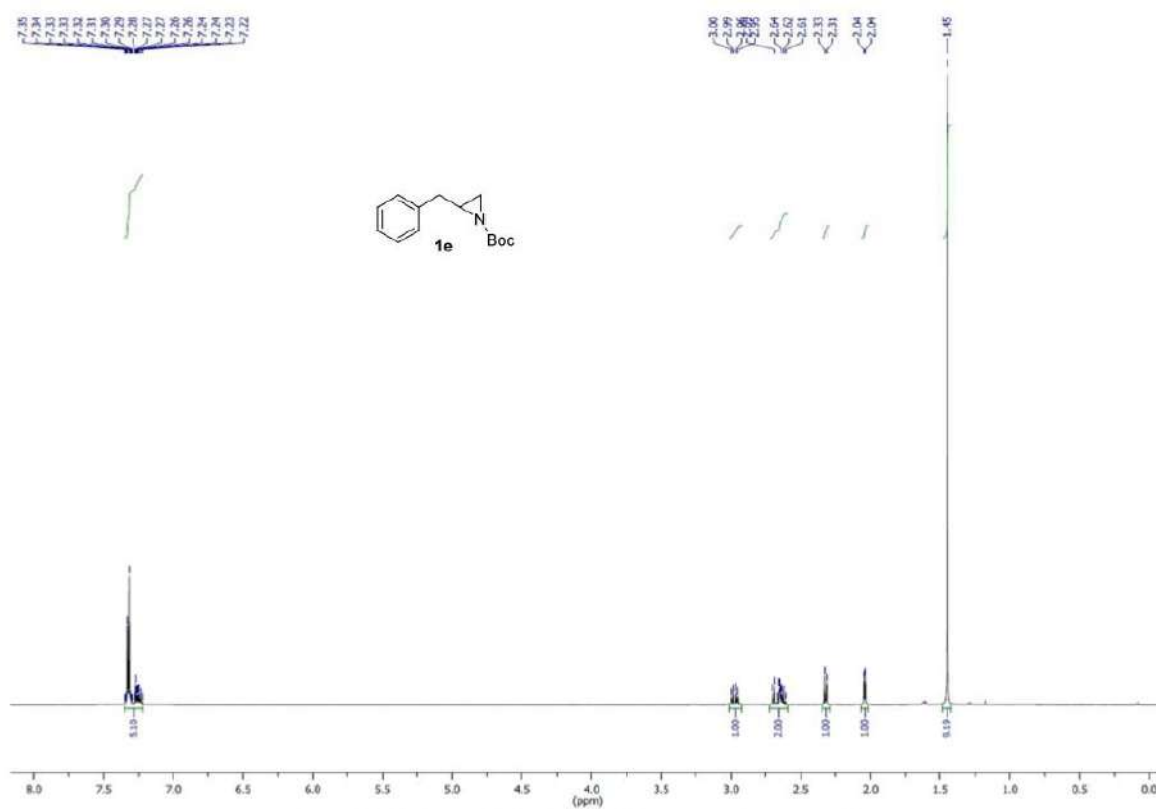


Figure S10. <sup>13</sup>C NMR (CDCl<sub>3</sub>, 101 MHz) spectrum of compound **1d**.





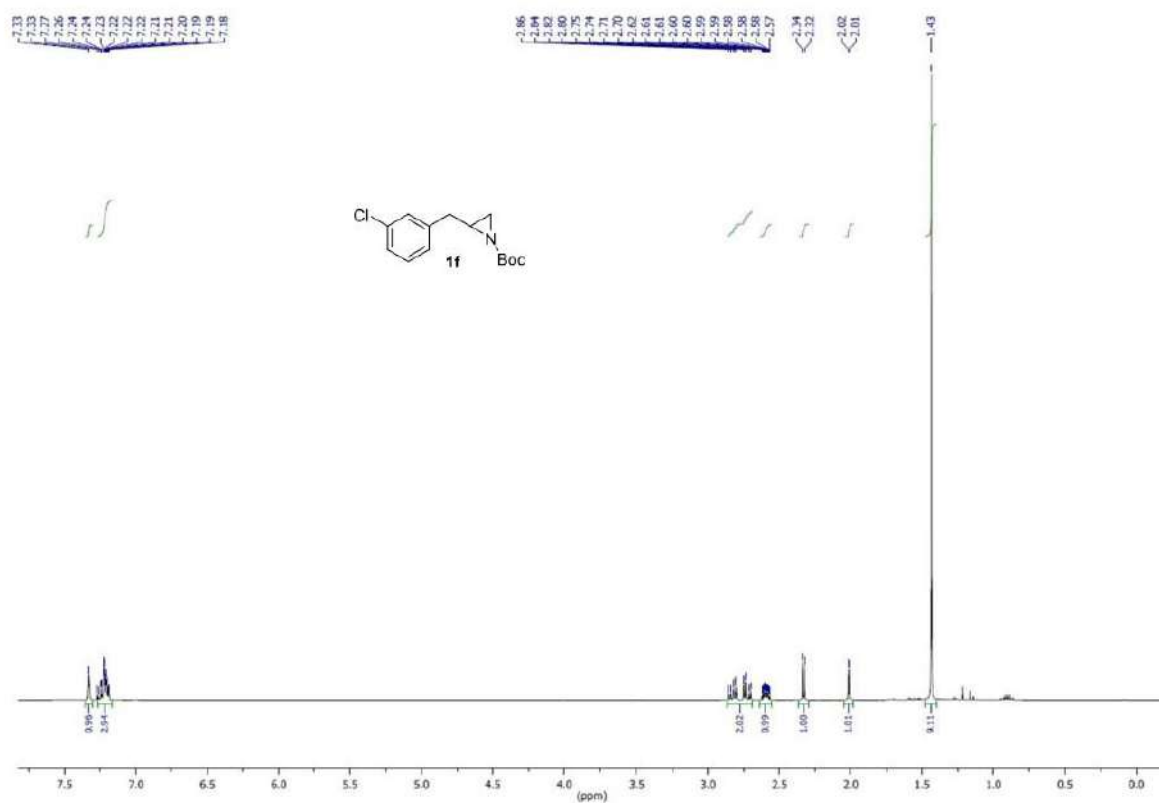


Figure S13. <sup>1</sup>H NMR (CDCl<sub>3</sub>, 400 MHz) spectrum of compound **1f**.

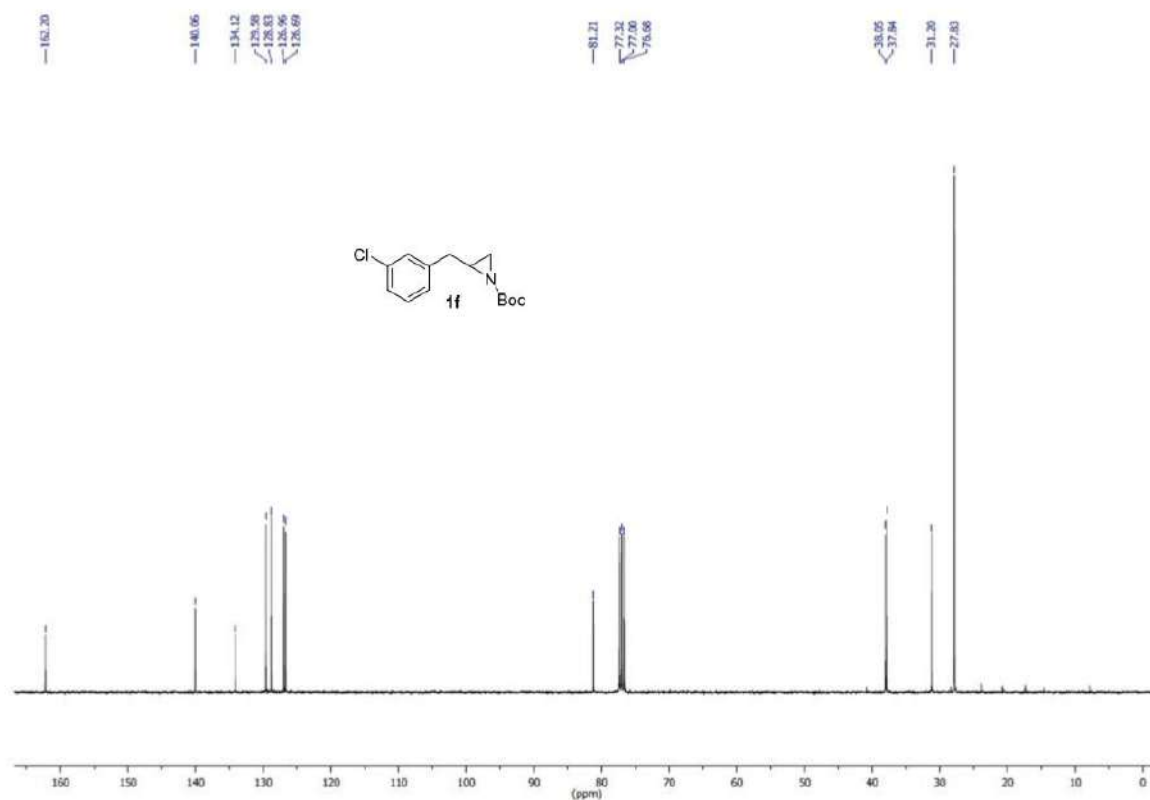


Figure S14. <sup>13</sup>C NMR (CDCl<sub>3</sub>, 101 MHz) spectrum of compound **1f**.

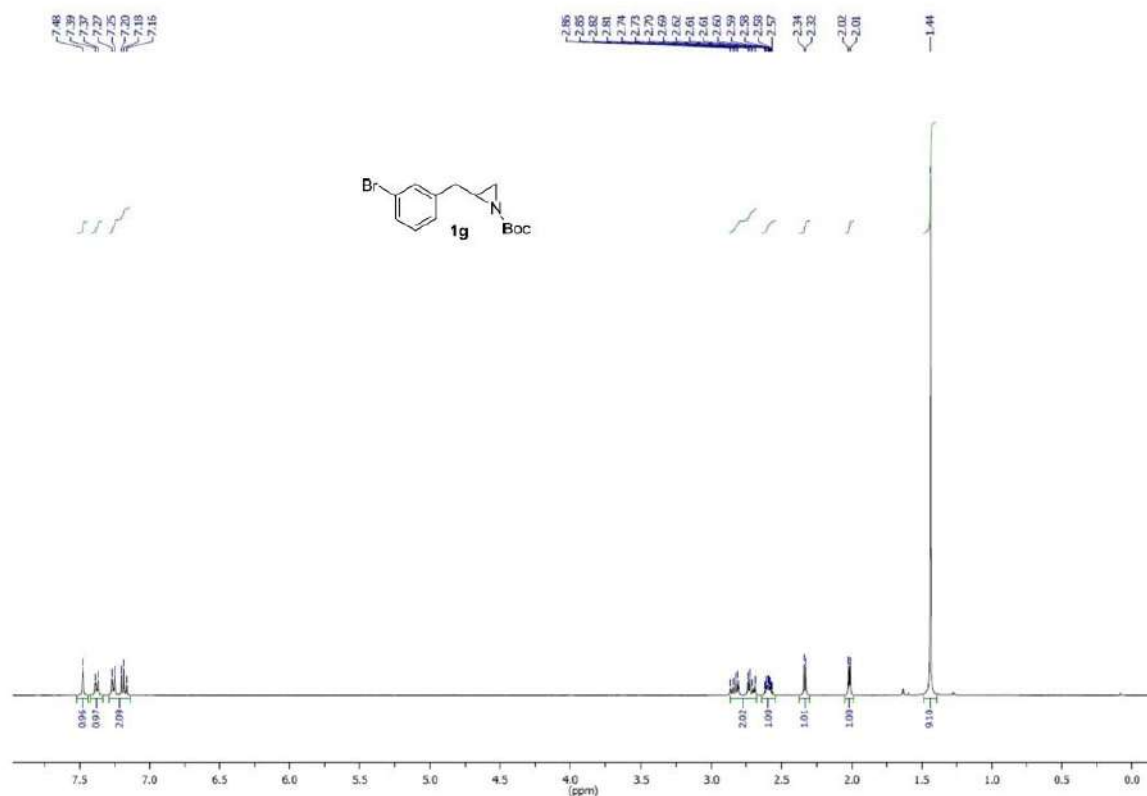


Figure S15. <sup>1</sup>H NMR (CDCl<sub>3</sub>, 400 MHz) spectrum of compound **1g**.

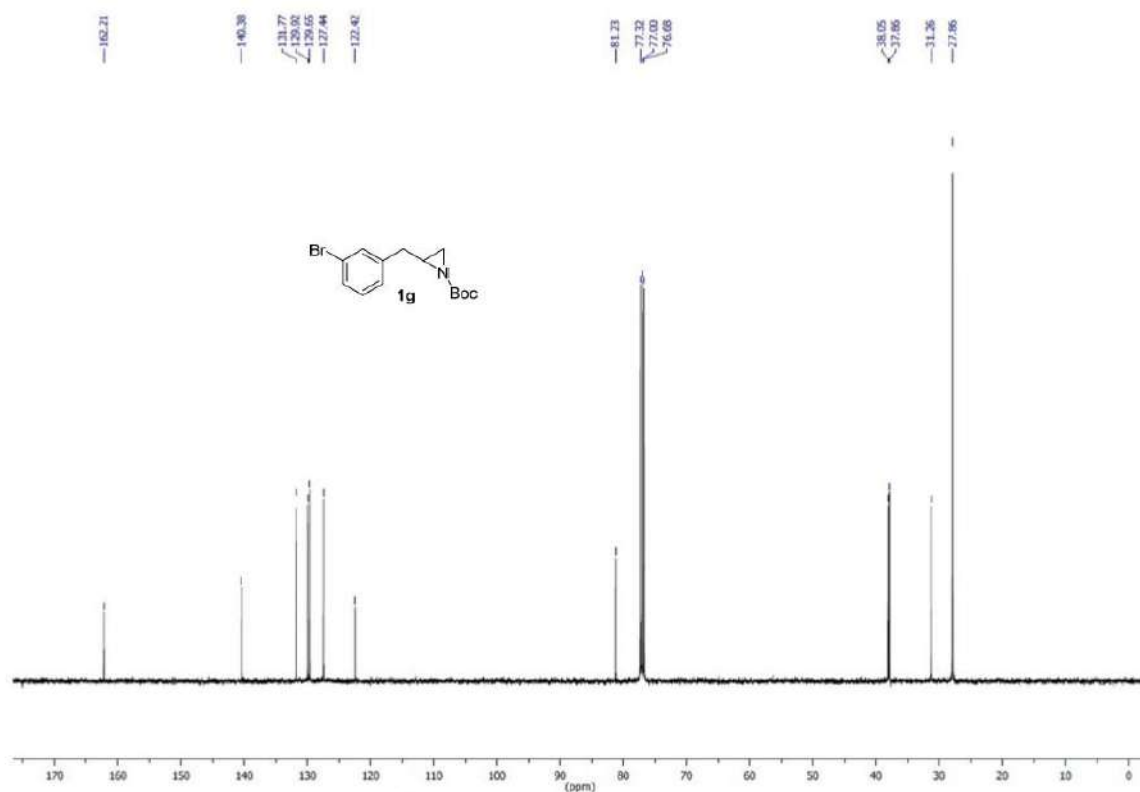
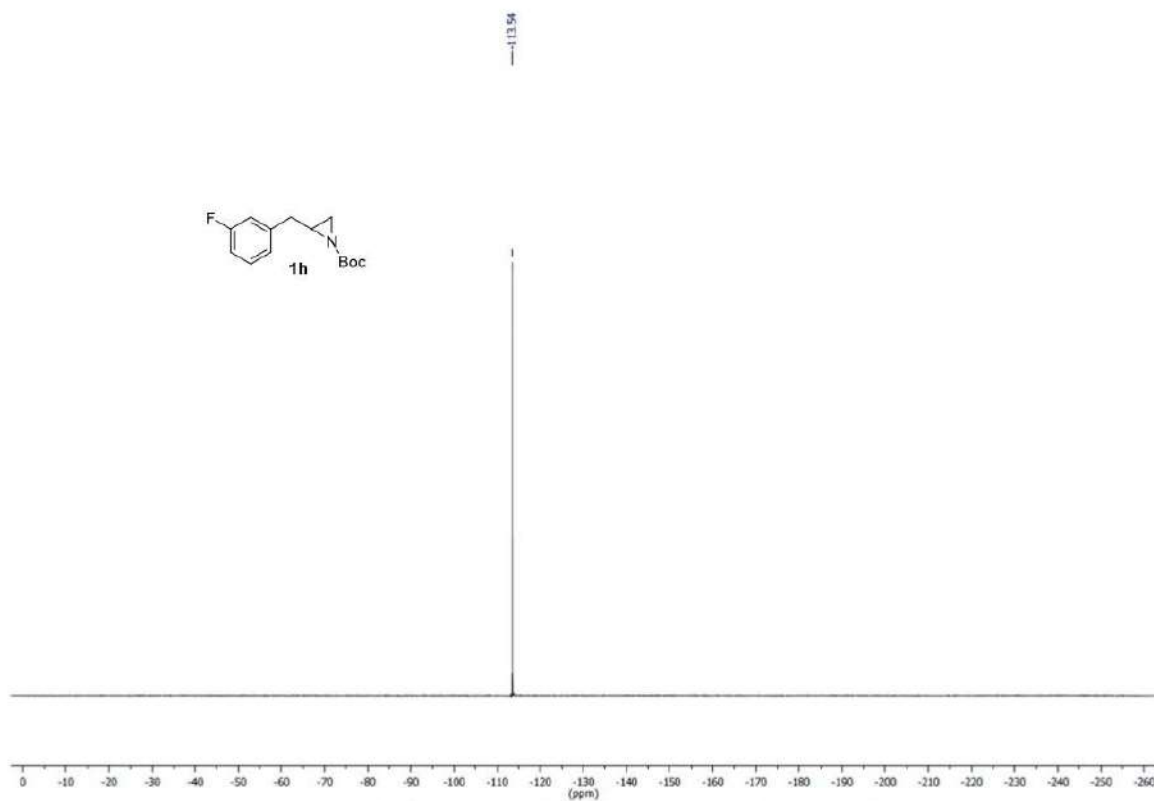


Figure S16. <sup>13</sup>C NMR (CDCl<sub>3</sub>, 101 MHz) spectrum of compound **1g**.





**Figure S19.**  $^{19}\text{F}\{^1\text{H}\}$  NMR ( $\text{CDCl}_3$ , 376 MHz) spectrum of compound **1h**.

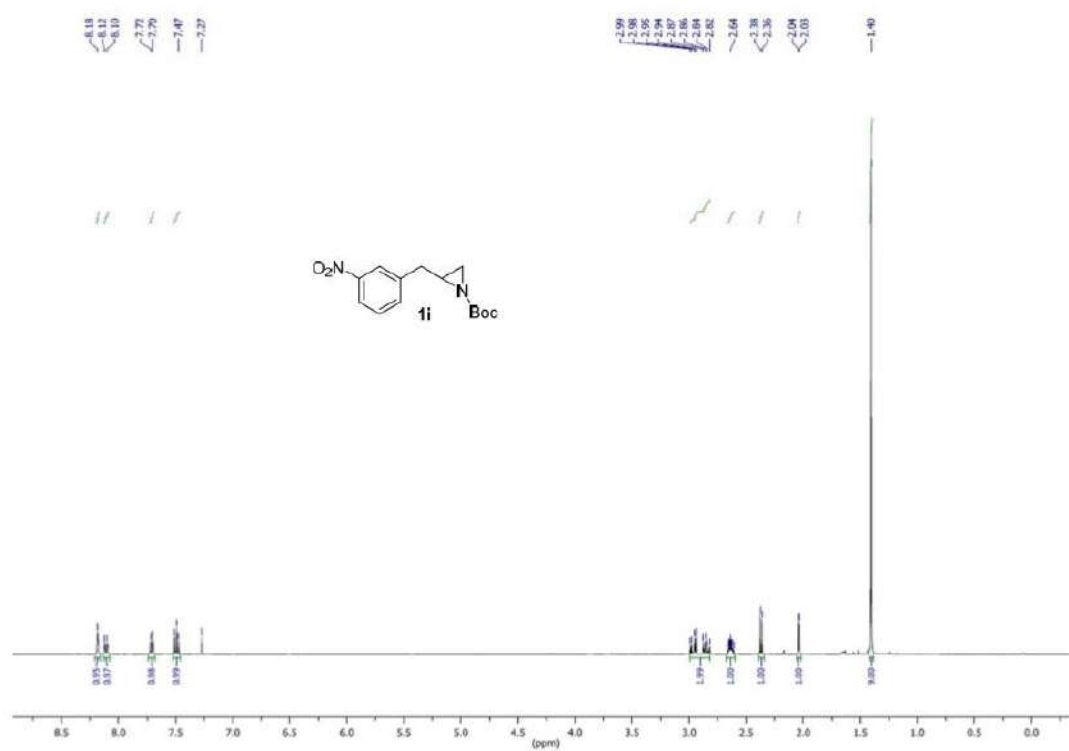


Figure S20. <sup>1</sup>H NMR (CDCl<sub>3</sub>, 400 MHz) spectrum of compound 1i.

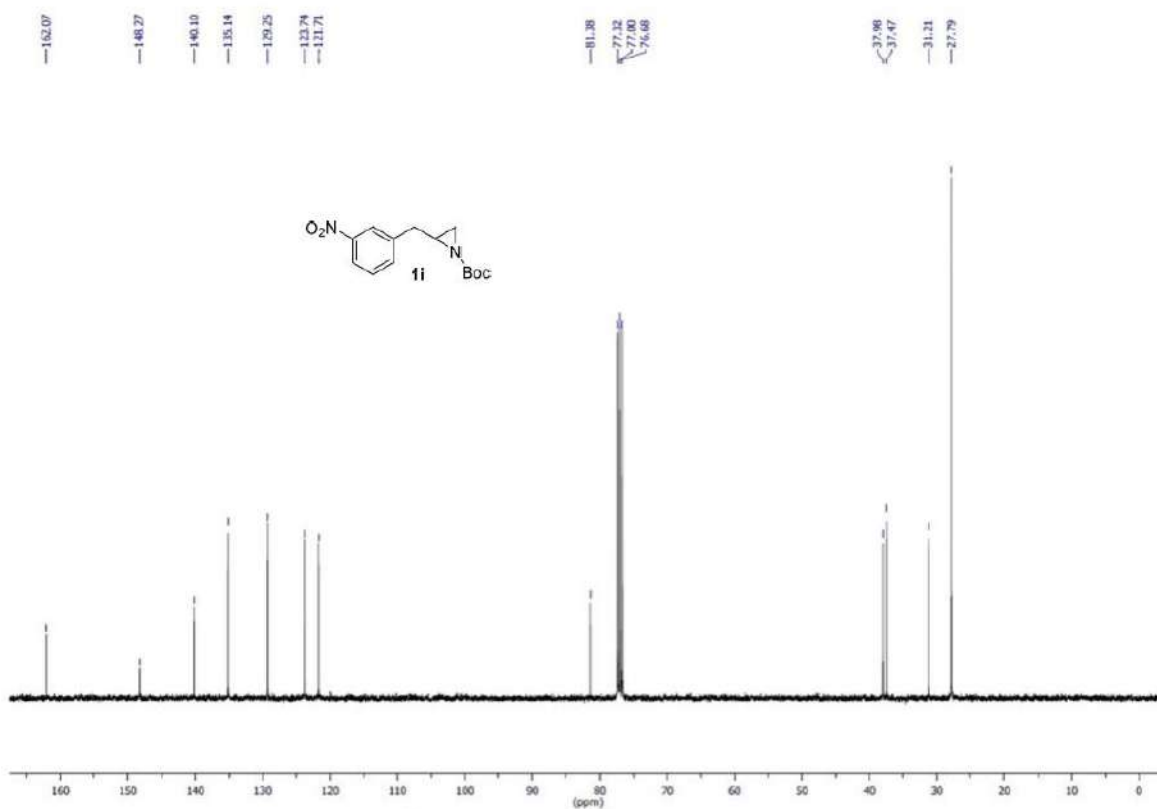
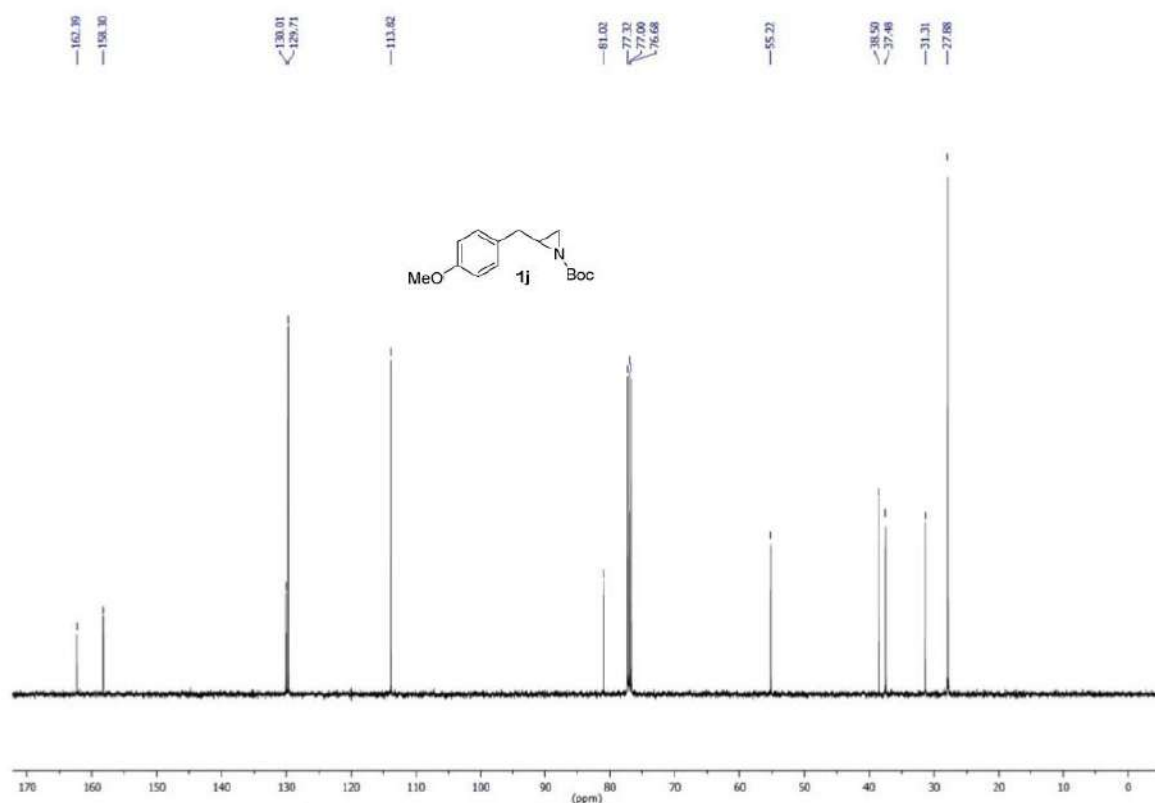
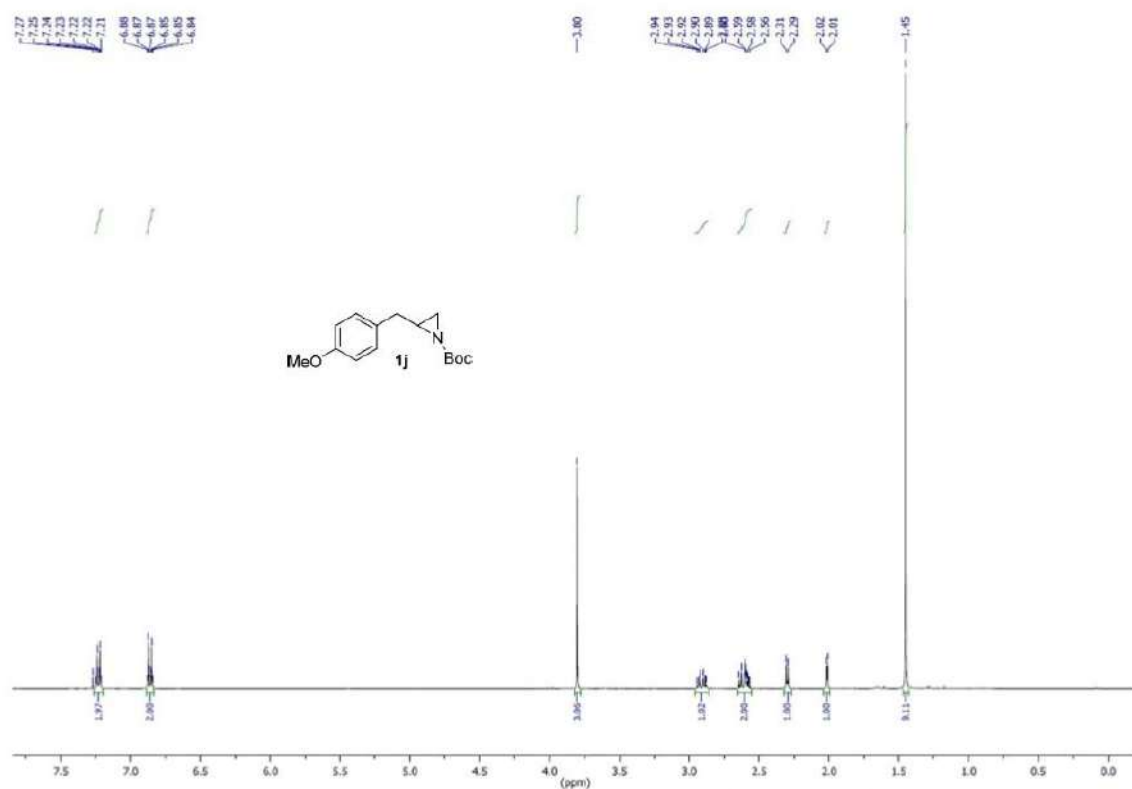
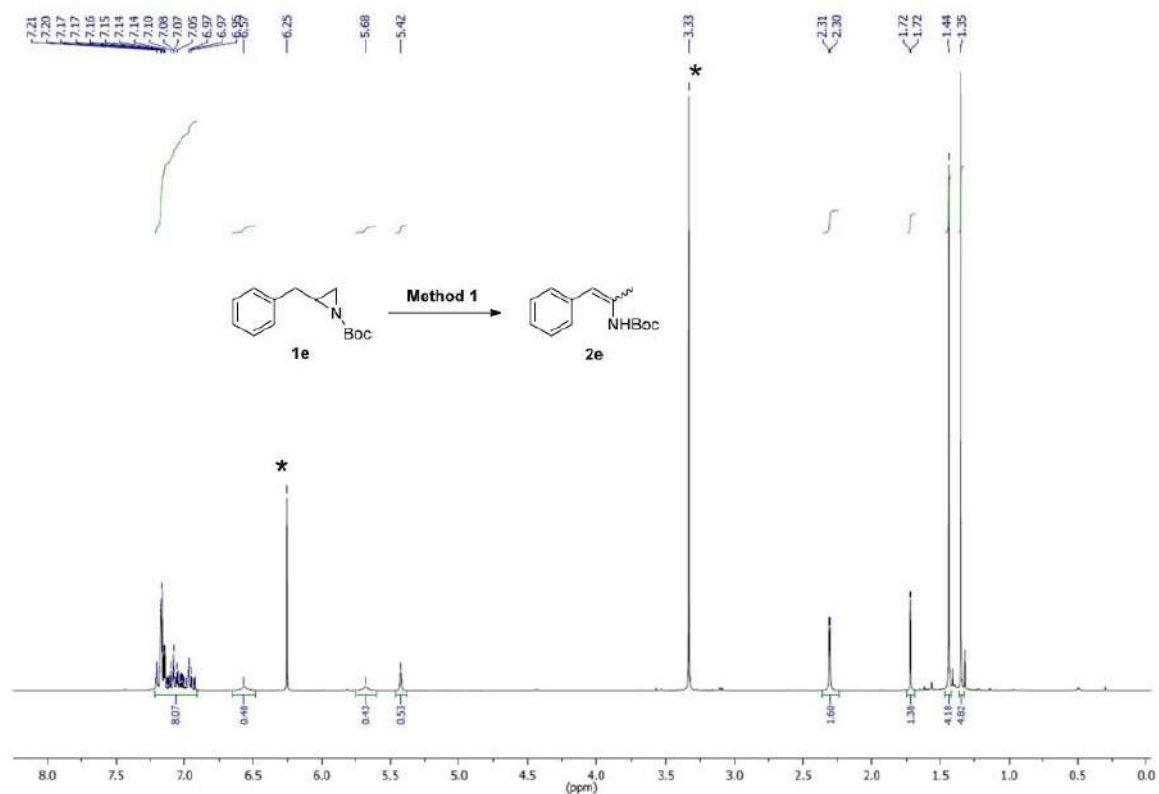
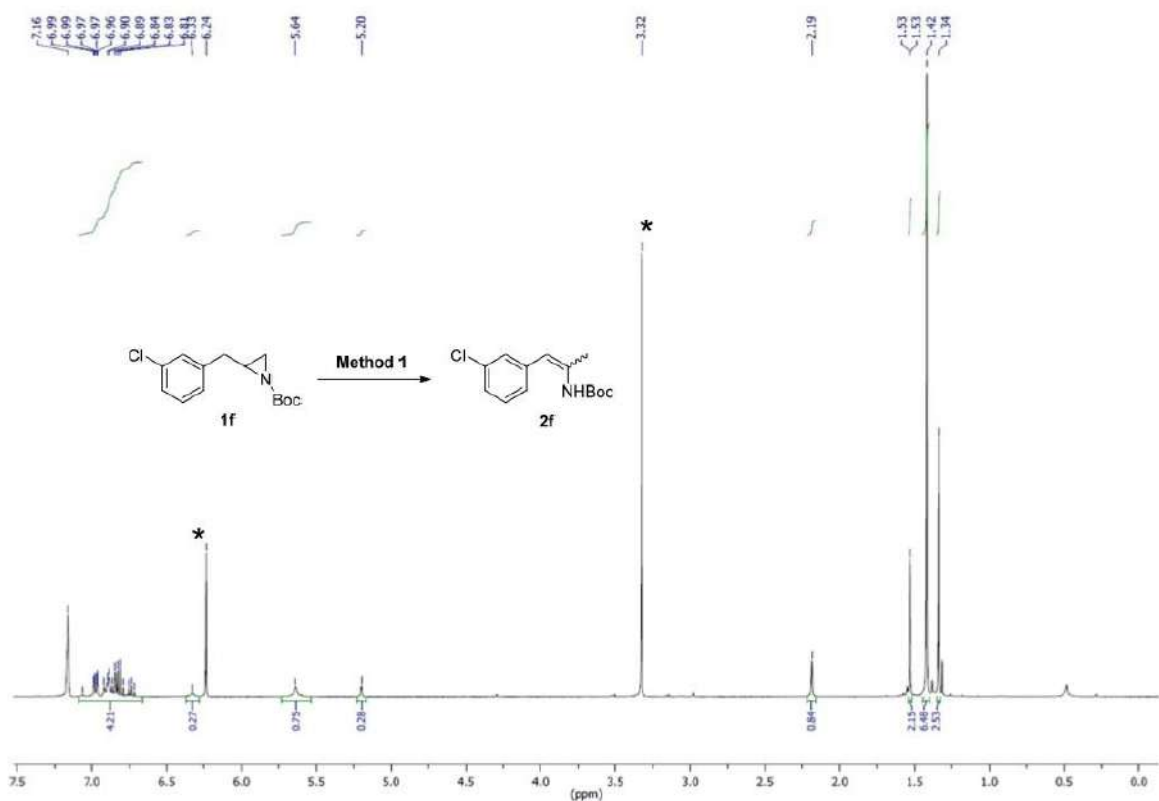


Figure S21. <sup>13</sup>C NMR (CDCl<sub>3</sub>, 101 MHz) spectrum of compound 1i.

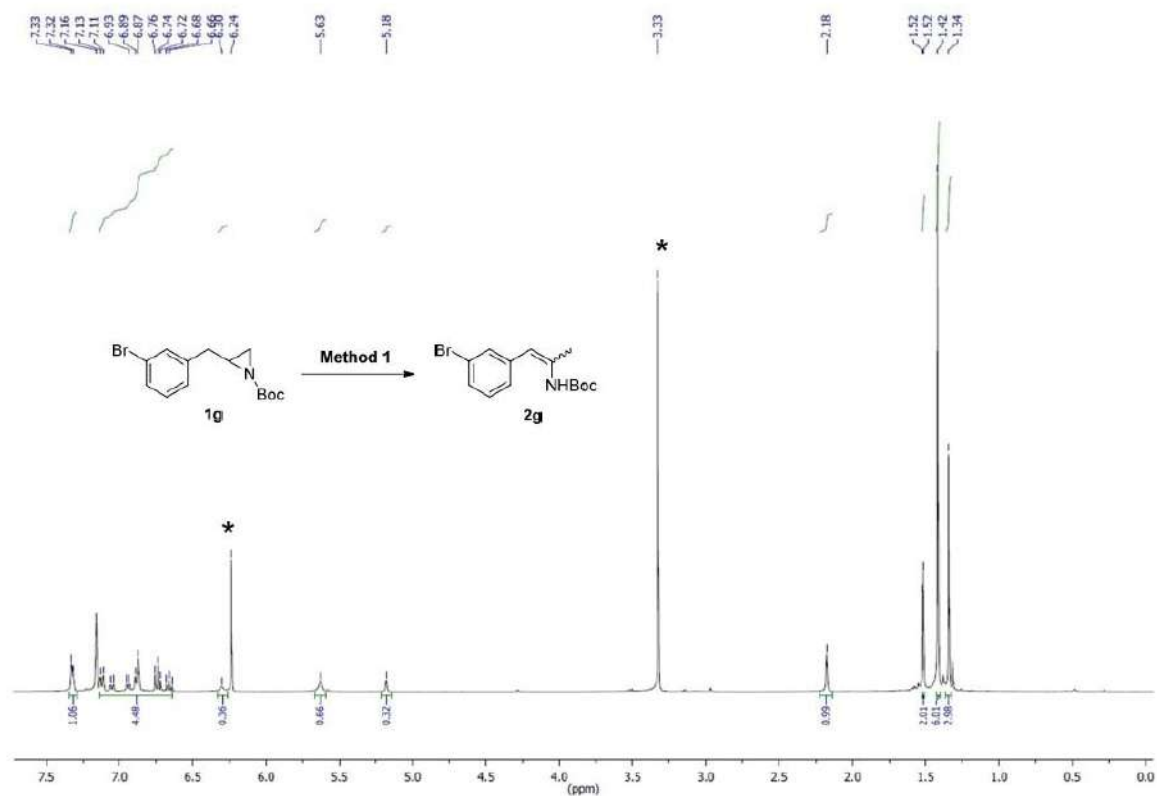




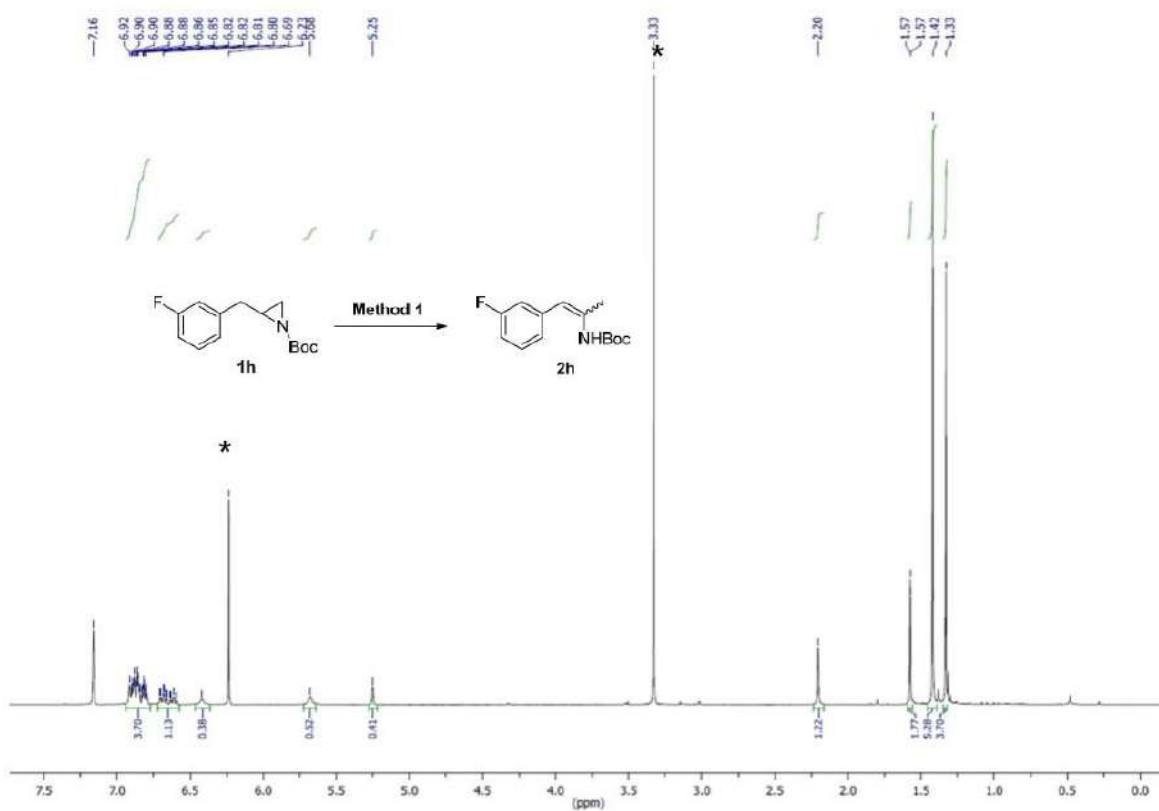
**Figure S24.**  $^1\text{H}$  NMR ( $\text{C}_6\text{D}_6$  (#), 400 MHz) spectrum: isomerization of **1e** into **2e** including the internal standard (\*).



**Figure S25.**  $^1\text{H}$  NMR ( $\text{C}_6\text{D}_5$  (#), 400 MHz) spectrum: isomerization of **1f** into **2f** including the internal standard (\*).



**Figure S26.** <sup>1</sup>H NMR (C<sub>6</sub>D<sub>6</sub> (#), 400 MHz) spectrum: isomerization of **1g** into **2g** including the internal standard (\*).



**Figure S27.** <sup>1</sup>H NMR (C<sub>6</sub>D<sub>6</sub> (#), 400 MHz) spectrum: isomerization of **1h** into **2h** including the internal standard (\*).



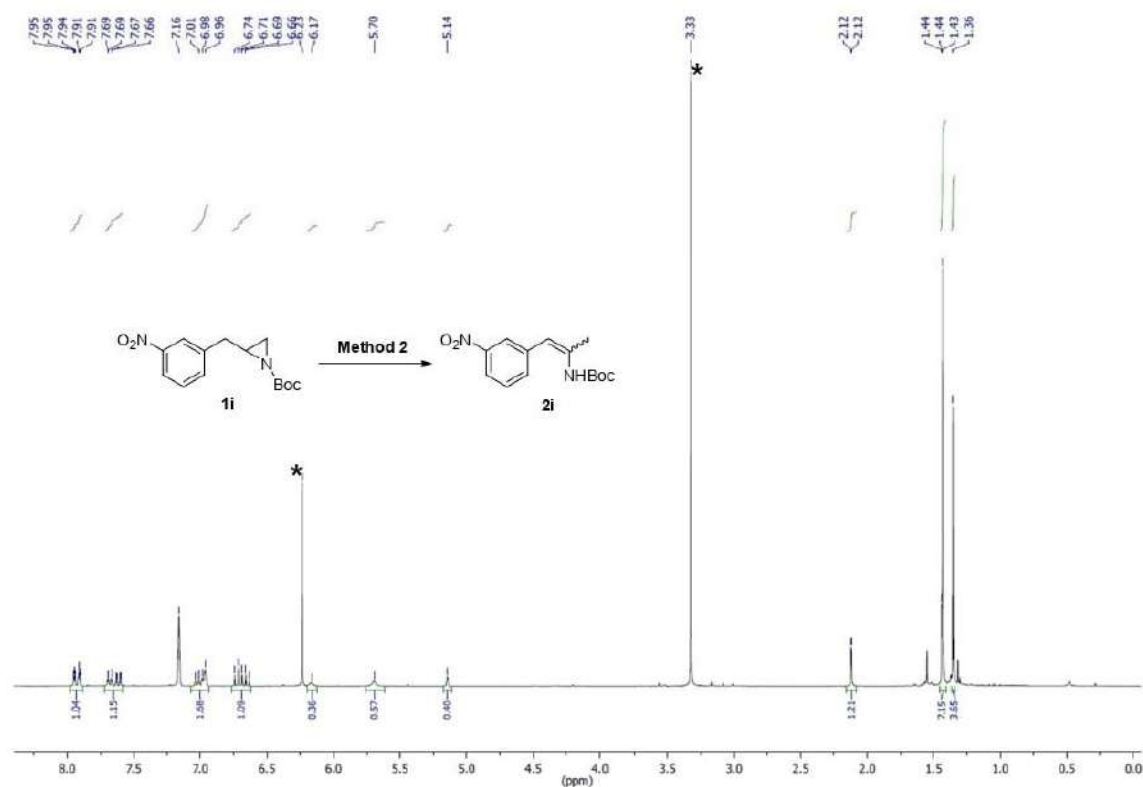


Figure S28. <sup>1</sup>H NMR (C<sub>6</sub>D<sub>6</sub> (#), 400 MHz) spectrum: isomerization of **1i** into **2i** including the internal standard (\*).

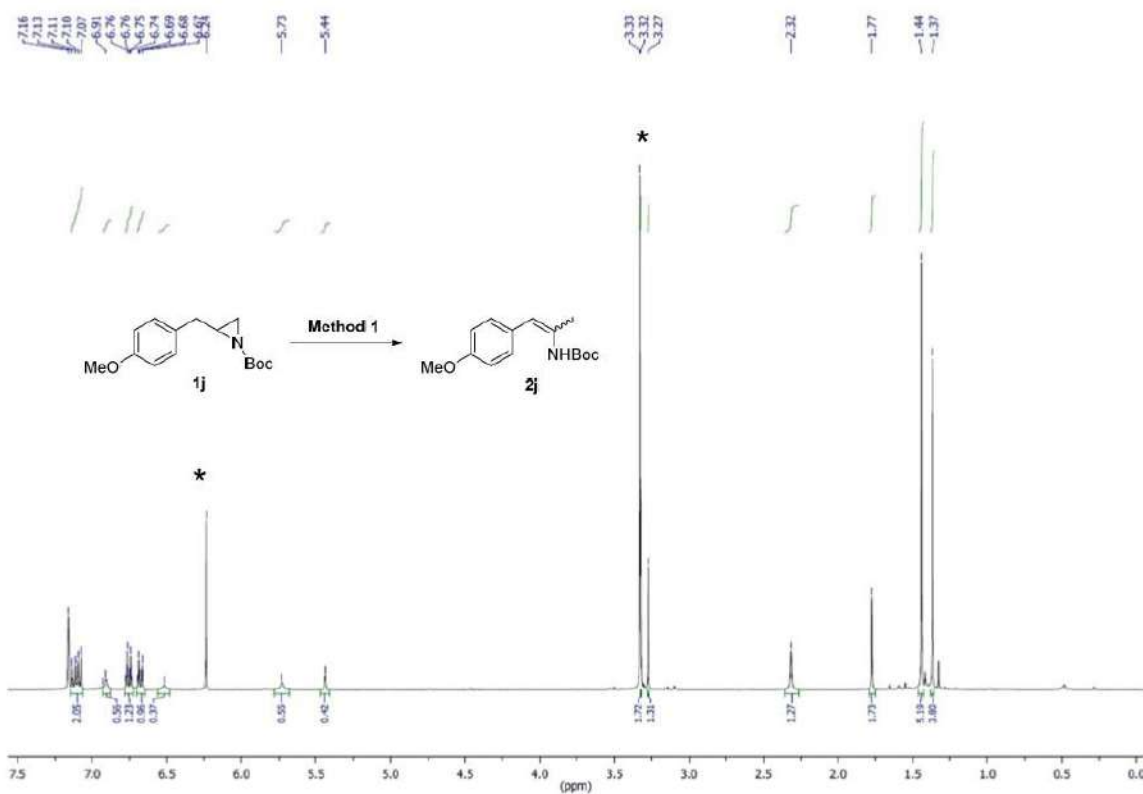


Figure S29. <sup>1</sup>H NMR (C<sub>6</sub>D<sub>6</sub> (#), 400 MHz) spectrum: isomerization of **1j** into **2j** including the internal standard (\*).

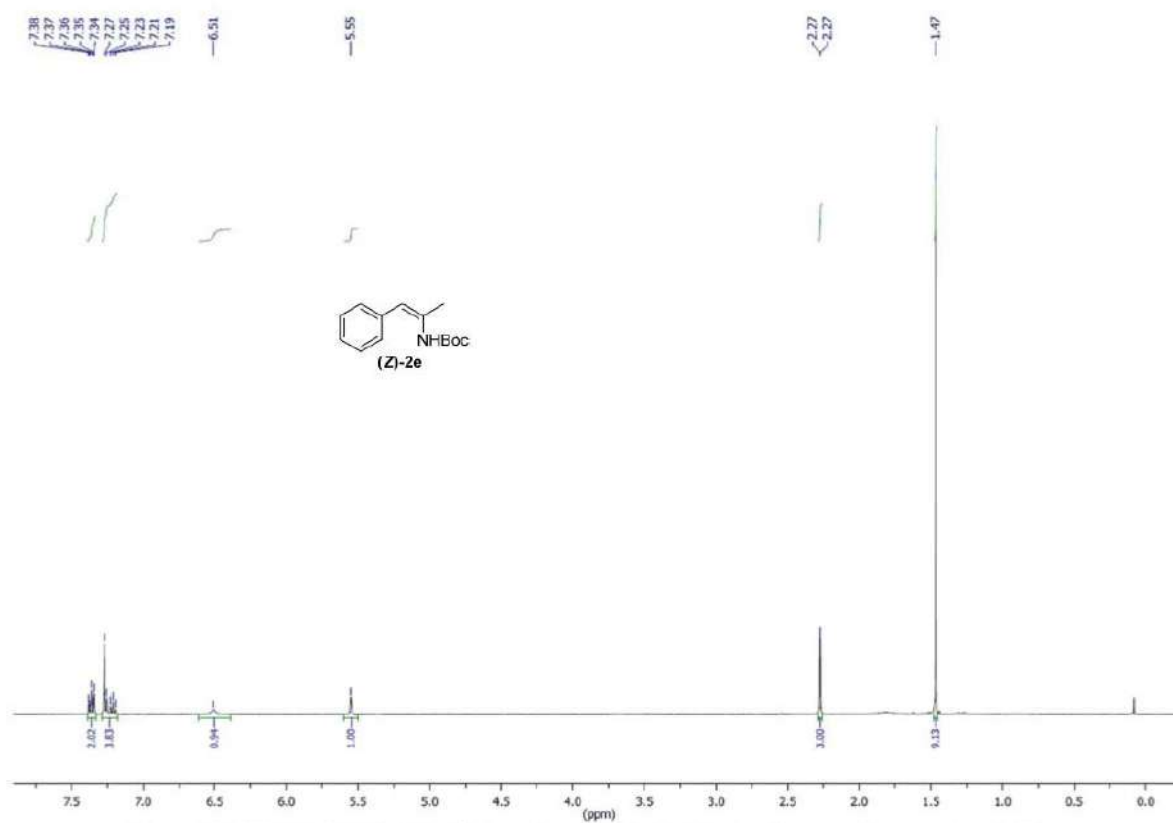


Figure S30. <sup>1</sup>H NMR (CDCl<sub>3</sub>, 300 MHz) spectrum: isolated (Z)-2e from the up-scaling experiment of 1e.

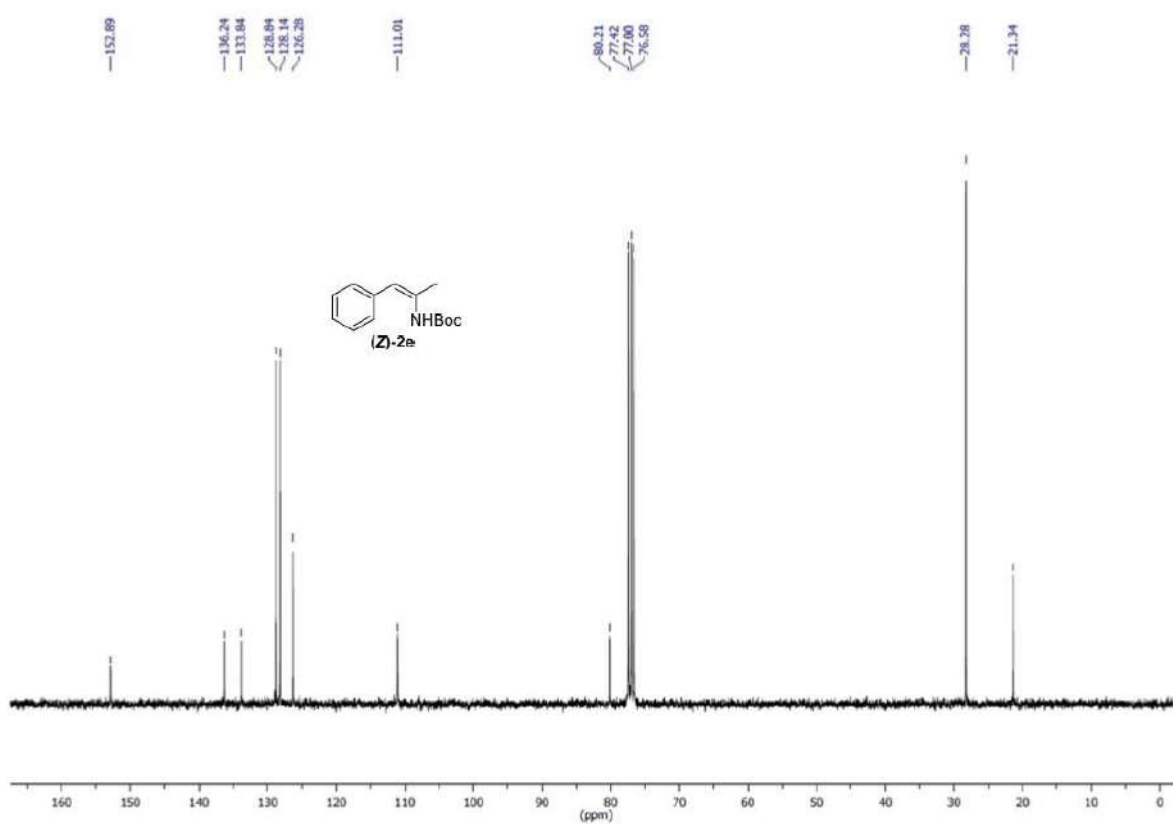


Figure S31. <sup>13</sup>C NMR (CDCl<sub>3</sub>, 75 MHz) spectrum: isolated (Z)-2e from the up-scaling experiment of 1e.

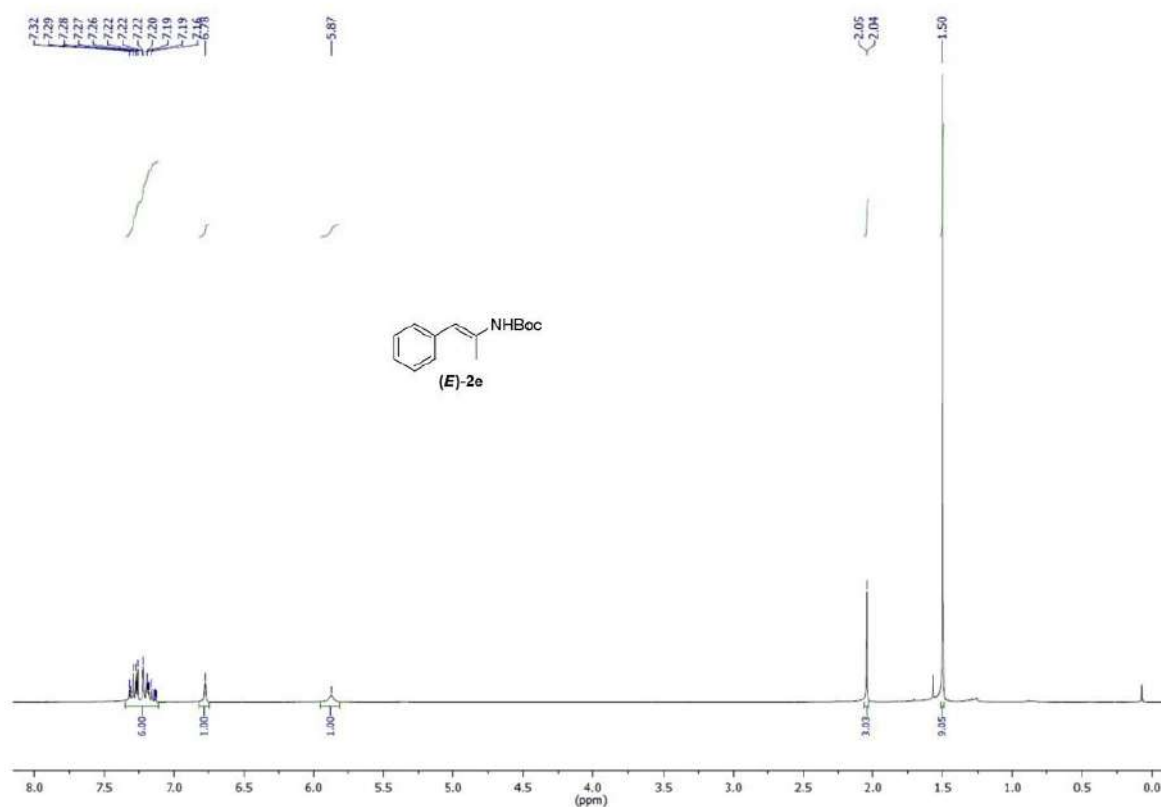


Figure S32. <sup>1</sup>H NMR (CDCl<sub>3</sub>, 300 MHz) spectrum: isolated (E)-2e from the up-scaling experiment of 1e.

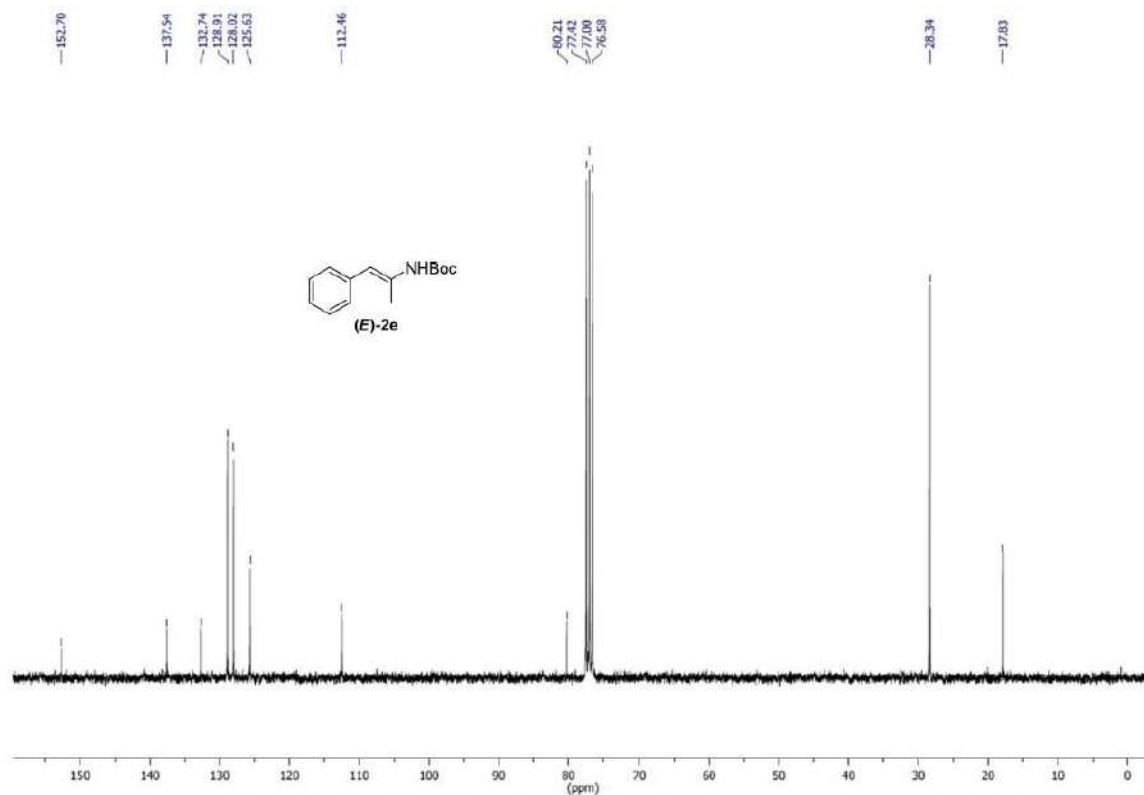


Figure S33. <sup>13</sup>C NMR (CDCl<sub>3</sub>, 75 MHz) spectrum: isolated (E)-2e from the up-scaling experiment of 1e.

## 8. References

1. Jürgens, E.; Wucher, B.; Rominger, F.; Törnroos, K. W.; Kunz, D. Selective rearrangement of terminal epoxides into methylketones catalysed by a nucleophilic rhodium-NHC-pincer complex. *Chem. Commun.* **2015**, *51*, 1897-900.
2. Tian, Y.; Jürgens, E.; Kunz, D. Regio- and chemoselective rearrangement of terminal epoxides into methyl alkyl and aryl ketones. *Chem. Commun.* **2018**, *54*, 11340-11343.
3. Tian, Y.; Jürgens, E.; Mill, K.; Jordan, R.; Maulbetsch, T.; Kunz, D. Nucleophilic Isomerization of Epoxides by Pincer-Rhodium Catalysts: Activity Increase and Mechanistic Insights. *ChemCatChem* **2019**, *11*, 4028-4035.
4. Buckley, B. R.; Patel, A. P.; Wijayantha, K. G. U. Observations on the Modified Wenker Synthesis of Aziridines and the Development of a Biphasic System. *J. Org. Chem.* **2013**, *78*, 1289-1292.
5. Bates, G. S.; Varelas, M. A. A mild, general preparation of N-acyl aziridines and 2-substituted 4(S)-benzyloxazolines. *Can. J. Chem.* **1980**, *58*, 2562-2566.
6. Okoromoba, O. E.; Li, Z.; Robertson, N.; Mashuta, M. S.; Couto, U. R.; Tormena, C. F.; Xu, B.; Hammond, G. B. Achieving regio- and stereo-control in the fluorination of aziridines under acidic conditions. *Chem. Commun.* **2016**, *52*, 13353-13356.
7. Sasaki, M.; Yudin, A. K. Oxidative Cycloamination of Olefins with Aziridines as a Versatile Route to Saturated Nitrogen-Containing Heterocycles. *J. Am. Chem. Soc.* **2003**, *125*, 14242-14243.
8. Braga, A. L.; Lüdtke, D. S.; Paixão, M. W.; Alberto, E. E.; Stefani, H. A.; Juliano, L. Straightforward Synthesis of Non-Natural Selenium Containing Amino Acid Derivatives and Peptides. *Eur. J. Org. Chem.* **2005**, 4260-4264.
9. Cañellas, S.; Alonso, P.; Pericàs, M. À. Development of C<sub>2</sub>-Symmetric Chiral Bifunctional Triamines: Synthesis and Application in Asymmetric Organocatalysis. *Org. Lett.* **2018**, *20*, 4806-4810.

## Abbreviations

acac	acetylacetonate
bimca	1,8-bis(imidazolin-2-ylidene)-3,6-di( <i>tert</i> -butyl)carbazolide
Boc	<i>tert</i> -butyloxycarbonyl
b.p.	boiling point
Cbz	benzyloxycarbonyl
COD	1,5-cyclooctadiene
COSY	correlation spectroscopy
DCM	dichloromethane
DMF	N,N'-dimethylformamide
DMSO	dimethyl sulfoxide
eq	equivalent
EtOAc	ethyl acetate
FG	functional group
HMBC	heteronuclear multiple bond correlation
HOMO	highest occupied molecular orbital
HSQC	heteronuclear single quantum coherence
<i>i</i> Bu	2-methylpropyl
-I-effect	electron-withdrawing inductive effect
<i>i</i> Pr	<i>iso</i> -propyl
KHMDS	potassium bis(trimethylsilyl)amide
LiHMDS	lithium bis(trimethylsilyl)amide
LUMO	lowest unoccupied molecular orbital
<i>m</i> -CPBA	<i>meta</i> -chloroperoxybenzoic acid
+M-effect	mesomeric effect
m.p.	melting point
<i>n</i> Bu	butyl
NHCs	N-heterocyclic carbenes
<sup>n</sup> <i>J</i>	coupling constant over n bonds
NMR	nuclear magnetic resonance
NOE	nuclear overhauser effect
PG	protecting group

## Abbreviations

---

rt	room temperature
<i>t</i> Bu	<i>tert</i> -butyl
TEA	triethylamine
Tf	trifluoromethanesulfonate
THF	tetrahydrofuran
Ts	4-toluenesulfonyl

## List of Publications

### Journal Papers

Y. Tian, E. Jürgens, D. Kunz, Regio- and chemoselective rearrangement of terminal epoxides into methyl alkyl and aryl ketones, *Chem. Commun.*, **2018**, *54*, 11340-11343.

Y. Tian, E. Jürgens, K. Mill, R. Jordan, T. Maulbetsch, D. Kunz, Nucleophilic Isomerization of Epoxides by Pincer-Rhodium Catalysts: Activity Increase and Mechanistic Insights, *ChemCatChem*, **2019**, *11*, 4028-4035.

Y. Tian, T. Maulbetsch, R. Jordan, K. W. Törnroos, D. Kunz, Synthesis and Reactivity of Cobalt(I) and Iridium(I) Complexes Bearing a Pentadentate *N*-Homoallyl Substituted Bis(NHC) Pincer-Ligand. *Organometallics*, **2020**, *39*, 1221-1229.

Y. Tian, D. Kunz, Nucleophilic Rh<sup>I</sup> Catalyzed Selective Isomerization of Terminal Aziridines to Enamides, *ChemCatChem*, **2020**, DOI: 10.1002/cctc.202000597.

### Presentations

#### Oral presentation

Homogeneous Catalysis with Group 9 Bis(NHC)-Pincer Complexes, inorganic seminar, University of Tübingen, **2019**.

#### Poster presentations

Rh-Catalyzed Regio- and Chemoselective Rearrangement of Epoxides and Aziridines, 20<sup>th</sup> Organometallic Catalysis Directed Towards Organic Synthesis (OMCOS), July 21-25, **2019**, Heidelberg, Germany.

Rh-Catalyzed Regio- and Chemoselective Rearrangement of Terminal Epoxides into Methyl Alkyl and Aryl Ketones, 28<sup>th</sup> International Conference on Organometallic Chemistry (ICOMC), July 15-20, **2018**, Florence, Italy.

## *List of Publications*

---

A Highly Active and Selective Catalyst for the Nucleophilic Meinwald Rearrangement of Terminal Epoxides into Methyl Ketones, ACS on campus, October 10-11, **2018**, Heidelberg, Germany.

Rhodium Catalyzed Meinwald Rearrangement of Terminal Epoxides to Ketones, Anglo-German Inorganic Chemistry Conference (AGICHEM), August 6-9, **2017**, Göttingen, Germany.



## **Acknowledgement**

This PhD thesis has been achieved with the sincere help and support from the people who are acknowledged here.

I am extremely grateful to Prof. Dr. Doris Kunz, for accepting me as a doctoral candidate in her group, providing such interesting research topics and being so supportive not only in the lab but also during daily life. The enlightening guidance and constant encouragement from her throughout these years enabled me to develop my research expertise and to gain scientific experience in the field of organometallic chemistry. Without her extensive knowledge and invaluable supervisions, it would not be possible to complete this thesis.

The thanks goes to Prof. Dr. Reiner Anwander for kindly reviewing this thesis.

Thanks to the dear group members Ronja Jordan, Theo Maulbetsch, Fabio Mazzotta, Manfred Steimann, former group members and the members from Prof. Dr. Michael Seitz's group for providing such a harmonious and cooperative work atmosphere. The special thanks goes to Ronja Jordan for helping me to translate the abstract in this thesis and measuring single crystals together with Theo Maulbetsch, and Fabio Mazzotta as well for the kind help of measuring VT NMR spectra.

All my practical students Nina Franziska Liska, Mario Robin Rapp, Nicholas R. Wiedmaier, Xiaoli Su, Jan Grammel and Christina Breitenstein and Felix Kracht are thanked as well for their hard working and cooperation.

I would like to thank Dr. Klaus Eichele, Kristina Strohmaier, and Dr. Wolfgang Leis for special NMR measurements.

I appreciate the help from Dr. Dorothee Wistuba and Dr. Peter Haiss for the mass spectrometry, and Wolfgang Bock for the elemental analyses.

## *Acknowledgement*

---

The thanks also go to Prof. Dr. Karl Törnroos for helping me with X-ray measurement and analysis.

Thanks to Sabine Ehrlich for coordinating all administration affairs.

I am grateful to the China Scholarship Council for providing me financial support.

I would like to express my deep thanks to my lovely family, especially my parents for their endless love, and for their support and understanding for every decision that I have made.

Most of all, I would like to thank my dearest fiancé, Peng Zhang, who shares every exciting moments and accompanies me all these years even though we are in different countries.

## **Personal Contribution**

### **Publication 1:**

All the reactions and analyses described were planned and conducted by myself. Analyses include one dimensional ( $^1\text{H}$ ,  $^{13}\text{C}\{\text{H}\}$ ,  $^{19}\text{F}\{\text{H}\}$ ) and two dimensional ( $^1\text{H}$ ,  $^{13}\text{C}$ -HSQC,  $^1\text{H}$ ,  $^{13}\text{C}$ -HMBC,  $^1\text{H}$ ,  $^1\text{H}$ -COSY,  $^1\text{H}$ ,  $^1\text{H}$ -NOE) NMR spectroscopy. Publication was written by myself and corrected by Prof. Dr. Doris Kunz. The rhodium complex  $[\text{Rh}(\text{bimca}^{\text{Homo}})]$  was designed by Eva Jürgens.

DFT calculations were made by Prof. Dr. Doris Kunz. Elemental analyses were performed by Wolfgang Bock.

### **Publication 2:**

All the reactions and analyses described were planned and conducted by myself. Analyses include one dimensional ( $^1\text{H}$ ,  $^{13}\text{C}\{\text{H}\}$ ,  $^{19}\text{F}\{\text{H}\}$ ) and two dimensional ( $^1\text{H}$ ,  $^{13}\text{C}$ -HSQC,  $^1\text{H}$ ,  $^{13}\text{C}$ -HMBC,  $^1\text{H}$ ,  $^1\text{H}$ -COSY,  $^1\text{H}$ ,  $^1\text{H}$ -NOE) NMR spectroscopy. Publication was written by myself and corrected by Prof. Dr. Doris Kunz. The  $\text{bimca}^{\text{Me,Homo}}$  ligand was designed by Eva Jürgens and Katharina Mill.

DFT calculations were made by Prof. Dr. Doris Kunz. All the X-ray structure analyses were done by Theo Maulbetsch and Ronja Jordan. Elemental analyses were performed by Wolfgang Bock.

### **Publication 3:**

All the reactions and analyses described were planned and conducted by myself. Analyses include one dimensional ( $^1\text{H}$ ,  $^{13}\text{C}\{\text{H}\}$ ,  $^{19}\text{F}\{\text{H}\}$ ) and two dimensional ( $^1\text{H}$ ,  $^{13}\text{C}$ -HSQC,  $^1\text{H}$ ,  $^{13}\text{C}$ -HMBC,  $^1\text{H}$ ,  $^1\text{H}$ -COSY,  $^1\text{H}$ ,  $^1\text{H}$ -NOE) NMR spectroscopy. Publication was written by myself and corrected by Prof. Dr. Doris Kunz.

DFT calculations were made by Prof. Dr. Doris Kunz. All the X-ray structure analyses were done by Prof. Dr. Karl W. Törnroos, Theo Maulbetsch and Ronja Jordan. Elemental analyses were performed by Wolfgang Bock.

**Publication 4:**

All the reactions and analyses ( $^1\text{H}$ ,  $^{13}\text{C}\{\text{H}\}$ ,  $^{19}\text{F}\{\text{H}\}$  NMR spectroscopy) described were planned and conducted by myself. Publication was written by myself and corrected by Prof. Dr. Doris Kunz.

## Curriculum Vitae

---

### Yingying Tian

**Born:** August 1989, AnHui Province, China

**Address:** Institute of Inorganic Chemistry,  
University of Tuebingen  
Auf der Morgenstelle 18, 72076 Tuebingen, Germany

**Telephone:** +49 17630177953

**E-mail:** [yingying.tian@student.uni-tuebingen.de](mailto:yingying.tian@student.uni-tuebingen.de)

**ORCID:** <https://orcid.org/0000-0001-8894-576X>

---

### Education

10/2016–Present **PhD Student** (Advisor: Prof. Dr. Doris Kunz)

Institute of Inorganic Chemistry, University of Tuebingen, Germany

*Thesis:  $C_{NHC}NC_{NHC}$ -Pincer Complexes of Group 9 and Their Catalytic Activities in Homogeneous Catalysis*

08/2013–07/2016 **Master** (Advisor: Prof. Dr. Qian Cai)

Guangzhou Institutes of Biomedicine and Health, Chinese Academy of Sciences, China

*Thesis: Transition-Metal Catalyzed Asymmetric Aryl Carbon-Heteroatom Coupling Reactions*

09/2008–07/2012 **Bachelor** (Advisor: Prof. Dr. Shihua Zhong)

Pharmaceutical Engineering, Hunan Normal University, China

*Thesis: Studies on Synthesis and Properties of Macroporous Crosslinked Resin Modified by Validoxylamine A and Absorption for Salicylic Acid*

---

### Main Honors

2016 PhD sponsorship, China Scholarship Council

2015 Excellent Student, Chinese Academy of Sciences

### Professional Skills

- Solid knowledge of Schlenk techniques and glovebox handling
- Design and synthesis of organometallic complexes and structure characterization (NMRs, GC-MS, MS, IR, UV, etc.)
- Homogeneous catalytic reaction development and mechanistic study
- Multiple-step synthesis
- Purification skills including recrystallization and column chromatography
- Proficient in computer skills (Scifinder, EndNote, Mercury, Topspin, MestReNova, ChemDraw, Origin, ACD Labs and Microsoft Office)
- Excellent in English speaking, writing and reading

### Supervisor Experience

- Since 2017 Supervisor to master students in their practical courses
- 2018 Laboratory demonstrator to high school students
- 2019 Laboratory demonstrator to high school students

### Publications

#### Journal Papers

- 1) **Y. Tian**, E. Jürgens, D. Kunz, Regio- and chemoselective rearrangement of terminal epoxides into methyl alkyl and aryl ketones, *Chem. Commun.*, **2018**, 54, 11340.
- 2) **Y. Tian**, E. Jürgens, K. Mill, R. Jordan, T. Maulbetsch, D. Kunz, Nucleophilic Isomerization of Epoxides by Pincer-Rhodium Catalysts: Activity Increase and Mechanistic Insights, *ChemCatChem*, **2019**, 11, 4028.
- 3) **Y. Tian**, T. Maulbetsch, R. Jordan, K. W. Törnroos, D. Kunz, Synthesis and Reactivity of Cobalt(I) and Iridium(I) Complexes Bearing a Pentadentate *N*-Homoallyl Substituted Bis(NHC) Pincer-Ligand, *Organometallics*, **2020**, 39, 1221.
- 4) **Y. Tian**, D. Kunz, Nucleophilic Rh<sup>I</sup> Catalyzed Selective Isomerization of Terminal Aziridines to Enamides, *ChemCatChem*, **2020**, DOI: 10.1002/cctc.202000597.

- 5) J. Liu, **Y. Tian**, J. Shi, S. Zhang, Q. Cai, An Enantioselective Synthesis of Spiroblactams through Copper-Catalyzed Intramolecular Double N-Arylation and Phase Separation. *Angew. Chem. Int. Ed.*, **2015**, 37, 10917.

### **Conference Participation**

1) **Y. Tian**, E. Jürgens, D. Kunz, Rh-Catalyzed Regio- and Chemoselective Rearrangement of Epoxides and Aziridines, 20<sup>th</sup> Organometallic Catalysis Directed Towards Organic Synthesis (OMCOS), July 21-25, **2019**, Heidelberg, Germany. (Poster)

2) **Y. Tian**, E. Jürgens, D. Kunz, Rh-Catalyzed Regio- and Chemoselective Rearrangement of Terminal Epoxides into Methyl Alkyl and Aryl Ketones, 28<sup>th</sup> International Conference on Organometallic Chemistry (ICOMC), July 15-20, **2018**, Florence, Italy. (Poster)

3) **Y. Tian**, E. Jürgens, D. Kunz, A Highly Active and Selective Catalyst for the Nucleophilic Meinwald Rearrangement of Terminal Epoxides into Methyl Ketones, ACS on campus, October 10-11, **2018**, Heidelberg, Germany. (Poster)

4) **Y. Tian**, E. Jürgens, D. Kunz, Rhodium Catalyzed Meinwald Rearrangement of Terminal Epoxides to Ketones, Anglo-German Inorganic Chemistry Conference (AGICHEM), August 6-9, **2017**, Göttingen, Germany. (Poster)

5) **Y. Tian**, Summer School on Chiral Reagents, Nankai University, July 12-20, **2015**, Tianjin, China.

---

### **Oral presentation**

Homogeneous Catalysis with Group 9 Bis(NHC)-Pincer Complexes, inorganic seminar, University of Tübingen, **2019**.